Washington University in St. Louis
Washington University Open Scholarship

All Theses and Dissertations (ETDs)

1-1-2012

Investigation of the Structure of Alkyne Self-Assembled Monolayers on Gold and the Development of Matrix-Enhanced Secondary Ion Mass Spectrometry Methods

Jennifer Dertinger
Washington University in St. Louis

Follow this and additional works at: https://openscholarship.wustl.edu/etd

Recommended Citation

Dertinger, Jennifer, "Investigation of the Structure of Alkyne Self-Assembled Monolayers on Gold and the Development of Matrix-Enhanced Secondary Ion Mass Spectrometry Methods" (2012). *All Theses and Dissertations (ETDs)*. 569.
https://openscholarship.wustl.edu/etd/569

This Dissertation is brought to you for free and open access by Washington University Open Scholarship. It has been accepted for inclusion in All Theses and Dissertations (ETDs) by an authorized administrator of Washington University Open Scholarship. For more information, please contact digital@wumail.wustl.edu.

WASHINGTON UNIVERSITY IN ST LOUIS

Department of Chemistry

Dissertation Examination Committee:

Amy V. Walker, Advisor, Co-chair

Michael Gross, Co-chair

Joesph Ackerman

Robert Blankenship

Mark Conradi

Kevin Moeller

Investigation of the Structure of Alkyne Self-Assembled Monolayers on Gold and the Development of Matrix-Enhanced Secondary Ion Mass Spectrometry Methods

By

Jennifer Joan Dertinger

A dissertation presented to the
Graduate School of Arts and Sciences
of Washington University in
partial fulfillment of the
requirements for the degree
of Doctor of Philosophy

May 2012

Saint Louis, Missouri

ABSTRACT OF THE DISSERTATION

Characterization of thin films is critical to the understanding of many technological and biological processes. The focus of this dissertation is to develop methods to characterize very low concentration species present on surfaces.

A reflection adsorption infrared spectroscopy (RAIRS) system was constructed and tested. The instrument comprises an Fourier transform infrared (FTIR) spectrometer, an optical pathway and a vacuum chamber. The RAIRS system is designed to investigate *in situ* the interaction of vapor-deposited metals and gases, such as CVD precursors, with organic thin films, and so a vacuum chamber is required. To accommodate the vacuum chamber, an external IR optical pathway was designed and assembled because there was not enough room in the internal optical pathway of the FTIR spectrometer.

The synthesis and characterization of terminal alkyne monolayers (TAMs) adsorbed on gold was investigated by RAIRS, single wavelength ellipsometry, time-of-flight secondary ion mass spectrometry (TOF SIMS) and x-ray photoelectron spectroscopy (XPS). TAMs have the potential to transform surface functionalization for many technological applications because they have increased temperature stability and electrical conductance. However, the data suggest that TAMs are not well-ordered and can be oxidized, which may limit their application. For TAMs with less than 11 methylene units in the backbone, the adsorbed layer is highly disordered, oxidized and has a multilayer structure. Longer chain length TAMs form disordered monolayers on gold. As the methylene chain length increases, the conformational order of the TAMs increases with the alkynes in an upright conformation and bound to the surface via a Au-$C\equiv C$- bond.

The use of room temperature ionic liquids (ILs) as matrices in TOF SIMS was examined to further characterize biological thin films. The data indicate that the secondary ion intensities of lipids, steroids, peptides, proteins and proteins are significantly enhanced using IL matrices. Secondary ion enhancements of at least an order of magnitude are typically observed. Limits of detection are also greatly improved. For example, the limits of detection of 1,2-dipalmityl-sn-glycero-phosphocholine (DPPC) and 1,2-dipalmityl-sn-glycero-phosphoethanolamine (DPPE) were at least two orders of magnitude better. The data also show that ILs are suitable matrices for imaging SIMS. The IL matrices did not cause changes to the sample surface; no “hot spots” were observed.

The mechanism of the secondary ion intensity enhancements using IL matrices was then investigated to optimize use in characterization. Only protic ILs, which are formed by the transfer of a proton from a Brønsted acid to base, were observed to increase analyte signals. The matrix enhancement mechanism therefore involves the transfer of protons from, or to, the analyte, to, or from the matrix. The magnitude of the analyte signal enhancements is dependent on the chemistry of the matrix cation, anion and analyte. The pK_a of the matrix acid and base do not appear to have a strong effect on the ion-intensity enhancements. The results also indicate that the chemical identity of the matrix anion has a stronger effect on analyte signal enhancements than the matrix cation.

Acknowledgements

I would like to offer my deepest gratitude to my advisor, Dr. Amy V. Walker. She has been a mentor in every sense of the word, caring about her students while guiding their studies. Words cannot express how much she has shaped my life, professionally and personally.

I would like to thank the members of my committee, Dr. Michael Gross, Dr. Joesph Ackerman, Dr. Kevin Moeller, Dr. Robert Blankenship and Dr. Mark Conradi, for their time and insights into my research and this dissertation. A special thank you to Dr. Gross for agreeing to serve as the co-chair.

Additionally, I would like to thank the many people who helped make the research in this dissertation possible.

The construction of the RAIRS chamber was assisted by the machinists in two machine shops. Thank you to Jim Linders (WU), who provided much insight and wisdom, Larry Guerdan (WU), and Dave Stimson (UTD).

The administrative staff in both the Washington University in St. Louis Chemistry Department and the Materials Science and Engineering Department at the University of Texas at Dallas, have been extremely helpful, providing support and assistance with the multitude of paperwork needed.

The graduate students in my group- Gabriella Nagy, Chuanzhen Zhou, Peng Lu, Zhiwei Shi, Jing Yang, and Ricardo Pineda García- have been both friends and colleagues. Their assistance has been invaluable. Several undergraduates have assisted as well. Thank you to Charlie Barrows, Ely Shapiro, Paul Kunnath, Katie Borner and Kristen Genter.

I would like to thank the faculty, staff and students of the University of Texas at Dallas Materials Science Department. They made me feel a part of the department, and became my friends. A special thanks to the Quevedo group for teaching me Spanish. It will be a skill that I will use throughout my life.

Finally, I would like to thank my parents, Barbara and Thomas Dertinger. I would not be the person I am today without them.

Table of Contents

Foreword

Thesis Abstract……………………………………………………………..…..…ii

Acknowledgments…………………………………………………………..……v

Table of Contents…………………………………………………………..….vii

List of Tables……………………………………………………………………xvi

List of Figures…………………………………………………………………xvii

Abbreviations…………………………………………………………………xxiv

Chapter 1

Introduction

1.1 Characterization……………………….……………………………………1

1.2 Research Objectives…………………………………………………………...3

1.3 References…………………………………..…………………………….5

Chapter 2

Time of Flight Secondary Ion Mass Spectrometry

2.1 Introduction ………………...……………………….…………………………...11

2.2 The Basic Principle of SIMS………………………...12

2.3 Mass Spectrometric Imaging………………………………...………………13

2.4 Time of Flight Secondary Ion Mass Spectrometer………………………………..13

2.4.1 Vacuum System……………………………………………………………14

2.4.2 Primary Ion Source…………………………………………...…………..…15

2.4.3 Time of Flight Analyzer……………………………………………………19

2.5 References…………………………………………………………………22

Chapter 3

Construction of a High Vacuum Chamber for Reflection Absorption Infrared Spectroscopy (RAIRS)

Abstract…………………………………………….…………………26

3.1 Introduction……………………………………………..……………27

3.2 IR excitation of molecules……………………………….…………27

3.3 Fourier Transform Infrared Spectroscopy……………………...………30

3.4 Reflection Absorption Infrared Spectroscopy……………….……………32

3.5 Construction of a RAIRS Instrument Equipped with a Vacuum System……34

3.5.1 IR Optical Pathway……………………………………………….……..35

3.5.2 Vacuum System…………………………………………………………37

3.5.2.1 Gas Handling System……………………………….……38

3.5.2.2. Quantification of Metal Deposition……………….…….38

3.5.2.3 Vacuum System…………………………….....…..40

3.6 Design and Construction of the Sample Holder…………………………..41

3.7 Testing…………………………………………………………….…….46

3.7.1 IR spectra of Octadecanethiol Adsorbed on Au………………..…46

3.7.2 Heating and Cooling of the Sample………………………….….47

3.8 Conclusions……………………………………………………..……49

3.9 References…………………………………………………...…….49

Chapter 4

Formation and Structure of Terminal Alkyne Self-Assembled Monolayers on Au

Abstract……………………………………………………………………..54

4.1 Introduction…………………………………………….……………….55

4.2 Experimetal…………………………………….…………………57

4.2.1 Materials……………………………………….…………………..57

4.2.2 Monolayer Synthesis……………………………………………….58

4.2.3 Single Wavelength Ellipsometry…………………………………..58

4.2.4 X-ray Photoelectron Spectroscopy…………………...…………58

4.2.5 Reflection absorption infrared spectroscopy…………...………….59

4.2.6 Time-of-Flight Secondary Ion Mass Spectrometry………………..59

4.3 Results……………………………………………………………………..59

4.3.1 Ellipsometry………………………………………………………..59

4.3.2 XPS…………………………………………………………….…..62

4.3.3 Reflection Absorption Infrared Spectroscopy…………………..…67

4.3.4 Time-of-Flight Mass Spectrometry…………………….……….69

4.4 Discusssion…………………………………………………….…….71

4.5 Conclusions………………………………………………………………..74

4.6 References………………………………………………………..…..74

Chapter 5

Matrix-Enhanced Secondary Ion Mass Spectrometry (ME SIMS) Using Room Temperature Ionic Liquid Matrices

Abstract……………………………………………………………………..83

5.1 Introduction…………………………………………………………..84

5.2 Experimental………………………………………………………....89

5.2.1 Materials……………………………………………………...89

5.2.2 Preparation of Ionic Liquids…………………………………….89

5.2.3 Sample Preparation…………………………………...………90

5.2.4 Time-of-Flight Secondary Ion Mass Spectrometry……………..…90

5.3 Results and Discussion…………...…………………………………….91

5.3.1 Molecular and Fragment Ions……...………………………………91

5.3.2 Imaging…………………………….……..…………………102

5.4 Mechanism……………………………………...…………………..104

5.5 Conclusions……………………………………...………………….106

5.6 References…………………………………………..………………107

Chapter 6

Proton Transfer in Matrix-Enhanced Secondary Ion Mass Spectrometry Using Ionic Liquid Matrices

` Abstract…………………………………………………………...……….114

6.1 Introduction……………………………………………………………………115

6.2 Experimental…………………………………………………………………..119

6.2.1 Materials…………………………………....……………….119

6.2.2 Preparation of Ionic Liquids……………………..…………….119

6.2.3 Sample Preparation……………………………...…………..120

6.2.4 Time of Flight Secondary Ion Mass Spectrometry……..………...120

6.3 Results and Discussion……………………………………………….………121

6.4 Conclusions………………………………………………………...……137

6.5 References……………………………………………………………………..138

Chapter 7

Toward the Rational Design of Ionic Liquid Matrices for Secondary Ion Mass Spectrometry: Role of the Anion

Abstract……………………………………………………………………….141

7.1 Introduction……………………………………………………………………142

7.2 Experimental…………………………………………………………………..147

7.2.1 Materials…………………………………………………....... 147

7.2.2 Ionic Liquid Preparation……………………………………… 147

7.2.3 Sample Preparation…………………………………………….... 148

7.2.4 Time of Flight Secondary Ion Mass Spectrometry………..……..148

7.3 Results and Discussion………………………………………..………149

7.3.1 pK_a of Matrix Acid……………………………………………152

7.3.2 Chemical Identity of Substituents on the Benzene Ring of the Anion ………………………………………………………..154

7.3.3 Position of Substituents on the Benzene Ring of the Anion…..….156

7.3.4 Number of Substituents on the Benzene Ring of the Anion…..….156

7.4 Conclusions……………………………………………………….. 161

7.5 References……………………………………………………… 162

Chapter 8

Examining High Molecular Weight Species Using Ionic Liquid Matrices in Time-of-Flight Secondary Ion Mass Spectrometry

Abstract……………………………………………………………... 168

8.1 Introduction………………………………………………………169

8.2 Experimental……………………………………………………..174

8.2.1 Materials…………………………………………………….174

8.2.2 Ionic Liquid Preparation……………………………………….174

8.2.3 Sample Preparation…………………………...………..175

8.2.4 Time of Flight Secondary Ion Mass Spectrometry……….………175

8.3 Results and Discussion……………………………………………..176

8.3.1 Polymers…………………………………………….……176

8.3.1.1 Low Molecular Weight Polymers: Polystyrene and Polyisoprene…………………………………………………176

3.1.1.2 Polypropylene Glycol and Polyethylene Oxide………...178

3.1.1.3 High Molecular Weight Polymers……………………...180

8.3.2 Proteins……………………………….…………..181

8.3.2.1 Bradykinin………………………………...…….181

8.3.2.2 Other Proteins…………………………..…185

8.4 Conclusions…………………………………………………185

8.5 References…………………………………………………..186

Chapter 9

9.1 Conclusions…………………………………………………191

9.2 Future Work…………………………………………….........193

9.3 References……………………………………………………………..194

Appendices

Appendix 1 Design of RAIRS instrument……………………………………………..197

Appendix 2 Characterization of Terminal Alkyne Monolayers………………………200

Appendix 3 Characterization of Ionic Liquids………………………………………..206

Appendix 4 Complete Matrix and Analyte Spectra…………………………………..255

Appendix 5 Fragment Ions of Deuterated Species……………………………………423

List of Tables

3.1 Vibrational stretches of octadecanethiol monolayer ……………………………47

4.1 Ellipsometric film thickess of the alkyne monolayers adsorbed on Au …………61

4.3 Peak Positions for alkyne IR modes in the gas phase and adsorbed on Au ……..69

6.1 Proton affinity, gas phase basicity and pK_a of various imidazoles …………….136

7.1 Summary of enhancements of quasimolecular ions for analytes using IL matrices ………………………………………………………………………...150

8.1 Structure of polymers studied. …………………………………………………172

8.2 Structure of proteins studied …………………………………………………...172

List of Figures

2.1 A schematic of the SIMS process……………………………………………..11

2.2 A schematic of the ION TOF IV vacuum system………………………………..14

2.3 A schematic of the liquid metal ion source………………………………………16

2.4 A schematic of the ion optics of the liquid metal ion gun………………………17

2.5 A schematic diagram of the bunching process…………………………………..18

2.6 A schematic of the time-of-flight mass analyzer equipped with a reflectron…...21

3.1 Six possible vibrational modes observed by IR spectroscopy…………………...29

3.2 A Michelson interferometer……………………………………………………...31

3.3 A schematic diagram of the electric fields of the incident and reflected IR beam at a bare metal surface……………………………………………………………..34

3.4 A schematic of the infrared spectroscopy system………………………………..34

3.5 RAIRS chamber. a) Front, b) side, c) top schematics and d) picture of instrument……………………………………………………………………….39

3.6 Pumping diagram of the RAIRS vacuum chamber and gas line………………...40

3.7 A schematic of the sample manipulation system. The sample platen is placed on the variable temperature sample holder, which is then lowered onto the sample guide for IR analyses……………………………………………………………42

3.8 A schematic of the sample platen……………………………………………..42

3.9 The copper block with cooling lines of the sample holder………………………44

3.10 Insulating Delrin piece of the sample holder……………………………………44

3.11 Sample guide ring of the sample holder system…………………………………45

3.12 RAIRS spectra of an octadecanethiol monolayer on gold…….…………………46

3.13 The variation of the sample temperature with a) the pressure of cooled nitrogen gas; and b) the temperature of heated nitrogen gas………………………………48

4.1 Reaction to form acetylide anion……………………………………………...57

4.2 Ellipsometric film thickness of the alkyne monolayers of experimental and literature values…………………………………………………………………..61

4.3 C 1s XPS spectrum of a dodecyne monolayer on Au showing curves fitted to the experimental data………………………………………………………………..63

4.4 Fraction of the –CH$_2$-, CO, COO signals in the C1 XPS spectrum as a function of chain length……………………………………………………………………64

45 Fractional intensity of the C 1s peak (I(C 1s)$_n$/I(C 1s)$_{18}$ as a function of chain length……………………………………………………………………………..66

4.6 IRS spectra as a function of chain length for alkyne monolayers adsorbed on Au: a) 2800 – 3000 cm^{-1} and b) 2120-2000 cm^{-1}……………………………………68

4.7 High mass resolution negative ion spectra centered at *m/z* 255.5 and *m/z* 420 as a function of chain length for alkyne monolayers adsorbed on Au………………..71

5.1 SIMS images of DPPC, a phospholipid, mixed with sinapinic acid, a MALDI matrix. Area of analysis: 100 x 100 μm^2: 128 x 128 pixels. Primary ion: Bi^+. Primary ion energy: 25 keV………………………………………….........................86

5.2 Structures of a) trip CHCA, b) MI CHCA, c) DPPC, d) DPPE, e) cholesterol, f) Lys (Des-Arg9-Leu8) bradykinin, and g) angiotensin I………………………88

5.3 High mass resolution SIMS spectra of the quasimolecular ions of a) DPPE, b) DPPC, and c) cholesterol in MI CHCA and trip CHCA matrices, and with no matrix applied. Concentration of DPPE and DPPC: 0.5 mg/ml. Concentration of cholesterol: 1.0 mg/ml………………………………………………...………92

5.4 The enhancement of the quasimolecular ion intensities of a) DPPC and b) DPPE with analyte concentration…………………………………………………….95

5.5 The ion intensity enhancement of representative fragment ions and molecular ions at four different concentrations of analyte (1, 0.5, 0.1 and 0.05 mg/ml) for

a) DPPC, b) DPPE and c) cholesterol with MI CHCA…………………………..97

5.6 SIMS spectra of lys (Des-Arg9-Leu8) bradykinin using a) MI CHCA, b) trip CHCA and c) no matrix………………………………………………………99

5.7 Negative TOF SIMS images of DPPE ($(M - H)^-$, *m/z* 690) and the matrix ($(CHCA - H)^-$, *m/z* 188)……………………………………………………..100

5.8 Normalized ion intensities of the molecular and characteristic fragment ions of DPPE, DPPC and MI CHCA………………………………………………102

5.9 The optical and negative mass spectrometric images of a red onion skin treated with a) no matrix, b) MI CHCA, or c) trip CHCA……………………………..104

6.1 Structures of a) DPPC; b) d62 DPPC; and c) d75 DPPC………………………118

6.2 Structures of the ionic liquid matrices employed: a) MI CHCA; b) dMI CHCA; c) MI_2 CHCA; d) EI CHCA; e) BI CHCA; and f) trip CHCA…………………118

6.3 Variation of quasimolecular ion intensities with mixing time: a) $(DPPC + H)^+$; b) $(CHCA - H)^-$; and c) $(MI + H)^+$……………………………………………..124

6.4 SIMS spectra from *m/z* 732 to *m/z* 737 of DPPC using MI CHCA, trip CHCA, dMI CHCA and MI_2CHCA as matrices. A control sample (“no matrix”) is shown for reference……………………………………………………………….127

6.5 Variation of the ion intensities of $(DPPC)^+$ and $(DPPC - H)^+$ with mixing time…………………………………………………………………………..128

6.6 SIMS spectra of the molecular ion intensities of a) d62 DPPC and b) d75 DPPC using using MI CHCA, dMI CHCA and MI_2CHCA as matrices. A control sample ("no matrix") is shown for reference………………………………………130

6.7 SIMS spectra from *m/z* 187 to *m/z* 191 showing the $(CHCA – H)^-$ ion region for DPPC, d62 DPPC and d75 DPPC with MI CHCA as the matrix…………….132

6.8 SIMS spectra of the protonated cation intensities a) $(MI + H)^+$ and $(MI + 2)^+$, and b) $(dMI + H)^+$ and $(dMI + D)^+$ using DPPC, d62 DPPC and d75 DPPC as the analytes……………………………………………………………………133

6.9 a) Variation of secondary ion enhancements for the protonated molecular ion of DPPC and d62 DPPC with matrix cation. b) Variation of the ratio of I((cation + $D)^+$ to I$(cation + H)^+$ with matrix cation using d62 DPPC……………………..137

7.1 The structure and pK_a of the matrix acids employed, and the abbreviations used for the matrix anions………………………………………………………145

7.2 The structures of a) DPPC, b) DPPE, c) leucine enkaphalin, d) bradykinin, e) polystyrene, f) polypropylene glycol, and g) cholesterol……………………146

7.3 TOF SIMS spectra of the quasimolecular ions of a) DPPC, and b) DPPE in MI PA and MI CHCA matrices, and with no matrix applied……………………………154

7.4 TOF SIMS spectra of the quasimolecular ions of a) cholesterol, b) DPPC, and c) DPPE in MI PA, MI MA and MI OA matrices, and with no matrix applied..158

7.5 TOF SIMS spectra of the quasimolecular ions of a) DPPC, and b) DPPE in MI CHCA and MI CMCA matrices, and with no matrix applied…………………160

8.1 The structure of ionic liquid matrices used a) MI CHCA, b) trip CHCA, c) MI DHB and d) trip DHB…………………………………………….……………173

8.2 SIMS spectra of the PS 1110 oligomer ion region using MI CHCA, trip CHCA, MI DHB, and trip DHB matrices, and with a control (no matrix applied)……177

8.3 SIMS spectra of polyisoprene oligomer ion region using MI CHCA, trip CHCA, MI DHB, and trip DHB matrices, and with a control (no matrix applied)…….178

8.4 SIMS spectra of PPG oligomer ion region using MI CHCA, trip CHCA, MI DHB, and trip DHB matrices, and with a control (no matrix applied)…………179

8.5 The oligomer and n-mer region of PPG with trip DHB and no matrix applied. The * denote oligomer ions. A and B denote two different series of n-mer ions, and their structure is shown…………………………………………………180

8.6 The protonated (a) and deprotonated (b) molecular ion enhancements of bradykinin (2-7), bradykinin (2-9), bradykinin ("1-9"), Lys-(Des-Arg9-Leu8) bradykinin ("Lys-Leu") and Lys-(Des-Arg9) bradykinin ("Lys-Phe") using MI CHCA, MI DHB, trip CHCA and trip DHB…………………………..184

Abbreviations

^{1}H NMR	Proton Nuclear Magnetic Resonance
AFM	Atomic force microscopy
BI	1-butylimidazole
BI CHCA	1-butylimidazolium α-cyanohydroxycinnamate
CA	Caffeic acid
CHCA	α-cyanohydroxycinnamic acid
CMCA	α-cyanomethoxycinnamic acid
d 62 DPPC	1,2-Dipalmitoyl(d62)-*sn*-glycero-3-phosphocholine
d75 DPPC	1,2-dipalmitoyl(d62)-*sn*-glycero-3-phosphocholine-1,1,2,2-d4-N,N,N-trimethyl-d9
DDY	Dodecyne
DHB	2,5 Dihydroxybenzoic acid
dMI	1-methylimidazolium-d6
dMI CHCA	1-methylimidazolium-d6 α-cyanohydroxycinnamate
DPPC	1,2- Dipalmitoyl-sn-glycero-3-phosphocholine
DPPE	1,2- Dipalmitoyl-sn-glycero-3-phosphoethanolamine
DY	Decyne
EI	1-ethylimidazole
EI CHCA	1-ethylimidazolium α-cyanohydroxycinnamate
FA	Ferulic acid
FMCA	4-(Trifluoromethyl)cinnamic acid

FTIR	Fourier transform infrared spectroscopy
GRHF	Growth Hormone Releasing Factors
GIXRD	Grazing incidence x-ray diffraction
HDY	Hexadecyne
IL	Ionic Liquid
IR	Infared Spectroscopy
IRS	Infrared Spectroscopy
LE	Leucine Enkephalin
LMIG	Liquid Metal Ion Gun
LMIS	Liquid Metal Ion Source
MA	*m*-coumaric acid
MALDI	Matrix assisted laser desorption ionization mass spectrometry
MCA	4-methylcinnamic acid
MCP	Multichannel plate
ME SIMS	Matrix enhanced Secondary ion mass spectrometry
meta-SIMS	metal enhanced secondary ion mass spectrometry
MI CA	1-methylimidazolium caffeiate
MI CHCA	1-methylimidazolium α-cyanohydroxycinnamate
MI CMCA	1-methylimidazolium α-cyanomethoxycinnamate
MI DHB	1-methylimidazolium 2,5- Dihydroxybenzoate
MI FA	1-methylimidazolium ferulate
MI FMCA	1-methylimidazolium 4-(Trifluoromethyl)cinnamate
MI MA	1-methylimidazolium m-coumarate

MI MCA	1-methylimidazolium 4-methylcinnamate
MI MXCA	1-methylimidazolium 4-methoxycinnamate
MI OA	1-methylimidazolium o-coumarate
MI PA	1-methylimidazolium p-coumarate
MI SA	1-methylimidazolium sinapinate
MI TMCA	1-methylimidazolium 3,4,5 trimethoxycinnamate
MI_2CHCA	di-1-methylimidazolium α-cyanohydroxycinnamate
MS	Mass spectrometry
MXCA	4-methoxycinnamic acid
OA	*o*-coumaric acid
ODT	Octadecanethiol
ODY	Octadecyne
OY	Octyne
PA	*p*-coumaric acid
PDMPO	Poly(2,6-dimethyl-p-phenylene oxide)
PEO	Polyethylene oxide
PET	Poly(ethylene terephtalate)
PI	Polyisoprene
PMMA	Poly (methylmethacyralate)
PPG	Polypropylene glycol
PS	Polystyrene
QCM	Quartz crystal microbalance
RAIRS	reflection absorption infrared spectroscopy

ROI	Region of Interest
RTIL	Room temperature Ionic Liquid
SA	Sinapinic acid
SAM	Self-assembled monolayer
SEM	Scanning electron microscopy
SERS	Surface-enhanced Raman scattering
SI	Secondary Ions
SIMS	Secondary Ion Mass Spectrometry
SPM	Scanning probe microscopy
STM	Scanning tunneling microscopy
SWE	Single wave ellipsometry
TAM	Terminal alkyne monolayer
TDY	Tetradecyne
TEM	Transmission electron microscopy
TMCA	3,4,5 trimethoxycinnamic acid
TOF	Time of flight
TOF SIMS	Time of flight secondary ion mass spectrometry
trip	Tripropylamine
trip CA	Tripropylammonium caffeiate
trip CHCA	Tripropylammonium α-cyanohydroxycinnamate
trip CMCA	Tripropylammonium α-cyanomethoxycinnamate
trip DHB	Tripropylammonium 2,5- Dihydroxybenzoate
trip FA	Tripropylammonium ferulate

trip FMCA	Tripropylammonium 4-trifluoromethylcinnamate
trip MA	Tripropylammonium m-coumarate
trip MCA	Tripropylammonium 4-methylcinnamate
trip MXCA	Tripropylammonium 4-methoxycinnamate
trip OA	Tripropylammonium o-coumarate
trip PA	Tripropylammonium p-coumarate
trip SA	Tripropylammonium sinapinate
trip TMCA	Tripropylammonium 3,4,5, trimethoxycinnamate
XPS	X-ray photoelectron spectroscopy
XRF	X-ray fluorescence

Chapter 1

Introduction

1.1. Characterization

The analysis of thin films and biological samples has many applications in molecular/organic electronics[1-7], solar cells[8-11], sensing[12-18], biological applications[12,19-30], and computer memory[6,17,18]. The complete characterization of complex samples, such as a biological tissue or an electronic device, requires the determination of both their physical and chemical structure. Further, by understanding their structure one gains insights into their mechanical[1,4,5,7], electrical[1,3-5,7,18,31], optical[8-11] and biological properties[20-23,25-28,32].

Physical characterization methods investigate the structure of the material including the position of atoms on the surface, the crystallinity of the layer and the topography.[33] Physical characterization methods can be further divided into indirect and direct methods. To obtain the physical structure, indirect methods require that the data collected are compared to a model of the data. An example of an indirect physical characterization method is grazing incidence x-ray diffraction (GIXRD), which measures the crystalline structure of thin films.[33] In this technique, x-rays impinge on a sample at a small incident angles, and a diffraction pattern of the surface layer is obtained. In direct methods the position of the atoms or molecules and topography of the sample is directly observed. Examples of these techniques include scanning tunneling microscopy (STM), atomic force microscopy (AFM), scanning electron microscopy (SEM) and transmission electron microscopy (TEM).[33] STM and AFM are examples of scanning probe microscopies (SPMs) and have lateral resolutions of Angstroms (10^{-10} m).[33] In these methods a sharp probe tip is scanned across a sample surface. The tip is in very close proximity to the surface because the SPM employs near-field interactions between the tip and sample.[33] In STM, the tunneling current is between the tip and surface is employed to determine the sample topography, while in AFM the force between the tip and the surface is used to image the sample. SEM employs a focused, collimated, high-energy electron beam that is rastered across the sample, and the scattered electrons are employed to construct an image of the surface with nm resolution. Transmission electron microscopy (TEM) is used to image to obtain sub-Angstrom resolution images of thin samples (< 500 Å thick), and provides information on the crystallinity and orientation of nanoscale objects.[33]

Chemical characterization methods are employed to determine the elemental and molecular composition of samples. Examples of chemical characterization techniques include infrared spectroscopy (IRS), Raman scattering, x-ray photoelectron spectroscopy (XPS), secondary ion mass spectrometry (SIMS), and X-ray fluorescence (XRF).[33] IRS and Raman scattering provide information about the characteristic vibrational modes of the bonds and groups present in compounds. SIMS is a desorption mass spectrometry method and is complementary to IRS and Raman scattering.[33] In this method, an energetic primary ion strikes a sample surface, leading to the ejection of secondary species, including positive and negative ions, which are characteristic of the sample chemistry.[34-40] By scanning a focused primary ion beam across the surface, an image of the sample chemistry can be obtained.[41-44] XPS and XRF provide information on the elemental composition of materials.[33] In these methods, an x-ray beam is incident on a sample. Upon x-ray adsorption, an electron (XPS) or a photon (XRF) are emitted, and they are characteristic of the elements present in the materials.[33]

1.2 Research Objectives

In this thesis, two surface analysis methods were investigated to analyze complex samples. A reflection absorption infrared spectrometry system was constructed. As a demonstration of its use, terminal alkyne monolayers adsorbed on Au were synthesized and characterized. Second ionic liquid matrix-enhanced secondary ion mass spectrometry was developed to characterize and image biological samples.

This thesis is organized in the following way. Chapter 2 describes time-of-flight secondary ion mass spectrometry (TOF SIMS) including its advantages and disadvantages, and the instrument used in these studies.

In Chapter 3 the construction of a reflection absorption infrared (RAIRS) spectrometer is described. The infrared system is designed to examine *in-situ* the interaction of vapor-deposited metals and reactive gases, including chemical vapor deposition precursors. This requires that the sample is housed in a vacuum chamber. To accommodate the vacuum chamber, an external optical IR pathway was constructed because there is not enough room in the internal interferometric optical pathway of the FTIR spectrometer.

Chapter 4 describes the synthesis and characterization of terminal alkyne monolayers (TAMs) adsorbed on gold substrates. The structure of a homogolous series of six n-terminal alkynes was investigated using XPS, single wavelength ellipsometry, TOF SIMS and RAIRS. Alkanethiolate self-assembled monolayers (SAMs) were used to functionalize surfaces in applications ranging from sensing to organic/molecular electronics. Terminal alkyne monolayers (TAMs) have the potential to revolutionize surface functionalization through greatly increased monolayer temperature stability and electrical conductance. However, our studies suggest that TAMs have more conformational disorder than alkanethiolate SAMS, which may limit their technological applications.

In Chapter 5 the use of ionic liquids as matrices in TOF SIMS is investigated. Two ionic liquid (IL) matrices derived from the MALDI matrix α-cyano-4-hydroxycinnamic acid (CHCA) were employed: 1-methylimidazolium α-cyano-4-hydroxycinnamate (MI CHCA) and tripropylammonium α-cyano-4-hydroxycinnamate (trip CHCA). The molecular ion intensities of biologically-relevant phospholipids, peptides and cholesterol are enhanced by at least an order of magnitude. Further, limits of detections were also significantly improved. For example the detection limit of 1,2-dipalmityl-sn-glycero-phosphocholine (DPPC) were 1000x better. The data also show that the IL matrices are suitable for SIMS imaging.

The mechanism for the enhancement of molecular ions in TOF SIMS is investigated in Chapters 6 and 7. Only protic ILs, which are formed by the transfer of a proton from a Brønsted acid to base, are observed to increase analyte signals. The matrix enhancement mechanism thus involves in part the transfer of protons from, or to, the analyte, to, or from the matrix. The magnitude of the analyte signal enhancement is partly dependent on the chemistry of both the matrix cation and anion. The pK_a of the matrix acid and base do not appear to have a strong effect on the analyte ion intensity enhancement. Further, the identity matrix cation does not significantly alter the magnitude of the analyte signal enhancements. Rather, the structure of the anion appears to greatly affect the analyte ion enhancements.

In Chapter 8 we investigate the analyte signal enhancements of polymers and proteins using by IL matrix-enhanced SIMS. Six polymers including polyisoprene, polypropylene glycol, and polystyrene were studied to determine the ion intensity enhancements of the *n*-mer and oligomer ions based on the polymer molecular weight and their chemistry. In addition, the molecular ion intensity enhancements of various proteins including bradykinin, angiotensin, insulin and cytochrome c were investigated. Using bradykinins with different terminal acids, we found that molecular ion intensities are significantly enhanced by using IL matrices if the N or C terminal amino acid can accept (or donate) a proton. Chapter 9 discusses the conclusions from this thesis, and suggests further studies that can be performed.

1.3 References

(1) Cao, Q.; Kim, H.-s.; Pimparkar, N.; Kulkarni, J. P.; Wang, C.; Shim, M.; Roy, K.; Alam, M. A.; Rogers, J. A., Medium-scale carbon nanotube thin-film integrated circuits on flexible plastic substrates. *Nature* **2008**, *454*, 495-502.

(2) Catchpole, K. R.; McCann, M. J.; Weber, K. J.; Blakers, A. W., A review of thin-film crystalline silicon for solar cell applications. Part 2: Foreign substrates. *Solar Energy Materials & Solar Cells* **2001**, *68*, 173-215.

(3) Cho, J. H.; Lee, J.; Xia, Y.; Kim, B.; He, Y.; Renn, M. J.; Lodge, T. P.; Frisbie, C. D., Printable ion-gel gate dielectrics for low-voltage polymer thin-film transistors on plastic. *Nature Materials* **2006**, *7*.

(4) Dimitrakopoulos, C. D.; Malenfant, P. R. L., Organic Thin Film Transistors for Large Area Electronics. *Adv. Mater.* **2002**, *14*, 99-117.

(5) Dimitrakopoulos, C. D.; Mascaro, D. J., Organic thin-film transistors: A review of recent advances. *IBM J. Res. & Dev.* **2001**, *45*, 11-27.

(6) Hwang, C. S.; Park, S. O.; Cho, H.-J.; Kang, C. S.; Kang, H.-K.; Lee, S. I.; Lee, M. Y., Deposition of extremely thin (Ba,Sr)TiO_3 thin films for ultra-large-scale integrated dynamic random access memory application. *Appl. Phys. Lett* **1995**, *67*, 2819-2821.

(7) Maheshwari, V.; Saraf, R. F., High-Resolution Thin-Film Device to Sense Texture by Touch. *Science* **2006**, *312*, 1501-1504.

(8) Aberle, A. G., Thin-film solar cells. *Thin Solid Films* **2009**, *517*, 4706-4710.

(9) Birkmire, R. W.; Eser, E., Polycrystalline Thin Film Solar Cells: Present Status and Future Potential. *Annu. Rev. Mater. Sci.* **1997**, *27*, 625-633.

(10) Bloss, W. H.; Pfeisterer, F.; Schubert, M.; Walter, T., Thin-film Solar Cells. *Progress in Photovoltaics: Research and Applications* **1995**, *3*, 3-24.

(11) Green, M. A., Thin-film solar cells: review of materials, technologies, and commercial status. *J. Mater. Sci: Mater Electron* **2007**, *18,* S15-S19.

(12) Jobst, G.; Moser, I.; Varahram, M.; Svasek, P.; Aschauer, E.; Trajanoski, Z.; Wach, P.; Kotanko, P.; Skrabal, F.; Urban, G., Thin-Film Microbiosensors for Glucose-Lactate Monitoring. *Anal. Chem.* **1996**, *68*, 3173-3179.

(13) Sakai, G.; Baik, N. S.; Miura, N.; Yamazoe, N., Gas sensing properties of tin oxide thin films fabricated from hydrothermally treated nanoparticles. Dependence of CO and H_2 response on film thickness. *Sensors and Actuators B* **2001**, *77*, 116-121.

(14) Shen, W.; Zhao, Y.; Zhang, C., The preparation of ZnO based gas-sensing thin films by ink-jet printing method. *Thin Solid Films* **2005**, *483* 382-387.

(15) Tien, L. C.; Sadik, P. W.; Norton, D. P.; Voss, L. F.; Pearton, S. J.; Wang, H. T.; Ren, B. S. K. F.; Jun, J.; Lin, J., Hydrogen sensing at room temperature with Pt-coated ZnO thin films and nanorods. *Appl. Phys. Lett* **2005**, *87*, 222106.

(16) O'Hara, J. F.; Singh, R.; Brener, I.; Smirnova, E.; Han, J.; Taylor, A. J.; Zhang, W., Thin-film sensing with planar terahertz metamaterials: sensitivity and limitations. *Optics Express* **2008**, *16*, 1786-1795.

(17) Albert, F. J.; Katine, J. A.; Buhrman, R. A.; Ralph, D. C., Spin-polarized current switching of a Co thin film magnet. *Appl. Phys. Lett* **2000**, *77*, 3809-3811.

(18) Ouyang, J.; Chu, C.-W.; Szmanda, C. R.; Ma, L.; Yang, Y., Programmable polymer thin film and non-volatile memory device. *Nature Materials* **2004**, *3*, 918-922.

(19) Boisselier, E.; Astruc, D., Gold nanoparticles in nanomedicine: preparations, imaging, diagnostics, therapies and toxicity. *Chem Soc Rev* **2009**, *38*, 1759-1782.

(20) Boxer, S. G.; Kraft, M. L.; Weber, P. K., Advances in Imaging Secondary Ion Mass Spectrometry for Biological Samples. *Annu. Rev. Biophys.* **2009**, *38*, 53-74.

(21) Canavan, H. E.; Cheng, X.; Graham, D. J.; Ratner, B. D.; Castner, D. G., Surface Characterization of the Extracellular Matrix Remaining after Cell Detachment from a Thermoresponsive Polymer. *Langmuir* **2005**, *21*, 1949-1955.

(22) Kasemo, B., Biological surface science. *Surface Science* **2002**, *2002*, 656-677.

(23) Lu, H. B.; Campbell, C. T.; Graham, D. J.; Ratner, B. D., Surface Characterization of Hydroxyapatite and Related Calcium Phosphates by XPS and TOF-SIMS. *Anal. Chem.* **2000**, *72*, 2886-2894.

(24) Moghimi, S. M.; Hunter, A. C.; Murray, J. C., Nanomedicine: current status and future prospects. *The FASEB Journal* **2005**, *19*, 311-330.

(25) Ratner, B. D., Surface Characterization of Biomaterials by Electron Spectroscopy for Chemical Analysis. *Analysis of Biomedical Engineering* **1983**, *11*, 313-336.

(26) Rezania, A.; Johnson, R.; Lefkow, A. R.; Healy, K. E., Bioactivation of Metal Oxide Surfaces. 1. Surface Characterization and Cell Response. *Langmuir* **1999**, *15*, 6931-6939.

(27) Sunada, K.; Watanabe, T.; Hasimoto, K., Batericidal Activity of Copper-Deposited TiO_2 Thin Film under Weak UV Light Illumination. *Environ. Sci. Technol.* **2003**, *37*, 4785-4789.

(28) Sung, H.-W.; Chen, C.-N.; Huang, R.-N.; Hsu, J.-C.; Chang, W.-H., In vitro surface characterization of a biological patch fixed with a naturally occurring crosslinking agent. *Biomaterials* **2000**, *21*, 1353-1362.

(29) Voldman, J.; Gray, M. L.; Scmidt, M. A., Microfabrication in Biology and Medicine. *Annu. Rev. Biomed. Eng.* **1999**, *01*, 401-425.

(30) Roy, I.; Ohulchanskyy, T. Y.; Bharali, D. J.; Pudavar, H. E.; Mistretta, R. A.; Kaur, N.; Prasad, P. N., Optical tracking of organically modified silica nanoparticles

as DNA carriers: A nonviral, nanomedicine approach for gene delivery. *PNAS* **2004**, *102*, 279-284.

(31) Austin, M. D.; Chou, S. Y., Fabrication of 70nm channel length polymer organic thin-film transistors using nanoimprint lithography. *Appl. Phys. Lett* **2002**, *81*, 4431-4433.

(32) Dixhit, R. P.; Puthli, S. P., Oral strip technology: Overview and future potential. *Journal of Controlled Release* **2009**, *139*, 94-107.

(33) Leng, Y. *Materials Characterization: Introduction to Microscopic and Spectroscopic Materials*; John Wiley & Sons (Asia) Pte Ltd: Singapore, 2008.

(34) Belu, A. M.; Graham, D. J.; Castner, D. G., Time-of-flight secondary ion mass spectrometry: techniques and applications for the characterization of biomaterial surfaces. *Biomaterials* **2003**, *24*, 3635-3653.

(35) Adriaens, A.; Van Vaeck, L.; Adams, F., Static Secondary Ion Mass Spectrometry (S-SIMS) Part 2: Material Science Applications. *Mass Spectrometry Reviews* **1999**, *18*, 48-81.

(36) Benninghoven, A., Surface Investigation of Solids by the Stastical Method of Secondary Ion Mass Spectrometry. *Surface Science* **1973**, *1973*, 427-457.

(37) Benninghoven, A., Developments in Secondary Ion Mass Spectroscopy and Applications to Surface Studies. *Surface Science* **1975**, *53*, 596-625.

(38) Benninghoven, A., Chemical Analysis of Inorganic and Organic Surfaces and Thin Films by Static Time-of-Flight Secondary Ion Mass Spectrometry (TOF-SIMS). *Angew. Chem. Int. Ed. Engl.* **1994**, *33*, 1023-1043.

(39) Benninghoven, A.; Rudemauer, F. G.; Werner, H. W. *Secondary Ion Mass Spectrometry: Basic Concepts, Instrumental Aspects, Applications and Trends*; John Wiley & Sons: New York, NY, 1987.

(40) Williams, P., Secondary Ion Mass Spectrometry. *Annual Review of Materials Science* **1985**, *15*, 517-548.

(41) Belu, A. M.; Davies, M. C.; Newton, J. M.; Patel, N., TOF-SIMS Characterization and IMaging of Controlled-Release Drug Delivery Systems. *Analytical Chemistry* **2000**, *72*, 5625-5638.

(42) Gillen, G.; Bennett, J.; Tarlov, M. J.; Donald R.F. Burgess, J., Molecular Imaging Secondary Ion Mass Spectrometry for the Characterization of Patterned Self-Assembled Monolayers on Silver and Gold. *Analytical Chemistry* **1994**, *66*, 2170-2174.

(43) Schueler, B., Microscopic Imaging by Time-of-Flight Secondary Ion Mass Spectrometry. *Microsc. Microanal. Microstruct.* **1992**, *3*, 119-139.

(44) Walker, A. V., Why is SIMS Underused in Chemical and Biological Analysis? Challenges and Opportunities. *Analytical Chemistry* **2008**, *80*, 8865-8870.

Chapter 2

Time of Flight Secondary Ion Mass Spectrometry

2.1 Introduction

Secondary ion mass spectrometry (SIMS) is one of the desorption mass spectrometries. It is used in wide variety of fields including geochemistry[1], cosmology[2], organic electronics, and materials science[3] to analyze electronics[4-6], polymers[7], geological materials[1] and biomolecules[8,9]. In this technique energetic primary ions strike a sample surface leading to the ejection of secondary species – neutrals, positive and negative ions, and electrons. Figure 1 displays a schematic of the SIMS process. The ejected positive or negative secondary ions are then extracted and detected by using a mass analyzer. The majority of the sputtered species (~96 %) are neutrals. The ejected ions (~4 %) may be fragment, molecular or cluster ions.

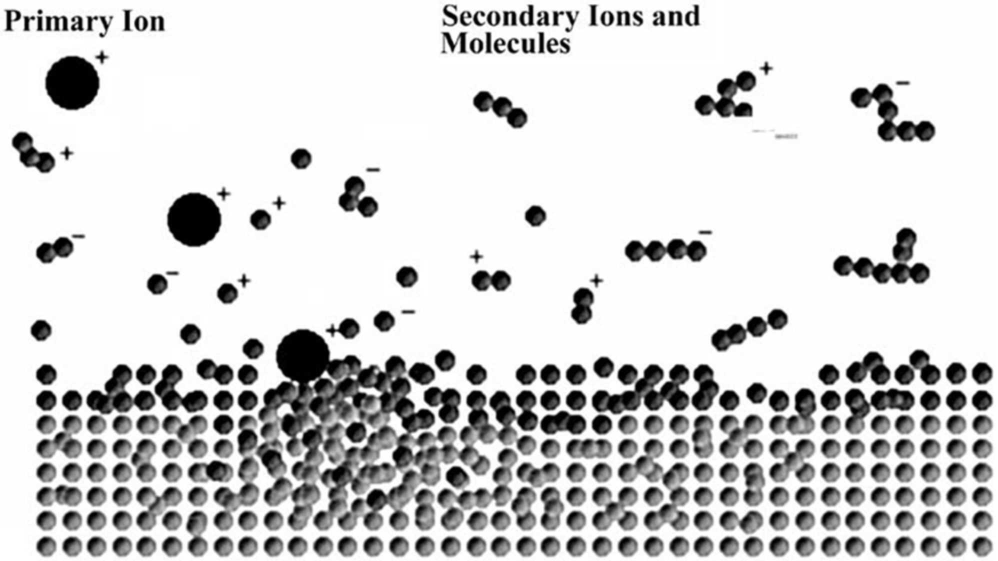

Figure 1: A schematic of the SIMS process. Figure used with permission.[10]

The first reports of surface sputtering by gaseous ions were in the mid-19th century.[11] In 1949, Herzog and co-workers[12] produced the first SIMS instruments. However, it only detected elemental and small fragment ions. There were two major developments that made it possible to desorb intact molecular ions from large organic molecules. In the late 1960s Benninghoven and coworkers[12-15] developed a single ion counting system, which allowed SIMS spectra to be obtained under low ion beam current conditions ("static" SIMS). Under these conditions, most of the sample surface is undamaged by the primary ion beam, and one can softly ionize the surface layer leading to the ejection of molecular ions. Second, time-of-flight instruments were developed in which ions at every mass are detected in parallel.[16-18]

2.2 The Basic Principle of SIMS

The formation of secondary ions by an incident primary ion beam incident on a surface is a complex process and is dependent on a number of parameters. The type and number of secondary ions produced are strongly dependent on the primary ion-beam properties including its energy, current density and type. Since the ionization and emission of species occurs in the top layers of the sample, the yield of secondary ions is also influenced by the electronic state of the substrate (the matrix). The secondary ion current, $I_m^{\pm}$ is, therefore, given by

$$I_m^{\pm} = I_p\, Y^m\, \eta^{\pm}\, \alpha^{\pm}\, \theta_m \qquad \text{Equation 2.1}$$

where I_p is the primary ion current, Y_m is the sputter yield, $\eta^{\pm}$ is the ion transmission efficience for positive (+) or negative (-) ions, $\alpha^{\pm}$ is the ionization probability of species m, and θ_m is the surface fractional coverage of species m.

SIMS is employed in one of two modes that are defined by the primary ion beam dose employed.[19] In static SIMS the ion dose is less 1 x 10^{13} ions cm^{-2} and thus < 1% of the surface is impacted, which allows intact molecular ions and large fragment ions to be observed.[20,21] Dynamic SIMS uses higher primary ion beam doses, allowing for depth profiling of materials.[22-24]

2.3 Mass Spectrometric Imaging

An important application of SIMS is mass spectrometric imaging. Mass spectrometric images can be obtained by both ion microscopes and ion microprobes. In an ion microscope an ion-optical collection system preserves the spatial relationship of the desorbed ions between a sample and a detector. The ion optics employed are very similar to the lens system used in an optical microscope.

A complementary imaging technique is the ion microprobe. In this technique the ion beam is rastered, or scanned, across the sample surface. An image of the sample is built up from the chemical information acquired at each pixel in a similar way to a photograph obtained using a CCD. This approach places less restrictions on the type of mass analyzer used and takes advantage of the small ion beam diameters generated using liquid metal ion guns.

2.4 Time-of-Flight Secondary Ion Mass Spectrometer

All TOF SIMS analyses in this thesis were performed using an ION TOF IV instrument (ION TOF Inc., Chestnut Hill, NY) equipped with a $Bi_m{}^n{}_+$ (m = 1-6, n = 1,2) liquid metal ion gun. A brief description of the components of the ION TOF IV is given in the following sections.

2.4.1 Vacuum system

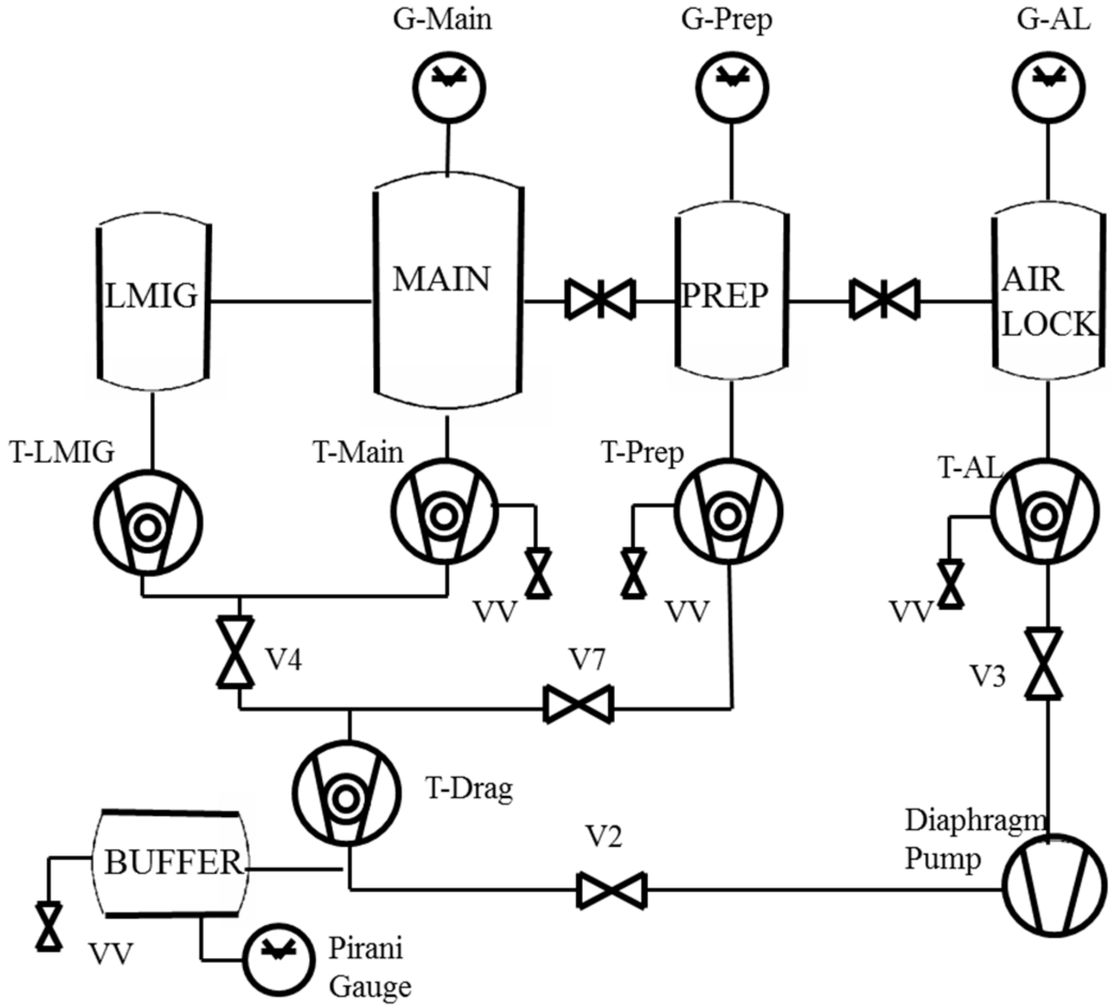
G-Main
G-Prep
G-AL
LMIG
MAIN
PREP
AIR
LOCK
T-LMIG
T-Main
T-Prep
T-AL
VV
VV
VV
V4
V7
V3
T-Drag
V2
Diaphragm
Pump
BUFFER
VV
Pirani
Gauge

Figure 2. A schematic diagram of the ION TOF IV vacuum system.

The spectrometer consists of an ultrahigh vacuum system with three connected chambers: a loadlock, a preparation chamber, and an analysis chamber. All chambers are separated by gate valves. Figure 2 displays a diagram of the vacuum system. The sample is introduced into the vacuum system via loadlock, which is pumped by a turbo pump (Pfeiffer TMU 260, 240 l/s N_2). Once the pressure of this chamber has reached ~2 x 10^{-6} mbar, the sample is transferred into the preparation chamber, which is pumped by a second, larger turbo pump (Leybold Turbovac 340M, 460 l/s N_2). The primary use of this chamber is to allow the sample to reach vhv pressures (~1 x 10^{-9} mbar). It can also be used to vapor-deposit metals and other compounds, such as CVD precursors, *in situ* on the sample. Finally, the sample is transferred to the analysis chamber for SIMS measurements. The analysis chamber is also pumped by a turbo pump (Leybold Turbovac 340M, 460 l/s N_2). The turbo pumps of the three chambers are backed by a drag pump (Pfeiffer TMU 064, 60 L/s N_2) through a buffer chamber to a diaphragm pump (Vacuubrandt MD4). The pressures in the analysis chamber is monitored using a cold cathode gauge, while the pressures in the loadlock and preparation chambers are measured using all range gauges.

2.4.2 Primary Ion Source

In a liquid metal ion gun (LMIG) a metal (or very low melting point alloy), in our case Bi, is melted. Once melted the metal wets a very sharp tungsten tip. A large electric field is applied to the tip leading to the formation of ions in a Taylor cone (Figure 3, extractor). The ion current is measured by using an ammeter and controlled using a suppressor" potential, which in effect reduces the magnitude of the extraction field.

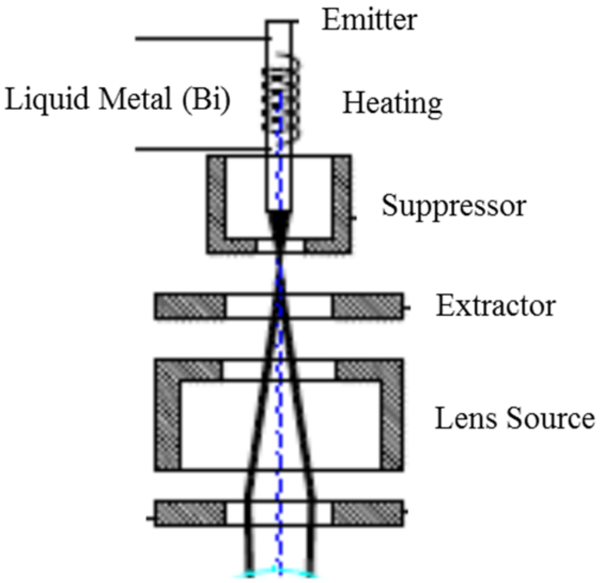
Emitter
Liquid Metal (Bi)
Heating
Suppressor
Extractor
Lens Source

Figure 3. A schematic diagram of a liquid metal ion source. Figure used with permission.[25]

After the ion beam is formed, ion optics are employed to focus the ion beam on the sample. Three lenses are employed: lens source, lens magnification, and lens target (Figure 4).

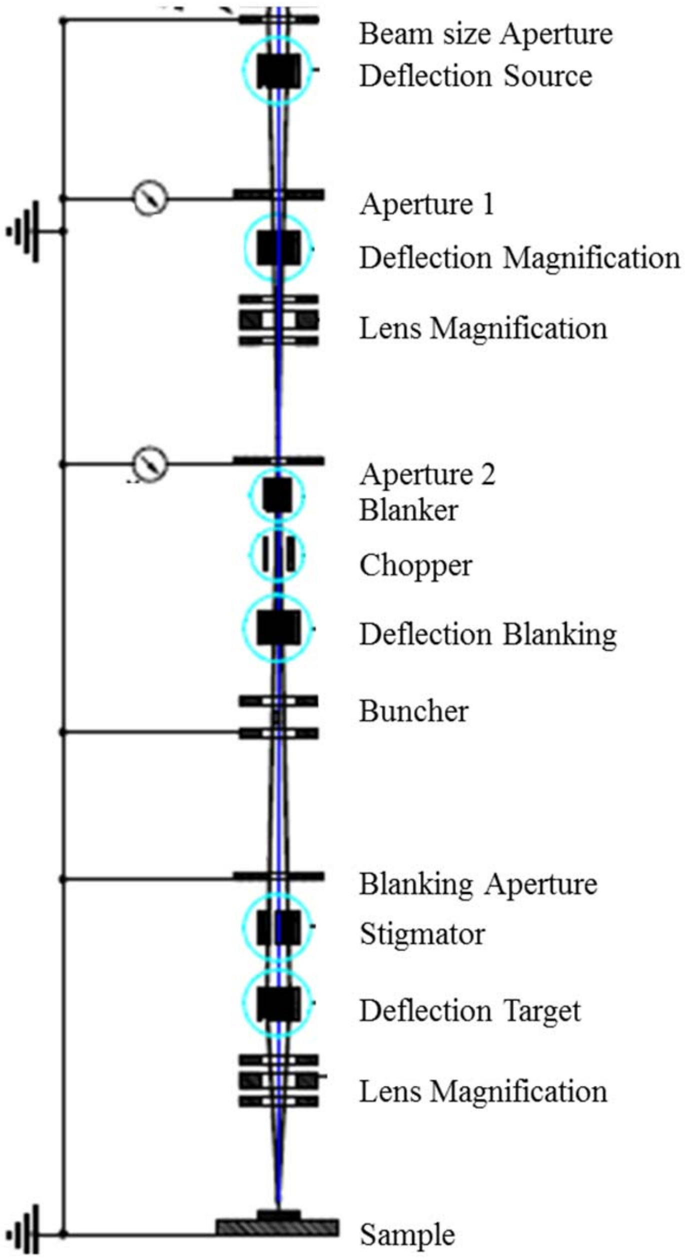
Beam size Aperture
Deflection Source
Aperture 1
Deflection Magnification
Lens Magnification
Aperture 2
Blanker
Chopper
Deflection Blanking
Buncher
Blanking Aperture
Stigmator
Deflection Target
Lens Magnification
Sample

Figure 4. Schematic of the ion optics of the ION TOF IV ion gun. Figure used with permission.[25]

Since the ION TOF employs a time-of-flight mass analyzer, the primary ion beam must be chopped into a series of pulses. The beam is first made into pulses of ~20 ns using a beam blanker that performs high-speed motionless beam blanking. The blanker consists of two plates. One plate is maintained at 0 V while the other has a voltage applied to it. The voltage generates an electric field that steers the primary ion beam into the plate. To form a pulse, the voltage on this plate is reduced to 0 V for a set time, allowing a pulse of ions to proceed towards the sample. The pulse width of the ion packet is further compressed to ~600 ps using a buncher. The buncher reduces the energy spread of the ion packet.

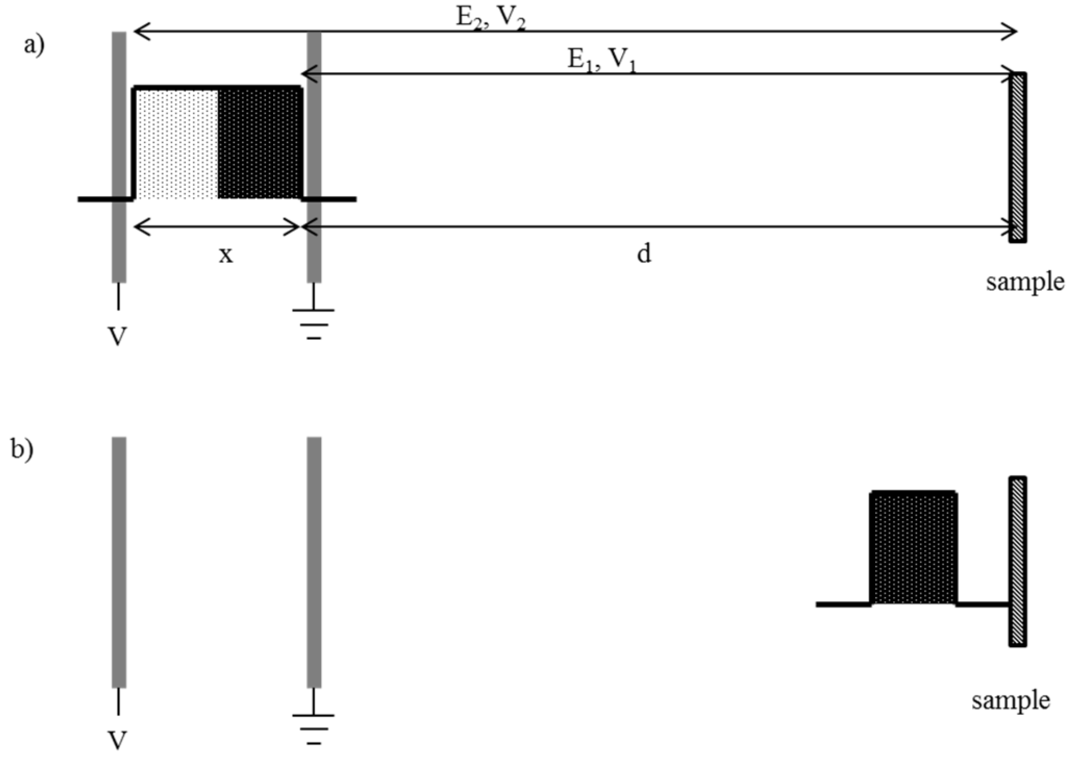

Figure 5. A schematic diagram of the bunching process.

Once an pulse of ions, with energy $E_1 = eV_1$ enters and fills the area between two plates, a voltage V is applied to the back electrode. This applied voltage accelerates the back of the ion packet towards the front of the pulse and so at the sample the ion pulse has a compressed width. This results in large improvements in the mass resolution observed in the SIMS spectra. The bunching voltage, V, is calculated in the following way. The distance of the front bunching plate to the sample is x, while the distance from the back buncher electrode to the sample is x + d. At the sample the front of the primary ion pulse has an The front of E_1, while the back of the pulse has a higher kinetic energy, $E_2 = eV_2 = e\ (V_1 + V)$. The kinetic energies of the front and back of the pulse can be re-written in terms of their velocities, v_1 and v_2, which in turn can be described by the distance that the ions have traveled from the buncher and their time of arrival, t. Thus, the energy of the front of the packet is given by

$$E_1 = eV_1 = \frac{1}{2} m v_{12}^2 = \frac{1}{2} m \frac{d^2}{t^2}$$

and the energy of the packet is

$$E_2 = eV_{12} = \frac{1}{2} m v_{12}^2 = \frac{1}{2} m \frac{(x+d)^2}{t^2}$$

Since $V_2 = V_1 + V$ and the ratio of the kinetic energies of the ions is $\frac{E_{12}}{E1} = \frac{V_2}{V_1} = \frac{(x+d)^2}{d^2}$, the bunching voltage, V, required is

$$V = V_1 \left(\frac{(x+d)^2}{d^2} - 1\right) \approx V_1 \frac{2x}{d}.$$

Finally, it is important to note that bunching cannot be employed in imaging mass spectrometry because the primary beam is no longer monoenergetic, which causes the primary ion beam diameter to widen significantly from ~100 nm to several μm.

2.4.3 Time of Flight Analyzer

After the secondary ions are generated, they are extracted into a time-of-flight mass analyzer using 2000 V. In a time-of-flight analyzer, the time of arrival of ions is measured. If the secondary ions are generated with the same kinetic energy and are singly charged, the time of flight, t, of the ion is proportional to the square root of the mass of the ion, $m^{1/2}$. However, in practice there are many instrumental variables that influence the flight time of the ion and so the time of flight of a singly charged ion with mass-to-charge ratio, *m/z* is

$$t = a(m/z)^{1/2} + c$$

However, ejected secondary ions have a small energy distribution due to uncertainties in the time of creation of the ion and the position of creation of the ion in the extraction field. To compensate for this energy spread a reflectron is employed.

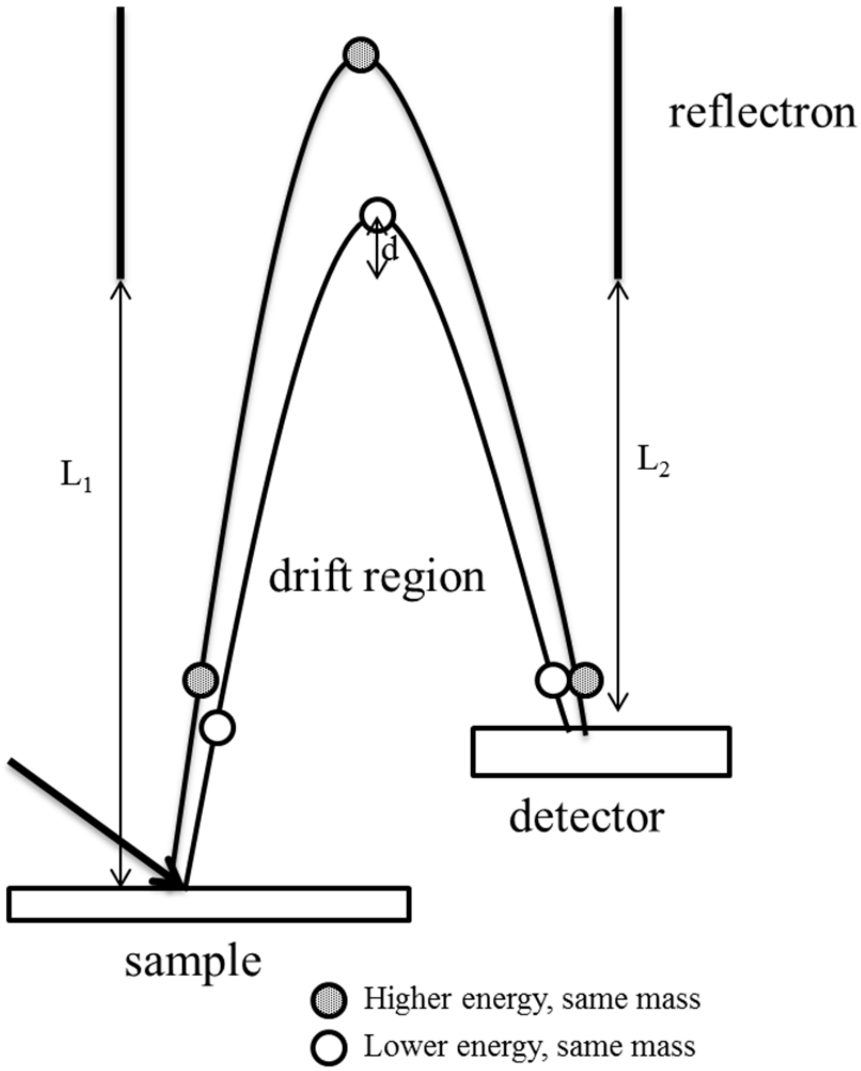
reflectron
d
L_1
L_2
drift region
detector
sample
Higher energy, same mass
Lower energy, same mass

Figure 4. A schematic diagram of a time-of-flight mass analyzer equipped with a reflectron.

In a reflectron mass analyzer there is are two field-free regions with lengths L_1 and L_2 separated by an ion mirror with a variable energy gradient. Ions with a large kinetic energy penetrate more deeply into the reflectron before stopping and being reflected with a potential V into the second field free region. In contrast ions with a lower energy penetrate less deeply into the reflectron being stopping and being reflected into the second field free region. The time of flight through the mass analyzer is now given by $t = (\frac{m_a}{2eV})^{1/2}[L_1 + L_2 + 4d]$

where d is the distance that the ion penetrates into the reflectron. Thus, secondary ions with different kinetic energies arrive at the detector simultaneously. After the secondary ions exit the flight tube, they are re-accelerated to 10 keV so that heavy ions can be efficiently detected by a multichannel plate (MCP). The MCP amplifies the generated secondary ions into a detectable pulse of electrons, which in turn is amplified and converted into photons by a scintillator. These photons are detected by a photomultiplier that converts the photons back into an electron pulse (current). The current is a measure of the intensity of the secondary ion siganl, while the time of arrival of the secondary ion corresponds to the mass-to-charge ratio.

2.5 References

(1) Toporski, J.; Steele, A., *Org. Geochem.* **2004**, *35*, 793-811.

(2) Stephan, T., *Planet Space Science* **2001**, *49*, 859-906.

(3) Adriaens, A.; Van Vaeck, L.; Adams, F., Static Secondary Ion Mass Spectrometry (S-SIMS) Part 2: Material Science Applications. *Mass Spectrometry Reviews* **1999**, *18*, 48-81.

(4) Haick, H.; Ghabboun, J.; Niitsoo, O.; Cohen, H.; Cahen, D.; Vilan, A.; Hwang, J.; Wan, A.; Amy, F.; Kahn, A., *Journal of Physical Chemistry B* **2005**, *109*, 9622-9630.

(5) Zhou, C.; Nagy, G.; Walker, A. V., *Journal of the American Chemical Society* **2005**, *127*, 12160-12161.

(6) Zhu, Z.; Allara, D. L.; Winograd, N., *Applied Surface Science* **2006**, *252*, 6686-6688.

(7) Vaeck, L. V.; Adriaens, A.; Gijbels, R., Static Secondary Ion Mass Spectrometry (S-SIMS) Part 1: Methodology and Structural Interpretation. *Mass Spectrometry Reviews* **1999**, *18*, 1-47.

(8) Winograd, N., Prospects for imaging TOF-SIMS: from fundamentals to biotechnology. *Applied Surface Science* **2003**, *203-204*, 13-19.

(9) Borner, K.; Malmberg, P.; Mansson, J.-E.; Nygren, H., *Internation Journal of Mass Spectrometry* **2007**, *260*, 128-136.

(10) Belu, A. M.; Graham, D. J.; Castner, D. G., time-of-flight secondary ion mass spectrometry: techniques and applications for the characterization of biomaterial surfaces. *Biomaterials* **2003**, *24*, 3635-3653.

(11) Herzog, R. F. K.; Viehbock, F. P., Ion Source for Mass Spectrography. *Phys. Rev.* **1949**, *76*, 855-856.

(12) Liebl, H. J.; Herzog, R. F. K., Sputtering Ion Source for Solids. *Journal of Applied Physics* **1963**, *34*, 2893-2896.

(13) Benninghoven, A., Surface Investigation of Solids by the Stastical Method of Secondary Ion Mass Spectrometry. *Surface Science* **1973**, *1973*, 427-457.

(14) Benninghoven, A., Developments in Secondary Ion Mass Spectroscopy and Applications to Surface Studies. *Surface Science* **1975**, *53*, 596-625.

(15) Benninghoven, A.; Sichtermann, W. K., Detection, Identification and Structural Investigation of Biologically Important Compounds by Secondary Ion Mass Spectrometry. *Analytical Chemistry* **1978**, *50*.

(16) Wu, K. J.; Odom, R. W., Matrix-Enhanced Secondary Ion Mass Spectrometry: A Method for Molecular Analysis of Solid Surfaces. *Analytical Chemistry* **1996**, *68*, 873-882.

(17) Schueler, B., Microscopic Imaging by Time-of-Flight Secondary Ion Mass Spectrometry. *Microsc. Microanal. Microstruct.* **1992**, *3*, 119-139.

(18) Wollnik, H., Time-of-flight mass analyzers. *Mass Spectrometry Reviews* **1993**, *12*, 89-114.

(19) Gross, M. L.; Caprioli, R. M. In *The Encyclopedia of Mass Spectrometry: Molecular Ionization Methods*
Elsevier Science & Technology Books: Burlington, VT, 2006; Vol. 6, p 535-546.

(20) Vickerman, J. C. *ToF SIMS: Surface Analysis by Mass Spectrometry*; IM Publications and Surface Spectra Limited: Chichester and Manchester, UK, 2001.

(21) Vaeck, L. V.; Adriaens, A.; Gijbels, R., Static Secondary Ion Mass Spectrometry: (S-SIMS) Part 1. Methodology and Structural Interpretation. *Mass Spectrometry Reviews* **1999**, *18*, 1-47.

(22) Brison, J.; Houssiau, L., On the understanding and the optimization of ToF-SIMS depth profiles by cosputtering cesium and xenon. *Surface and Interface Analysis* **2006**, *38*, 1715-1719.

(23) Cheng, J.; Winograd, N., Depth Profiling of Peptide Films with TOF-SIMS and a C_{60} probe. *Analytical Chemistry* **2005**, *77*, 3651-3659.

(24) Hinder, S. J.; Lowe, C.; Watts, J. F., ToF-SIMS depth profiling of a complex polymeric coating employing a C_{60} sputter source. *Surface and Interface Analysis* **2007**, *39*, 467-475.

(25) GmbH, I. T. Münster, Germany.

Chapter 3

Construction of a High Vacuum Chamber for Reflection Absorption Infrared Spectroscopy (RAIRS)

Abstract

A reflection absorption infrared spectroscopy (RAIRS) system was constructed. The infrared system is designed to examine *in-situ* the interaction of vapor-deposited metals and reactive gases, including chemical vapor deposition precursors. The RAIRS system is composed of two parts: a vacuum chamber, which houses the sample, and an optical pathway. A sample holder was designed and constructed that allows the sample to be cooled to 93 K and heated to 378 K. As a demonstration, an infrared spectrum of an octadecanethiol self-assembled monolayer was obtained with a signal-to-noise ratio of greater than 14.

3.1 Introduction

Infrared spectroscopy (IRS) is widely used in applications including catalysis[1-5], food technology[6,7], energy storage[5,8,9] and organic/molecular electronics[10-12]. In this technique, the absorption of infrared light by molecules is measured as a function of frequency. The frequency and intensity of the light absorption is characteristic of the bonds and groups present in the compound.[13] Since IRS is a non-destructive technique and does not require a vacuum chamber, it is a versatile technique for surface analysis.[14] However, most surfaces are opaque to IR experiments, and so transmission experiments cannot be performed. Thus, most studies of surfaces employ reflection mode experiments (reflection absorption infrared spectroscopy, RAIRS).

In this chapter the construction of a reflection absorption infrared spectroscopy system is discussed. The infrared system is designed to examine *in-situ* the interaction of vapor-deposited reactive gases, including chemical vapor deposition precursors, and metals, which requires that the sample is housed in a vacuum chamber. To accommodate the vacuum chamber, an external IR beam is employed because there is not enough room in the internal interferometric optical pathway of the FTIR spectrometer. A variable sample holder was constructed so that the sample can be cooled to 93 K and heated to 378 K. As a demonstration, an infrared spectrum of an octadecanethiol self-assembled monolayer was obtained with a signal-to-noise ratio of greater than 14

3.2 IR excitation of molecules

Vibrational energy levels of molecules are quantized, and for most molecules, the differences in these levels correspond to energies in the mid-IR region. To absorb IR radiation, a molecule must have a net change in its dipole moment as it vibrates or rotates.[13] The number of vibrational modes in a molecule is determined by its shape. Linear and non-linear molecules have 3N-5 and 3N-6 vibrations, respectively, where N is the number of atoms in the molecule.[13] For example the linear CO molecule has 1 vibrational mode, while the non-linear CH_4 molecule has 9 vibrational modes. There are two basic types of vibrational modes: stretches and bends (Figure 1). Stretch modes involve changes in the interatomic distances between the atoms along the bond axis and can be divided into symmetric and asymmetric modes. Bending modes are characterized by a change in the angle between two bonds, and there are four types: scissors, wags, rocks and torsion (twist).[13]

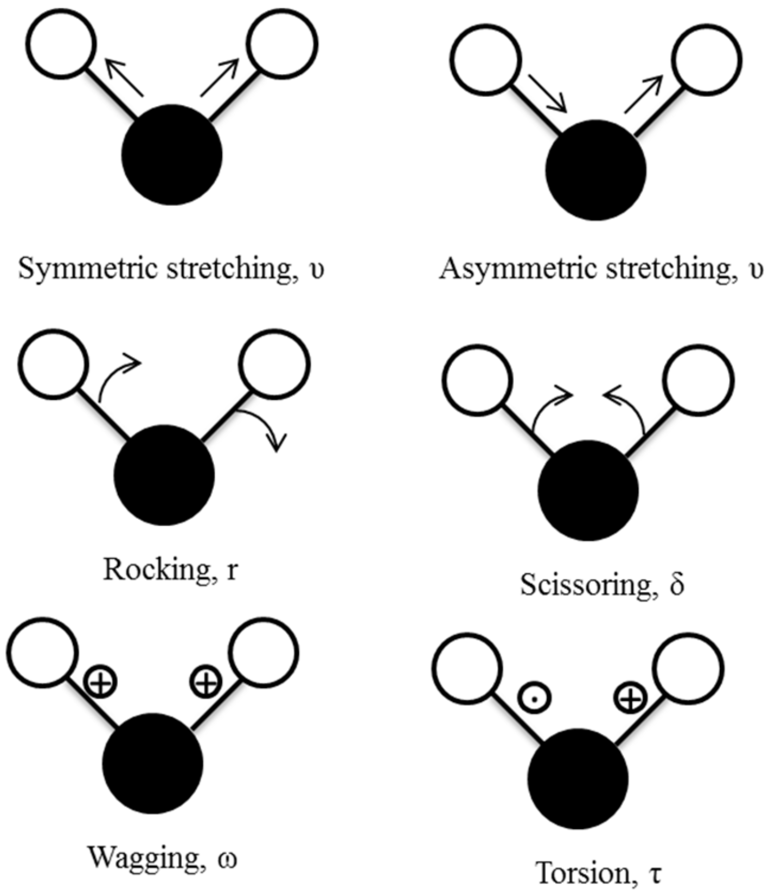

Symmetric stretching, υ

Asymmetric stretching, υ

Rocking, r

Scissoring, δ

Wagging, ω

Torsion, τ

Figure 1: A schematic of the 6 possible vibrational modes. The arrows point to the direction of the atoms moving in the plane of the paper, while atoms that are moving out of the plane of the paper are denoted by a circle with a dot (atoms moving towards the viewer) and a circle with the + (atom moving away from the viewer).

While the vibrational energies of molecules are quantized, the frequency of the modes are often modeled using classical mechanics. For a diatomic molecule, AB, the frequency of the vibration can be calculated using Hooke’s Law. The two atoms are considered to be attached to each other by a spring. The vibrational frequency of the spring is given by

$$\tilde{\upsilon} = \frac{1}{2\pi c}\sqrt{k/\mu}$$ **Equation 3.1**

where $\tilde{\upsilon}$ (= $1/\lambda$) is the wavenumber corresponding to the frequency of the vibration, c is the speed of light, k is the force constant of the bond and μ is the reduced mass of AB. The reduced mass of AB is

$$\mu = \frac{m_A m_B}{m_A + m_B}$$ **Equation 3.2**

where m_A and m_B are the masses of A and B, respectively.[13]

3.3 Fourier Transform Infrared Spectroscopy

Commercial infrared spectrometers are Fourier transform infrared (FTIR) instruments. FTIRs have three advantages: they measure all wavelength simultaneously (Fellgett advantage), the optical throughput is high (Jacquinot advantage) and the wavelengths of light can be precisely measured.[14] In an FTIR instrument there is a Michelson interferometer, which is schematically shown in Figure 3. Light emitted by a globar (source) impinges on a beam splitter, which is a thin semi-reflective film (typically KBr in IR instruments).[13,15] The beam splitter divides the light into beams whose relative length can be varied. One beam is reflected by a fixed mirror, M_1, at a distance $L_1/2$ from the beam splitter. A second beam is returned to the beam splitter by a movable mirror, M_2, which is a distance $L_2/2$ from the splitter. At the beam splitter, the light recombines to form a coherent light beam, B. The interference observed for light with wavelength λ is dependent on the path difference, δ, between the two mirrors.[14] Constructive interference is observed when δ is an integral number of path length ($\delta = n\lambda$) and destructive when $\delta = (n + \frac{1}{2})\lambda$.[13] For a monochromatic light, the interference between the two beams will vary sinusoidally as mirror M_2 moves. For polychromatic light, the plot of beam intensity versus mirror position (wavelength) is called an interferogram. When beam B impinges on the sample, light is absorbed as the characteristic vibrational modes are excited, which alters the intensities of the interferogram.[13]

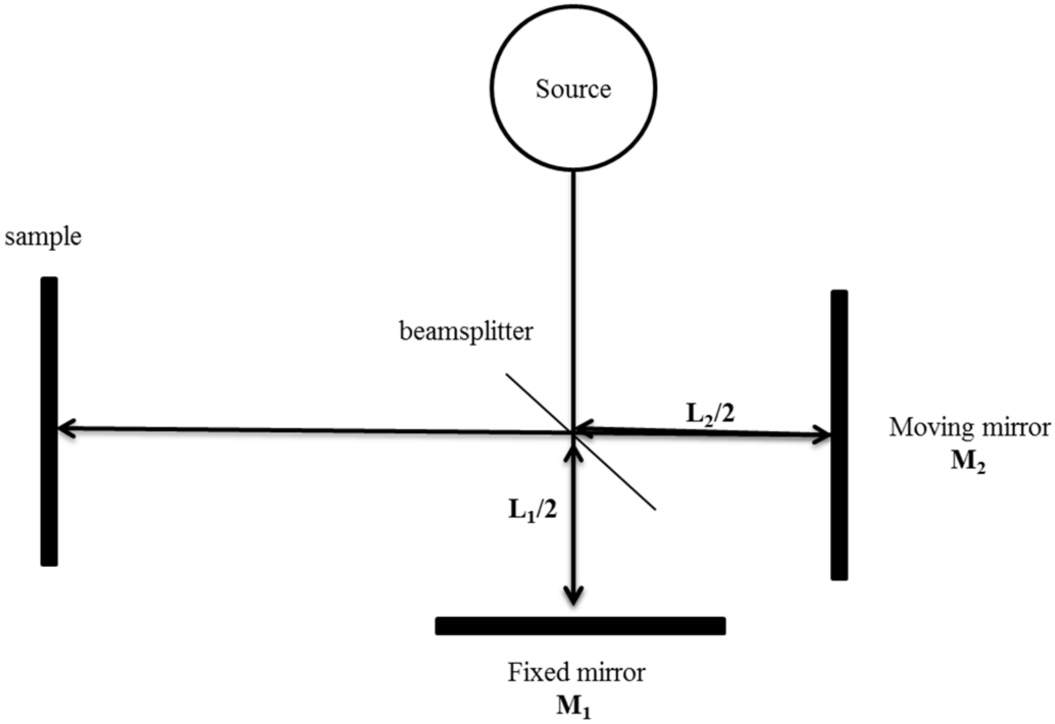
Source
sample
beamsplitter
$L_2/2$
Moving mirror
M_2
$L_1/2$
Fixed mirror
M_1

Figure 2 A schematic of a Michelson interferometer.

To convert the interferogram from wavelength (time) to the frequency domain the data is Fourier transformed.[14] The Fourier transform from the time domain to the frequency domain is

$$f(\omega) = \int_{-\infty}^{\infty} f(t)e^{2\pi i\omega t}dt$$ **Equation 3.7**

where f(ω) is the function in the frequency domain, and f(t) is the function in the time domain. Typically, only positive path differences are employed in the data analysis, and in this case, the Fourier transform is given by

$$\mathrm{f}(\omega) = 2\int_{0}^{\infty} \mathrm{f}(\mathrm{t})\mathrm{e}^{2\pi \mathrm{i}\omega \mathrm{t}}\mathrm{dt}$$

3.4 Reflection Absorption Infrared Spectroscopy

The theory of RAIRS was developed by Francis and Ellison [16], and Greenler [17,18] in the 1950s and 1960s. The intensity of the IR absorption is dependent only on the interaction of the IR light with molecular vibrations that are perpendicular to the surface. This is known as the “surface selection” rule and allows the determination of molecular orientation on the surface by using the intensity of the IR absorption bands.[19-21] Greenler showed that upon reflection from a metal surface, IR p(parallel)-polarized light strongly interacts with the perpendicular component of the electric field (E_p) of the surface. This interaction is strongly dependent upon the incident angle of the IR light, with the strongest interaction occurring at near-glancing incident angles, 80° - 88°.[20] On reflection the s(perpendicular)-polarized component of the light (E_s) reverses phase by ~ 180° to E_s’ (Figure 3) at all angles of incidence and so the vector sum of E_s and E_s’ is close to zero. In contrast p-polarized light undergoes a phase change (from E_p to E_p’) that is strongly dependent on the incident angle of the IR beam. Here the vector sum of E_p and E_p’ will vary with incident angle. In Figure 3, it can be seen that at grazing incident angles the perpendicular component of E_p will approximately double upon reflection (E_p (total) ≈ E_p + E_p’ ≈ 2 E_p) but the tangential component of E_p will remain insignificant upon reflection.[20] From the above discussion, it can be seen that several experimental conditions are required for RAIRS:

1) The substrate must be a good reflector. It can be a polished metal or semiconductor so long as the material is not IR transparent.
2) The IR light used should be p-polarized to eliminate any small contribution to the IR spectrum by s-polarized light.
3) The angle of incidence of the IR beam should be close to grazing (i.e. near to the Brewster angle, the angle at which the reflected light is completely polarized).

Finally, the IR absorption cross-sections of the organic-film functional groups at their characteristic frequencies must be sufficiently large so that the resultant signal-to-noise ratio allows adequate energy resolution, typically 2-4 cm^{-1}, to be used so that changes in the chemical composition and structure of the film can be observed.

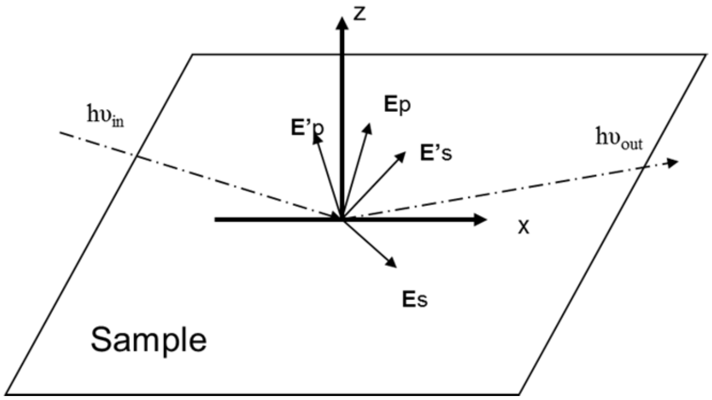
z
hυin
E'p
Ep
E's
hυout
x
Es
Sample

Figure 3. A schematic diagram of the electric fields of the incident and reflected IR beam at a bare metal surface. E_s and E_p are the s- and p-polarized components of the incident IR light; E_s' and E_p' are the corresponding components of the reflected IR radiation. The metal surface is in the xy plane and the plane of incidence is xz.

3.5 Construction of a RAIRS Instrument Equipped with a Vacuum System

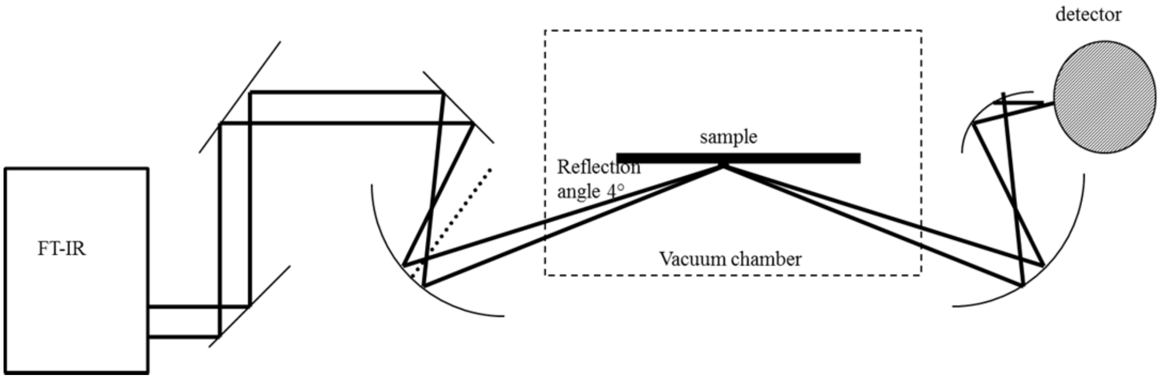
detector
sample
Reflection
angle 4°
FT-IR
Vacuum chamber

Figure 4. A schematic of the infrared spectroscopy system.

The infrared system is designed to examine *in-situ* the interaction of vapor-deposited metals and reactive gases, including chemical vapor deposition precursors. This requires that the sample is housed in a vacuum chamber. To accommodate the vacuum chamber an external IR beam is required because there is not enough room in the internal interferometric optical pathway of the FTIR spectrometer. There are two major components of the IR system, the vacuum chamber and the optical pathway. Each component is discussed in detail in the following sections.

3.5.1 IR Optical Pathway

The use of an external IR beam imposes two major design criteria that need to be addressed:

1) The intensity of the light that reaches the detector must be maximized.
2) Contaminant IR absorbances from gases present in the atmosphere, e.g. water vapor and carbon dioxide, must be greatly reduced/eliminated.

To maximize the amount of light that reaches the detector a Varian FTS 7000 (Digilab Inc.) FTIR spectrometer was employed which has a 10x higher optical throughput than other available FTIR spectrometers.[22] To reduce IR absorbances by atmospheric gases such as H_2O vapor and CO_2, the entire optical pathwaywas contained in a nitrogen gas-purged box.

In the experiment, the IR beam is reflected from the surface close to the Brewster angle (i.e. at grazing incidence to the sample surface (~84 - 86°)). This maximizes the experimental sensitivity to the organic thin film since:

1) In the reflection geometry the IR beam passes through the surface layer once before being reflected and again on its outward journey, and so interacts with the sample surface twice.

2) By using a grazing incidence geometry, there is a rapid increase with incident angle in the path length of the IR light through the sample.

Figure 4 displays the detailed optical pathway. Upon exiting the IR spectrometer, the IR beam first passes through an aperture to ensure that it is collimated. For ease in alignment, the IR beam is reflected off several mirrors before passing into the vacuum chamber, and again upon exit before reaching the HgCdTe (MCT) detector (Varian) (frequency range ~ 700 – 10,000 cm^{-1}). Before reaching the sample surface, the IR beam was first reflected from three planar mirrors set at 45° to the IR beam to rotate the light path by 180°. It was then be reflected from an off-axis parabolic mirror (Janos Technology Inc.) (focal length 12” and rotation angle 30°) to focus it onto the center of the sample surface. After reflection, the IR beam was reflected from a second off-axis parabolic mirror (Janos Technology Inc.) (focal length 12” and rotation angle 30°) onto an off-axis parabolic collection mirror (Janos Technology Inc.) (focal length 2” and rotation angle 90°) to focus the IR light onto the external MCT detector. All the mirrors used were gold-coated since gold has a uniform reflectance over the entire IR frequency range.[23] To allow IR light to pass through the vacuum chamber, differentially pumped KBr windows (Harrick Scientific Corp.) were employed, which are transparent to IR wavelengths.[13]

To maximize the light passing to the detector (and, therefore, the sensitivity of the experiment), the optical pathway is aligned using the internal FTIR spectrometer HeNe laser. (In a FTIR spectrometer a HeNe laser is used to align the Fabry-Perot interferometer; the laser beam can further be used to align optics that are external to the spectrometer.) To further “fine tune” the alignment, the IR beam itself and an IR scope (FJW Optical Systems) was employed.

3.5.2 Vacuum System

The vacuum system was designed with two different levels. A schematic of the chamber is shown in Figure 5. On the upper level, there was a quick access port to introduce samples into the vacuum. Once the sample was put inside the vacuum chamber, it was lowered to a second level for IR analysis. On this level, there was a Knudsen source for metal vapor-deposition and a gas doser for background gas dosing (section 3.5.2.1). To quantify the amount of vapor-deposited metal, a quartz crystal microbalance (QCM) (Maxtek Inc.) (section 3.5.2.2) was also to be installed on this level.

The sample manipulator is capable of moving in four directions - along the x,y,z axes and one rotation axis - for precise sample alignment and movement from the sample introduction (upper) level to the IR analysis (lower) level. Upon moving the sample, there was always a small chance that it will become misaligned. To avoid this problem, a precision xyz manipulator (McAllister Technical Services) with a repeatability of $< 5 \times 10^{-4}$ inches in the x,y (horizontal) and z (vertical) directions and a sample guide (see section 3.6.X) were employed. The sample mount was employed to cool and heat the sample from 93 K to 378 K (see section 3.4.2).

3.5.2.1 Gas Handling System

The pressure of a gas introduced into the vacuum chamber is precisely controlled by using a leak valve. The gas handling system consists of three ports for attaching both gas and liquid-vapor (e.g. water vapor) sources. The gas handling system was pumped by a rotary pump (single stage rotary pump, Leybold Trivac D16B, 13 cfm) and has a base pressure of 1×10^{-4} torr.

3.5.2.2 Quantification of Metal Deposition

A quartz crystal microbalance (QCM) was to be employed to quantify the amount of metal vapor-deposited on the surface. A QCM is an oscillating, gold-coated quartz crystal which was placed in the vacuum chamber close to the sample (see Figure 3). Upon vapor deposition of metal atoms, the QCM frequency changes.[24] From the frequency change, the amount of material deposited is determined.

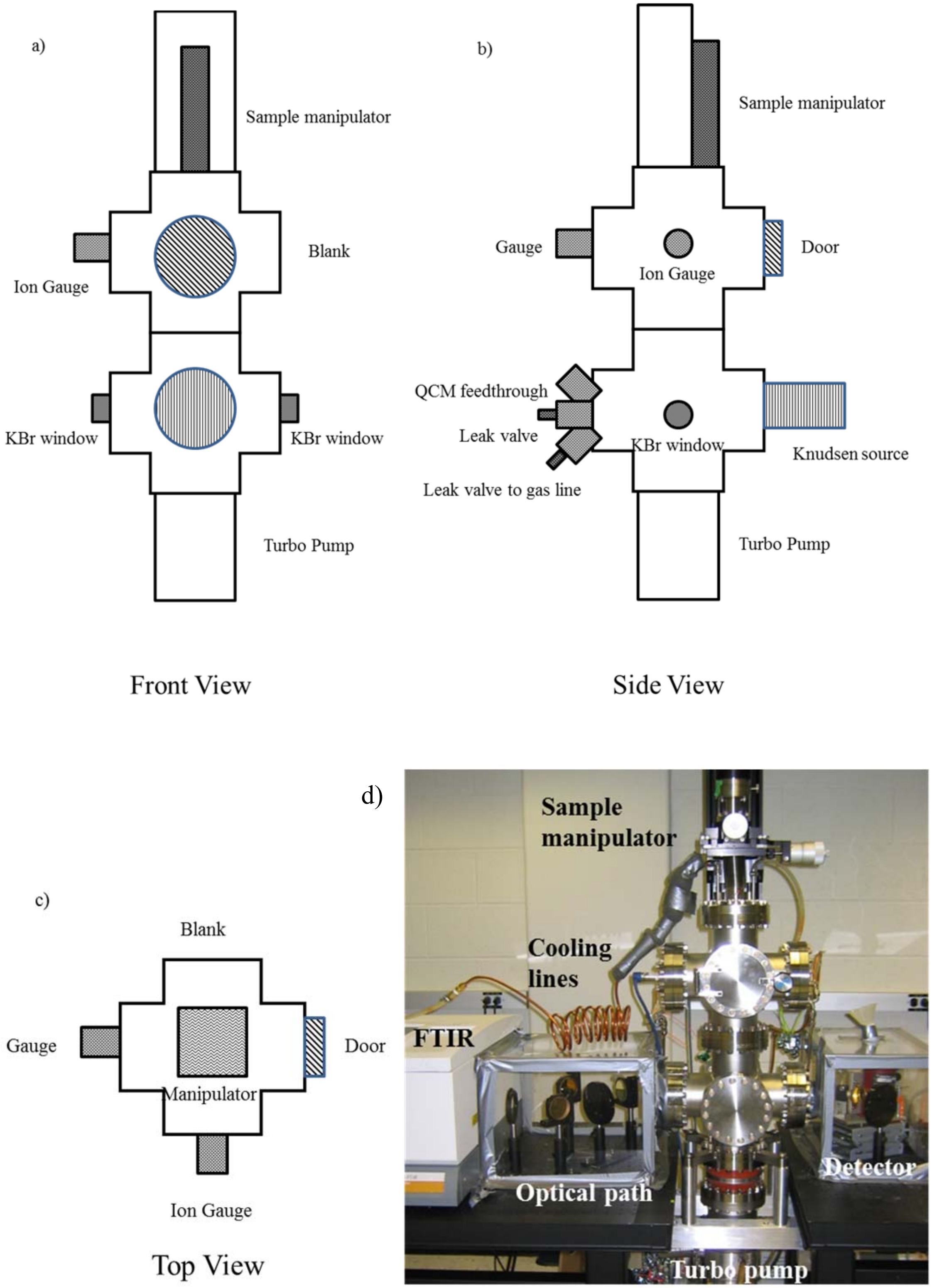
a)
Sample manipulator
Blank
Ion Gauge
KBr window
KBr window
Turbo Pump
b)
Sample manipulator
Gauge
Ion Gauge
Door
QCM feedthrough
Leak valve
KBr window
Knudsen source
Leak valve to gas line
Turbo Pump
c)
Blank
Gauge
Door
Manipulator
Ion Gauge
d)
Sample manipulator
Cooling lines
FTIR
Optical path
Detector
Turbo pump

Front View

Side View

Top View

Figure 5. RAIRS chamber. a) Front, b) side, c) top schematics, d) picture of instrument.

3.5.2.3 Vacuum system

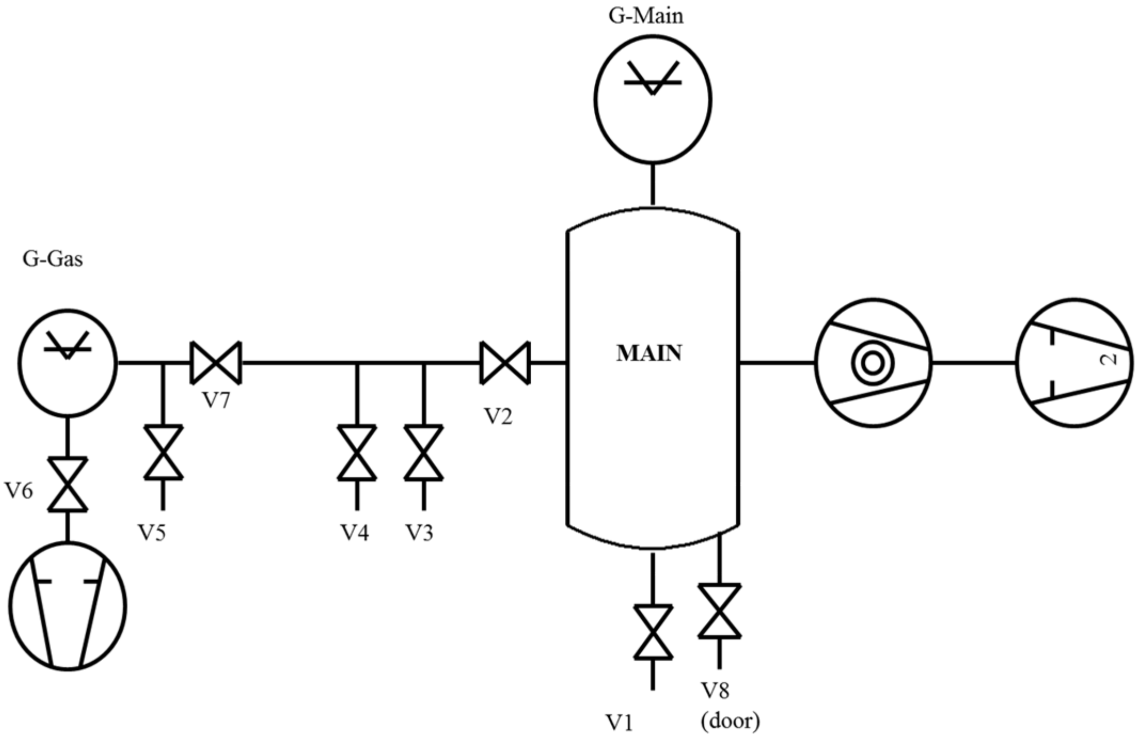

Figure 6. A schematic of the pumping used in the IR system.

Figure 6 displays the pumping diagram of the system. The main chamber was pumped with a turbomolecular pump, Leybold Turbovac 151 (145 L/s, N_2), which was backed a dual stage rotary vane pump, Leybold Trivac D25B (21 cfm). The base pressure of the chamber was 1.9 x 10^{-8} torr and was limited by both the leak rate of the door (V8) and the leak rate of the sample manipulator bellows. The pressure of the chamber was measured by an ion gauge (Granville Phillips) (G-Main). There was a gas line attached to the main chamber (see section 3.5.1). Valve V1 was employed to vent the chamber to dry nitrogen.

3.6. Design and Construction of the Sample Holder

The sample holder was constructed to meet the following design criteria:

1) For ease of introduction into the vacuum chamber, the sample was placed on a removable holder.
2) For IR spectroscopy, the sample must automatically be aligned correctly after moving from the top level of the chamber (sample introduction level) to the bottom level (analysis level).
3) The sample can be cooled to liquid nitrogen temperatures and heated to above 100 °C.

To address these issues, a sample manipulation system was constructed with three components: a sample platen, a sample holder and a sample guide. A schematic of the sample manipulation system is shown in Figure 7.

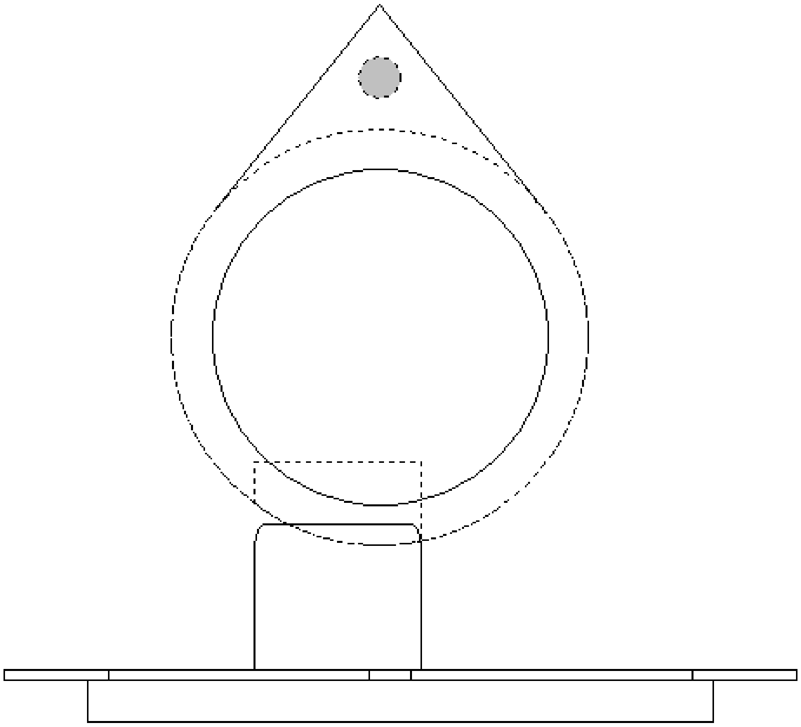

Figure 7. A schematic of the sample manipulation system. The sample platen is placed on the variable temperature sample holder, which is then lowered onto the sample guide for IR analyses. The guide ensures that the sample is in the correct position for RAIRS.

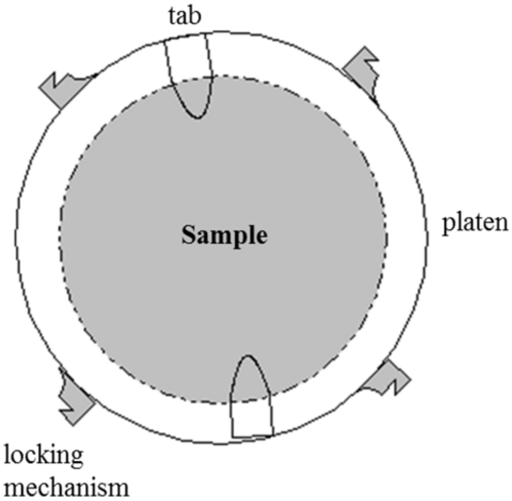

Figure 8. A schematic of the sample platen. The grey circle represents the sample. Drawn to scale.

The sample substrate was attached to a platen (Figure 8; diameter 2.5” and thickness 1/8”) using two tabs (Figure 8; dimensions ½” x ¼” x $^{1}/_{16}$”). To attach the platen to the sample holder, there were four tabs which comprise a locking mechanism (Figure 8). The tabs and locking mechanism are at 45° to each other so that they do not interfere with the IR beam impinging on the sample.

The sample platen was attached to the sample holder, which has two components: a metallic block and an insulating piece. The copper block (diameter 2”; thickness 3/8”) is employed to heat and cool the sample by using gaseous nitrogen via $^{1}/_{8}$” diameter stainless steel tubes soldered to the block. The platen was locked to a stainless steel ring (¼” wide) surrounding the copper block (Figure 9). The temperature of the sample was measured using a K-type thermocouple, which was attached between the sample and the platen/block. To insulate the metallic block from the chamber both thermally and electrically, the block was attached to an insulating piece, composed of Delrin (Figure 10). This piece has two other purposes. First, it attached the holder to the 4-axis sample manipulator via a ¼” screw. Second, for IR analyses, a hole cut in the Delrin allowed the precise alignment of the sample holder in the guide (Figure 10).

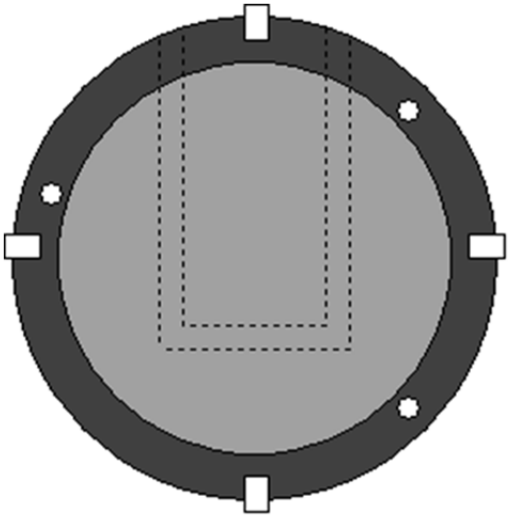

Figure 9. The copper block with cooling lines of the sample holder. Figure is drawn to scale. The light grey is copper, and the dark grey is stainless steel. The 4 white rectangles represent the locking mechanism. Dashed lines represent the cooling lines.

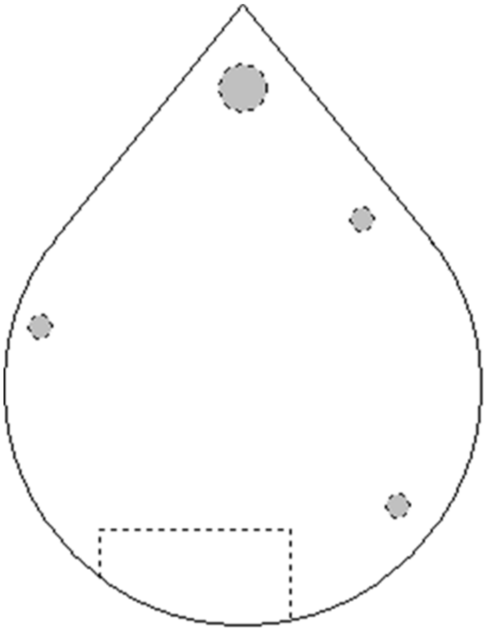

Figure 10: A schematic of the insulating block Figure is drawn to scale.

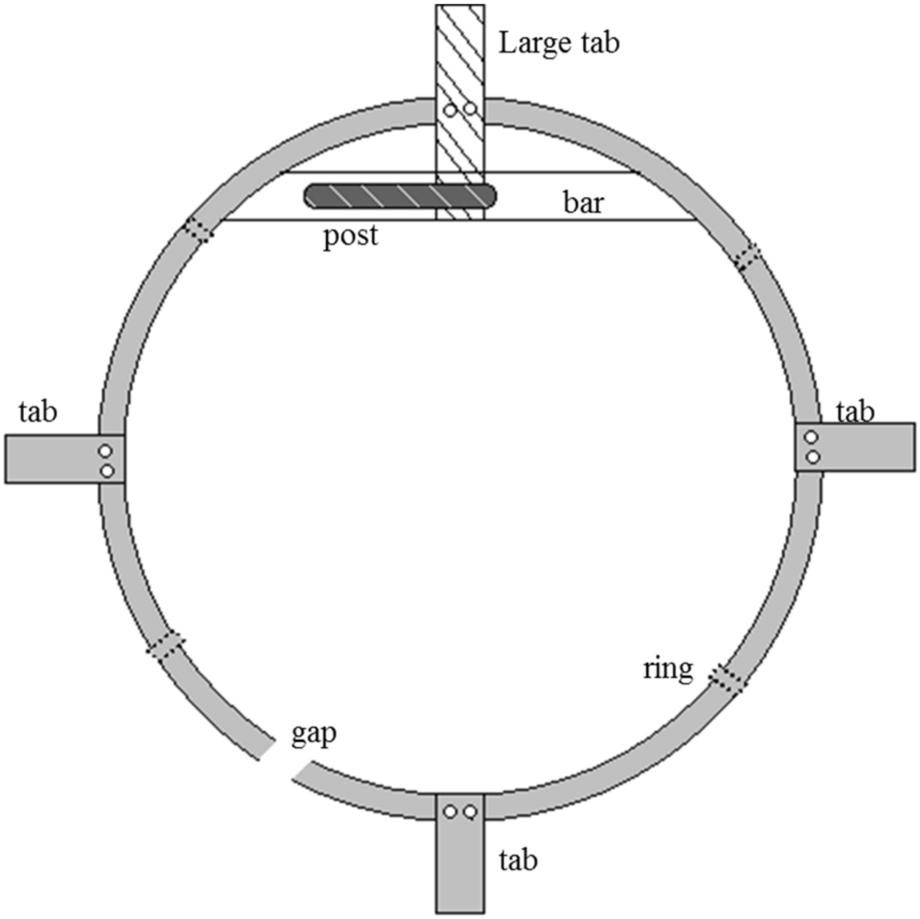

Figure 11: A top view of the sample guide. Figure is drawn to scale.

At the bottom of the chamber, there is a sample guide that was used to align the sample for IR analyses. Upon lowering the sample holder into position, a hole in the Delrin block fit snuggly into a guide post, ensuring the precise positioning of the sample. The guide post was attached to a stainless steel ring (inner diameter 3.5; width $^{1}/_{8}$" ; height ¼") with four tabs attached which sat at the bottom of the chamber (Figure 11). (To aid in fitting it into the chamber, there is a gap of $^{1}/_{8}$".). The tabs were employed to ensure that the ring is level and to add stability to the ring when the sample holder was moved into position (dimension 3 tabs: ¼" x 5/8" x $^{1}/_{10}$" ; 1 extended tab (¼" x 1 ¼" x $^{1}/_{10}$") Attached to the stainless steel ring was a bar (dimensions: 2 .875"x ¼"x ¼"). The bar holds the guide post off center by ½”. It is composed of a stainless steel piece with dimensions 1.125” x 0.125” x 0.87”.

3.7 Testing

3.7.1 IR spectra of Octadecanethiol Adsorbed on Au

As a demonstration of the constructed IRS system, the infrared spectrum of an octadecanethiolate self-assembled monolayer (ODT) SAM) ($CH_3(CH_2)_{17}S$-Au) was acquired. As a measure of the noise in the spectrum, the standard deviation of the IR signal was determined to be 0.00014 absorbance units from 4000 to 4500 cm^{-1}. Figure 12 displays the C-H stretch region of the IR spectrum. It can be clearly seen that the IR peaks are well-resolved and have low noise. The signal-to-noise ratio is calculated to be greater than fourteen. Further, the IR peak positions are the same as those observed for ODT SAMs adsorbed on Au (Table 1).[25-27]

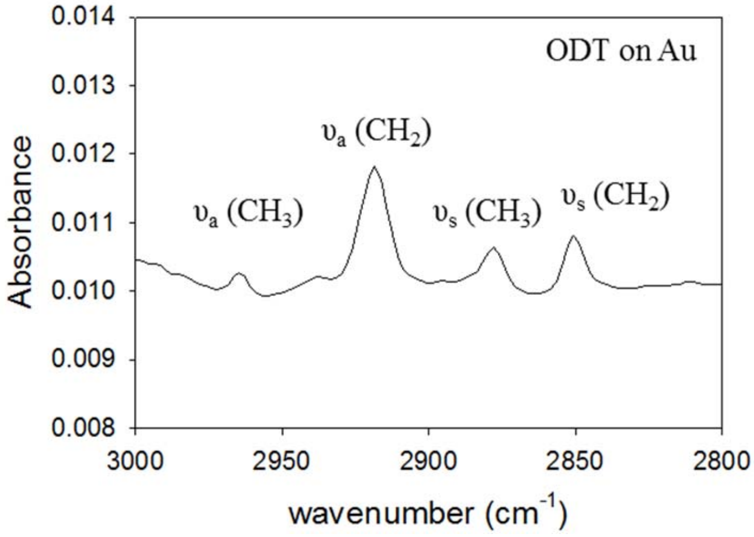

Figure 12. A RAIRS spectrum of an ODT monolayer on gold.

.

Stretch	Experimental	Literature[25,26]
υ_a (CH_3)	2964 cm^{-1}	2964 cm^{-1}
υ_a (CH_2)	2918 cm^{-1}	2918 cm^{-1}
υ_s (CH_3)	2879 cm^{-1}	2878 cm^{-1}
υ_s (CH_2)	2850 cm^{-1}	2850 cm^{-1}

Table 1. The vibrational frequencies of the C-H stretches of an ODT SAM adsorbed on Au.

3.7.2. Heating and Cooling of the Sample

The temperature studies were performed as follows. For all experiments a 3/8" diameter vinyl tube was connected to a regulated N2 source. The tube was then connected to a coppuer tube fashioned into a coil. The coil was made out of 5' of Cu tubing and the coil itself is 10 ¼" wide and 3 3/4" tall. There were 9 loops.The tube was then connected to a feed through in the chamber. This connection was insulated. For the cooling experiments the coil was submersed into lN2. The heating experiments had a 10 foot heating tape wound through the coil, which was then attached to a variac.

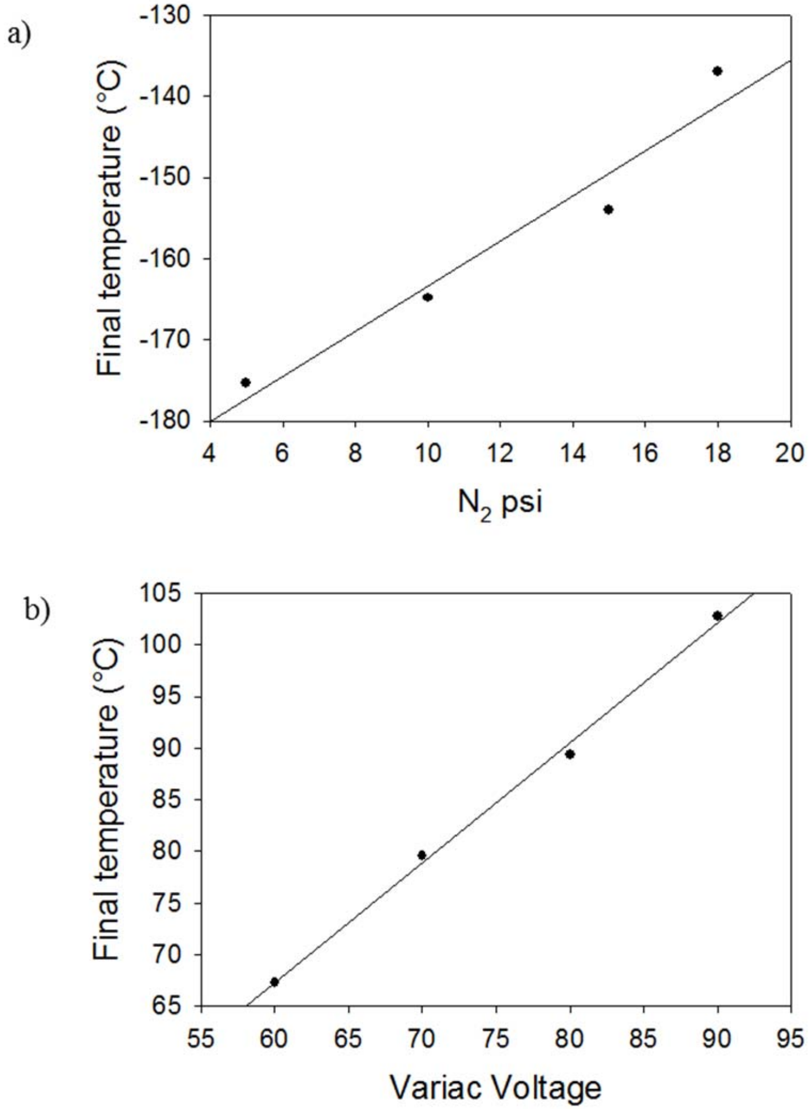

Figure 13. The variation of the sample temperature with a) the pressure of cooled nitrogen gas; and b) the temperature of heated nitrogen gas. As a measure of the nitrogen gas temperature, the voltage of the variac was used.

To heat and cool the sample, nitrogen gas is passed through the copper block of the sample holder. To cool the sample cold nitrogen gas is passed through the copper block. Using this method after 15 – 30 mins, the lowest temperature obtained was -180°C (93 K). The temperature was dependent on the pressure of the nitrogen flowing through the sample holder. The lowest temperature obtained was at the lowest gas pressure employed, 5 psi (Figure 13a).

To heat the sample, a constant pressure of nitrogen gas, 10 psi was employed. The gas was heated using resistive heating tape powered by a variac (KRM, 2090VR). After 60 mins, the maximum temperature was obtained, and was dependent on the voltage applied (Figure 13b). At 90 V, the maximum temperature achieved was 105 °C (378 K).

For both heating and cooling, the temperature of the sample was stable for at least 5 mins, which was sufficient time to obtain an IR spectrum.

3.8. Conclusions

A infrared spectrometry system was constructed and tested. The instrument is composed of two parts: a vacuum chamber, which houses the sample, and an optical pathway. A sample holder was constructed so that the sample can be heated and cooled from 378 K to 93 K, and allows for the reproducible positioning of the sample in the optical pathway. As a demonstration of the system, a IR spectrum of an ODT SAM adsorbed on Au was obtained.

3.9. References

(1) Barros, R. B. d.; Garcia, A. R.; Ilharco, L. M., Reactivity of methanol on clean Ru (001) studied by RAIRS: effect of deuterium substitution. *Surface Science* **2003**, *532-535*, 185-190.

(2) Chesters, M. A.; Parker, S. F.; Raval, R., Fourier Transform Reflection-Absorption Infrared Spectroscopy of Adsorbates on Cu(100) and Cu(111). *Surface Science* **1986**, *165*, 179-190.

(3) Higgs, V.; Hollins, P.; Pemble, M. E.; Pritchard, J., Formation of a Surface Nitride of Copper(111) and its Influence on Carbon Monoxide Adsorption: Investigation by LEED, RAIRS and EELS. *Journal of Electron Spectroscopy and Related Phenomena* **2986**, *39*, 137-144.

(4) Lee, I.; Zaera, F., Infrared Spectroscopy Characterization of the Chemistry of C_4 Hyrdocarbons on Pt(111) Single-Crystal Surfaces. *J. Phys. Chem. C* **2007**, *111*, 10062-10072.

(5) Wachs, I. E., Raman and IR studies of surface metal oxide species on oxide supports: Supported metal oxide catalysts. *Catalysis Today* **1996**, *27*, 437-455.

(6) Huang, H.; Yu, H.; Xu, H.; Ying, Y., Near infrared spectroscopy for on/in-line monitoring of quality in food and beverages: A review. *Journal of Food Engineering* **2008**, *87*, 303-313.

(7) Rodriguez-Otero, J. L.; Hermida, M.; Centeno, J., Analysis of Dairy Products by Near-Infrared Spectroscopy: A Review. *Journal of Agricultural and Food Chemistry* **1997**, *45*, 2815-2819.

(8) Nijem, N.; Veyan, J.-F.; Kong, L.; Li, K.; Pramanik, S.; Zhao, Y.; Li, J.; Langreth, D.; Chabal, Y. J., Interation of Molecular Hydrogen with Microporous Metal Organic Framework Materials at Room Temperature. *Journal of the American Chemical Society* **2010**, *132*, 1654-1664.

(9) Chaudhuri, S.; Rangan, S.; Veyan, J.-F.; Muckerman, J. T.; Chabal, Y. J., Formation and Bonding of Alane Clusters on Al(111) Surfaces Studied by Infrared Absorption Spectroscopy and Theoretical Modeling. *Journal of the American Chemical Society* **2008**, *130*, 10576-10587.

(10) Weldon, M. K.; Marsico, V. E.; Chabal, Y. J.; Hamann, D. R.; Christman, S. B.; Chaban, E. E., Infrared spectroscopy as a probe of fundamental processes in microelectronics: silicon wafer cleaning and bonding. *Surface Science* **1996**, *368*, 163-178.

(11) Bliznyuk, V. N.; Carter, S. A.; Scott, J. C.; Klärner, G.; Miller, R. D.; Miller, D. C., Electrical and Photoinduced Degradation of Polyfuorene Based Films and Light-Emitting Devices. *Macromolecules* **1999**, *32*, 361-369.

(12) Richter, C. A.; Hacker, C. A.; Richter, L. J., Electrical and Spectroscopic Characterization of Metal/Monolayer/Si Devices. *J. Phys. Chem. B* **2005**, *109*, 21836-21841.

(13) Leng, Y. *Materials Characterization: Introduction to Microscopic and Spectroscopic Materials*; John Wiley & Sons (Asia) Pte Ltd: Singapore, 2008.

(14) Strobel, H. A. *Chemical Instrumentation: A Systematic Approach*; John Wiley & Sons: New York, NY, 1989.

(15) Michelson, A. A.; Morley, E. W., On the Relative Motion of the Earth and the Luminiferous Ether. *The American Journal of Science* **1887**, *34*, 333-345.

(16) Francis, S. A.; Ellison, A. H., Infrared Spectra of Monolayers on Metal Mirrors. *Journal of the Optical Society of America* **1959**, *49*, 131-135.

(17) Greenler, R. G., Infrared Study of Adsorbed Molecules on Metal Surfaces by Reflection Techniques. *Journal of Chemical Physics* **1966**, *44*, 310-315.

(18) Greenler, R. G., Reflection Method for Obtaining the Infrared Spectrum of a Thin Layer on a Metal Surface. *Journal of Chemical Physics* **1969**, *50*, 1963-1968.

(19) Chabal, Y. J., Surface Infrared Spectroscopy. *Surface Science Reports* **1988**, *8*, 211-357.

(20) Greenler, R. G., Infrared Study of Adsorbed Molecules on Metal Surfaces by Reflection Techniques. *The Journal of Chemical Physics* **1966**, *44*, 310-315.

(21) Greenler, R. G., Design of a reflection-absorption experiment for studying the ir spectrum of molecules adsorbed on a metal surface. *Journal of Vacuum Science and Technology* **1975**, *12*, 1410-1417.

(22)

(23) Moore, J. H.; Davis, C. C.; Coplan, M. A. *Building Scientific Apparatus*; 2nd ed.; Addison-Wesley Publishing Company, Inc.: Redwood City, California, 1989.

(24) Lu, C.-S.; Lewis, O., Investigation of film thickness determination by oscillating quart resonators with large mass load. *J. Appl. Phys.* **1972**, *43*, 4385-4390.

(25) Han, J.; Wang, X.; Kwok, D. Y. In *2004 International Conference on MEMS, NANO and Smart Systems (ICMENS '04)* 2004.

(26) Laibinis, P. E.; Whitesides, G. M.; Allara, D. L.; Tao, Y.-T.; Parikh, A. N.; Nuzzo, R. G., Comparison of the Structures and Wetting Properties of Self-Assembled Monolayers of n-Alkanethiols on the Coinage Metal Surfaces, Cu, Ag, Au. *J. Am. Chem. Soc.* **1991**, *113*, 7152-7167.

(27) Walker, A. V.; Tighe, T. B.; Cabarcos, O. M.; Reinard, M. D.; Haynie, B. C.; Uppili, S.; Winograd, N.; Allara, D. L., The Dynamics of Noble Metal Atom Penetration through Methoxy-Terminated Alkanethiolate Monolayers. *J. Am. Chem. Soc.* **2004**, *126*, 3954-3963.

Chapter 4

Formation and Structure of Terminal Alkyne Self-Assembled Monolayers on Au

Abstract A new class of self-assembled monolayer, terminal alkyne monolayers (TAMs) ($HC{\equiv}C(CH_2)_nCH_3$, n = 5, 7, 9, 11, 13, 15) adsorbed on Au, was synthesized and characterized using single wavelength ellipsometry, reflection absorption infrared spectroscopy (RAIRS), x-ray photoelectron spectroscopy (XPS) and secondary ion mass spectrometry (SIMS). For TAMs with less than 11 methylene units ($n < 11$) in the backbone, the adsorbed layer is highly disordered, oxidized and has a multilayer structure. Longer chain length TAMs ($n \geq 11$) form disordered monolayers on gold. As the methylene chain length increases, the conformational order of the TAMs increases. The molecules have an upright conformation and bind to the surface via a Au-C≡C-bond. Some oxidized species are present in the TAM. The implications for the chemical stability of TAMs are discussed.

4.1. Introduction

For many years, the formation of well-ordered, densely packed self-assembled monolayers (SAMs) on metal and semiconductor substrates has been of great interest.[1,2] SAMs are used to functionalize surfaces in applications ranging from sensing[3-7] to organic/molecular electronics[8-22] to anti-corrosion coatings[2] to lithography[23-31]. The assembly of these layers is mediated by the interplay of molecule-molecule interactions, molecule-substrate attachment and SAM-ambient interface energetics.[2] Attachment chemistries include covalent-polar interactions (e.g. alkanethiols on Au[1,2] or GaAs[32]) and Brønsted acid-base interactions, e.g. alkylphosphonic acids adsorbed on titanium dioxide.[33]

To date, the most widely studied SAMs are those dervived from alkanethiols adsorbed on both metal surfaces, including Au, Ag, Cu, Pd and Pt[1,2,32], and semiconductor substrates, such as GaAs[2,32] and InAs[34,35]. Thiol-based SAMs have several limitations. First, they are not stable above ~70 °C.[1,36,37] At between 100 and 140 °C, alkanethiolate SAMs undergo a melting transition to a liquid-like state.[1,36] Further, as the temperature of the SAMs is increased, the number of gauche defects increases, and the number of interstitial defects decreases with a concomitant increase in observed domain sizes.[37] Gauche defects created at temperatures above 77 °C remain present in the sample even upon cooling. Second, for electronic applications it is preferable to have a SAM linker with π-bond character which facilitates electronic state mixing between the molecule and substrate.[38,39]

It was recently demonstrated that terminal alkynes can form self-assembled monolayers on gold.[39-41] Zhang and co-workers[39] showed that terminal alkyne monolayers (TAMs) form relatively organized and stable SAMs on Au, determined by using water contact angle measurements, ellipsometry, electrochemical blocking and infrared spectroscopy (IRS). A second study using x-ray photoelectron spectroscopy (XPS), scanning tunneling microscopy (STM) and IRS also demonstrated that ethynylbenzene and 1,4-ethynylbenzene form bound monolayers on gold.[41] The data suggest that alkyne molecules adsorbed on Au have an upright orientation mediated via an end-on interaction between the alkyne and gold.[39] However, the chemistry of the binding to the gold remains unclear. Theoretical analyses of the adsorption of ethynylbenzene on Au suggest that a vinylidene/Au (-HC=C-Au) interaction is the most stable.[42] This interaction involves a 1,2-hydride shift to form a carbene that then datively bonds to the gold. However, later experiments suggest that both ethnylbenzene and 1,4-ethynylbenzene form TAMs via an oxidation reaction facilitated by the Au substrate.[41] The data suggest that the layer is composed of oxygen-containing hydrocarbons such as phenylacetic acid and phenyloxirane. In contrast, using surface-enhanced Raman scattering (SERS), Lim and co-workers [43] determined that diethynylbenzene monolayers bind to gold nanoparticles via a -C≡C-Au bond.

In this chapter, the synthesis and structure of TAMs adsorbed on Au was investigated using a homologous series of alkynes, $HC{\equiv}C(CH_2)_nCH_3$ (n = 5,7,9,11,13,15). The TAMs are adsorbed on Au by a solution-phase method. Briefly, acetylide anions are produced *in situ* by the reaction of the terminal alkynes with ammonium hydroxide (Figure 1). These acetylide anions then chemisorb on the gold substrate. Ellipsometry, reflection absorption infrared absorption (RAIRS) spectroscopy, x-ray photoelectron spectroscopy (XPS) and secondary ion mass spectrometry (SIMS) were employed to investigate the deposited TAM layers. For TAMs with less than 11 methylene units ($n < 11$) in the backbone, the adsorbed layer has a multilayer structure and contains both unoxidized and oxidized alkynes. Longer chain length TAMs ($n \geq 11$) form disordered monolayers on gold, and the conformational order of the TAMs increases with the number of methylene units in the backbone. The molecules have an upright conformation and bind to the surface via a Au-C≡C- bond. Some oxidized alkyne species are also present in the TAM.

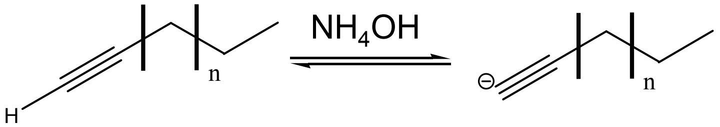

Figure 1. Schematic of the reaction to form acetlyide anions.

4.2. Experimental

4.2.1 Materials

Octyne, decyne, dodecyne and tetradecyne were purchased from Sigma Aldrich (St. Louis, MO). Hexadecyne and octadecyne were obtained from TCI America (Portland, OR). Ammonium hydroxide and n-propanol were acquired from JT Baker (CMOS grade) (Phillipsburg, NJ) and VWR (Radnor, PA), respectively. All chemicals were used without further purification. Gold (99.999%) was obtained from Alfa Aesar (Ward Hill, MA). Chromium rod was purchased from R.D. Mathis Inc. (Long Beach, CA). Single side polished silicon wafers (<111> orientation) were acquired from Addison Engineering (San Jose, CA).

4.2.2 Monolayer Synthesis

SAMs with different alkyl chain lengths and terminal groups on Au were prepared using a procedure based on the synthesis of ethynylbenzene monolayers on Au reported by McDonagh and co-workers.[41] Briefly, Cr (~10 nm) and Au (~100-200 nm) were sequentially thermally deposited onto clean Si native oxide-covered wafers. In an anaerobic chamber, the gold substrate was immersed in a *n*-propanoic solution containing 3 mM of the corresponding alkyne and 3 μl of ammonium hydroxide per ml of *n*-propanol. The substrates were immersed in the solution for 24 hours at 45 ± 2°C. After removing from the alkyne solutions, the substrates were sonicated in *n*-propanol for 2 mins, rinsed with copious *n*-propanol and dried with a N_2 stream.

4.2.3 Single Wavelength Ellipsometery

The thickness of alkyne monolayers were determined using single wavelength ellipsometry on a

Gaertner LSE Stokes Ellipsometer (Gaertner Scientific Corp., Skokie, IL). The HeNe laser light (λ = 632.8 nm) was incident on the sample at 70°. Layer thicknesses were calculated using an isotropic three layer model (air/hydrocarbon/Au) using standard hydrocarbon optical constants, $n_f = 1.5$ and $k_f = 0.0$.

4.2.4 X-ray photoelectron spectroscopy

Photoelectron specta were obtained on a Perkin Elmer PHI 5600 ESCA system using a monochromatic Al Kα source (E_p = 1486.6 eV). Typically, the pressure of the chamber was $< 6 \times 10^{-10}$ mbar during analysis. All XPS spectra were measured with a pass energy of 58.7 eV and energy step of 0.125 eV. The data were collected at 45˚ to the normal of the sample surface. All spectra were referenced to the Au $4f_{7/2}$ core-level peak at 84 eV.

4.2.5 Reflection absorption infrared spectroscopy

The RAIRS spectra were recorded by using a Fourier transform instrument (FT-IR7000, Varian, Palo Alto, CA) interfaced via custom optics to a vacuum chamber (base pressure: 2 x 10^{-8} torr) with differentially pumped KBr windows. To reduce IR absorbance by water vapor, carbon dioxide and other atmospheric gases, the optical pathway is contained in a dry nitrogen gas-purged box. The infrared beam is incident on the sample at ~86° and detected using an MCT detector (wavenumber range: ~750 cm^{-1} to 4000 cm^{-1}).

4.2.6 Time-of-Flight Secondary Ion Mass Spectrometry

TOF SIMS analyses were conducted using a TOF SIMS IV (ION TOF Inc., Chestnut Ridge, NY) instrument equipped with a Bi_n^{m+} (n = 1 – 7, m = 1, 2) liquid metal ion gun. The instrument consisted of an airlock, a preparation chamber, and an analysis chamber, which were separated by gate valves. The preparation and analysis chambers were maintained at less than 8 x 10^{-9} mbar to avoid sample contamination. The primary Bi^+ ions had a kinetic energy of 25 keV and were rastered across a 100 x 100 μm^2 area. The total accumulated primary ion dose was less than 1 x 10^{10} ions/cm^2, which is within the static SIMS regime.[44] The secondary ions were extracted into a time-of-flight mass spectrometer by using 2000 V and reaccelerated to 10 keV before reaching the detector.

4.3 Results

4.3.1 Ellipsometry

The thickness of each TAM formed on Au was investigated with single wavelength ellipsometry (SWE) measurements. Using a refractive index of n_r = 1.50 for the hydrocarbon layer [32,39] and an isotropic three layer model (air/TAM/Au), we observe that the film thickness is approximately constant for alkynes with less than ~9 methylene units in the backbone ($n \leq 9$) (Figure 2 and Table 1). The thickness of these layers is larger than the calculated molecular length (Table 1) suggesting that multilayers are forming. For longer chain alkynes, the thickness of the layer is less than the calculated molecular length (Table 1), indicating that a monolayer forms. This is in contrast to previous studies where it was observed that the TAM thickness increased linearly with the number of methylene units in the backbone.[39] For these longer chain alkynes a plot of film thickness versus chain length yields a line with a slope of 2.29 Å/C and an intercept of -11.23 Å using $n = 11 – 15$ (goodness of fit, $R^2 = 0.9999$) (Figure 2, dotted line) and a slope of 1.30 Å/C and intercept 2.25 Å using $n = 9 – 15$ (goodness of fit, $R^2 = 0.7779$) (Figure 2, dashed line). Neither of these fits is particularly satisfying. The slope obtained using $n = 11 – 15$ (2.29 Å/C) is similar to that observed for *n*-alkanethiols adsorbed on GaAs (001) (slope 2.1 – 2.3 Å/C) but is very large when compared to other monolayer systems.[32] In contrast, the best fit slope for $n = 9 – 15$ is similar to that observed for *n*-alkanethiols adsorbed on Au (1.19 Å/C) [32,45] and for TAMS adsorbed on Au (1.13 Å/C) measured by Zhang and co-workers.[39]

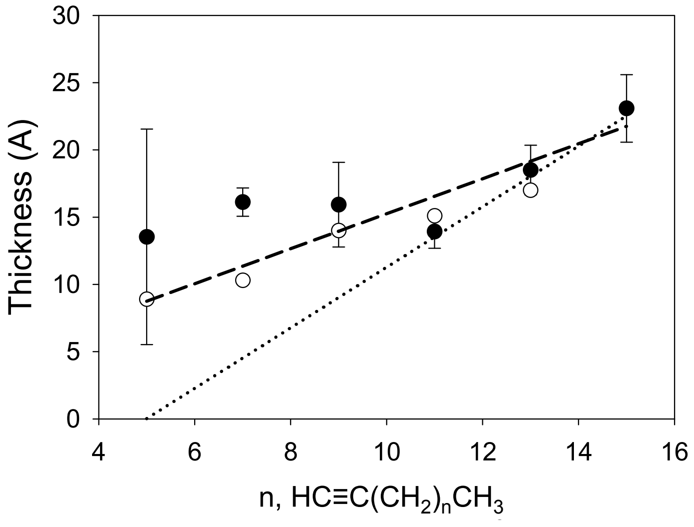

Figure 2. Ellipsometric film thickness of the alkyne monolayers. Black circles are obtained in this work. The fits to the ellipsometric film thickness are shown as dotted and dashed lines. For reference, the open circles are the film thicknesses obtained by the Zhang et al.[39]

Alkyne, $HC{\equiv}C(CH_2)_nCH_3$	**n**	**Film Thickness (Å)**	**Molecular Length (Å)[a]**	**Zhang et al Film Thickness (Å)[a]**
octyne	3	13.5 ± 8.0	10.4	8.9
decyne	5	16.1 ± 1.1	12.8	10.3
dodecyne	7	15.9 ± 3.1	15.3	14.0
tetradecyne	11	13.9 ± 1.3	17.8	15.1
hexdecyne	13	18.5 ± 1.8	20.2	17.0
octadecyne	15	23.1 ± 2.5	22.7	-

Table 1. Ellipsometric film thickness of the alkyne monolayers adsorbed on Au.

[a]The experimental ellipsometric film thickness and theoretical molecular length were obtained from Zhang et al.[39]

The intercept for the thickness trends derived from ellipsometric data are normally interpreted to be the limiting value for alkyne-substrate interface. Using the fit for n = 11 – 15, the intercept is a large negative number (-11.23 Å), which suggests that this interpretation is not valid. For n = 9 – 15, the intercept is more reasonable, 2.25 Å, and is similar to that observed for *n*-alkanethiols on gold (~2 Å). [32,45] However, the fit for this range of alkyne molecules is much worse.

Given the differences in the calculated slopes and intercepts obtained for TAMS, it is not entirely clear that a simple isotropic three layer model is appropriate to determine layer thicknesses. These data suggest that a more complex model, which includes less dense monolayers, defects and contributions from the TAM-Au interfaces, may need to be considered.

4.3.2 XPS

XPS spectra were recorded of freshly prepared TAMs adsorbed on Au. For each TAM studied, the fitted C 1s spectra show that the spectra consist of three peaks with binding energies 284.4 eV, 286.2 eV and 289.2 eV. Figure 3 displays are representative C 1s spectrum: the C1s spectral region from dodecyne adsorbed on Au. Previous experiments of alkanethiolate SAMs adsorbed on Au indicate that signal at 284.3 eV is due to the carbons of the methylene backbone ($-\underline{C}H_2-$).[32,46-49] The peak at 289.2 eV is characteristic of a carbon atom in a carboxylic acid or ester ($\underline{C}OO$).[41,50] We assign the peak at 286.2 eV to $\underline{C}O$ bonds present in the layer. This assignment is speculative although it is similar to the binding energies of C-O bonds in poly(ethylene terephthalate) (PET).[50]

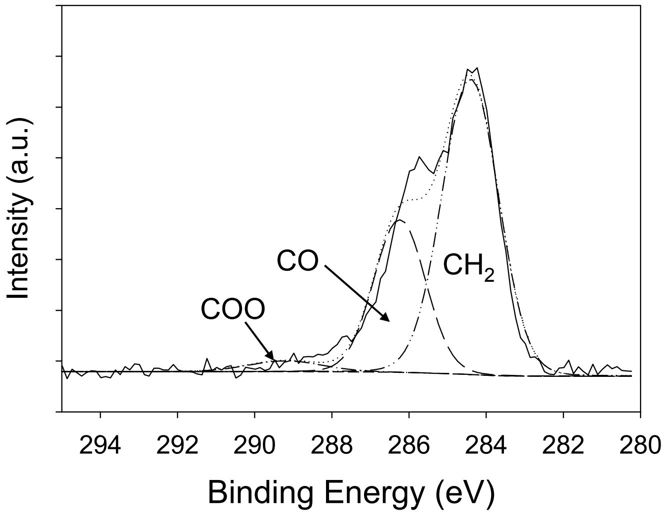

Figure 3. C 1s XPS spectrum of a dodecyne monolayer on Au showing curves fitted to the experimental data.

The intensity of peak C decreases with increasing methylene chain length from 5% of the total C 1s intensity for octyne and decyne TAMs to 1.6 % for octadecyne TAMs suggesting that the level of oxidation in the TAM decreases with increasing chain length (Figure 4). In contrast, the relative intensity of the C̲O peak (binding energy = 286.2 eV) first increases with increasing chain length reaching a maximum for dodecyne TAMs (n = 9) before decreasing. These results suggest that the for longer methylene chain length TAMs (n ≥ 10) that the amount of oxidized species decreases. Since the intensities of the peaks at 286.2 eV and 289.2 eV have different dependencies on the TAM chain length, the data also indicate that there are more than one oxidized species on the surface.

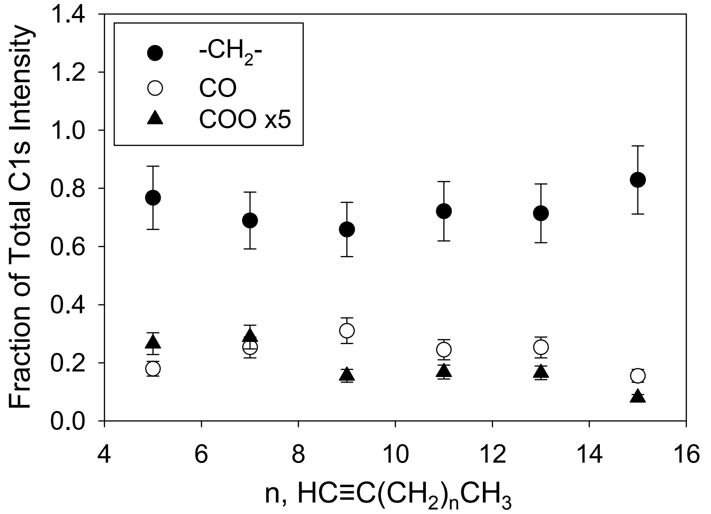

Figure 4. Fraction of the $–\underline{C}H_2$-, $\underline{C}O$, $\underline{C}OO$ signals in the C1 XPS spectrum as a function of chain length.

Since the C1s cross-section is constant for all atoms in TAMs for our condition of a 45° photoelectron exit angle, we expect that the C 1s peak intensites (peak areas) are correlated with the methylene chain length via the attenuation relationship:[51]

$$I = \int_0^{z_d} \rho_0 \exp\left(-\frac{z}{\lambda\cos\theta}\right)dz$$

Equation 4.1

where z is the distance in the alkyl chain matrix from the Au/alkyne interface towards the vacuum, z_d is the thickness of the alkyl chain matrix, ρ_0 is the intrinsic C 1s photoemission intensity per unit thickness (dI/dz_0) with no overlayer attenuation, λ is the C 1s photoelectron attenuation length (= 35.4 Å) and θ is the photoelectron exit angle. The ratio of the C1s signal for a TAM with n methylene units to the C1s signal intensity for an octadecyne SAM is

$$\frac{I_n}{I_{18}} = \frac{\int_0^{nd_C} \rho_0 \exp\left(-\frac{nd_c}{\lambda\cos\theta}\right) d(nd_c)}{\int_0^{16d_c} \rho_0 \exp\left(-\frac{nd_c}{\lambda\cos\theta}\right) d(nd_c)}$$

$$= \frac{\left(e^{-n\alpha}-1\right)}{\left(e^{-16\alpha}-1\right)} = x\left(e^{-n\alpha}-1\right)$$

Equation 4.2

where d_C is the thickness of the alkyl matrix per C atom, n is the number of C atoms in the alkyl chain, α is d_c/λ and $x = (e^{-16\alpha} - 1)$. Re-arranging, I_n/I_{18} is related to the number of Cs in the alkyl backbone by

$$\ln\left(\frac{I_n}{I_{18}}+1\right) = -n\alpha+\ln x$$

Equation 4.3

Thus, a plot of $\ln(I_n/I_{18} + 1)$ versus n will yield a straight line with a gradient of α. For $n \geq 11$, we find that α is 0.02622 and the C 1s peak intensities are correlated with the methylene chain length (Figure 5). However, for shorter chain lengths, the C 1s intensity deviates to higher values suggesting that there is more C present on the surface than expected for monolayer formation. This suggests that there are multilayers on the surface in agreement with the ellipsometric data.

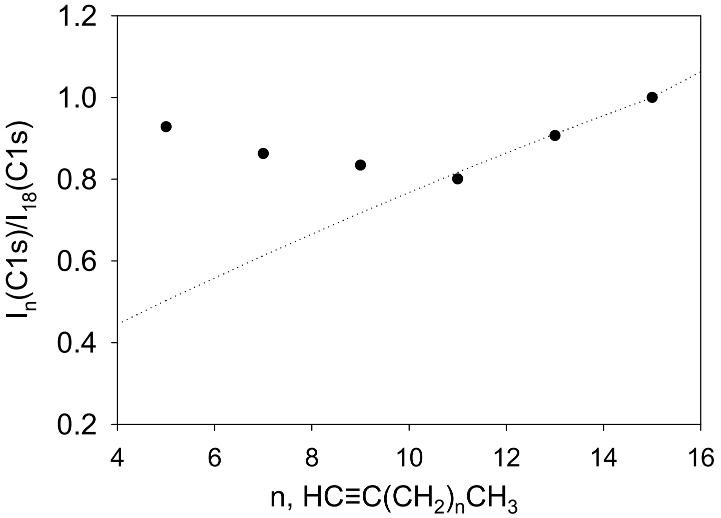

Figure 5. Fractional intensity of the C 1s peak (I(C 1s)$_n$/I(C 1s)$_{18}$ as a function of chain length. The dotted line is the theoretical dependence based on a constant monolayer coverage and film density for all values of n and references to the C 1s intensity of the octadecyne layer.

We also observe signals in the O 1s region. Deconvolution of the experimental data yields two peaks at 532.4 eV and 530.8 eV. The peak at 532.4 eV is consistent with the binding energies of O reported for poly(vinyl alcohol) and poly(methyl acrylate).[52] The signal at 530.8 eV is similar to the binding energies reported for O in ketones.[52] Further, the intensities of the O 1s peaks increase with increasing methylene chain length and reach a maximum for dodecyne TAMs before decreasing. The data are consistent with the above conclusions and suggest that there is more than one oxidized species on the surface.

No signals due to any N species, which may arise from ammonium hydroxide, were observed indicating that it does not react with the alkynes to form N containing organic compounds nor does it bind to the Au surface. Further, the Au $4f_{7/2}$ peak indicates that the Au surface is not oxidized during monolayer formation.

4.3.3 Reflection Absorption Infrared Spectroscopy

Changes in the stretching mode peaks with alkyl chain length provide a qualitative measure of the conformational order of each TAM. The peak frequencies are summarized in Table 2 and the spectra are shown in Figure 6a. In general, TAMs have broad C-H stretches with frequencies that are higher than those observed for well-ordered alkanethiolate SAMs on gold [45-49] (Table 2). However, the frequencies are lower than those observed for gas phase alkynes [53] (Table 2). Taken together, these data indicate that TAMs are disordered and in a liquid-like state. For $n \geq 11$ the peak frequency and absorbance of the asymmetric and symmetric CH_2 stretches decrease, indicating an increase in conformational order and monolayer organization. Further, for long chain alkynes ($n \geq 11$) an increase in the intensity of $\nu_{C\equiv C}$ ($C\equiv C$ stretch, 2136 cm^{-1}) is also detected, which also suggests that the TAMs are becoming ordered and have an upright orientation on the Au surface (Figure 6b). This is consistent with both the trends in monolayer thickness (Figure 2) and the decrease in oxidized species present on the surface (Figure 4).

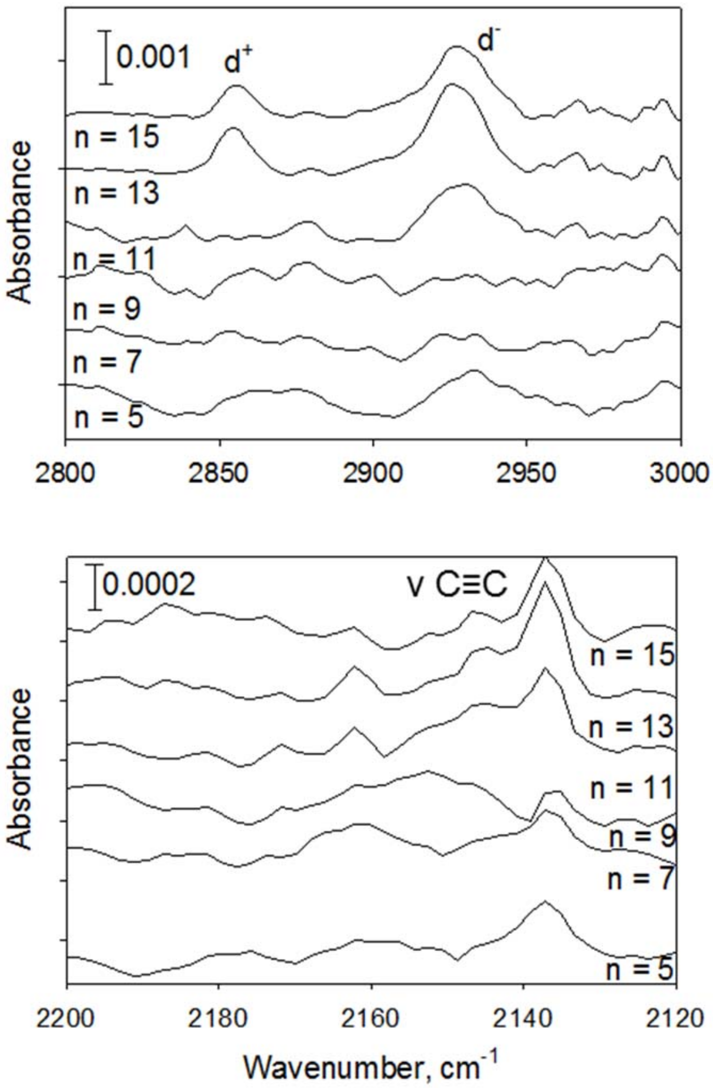

Figure 6. IRS spectra as a function of chain length for alkyne monolayers adsorbed on Au: a) 2800 – 3000 cm^{-1} and b) 2120-2000 cm^{-1}.

	Hexadecanethiol Adsorbed on Au[a]	**Alkyne Gas Phase[b]**	**$HC\equiv C(CH_2)_nCH_3$ on Au, cm^{-1}**					
Mode			**n = 5**	**n = 7**	**n = 9**	**n = 11**	**n = 13**	**n = 15**
$CH_2\ d^-$	2919	2930-2960	2932	2931	2931	2930	2926	2927
$CH_2\ d^+$	2851	2860 -2885	2862c	2860 c	2861	2861	2853	2854
$CH_3\ r_a^-$	2965	2960-2991	d	d	d	2965	2966	2966
$CH_3\ r_b^-$	~2958		d	d	d	2952	2954	2954
$CH_3\ r^+$, FR	2938		2874c	2875c	2876c	2878	2880	2879
$\nu \equiv C\text{-}H$		3325-3340	-	-	-	-	-	-
$\nu\ C\equiv C$		2132-2162	d	d	d	2137	2137	2137
$2\ \delta\equiv C\text{-}H$		1247-1257	-	-	-	-	-	-

Table 2. Peak positions for alkyne IR modes in the gas phase and adsorbed on Au. Also shown for reference are the positions of the C-H stretch modes for hexadecanethiol adsorbed on Au.

[a]Obtained from ref. [54]. [b]Obtained from ref. [53]. [c]The mode is very broad and weak. [d]The mode is not clearly observed.

4.3.4 Time-of-Flight Mass Spectrometry

In the positive and negative SIMS spectra the ions associated with the TAMs are found mostly below a mass-to-charge ratio (*m*/*z*) of 200. Prominent features in the mass spectra include fragment ions of the methylene chain and are characterized by ions with the general formula $(CH_2)_x(CH)_y^+$, $(CH_2)_xCH_3^+$ and $(CH_2)_x^+$. Several oxygen containing ions, including $CO(CH_2)_x^+$, $(CH_2)_xO^-$ and CO_2^-, are also observed indicating that oxidized alkyne species are adsorbed on the Au surface. These ions are often observed in monolayers with ester, carboxylic acid and alcohol groups.

In contrast to alkanethiolate SAMs adsorbed on Au, at higher masses (*m/z* > 200) no characteristic quasimolecular and cluster ions were observed, such as $AuM^{\pm}$, Au_2M^-,

AuM_2^- and $M^\pm$ where M denotes the alkyne molecule, $-C\equiv C(CH_2)_nCH_3$. However, several Au-containing fragment ions indicative of the TAM binding to the substrate are detected. In the positive and negative-ion spectra we observe ions with the formula $[Au_xC_2H_2]^\pm$ (Figure 7a). Since these ions have the same formula and appear in both positive and negative-ion spectra, this suggests that the charge is present on the Au and the alkyne binds to the surface via a Au-C≡C- bond. In the mass spectra Au-, O- and C- ions are also detected (Figure 7b) indicating that a proportion of the alkynes are oxidized and bind to the surface via, for example, a carboxylic acid in agreement with the XPS data (C1s Figure 3) and previous studies of ethynylbenzene adsorption Au substrates.

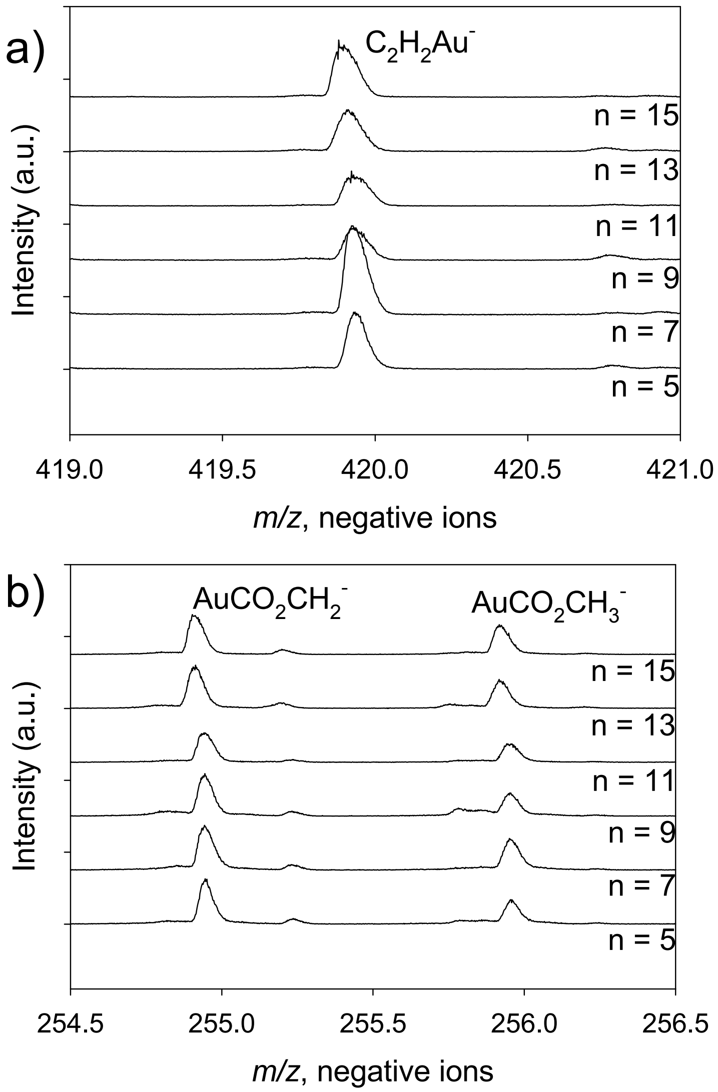

Figure 7. High mass resolution negative ion spectra centered at *m/z* 255.5 and *m/z* 420 as a function of chain length for alkyne monolayers adsorbed on Au.

4.4. Discussion

For the homologous series of terminal alkyne monolayers adsorbed on Au, the combination of ellipsometric, XPS, RAIRS and SIMS measurements are all consistent with a structural trend in which chains with more than 11 methylene units form disordered monolayers, which have an upright orientation. As the chain length increases, the conformational order is also observed to increase. For shorter chain lengths, monolayers are observed not to form. Rather, multilayer adsorption is detected; the film thicknesses are higher than the molecular length (Table 1; Figure 2). This is consistent with the oligomerization of the alkynes, which has been extensively studied in bulk and in functionalized SAMs. [55-57]

This behavior is in sharp contrast to alkanethiolate SAMs adsorbed on metals and semiconductors. [1,2,32] In general, these SAMs form monolayers on the substrate for all chain lengths. However, it is interesting to note that TAMs with more than 10 methylene units in the backbone start to form ordered layers. Similarly alkanethiolate SAMs with more than 9 or 10 methylene units are observed to form ordered monolayers. [1,2] This observation suggests that the formation and ordering of TAMs and alkanethiolate SAMs are both driven by the same process, hydrogen bonding between the alkane chains.

To date the binding of TAMs to Au has been unclear. Zhang and co-workers [39] and Lim and co-workers[43] suggested that the alkyne molecules adsorb on Au via Au-C≡C- bond. However, DFT calculations of ethynylbenzene adsorption on Au indicated that a vinylidene/Au (-HC=C-Au) interaction is the most stable.[42] Finally McDonaugh *et al*[41] observed that oxidized species of ethynylbenzene and 1,4-ethynylbenzene adsorbed to Au. Our data clearly indicate for terminal alkyne monolayers that both unoxidized and oxidized species adsorb on the surface. The SIMS data indicate that a proportion of the alkynes adsorb to the Au surface via a Au-C≡C- bond (Figure 7a). The IR data is consistent with this observation; for long chain alkynes ($n > 11$) a C≡C stretch was observed indicating that the alkyne had an erect orientation and was bound to the surface via a Au-C≡C- bond (Figure 6b). However, both the SIMS and XPS data show that oxidized species are present on the surface (Figure 3 and 7b). The chemical identity of the oxidized species is not clear. The C1s XPS spectra indicate that C-O and C=O bonds are present, with a C-O binding energy similar to that in PET. In PET the C-O bond is in the backbone of the polymer, -C-O-CH_2-CH_2.[50] The O1s spectra confirm that there are two oxidized species present. In SIMS, Au-, C- and O- containing ions, such as $AuCO_2CH_x^-$ (x = 2, 3) ions (Figure 7b), are observed which suggest that the oxidized alkyne is a carboxylic acid. Taken together with the XPS data, this suggests the alkyne undergoes a reaction to form a carboxylic acid, which binds to the surface via a Au-C(=O)OC bond.

From the above discussion, it is clear that the TAMs are likely to be less stable than alkanethiolate SAMs adsorbed on Au. Zhang *et al* [39] reported that TAMs are electrochemically stable and prevented the aggregation of Au nanoparticles in solution for up to 8 weeks. However, recent experiments indicate that dodecyne adsorbed on Au can be easily replaced by ferrocenylundecanethioacetate and ferrocenylundecanethiolate. [40] The amount of displacement by these molecules was observed to be dependent on the concentration of the thioacetate and thiolate and reached an equilibrium value. The authors suggested that the reaction was limited by the deprotection of the thioacetate to form a thiol. At lower concentrations the amount of thiolate available to replace the adsorbed.[40] However this does not explain why the replacement reaction reached an equilibrium value. One possible reason is that the ferrocenylundecanethioacetate quickly replaced the oxidize alkyne species present on the surface, and the displacement of the adsorbed, unoxidized alkyne is much slower.

It should be noted that, while the acetylide anion mechanism presented above explains the data, it may not be the only mechanism that is occuring in these experiments. Hydrogenation can occur at the alkyne, with the water present in the ammonium hydroxide. Also oxidative addition could occur to give olefin products. These may be side products in the reaction which additionally explain the side products observed.

4.5. Conclusions

The chemisorption of terminal alkynes ($HC\equiv C(CH_2)_nCH_3$, $n = 5,7,9,11,13,15$) on gold surfaces has been demonstrated under solution conditions. Long chain length terminal alkynes ($n \geq 11$) form disordered monolayers on gold. As the methylene chain length increases, the conformational order of the terminal alkyne monolayers (TAMs) increases. The molecules have an upright conformation and bind to the surface via a Au-C≡C- bond. Some oxidized species are present in the TAM, which are tentatively identified as carboxylic acids. For TAMs with less than 11 methylene units ($n < 11$) in the backbone, the adsorbed layer is highly disordered, oxidized and has a multilayer structure.

4.6. References

(1) Schreiber, F., Structure and Growth of Self-Assembling Monolayers. *Prog. Surf. Sci.* **2000**, *65*, 151-256.

(2) Ulman, A., Formation and Structure of Self-Assembled Monolayers. *Chem. Rev.* **1996**, *96*, 1533-1554.

(3) Widge, A. S.; Jeffries-El, M.; Cui, X.; Lagenaur, C. F.; Matsuoka, Y., Self-Assembled Monolayers of Polythiophene Conductive Polymers Improve Biocompatibility and Electrical Impedance of Neural Electrodes. *Biosens. Bioelectron.* **2007**, *22*, 1723-1732.

(4) Pearton, S. J.; Ren, F.; Wang, Y.-L.; Chu, B. H.; Chen, K. H.; Chang, C. Y.; Lim, W.; Lin, J.; Norton, D. P., Recent Advances in Wide Bandgap Semiconductor Biological and Gas Sensors. *Progress in Materials Science* **2009**, *55*, 1-59.

(5) Mirsky, V. M.; Vasjari, M.; Novotny, I.; Rehacek, V.; Tvarozek, V.; Wolfbeis, O. S., Self-Assembled Monolayers as Selective Filters for Chemical Sensors. *Nanotechnology* **2002**, *13*, 175-178.

(6) Mrksich, M.; Whitesides, G. M., Patterning Self-Assembled Monolayers Using Microcontact Printing - A New Technology for Biosensors. *Trends Biotechnol.* **1995**, *13*, 228-235.

(7) Palyvoda, O.; Chen, C.-C.; Auner, G. W., Culturing Neuron Cells on Electrode with Self-Assembly Monolayer. *Biosens. Bioelectron.* **2007**, *22*, 2346-2350.

(8) Carroll, R. L.; Gorman, C. B., The Genesis of Molecular Electronics. *Angew. Chem., Int. Ed. Engl.* **2002**, *41*, 4378-4400.

(9) Gorman, C. B.; Carroll, R. L.; Fuierer, R. R., Negative Differential Resistance in Patterned Electroactive Self-Assembled Monolayers. *Langmuir* **2001**, *17*, 6923-6930.

(10) Reed, M. A., Molecular-Scale Electronics. *Proc. IEEE* **1999**, *87*, 652-658.

(11) Reed, M. A.; Chen, J.; Rawlett, A. M.; Price, D. W.; Tour, J. M., Molecular Random Access Memory Cell. *Appl. Phys. Lett.* **2001**, *78*, 3735-3737.

(12) Reinerth, W. A.; Jones, L., II; Burgin, T. P.; Zhou, C.-w.; Muller, C. J.; Deshpande, M. R.; Reed, M. A.; Tour, J. M., Molecular Scale Electronics: Syntheses and Testing. *Nanotechnology* **1998**, *9*, 246-250.

(13) Tour, J. M.; Rawlett, A. M.; Kozaki, M.; Yao, Y.; Jagessar, R. C.; Dirk, S. M.; Price, D. W.; Reed, M. A.; Zhou, C.-W.; Chen, J.; Wang, W.; Campbell, I., Synthesis and Preliminary Testing of Molecular Wires and Devices. *Chem. Eur. J.* **2001**, *7*, 5118-5134.

(14) Tour, J. M.; Reinerth, W. A.; Jones, L., II; Burgin, T. P.; Zhou, C.-W.; Muller, C. J.; Deshpande, M. R.; Reed, M. A., Recent Advances in Molecular Scale Electronics. *Ann. N. Y. Acad. Sci.* **1998**, *852*, 197-205.

(15) Zareie, M. H.; Ma, H.; Reed, B. W.; Jen, A. K.-Y.; Sarikaya, M., Controlled Assembly of Conducting Monomers for Molecular Electronics. *Nano Letts.* **2003**, *3*, 139-142.

(16) Zhou, C.; Deshpande, M. R.; Reed, M. A.; Jones, L., II; Tour, J. M., Nanoscale Metal/Self-Assembled Monolayer/Metal Heterostructures. *Appl. Phys. Lett.* **1997**, *71*, 611-613.

(17) Stewart, M. P.; Maya, F.; Kosynkin, D. V.; Dirk, S. M.; Stapleton, J. J.; McGuiness, C. L.; Allara, D. L.; Tour, J. M., Direct Covalent Grafting of Conjugated Molecules onto Si, GaAs, and Pd Surfaces from Aryldiazonium Salts. *J. Am. Chem. Soc.* **2003**, *126*, 370-378.

(18) Tour, J. M., Molecular Electronics. Synthesis and Testing of Components. *Acc. Chem. Res.* **2000**, *33*, 791-804.

(19) Tour, J. M., Conjugated Macromoleculles of Precise Length and Constitution. Organic Synthesis for the Construction of Nanoarchitectures. *Chem. Rev.* **1996**, *96*, 537-553.

(20) Tour, J. M.; Kozaki, M.; Seminario, J. M., Molecular Scale Electronics: A Synthetic/Computational Approach to Digital Computing. *J. Am. Chem. Soc.* **1998**, *120*, 8486-8493.

(21) Tour, J. M.; Van Zandt, W. L.; Hushband, C. P.; Husband, S. M.; Wilson, L. S.; Franzon, P. D.; Nackashi, D. P., Nanocell Logic Gates for Molecular Computing. *IEEE Transactions on Nanotechnology* **2002**, *1*, 100-109.

(22) Wassel, R. A.; Gorman, C. B., Establishing the Molecular Basis for Molecular Electronics. *Angew. Chem., Int. Ed. Engl.* **2004**, *43*, 5120-5123.

(23) Lercel, M. J.; Craighead, H. G.; Parikh, A. N.; Seshadri, K.; Allara, D. L., Sub-10nm Lithography with Self-Assembled Monolayers. *Appl. Phys. Lett.* **1996**, *68*, 1504-1506.

(24) Lercel, M. J.; Craighead, H. G.; Parikh, A. N.; Seshadri, K.; Allara, D. L., Plasma Etching with Self-Assembled Monolayer Masks for Nanostructure Fabrication. *J. Vac. Sci. Technol. A* **1996**, *14*, 1844-1849.

(25) Lercel, M. J.; Redinbo, G. F.; Pardo, F. D.; Rooks, M.; Tiberio, R. C.; Simpson, P.; Craighead, H. G.; Sheen, C. W.; Parikh, A. N.; Allara, D. L., Electron Beam Lithography with Monolayers on Alkylthiols and Alkylsiloxanes. *J. Vac. Sci Technol. B* **1994**, *12*, 3663-3667.

(26) Lercel, M. J.; Rooks, M.; Tiberio, R. C.; Craighead, H. G.; Sheen, C. W.; Parikh, A. N.; Allara, D. L., Pattern Transfer of Electron Beam Modified Self-Assembled Monolayers for High-Resolution Lithography. *J. Vac. Sci Technol. B* **1995**, *13*, 1139-1143.

(27) Lercel, M. J.; Tiberio, R. C.; Chapman, P. F.; Craighead, H. G.; Sheen, C. W.; Parikh, A. N.; Allara, D. L., Self-Assembled Monolayer Electron-Beam Resists on GaAs and SiO_2. *J. Vac. Sci Technol. B* **1993**, *11*, 2823-2828.

(28) Zhou, C.; Trionfi, A.; Jones, J. C.; Hsu, J. W. P.; Walker, A. V., Comparison of Chemical Lithography Using Alkanethiolate Self-Assembled Monolayers on GaAs (001) and Au. *Langmuir* **2009**, *26*, 4523-4528.

(29) Zhou, C.; Walker, A. V., UV Photooxidation of Photopatterning of Alkanethiolate Self-Assembled Monolayer Adsorbed on GaAs (001). *Langmuir* **2007**, *23*, 8876-8881.

(30) Zhou, C.; Walker, A. V., UV Photooxidation of a Homologous Series of n-Alkanethiolate Monolayers on GaAs (001): A Static SIMS Investigation. *J. Phys. Chem. C* **2007**, *112*, 797-805.

(31) Zhou, C.; Walker, A. V., Dependence of Patterned Binary Alkanethiolate Self-Assembled Monolayers on “UV Photopatterning” Conditions, and Evolution with Time, Terminal Group and Methylene Chain Length. *Langmuir* **2006**, *22*, 11420-11425.

(32) McGuiness, C. L.; Blasini, D.; Masejewski, J. P.; Uppili, S.; Cabarcos, O. M.; Smilgies, D.; Allara, D. L., Molecular Self-Assembly at Bare Semiconductor Surfaces: Characterization of a Homologous Series of n-Alkanethiolate Monolayers on GaAs(001). *ACS Nano* **2007**, *1*, 30-49.

(33) Gawalt, E. S.; Avaltroni, M. J.; Koch, N.; Schwartz, J., Self-Assembly and Bonding of Alkanephosphonic Acids on the Native Oxide Surface of Titanium. *Langmuir* **2001**, *17*, 5736-5738.

(34) Petrovykh, D. Y.; Smith, J. C.; Clark, T. D.; Stine, R.; Baker, L. A.; Whitman, L. J., Self-Assembled Monolayers of Alkanethiols on InAs. *Langmuir* **2009**, *25*, 12185-12194.

(35) Knoben, W.; Brongersma, S. H.; Crego-Calama, M., Preparation and Characterization of Octadecanethiol Self-Assembled Monolayers on Indium Arsenide (100). *J. Phys. Chem. C* **2009**, *113*, 18331-18340.

(36) Bensebaa, F.; Ellis, T. H.; Badia, A.; Lennox, R. B., Probing the Different Phases of Self-Assembled Monolayers on Metal Surfaces: Temperaure Dependence of the C-H Stretching Modes. *J. Vac. Sci. Technol. A* **1995**, *13*, 1331-1336.

(37) Yamada, Y.; Wano, H.; Uosaki, K., Effect of Temperature on Structure of the Self-Assembled Monolayer of Decanethiol on Au(111) Surface. *Langmuir* **2000**, *16*, 5523-5525.

(38) Chu, C.; Ayres, J. A.; Stefanescu, D. M.; Walker, B. R.; Gorman, C. B.; Parsons, G. N., Enhanced Conduction through Isocyanide Terminal Groups in Alkane and Biphenylene Molecules Measured in Molecule/Nanoparticle/Molecule Junctions. *J. Phys. Chem. C* **2007**, *111*, 8080-8085.

(39) Zhang, S.; Chandra, K. L.; Gorman, C. B., Self-Assembled Monolayers of Terminal Alkynes on Gold. *J. Am. Chem. Soc.* **2007**, *129*, 4876-4877.

(40) Tucker, E. Z.; Gorman, C. B., Terminal Alkynes as an Ink or Background SAM in Replacement Lithography: Adventitious versus Directed Replacement. *Langmuir* **2010**, *26*, 15027-15034.

(41) McDonagh, A. M.; Zareie, H. M.; Ford, M. J.; Barton, C. S.; Ginic-Markovic, M.; Matisons, J. G., Ethynylbenzene Monolayers on Gold: A Metal-Molecule Binding Motif Derived from a Hydrocarbon. *J. Am. Chem. Soc.* **2007**, *129*, 3533-3538.

(42) Ford, M. J.; Hoft, R. C.; McDonagh, A., Theoretical Study of Ethynylbenzene Adsorption on Au(111) and Implications for a New Class of Self-Assembled Monolayer. *J. Phys. Chem. B* **2005**, *109*, 20387-20392.

(43) Lim, J. K.; Joo, S.-W.; Shin, K. S., Concentration dependent Raman study of 1,4-diethynylbenzene on gold nanoparticle surfaces. *Vibrational Spectroscopy* **2007**, *43*, 330-334.

(44) *ToF-SIMS: Surface Analysis by Mass Spectrometry*; Vickerman, J. C.; Briggs, D., Eds.; IM Publications and Surface Spectra Limited: Chichester and Manchester, UK, 2001.

(45) Laibinis, P. E.; Whitesides, G. M.; Allara, D. L.; Tao, Y.-T.; Parikh, A. N.; Nuzzo, R. G., Comparison of the Structures and Wetting Properties of Self-Assembled Monolayers of *n*-Alkanethiols on the Coinage Metal Surfaces, Cu, Ag, Au. *J. Am. Chem. Soc.* **1991**, *113*, 7152-7167.

(46) Fisher, G. L.; Hooper, A. E.; Opila, R. L.; Allara, D. L.; Winograd, N., The Interaction of Vapor-Deposited Al Atoms with CO_2H Groups at the Surface of a Self-Assembled Alkanethiolate Monolayer on Gold. *J. Phys. Chem. B* **2000**, *104*, 3267-3273.

(47) Fisher, G. L.; Hooper, A. E.; Opila, R. L.; Jung, D. R.; Allara, D. L.; Winograd, N., The Interaction Between Vapor-Deposited Al Atoms and Methylester-

Terminated Self-Assembled Monolayers Studied by ToF-SIMS, XPS and IRS. *J. Electron Spectrosc. Relat. Phenom.* **1998**, *98-99*, 139-148.

(48) Fisher, G. L.; Walker, A. V.; Hooper, A. E.; Tighe, T. B.; Bahnck, K. B.; Skriba, H. T.; Reinard, M. D.; Haynie, B. C.; Opila, R. L.; Winograd, N.; Allara, D. L., Bond Insertion, Complexation and Penetration Pathways of Vapor-Deposited Aluminum Atoms with HO- and CH_3O- Terminated Organic Monolayers. *J. Am. Chem. Soc.* **2002**, *124*, 5528-5541.

(49) Hooper, A.; Fisher, G. L.; Konstadinidis, K.; Jung, D.; Nguyen, H.; Opila, R.; Collins, R. W.; Winograd, N.; Allara, D. L., Chemical Effects of Methyl and Methyl Ester Groups on the Nucleation and Growth of Vapor-Deposited Aluminum Films. *J. Am. Chem. Soc.* **1999**, *121*, 8052-8064.

(50) Kono, M.; Wong, P. C.; Li, Y. S.; Mitchell, K. A. R., X-ray Photoelectron Spectroscopy Studies of the Stability of Al/Mg/PET Interfaces. *Surf. Rev. Letts.* **2000**, *7*, 227-233.

(51) Hofmann, S. In *Practical Surface Analysis by Auger and X-ray Photoelectron Spectroscopy*; Briggs, D., Seah, M. P., Eds.; John Wiley & Sons, Ltd: Chichester, UK, 1983, p 141-180.

(52) NIST X-ray Photoelectron Spectroscopy Database version 3.5, http:/http://srdata.nist.gov/xps/, 02/03/12 9:00 am

(53) Nyquist, R. A., Infrared Spectra-Structure Correlations for 1-Alkynes. A*ppl. Spectrosc.* 1**985,** 3*9,* 1088-1089.

(54) Nuzzo, R. G.; Dubois, L. H.; Allara, D. L., Fundamental Studies of Microscopic Wetting on Organic Surfaces. 1. Formation and Structural Characterization of a Self-Consistent Series of Polyfunctional Organic Monolayers. J. *Am. Chem. Soc.* 1**990,** 1*12,* 558-569.

(55) Vyklický, L.; Afzali-Ardakani, A.; Kagan, C. R., Self-Assembly and Oligomerization of Alkyne-Terminated Molecules on Metal and Oxide Surfaces. L*angmuir* 2**005,** 2*1,* 11574-11577.

(56) Chan, K. C.; Kim, T.; Schoer, J. K.; Crooks, R. M., Polymeric Self-Assembled Monolayers. 3. Pattern Transfer by Use of Photolithography, Electrochemical Methods, and an Ultrathin, Self-Assembled Diacetylenic Resist. J. *Am. Chem. Soc.* 1**995,** 1*17,* 5875-5876.

(57) Kim, T.; Chan, K. C.; Crooks, R. M., Polymeric Self-Assembled Monolayers. 4. Chemical, Electrochemical, and Thermal Stability of w-Functionalized, Self-Assembled Diacetylenic and Polydiacetylenic Monolayers. J. *Am. Chem. Soc.* 1**997,** 1*19,* 189-193.

Chapter 5

Matrix- Enhanced Secondary Ion Mass Spectrometry (ME SIMS) using Room Temperature Ionic Liquid Matrices

[Portions of this work have been previously published by Jennifer J.D. Fitzgerald, Paul Kunnath and Amy V. Walker, *Analytical Chemistry*, **2010**, *82*, 4413-4419]

Abstract. Room temperature ionic liquids (ILs) are used in a wide variety of applications including as matrices in matrix assisted laser desorption ionization (MALDI) mass spectrometry. The use of ionic liquids (ILs) as matrices has been investigated in TOF SIMS. Two ionic liquid matrices derived from the MALDI matrix α-cyano-4-hydroxycinnamic acid (CHCA) were employed in these studies: 1-methylimidazolium α-cyano-4-hydroxycinnamate (MI CHCA) and tripropylammonium α-cyano-4-hydroxycinnamate (trip CHCA). The molecular ion intensities of biologically-relevant analytes including phospholipids, cholesterol and peptides, were greatly enhanced. Further detection limits were also improved. For example, the limits of detection of 1,2-dipalmityl-sn-glycero-phosphocholine (DPPC) and 1,2-dipalmityl-sn-glycero-phosphoethanolamine (DPPE) were at least two orders of magnitude better. The data also suggest that IL matrices are suitable for imaging SIMS. The IL matrices did not cause changes to the sample surface; no "hot" spots were observed in the SIMS spectra. To demonstrate their use in imaging SIMS, an onion skin was imaged.

5.1 Introduction

Mass spectrometric imaging provides information about the spatial distribution of molecules and elements present on sample surfaces without the use of chemical tags, such as fluorescent labels. It can be used for lipid[1-3], peptide[4-7], pharmaceuticals[8], polymers[9,10] and semiconductor materials imaging[11]. Two different types of ionization methods are currently used for MS images: matrix assisted laser desorption ionization (MALDI)[4-9] and secondary ion mass spectrometry (SIMS)[8,9,11,12].

MALDI is routinely employed to analyze biological samples because it can easily ionize high molecular weight species, such as proteins and oligonucleotides.[13] In imaging MALDI an image is obtained by scanning a sample through a laser beam.[8,9] The spatial resolution is limited by the laser spot size, which is typically ~25 µm.[5,7,8] Since the typical size of individual cell components is less than ~250 µm, it is difficult to obtain the spatial distribution of molecules within a cell or nanoscale object. One disadvantage of MALDI imaging is that the sample must be carefully prepared to maintain the spatial distribution of compounds.[14,15]

SIMS has some advantages over MALDI for imaging. SIMS does not require the use of a matrix, and the lateral resolution is better, as high as ~200 nm. In SIMS, imaging is normally performed in microprobe configuration in which a high energy focused primary ion beam is rastered across the sample surface. In this configuration lateral resolution is determined by a number of factors including the ionization probability of the analyte and its concentration, and the ion-beam diameter, as well as other instrumental factors. One of the disadvantages of SIMS is that the ionization probability of intact molecules with mass-to-charge greater than 500 is extremely low.

In these cases the lateral resolution is determined by the amount of signal that can be generated per pixel. This leads to lateral resolutions that are much lower than the primary ion beam diameter.[10,15] Cluster ion beams, such as Au_n^{+}[15,16], C_{60}^{x+}[15,17,18], SF_5^{+}[15], and Bi_n^{x+}[15,19], greatly improve secondary ion production from molecules particularly at high mass. This has led to increased image contrast and an increase in experimental lateral resolutions to 400nm.[20] However, this lateral resolution is still much larger than the primary beam diameter. [15]

Another method to increase secondary ion intensities (by increasing analyte ionization probabilities) is to use a chemical pretreatment. In matrix enhanced SIMS (ME SIMS) a matrix, such as 2,5 dihydroxybenzoic acid (DHB)[21], glycerol[22] or hydrochloric acid[23], is either mixed with or sprayed onto the analyte surface. Quasimolecular ions of proteins with *m/z* up to 10,000 have been detected using this method.[21] However, ME SIMS is unsuitable for imaging because solid matrices can crystallize on the sample surface. This causes the recorded distribution of molecules and atoms present on the surface to be different from the original (“true”) distribution. This is often manifested by the formation of “hot spots”, which are areas where the recorded ion intensities are much larger than elsewhere on the surface (Figure 1).[21,24,25]

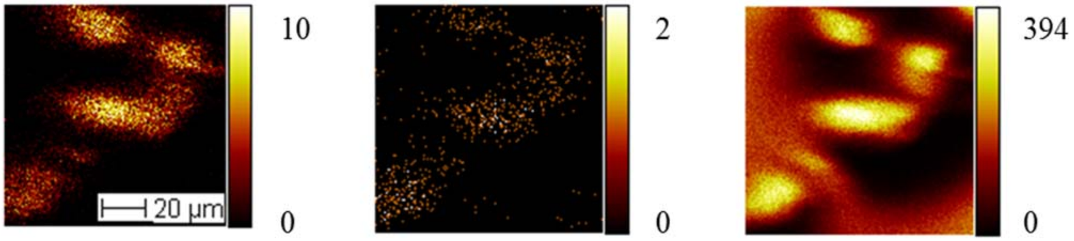

m/z 225 $[C_{11}H_{13}O_5]^+$ Sinapinic Acid

m/z 734 $[C_{40}H_{81}NPO_8]^+$ DPPC

Total ion image

Figure 1. SIMS images of DPPC, a phospholipid, mixed with sinapinic acid, a MALDI matrix. Area of analysis: 100 x 100 μm^2: 128 x 128 pixels. Primary ion: Bi^+. Primary ion energy: 25 keV. All images are shown using a heat scale with maximum and minimum counts for each pixel shown on the scale bar. Unpublished data by Sarah Machover, Amy V Walker.

Addition of metals, such as gold and silver can also increase molecular ion intensities (meta-SIMS)[26-29]. Although meta-SIMS is suitable for imaging, Adriaensen *et al*[26] have shown that meta-SIMS ion yields are time-dependent. [26] Metal-analyte adducts are often formed making it difficult to interpret the data.

Room temperature ionic liquids (ILs) have been demonstrated to be effective MALDI matrices.[27-32] They can be used with a wide variety of analytes including oligonucleotides[30], peptides[30], proteins[30], lipids[31], oligiosaccaraides[32], glycocongugates[32], and polymers[32]. In MALDI, the performance of the ILs have been shown to be as good, if not better, than the analogous solid matrix. For example, using the solid matrix α-cyano-4-hydroxycinnamic acid (CHCA), the detection limit of bradykinin was 10 pmol/ml.[33] Using an IL matrix, 1-methylimidazolium α-cyano-4-hydroxycinnamate (MI CHCA) the detection limit was < 1 fmol/ml.[33]

In addition, ionic liquids are attractive as matrices for imaging mass spectrometry. They have very low vapor pressure and so can be employed in the high vacuum.[33,34] Since they are liquids, they do not alter the sample surface density by crystallizing. This leads to little to no “hot spot” formation.[33] Finally, ILs are composed of preformed ions and so there is little mass interferences due to the fragmentation of the matrix.[33]

In this chapter, the use of ionic liquids are described as a new class of matrices in SIMS. Two different ILs matrices were chosen: 1-methylimidazolium α-cyano-4-hydroxycinnamate (MI CHCA) and tripropylammonium α-cyano-4-hydroxycinnamate (trip CHCA) (Figure 1). These IL matrices are derived from the MALDI matrix CHCA and have been shown to be effective MALDI matrices for the analytes polyethylene glycol, bradykinin and human insulin.[33] The analytes chosen were 1,2-dipalmitoyl-*sn*-glycero-3-phosphocholine (DPPC) ($(M + H)^+$, *m/z* 734.04), 1,2-dipalmitoyl-*sn*-glycero-3-phosphoethanolamine (DPPE) ($(M - H)^-$, *m/z* 691.95), cholesterol ($(M - H)^+$, *m/z* 386.85), lys (Des-Arg9-Leu8) bradykinin ($(M + H)^+$, *m/z* 997.6), and angiotensin I ($(M + H)^+$, *m/z* 1295.3) (Figure 2). These analytes represent three classes of biomolecules - phospholipids, steroids and peptides. DPPC, DPPE and cholesterol are commonly found in cell walls[24,35], while DPPC and DPPE are the most abundant lipids in the inner leaflet of the plasma membrane[35], while cholesterol plays a critical role in the formation of lipid domains and helps establish proper membrane fluidity and permeability.[36] Bradykinin and angiotensin I, are important in vascular signaling and the regulation of blood pressure.[37,38] The data show that use of IL matrices greatly enhances quasimolecular ion intensities, and and also substantially improves limits of detection. Signal intensities are at a least an order of magnitude better, while detection limits are improved by ~3 orders of magnitude. Further, no “hot spots” are in the spectra indicating that IL matrices are suitable for MS imaging. To demonstrate this, an onionskin membrane was imaged.

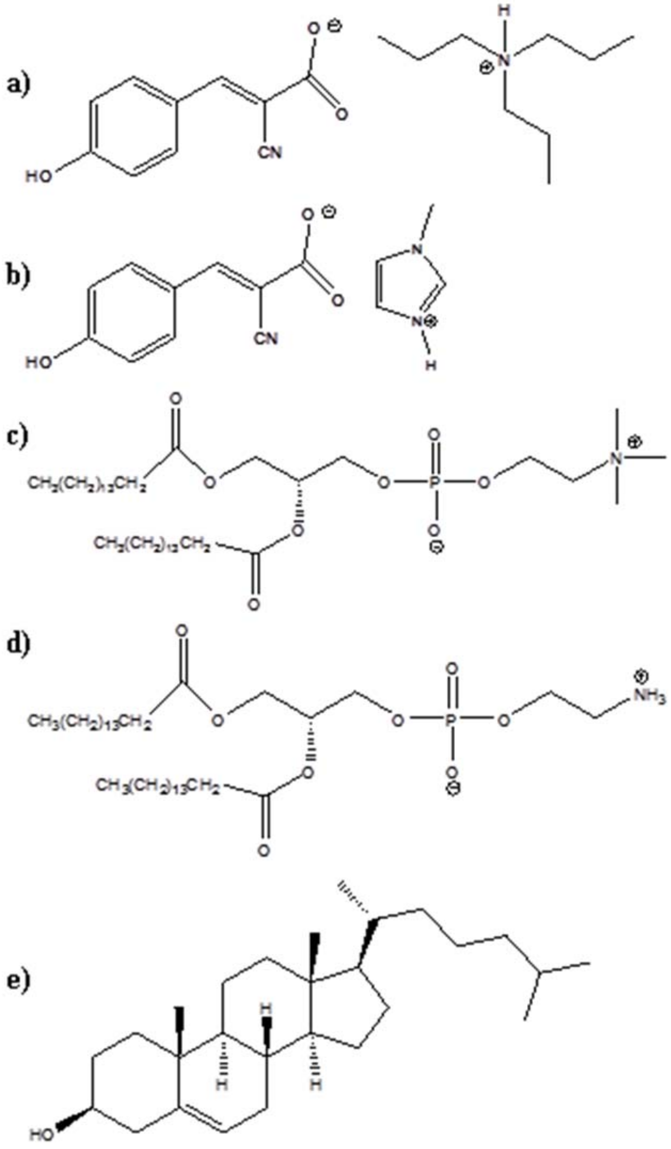

f) Lys-Arg-Pro-Pro-Gly-Phe-Ser-Pro-

g) Asp-Arg-Val-Tyr-Ile-His-Pro-Phe-His-

Figure 2. Structures of a) trip CHCA, b) MI CHCA, c) DPPC, d) DPPE, e) cholesterol, f) Lys (Des-Arg9-Leu8) bradykinin, and g) angiotensin I.

5.2 Experimental

5.2.1 Materials

Tripropylamine (99%), 1-methylimidazole (99%), α-cyano-4-hydroxycinnamic acid (97%) (CHCA) and cholesterol (99%) were purchased from Sigma Aldrich (St. Louis, MO). 1,2-Dipalmitoyl-*sn*-glycero-3-phosphocholine (DPPC) and 1,2-dipalmitoyl-*sn*-glycero-3-phosphoethanolamine (DPPE)were obtained from Avanti Polar Lipids Inc. (Alabaster, AL). Lys-(Des-Arg9-Leu8) bradykinin and angiotensin I were purchased from American Peptide (Sunnyvale, CA). HPLC-grade methanol and chloroform were acquired from Omnisolv (Charlotte, NC), and silicon wafers (<111> orientation, single side polished) were obtained from Addison Engineering (San Jose, CA). All chemicals were used without further purification except the silicon wafers. These were etched using RA1 etch (1:1:2 $NH_4OH:H_2O_2:H_2O$), rinsed with water and ethanol, and dried using nitrogen gas before use. The onion skin membrane was obtained from a red onion (Schnuck Markets Inc., St. Louis, MO).

5.2.2 Preparation of Ionic Liquids

Ionic liquids were synthesized using the method described by Armstrong *et al.*[33] Briefly, MI CHCA and trip CHCA were formed by first dissolving 0.5 g of CHCA (0.00265 mole) in 15 ml of methanol. To synthesize MI CHCA, an equimolar amount of 1-methylimidazole (212 µl, 0.00265 mole) was dissolved in the CHCA solution. Similarily, to prepare trip CHCA an equimolar amount of tripropylamine (505 µl, 0.00265 moles) was added to the CHCA solution. After sonication for 2 min, the methanol was evaporated, leaving the IL. Prior to use, the ionic liquids were characterized by using TOF SIMS, ^{1}H NMR, and IR spectroscopy (see appendix 3).

5.2.3 Sample Preparation

To investigate the detection limits and signal intensity enhancements of DPPC, DPPE and cholesterol, three sets of sample were prepared: one for each matrix (either trip CHCA or MI CHCA) and a control (no matrix added). For "matrix-enhanced" samples, 100 μl of IL solution (0.5 M) were mixed with 100 μl of the analyte solution. The concentration of the analyte was varied from 1 mg/ml to 1 x 10^{-5} mg/ml. The solvent employed was 1:1 methanol:choloroform (v/v). For the control samples 100 μl of the methanol/chloroform solution was mixed with the 100 μl of the analyte solution. After mixing, the 200 μl sample solution was then spun coat onto a ~0.5 cm^2 Si substrate for 6 s at 500 rpm and 20 s at 2000 rpm using a KW-4A spin coater (Chemat Technologies, Northridge, CA). Angiotensin I and bradykinin were prepared in a similar manner, but with only single analyte concentration of 1 mg/ml.

For imaging, three onionskin samples were prepared placing a piece of membrane on an ~1 cm^2 Si substrate. The matrix solution (500 μl ; 0.2 M; MI CHCA or trip CHCA) was spun coat on the sample for 30 s at 2000 rpm. The control sample was prepared by spin coating 500 μl of the methanol/choloroform solvent onto the membrane.

5.2.4 Time-of-Flight Secondary Ion Mass Spectrometry

Spectra were obtained using a TOF SIMS IV (ION TOF, Inc., Chestnut Ridge, NY) equipped with a Bi liquid metal ion gun. Briefly the instrument consisted of a loadlock, preparation chamber, and analysis chamber each separated by a gate valve. The main chamber was kept at $< 8x10^{-9}$mbar to prevent sample contamination. The primary Bi^+ ion had a kinetic energy of 25 keV. The primary ion dose of less was less than 1 x 10^{-10} ions cm^{-2}, which is within the static SIMS regime.[12] The secondary ions were extracted from the surface by using 2000 V and were reaccelerated to 10 keV before reaching the detector.

High resolution mass spectra and images were obtained using analysis areas of (100 x 100) μm^2 (500 x 500) μm^2(128 pixels x 128 pixels), respectively. The high resolution mass spectra had a mass resolution (or mass resolving power; $m/\Delta m$) of 4850 for ions of *m/z* 29, while the imaging mass spectra had a unit mass resolution (Δm). The secondary ion intensities reported are the averages of the data obtained from one sample with three randomly selected areas per sample. The detection limit of the analyte was determined by finding the lowest concentration for which the quasimolecular ion signal has a signal-to-noise ratio of 2.

To investigate the spatial variation of the matrix and analyte signals, the DPPE and DPPC (1 mg/ml) mass spectra were studied in more detail. For each (100 x 100) μm^2 area, five (20 x 20) μm^2 nonoverlapping regions were selected and the intensities of the quasimolecular, characteristic fragment, and matrix ions obtained. For each (20 x 20) μm^2 area, the data shown represent the average of the signal intensities over the three spots examined.

5.3 Results and Discussion

5.3.1 Molecular and Fragment Ions

Figure 1 displays the protonated and deprotonated molecular ions of DPPC (*m/z* 734.6, $[M + H]^+$), DPPE (*m/z* 690.5, $[M - H]^-$) and cholesterol (*m/z* 385.4, $[M - H]^-$). The data clearly show that both MI CHCA and trip CHCA are effective matrices and in general the signal intensity enhancement is larger using MI CHCA as a matrix.

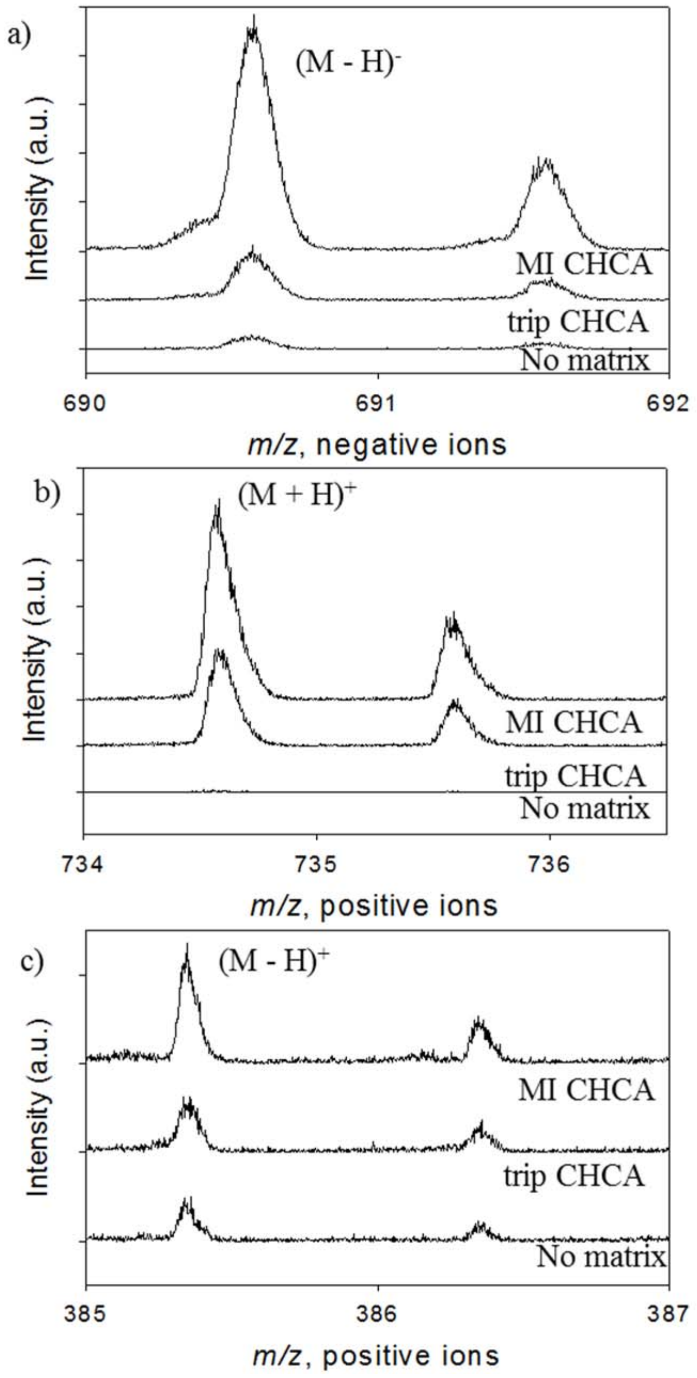

Figure 3. High mass resolution SIMS spectra of the quasimolecular ions of a) DPPE, b) DPPC, and c) cholesterol in MI CHCA and trip CHCA matrices, and with no matrix applied. Concentration of DPPE and DPPC: 0.5 mg/ml. Concentration of cholesterol: 1.0 mg/ml.

The enhancement observed is dependent on the concentration of the analyte (i.e. it is dependent on the matrix-to-analyte ratio). To investigate this effect, the molar matrix ratio was varied from ~350:1 to ~3.5 x 10^7:1 (matrix/analyte). The samples were prepared in the following way. To a 100 µl aliquot of the matrix solution, 100 µl of analyte of varying concentration (1 to 1 x 10^{-5} mg/ml) was added and thoroughly mixed. The resulting solution was then spun coat onto a clean Si substrate.

Figure 4 displays an example of the data obtained: the variation of the enhancement in the quasimolecular ion intensities of DPPC and DPPE with analyte concentration. The signal intensity enhancement is calculated using

Enhancement= $I(M \pm H)^{\pm}_{\text{matrix}}/I(M \pm H)^{\pm}_{\text{control}}$ **Formula 5.1**

where $I(M \pm H)^{\pm}$ is the intensity (peak area) of the quasimolecular ions of DPPC and DPPE. In Figure 4 it can been seen that the largest signal intensities are observed for concentrations ≥0.1 mg. At concentrations ≤0.01 mg/ml, the signal intensity enhancements are 10-20x and 3-15x for MI CHCA and trip CHCA, respectively. For cholesterol, the enhancement of the deprotonated molecular ion intensity is smaller, typically 3-10x.

The signal intensity enhancements appear to be affected by other experimental variables. Variations in the ion intensity enhancements are observed particularly at high analyte concentrations. For example, at a DPPC concentration of 1mg/ml, the enhancement of the protonated molecular ion varies from 100x to 300x when using MI CHCA. This is most likely due to uneven mixing of the analyte and matrix in solution or small changes in the thickness of the spun coat film. No “hot spots” were observed.

The detection limit of DPPC, DPPE and cholesterol were improved using IL matrices. It was determined by finding the analyte concentration for which the quasimolecular ion signal had a signal-to-noise ratio of at least 2. For DPPC, without matrix the limit of detection was 4 x 10^{-2} mg/ml corresponding to 5.3 nmol. (Note: This is the total amount of analyte in solution and not the amount present on the Si substrate which is less due to losses in the spin coating process.) Using the matrices, we found the detection limit is 1000x better: for MI CHCA and trip CHCA the limits of detection were 2.7 pmol (2 x 10^{-5} mg/ml) and 5.3 pmol (4 x 10^{-5}mg/ml), respectively. Assuming that all of the DPPC is deposited evenly across the Si substrate (~0.5 cm^2), for a (100 x 100) μm^2 analysis area, this corresponds to 0.54 and 1.1 fmol of DPPC for MI CHCA and trip CHCA, respectively.

This is ~10x lower than the reported smallest amounts of analyte detected using ME SIMS and a traditional MALDI matrix (50 fmol bovine insulin using 2,5 DHB as the matrix) and a 1000 fold increase in a limit of detection from not using any matrix. Similarly, for DPPE the detection limit was improved. Without a matrix the limit of detection was 5.8 nmol (4 x 10^{-2} mg/ml). Using MI CHCA, the detection limit was 1000x better, 5.8 pmol (4 x 10^{-5} mg/ml), while it was higher for trip CHCA, 29 pmol (2 x 10^{-4} mg/ml), a 200x improvement. For cholesterol, using the matrices all analyte concentrations were detected, so the limit of detection was <10^{-5} mg/ml, which was the smallest analyte concentration used. Without a matrix, the detection limit was 6 x 10^{-5} mg/ml (16 pmol).

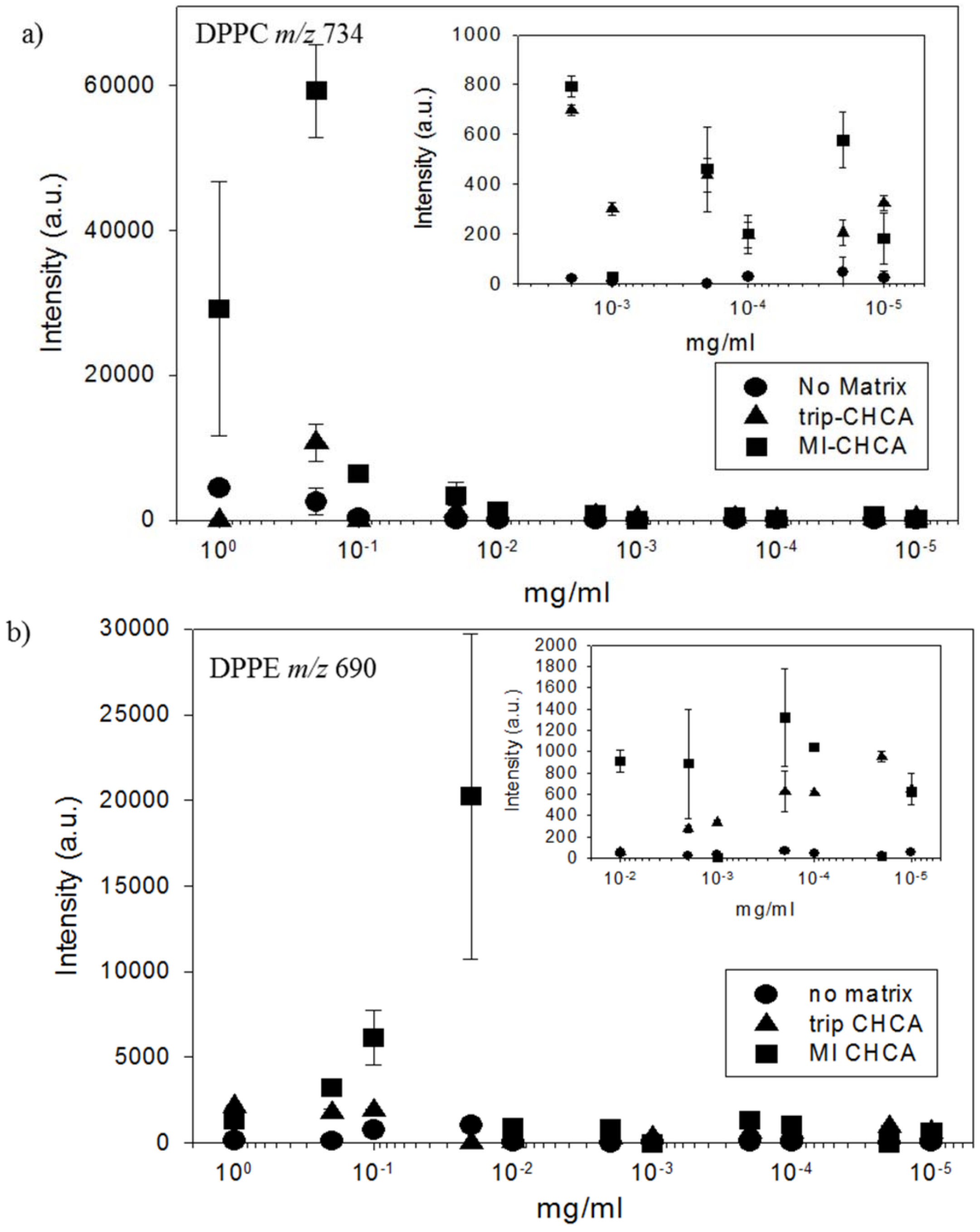

Figure 4. The enhancement of the quasimolecular ion intensities of a) DPPC and b) DPPE with analyte concentration.

Fragment ion intensities were also increased using MI CHCA and trip CHCA matrices. Figure 5 displays the enhancements of characteristic fragment ions of DPPC, DPPE and cholesterol at several different analyte concentrations. As in Figure 4, the signal intensity enhancement is calculated using

Enhancement= $I(X\pm)^{\pm}_{matrix}/I(X\pm)^{\pm}_{control}$ **Equation 5.2**

where $I(ion^{+})$ is the intensity signal (peak area) of $X^{\pm}$. For DPPC, the enhancement of fragment ions, characteristic of the headgroup, *m/z* 184 ($C_5H_{15}NPO_4^{+}$), and *m/z* 224 ($C_8H_{19}NPO_4^{+}$) for DPPC as well as the tail group, *m/z* 552 ($C_{35}H_{67}O_4^{+}$) were substantially smaller than the enhancement observed for the protonated molecular ion, $(M + H)^{+}$, suggesting that the extent of fragmentation decreases using an IL matrix. In contrast to the quasimolecular ion intensity, the intensity enhancement of these fragment ions remains approximately constant with decreasing DPPC concentration (Figure 5a). Similar behavior is observed for DPPE: the intensity enhancements of the characteristic ions of the headgroup (*m/z* 148 $C_2H_9NPO_4^{+}$) and tailgroup (*m/z* 552) are much smaller that for the quasimolecular ion, $(M - H)^{-}$ (Figure 5b). However, in contrast to the DPPC, the enhancement of the characteristic fragment ions decreasing DPPE concentration. In contrast to DPPC and DPPE, for cholesterol the fragment ion abundance, $(M - H_2O + H)^{+}$ (*m/z* 369), was approximately the same as that of the quasimolecular ion.

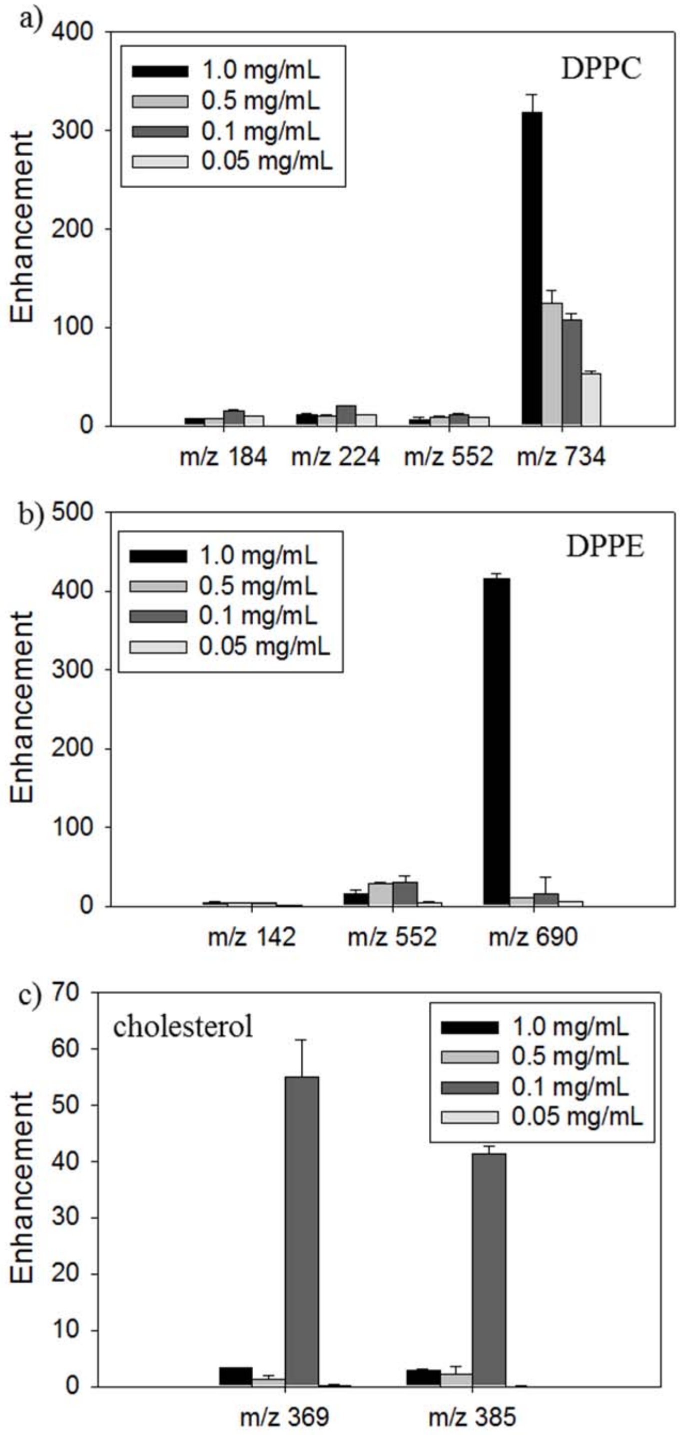

Figure 5. The ion intensity enhancement of representative fragment ions and molecular ions at four different concentrations of analyte (1, 0.5, 0.1 and 0.05 mg/ml) for a) DPPC, b) DPPE and c) cholesterol with MI CHCA.

TOF SIMS analyses were also performed for lys (Des-Arg9-Leu8) bradykinin (*m/z* 997.6 $(M + H)^+$) and angiotensin I (*m/z* 1296 $(M + H)^+$) using trip CHCA and MI CHCA matrices. Both peptides were analyzed at 1 mg/ml concentration. In the area occupied by the sample for analysis, this corresponds to 2×10^{-8} mol and 1.5×10^{-8} mol of analyte, respectively. Figure 6 displays the SIMS spectra of bradykinin using trip CHCA and MI CHCA matrices. It can be clearly seen that an intense quasimolecular ion, $(M + H)^+$ is observed as well as sodiated molecular ion, ($(M + Na)^+$, *m/z* 1020.6) were observed when using both IL matrices. For the neat analyte a very low intensity protonated molecular ion is observed but no sodiated ion (Figure 6c).

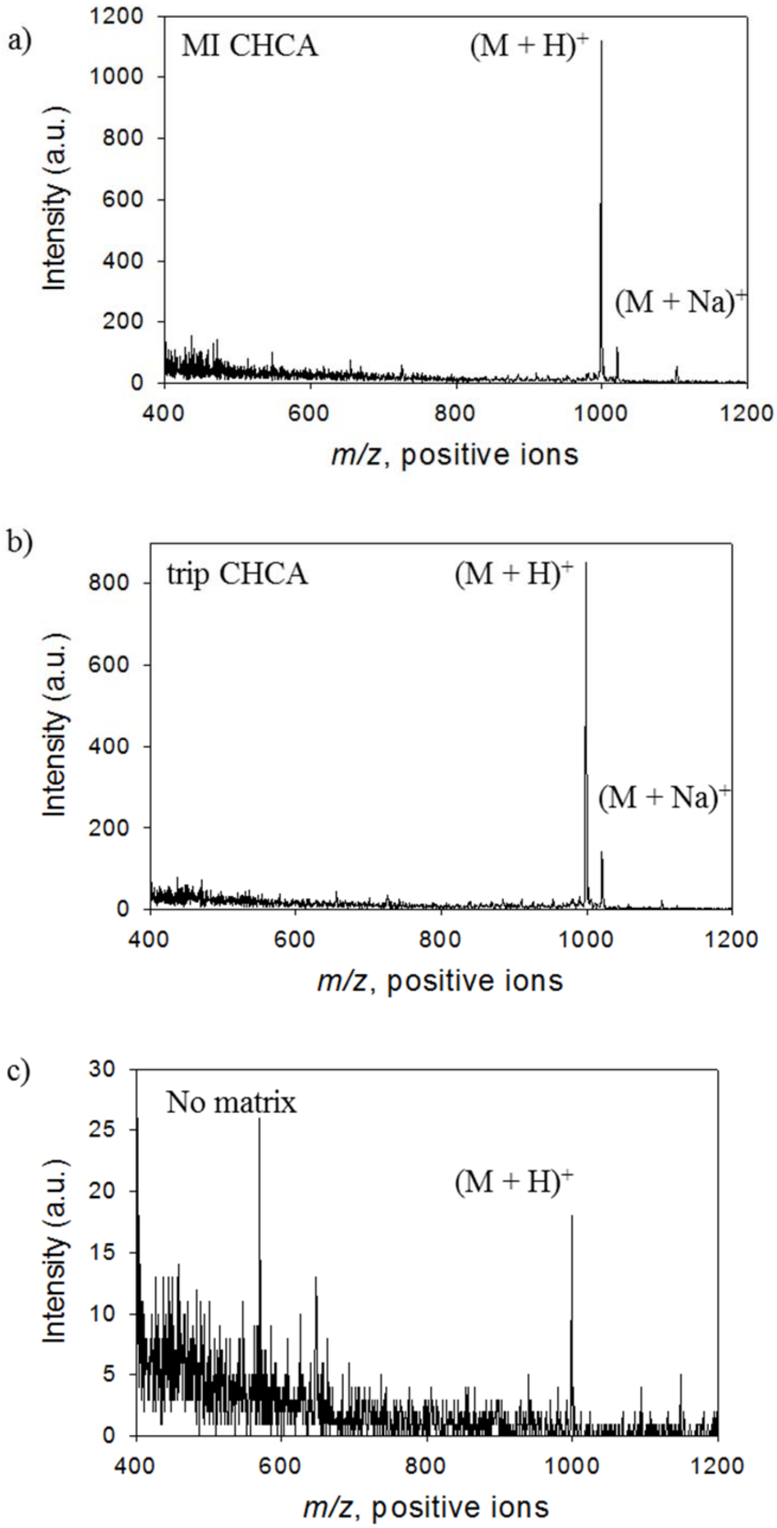

Figure 6. SIMS spectra of lys (Des-Arg9-Leu8) bradykinin using a) MI CHCA, b) trip CHCA and c) no matrix.

However, IL matrices are not always effective in SIMS. For angiotensin I ([M + H]$^+$ *m/z* 1290) no (M + H)$^+$ ions were observed in the neat analyte spectrum or using MI CHCA as a matrix in the positive-ion spectra. Using trip CHCA as a matrix, an (M + H)$^+$ ion was observed in the positive-ion spectrum with a low intensity (signal-to-noise ratio = 5).

5.3.2 Imaging

The data indicate that the analyte and matrix ion intensites are uniform across the sample. Figure 7 clearly shows that the ion intensities of DPPE ((M – H)$^-$, *m/z* 690) and the matrix ((CHCA – H)$^-$ *m/z* 188) are approximately constant indicating that there are no "hot spots."

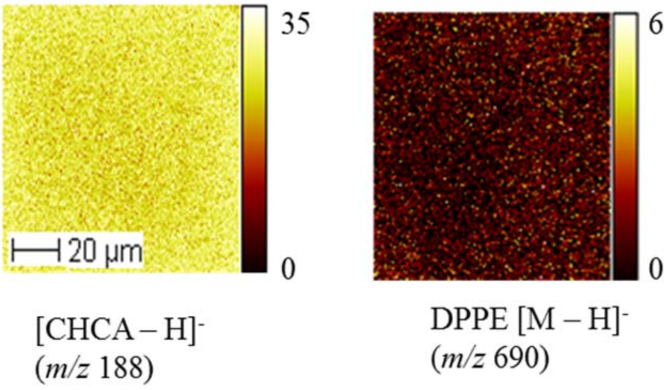

[CHCA – H]$^-$
(*m/z* 188)

DPPE [M – H]$^-$
(*m/z* 690)

Figure 7. Negative TOF SIMS images of DPPE ((M – H)$^-$, *m/z* 690) and the matrix ((CHCA – H)$^-$, *m/z* 188). The images are shown on a heat scale, and the scale bar shows the minimum and maximum counts per pixel. Concentration of DPPE solution: 1 mg/ml. Area of analysis: (100 x 100) μm^2.

To investigate further the spatial variation of the analyte and matrix ions, the DPPC and DPPE spectra were examined in detail. For each (100 x 100) μm^2 analysis area, five non-overlapping (20 x 20) μm^2 were selected. For each (20 x 20) μm^2 area, the signal intensities corresponding to the quasimolecular, characteristic fragment and matrix ions were averaged over the three analysis areas used per sample. Figure 8 displays the results obtained using MI CHCA as a matrix. The data clearly show that the signal intensities are constant across the analysis area indicating that ILs are suitable for imaging applications.

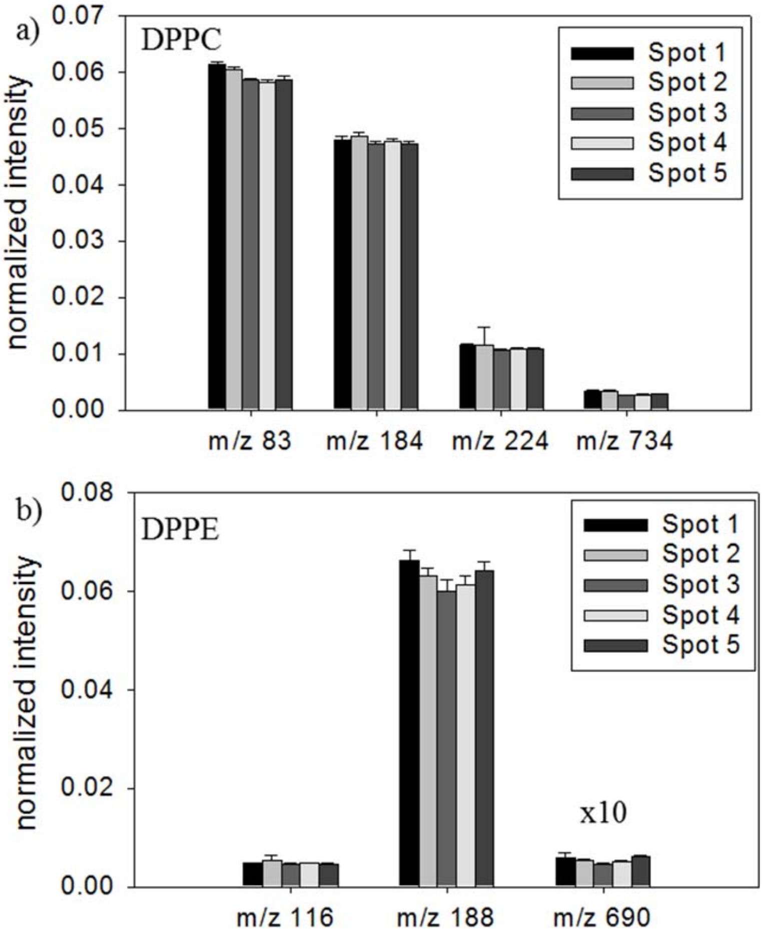

Figure 8. Normalized ion intensities of the molecular and characteristic fragment ions of DPPE, DPPC and MI CHCA.

The concentration of the phospholipid solutions was 1 mg/ml. For the DPPC sample (a), the ion intensities studied were those for ions of *m/z* 184 ($C_5H_{15}NPO_4^+$), and *m/z* 224 ($C_8H_{19}NPO_4^+$), characteristic ions of DPPE, and the matrix ion $(CHCA – H)^-$ (*m/z* 188). For DPPC, the signal intensities examined were the matrix ion $(MI + H)^+$ (*m/z* 83) and $(C_5H_8O_3)^-$ (*m/z* 116), characteristic ions of DPPC. The signal intensities were normalized to the total number of ion counts to compensate for any small changes in the ion dose.

5.4 Imaging

To demonstrate this application, three onionskin membranes were imaged. Two samples were prepared by spin coating either MI CHCA or trip CHCA on top of the onionskin while the third sample, the control, was prepared with application of only the solvent. In the positive ion mass spectra for the MI CHCA and trip CHCA coated samples, the signal intensities corresponding to $(\mathrm{MI} + \mathrm{H})^+$ (*m/z* 83) and $(\mathrm{trip} + \mathrm{H})^+$ (*m/z* 144) were approximately constant over the sample, indicating that the matrix is evenly coated across it.

Figure 9 displays optical and negative ion TOF SIMS images of the onion skin membranes. For the control sample, very low signal intensities were observed and there is no localization of ions such as CN^- (*m/z* 26) which are characteristic of proteins present in the cell nuclei. In contrast, for the MI CHCA and trip CHCA samples ions characteristic of proteins including CN^- (*m/z* 26), and the b ions of (Gly-Ser) (*m/z* 144) and (Ser-Cys) (*m/z* 189) were detected. These ions are co-localized in well-defined areas and most likely arise from the cell nuclei. In some cases, these areas are within the cell while other areas are located at the cell wall, suggesting that some of the cells “burst” upon introduction into the vacuum. It is interesting to note that these features are not clearly defined in the optical images but can be easily observed in ME SIMS.

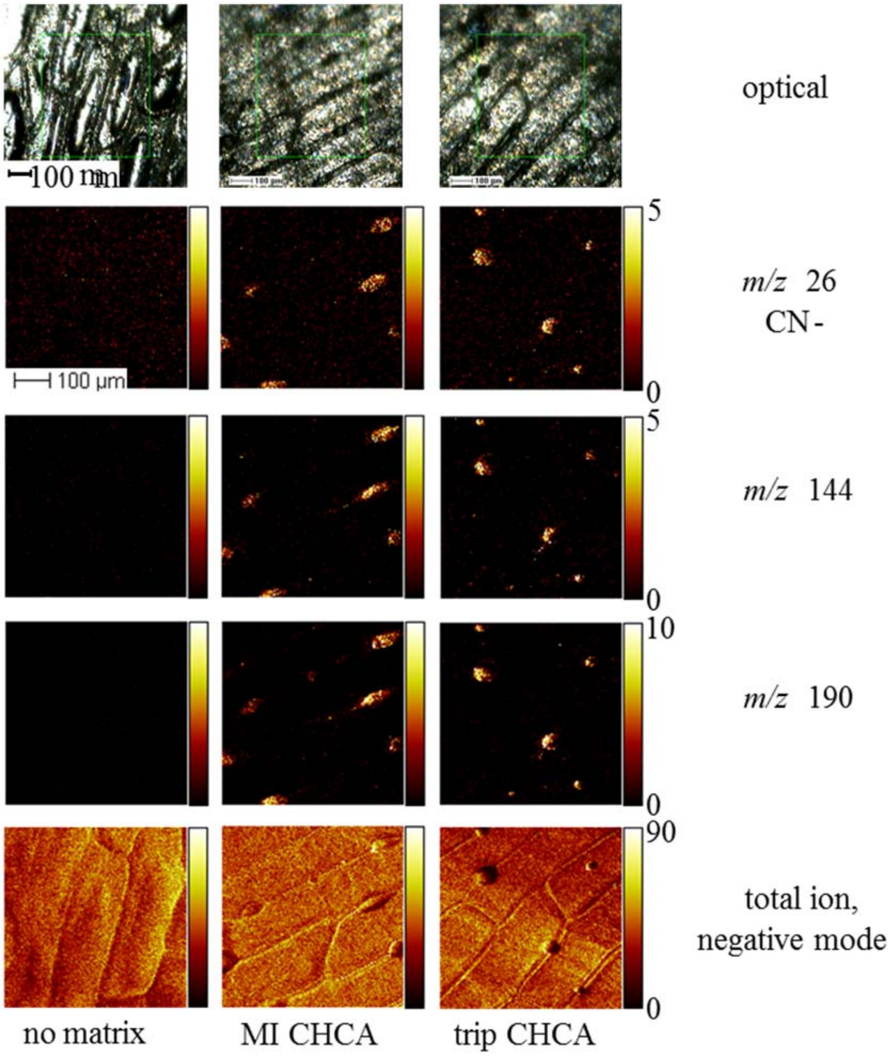

Figure 9. The optical and negative mass spectrometric images of a red onion skin treated with a) no matrix, b) MI CHCA, or c) trip CHCA.

5.5 Mechanism

It is clear that the mechanism of ion yield enhancement using ionic liquids is different in MALDI and SIMS. This is because the secondary ions are generated in a different way. In MALDI, a pulsed laser is employed. Secondary ions are generated via collisions between neutral analytes and matrix ions in the expansion plume as the sample (matrix/analyte mixture) is ablated from the surface.[39] In contrast, in TOF SIMS a pulsed primary ion beam is employed. Primary ions impinging on the surface cause a collision cascade within the sample which leads to the ejection of secondary species – neutrals, electrons and secondary ions.[40] However, there are some similarities in the behaviors observed using ionic liquid matrices in SIMS and MALDI.[32,41,42] First, the detection limit of phospholipids is several orders of magnitude better using IL matrices (Figure 4). Second, the extent of fragmentation is significantly reduced for most analytes (Figure 5). In MALDI, it is believed that ionization is promoted by available matrix protons; ionic liquids with an acidic proton promote the production of the desired gas-phase protonated quasimolecular ion, $(M + H)^+$.[42] In SIMS, it is also likely that ionization is promoted via the transfer of protons from (or to) the matrix. We observe that the intensities of protonated, or deprotonated, molecular ions of DPPC, DPPE, cholesterol and bradykinin are significantly increased using IL matrices (Figures 2 and 6). Further, for cholesterol similar ion intensity enhancements are observed for the characteristic fragment ion $(M – H_2O + H)^+$ (*m/z* 369) as for the quasimolecular ion $(M - H)^+$ (*m/z* 385) (Figure 4). The formation of this ion also requires the transfer of a proton from the surrounding matrix to the analyte. For DPPC, we note that the formation of the fragment ion characteristic of the headgroup (*m/z* 184) also involves the transfer of a proton from the molecular environment. However, its ion intensity is only increased ~5x – 10x which is much smaller than the enhancement observed for the quasimolecular ion, $(M + H)^+$ (*m/z* 734) (Figure 4). The most likely reason for this is that the formation of this fragment ion involves an intramolecular rearrangement, and not just a proton transfer.[43]

The chemical nature of the cation portion (protonated amine) of the matrix also appears to have an influence on secondary ion intensities. However there appears to be no relationship between the pK_a of the matrix components and the secondary ion signal intensities. The pK_a of methylimidazole is 6.95, while the pK_a of tripropylamine is 10.89.[42] The pK_a of CHCA (matrix base) is ~2.[44,45] Upon formation of the ionic liquid the matrix anion (CHCA) becomes almost completely deprotonated, and the matrix cation (trip or MI) is almost completely protonated. Upon addition of DPPC (pK_a = 2 -3)[46] there will be a competition between CHCA and DPPC to donate protons to the MI or trip amine groups to form the cation. Thus one would expect to see an increase in deprotonated molecular ions, such as $(M - H)^-$. Further the pK_a of MI and trip cannot account for the observed differences in the ion intensity enhancements observed. Upon formation of the ionic liquid, the matrix base with the lower pK_a (MI) will be slightly less protonated than the base with the higher pK_a (trip). This suggests that there will be more uncharged MI available for the donation of protons, but this is a vanishingly small effect. Thus, the pK_a of the matrix can not explain the observed matrix effects. The mechanism of matrix enhancement will be further explored in chapters 6 and 7.

5.6 Conclusion

The use of two room temperature ionic liquids derived from the MALDI matrix CHCA was investigated in TOF SIMS. The data indicate that molecular ion intensities of DPPC, DPPE, cholesterol and bradykinin are increased using IL matrices, indicating that ILs are broadly applicable effective matrices for ME SIMS. Further, using IL matrices the detection limits of DPPC, DPPE and cholesterol are improved by several orders of magnitude. The formation of fragment ions is also suppressed for the phospholipids and peptide samples. However, for cholesterol the signal intensity enhancement of the characteristic fragment ion, $(M - H_2O + H)^+$, is similar to that observed for the quasimolecular ion, $(M - H)^+$.

In contrast to solid matrices, such as sinapinic acid (Figure 1), the data indicate that the ion intensities are uniform across the sample surface, and ILs are suitable matrices for SIMS imaging. To demonstrate this application, onion-skin membranes were imaged. Using IL matrices, fragment ions characteristic of proteins, most likely from the cell nuclei, were observed which were not observed in SIMS images of control samples (no matrix applied).

The data indicate that ionization is promoted by proton transfer from (or to) the matrix. However there appears to be no relationship between the pK_a of the matrix and the secondary ion intensity enhancement observed.

5.6 References

(1) Brunelle, A.; Laprévote, O., Recent Advances in Biological Tissue Imaging with Time-of-Flight Secondary Ion Mass Spectrometry: Polyatomic Ion Sources, Sample Preparation and Applications. *Current Pharmaceutical Design* **2007**, *13*, 3335-3343.

(2) Brunelle, A.; Laprévote, O., Lipid Imaging with cluster time-of-flight secondary ion mass spectrometry. *Analytical Bioanalytical Chemistry* **2009**, *393*, 31-35.

(3) Jackson, S. N.; Woods, A. S., Direct profiling of tissue lipids by MALDI-TOFMS. *Journal of Chromatography B* **2009**, *877*, 2822-2829.

(4) Caprioli, R. M.; Farmer, T. B.; Gile, J., Molecular Imaging of Biological Samples: Localization of Peptides and Proteins Using MALDI-TOF MS. *Anal. Chem.* **1997**, *69*, 4751-4760.

(5) Chaurand, P.; Schwartz, S. A.; Caprioli, R. M., Imaging mass spectrometry: a new tool to investigate the spatial organization of peptides and proteins in mammalian tissue sections. *Curr. Opin. Chem. Biol.* **2002**, *6*, 676-681.

(6) Goodwin, R. J. A.; Pennington, S. R.; Pitt, A. R., Proteins and peptides in pictures: Imaging with MALDI mass spectrometry. *Proteomics* **2008**, *8*, 3785-3800.

(7) Stoeckli, M.; Chaurand, P.; Hallahan, D. E.; Caprioli, R. M., Imaging mass spectrometry: A new technology for the analysis of protein expression in mammalian tissues. *Nature Medicine* **2001**, *7*, 493-496.

(8) Rubakhin, S. S.; Jurchen, J. C.; Monroe, E. B.; Sweedler, J. V., Imaging mass spectrometry: fundamentals and applications to drug discovery. *Drug Discovery Today* **2005**, *10*, 823-837.

(9) McDonnell, L. A.; Heeren, R. M. A., Imaging mass spectrometry. *Mass Spectrom. Rev.* **2007**, *26*, 606-643.

(10) Pacholski, M. L.; Winograd, N., Imaging with Mass Spectrometry. *Chem. Rev. (Washington, D. C.)* **1999**, *99*, 2977-3005.

(11) Winograd, N., Prospects for imaging TOF-SIMS: from fundamentals to biotechnology. *Applied Surface Science* **2003**, *203-204*, 13-19.

(12) Walker, A. V., Why is SIMS Underused in Chemical and Biological Analysis? Challenges and Opportunities. *Analytical Chemistry* **2008**, *80*, 8865-8870.

(13) Todd, P. J.; Schaaff, T. G.; Chaurand, P.; Caprioli, R. M., Organic ion imaging of biological tissue with secondary ion mass spectrometry and matrix-assisted laser desorption/ionization. *J. Mass Spectrom.* **2001**, *36*, 355-369.

(14) Kaletaş, B. K.; Wiel, I. M. v. d.; Stauber, J.; Dekker, L. J.; Güzel, C.; Kros, J. M.; Luider, T. M.; Heeren, R. M. A., Sample preparation issues for tissue imaging by imaging MS. *Proteomics* **2009**, *9*, 2622-2633.

(15) Kollmer, F., Cluster primary ion bombardment of organic materials. *Appl. Surf. Sci.* **2004**, *231-232*, 153-158.

(16) Nagy, G.; Gelb, L. D.; Walker, A. V., An Investigation of Enhanced Secondary Ion Emission Under Au_n^+ (n = 1-7) Bombardment. *J. Am. Soc. Mass Spectrom.* **2005**, *16*, 733-742.

(17) Sun, S.; Szakal, C.; Smiley, E. J.; Postawa, Z.; Wucher, A.; Garrison, B. J.; Winograd, N., Spttering of Ag C_{60}^+ and Ga^+ projectile bombardment. *Appl. Surf. Sci.* **2004**, *231-232*, 64-67.

(18) Wong, S. C. C.; Hill, R.; P.Blenkinsopp; Lockyer, N. P.; Weibel, D. E.; Vickerman, J. C., Development of a C_{60}^+ ion gun for static SIMS and chemical imaging. *Appl. Surf. Sci.* **2003**, *203-204*, 219-222.

(19) Nagy, G.; Walker, A. V., Enhanced secondary ion emission with a bismuth cluster ion source. *Int. J. Mass Spectrom.* **2007**, *262*, 144-153.

(20) Touboul, D.; Kollmer, F.; Niehuis, E.; Brunelle, A.; Laprévote, O., Improvement of Biological Time-of-Flight-Secondary Ion Mass Spectrometry Imaging with a Bismuth Cluster Ion Source. *Journal of the American Society of Mass Spectrometry* **2005**, *16*, 1608-1618.

(21) Wu, K. J.; Odom, R. W., Matrix-Enhanced Secondary Ion Mass Spectrometry: A Method for Molecular Analysis of Solid Surfaces. *Analytical Chemistry* **1996**, *68*, 873-882.

(22) Tantsyrev, G. D.; Pronchev, G. B., Using a Water-Glycerol Matrix in Secondary-Ion Mass Spectrometry for Determining Organic Compounds. *J. Anal. Chem.* **1996**, *51*, 961-963.

(23) Seki, S.; Kambara, H., Acid Spray for Enhancement of MH^+ Ion Intensity in Secondary Ion Mass Spectrometry. *Shitsuryo Bunseki* **1987**, *35*, 84-89.

(24) Hanton, S. D.; Clark, P. A. C.; Owens, K. G., Investigations of Matrix-Assisted Laser Desorption/Ionization Sample Preparation by Time-of-Flight Secondary Ion Mass Spectrometry. *Journal of the American Society of Mass Spectrometry* **1999**, *10*, 104.

(25) Luxembourg, S. L.; McDonnell, L. A.; Duursma, M. C.; Guo, X.; Heeren, R. M. A., Effect of Local Matrix Crystal Variations in Matrix-Assisted Ionization Techniques for Mass Spectrometry. *Analytical Chemistry* **2003**, *75*, 2333-2341.

(26) Adriaensen, L.; Vangaever, F.; Gijbels, R., Metal-Assisted Secondary Ion Mass Spectrometry: Influence of Ag and Au Deposition on Molecular Ion Yields. *Anal. Chem.* **2004**, *76*, 6777-6785.

(27) Delcorte, A.; Bour, J.; Aubriet, F.; Muller, J.-F.; Bertrand, P., Sample Metallization for Performance Improvement in Desorption/Ionization of Kilodalton Molecules: Quantitatve Evaluation, Imaging Secondary Ion MS, and Laser Ablation. *Anal. Chem.* **2003**, *75*, 6875-6885.

(28) Delcorte, A.; Médard, N.; Bertrand, P., Organic Secondary Ion Mass Spectrometry: Sensitivity Enhancement by Gold Deposition. *Anal. Chem.* **2002**, *74*, 4955-4968.

(29) Heile, A.; Lipinsky, D.; Wehbe, N.; Delcorte, A.; Bertrand, P.; Felten, A.; Houssiau, L.; Piraux, J.-J.; Mondt, R. D.; Vaeck, L. V.; Arlinghaus, H. F., Metal-assisted SIMS and cluster ion bombardment for ion yield enhancement. *Appl. Surf. Sci.* **2008**, *255*, 941-943.

(30) Li, Y. L.; Gross, M. L., Ionic-Liquid Matrices for Quantitative Analysis by MALDI-TOF Mass Spectrometry. *J. Am. Soc. Mass Spectrom.* **2004**, *15*, 1833-1837.

(31) Li, Y. L.; Gross, M. L.; Hsu, F.-F., Ionic-Liquid Matrices for Improved Analysis of Phospholipids by MALDI-TOF Mass Spectrometry. *J. Am. Soc. Mass Spectrom.* **2005**, *16*, 679-682.

(32) Mank, M.; Stahl, B.; Boehm, G., 2, 5-Dihydroxybenzoic Acid Butylamine and Other Ionic Liquid Matrixes for Enhanced MALDI-MS Analysis of Biomolecules. *Analytical Chemistry* **2004**, *76*, 2938-2950.

(33) Armstrong, D. W.; Zhang, L.-K.; He, L.; Gross, M. L., Ionic Liquids as Matrixes for Matrix-Assisted Laser Desorption/ Ionization Mass Spectrometry. *Analytical Chemistry* **2001**, *73*, 3679-3685.

(34) Smith, E. F.; Rutten, F. J. M.; Villar-Garcia, I. J.; Briggs, D.; Licence, P., Ionic Liquids in Vacuo: Analysis of Liquid Surfaces Using Ultra-High-Vacuum Techniques. *Langmuir* **2006**, *22*, 9386-9392.

(35) Roddy, T. P.; Donald M. Cannon, J.; Ostrowski, S. G.; Ewing, A. G.; Winograd, N., Proton Transfer in Time-of-Flight Secondary Ion Mass Spectrometry

Studies of Frozen-Hydrated Dipalmitoylphosphatidylcholine. *Analytical Chemistry* **2003**, *75*, 4087-4094.

(36) Leah, E., *Lipidomics Gateway* **2009**, *1*.

(37) Dendorfer, A.; Wolfrum, S.; Wagemann, M.; Qadri, F.; Dominiak, P., Pathways of bradykinin degradation in blood and plasma of normotensive and hypertensive rats. *Am J Physiol Heart Circ Physiol* **2001**, *280*, H2182-8.

(38) Paul, M.; Mehr, A. P.; Kreutz, R., Physiology of local renin-angiotensin systems. *Physiol. Rev.* **2006**, *86*, 747-803.

(39) Zenobi, R.; Knochenmuss, R., Ion Formation in MALDI Mass Spectrometry. *Mass Spectrom. Rev.* **1998**, *17*, 337-366.

(40) Walker, A. V. In *The Encyclopedia of Mass Spectrometry: Molecular Ionization Methods*; Gross, M. L., Caprioli, R. M., Eds.; Elsevier Science & Technology Books: Burlington, USA, 2007; Vol. 6, p 535-551.

(41) Li, Y. L.; Gross, M. L.; Hsu, F.-F., Ionic-Liquid Matrices for Improved Analysis of Phospholipids by MALDI-TOF Mass Spectrometry. *J. Am. Soc. Mass Spectrom.* **2005**, *16*, 679-682.

(42) Armstrong, D. W.; Zhang, L.-K.; He, L.; Gross, M. L., Ionic Liquids as Matrices for Matrix-Assisted Laser Desorption/ionization Mass Spectrometry. *Anal. Chem.* **2001**, *73*, 3679-3686.

(43) Sostarecz, A. G.; Cannon, D. M., Jr.; McQuaw, C. M.; Sun, S.; Ewing, A. G.; Winograd, N., Influence of Molecular Environment on the Analysis of Phospholipids by Time-of-Flight Secondary Ion Mass Spectrometry. *Langmuir* **2004**, *20*, 4926-4932.

(44) Guo, Z.; He, L., A Binary Matrix for Background Suppression in MALDI-MS of Small Molecules *Anal. Bioanal. Chem.* **2007**, *387*, 1939-1944.

(45) Lou, X.; van den Hout, K. P.; van Houtem, M. H. C. J.; van Dongen, J. L. J.; Vekemans, J. A. J. M.; Meijer, E. W., Radical Cation Formation in Characterization of Novel C_3-Symmetric Disks and Their Precursors by Matrix-Assisted Laser Desorption/Ionization Time-of-Flight Mass Spectrometry. *J. Mass Spectrom.* **2006**, *41*, 659-669.

(46) Köhler, U.; Mantsch, H. H.; Casal, H. L., Infrared Spectroscopic Characterization of the Interaction of Ascorbyl Palmitate with Phospholipid Bilayers. *Can. J. Chem.* **1988**, *66*, 983-988.

Chapter 6

Proton Transfer in Matrix-Enhanced Secondary Ion Mass Spectrometry Using Ionic Liquid Matrices

Abstract: Room temperature ionic liquids (ILs) have been demonstrated to be effective matrices in SIMS. In this chapter we examine the role of proton transfer in the mechanism of secondary ion enhancement when using the analyte DPPC. We employ hydrogenated and deuterated DPPC and ILs to determine the origin of proton transfer from and to DPPC. The data indicate that protons from the matrix acid transfer to DPPC in solution leading to an increase in the secondary ion intensity of the protonated molecular ion, $(DPPC + H)^+$. The chemical identity of the matrix cation also affects analyte signal intensities. Using deuterated DPPC, we observe that protons (deuterium) from the DPPC tail group react with the cation of the IL liquid leading to an increase in $(cation + D)^+$ ion intensities. The data suggest that the transfer kinetics of deuterium (hydrogen) is correlated with the secondary ion enhancements observed. The highest secondary ion enhancements are observed for the least sterically hindered cation. The proton affinity and pK_a of the cation do not appear to have a large effect on the analyte signal intensity, suggesting that in SIMS, steric factors are important in determining the efficacy of the IL matrix.

6.1. Introduction

Room temperature ionic liquids (ILs) recently have been demonstrated to act as effective matrices for both matrix-assisted laser desorption ionization (MALDI)[1] and matrix enhanced secondary ion mass spectrometry (ME SIMS)[2]. They can be employed with a wide variety of analytes including lipids[2,3], proteins[1,4], peptides[1,2,4], sterols[2], oligonucleotides[5,6], polymers[1,7], carbohydrates[4], oligosaccharides[7] and glycoconjugates[7]. In SIMS, molecular ion yields are improved by at least an order of magnitude. For example, the protonated molecular ion of 1,2-dipalmitoyl-sn-glycero-3-phosphocholine (DPPC), $(M + H)^+$ (*m/z* 734.57) is enhanced up to 300x [2]. The detection limits are also improved: for DPPC and another phospholipid 1,2-dipalmitoyl-sn-glycero-3-phosphoethanolamine (DPPE) are at least two orders of magnitude better using IL matrices.[2] Indeed, protonated DPPC was detected with <1 fmol of DPPC in the analysis area. This allowed the detection of femtomolar amounts of analyte. Similarly in MALDI, limits of detection were also greatly improved. Using an IL matrix the detection limit of bradykinin was measured to be more than 3 orders of magnitude better, <1 fmol/ml, than using the analogous solid α-cyano-4-hydroxycinnamic acid (CHCA) matrix.[1] Further, less fragmentation is observed in the mass spectra using ionic matrices.[1,2] The data also indicated that IL matrices are suitable for both MALDI[1] and SIMS[2] imaging. The IL matrices did not cause changes to the sample surface via matrix crystallization or other processes; no hot spots were observed.

At first glance, it appears that the mechanism of matrix enhancement will be different for SIMS and MALDI. In SIMS, a pulsed ion beam is typically employed.[8] Secondary ions are generated via a collision cascade within the sample, and this leads to the ejection of secondary ions, neutrals and electrons. The generated secondary ions are characteristic of the sample chemistry. For MALDI, a pulsed laser source is employed.[9] Secondary ions are generated via collisions between the neutral analytes and matrix ions in the expansion plume as the sample (analyte/matrix mixture) is ablated. However, there are similarities in the behavior of IL matrices in SIMS and MALDI.[1-3,7] In MALDI it is likely that ionization is promoted via available matrix protons. Armstrong and co-workers[1] demonstrated that only ILs with acidic protons promote the formation of gas-phase protonated molecular ions, $(M + H)^+$. In SIMS, it is also believed that ionization is promoted via the transfer of protons to, or from, the matrix [2]. The intensities of protonated, or deprotonated, molecular ions of phospholipids, proteins and sterols are significantly increased by using IL liquids. Second, for cholesterol similar signal intensity enhancements are observed for the characteristic fragment ion $(M - H_2O + H)^+$ (*m/z* 369.35) and the deprotonated molecular ion, $(M - H)^+$ (*m/z* 385.35).[2] The formation of these ions also involves the proton transfer between the surrounding matrix and the analyte.

While it is clear that the chemical nature of both the cation and anion portions of the IL liquid influence secondary ion intensities [1,2,4], there are many questions that remain to be answered about the reaction pathways involved. For example, there appears to be no relationship between the pK_a of the matrix and the secondary ion intensity enhancements observed [1,2]. The pK_as of CHCA (a matrix conjugate base) and 1-methylimidazole (MI, a matrix conjugate acid) are ~1.1 and 7.01, respectively [10]. Upon formation of the IL, the CHCA becomes almost totally deprotonated, and the matrix base (MI) is almost completely protonated. The pK_a of the phosphonic ester group of phospholipids, such as

DPPE and DPPC, is 2-3.[11] Upon mixing of the phospholipid with the IL matrix, CHCA will donate a proton to the phosphate group leading to an increase in the intensity of protonated molecular ions, $(M + H)^+$. This is experimentally observed for DPPC but not for DPPE, where an increase in the deprotonated molecular ions, $(M - H)^-$ is observed.[2]

In this chapter, we investigate the role of proton transfer in secondary ion enhancements observed for DPPC using IL matrices in SIMS. Deuterated DPPC and IL matrices are employed to determine the origins of proton transfer to and from DPPC. Figures 1 and 2 display the structures of the DPPCs and ionic liquids used. The data indicate that protons from the matrix acid, CHCA, to DPPC leading to a substantial increase in the ion intensity of the protonated molecular ion, $(DPPC + H)^+$. Using deuterated DPPCs, we demonstrate that the tail groups dehydrogenate (lose D) leading to the formation of C=C bonds. The desorbed D then reacts with the IL cation, and is involved in inter- and intra- molecular reactions to form characteristic fragment ions of DPPC. Further, the ability of the matrix cation to accept (or donate) protons in an exchange is correlated with the analyte signal intensity enhancements. These measurements show that both the matrix cation and anion play significant roles in determining the magnitude of secondary ion yield enhancements observed in SIMS using IL matrices.

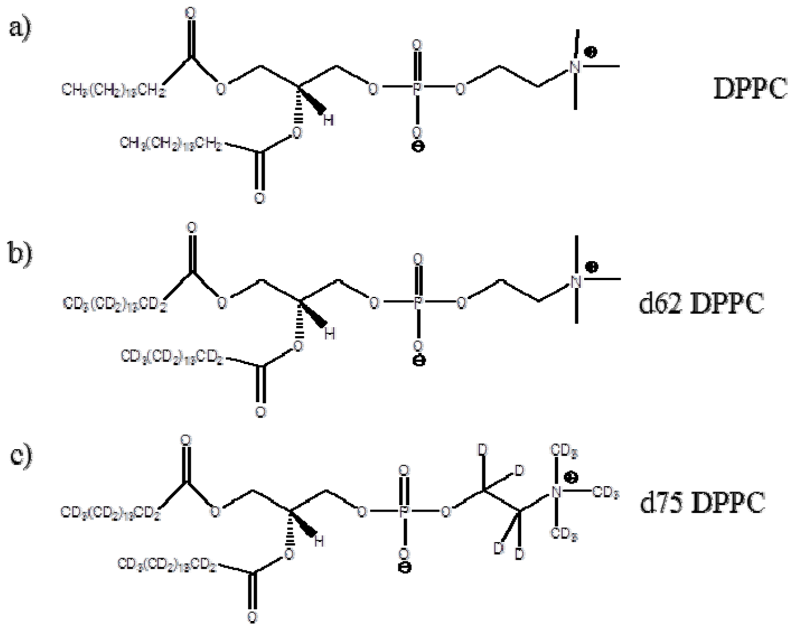
a)
DPPC
b)
d62 DPPC
c)
d75 DPPC

Figure 1. Structures of a) DPPC; b) d62 DPPC; and c) d75 DPPC.

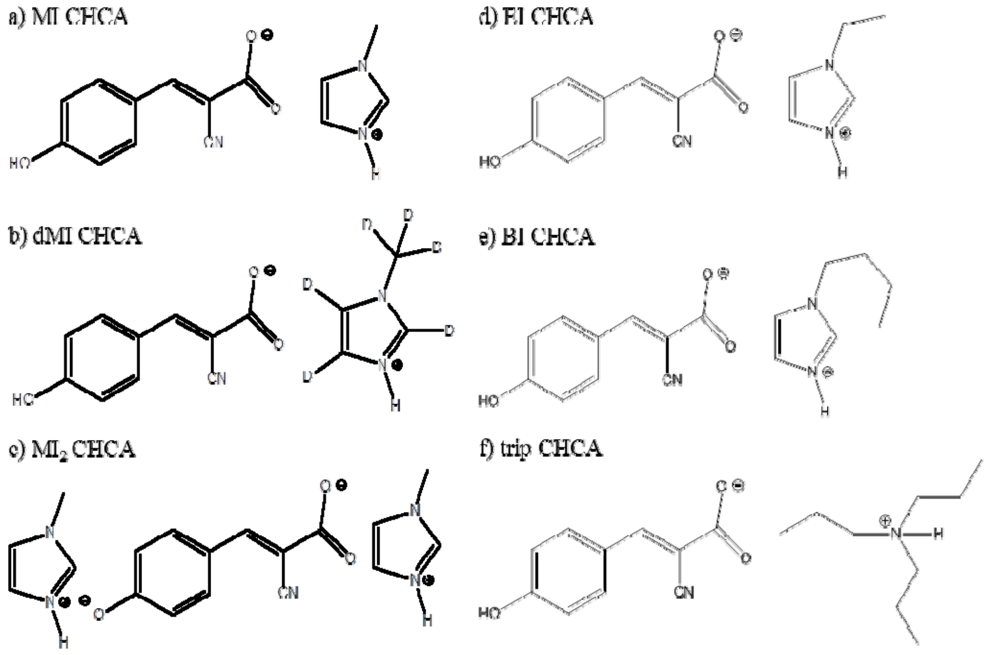
a) MI CHCA
b) dMI CHCA
c) MI$_2$ CHCA
d) EI CHCA
e) BI CHCA
f) trip CHCA

Figure 2. Structures of the ionic liquid matrices employed: a) MI CHCA; b) dMI CHCA; c) MI$_2$ CHCA; d) EI CHCA; e) BI CHCA; and f) trip CHCA.

6.2. Experimental

6.2.1 Materials

1-methylimidazole (99%), tripropylamine (99%), α-cyanohydroxycinnamic acid (97%) and 2,5 Dihydroxybenzoic acid (98%) were purchased from Sigma Aldrich (St. Louis, MO). 1,2-dipalmitoyl-*sn*-glycero-3-phosphocholine (DPPC), 1,2-dipalmitoyl(d62)-*sn*-glycero-3-phosphocholine (d62 DPPC),and 1,2-dipalmitoyl(d62)-*sn*-glycero-3-phosphocholine-1,1,2,2-d4-N,N,N-trimethyl-d9 (d75 DPPC were obtained from Avanti Polar Lipids, Inc. (Alabaster, AL). 1-methylimidazole-d_6 (98%) was obtained from CDN isotopes (Pointe-Claire, Quebec, Canada). HPLC grade methanol and chloroform were purchased from VWR (Radnor, PA) and Omnisolv (Charlotte, NC), respectively. Single side polished <111> Si wafers were purchased from Addison Engineering (San Jose, CA). All chemicals were used without further purification.

6.2.2. Preparation of Ionic Liquids

All ionic liquids were prepared using a method described by Armstrong and co-workers [1,4,6]. Briefly, 0.5g of α-cyanohydroxycinnamic acid (CHCA, 0.00265 moles) were dissolved in 15 ml of methanol. Equimolar amounts of the base (210 µl (0.00265 moles) of MI or dMI; 505 µl (0.00265 moles tripropylamine) were added to the methanolic solution of CHCA. After sonicating the resulting solution, the methanol was evaporated, leaving the ionic liquid. MI_2CHCA was prepared in a similar manner to that described above with 420 µl of MI (0.0053 moles) added to the 0.00265 moles of CHCA. Prior to use the ILs were characterized using time-of-flight secondary ion mass spectrometry (TOF SIMS), ^1H NMR and infrared spectroscopy.

6.2.3. Sample Preparation

For each "matrix enhanced" sample, 400 µl of 0.5 M IL solution was mixed with 400 µl of analyte solution (concentration: 1mg/ml). The solvent employed was 1:1 methanol/chloroform (v/v). For control samples a 400 µl aliquot of the methanol/chloroform solution was mixed with 400 µl of analyte solution. Once mixed the sample (total volume: 800 µl) was spun coat onto a ~1cm^2 Si substrate for 6 s at 250 rpm and 20 s at 3000 rpm using a KW-4A Spin Coater (Chemat Technology, Inc., Northridge, CA).

6.2.4 Time of Flight Secondary Ion Mass Spectrometry

TOF SIMS spectra were taken on an ION TOF IV (ION TOF USA, Chestnut Ridge, NY) equipped with a Bi primary ion gun. Briefly the instrument consists of a loadlock chamber, preparation chamber and main chamber, all separated by gate valves. During experiments, the main chamber was maintained at $\leq 1 \times 10^{-8}$ mbar to prevent sample contamination. The primary Bi_3^+ ion had a kinetic energy of 25 keV. The mass spectra were obtained in the static regime [8] with a primary ion dose of less than 1×10^{10} ions$\cdot$cm^{-2}. The generated secondary ions were extracted from the surface by using 2000 V and reaccelerated to 10 keV before reaching the detector.

High resolution mass spectra were obtained using an analysis area of (100 x 100) µm^2. The mass resolution (or resolving power; m/Δm) at *m/z* 29 was 3000. The secondary ion intensities reported are the averages of the data from one sample with at least three randomly selected areas per sample analyzed. The error bars reported are the standard deviation of the data. Mass spectra shown are representative of the data collected.

6.3. Results and Discussion

Previous studies indicate that analyte ionization is promoted via the transfer of protons to, or from, the matrix. A protic ionic liquid is a complex mixture of molecular species («1 % of the ionic liquid), ion pairs and ions [12]. Thus, proton transfer can occur between the molecular components of the ionic liquid and the analyte as well as with the ions present. For example using DPPC as the analyte and MI CHCA as the ionic liquid matrix the following reactions are possible:

$$\mathrm{DPPC}^0_{\mathrm{ads}} \rightarrow \mathrm{DPPC}^0_{\mathrm{g}} \xrightarrow{H^+} (\mathrm{DPPC} + \mathrm{H})^+_{\mathrm{g}} \qquad \textbf{Equation 6.1}$$

$$\mathrm{DPPC}^0_{\mathrm{ads}} + \mathrm{CHCA}^0_{\mathrm{ads}} \rightarrow (\mathrm{DPPC} + \mathrm{H})^+_{\mathrm{g}} + (\mathrm{CHCA} - \mathrm{H})^-_{\mathrm{g}} \qquad \textbf{Equation 6.2}$$

$$\mathrm{DPPC}^0_{\mathrm{ads}} + \mathrm{MI}^0_{\mathrm{ads}} \rightarrow (\mathrm{DPPC} - \mathrm{H})^-_{\mathrm{g}} + (\mathrm{MI} + \mathrm{H})^+_{\mathrm{g}} \qquad \textbf{Equation 6.3}$$

$$\mathrm{DPPC}^0_{\mathrm{ads}} + (\mathrm{CHCA} - \mathrm{H})^0_{\mathrm{ads}} \rightarrow (\mathrm{DPPC} - \mathrm{H})^-_{\mathrm{g}} + \mathrm{CHCA}^0_{\mathrm{g\ or\ ads}} \qquad \textbf{Equation 6.4}$$

$$\mathrm{DPPC}^0_{\mathrm{ads}} + (\mathrm{MI} + \mathrm{H})^+_{\mathrm{ads}} \rightarrow (\mathrm{DPPC} + \mathrm{H})^+_{\mathrm{g}} + \mathrm{MI}^0_{\mathrm{g\ or\ ads}} \qquad \textbf{Equation 6.5}$$

$$\mathrm{CHCA}^0_{\mathrm{ads}} + \mathrm{MI}^0_{\mathrm{ads}} \rightarrow (\mathrm{CHCA} - \mathrm{H})^-_{\mathrm{g\ or\ ads}} + (\mathrm{MI} + \mathrm{H})^+_{\mathrm{g\ or\ ads}} \qquad \textbf{Equation 6.6}$$

where $(\mathrm{DPPC} + \mathrm{H})^+$ and $(\mathrm{MI} + \mathrm{H})^+$ are the protonated molecular ions of DPPC and MI, respectively, and $(\mathrm{CHCA} - \mathrm{H})^-$ is the deprotonated molecular ions of CHCA. The subscripts *ads* and *g* denote adsorbed and gas phase species, respectively. Equation 1 describes the gas-phase protonation of DPPC to form $(\mathrm{DPPC} + \mathrm{H})^+$. Equations 2 – 6 describe processes that occur on the substrate surface in the ionic liquid. Equation 2 describes the protonation of DPPC via the transfer of a proton from CHCA, while equations 3 and 4 illustrate the formation of a deprotonated DPPC molecular ion, $(\mathrm{DPPC} - \mathrm{H})^-$. The $\mathrm{pK_a}$ of CHCA is ~1.1 [10] while the $\mathrm{pK_a}$ of the DPPC phosphonic ester group is

2-3.[11] Thus it is likely that protons will transfer from CHCA to DPPC leading to the formation of (DPPC + H)$^+$ and (CHCA – H)$^-$ ions (equation 2). Similarly, the relative values of the pK$_a$s of DPPC and MI (pK$_a$ = 7.01 [10]) suggest that a proton will transfer from DPPC to MI (equation 3). Equation 5 describes the transfer, or exchange, of protons between DPPC and the IL cation, (MI + H)$^+$. Although the pK$_a$ of the DPPC choline group is 13.9[13], this reaction is less likely because the choline is already protonated. Finally, equation 6 illustrates the acid-base reaction between CHCA and MI (formation of the protic IL).

If proton transfer occurs between the IL and analyte in solution, we predict that the quasimolecular ion intensities of analytes, such as DPPC, will vary as a function of mixing time, which we define as the length of time the IL and analyte are mixed together in the methanol/chloroform solution prior to spin coating on the Si substrate. In contrast, if the DPPC is first ablated from the surface and protonated in the gas phase (equation 1) it is expected that the secondary ion yields of the analyte will not depend on the mixing time. To test whether proton transfer occurs between the IL and analyte in solution the following experiment was performed. A solution of DPPC (concentration 1 mg/ml) was mixed with 0.5 M MI CHCA for times from 30 s to 1800 s (30 min). At each time point, a 400 µl aliquot was removed from the solution, immediately spun coat onto a Si substrate and transferred to the TOF SIMS instrument for analysis. Figure 3a displays the variation of the protonated molecular ion of DPPC, (DPPC + H)$^+$ (*m/z* 734.46) with mixing time. It can be clearly seen that initially the (DPPC + H)$^+$ ion intensity increases and then remains approximately constant until a mixing time of 600 s. At longer mixing times, the ion intensity decreases significantly. After 1800 s (30 min) the ion intensity of

$(DPPC + H)^+$ is approximately that of the control sample, a DPPC sample without IL added. Since the intensity of $(DPPC + H)^+$ changes with mixing time, the gas phase protonation of DPPC (equation 1) does not appear to be a major reaction pathway in the secondary ion yield enhancements observed using IL matrices. Subsequent experiments employed mixing times between 60 and 300 s (1 and 5 min) to maximize the analyte quasimolecular ion intensities.

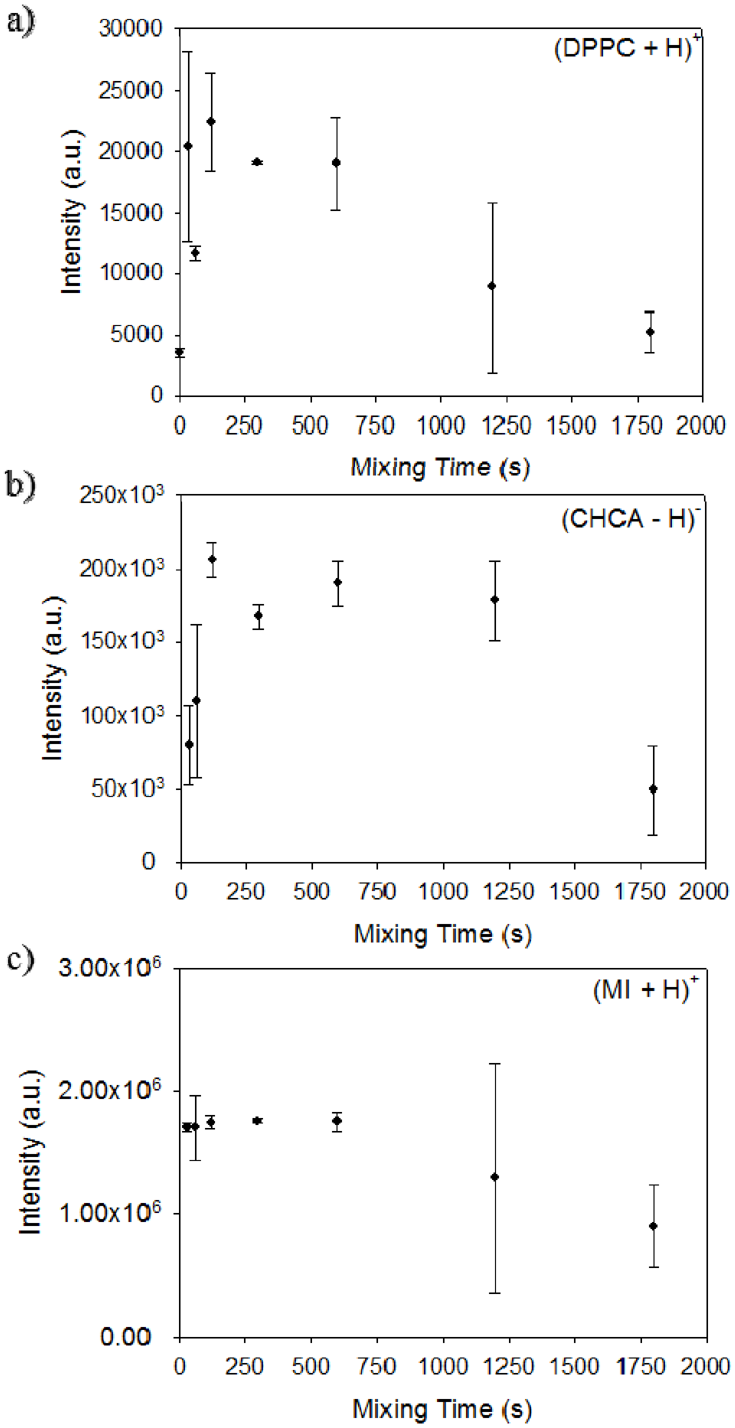

Figure 3. Variation of quasimolecular ion intensities with mixing time: a) (DPPC + H)$^+$; b) (CHCA – H)$^-$; and c) (MI + H)$^+$. The ion intensity of (DPPC + H)$^+$ for a control sample without matrix is shown in a) at 0s mixing time.

The increase, and decrease, in the $(DPPC + H)^+$ ion intensity is mirrored by the deprotonated molecular ion of the matrix acid, $(CHCA - H)^-$ (Figure 3b). There is a rapid rise in the ion intensity of $(CHCA - H)^-$ in the first two minutes (120 s) of mixing. At later times, the intensity of $(CHCA - H)^-$ remains approximately constant until a mixing time of ~20 mins (1200 s) whereupon it significantly decreases. These observations suggest that CHCA transfers a proton to DPPC leading to an increase in the ion intensities of $(CHCA - H)^-$ and $(DPPC + H)^+$ (equation 2). This is also consistent with the relative pK_as of CHCA and DPPC. In solution DPPC is a zwitterion with a negatively charged phosphate group and a positively charged choline headgroup [14]. CHCA has a lower pK_a than the phosphate group of DPPC, and so a proton will transfer from CHCA to the negatively charged phosphonic ester group neutralizing it. Thus, a protonated positively charged molecule of DPPC forms, $(DPPC + H)^+$.

In contrast to the quasimolecular ions of DPPC and CHCA, the ion intensity of the matrix cation, $(MI + H)^+$ initially remains constant (Figure 3c). This suggests that protons are not transferred from MI to DPPC either via reaction 3 or 5, which is consistent with the relative pK_as of MI and DPPC. Further, no $(DPPC - H)^-$ ions are observed in the negative SIMS spectra (data not shown). Since $(DPPC - H)^-$ ions are also a product of reaction 4, this pathway also is not operative. These data also suggest that reaction 6 is not a major reaction pathway: while the $(CHCA - H)^-$ ion intensity increases with time, the intensity of $(MI + H)^+$ remains constant. At long mixing times (≥600 s) the ion intensity of $(MI + H)^+$ decreases significantly in a similar manner to that observed for $(DPPC + H)^+$ and $(CHCA - H)^-$.

At long mixing times (≥600 s) significant decreases in all ion intensities are observed. This suggests that another slower process is occurring in solution. One possible process is that the DPPC – MI CHCA solution undergoes a slow re-arrangement in solution forming ion pairs and other charge-shielded structures leading to a decrease in the observed ion intensities.

While the transfer of a proton from CHCA to DPPC can explain the observed increase in $(DPPC + H)^+$ ion intensity, there are several features of the mass spectra that cannot be explained by this proton transfer. First, an increase in the ion intensities of $(DPPC - H)^+$ and $(DPPC)^+$ are also observed (Figure 4). These ions also vary with mixing time in a similar manner to that observed for $(DPPC + H)^+$ (Figure 5). Second from the above discussion, it could be concluded that the matrix ion does not play a significant role in the signal enhancement observed. However, in both SIMS and MALDI the chemical identity of the matrix cation affects the observed analyte quasimolecular ion intensities and limits of detection [1,2,4]. For example in Figure 4, the intensity of $(DPPC + H)^+$ is largest when MI CHCA is employed. The ion intensity enhancement of $(DPPC + H)^+$ is ~8x, ~6.5x and ~5x using MI CHCA, trip CHCA and dMI CHCA, respectively. The ion yield enhancement is calculated using

$$\text{enhancement} = \frac{I((M{+}H)^{+}_{\text{matrix}})}{I((M{+}H)^{+}_{\text{no matrix}})} \qquad \textbf{Equation 6.7}$$

where $I((M + H)^+)$ is the signal intensity (peak area) corresponding the protonated molecular ion of DPPC. Third, the protonated molecular ion intensity of DPPC is also observed to increase when MI_2CHCA is employed as a matrix (Figure 4). In MI_2CHCA, there are no labile protons available from the matrix anion, $CHCA^{2-}$. This suggests a proton is transferred from $(MI + H)^+$ to DPPC (reaction 5) which is inconsistent with the relative of pK_as of CHCA and DPPC. One possible reason for the increase in the $(DPPC + H)^+$ intensity is that a proton transfers to DPPC from neutral CHCA or $(CHCA - H)^-$ which are also present in solution. This is consistent with the results of the previous experiment as well as the relative pK_as of CHCA and DPPC.

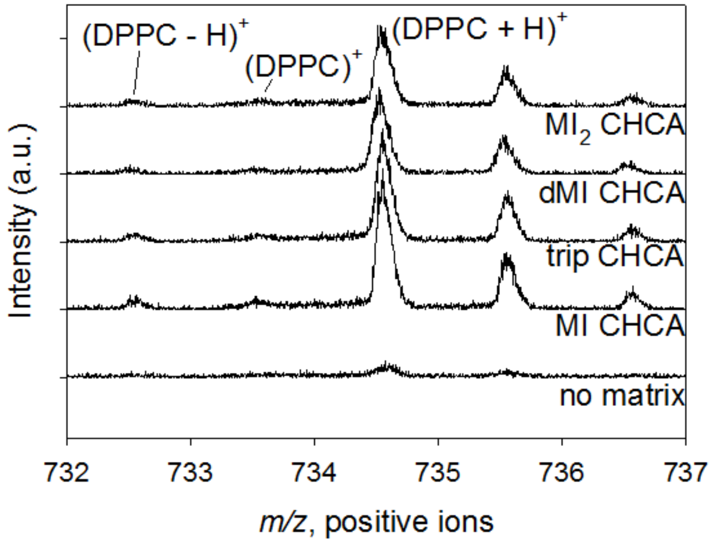

Figure 4. SIMS spectra from *m/z* 732 to *m/z* 737 of DPPC using MI CHCA, trip CHCA, dMI CHCA and MI_2CHCA as matrices. A control sample (“no matrix”) is shown for reference.

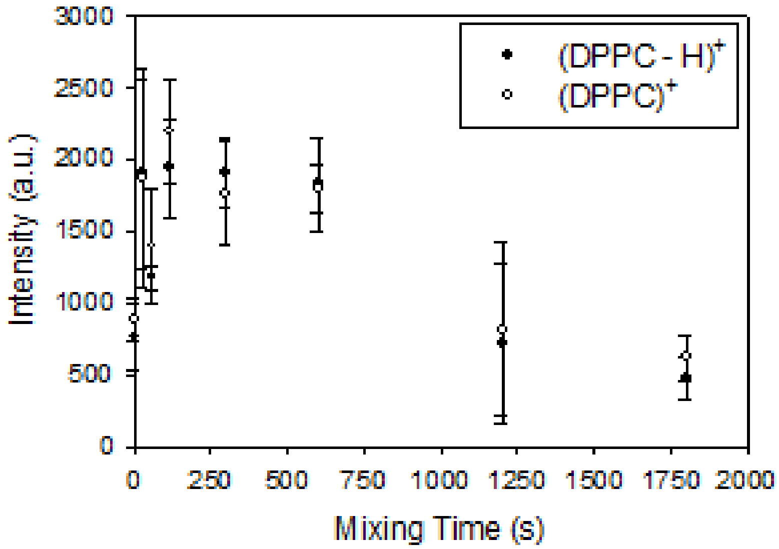

Figure 5. Variation of the ion intensities of $(DPPC)^+$ and $(DPPC – H)^+$ with mixing time. The ion intensities for a control sample without a matrix are shown at 0s mixing time.

To address these issues deuterated DPPCs (d62 DPPC and d75 DPPC) were employed as analytes. The head and tail groups of d75 DPPC are deuterated while d62 DPPC has only a deuterated tail group (Figure 1). In Figure 6, in the spectra of d62 and d75 DPPC it can be seen that various molecular ions are observed. In the control spectra (Figure 6, “no matrix”), ions are observed with the general formula $(M – xD)^+$, $(M – xD + H)^+$ (x = 1,2), M^+ and $(M + H)^+$, where M = d75 DPPC ($C_{40}H_5NO_8PD_{75}$, *m/z* 809.03) or d62 DPPC ($C_{40}H_{18}NO_8PD_{62}$, *m/z* 795.95). Since similar ions are observed for d75 and d62 DPPC, this suggests that in the SIMS process the tail group becomes dehydrogenated leading to the formation of C=C bonds. Thus it seems likely that $(DPPC – H)^+$ and $(DPPC)^+$ ions observed in Figure 4 are more correctly written as $(DPPC – 2H + H)^+$ and $(DPPC – H + H)^+$, and arise from the dehydrogenation of the tail group and the addition of a proton to the DPPC phosphate group from the IL matrix. Similarly, the observation of $(DPPC)^+$ ions suggests that it is formed via the loss of one hydrogen from the tail group and the addition of a proton to the phosphate group. Using an IL matrix a larger range of molecular ions is observed: up to four D are lost from both d62 and d75 DPPC (Figure 6). The most likely reason that more molecular ions are observed is that the ion intensities are significantly increased using IL matrices. This allows the detection of ions such as $(M – 4D)^+$ not seen in the spectra with no matrix applied. The data also confirm that a proton transfers from CHCA to DPPC. In the mass spectra we observe high intensities of $(M – xD +H)^+$ and $(M + H)^+$ ions for all matrices employed including dMI CHCA (Figure 6).

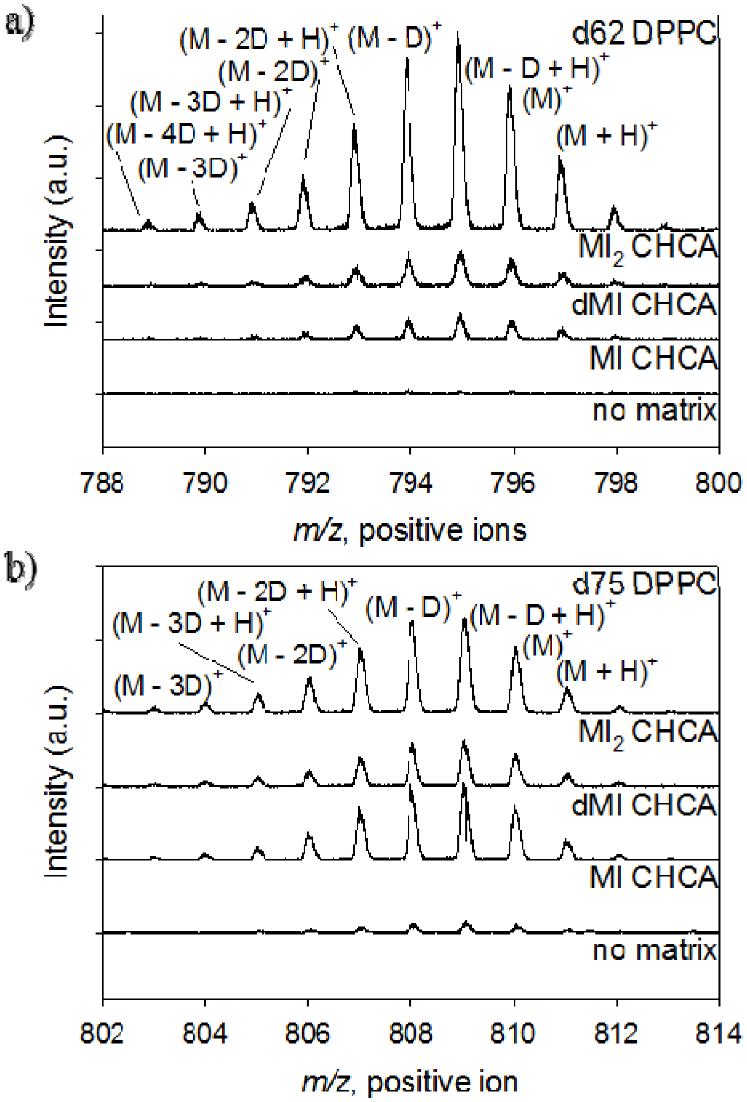

Figure 6. SIMS spectra showing the molecular ion intensities of a) d62 DPPC and b) d75 DPPC by using MI CHCA, dMI CHCA and MI_2CHCA as matrices. A control sample (“no matrix”) is shown for reference.

Deuterium which originates from the tail group of d75 and d62 DPPC can further react with the matrix or DPPC leading to the formation of deuterated ions. There does not appear to be H-D exchange with the IL anion. For example, using MI_2CHCA there is no increase in the ion intensity of *m/z* 189 ((CHCA – H + 1)$^-$ or (CHCA – 2H + D)$^-$) which arises from the reaction of D with CHCA^{2-} (Figure 7). Rather, it appears that D reacts with the IL cation, and is involved in intra- and inter-molecular reactions leading to the formation of deuterated DPPC fragment ions. For example, in the spectra of d62 DPPC in an MI CHCA matrix, we observe a significant increase in the ion intensity of $[C_5H_{14}DNPO_4]^+$ (*m/z* 185.08), a characteristic *deuterated* fragment ion of the DPPC head group. Since D is only present in the tail group of d62 DPPC, this suggests that the fragment ion was formed via intramolecular transfer of D from the tail group. We also observe an increase in the intensities of ions characteristic of deuterated IL cations, such as (MI + 2)$^+$. In Figure 8a, it can be clearly seen that the (MI + 2)$^+$ ion intensity is ~2x larger in the spectra of d75 DPPC than in the spectrum of fully hydrogenated DPPC. Further, the (MI + 2)$^+$ peak intensity increases with the level of deuteration in the analyte: the intensity of (MI + 2)$^+$ is larger for d75 DPPC than d62 DPPC, which in turn is larger than for DPPC. To confirm that deuterium (hydrogen) transfers from DPPC to the matrix cation, MI, we employed a deuterated matrix cation, dMI, and measured the (dMI + 2)$^+$ ion intensity in the spectra of DPPC, d62 DPPC and d75 DPPC. In the latter spectra, the intensity of (dMI + H)$^+$ is due to either the transfer of a proton from CHCA to dMI in the formation of the ionic liquid or from gas-phase processes. In contrast, the (dMI + 2)$^+$ intensity will be mainly due to the transfer of deuterium from the deuterated analyte to the matrix cation. In Figure 8b, it can be clearly seen that the (dMI + 2)$^+$ intensity significantly increases as the number of D increases in the analyte confirming that D transfers from DPPC to the matrix cation. The transfer of deuterium from DPPC to the IL cation does not appear to vary with mixing time in solution. Using d62 DPPC, we observed that the ratio of $(MI + 2)^+$ to $(MI + H)^+$ remains approximately constant with time (data not shown). This suggests that the addition of D to, or exchange of D with, MI to form $(MI + D)^+$ arises from a gas-phase process.

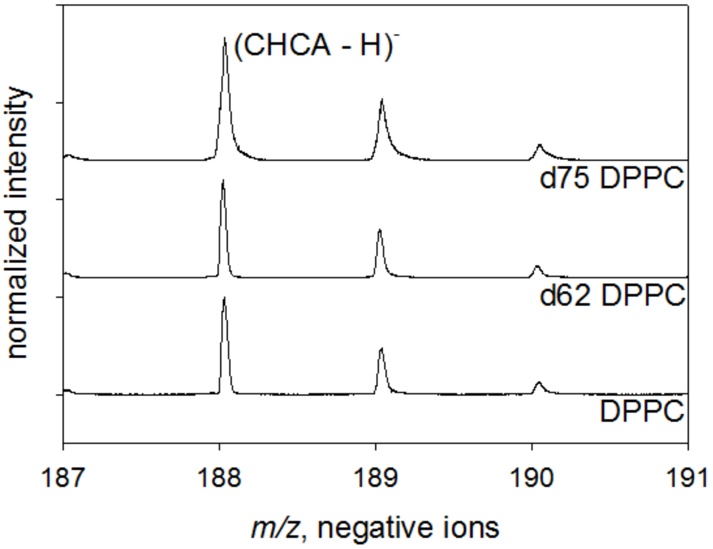

Figure 7. SIMS spectra from *m/z* 187 to *m/z* 191 showing the $(CHCA – H)^-$ ion region for DPPC, d62 DPPC and d75 DPPC with MI CHCA as the matrix. The spectra are normalized to the intensity of $(CHCA – H)^-$ to make clear any changes in the $(CHCA – H + 1)^-$ and $(CHCA – H + 2)^-$ ion intensities.

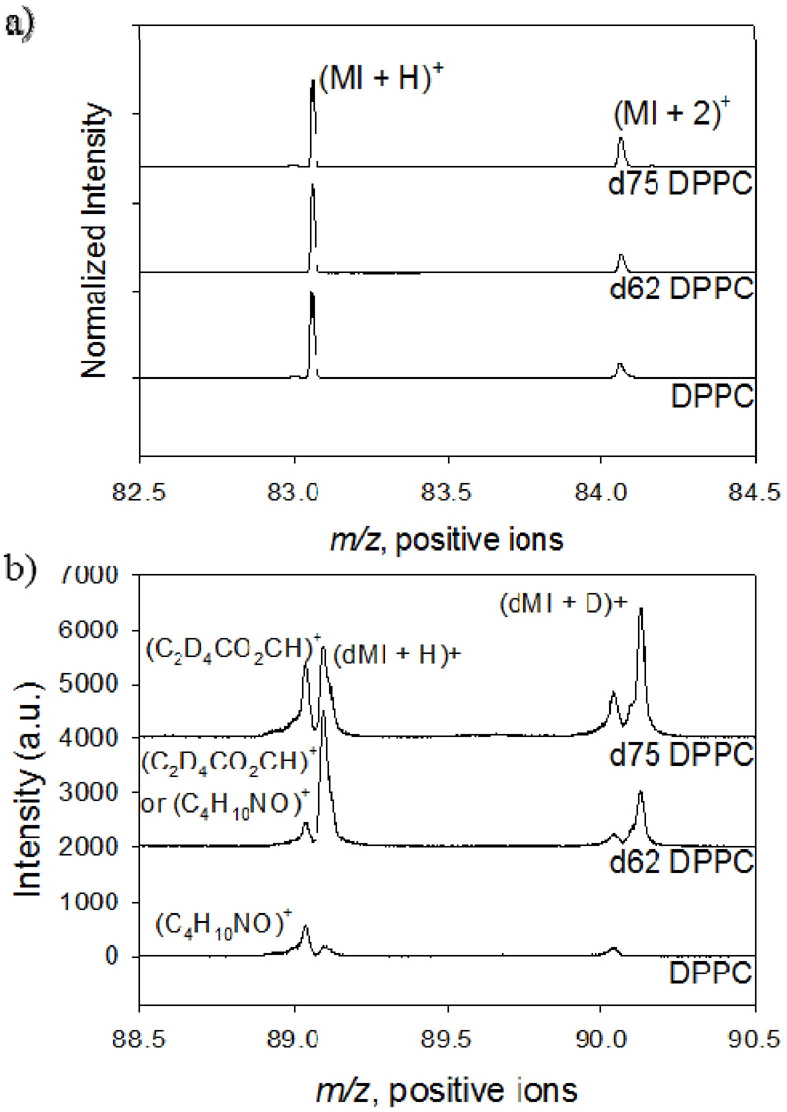

Figure 8. SIMS spectra of the protonated cation intensities a) $(MI + H)^+$ and $(MI + 2)^+$, and b) $(dMI + H)^+$ and $(dMI + D)^+$ using DPPC, d62 DPPC and d75 DPPC as the analytes.

These observations suggest that one possible reason that the chemical identity of the matrix cation affects the secondary ion yield enhancements observed by altering the proton, or deuterium, reaction kinetics between the ionic liquid and the analyte. To investigate the effect of the matrix cation on molecular ion intensities, we employed four different cations based on 1-methylimidazole (MI), 1-ethylimidazole (EI), 1-butylimidazole (BI) and tripropylammine (trip). The structures of these cations are shown in Figure 2. Figure 9a displays the yield enhancements of the protonated molecular ion of DPPC, $(\mathrm{DPPC} + \mathrm{H})^+$. It can be clearly seen that the highest and lowest secondary ion intensity enhancements are observed using MI CHCA and trip CHCA matrices, respectively. For d62 DPPC, similar trends are observed (Figure 9a). To explore the proton, or deuterium, reaction kinetics between the analyte and matrix cation, we employed d62 DPPC as an analyte and calculated the ratio of the ion intensities of $(\mathrm{cation} + \mathrm{D})^+$ to $(\mathrm{cation} + \mathrm{H})^+$. The $(\mathrm{cation} + \mathrm{D})^+$ ion intensity was calculated from the $(\mathrm{cation} + 2)^+$ ion intensity in the following way. There are two contributions to the $(\mathrm{cation} + 2)^+$ ion intensity. First, this ion can arise from the reaction of D with the matrix cation. Second, there is a contribution from the naturally occurring isotope contributions of $^{12}\mathrm{C}$ and $^2\mathrm{H}$ (D) from the $(\mathrm{cation} + \mathrm{H})^+$ ion. Thus, the intensity of the $(\mathrm{cation} + 2)^+$ can be described as:

$$I\left(\left(\mathrm{cation}+2\right)^+\right)=I\left(\left(\mathrm{cation}+\mathrm{D}\right)^+\right)+I\left(\left(\mathrm{cation}+\mathrm{H}\right)^+_{isotope}\right) \qquad \textbf{Equation 6.8}$$

where $I(X^+)$ is ion intensity (peak area) of the X^+ ion. Re-arranging this equation, the ion intensity of $(\mathrm{cation} + \mathrm{D})^+$ peak is:

$$I\left(\left(\mathrm{cation}+\mathrm{D}\right)^+\right)=I\left(\left(\mathrm{cation}+2\right)^+\right)-I\left(\left(\mathrm{cation}+\mathrm{H}\right)^+_{isotope}\right) \qquad \textbf{Equation 6.9}$$

The intensity of the $(\mathrm{cation} + 2)^+$ is experimentally measured. The ion intensity of $(\mathrm{cation} + \mathrm{H})^+_{\mathrm{isotope}}$ is calculated from the intensity of $(\mathrm{cation} + \mathrm{H})^+$ using the following equation:

$$I\left(\left(\text{cation} + \text{H}\right)^{+}_{isotope}\right) = \left[a\left(\frac{^{13}C}{^{12}C}\right) + b\left(\frac{^{2}H}{^{1}H}\right)\right] I\left(\left(\text{cation} + \text{H}\right)^{+}\right)$$ **Equation 6.10**

Where a and b are the number of carbons and hydrogen atoms in the matrix cation, and ^{13}C/^{12}C and ^{2}H/^{1}H are the isotope abundance ratios of the ^{13}C to ^{12}C and ^{2}H to ^{1}H, respectively. Therefore, the ion intensity of (cation + D)$^{+}$ peak is given by:

$$I\left(\left(\text{cation} + \text{D}\right)^{+}\right) = I\left(\left(\text{cation} + 2\right)^{+}\right) - \left[a\left(\frac{^{13}C}{^{12}C}\right) + b\left(\frac{^{2}H}{^{1}H}\right)\right] I\left(\left(\text{cation} + \text{H}\right)^{+}\right)$$ **Equation 6.11**

Figure 9b displays the ratio of (cation + D)$^{+}$ to (cation + H)$^{+}$ ion intensities for each cation determined from the mass spectra of d62 DPPC. The ratio is largest for MI and EI, and substantially smaller for BI and trip. We note that the ion intensity of (EI + 2)$^{+}$ is anomalously large due to an isobaric interference with a tail group fragment of d62 DPPC, $CD_3(CD_2)^{+}$. Consequently the true intensity of (EI + D)$^{+}$ is likely smaller than calculated here. The data suggest that the transfer of D from d62 DPPC to the IL cation is correlated with the secondary ion yield enhancements observed. The largest ion intensity ratio of (cation + D)$^{+}$ to (cation + H)$^{+}$ and the highest secondary ion enhancement are observed for the least sterically hindered cation, MI. The ion intensity ratio is smallest for the most sterically hindered cation, trip, and the smallest ion yield enhancements are observed for this cation. In MALDI steric factors have been shown to affect the analyte signal intensity.[4]. We observe that cations with less steric hindrance result in higher analyte signal intensities. However, the preferred steric hindernce contrasts with Crank and Armstrong.[4] Steric effects may not be the sole factor in determining the analyte ion intensities observed. Crank and Armstrong [4] also suggested that both the pK$_a$s and the gas proton affinity (PA) of the matrix cation affect the ion intensities observed. They observed that cations must generally have both a high pK_a (≥ 11) and PA (>930 $kJmol^{-1}$) for the generation of high analyte signal intensities. Table 1 displays the pK_a, proton affinities and gas phase basicities of the cations employed in this study. In contrast to Armstrong and Crank [4] we observe that the best performing cation, MI, has a low pK_a and PA. Further, there does not appear to be a clear trend between that pK_a and PA of the matrix cation. This suggests that in SIMS steric factors are the most important in determining the performance of the matrix.

	pK_a	**PA ($kJ\ mol^{-1}$)**	**GB ($kJ\ mol^{-1}$)**
MI	7.01	959.6	927.7
EI	7.08	~950[a]	NA
BI	7.09	987	954.9
trip	9.99	991	960.1

[a] H.J. Singh, U. Mukherjee, J. Molecular Modeling, 17 (2011) 2687-2692.

Table 1: IL azoles and ammonium properties arranged by increasing pK_a. In the proton affinity (PA) and gas phase basicity (GB) columns NA indicates not available. The pK_as were obtained from [10], while the PAs and GBs were obtained from [15] except where indicated.

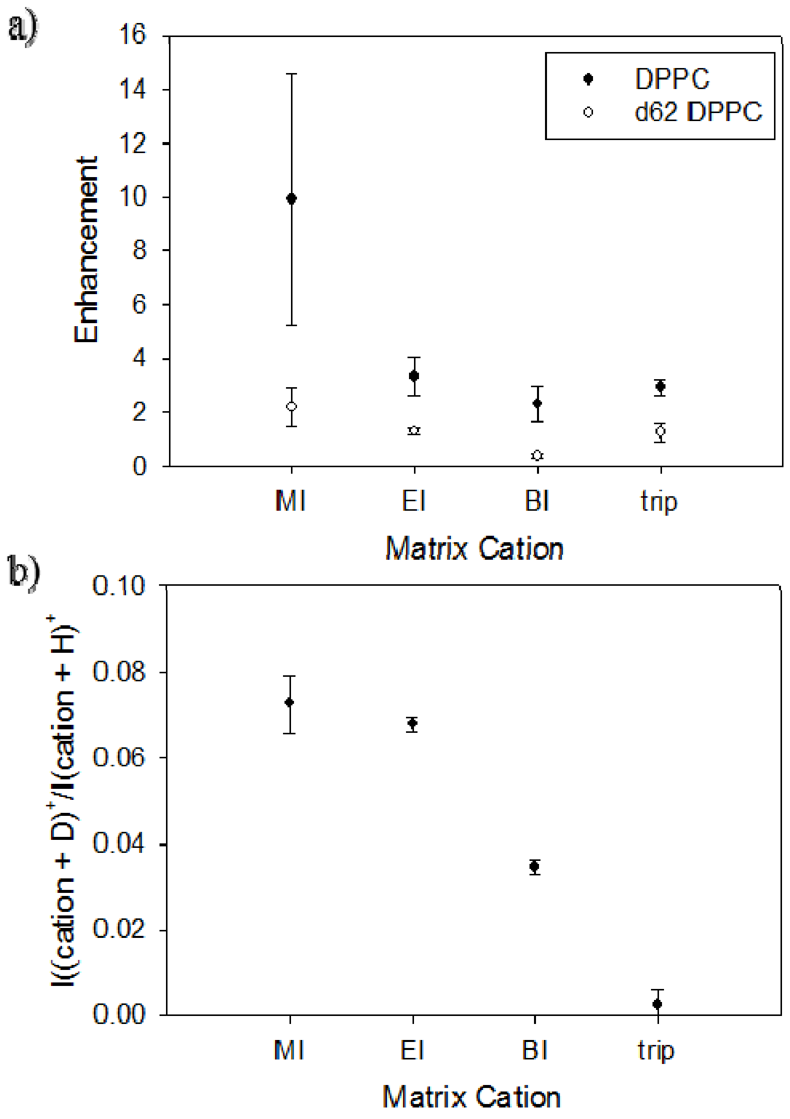

Figure 9. a) Variation of secondary ion enhancements for the protonated molecular ion of DPPC and d62 DPPC with matrix cation. b) Variation of the ratio of I((cation + D)$^+$ to I(cation + H)$^+$ with matrix cation using d62 DPPC.

6.4. Conclusions

We have investigated the reaction pathways involved in quasimolecular ion signal enhancements using ionic liquid matrices. The analyte signal intensity is dependent of the mixing time of the analyte with the IL in solution. The data indicate that protons transfer from the molecular component of the IL anion, CHCA, to the analyte, DPPC, leading to an increase in the ion intensities of $(CHCA - H)^-$ and $(DPPC + H)^+$. The chemical identity of the IL cation also affects the analyte signal intensity. Using d62 DPPC we observe that protons (deuterium) from the DPPC tail group react, or exchange, with the cation of the IL liquid leading to an increase in $(\text{cation} + D)^+$ ion intensities. The data indicate that the deuterium (hydrogen) transfer kinetics is correlated with the observed analyte secondary ion enhancements. The highest secondary ion enhancements are observed for the least sterically hindered cation, MI. There does not appear to be any correlation between the analyte ion intensity and proton affinity or pK_a of the cation suggesting that, in SIMS, steric factors are the most important in determining the efficacy of the IL matrix.

6.5 References

(1) Armstrong, D. W.; Zhang, L.-K.; He, L.; Gross, M. L., Ionic Liquids as Matrixes for Matrix-Assisted Laser Desorption/ Ionization Mass Spectrometry. *Analytical Chemistry* **2001**, *73*, 3679-3685.

(2) Fitzgerald, J. J. D.; Kunnath, P.; Walker, A. V., Matrix-Enhanced Secondary Ion Mass Spectrometry (ME SIMS) using Room Temperature Ionic Liquid Matrices. *Anal. Chem.* **2010**, *82*, 4413-4419.

(3) Li, Y. L.; Gross, M. L.; Hsu, F.-F., Ionic-Liquid Matrices for Improved Analysis of Phospholipids by MALDI-TOF Mass Spectrometry. *J. Am. Soc. Mass Spectrom.* **2005**, *16*, 679-682.

(4) Crank, J. A.; Armstrong, D. W., Towards a Second Generation of Ionic Liquid Matrices (ILMs) for MALDI-MS of Peptides, Proteins and Carbohydrates. *J. Am. Soc. Mass Spectrom.* **2009**, *20*, 1790-1800.

(5) Li, Y. L.; Gross, M. L., Ionic-Liquid Matrices for Quantitative Analysis by MALDI-TOF Mass Spectrometry. *J. Am. Soc. Mass Spectrom.* **2004**, *15*, 1833-1837.

(6) Carda-Broch, S.; Berthod, A.; Armstrong, D. W., Ionic matrices for matrix-assisted laser desorption/ionization time-of-flight detection of DNA oligomers. *Rapid Communications in Mass Spectrometry* **2003**, *17*, 553-560.

(7) Mank, M.; Stahl, B.; Boehm, G., 2, 5-Dihydroxybenzoic Acid Butylamine and Other Ionic Liquid Matrixes for Enhanced MALDI-MS Analysis of Biomolecules. *Anal. Chem.* **2004**, *76*, 2938-2950.

(8) Walker, A. V. In *The Encyclopedia of Mass Spectrometry: Molecular Ionization Methods*; Gross, M. L., Caprioli, R. M., Eds.; Elsevier Science & Technology Books: Burlington, USA, 2007; Vol. 6, p 535-551.

(9) Zenobi, R.; Knochenmuss, R., Ion Formation in MALDI Mass Spectrometry. *Mass Spectrom. Rev.* **1998**, *17*, 337-366.

(10) SciFinder, http:scifinder.cas.org. *January 17th, 2012, 9.05 am.*

(11) Tocanne, J.-F.; Teissié, J., Ionization of Phopholipids and Phospholipid-Supported Interfacial Lateral Diffusion of Protons in Membrane Model Systems. *Biochim. Biophys. Acta* **1990**, *1031*, 111-142.

(12) MacFarlane, D. R.; Seddon, K. R., Ionic Liquid - Progress on the Fundamental Issues. *Aust. J. Chem.* **2007**, *60*, 3-5.

(13) Dawson, R. M. C.; Elliott, D. C.; Elliott, W. H.; Jones, K. M. *Data for Biochemical Research*; Clarendon Press: Oxford, UK, 1959.

(14) Kaviratna, A. S.; Banerjee, R., The effect of acids on dipalmitoyl phosphatidylcholine (DPPC) monolayers and liposomes. *Colloids and Surfaces A: Physicochemical and Engineering Aspects* **2009**, *345*, 155-162.

(15) Hunter, E. P. L.; Lias, S. G., Evaluated Gas Phase Basicities and Proton Affinities of Molecules: An Update. *J. Phys. Chem. Ref. Data* **1998**, *27*, 413-656.

Chapter 7

Towards the Rational Design of Ionic Liquid Matrices for Secondary Ion Mass Spectrometry: Role of the Anion

Abstract: Protic ionic liquids (ILs) are effective matrices in SIMS. A protic IL is formed by the transfer of a proton from a Brønsted acid to a Brønsted base. The magnitude of the analyte signal enhancement is dependent on the chemical identities of the matrix cation and anion. The role of the IL anion structure on analyte signal enhancements has been systematically investigated using a variety of samples including lipids, sterols, polymers and peptides. Twenty four ILs were synthesized. The twelve matrix acids were based on cinnamic acid. Two bases were employed: 1-methylimidazole and tripropylamine. The pK_a of the matrix acid does not appear to have a strong effect on analyte ion intensities. Rather, we observe that adding a single hydroxyl group to the anion on the benzene ring leads to significantly increased molecular ion intensities. No analyte signal enhancements were observed for $–CH_3$, $–CF_3$ and $–OCH_3$ groups present on the anion benzene ring. The position of the –OH group on the anion benzene ring also alters molecular ion intensity enhancements. As well as the chemical identity and position of substituents, the number of substituents on the anion benzene ring also affects the analyte signal enhancements observed. These observations suggest that the activation of the benzene ring also plays a role in the analyte ion enhancements observed.

7.1 Introduction

There is considerable interest in the applications and properties of ionic liquids (ILs).[1-7] Applications of ILs include solvents for organic synthesis[2,5], lubricants[2,8-11], stationary phases in gas-liquid chromatography[1,2,7], synthesis of nanostructured materials[12], electrolytes in polymer membrane fuel cells[2,13-15] and as matrices in mass spectrometry[1,2,7,16-28]. There are two main classes of ionic liquids: aprotic, which contain no acid proton, and protic, which have an acidic proton on the cationic species.[2,4] Protic ionic liquids are complex liquids which contain both neutral (typically <1 %) and ionic species.[2-4] They have a proton available for hydrogen bonding, may have a non-negligible vapor pressure and some can even be distilled.[2]

Protic ionic liquids have been demonstrated to be effective matrices for both matrix assisted laser desorption/ionization (MALDI)[1,2,7,16-22] and secondary ion mass spectrometry (SIMS)[23,29]. Armstrong *et al.*[18] first reported in MALDI that ILs are effective matrices for the detection of polymers, proteins and peptides. Later studies have also shown that IL matrices can be employed for a wide variety of analytes including oligonucleotides[19,22,24,25], lipids[17,26], glycoconjugates[27] and carbohydrates[20,25,26,28]. Subsequently, ILs were demonstrated to be highly efficient matrices in SIMS with analyte signals from phospholipids, sterols and peptides enhanced by at least one order of magnitude.[23] IL matrices have a number of advantages over "traditional" solid matrices. The principal advantage of IL matrices is that they are liquids and so do not alter the sample chemistry.[18] Solid matrices, such as α-cyano-4-hydroxycinnamic acid (CHCA), co-crystallize with the analyte, which lead to a heterogeneous sample surface and "hot spot" formation – areas of greatly increased analyte ion intensities.[20,30,31] Second, they have a low vapor pressure and so can be used in a vacuum.[4,32] Third, there is little, or no, mass interference observed due to the fragmentation of the matrix[18,23] or the formation of matrix-molecule adducts[31,33]. This is because ILs are composed of pre-formed ions, and so in general there is little low mass interference from the ILs.

While there have been many reports of the use of IL matrices in MS[1,2,7,16-23,29], there have been few studies of the matrix enhancement mechanism.[20] An understanding of these mechanisms is critical for the design of new matrices as well as the development of quantitative analysis and imaging protocols. In both MALDI[18] and SIMS[23] the ionization of the analyte is promoted via available matrix protons. Further, it appears that the proton transfer occurs in solution, and in the case of 1,2 dipalmitoyl-*sn*-glycero-3-phosphocholine (DPPC) the proton transfers from the matrix acid to the analyte leading to the formation of protonated molecular ions, $(DPPC + H)^+$ (m/z 734.57).[29] In MALDI Crank and Armstrong[20] also observed that ILs with cations which have $pK_a \geq 11$ and proton affinity $\geq$930 kJ mol^{-1} are the most effective matrices. In contrast, in SIMS there does not appear to be a relationship between the pK_a and proton affinity of the IL cation and the matrix efficacy.[29] In this chapter, we systematically investigate the effect of anion structure and pK_a on the analyte signal enhancements observed in SIMS. Twenty four different ionic liquids were investigated. Twelve matrix acids based on cinnamic acid were tested with pK_as ranging from 0.80 to 4.65 (Figure 1). These include acids that act as solid MALDI matrices, such as CHCA, ferulic acid and sinapinic acid.[22,34] Two cations were used: 1-methylimidazolium (MI) and tripropylammonium (trip). The analytes employed include phospholipids, a sterol, polymers and peptides (Figure 2). The data show that 75 % of the tested ILs were effective matrices for phospholipids and peptides, and there was little difference in the magnitude of the enhancement if MI or trip was employed. Few matrices enhanced the n-mer and oligomer ions of the two polymers tested, polypropylene glycol 2220 (PPC) and polystyrene 1110 (PS). Our data clearly indicate that the chemical identities, positions and number of substituents on the anion benzene ring all affect the analyte signal intensities, indicating that the activation of the anion benzene ring is important in the design of IL matrices. Further, it appears that more effective matrices have anions with at least one substituent with a labile proton, such as –OH. The cation is not as important as the anion in designing new IL matrices for SIMS.

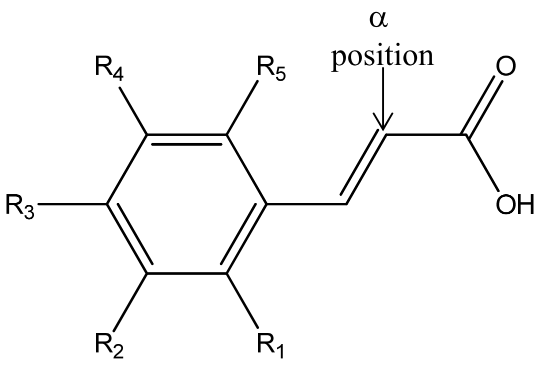

Acid	**Abbr.**	**Groups**	**pK$_a$**
α-Cyano-4-methoxycinnamic acid	CMCA	R_3=MeO; α = -CN	0.80
α-Cyano-4-hydroxycinnamic acid	CHCA	R_3=OH; α = -CN	0.85
4-trifluorothmethylcinnamic acid	FMCA	R_3=CF_3	4.21
m-coumaric acid	MA	R_2=OH	4.38
3,4,5-trimethoxy-cinnamic acid	TMCA	R_2=R_3=R_4= MeO	4.48
o-coumaric acid	OA	R_1=OH	4.51
sinapinic acid	SA	R_2=R_4= MeO; R_3=OH	4.53
methylcinnamic acid	MCA	R_3=Me	4.55
caffeic acid	CA	R_3=R_2=OH	4.58
ferulic acid	FA	R_3=OH; R_2=MeO	4.58
4-methoxycinnamic acid	MXCA	R_3=MeO	4.60
p-coumaric acid	PA	R_3=OH	4.65

Figure 1. The structure and pK$_a$ of the matrix acids employed, and the abbreviations used for the matrix anions. The pK$_a$ is the lowest pK$_a$ reported for the acid at 25 °C.

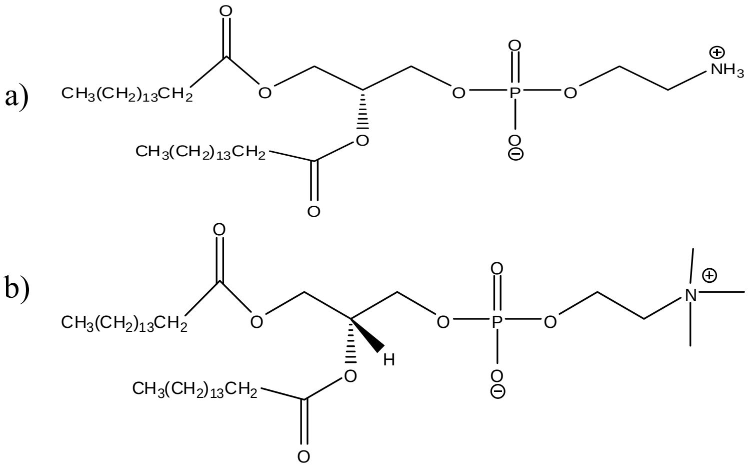
a)
CH3(CH2)13CH2
O
O
O
CH3(CH2)13CH2
O
O
O
P
O
O
⊖
⊕
NH3
b)
CH3(CH2)13CH2
O
O
O
H
CH3(CH2)13CH2
O
O
O
P
O
O
⊖
N
⊕

c) Tyr-Gly-Gly-Phe-Leu

d) Arg-Pro-Pro-Gly-Phe-Ser-Pro-Phe-Arg

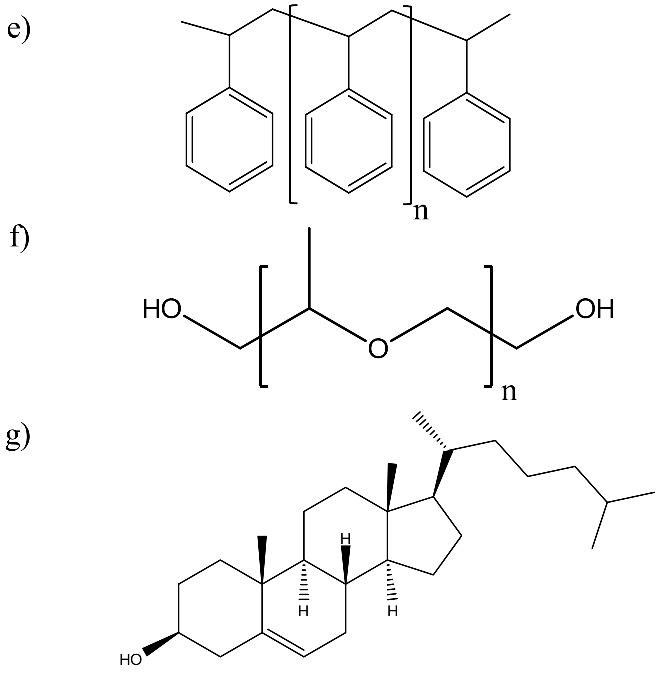
e)
n
f)
HO
O
OH
n
g)
H
H
H
HO

Figure 2. The structures of a) DPPC, b) DPPE, c) leucine enkaphalin, d) bradykinin, e) polystyrene, f) polypropylene glycol, and g) cholesterol.

7.2 Experimental

7.2.1 Materials

1-methylimidazole (99%), tripropylamine (98%), α-cyano-4-hydroxycinnamic acid (98%), α-cyano-4-methoxycinnamic acid, *p*-coumaric acid (98%), *m*-coumaric acid, *o*-coumaric acid, 4-methylcinnamic acid, ferulic acid (99%), sinapinic acid (98%), caffeic acid (98%), 3,4,5 trimethoxycinnamic acid (97%), trans-4-(trifluoromethyl)cinnamic acid (99%), 4-methoxycinnamic acid (98%), cholesterol, folic acid, bradykinin, leucine enkephalin, polystyrene, and polypropylene glycol were purchased from Sigma Aldrich (St. Louis, MO). 1,2-dipalmitoyl-*sn*-glycero-3-phosphocholine (DPPC) and 1,2-dipalmitoyl-*sn*-glycero-3-phosphoethanolamine (DPPE) were obtained from Avanti Polar Lipids, Inc. (Alabaster, AL). HPLC grade chloroform was obtained from Omnisolv (Charlotte, NC) and HPLC grade methanol was obtained from VWR (Radnor, PA). Single side polished <111> Si wafers were obtained from Addison Engineering (San Jose, CA). All chemicals were used without further purification.

7.2.2 Ionic Liquid Preparation

All ionic liquids were prepared using the synthesis described by Armstrong and coworkers.[18-20] Briefly, 0.5g of the acid was dissolved in 15ml of methanol. Equimolar amounts of the base (tripropylamine or 1-methylimidazole) were then added to the methanolic solution of the acid. After sonication of the resulting solution, the methanol was evaporated leaving the ionic liquid. Prior to use the ILs were characterized using ^{1}H NMR, infrared spectroscopy and time-of-flight secondary ion mass spectrometry.

7.2.3 Sample Preparation

For each “matrix enhanced” sample, a 400μl aliquot of 0.5 M IL was mixed with 400μl of analyte solution (concentration of 1 mg/ml). The solvent employed was 1:1 methanol:chloroform (v:v). For control samples a 400 μl aliquot of the analyte solution was mixed with an additional 400 μl of the solvent methanol/chloroform. Once mixed, the sample (total volume: 800μl) was spun coat onto a ~1 cm^2 Si wafer for 6s at ~300 rpm and 20s at 3000 rpm using a Chemat KW-4A spin coater (Chemat Technologies, Inc, Northridge, CA). To ensure that the maximum analyte signal intensities were obtained the solutions of the analyte and IL were mixed for 1-2 mins prior to spin coating.

7.2.4 Time of Flight Secondary Ion Mass Spectrometry

All TOF SIMS spectra were obtained using an ION TOF IV instrument (ION TOF USA, Chestnut Ridge, NY) equipped with a Bi primary ion gun. Briefly the instrument consists of a loadlock, a preparation chamber and an analysis chamber, each separated by gate valves. The pressure of the analysis chamber was maintained below 6.5 x 10^{-8} mbar. The primary Bi_3^+ ion had a kinetic energy of 25 keV and was contained within ~150 nm diameter. The mass spectra were obtained in the static regime[35,36] with a primary ion dose of <1 x 10^{10} ions cm^{-2}. The generated secondary ions were then extracted from the surface using 2000V and reaccelerated to 10keV before reaching the detector.

High mass resolution spectra were obtained using an analysis area of 100 μm x 100 μm. The mass resolution (or resolving power; m/Δm) was ~4000 at *m/z* 29. The reported secondary ion intensities are the averages of the data from several samples with at least three randomly selected areas analyzed per sample. Each sample had 3 positive and 3 negative spectra taken at randomly chosen spots within the sample. Mass spectra shown are representative of the data collected.

7.3 Results and Discussion

In this study twenty four ionic liquid matrices were tested for their efficacy in enhancing SIMS signals. The ILs were prepared from twelve different acids based on cinnamic acid (Figure 1) and two different bases, 1-methylimidazole and tripropylamine. To aid in the following discussion table 1 summarizes the results obtained. In Table 1 for each analyte "++" and "+" indicate that the quasimolecular ions are enhanced by >10 times and 5-10 times, respectively, while "-" and "0" indicate that the signal is not enhanced or not observed. The ion intensity enhancement was calculated using

$$\text{enhancement} = \frac{I(Q^{+}_{\text{matrix}})}{I(Q^{+}_{\text{no matrix}})}$$

Equation 7.1

where $I(Q^{+})$ is the intensity (peak area) of the quasimolecular ion. Most ILs greatly increased the quasimolecular ion intensities of the phospholipids, DPPC and DPPE, and the peptide, leucine enkephalin. The quasimolecular ion intensities of bradykinin and cholesterol are either slightly increased or not at all by the ILs tested. In general for polystyrene (PS) and polypropylene glycol (PPG) these IL matrices did not give rise to increased *n*-mer or oligomer ion intensities. Further, in Table 1 it can be clearly seen that changing the cation does not greatly alter the magnitude of the analyte signal enhancements for each anion. This observation suggests that the chemical identity of the cation is less important than the identity of the anion.

Analyte **Anion**	**DPPC**	**DPPE**	**LE**	**Bradykinin**	**PS**	**PPG**	**Cholesterol**
Cation: MI							
CMCA	+	++	++	-	++	0	-
CHCA	++	++	++	-	0	0	-
FMCA	-	-	-	-	0	0	-
MA	+	++	++	+	0	0	+
TMCA	+	++	++	-	0	0	-
OA	+	++	++	+	++	++	+
SA	+	++	++	+	0	0	-
MCA	-	-	-	-	+	0	-
CA	+	++	++	+	-	0	-
FA	+	++	++	+	0	0	-
MXCA	-	-	-	-	+	+	-
PA	+	++	++	+	0	0	-
Cation: trip							
CMCA	+	++	++	-	+	0	+

CHCA	++	++	++	-	0	0	-
FMCA	-	-	-	-	0	++	0
MA	+	++	++	+	0	0	+
TMCA	+	++	++	+	+	+	+
OA	+	+	++	-	+	++	+
SA	++	++	++	++	0	0	-
MCA	-	-	+	+	+	0	-
CA	++	++	++	+	0	0	+
FA	+	+	++	+	0	0	-
MXCA	-	-	-	-	0	0	-
PA	+	+	++	+	0	+	+

Table 1. Summary of enhancements of protonated and deprotonated molecular ions observed for a variety of analytes using IL matrices. The cations were 1-methylimidazolium (MI) and tripropylammonium (trip). The ability of the matrix to enhance quasimolecular ions is rated ++ 10+ times enhancement, + 1-10 times enhancement, - no enhancement and 0 no molecular ion observed.

It is interesting to note that by using IL matrices, the analyte signal intensities increase even when using a cluster primary ion beam, such as Bi_3^+ which was employed in this study. Cluster primary ion beams, such as Bi_3^+, have been demonstrated to greatly increase the secondary ion yields of analytes [37]. For example, using Bi_3^+ the quasimolecular ion yields of Irganox 1010, phenylalanine and polystyrene are increased between 10x and 100x times [37]. Using MI CHCA the enhancement of the protonated molecular ions of DPPC, $(DPPC + H)^+$, is up to 300x [23] and ~10-15x* using Bi^+ and Bi_3^+ primary ions, respectively. These results suggest that the enhancements are not multiplicative for cluster primary ions and ionic liquid matrices, i.e.

$$I\left(X^+\right) \neq a_{IL} b_{cluster} I\left(X^+\right)_{\text{no matrix,no cluster}}$$

Equation 7.2

where $I(X^+)$ is the ion intensity (peak area) of X^+, and a_{IL} and $b_{cluster}$ are the enhancement factors using an IL matrix and cluster primary ion respectively. Using IL matrices for some analytes, such as cholesterol, the ion intensity enhancement is 3-10x using Bi^+ [23]. Using Bi_3^+ primary ions similar ion intensity enhancements are observed. Consequently when using an IL and Bi_3^+ primary ion bombardment there is little, or no, enhancement is observed in the deprotonated molecular ion intensity, $(M – H)^+$ (*m/z* 385.35) (Table 1).

In the following sections we shall discuss the effect of the anion pK_a, chemical identity of substituents on the benzene ring and substituent position on the analyte quasimolecular ion intensity enhancements.

7.3.1 pK_a of Matrix Acid

We have previously demonstrated that protons transfer from the matrix acid to analytes in solution leading to an increase in the analyte quasimolecular ion signals [29]. This observation suggests that the pK_a of the matrix acid is an important factor in determining the ion intensity enhancements observed; the lower the pK_a of the matrix acid (A), the greater the extent of dissociation into H^+ and A^-. The generated H^+ ions then react with the analyte leading to an increase in the formation of quasimolecular ions.

To investigate the effect of the matrix acid pK_a on analyte signal intensities we compared the secondary ion intensity enhancements observed for two pairs of anions: PA and CHCA, and MXCA and CMCA. The structural difference between CHCA and CMCA, and PA and MXCA is the addition of a cyano group at the α position on the alkyl chain (Figure 1). This leads to a decrease in the pK_a of the matrix acid from ~4.6 to ~0.8 [38]. In Table 1 it can clearly be seen that CHCA, CMCA and PA significantly increase the quasimolecular ion intensities of DPPC, DPPE and LE. PA also slightly increases the molecular ion intensity of bradykinin (between 1-5x) while CHCA and CMCA do not. Thus, at first glance it appears that for MXCA and CHCA the pK_a of the matrix acid leads to significant differences in the analyte ion intensities observed. However, for MXCA it is observed that the *n*-mer and oligomer ions of PPG are enhanced, while for CMCA no *n*-mer and oligomer ions are observed indicating that the pK_a of the matrix acid is not a significant factor in determining analyte signal intensity. For PA and CHCA, the effect of the matrix acid pK_a is also subtle. Figure 3 displays the quasimolecular ion intensities of DPPC and DPPE using PA and CHCA as matrix anions. In general the analyte quasimolecular ion intensity enhancements are slightly larger for CHCA. However, in some cases the analyte signals are larger for PA than CHCA (Figure 3b). Taken together these data suggest that the pK_a of the matrix acid does not play a significant role in the analyte signal enhancements and suggests that other factors, such as the chemical identity of the anion substituents, are more important in determining the ion enhancements observed.

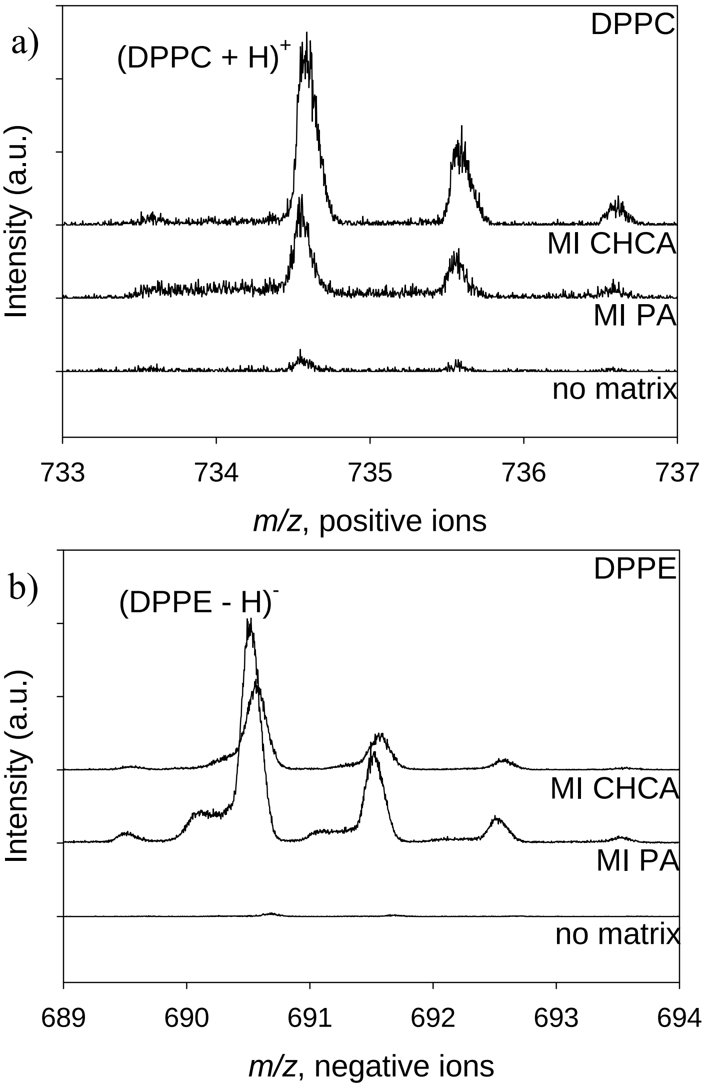

Figure 3. TOF SIMS spectra of the quasimolecular ions of a) DPPC, and b) DPPE in MI PA and MI CHCA matrices, and with no matrix applied.

7.3.2 Chemical Identity of Substituents on the Benzene Ring of the Anion

Four IL anions investigated had a different substituent at the para position of the benzene ring (Figure 1, R_3): FMCA (R_3 = -CF_3), MCA (R_3 = -CH_3), MXCA (R_3 = -OCH_3) and PA (R_3 = -OH). Only PA was observed to increase the quasimolecular ion intensities of DPPC, DPPE, LE, bradykinin, PPG and cholesterol (Table 1). Further, it appears that the ion intensity enhancements observed using trip PA are slightly larger than when using MI PA. In general MCA, MXCA and FMCA do not increase the quasimolecular ion intensities of the analytes tested, and in some cases the analyte signal is suppressed (Table 1).

There are two possible reasons for the observed behavior. First, the only anion which increased analyte ion intensities was one with a phenolic group (-OH), and so has a labile proton. In general the pK_a of this phenolic group is much higher than the carboxylic acid [39,40]. For example, for PA the pK_a of the phenolic group is ~9 [40] while for the carboxylic acid the pK_a is 4.65 [38]. Upon formation of trip PA it likely that some of the phenolic groups deprotonate by transferring a proton to the trip (pK_a = 9.99 [38]). In contrast for MI PA, the pK_a of MI is lower (7.01 [38]) than the PA phenolic group and no proton will be transferred. Thus, there are more sites available for proton exchange in trip PA, and so higher analyte ion intensities are observed. Second, the activation of the benzene ring may play a role in the observed analyte ion intensity enhancements. Strongly electron withdrawing groups, such as $-CF_3$, deactivate the benzene ring by creating regions of positive charge, which in turn prevent the reaction of the benzene ring with electrophiles, such as H^+ [41]. This may lead to a decrease in quasimolecular ion signals. In contrast, strongly activating substituents, such as –OH, activate the reaction of the benzene towards to electrophiles [41], and so improve the exchange of protons with the analyte increasing quasimolecular ion intensities.

7.3.3 Position of Substituents on the Benzene Ring of the Anion

The position of the anion phenolic group also affects the analyte signal intensities (Table 1). Three IL anions tested had the same chemical composition but differed in the position of the phenolic group on the benzene ring: PA, MA and OA. Cholesterol, PPG and PS ion intensities were strongly enhanced using OA (Figure 4a). Further, the analyte signals observed were approximately the same using PA and MA. Interestingly, both cholesterol and PS have benzene rings in their structures. Deprotonated negative molecular ion intensities are increased better by MA (Figure 4b); the quasimolecular ions of DPPE, leucine enkaphalin and bradykinin are strongly enhanced by MA. In the case of bradykinin both the protonated ($(M + H)^+$) and deprotonated ($(M - H)^-$) molecular ion intensities are strongly increased. For these analytes the order of signal enhancement is MA > PA > OA. The only analyte tested which is enhanced the most by PA is DPPC (Figure 4c). However, similar ion intensities are observed using MA with less signal enhancement observed for OA. There is no obvious reason why the position of the phenolic group alters the analyte molecular ion intensities observed. One possible reason is that the substituent position alters the formation of aggregates in solution [42,43], which alters proton transfer rates between the analyte and the anion in solution.

7.3.4 Number of Substituents on the Benzene Ring of the Anion

As well as the chemical identity and position of substituents on the anion benzene ring, the number of substituents also affects the analyte signal enhancements observed. For example, MXCA, which has one $-OCH_3$ group, does not in general increase analyte ion intensities (Table 1). In contrast, TMCA, which has three $-OCH_3$ groups, enhances the ion intensities of analytes such as DPPC, DPPE and LE (Table 1). Further, it is also interesting to note that MI MXCA weakly increased the oligomer ion intensities of PS and PPG, but MI TMCA does not. However, trip TMCA does increase the oligomer ion intensities of PS and PPG but no analyte signals are observed for trip MXCA. Since –OCH_3 groups do not possess a labile proton, these observations suggest that the activation of the anion benzene ring has an effect on the analyte signal enhancements observed.

The addition of –OH groups to the anion benzene ring do not appear to have a significant effect on the analyte ion intensity enhancements. CA has –OH groups at both the meta and ortho positions of the benzene ring. Thus it could be considered to be an anion in which a hydroxyl group has been added at the para position in MA or at the meta position in PA. In general similar analyte signal enhancements are observed for MA, PA and CA (Table 1). However for analytes that form deprotonated molecular ions ($(M – H)^-$), such as DPPE, LE and bradykinin, ILs with MA anions are the best matrices (Figure 4). This observation suggests that anions with less activated benzene rings are better matrices in this case.

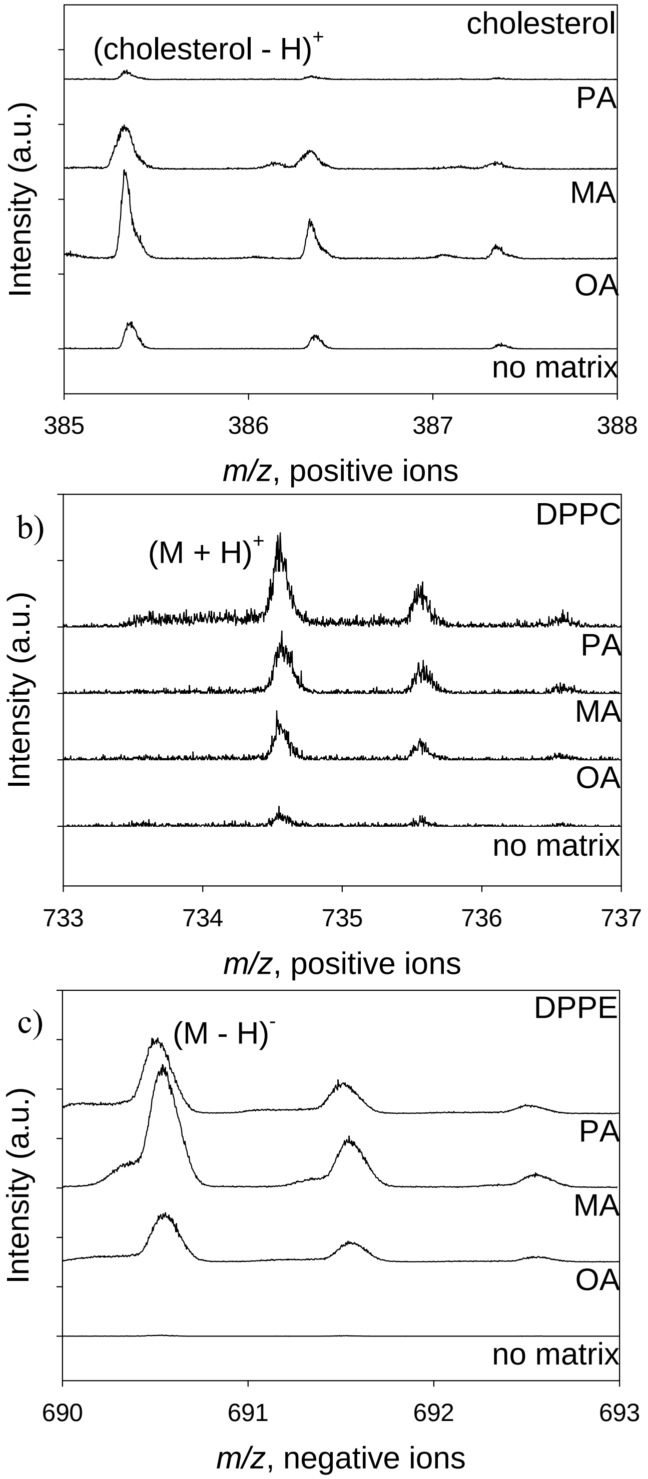

Figure 4. TOF SIMS spectra of the quasimolecular ions of a) cholesterol, b) DPPC, and c) DPPE in MI PA, MI MA and MI OA matrices, and with no matrix applied.

The substitution of –OH in place of –OCH_3 groups does appear to affect analyte ion enhancements observed. For example, in general CMCA gives rise to larger deprotonated molecular ion signals ($(M - H)^-$) than CHCA (analytes: DPPE, LE) (Figure 5b). In contrast, protonated molecular ion ($(M + H)^+$) intensities are better enhanced by CHCA than CMCA (Figure 5a). Again, these observations suggest that anions with less activated benzene rings are better matrices for increasing deprotonated molecular ion intensities. However this effect is subtle. For TMCA and SA, which differ by the substitution of a hydroxyl group for a methoxy group at R_3 (Figure 1), similar molecular ion intensity enhancements are observed for LE, DPPC and DPPC (Table 1).

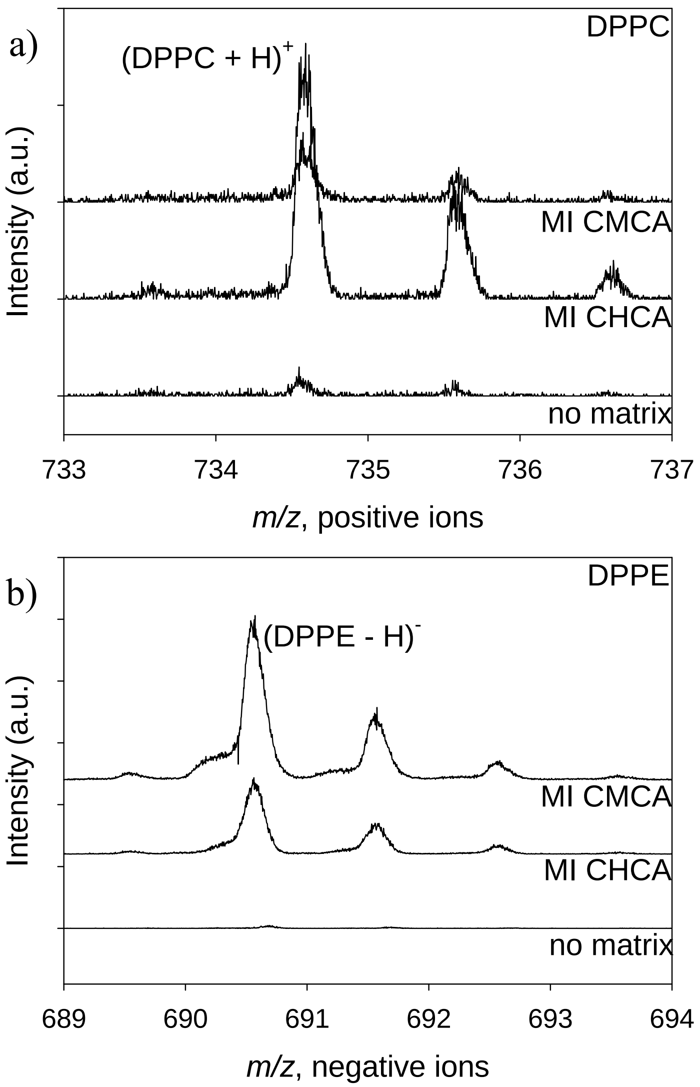

Figure 5. TOF SIMS spectra of the quasimolecular ions of a) DPPC, and b) DPPE in MI CHCA and MI CMCA matrices, and with no matrix applied.

The position of the –OCH_3 and –OH groups on the anion benzene ring does not appear to affect the analyte signal enhancements. FA has an –OH group at the R_3 position and an –OCH_3 group at R_2 while for CA the position of these groups is reversed (Figure 1). FA and CA enhance the molecular ions of DPPC, DPPE, bradykinin and LE similarly

(Table 1). Further, these anions do not enhance the analyte signals from PS, PPG and cholesterol.

7.4 Conclusions

We have investigated the role of the IL anion structure on analyte signal enhancements using a variety of samples including lipids, sterols, polymers and peptides. The pK_a of the anion acid, which is a measure of its ability to donate a proton in water to the matrix cation or analyte, does not appear to have a strong effect on the analyte ion intensities. In general, we observe that a single hydroxyl group, which has a labile proton, on the anion benzene ring leads to significantly increased molecular ion intensities. No analyte signal enhancements were observed for single $–CH_3$, $–CF_3$ and $–OCH_3$ groups present on the anion benzene ring. The position of the –OH group on the anion benzene ring also alters molecular ion intensity enhancements. Cholesterol, PPG and PS ion intensities were strongly enhanced using OA while the protonated molecular ion of DPPC is enhanced best by PA. The enhancement of negative deprotonated molecular ions ($(M – H)^-$) is best for MA. As well as the chemical identity and position of substituents, the number of substituents on the anion benzene ring also affects the analyte signal enhancements observed. For example, TMCA which has three $–OCH_3$ groups is an effective IL matrix while MXCA which has one $–OCH_3$ group is not. These observations suggest that the activation of the benzene ring also plays a role in the analyte ion enhancements observed.

7.5 References

(1) Anderson, J. L.; Armstrong, D. W.; Wei, G.-T., Ionic Liquids in Analytical Chemistry. *Anal. Chem.* **2006**, *78*, 2892-2902.

(2) Greaves, T. L.; Drummond, C. J., Protic Ionic Liquids: Properties and Applications. *Chem. Rev.* **2008**, *108*, 206-237.

(3) MacFarlane, D. R.; Seddon, K. R., Ionic Liquid - Progress on the Fundamental Issues. *Aust. J. Chem.* **2007**, *60*, 3-5.

(4) Johnson, K. E., What's an Ionic Liquid? *Interface* **2007**, *Spring 2007*, 38-41.

(5) Welton, T., Room-Temperature Ionic Liquids. Solvents for Synthesis and Catalysis. *Chem. Rev.* **1999**, *99*, 2071-2084.

(6) Wilkes, J. S., A short history of ionic liquids-from molten salts to neoteric solvents. *Green Chemistry* **2002**, *4*, 73-80.

(7) Soukup-Hein, R. J.; Warnke, M. M.; Armstrong, D. W. In *Annual Review of Analytical Chemistry*; Annual Reviews: Palo Alto, 2009; Vol. 2, p 145-168.

(8) Zhou, F.; Liang, Y.; Liu, W., Ionic liquid lubricants: designed chemistry for engineering applications. *Chem. Soc. Rev.* **2009**, *38*, 2590-2599.

(9) Ye, C.; Liu, W.; Chen, Y.; Yu, L., Room-temperature ionic liquids: a novel versatile lubricant. *Chem. Commun.* **2001**, 2244-2245.

(10) Kamimura, H.; Kubo, T.; Minami, I.; Mori, S., Effect and mechanism of additives for ionic liquids as new lubricants. *Tribology International* **2007**, *40*, 620-625.

(11) Qu, J.; Truhan, J.; Dai, S.; Luo, H.; Blau, P., Ionic liquids with ammonium cations as lubricants or additives. *Tribology Letters* **2006**, *22*, 207-214.

(12) Antonietti, M.; Kuang, D.; Smarsly, B.; Zhou, Y., Ionic Liquids for the Convenient Synthesis of Functional Nanoparticles and Other Inorganic Nanostructures. *Angew. Chem., Int. Ed. Engl.* **2004**, *43*, 4988-4992.

(13) Lin, B.; Cheng, S.; Qiu, L.; Yan, F.; Shang, S.; Lu, J., Protic Ionic Liquid-Based Hybrid Proton-Conducting Membranes for Anhydrous Proton Exchange Membrane Application. *Chem. Mater.* **2010**, *22*, 1807-1813.

(14) Ye, H.; Huang, J.; Xu, J. J.; Kodiweera, N. K. A. C.; Jayakody, J. R. P.; Greenbaum, S. G., New membranes based on ionic liquids for PEM fuel cells at elevated temperatures. *J. Power Sources* **2008**, *178*, 651-660.

(15) Subianto, S.; Mistry, M. K.; Choudhury, N. R.; Dutta, N. K.; Knott, R., Composite Polymer Electrolyte Containing Ionic Liquid and Functionalized Polyhedral Oligomeric Silsesquioxanes for Anhydrous PEM Applications. *ACS Applied Materials & Interfaces* **2009**, *1*, 1173-1182.

(16) Li, Y. L.; Gross, M. L., Ionic-Liquid Matrices for Quantitative Analysis by MALDI-TOF Mass Spectrometry. *J. Am. Soc. Mass Spectrom.* **2004**, *15*, 1833-1837.

(17) Li, Y. L.; Gross, M. L.; Hsu, F.-F., Ionic-Liquid Matrices for Improved Analysis of Phospholipids by MALDI-TOF Mass Spectrometry. *J. Am. Soc. Mass Spectrom.* **2005**, *16*, 679-682.

(18) Armstrong, D. W.; Zhang, L.-K.; He, L.; Gross, M. L., Ionic Liquids as Matrices for Matrix-Assisted Laser Desorption/ionization Mass Spectrometry. *Anal. Chem.* **2001**, *73*, 3679-3686.

(19) Carda-Broch, S.; Berthod, A.; Armstrong, D. W., Ionic matrices for matrix-assisted laser desorption/ionization time-of-flight detection of DNA oligomers. *Rapid Communications in Mass Spectrometry* **2003**, *17*, 553-560.

(20) Crank, J. A.; Armstrong, D. W., Towards a Second Generation of Ionic Liquid Matrices (ILMs) for MALDI-MS of Peptides, Proteins and Carbohydrates. *J. Am. Soc. Mass Spectrom.* **2009**, *20*, 1790-1800.

(21) Chan, K.; Lanthier, P.; Liu, X.; Sandhu, J. K.; Stanimirovic, D.; Li, J., MALDI Mass Spectrometry Imaging of Gangliosides in Mouse Brain Using Ionic Liquid Matrix. *Anal. Chim. Acta* **2009**, *639*, 57-61.

(22) Li, Y. L.; Gross, M. L. In *The Encyclopedia of Mass Spectrometry: Molecular Ionization Methods*; Gross, M. L., Caprioli, R. M., Eds.; Elsevier Science & Technology Books: Burlington, USA, 2007; Vol. 6, p 668-676.

(23) Fitzgerald, J. J. D.; Kunnath, P.; Walker, A. V., Matrix-Enhanced Secondary Ion Mass Spectrometry (ME SIMS) using Room Temperature Ionic Liquid Matrices. *Anal. Chem.* **2010**, *82*, 4413-4419.

(24) Laremore, T. N.; Zhang, F.; Linhardt, R. J., Ionic Liquid Matrix for Direct UV-MALDI-TOF-MS Analysis of Dermatan Sulfate and Chondroitin Sulfate Oligosaccharides. *Anal. Chem.* **2006**, *79*, 1604-1610.

(25) Tholey, A.; Heinzle, E., Ionic (liquid) matrices for matrix-assisted laser desorption/ionization mass spectrometry—applications and perspectives. *Anal. Bioanal. Chem.* **2006**, *386*, 24-37.

(26) Calvano, C. D.; Carulli, S.; Palmisano, F., Aniline/α-cyano-4-hydroxycinnamic acid is a highly versatile ionic liquid for matrix-assisted laser

desorption/ionization mass spectrometry. *Rapid Commun. Mass Spectrom.* **2009**, *23*, 1659-1668.

(27) Mank, M.; Stahl, B.; Boehm, G., 2, 5-Dihydroxybenzoic Acid Butylamine and Other Ionic Liquid Matrixes for Enhanced MALDI-MS Analysis of Biomolecules. *Anal. Chem.* **2004**, *76*, 2938-2950.

(28) Przybylski, C.; Gonnet, F.; Bonnaffé, D.; Hersant, Y.; Lortat-Jacob, H.; Daniel, R., HABA-based ionic liquid matrices for UV-MALDI-MS analysis of heparin and heparan sulfate oligosaccharides. *Glycobiology* **2010**, *20*, 224-234.

(29) Dertinger, J. J.; Walker, A. V., Proton Transfer in Matrix-Enhanced Secondary Ion Mass Spectrometry Using Ionic Liquid Matrices. *In preparation* **2012**.

(30) Luxembourg, S. L.; McDonnell, L. A.; Duursma, M. C.; Guo, X.; Heeren, R. M. A., Effect of Local Matrix Crystal Variations in Matrix-Assisted Ionization Techniques for Mass Spectrometry. *Anal. Chem.* **2003**, *75*, 2333-2341.

(31) McDonnell, L. A.; Heeren, R. M. A., Imaging Mass Spectrometry. *Mass Spectrom. Rev.* **2007**, *26*, 606-643.

(32) Smith, E. F.; Rutten, F. J. M.; Villar-Garcia, I. J.; Briggs, D.; Licence, P., Ionic Liquids in Vacuo: Analysis of Liquid Surfaces Using Ultra-High-Vacuum Techniques. *Langmuir* **2006**, *22*, 9386-9392.

(33) Adriaensen, L.; Vangaever, F.; Gijbels, R., Metal-Assisted Secondary Ion Mass Spectrometry: Influence of Ag and Au Deposition on Molecular Ion Yields. *Anal. Chem.* **2004**, *76*, 6777-6785.

(34) Cramer, R.; Dreisewerd In *The Encyclopedia of Mass Spectrometry: Molecular Ionization Methods*; Gross, M. L., Caprioli, R. M., Eds.; Elsevier Science & Technology Books: Burlington, USA, 2007; Vol. 6, p 646-661.

(35) *ToF-SIMS: Surface Analysis by Mass Spectrometry*; Vickerman, J. C.; Briggs, D., Eds.; IM Publications and Surface Spectra Limited: Chichester and Manchester, UK, 2001.

(36) Walker, A. V. In *The Encyclopedia of Mass Spectrometry: Molecular Ionization Methods*; Gross, M. L., Caprioli, R. M., Eds.; Elsevier Science & Technology Books: Burlington, USA, 2007; Vol. 6, p 535-546.

(37) Nagy, G.; Walker, A. V., Enhanced Secondary Ion Emission with a Bismuth Cluster Ion Source. *Int. J. Mass Spectrom.* **2007**, *262*, 144-153.

(38) SciFinder, http:scifinder.cas.org. *January 17th, 2012, 9.05 am.*

(39) Paramelle, D.; Cantel, S.; Enjabal, C.; Amblard, M.; Forest, E.; Heymann, M.; Geourjon, C.; Martinez, J.; Subra, G., A New Generation of Cross-linkers for Selective Detection by MALDI MS. *Proteomics* **2009**, *9*, 5384-5388.

(40) Erdemgil, F. Z.; Şanli, S.; Şanli, N.; Özkan, G.; Barbosa, J.; Guiteras, J.; Beltrán, J. L., Determination of pK_a Values of Some Hydroxylated Benzoic Acids in Methanol–Water Binary Mixtures by LC Methodology and Potentiometry. *Talanta* **2007**, *72*, 489-496.

(41) Ouellette, R. J. *Organic Chemistry, A Brief Introduction*; 2nd ed.; Prentice-Hall: Upper Saddle River, New Jersey, 1998.

(42) Greaves, T. L.; Kennedy, D. F.; Weerawardena, A.; Tse, N. M. K.; Kirby, N.; Drummond, C. J., Nanostructured Protic Ionic Liquids Retain Nanoscale Features in

Aqueous Solution While Precursor Brønsted Acids and Bases Exhibit Different Behavior. *J. Phys. Chem. B* **2011**, *115*, 2055-2066.

(43) Dupont, J., On the Solid, Liquid and Solution Structural Organization of Imidazolium Ionic Liquids. *Journal of the Brazilian Chemical Society* **2004**, *15*, 341-350.

Chapter 8

Ionic Liquid Matrices for Improved Detection of Proteins and Polymers in Time-of-Flight Secondary Ion Mass Spectrometry

Abstract

The analyte signal enhancements of polymers and proteins were investigated using IL matrix-enhanced SIMS. Six polymers, polyisoprene, polypropylene glycol, polyethylene oxide, poly(2,6-dimethyl-p-phenylene oxide), polymethyl methacrylate and polystyrene, were studied to examine the role of molecular weight and chemistry on the ion intensity enhancements of the *n*-mer and oligomer ions. The molecular weight of the polymer does not play a significant role in determining the magnitude of the signal enhancements. The analyte ion intensities enhancements are strongly dependent on the chemistry of the polymer side and end groups. Further it was observed that ILs based on the MALDI matrix 2,5 dihydroxybenzoic acid were the most effective matrices for polymers. The molecular ion intensity enhancements of proteins including bradykinin, angiotensin, insulin and cytochrome c were also investigated. Using bradykinins with different terminal amino acids, it is observed that molecular ion intensities are significantly enhanced using IL matrices if the N or C terminal amino acid can accept (or donate) a proton. No analyte signal enhancements were observed for proteins with complex structures, such as insulin.

8.1 Introduction

The analysis of the chemistry and spatial distribution of polymers and biomolecules have many technological applications from organic/molecular electronics to sensors.[1-4] Protein patterning is critical for the fabrication of protein and cell-based sensors, proteomic arrays and patterned biomaterials.[1] The surface composition of polymers is important for controlling properties including their anti-static, lubricating, biocidal, and UV stability.[2] Polymers and proteins can be thought of as high molecular weight compounds composed of a series of subunits, which can be systematically varied. For example, proteins are composed of twenty two different amino acids, which can be arranged in any order. Amino acids are molecules composed of a carboxylic acid, an amine group and a side chain that is specific to each amino acid. The protein is formed ("polymerized") via the reaction of an amine on one amino acid with the carboxylic acid of a second amino acid forming a peptide bond.

While SIMS is able to characterize the spatial distribution on species on surfaces, SIMS does not provide a unique molecular ion for proteins like MALDI.[5] The SIMS spectra of proteins are typically composed of complex fragmentation patterns which are dominated by amino acid fragment ions with $m/z < 300$. Since the amino acid composition of proteins is very similar, the interpretation of these spectra is not routine. However some useful information about polymer conformations can be obtained. For example, Tidwell *et al*[6] investigated the adsorption of albumin on titanium, gold, polytetrafluorethylene (PTFE) and a tetrofluoroethylene plasma polymer (TFE). They observed that the intensities of the albumin characteristic immonium ions varied significantly. On Ti $C_2NH_6^+$ and $C_4NH_8^+$ had the highest intensities while on Au and

PTFE $C_4NH_8^+$ was the highest intensity immonium cation. On TFE CNH_4^+, $C_2NH_6^+$ and $C_4NH_8^+$ had the same ion intensities. These results suggested that the orientation of the adsorbed protein affected the fragment ion distribution. More commonly, multivariate analysis techniques are employed to reduce the large set of correlated fragment ions into a more tractable number of associated variables, the principal components.[1,5,7-9] For example Wagner and co-workers [7-9] have employed PCA to differentiate the SIMS spectra of proteins adsorbed on a variety of substrates.

It is also difficult for polymers to obtain the molecular weight distribution without special sample preparation techniques.[10] In a similar manner to the analysis of proteins, SIMS spectra of polymers typically are composed of low *m/z* (*m/z* < 500) ions, which are both characteristic fragment and *n*-mer ions (combination of a small number of monomer units or monomer units plus fragement ions). These ions contain information about the microstructure of the polymer. For example, Hook and co-workers [11] have employed the statistical yield of *n*-mer ions to analyze the secondary and tertiary structure of polymers. Multivariate analysis methods are also employed to investigate structural changes in polymers when their chemistry is modified by methods such as plasma treatments.[12,13]

Oligomer ions of polymers can be detected in SIMS using a pretreatment method called cationization.[14-17] In this method, a thin layer of the polymer or protein is normally deposited on an etched silver, or other noble metal, substrate. The interaction of the metallic substrates with polymers results in the generation of oligomer distributions with $(M_x + Ag)^+$ up to *m/z* 8000.[17] Proteins and other biomolecules can also be detected using cationisation.[14,18,19] For example, McArthur co-workers investigated the effectivenessof cationization to generate the molecular ions of angiotensin II and substance P. [14]

Room temperature ionic liquids (ILs) have been demonstrated to be very effective matrices in SIMS.[20] The analyte signal enhancements of molecules with *m/z* 1500 are often greater than an order of magnitude, while detection limits are improved by several orders of magnitude. However, there have been no detailed studies of the use of IL matrices to enhance the SIMS spectra of polymers and proteins.

In this chapter the ion intensity enhancements of polymers and proteins are systematically investigated using four ionic liquid matrices: 1-methylimidazolium α-cyano-hydroxycinnamate (MI CHCA), tripropylammonium α-cyano-hydroxycinnamate (trip CHCA), 1-methylimidazolium 2,5 dihydroxybenzoate (MI DHB) and tripropylammonium 2,5 dihydroxybenzoate (trip DHB). The structures of the IL matrices are shown schematically in Figure 1. The IL anions were chosen because CHCA and 2,5 DHB are commonly used as MALDI matrices for the analysis of polymers and peptides[21,22] Five polymers, polyisoprene, polypropylene glycol, polymethyl methacrylate, polyethylene oxide and polystyrene, were studied to determine the ion intensity enhancements of the *n*-mer and oligomer ions based on the polymer molecular weight and their chemistry. Table 1 displays the structure of the polymers employed in this study. In addition, the molecular ion intensity enhancements of multiple proteins including bradykinin, angiotensin, insulin and cytochrome c were investigated. The proteins in this study are listed in Table 2, as well as their molecular weight and the chemistry of the terminal amino acids. Using bradykinins with different terminal acids it is observed that molecular ion intensities are significantly enhanced using IL matrices if the N or C terminal amino acid can accept (or donate) a proton.

Polymer	Name	MW	Proton Transfer?
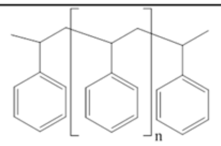	Polystyrene (PS)	1110	side chain
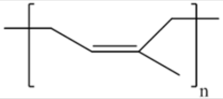	Polyisoprene (PI)	1120	-
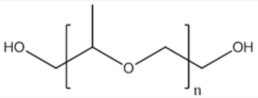	Polypropylene glycol (PPG)	2120	end groups
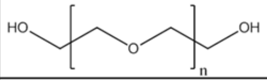	Polyethylene oxide (PEO)	~20000	end groups
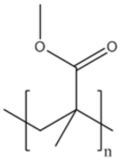	Poly(methyl methacrylate) (PMMA)	26000	side chain
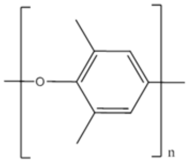	Poly(2,6-dimethyl-p-phenylene oxide) (PDMPO)	29500	backbone

Table 1. The structure of the different polymers used in this study, their molecular weight and the identity of site(s) where proton transfers may occur.

	Exact Mass	**N Terminus**	**C Terminus**
Angiotensin I	1295.7	Asp	Leu
Leucine Enkephalin	555.3	Tyr	Leu
β-endorphin	3462.8	Tyr	Glu
GHRF (1-44)	5036.6	Tyr	Ala
Ubiquitin	8564	Met	Gly
Cytochrome c	12327	Ser[a]	Lys[a]
Insulin	5729.6	Gly, Phe	Asn, Thr
Bradykinin	1059.6	Arg	Arg
Bradykinin 2-9	903.5	Pro	Arg

Bradykinin 2-7	600.3	Pro	Pro
Lys-(Des-Arg9, Leu8)-Bradykinin	997.6	Lys	Leu
Lys-(Des-Arg9)-Bradykinin	1031.5	Lys	Phe

Table 2. The molecular weight of the peptides and proteins employed in this study, and their terminal amino acids.

[a] The molecular weight of cytochrome c was obtained from ref. [23].

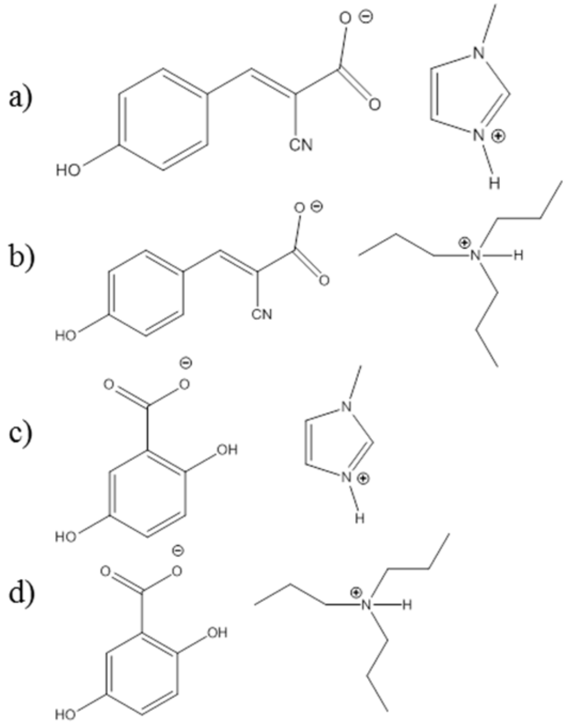

Figure 1. The structure of ionic liquid matrices used a) MI CHCA, b) trip CHCA, c) MI DHB and d) trip DHB\

8.2 Experimental

8.2.1 Materials

1-methylimidazole (99%), tripropylamine (99%), 2,5 dihydroxybenzoic acid (98%), α-cyanohydroxycinnamic acid (97%), bovine insulin, ubiquitin, and leucine enkephalin were purchased from Sigma Aldrich (St. Louis, MO). Polystyrene (MW 1110, M_n 990), polypropylene glycol (MW 2160, M_n 2050), polyethylene oxide (MW 33600, M_n 33000), poly(methyl methacrylate) (MW 17900, M_n 16200), poly(2,6-dimethyl-p-phenylene oxide) (MW 29500, M_n 18900), and polyisoprene (MW 1020, M_n 870) were purchased from Scientific Polymer, Ontario, NY. Bradykinin, bradykinin (2-9), bradykinin (2-7), Lys (Des-Arg9-Leu8) bradykinin, Lys (Des Arg 9) bradykinin, human growth factor (1-44) and angiotensin I were purchased from American Peptide Company (Sunnyvale, CA). HPLC grade methanol was purchased from VWR (Radnor, PA) and HPLC grade chloroform was purchased from Omnisolv (Charlotte, NC). Single side polished <111> Si wafers were purchased from Addison Engineering (San Jose, CA). All chemicals were used without further purification or modification.

8.2.2 Preparation of Ionic Liquids

All ionic liquids were prepared using a synthesis method described by Armstrong and co-workers.[24-27] Briefly, for each ionic liquid 0.5 g of the corresponding acid (CHCA or 2,5 DHB) was dissolved in 15 ml of methanol. The mixture was sonicated until all of the acid was dissolved. Equimolar amounts of the base (MI or trip) were added to the acid solutions and the resulting mixtures were sonicated for an additional minute. After evaporation of the solvent, the resulting ionic liquid was dissolved in a 1:1 (v:v) methanol and chloroform solution to 0.5 M concentration. The ionic liquids were characterized using ^{1}H NMR, FTIR and TOF SIMS.

8.2.3 Sample Preparation

For each "matrix enhanced" sample, a 400µl aliquot of 0.5 M IL was mixed with 400µl of analyte solution (concentration of 1 mg/ml). For proteins, the solvent employed was 1:1 methanol:chloroform (v:v) while for polymers it was choloroform. For control samples a 400 µl aliquot of the analyte solution was mixed with an additional 400 µl of the solvent methanol/choloroform. Once mixed, the sample (total volume: 800µl) was spun coat onto a ~1 cm^2 Si wafer for 6s at ~300 rpm and 20s at 3000 rpm using a Chemat KW-4A spin coater (Chemat Technologies, Inc, Northridge, CA). To ensure that the maximum analyte signal intensities were obtained the solutions of the analyte and IL were mixed for 1-2 mins prior to spin coating.

8.2.4 Time of Flight Secondary Ion Mass Spectrometry

TOF SIMS spectra were taken on an ION TOF IV (ION TOF USA, Chestnut Ridge, NY) equipped with a Bi liquid metal ion gun. Briefly, the instrument consists of a loadlock chamber, preparation chamber and main chamber, each separated by gate valves. During experiments the main chamber was maintained at $\leq 1 \times 10^{-8}$ mbar to prevent sample contamination. The primary ions used were Bi^+ and Bi_3^+ with a kinetic energy of 25 keV. The primary ion does was $<1 \times 10^{10}$ ions cm^{-2}, which is within the static regime.[28] The secondary ions were extracted to 2000V and reaccelerated to 10 keV before reaching the detector.

High resolution mass spectra were taken using an analysis area of (100 x 100) μm^2. The mass resolution (mass resolving power, $m/\Delta m$) at *m/z* 29 was 3000. The ion intensity enhancement is calculated using

Enhancement= $I(M \pm H)^{\pm}_{matrix}/I(M \pm H)^{\pm}_{control}$ **Formula 8.1**

where $I(M \pm H)^{\pm}$ is the intensity (peak area) of the protonated and deprotonated molecular ions. The secondary ion intensities reported are an average of three randomly selected areas on a sample, and the error is the estimated standard deviation.

8.3 Results and Discussion

8.3.1 Polymers

8.3.1.1. Low Molecular Weight Polymers: Polystyrene and Polyisoprene

The analyte signal enhancement of two polymers, polystyrene 1110 (PS) and polyisoprene (PI) with approximately the same MW (Table 1) were investigated. Figures 2 and 3 display the SIMS spectra of PS and PI. In the PI spectra, no *n*-mer or oligomer ions were observed using IL matrices or in the control spectrum (Figure 3). However, in the PS spectra, *n*-mer and oligomer ions were observed in the spectra without matrix (control) and using MI DHB and trip DHB matrices. No *n*-mer and oligomer ions are detected using MI CHCA and trip CHCA matrices indicating that the formation of these ions is suppressed. Taken together this data indicates that the mass of the polymer is not a factor in determining the magnitude of the analyte signal enhancements. Rather, the chemical structure of the analyte is important: PS has a benzene ring which can accept or donate protons whereas PI does not.

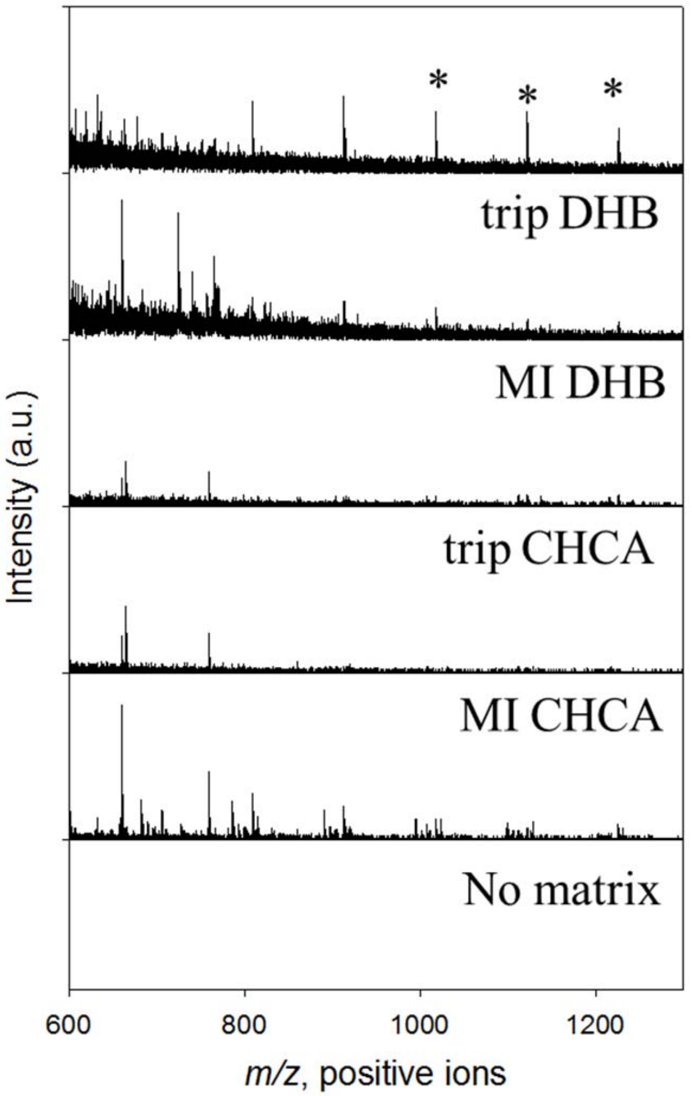

Figure 2. SIMS spectra of the PS 1110 oligomer ion region using MI CHCA, trip CHCA, MI DHB, and trip DHB matrices, and with a control (no matrix applied). The * denotes an oligomer ion. Primary ion: Bi_3^+.

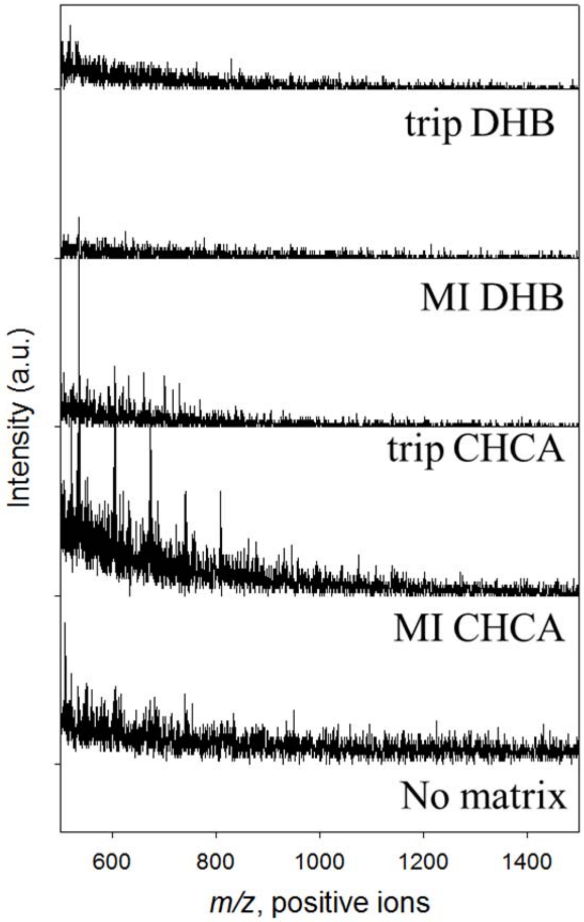

Figure 3. SIMS spectra of polyisoprene oligomer ion region using MI CHCA, trip CHCA, MI DHB, and trip DHB matrices, and with a control (no matrix applied). Note: Ions observed at *m/z* < 800 are cluster ions associated with the IL matrix. Primary ion: Bi_3^+.

3.1.1.2 Polypropylene Glycol and Polyethylene Oxide

Polypropylene glycol (PPG) and polyethylene oxide (PEO) have similar structures, but in this study had very different MWs (Table 1). In the SIMS spectra the *n*-mer regions of

PPG and PEO were observed using IL matrices. The oligomer region of PPG is also detected but not for PEO due to instrument restrictions. Figures 4 and 5 display an example of the data obtained: SIMS spectra of PPG. In Figure 4 it can be clearly seen that the *n*-mer and oligomer ions are better enhanced by MI DHB and trip DHB . Analyte signal enhancements of up to 100x were observed. MI CHCA and trip CHCA also increase analyte signals by a small factor, typically 2-3 x. In the *n*-mer region ($m/z < 1950$), two series of ions are observed, A and B (Figure 5). These series involve the loss of a terminal –OH group suggesting that proton transfer to and from the end of the polymer chain is important.

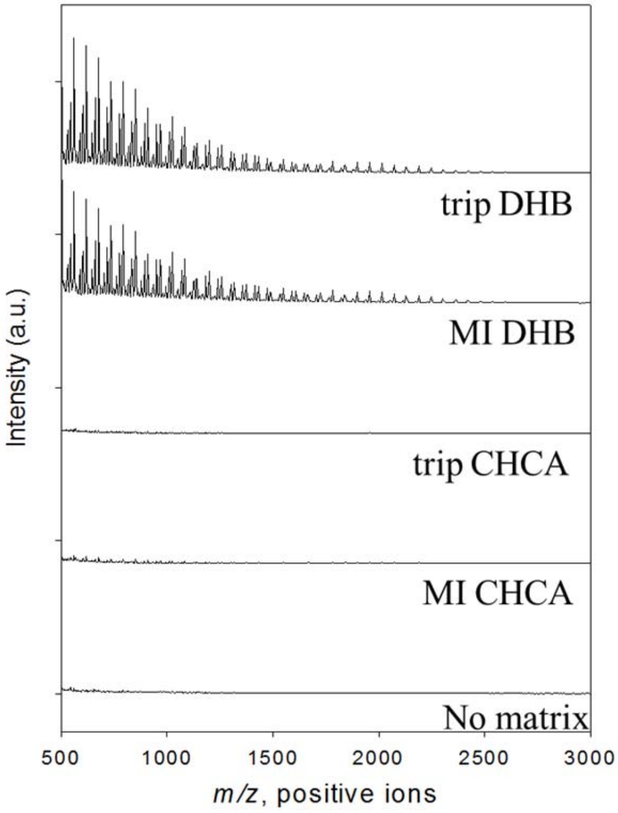

Figure 4. SIMS spectra of PPG oligomer ion region using MI CHCA, trip CHCA, MI DHB, and trip DHB matrices, and with a control (no matrix applied). Primary ion: Bi_3^+.

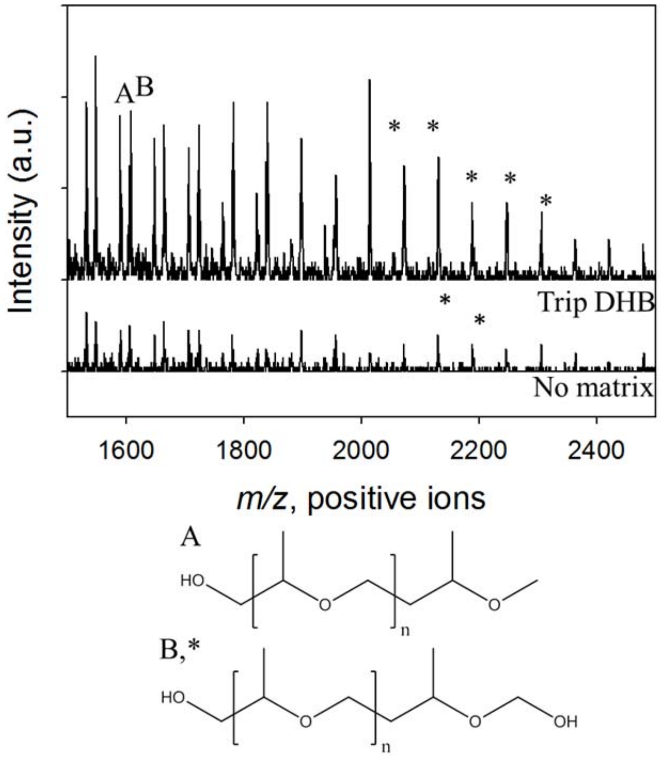

Figure 5. The oligomer and n-mer region of PPG with trip DHB and no matrix applied. The * denote oligomer ions. A and B denote two different series of n-mer ions, and their structure is shown above. Primary ion: Bi_3^+.

3.1.1.3 High Molecular Weight Polymers

Poly(2,6-dimethyl-p-phenylene oxide) (PDMPO) and poly(methylmethacrylate) (PMMA) are both high molecular weight polymers that have oxygen groups in the monomer unit (Table 1). In the SIMS spectra of PDMPO there are no ions observed above *m/z* 1000 with few *n*-mer ions detected below this mass-to-charge ratio. The *n*-mer ions of PMMA are enhanced by trip DHB up to approximately *m/z* 1400. Since these polymers both have groups that accept or donate protons, it was expected that a larger number of *n*-mer ions would be observed. However, the concentration of the analyte may have been too low to detect high intensities of *n*-mer and oligomer ions.

8.3.2 Proteins

8.3.2.1 Bradykinin

The analyte signal enhancements of five different bradykinins were investigated. Bradykinin, bradykinin (2-9) and bradykinin (2-7) have differing numbers of arginine and proline terminal groups (Table 2). Figure 6a displays the protonated molecular ion ($(M + H)^+$) intensity enhancements observed using MI CHCA, trip CHCA, MI DHB and trip DHB. It can be clearly seen that the largest signal increases are observed for bradykinin, which has two terminal arginines (Figure 6a, "1-9"). The protonated molecular ions of bradykinin (2-9), which has one terminal arginine, are enhanced slightly better than the molecular ions of bradykinin (2-7), which has two terminal prolines. Under our experimental conditions (pH 7) it is likely that at the C terminus of bradykinin and bradykinin (2-9) the side chain of arginine is protonated, while the carboxylic acid is deprotonated ($pK_a(\alpha\text{-COOH}) = 2.17$; $pK_a(\alpha\text{-NH}_3^+) = 9.04$; $pK_a(\text{side}) = 12.48$).[29] Thus a protonated molecular ion forms via the transfer of a proton from the IL to the carboxylate group at the C terminus. For bradykinin, which has an arginine at the N-terminus, the side group is also likely to be positively charged and so will have a larger signal enhancement that bradykinin (2-9), which has a proline group at the N-terminus ($pK_a(\alpha\text{-COOH}) = 1.99$; $pK_a(\alpha\text{-NH}_3^+) = 10.60$).[29] For bradykinin (2-7), which has two terminal proline groups, the addition of a proton to the carboxylate group at the N-terminus leads to the formation of a neutral species and so little, or no, enhancement of the $(M + H)^+$ ion is observed using IL matrices (Figure 6a). In the negative ion mass spectra, the deprotonated molecular ion ($(M - H)^-$) intensities of bradykinin (2-9) have the largest increases using IL matrices while little, or no, deprotonated molecular ion signal enhancements are observed for bradykinin (2-7) or bradykinin (Figure 6b). For bradykinin (2-9) the transfer of a proton to the IL matrix from the positively charged N-terminal arginine leads to the formation of a deprotonated molecular ion, $(M - H)^-$ because the C-terminal proline can not accept protons. In contrast for bradykinin, where the C-terminal arginine has a positively charged side group, the loss of a proton from the N-terminus leads to the formation of a neutral species. Similarly, no deprotonated molecular ion signal enhancements are observed for bradykinin (2-7) because the N-terminal proline cannot lose a proton.

The protonated and deprotonated molecular ion intensity enhancements of Lys-(Des-Arg9-Leu8) bradykinin and Lys-(Des-Arg9) bradykinin are consistent with the above analysis (Figure 6; Table 2). At the N terminus both Lys-(Des-Arg9-Leu8) bradykinin and Lys-(Des-Arg9) bradykinin have lysine groups ($pK_a(\alpha\text{-COOH}) = 2.18$; $pK_a(\alpha\text{-NH}_3^+) = 8.95$; $pK_a(\text{side}) = 10.79$),[29] while a the C terminus Lys-(Des-Arg9-Leu8) bradykinin and Lys-(Des-Arg9) bradykinin have leucine ($pK_a(\alpha\text{-COOH}) = 2.36$; $pK_a(\alpha\text{-NH}_3^+) = 9.60$)[29] and phenylalanine ($pK_a(\alpha\text{-COOH}) = 1.83$; $pK_a(\alpha\text{-NH}_3^+) = 9.13$)[29] groups, respectively. Thus both Lys-(Des-Arg9-Leu8) bradykinin and Lys-(Des-Arg9) bradykinin are likely to have a protonated side group and deprotonated carboxylic acid group at the N and C termini, respectively. Upon transfer of a proton from the IL matrix to the carboxylate group of the C terminus, a protonated molecular ion ($(M + H)^+$) will form leading to an analyte signal enhancement similar to that observed for bradykinin (2-9). Further, the transfer of a proton from the protonated lysine to the IL matrix leads to the formation of deprotonated molecular ions, $(M - H)^-$. In contrast, for Lys-(Des-Arg9) bradykinin the loss of a proton from the lysine terminal group does not lead to the formation of $(M - H)^-$ ions because in the SIMS process the side group of phenylalanine can be protonated via the formation of a tripropylium ion, $C_7H_7^+$, and so a neutral is formed.

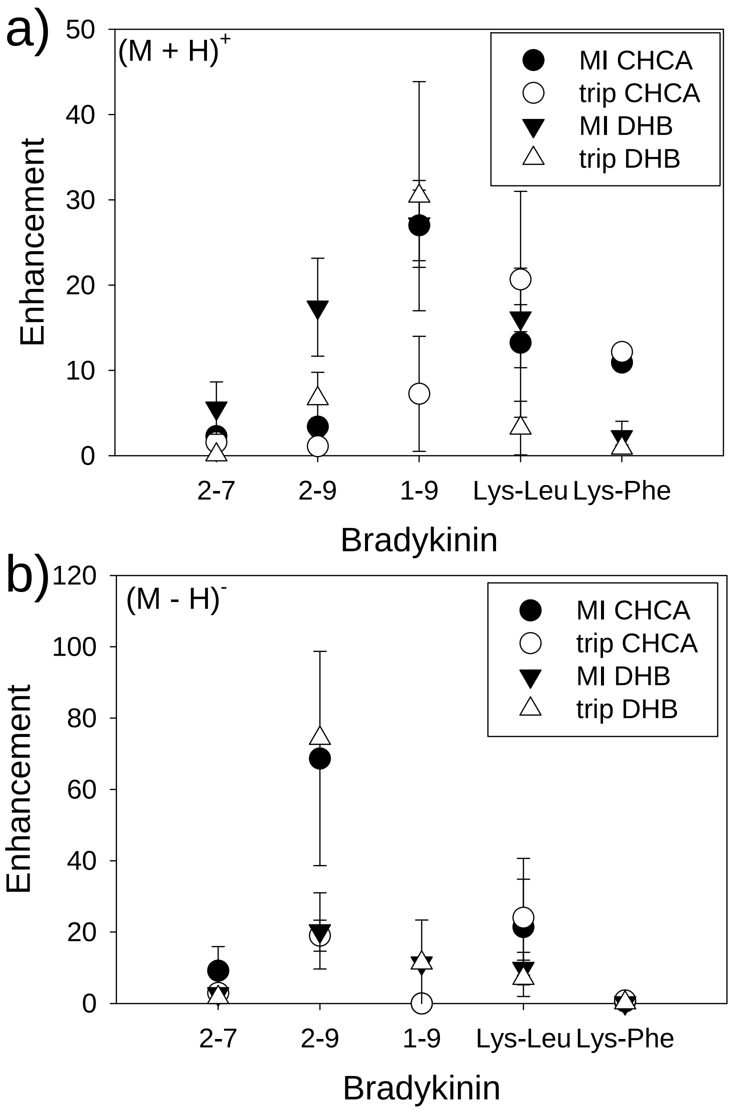

Figure 6. The protonated (a) and deprotonated (b) molecular ion enhancements of bradykinin (2-7), bradykinin (2-9), bradykinin ("1-9"), Lys-(Des-Arg9-Leu8) bradykinin ("Lys-Leu") and Lys-(Des-Arg9) bradykinin ("Lys-Phe") using MI CHCA, MI DHB, trip CHCA and trip DHB. Primary ion: Bi$^+$.

8.3.2.2 Other Proteins

The SIMS spectra of other proteins was also investigated using MI CHCA, trip CHCA, MI DHB and trip DHB IL matrices. Leucine enkephalin (*m/z* 555) and angiotensin I (*m/z* 1296) both have terminal amino acids which can accept or donate protons. Using Bi_3^+ primary ions quasimolecular ions of both proteins were observed. The analyte signal enhancement of leucine encephalin is discussed in further detail in chapter 7. However, using IL matrices no quasimolecular ions were observed for bovine insulin, β-endorphin, cytochrome c and ubiquitin. These proteins have complex structures and so may aggregated in the IL leading to greatly reduced proton transfer between the analyte and matrix.

8.4 Conclusions

The analyte signal enhancements of polymers and proteins were investigated using trip CHCA, trip DHB and MI CHCA, MI DHB matrices in SIMS. Five polymers, polyisoprene, polypropylene glycol, polyethylene oxide, polymethyl methacrylate and polystyrene, were studied to examine the role of molecular weight and chemistry on the ion intensity enhancements of the *n*-mer and oligomer ions. It was observed that the molecular weight of the polymer was not an important factor in determining the magnitude of the analyte signal enhancements observed. Rather, the chemistry of the polymer side and end groups were important in determining the ion intensity enhancement. Furthermore, it was observed that ILs based on 2,5 DHB were better matrices for polymers. There are no clear reasons for this and studies are ongoing to investigate these observations.

In addition, the molecular ion intensity enhancements of proteins including bradykinin, angiotensin, insulin and cytochrome c were investigated. Using bradykinins with different terminal amiono acids it is observed that molecular ion intensities are significantly enhanced using IL matrices if the N or C terminal amino acid can accept (or donate) a proton. Quasimolecular ions of proteins, such as insulin and cytochrome c, were not enhanced using the IL matrices studied, which may be caused by their aggregation in solution.

8.5 References

(1) Castner, D. G.; Ratner, B. D., Biomedical Surface Science: Foundations to Frontiers. *Surf. Sci.* **2002**, *500*, 28-60.

(2) Briggs, D. In *ToF-SIMS: Surface Analysis by Mass Spectrometry*; Vickerman, J. C., Briggs, D., Eds.; IM Publications and Surface Spectra Limited: Chichester and Manchester, UK, 2001.

(3) Walker, A. V., Why is SIMS Underused in Chemical and Biological Analysis? Challenges and Opportunities. *Anal. Chem.* **2008**, *80*, 8865-8870.

(4) Dertinger, J. J.; Walker, A. V., Proton Transfer in Matrix-Enhanced Secondary Ion Mass Spectrometry Using Ionic Liquid Matrices. *In preparation* **2012**.

(5) Chilkoti, A. In *ToF-SIMS: Surface Analysis by Mass Spectrometry*; Vickerman, J. C., Briggs, D., Eds.; IM Publications and Surface Spectra Limited: Chichester and Manchester, UK, 2001, p 627-650.

(6) Tidwell, C. D.; Castner, D. G.; Golledge, S. L.; Ratner, B. D.; Meyer, K.; Hagenhoff, B.; Benninghoven, A., Static Time-of-Flight Secondary Ion Mass

Spectrometry and X-ray Photoelectron Spectroscopy Characterization of Adsorbed Albumin and Fibronectin Films. *Surf. Interface Anal.* **2001**, *31*, 724-733.

(7) Wagner, M. S.; Castner, D. G., Characterization of Adsorbed Protein Films by Time-of-Flight Secondary Ion Mass Spectrometry with Principal Component Analysis. *Langmuir* **2001**, *17*, 4649-4660.

(8) Wagner, M. S.; Tyler, B. J.; Castner, D. G., Interpretation of Static Time-of-Flight Secondary Ion Mass Spectra of Adsorbed Protein Films by Multivariate Pattern Recognition. *Anal. Chem.* **2002**, *74*, 1824-1835.

(9) Lhoest, J.-B.; Wagner, M. S.; Tidwell, C. D.; Castner, D. G., Characterization of Adsorbed Protein Films by Time of Flight Secondary Ion Mass Spectrometry. *J. Biomed. Mater. Res.* **2001**, *57*, 432-440.

(10) Briggs, D. In *ToF-SIMS: Surface Analysis by Mass Spectrometry*; Vickerman, J. C., Briggs, D., Eds.; IM Publications and Surface Spectra Limited: Chichester and Manchester, UK, 2001, p 497-524.

(11) Hook, K. J.; Hook, T. J.; Wandass, J. H.; Gardella Jr, J. A., Secondary Ion Formation from Functional Polymer Systems in Static Secondary Ion Mass Spectrometry. *Appl. Surf. Sci.* **1990**, *44*, 29-41.

(12) Wagner, M. S.; Lenghaus, K.; Gillen, G.; Tarlov, M. J., Characterization and Ion-induced Degradation of Cross-Linked Poly(methyl methacrylate) Studied Using Time of light Secondary Ion Mass Spectrometry. *Appl. Surf. Sci.* **2006**, *253*, 2603-2610.

(13) Wagner, M. S.; Pasche, S.; Castner, D. G.; Textor, M., Characterization of Poly(L-lysine)-graft-Poly(ethylene glycol) Assembled Monolayers on Niobium

Pentoxide Substrates Using Time-of-Flight Secondary Ion Mass Spectrometry and Multivariate Analysis *Anal. Chem.* **2004**, *76*, 1483-1492.

(14) McArthur, S. L.; Vendettuoli, M. C.; Ratner, B. D.; Castner, D. G., Methods for Generating Protein Molecular Ions in ToF-SIMS. *Langmuir* **2004**, *20*, 3704-3709.

(15) Michel, R.; Luginbühl, R.; Graham, D. J.; Ratner, B. D., Self-Assembled Monolayers for Polymer and Protein Cationization with Time-of-Flight Secondary Ion Mass Spectrometry. *J. Vac. Sci. Technol. A* **2000**, *18*, 1114-1118.

(16) Michel, R.; Luginbühl, R.; Graham, D. J.; Ratner, B. D., New Substrates for Polymer Cationization with Time-of-Flight Secondary Ion Mass Spectrometry. *Langmuir* **2000**, *16*, 6503-6509.

(17) Hagenhoff, B. In *ToF-SIMS: Surface Analysis by Mass Spectrometry*; Vickerman, J. C., Briggs, D., Eds.; IM Publications and Surface Spectra Limited: Chichester and Manchester, UK, 2001, p 595-626.

(18) Benninghoven, A., Static SIMS Applications - From Silicon Single Crystal Oxidation to DNA Sequencing. *J. Vac. Sci. Technol. A* **1985**, *3*, 451-460.

(19) Benninghoven, A. In *ToF-SIMS: Surface Analysis by Mass Spectrometry*; Vickerman, J. C., Briggs, D., Eds.; Surface Spectra; IM Publications: Chichester, 2001.

(20) Fitzgerald, J. J. D.; Kunnath, P.; Walker, A. V., Matrix-Enhanced Secondary Ion Mass Spectrometry (ME SIMS) Using Room Temperature Ionic Liquid Matrices. *Analytical Chemistry* **2010**, *82*, 4413-4419.

(21) Cramer, R.; Dreisewerd In *The Encyclopedia of Mass Spectrometry: Molecular Ionization Methods*; Gross, M. L., Caprioli, R. M., Eds.; Elsevier Science & Technology Books: Burlington, USA, 2007; Vol. 6, p 646-661.

(22) Gross, J. In *The Encyclopedia of Mass Spectrometry: Molecular Ionization Methods*; Gross, M. L., Caprioli, R. M., Eds.; Elsevier Science & Technology Books: Burlington, USA, 2007; Vol. 6, p 662-668.

(23) Wakabayashi, S.; Matsubara, H.; Kim, C. H.; Kawai, K.; King, T. E., The Complete Amino Acid Sequence of Bovine Heart Cytochrome C_1. *Biochem. Biophys. Res. Commun.* **1980**, *97*, 1548-1554.

(24) Armstrong, D. W.; Zhang, L.-K.; He, L.; Gross, M. L., Ionic Liquids as Matrixes for Matrix-Assisted Laser Desorption/ Ionization Mass Spectrometry. *Analytical Chemistry* **2001**, *73*, 3679-3685.

(25) Carda-Broch, S.; Berthod, A.; Armstrong, D. W., Ionic matrices for matrix-assisted laser desorption/ionization time-of-flight detection of DNA oligomers. *Rapid Communications in Mass Spectrometry* **2003**, *17*, 553-560.

(26) Armstrong, D. W.; Zhang, L.-K.; He, L.; Gross, M. L., Ionic Liquids as Matrices for Matrix-Assisted Laser Desorption/ionization Mass Spectrometry. *Anal. Chem.* **2001**, *73*, 3679-3686.

(27) Crank, J. A.; Armstrong, D. W., Towards a Second Generation of Ionic Liquid Matrices (ILMs) for MALDI-MS of Peptides, Proteins and Carbohydrates. *J. Am. Soc. Mass Spectrom.* **2009**, *20*, 1790-1800.

(28) *ToF-SIMS: Surface Analysis by Mass Spectrometry*; Vickerman, J. C.; Briggs, D., Eds.; IM Publications and Surface Spectra Limited: Chichester and Manchester, UK, 2001.

(29) *CRC Handbook of Chemistry and Physics, 91st Edition*; Haynes, W. M., Ed.; CRC Press: Boca Raton, FL, 2010.

Chapter 9

Conclusions and Future Work

9.1 Conclusions

The analysis of thin films is important for wide variety of applications from biotechnology[1-13] to sensing[11,14-18] to organic electronics[19-24]. In this thesis two techniques have been investigated in detail: infrared spectroscopy (IRS) and secondary ion mass spectrometry (SIMS). In SIMS the distribution of molecular and elemental species can be obtained with ~200 nm lateral resolution.[25] IRS is complimentary to SIMS since it provides information about the bonds broken and made during chemical processes.[26]

A reflection absorption infrared spectroscopy (RAIRS) system was designed and constructed. It is composed of a optical pathway and a vacuum chamber. The vacuum chamber is necessary because it will be employed to examine *in situ* the interaction of vapor-deposited metals and gases, such as CVD precursors, with organic thin films. To facilitate these studies a sample holder was designed, built and tested so that the samples can be easily introduced into the vacuum chamber and be heated and cooled during experiments. As a demonstration of the RAIRS capabilities, an IR spectrum of an octadecanthiolate SAM adsorbed on Au was obtained.

A new class of self-assembled monolayer, terminal alkyne monolayers (TAMs) ($HC{\equiv}C(CH_2)_nCH_3$) adsorbed on Au, was synthesized and characterized using single wavelength ellipsometry, RAIRS, x-ray photoelectron spectroscopy (XPS) and SIMS. Terminal alkyne monolayers (TAMs) have the potential to revolutionize surface functionalization through greatly increased monolayer temperature stability and electrical conductance. The data indicates that the TAMs are more disordered than alkanethiolate self-assembled monolayers on Au. For TAMs with less than 11 methylene units in the backbone, the adsorbed layer is highly disordered, oxidized and has a multilayer structure. Longer chain length TAMs form disordered monolayers on gold. The molecules have an upright conformation and bind to the surface via a Au-C≡C- bond. Some oxidized species remain on the surface. These data suggest that the technological applications of TAMs may be limited.

Room temperature ionic liquids (ILs) are effective matrices in SIMS. The quasimolecular ion intensities of proteins, polymers, phospholipids, and peptides are enhanced by at least an order of magnitude using IL matrices. There is also a decrease in the fragmentation of analytes. The limit of detection of analytes is also greatly improved. For example, the detection limits of DPPC and DPPE were at least two orders of magnitude better. Since ILs are liquids, they do not cause changes to the chemistry of the sample surface and so can be employed in imaging SIMS. As a demonstration, a red onionskin membrane was imaged. Using IL matrices ions characteristic of proteins were observed, which could not otherwise be detected.

The mechanism of analyte signal enhancements using ion liquids involves the transfer of protons to, or from, the analyte to, or from, the matrix. Only protic ionic liquids, which have a labile proton, are effective matrices. Analyte/matrix samples are typically prepared by mixing a solution of the analyte with the matrix. The analyte signal enhancement is dependent on the mixing time in this solution, which indicates that the proton transfer occurs in solution. The chemistry of the matrix cation and anion are important in determining the magnitude of the analyte ion intensity enhancement. However the chemistry of the anion appears to be more important. The number, position and type of substituents present in the anion greatly effect ion intensity enhancements observed.

The analyte signal enhancements of polymers and proteins were also investigated using IL matrix-enhanced SIMS. Three polymers, polyisoprene, polypropylene glycol and polystyrene, were studied to examine the role of molecular weight and chemistry on the ion intensity enhancements of the *n*-mer and oligomer ions. In addition, the molecular ion intensity enhancements of proteins including bradykinin, angiotensin, insulin and cytochrome c were investigated. Using bradykinins with different terminal acids it is observed that molecular ion intensities are significantly enhanced using IL matrices if the N or C terminal amino acid can accept (or donate) a proton.

9.2 Future Work

A detailed understanding of the formation, structure, reactivity and manipulation of these promising TAMs is required to advance their application in nanolithography, sensing, electronics and other technologies. At present the use of TAMs on metal substrates, such as gold, appears to be limited by the formation of oxidized species. However, the synthesis of TAMs is not yet fully optimized. It is also important to develop methods to form TAMS on more technologically relevant substrates such as GaAs and InAs,

In this thesis it was demonstrated that IL are effective matrices for the enhancement of quasimolecular ions of biomolecules and polymers. However, few studies have attempted to understand and control the ionization of species using IL matrices. In SIMS and MALDI, only protic ILs are effective matrices: the ionization of the analyte is promoted by proton transfer from and to the IL matrix. The acidity and structure of the IL matrix will therefore influence the solubility and protonation of the analyte, and an understanding of their effects is critical in the design of new IL matrices for SIMS.

9.3 References

(1) Boxer, S. G.; Kraft, M. L.; Weber, P. K., Advances in Imaging Secondary Ion Mass Spectrometry for Biological Samples. *Annu. Rev. Biophys.* **2009**, *38*, 53-74.

(2) Rezania, A.; Johnson, R.; Lefkow, A. R.; Healy, K. E., Bioactivation of Metal Oxide Surfaces. 1. Surface Characterization and Cell Response. *Langmuir* **1999**, *15*, 6931-6939.

(3) Sunada, K.; Watanabe, T.; Hasimoto, K., Batericidal Activity of Copper-Deposited TiO_2 Thin Film under Weak UV Light Illumination. *Environ. Sci. Technol.* **2003**, *37*, 4785-4789.

(4) Voldman, J.; Gray, M. L.; Scmidt, M. A., Microfabrication in Biology and Medicine. *Annu. Rev. Biomed. Eng.* **1999**, *01*, 401-425.

(5) Kasemo, B., Biological surface science. *Surface Science* **2002**, *2002*, 656-677.

(6) Canavan, H. E.; Cheng, X.; Graham, D. J.; Ratner, B. D.; Castner, D. G., Surface Characterization of the Extracellular Matrix Remaining after Cell Detachment from a Thermoresponsive Polymer. *Langmuir* **2005**, *21*, 1949-1955.

(7) Sung, H.-W.; Chen, C.-N.; Huang, R.-N.; Hsu, J.-C.; Chang, W.-H., In vitro surface characterization of a biological patch fixed with a naturally occurring crosslinking agent. *Biomaterials* **2000**, *21*, 1353-1362.

(8) Boisselier, E.; Astruc, D., Gold nanoparticles in nanomedicine: preparations, imaging, diagnostics, therapies and toxicity. *Chem Soc Rev* **2009**, *38*, 1759-1782.

(9) Moghimi, S. M.; Hunter, A. C.; Murray, J. C., Nanomedicine: current status and future prospects. *The FASEB Journal* **2005**, *19*, 311-330.

(10) Ratner, B. D., Surface Characterization of Biomaterials by Electron Spectroscopy for Chemical Analysis. *Analysis of Biomedical Engineering* **1983**, *11*, 313-336.

(11) Jobst, G.; Moser, I.; Varahram, M.; Svasek, P.; Aschauer, E.; Trajanoski, Z.; Wach, P.; Kotanko, P.; Skrabal, F.; Urban, G., Thin-Film Microbiosensors for Glucose-Lactate Monitoring. *Anal. Chem.* **1996**, *68*, 3173-3179.

(12) Dixhit, R. P.; Puthli, S. P., Oral strip technology: Overview and future potential. *Journal of Controlled Release* **2009**, *139*, 94-107.

(13) Lu, H. B.; Campbell, C. T.; Graham, D. J.; Ratner, B. D., Surface Characterization of Hydroxyapatite and Related Calcium Phosphates by XPS and TOF-SIMS. *Anal. Chem.* **2000**, *72*, 2886-2894.

(14) Sakai, G.; Baik, N. S.; Miura, N.; Yamazoe, N., Gas sensing properties of tin oxide thin films fabricated from hydrothermally treated nanoparticles. Dependence of CO and H_2 response on film thickness. *Sensors and Actuators B* **2001**, *77*, 116-121.

(15) Tien, L. C.; Sadik, P. W.; Norton, D. P.; Voss, L. F.; Pearton, S. J.; Wang, H. T.; Ren, B. S. K. F.; Jun, J.; Lin, J., Hydrogen sensing at room temperature with Pt-coated ZnO thin films and nanorods. *Appl. Phys. Lett* **2005**, *87*, 222106.

(16) O'Hara, J. F.; Singh, R.; Brener, I.; Smirnova, E.; Han, J.; Taylor, A. J.; Zhang, W., Thin-film sensing with planar terahertz metamaterials: sensitivity and limitations. *Optics Express* **2008**, *16*, 1786-1795.

(17) Maheshwari, V.; Saraf, R. F., High-Resolution Thin-Film Device to Sense Texture by Touch. *Science* **2006**, *312*, 1501-1504.

(18) Shen, W.; Zhao, Y.; Zhang, C., The preparation of ZnO based gas-sensing thin films by ink-jet printing method. *Thin Solid Films* **2005**, *483* 382-387.

(19) Austin, M. D.; Chou, S. Y., Fabrication of 70nm channel length polymer organic thin-film transistors using nanoimprint lithography. *Appl. Phys. Lett* **2002**, *81*, 4431-4433.

(20) Cao, Q.; Kim, H.-s.; Pimparkar, N.; Kulkarni, J. P.; Wang, C.; Shim, M.; Roy, K.; Alam, M. A.; Rogers, J. A., Medium-scale carbon nanotube thin-film integrated circuits on flexible plastic substrates. *Nature* **2008**, *454*, 495-502.

(21) Dimitrakopoulos, C. D.; Malenfant, P. R. L., Organic Thin Film Transistors for Large Area Electronics. *Adv. Mater.* **2002**, *14*, 99-117.

(22) Dimitrakopoulos, C. D.; Mascaro, D. J., Organic thin-film transistors: A review of recent advances. *IBM J. Res. & Dev.* **2001**, *45*, 11-27.

(23) Cho, J. H.; Lee, J.; Xia, Y.; Kim, B.; He, Y.; Renn, M. J.; Lodge, T. P.; Frisbie, C. D., Printable ion-gel gate dielectrics for low-voltage polymer thin-film transistors on plastic. *Nature Materials* **2006**, *7*.

(24) Ouyang, J.; Chu, C.-W.; Szmanda, C. R.; Ma, L.; Yang, Y., Programmable polymer thin film and non-volatile memory device. *Nature Materials* **2004**, *3*, 918-922.

(25) Walker, A. V., Why is SIMS Underused in Chemical and Biological Analysis? Challenges and Opportunities. *Analytical Chemistry* **2008**, *80*, 8865-8870.

(26) Leng, Y. *Materials Characterization: Introduction to Microscopic and Spectroscopic Materials*; John Wiley & Sons (Asia) Pte Ltd: Singapore, 2008.

Appendix 1

Design of RAIRS instrument

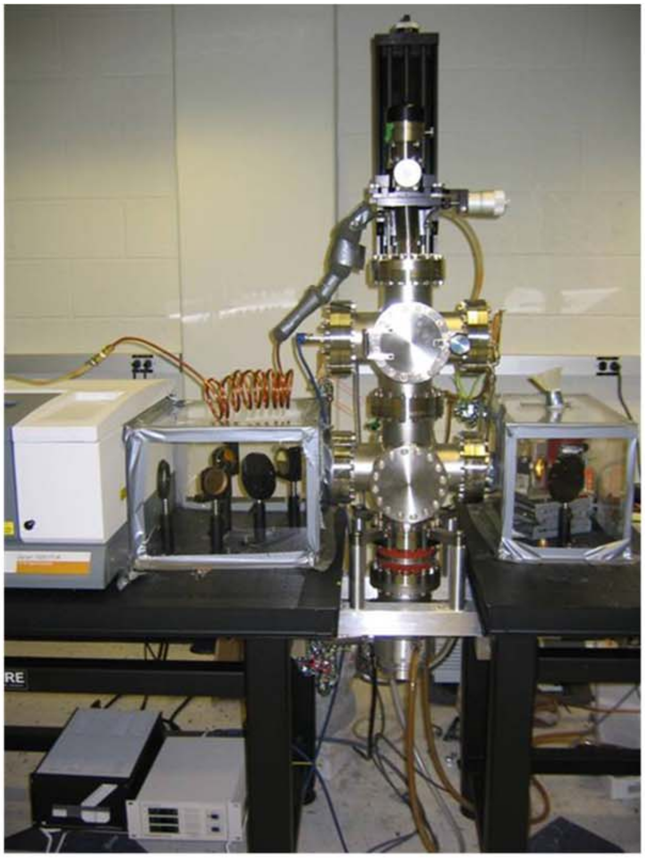

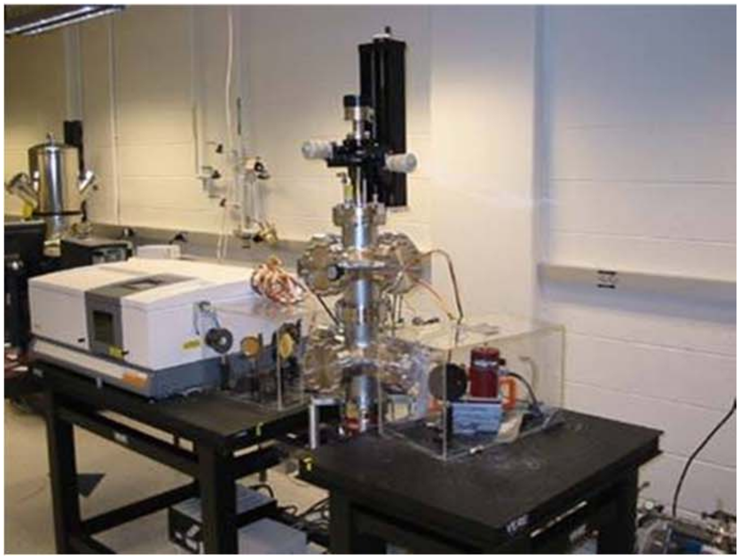

Appendix A1.1 Photographs of RAIRS instrument constructed.

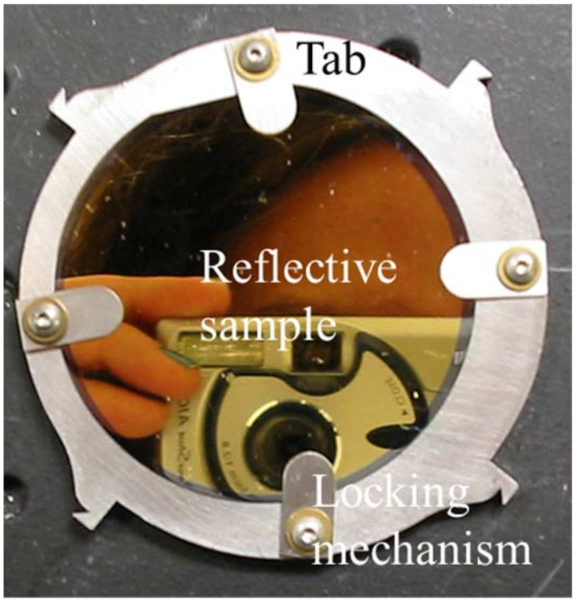
Tab
Reflective sample
Locking mechanism

Figure A1.2 Photograph of sample platen with sample loaded.

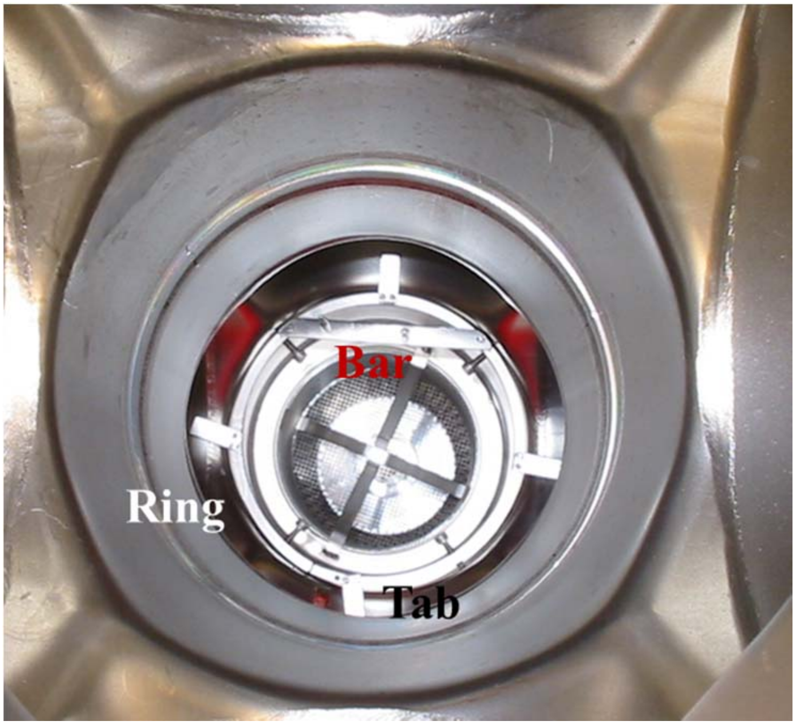
Bar
Ring
Tab

Figure A1.3 Photograph of sample guide ring inserted into the chamber.

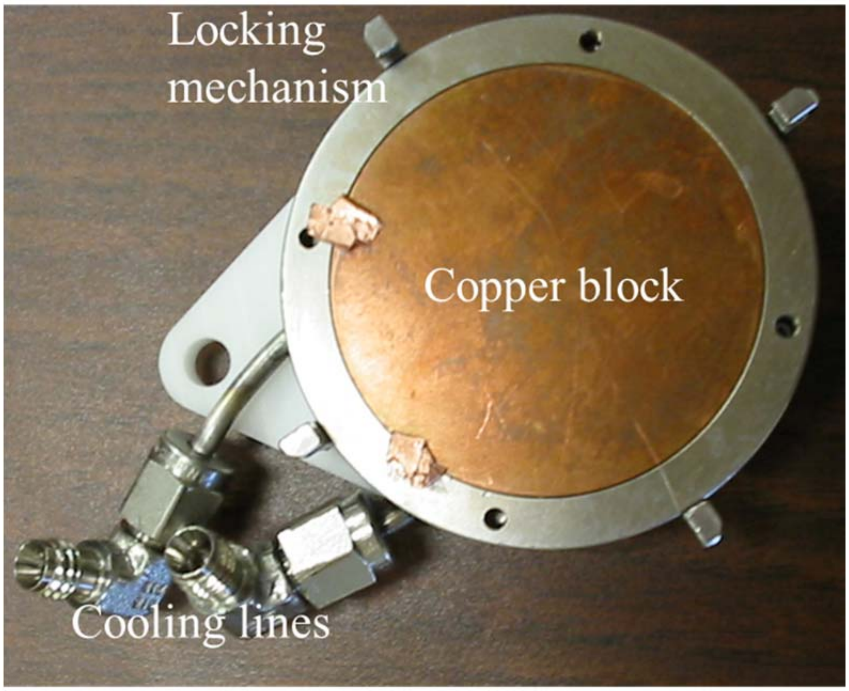
Locking
mechanism
Copper block
Cooling lines

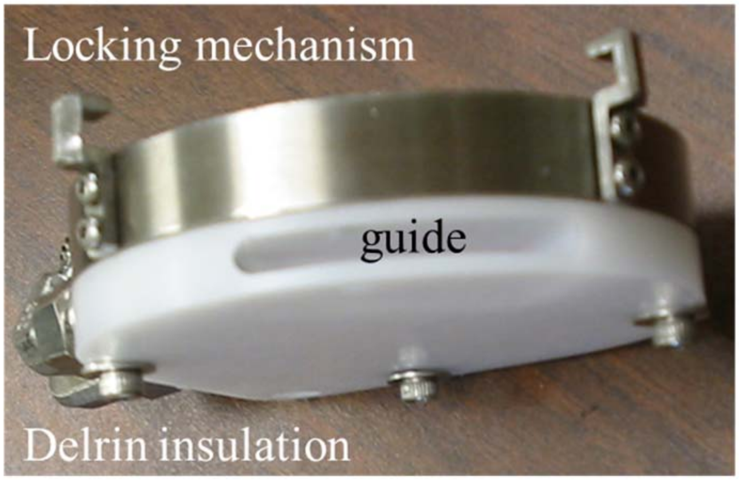
Locking mechanism
guide
Delrin insulation

Figure A1.4 Photographs of the copper block and insulating Delrin of the sample holder.

Appendix 2

Characterization of Terminal Alkyne Monolayers

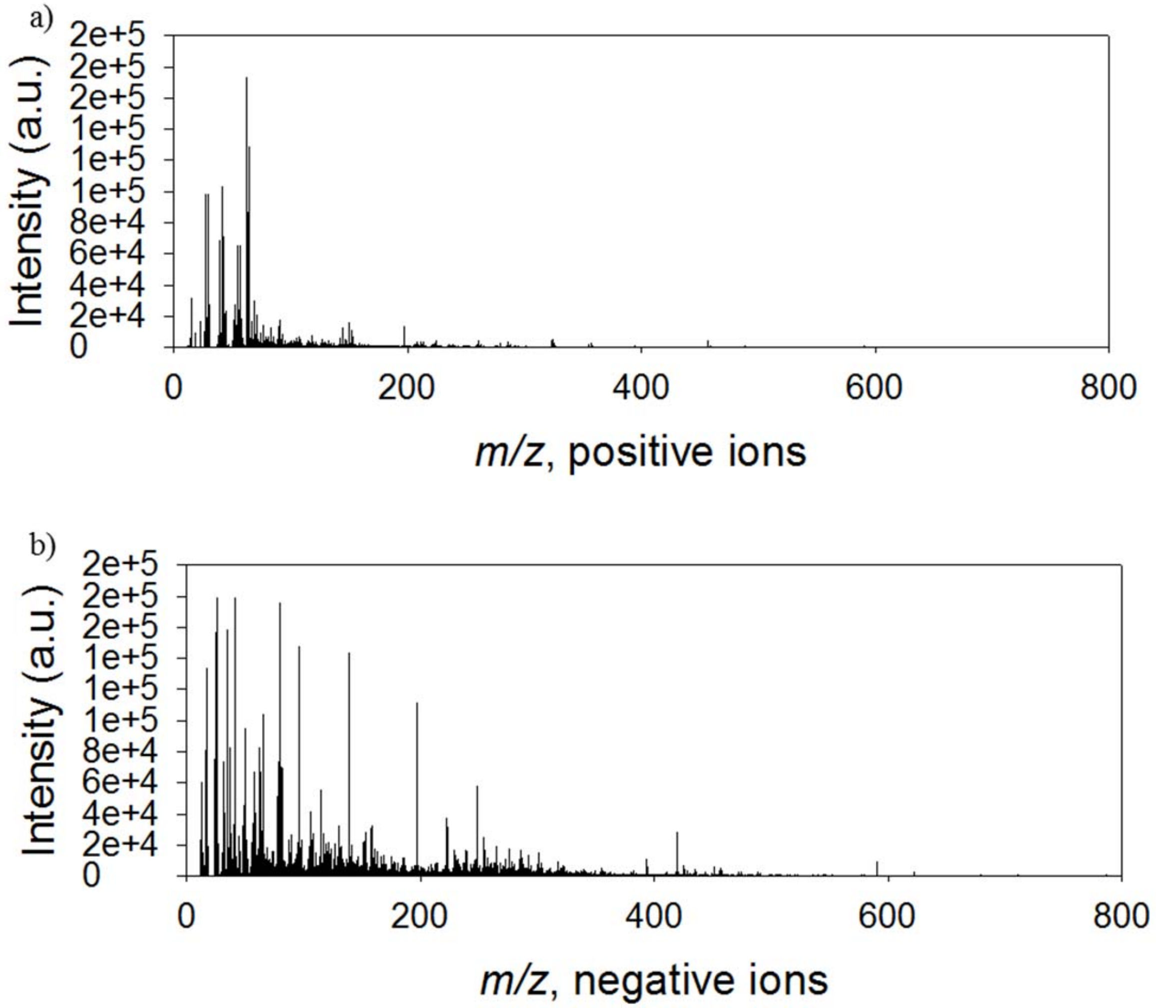

Figure A2.1 The a) positive and b) negative TOF SIMS spectra for octyne adsorbed on Au.

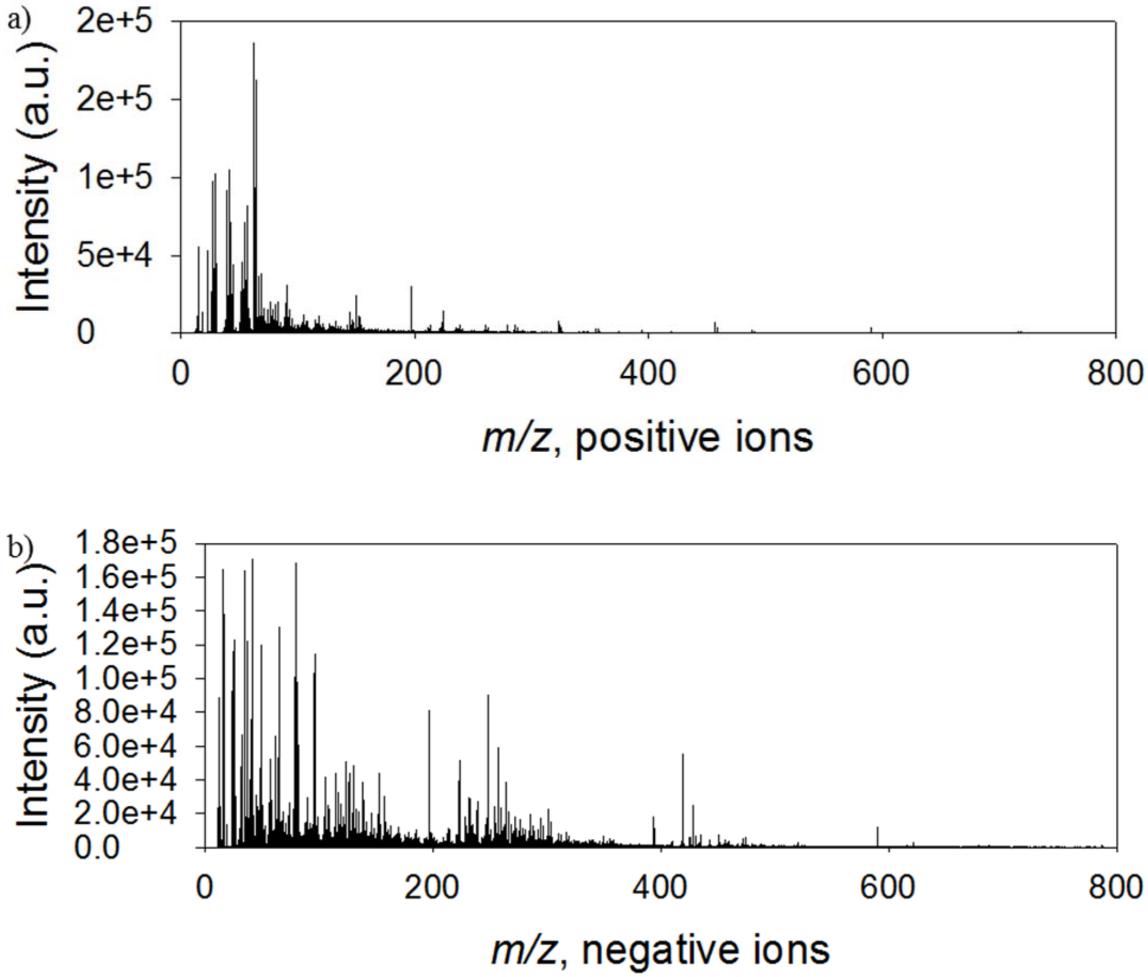

Figure A2.2 The a) positive and b) negative TOF SIMS spectra for decyne adsorbed on Au.

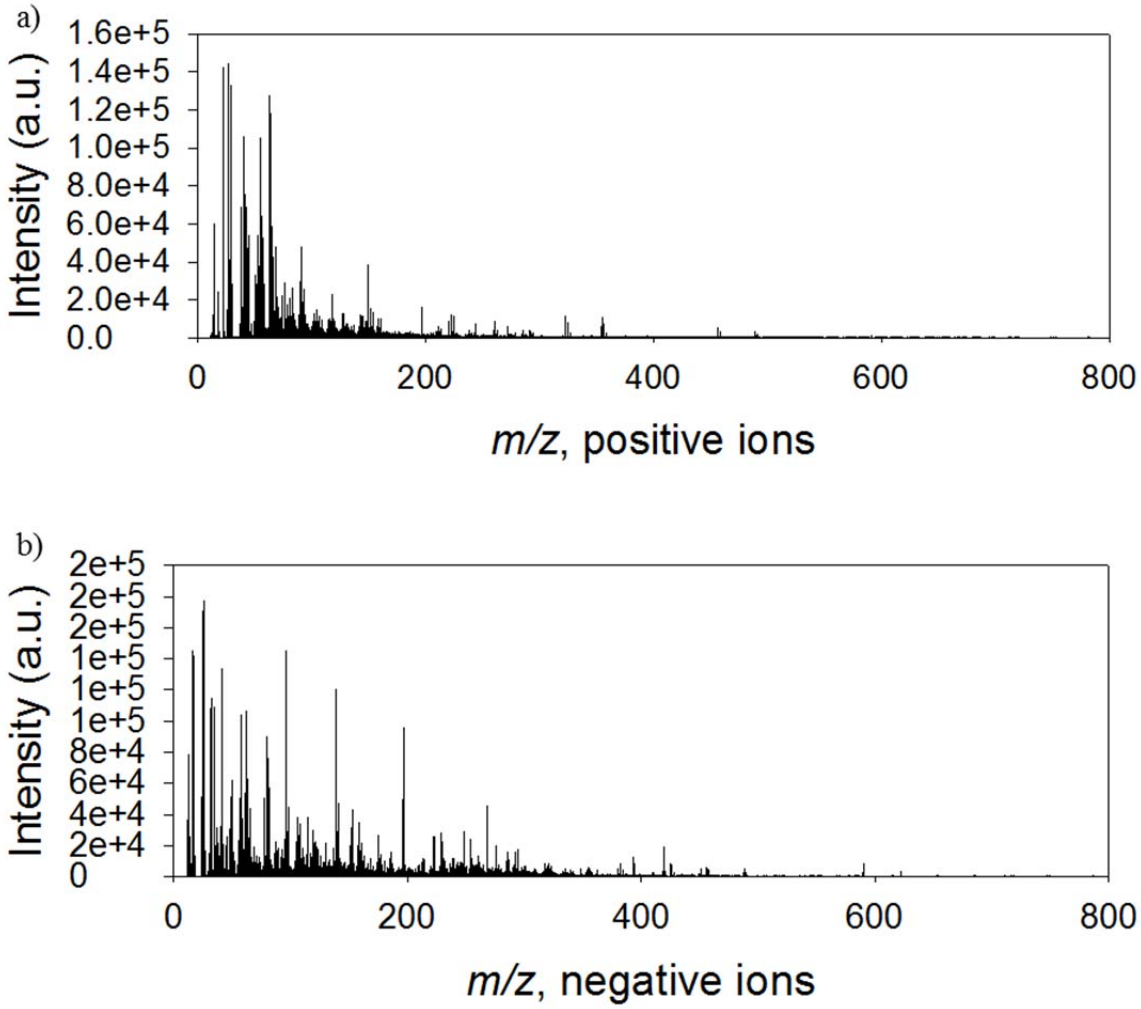

Figure A2.3 The a) positive and b) negative TOF SIMS spectra for dodecyne adsorbed on Au.

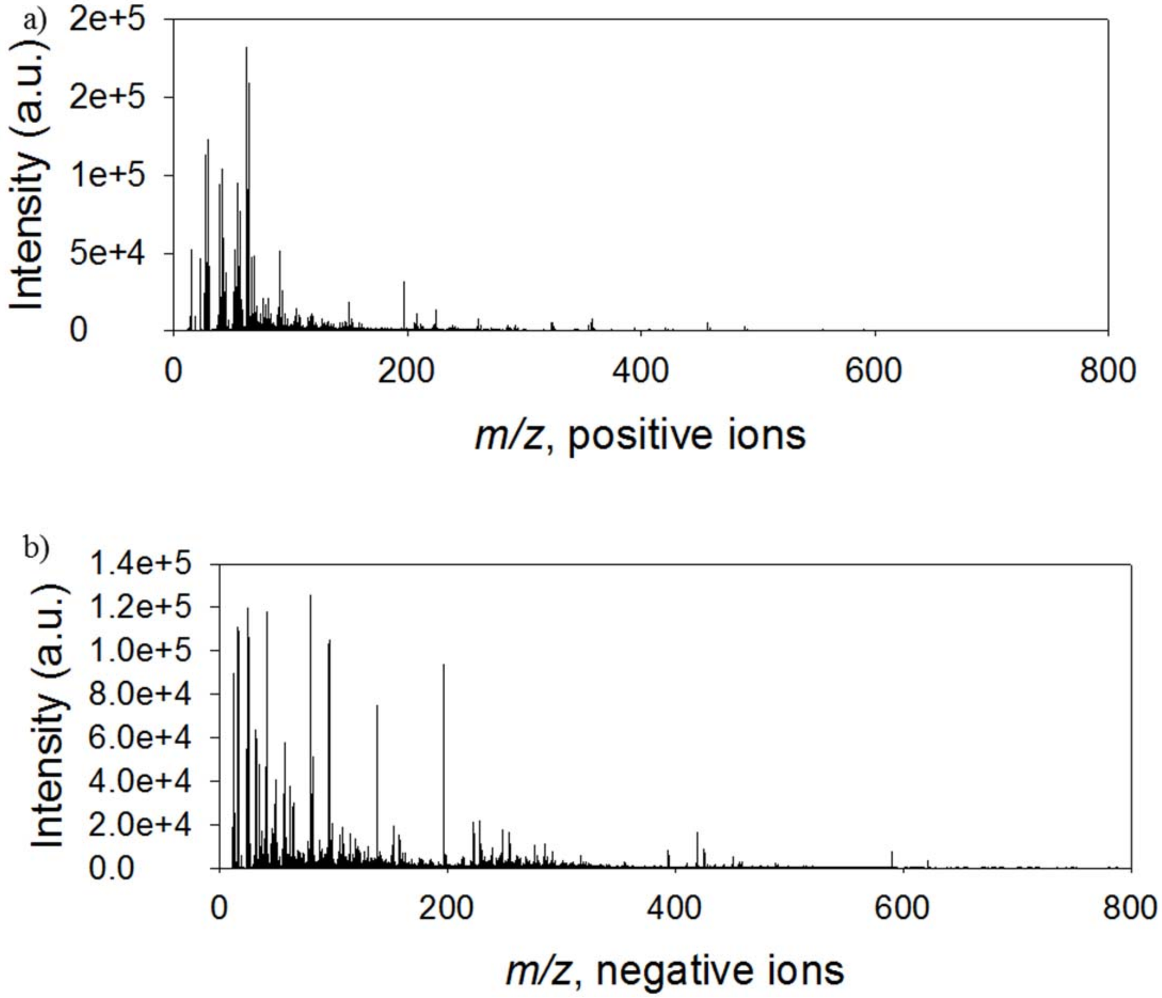

Figure A2.4 The a) positive and b) negative TOF SIMS spectra for tetradecyne adsorbed on Au.

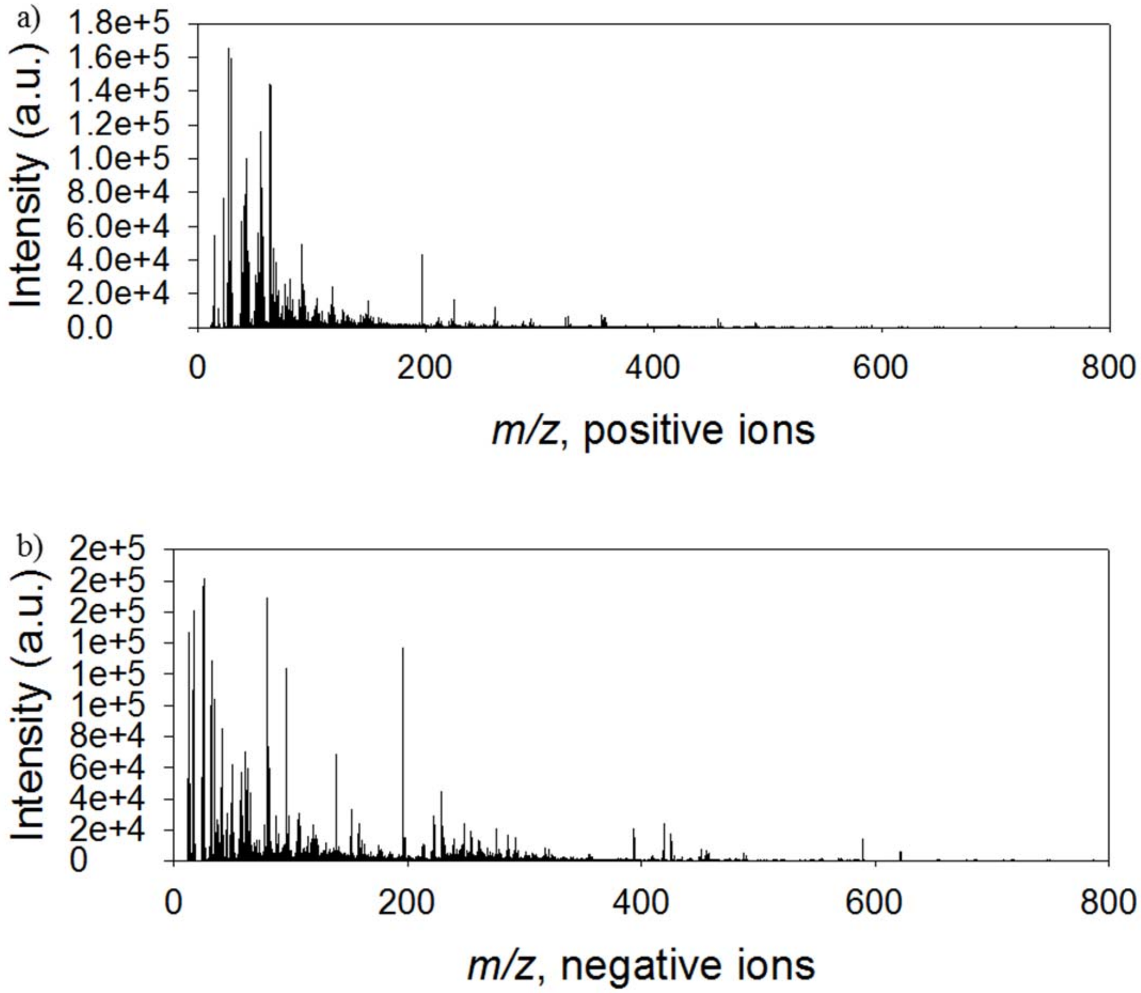

Figure A2.5 The a) positive and b) negative TOF SIMS spectra for heaadecyne adsorbed on Au.

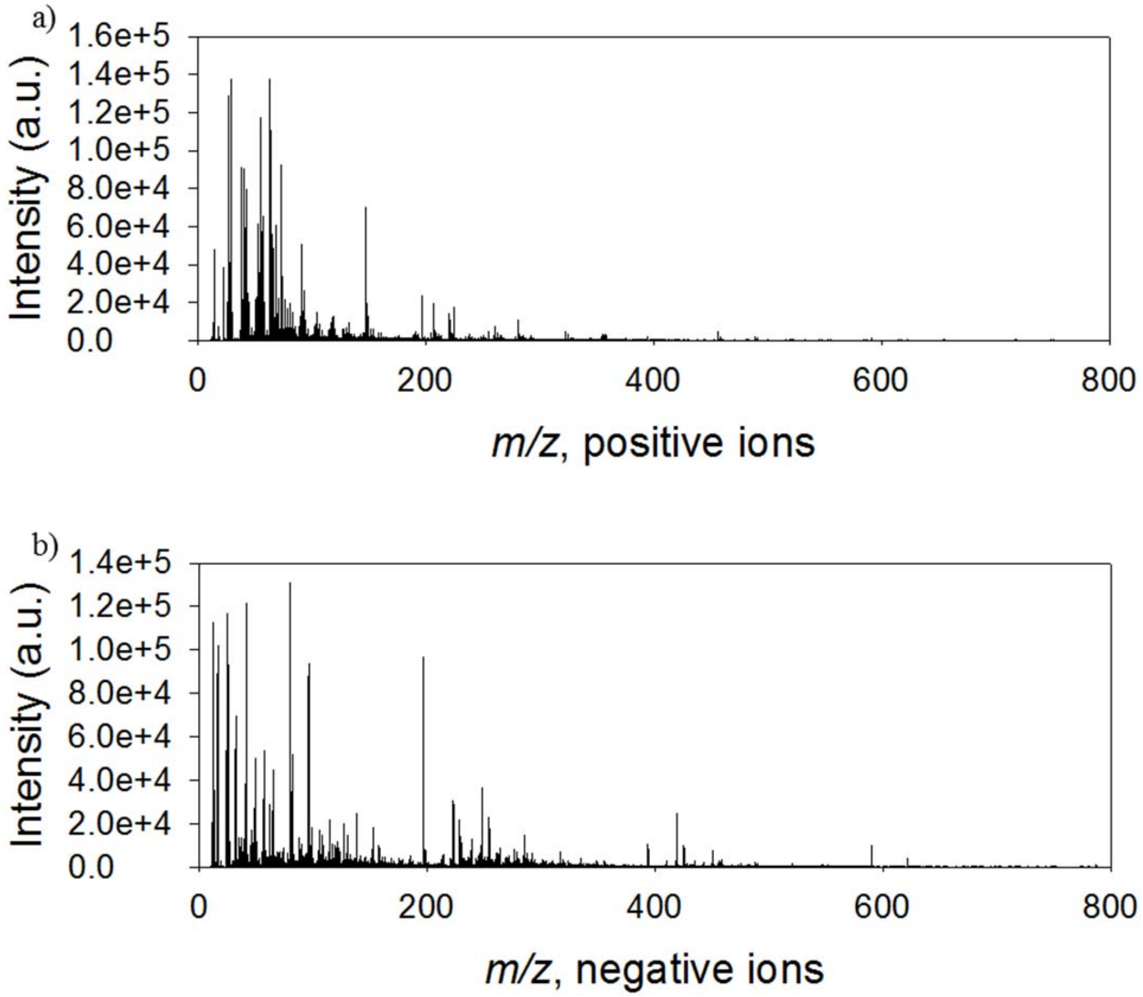

Figure A2.6 The a) positive and b) negative TOF SIMS spectra for octadecyne adsorbed on Au.

Appendix 3

Characterization of Ionic Liquids

All ionic liquids were characterized using ^{1}H NMR spectroscopy, IR spectroscopy and TOF SIMS. The full spectra for those characterizations is below in the following order. For each ionic liquid the positive mass spectrum will be first, followed by the negative mass spectrum, and the IR spectrum. On the second page will be the ^{1}H NMR spectra showing the proton shift. The ionic liquids are ordered alphabetically by acronym. The structure of the ionic liquid is given at the bottom of each page.

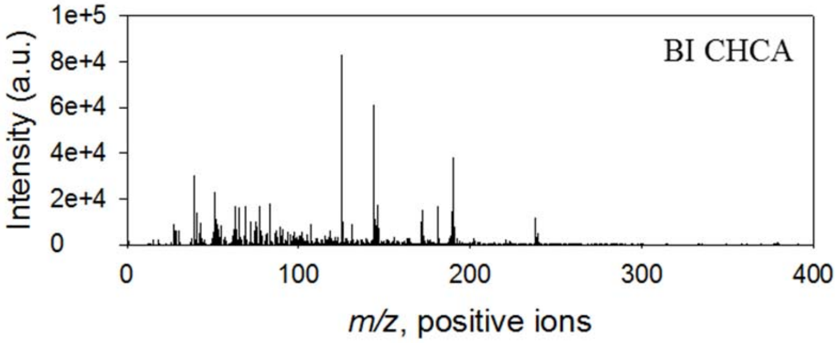
BI CHCA
Intensity (a.u.)
1e+5
8e+4
6e+4
4e+4
2e+4
0
0
100
200
300
400
m/z, positive ions

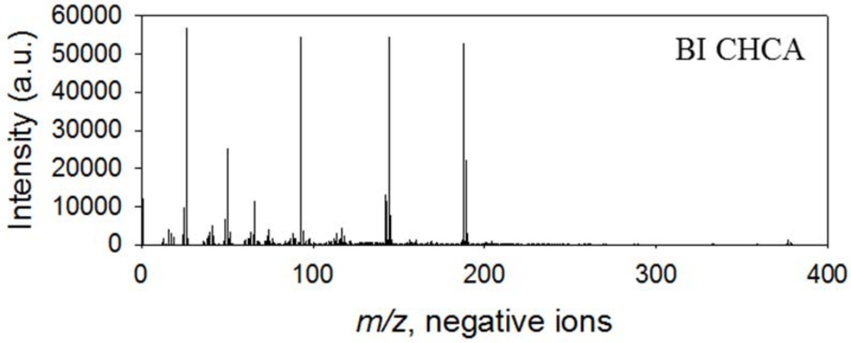
BI CHCA
Intensity (a.u.)
60000
50000
40000
30000
20000
10000
0
0
100
200
300
400
m/z, negative ions

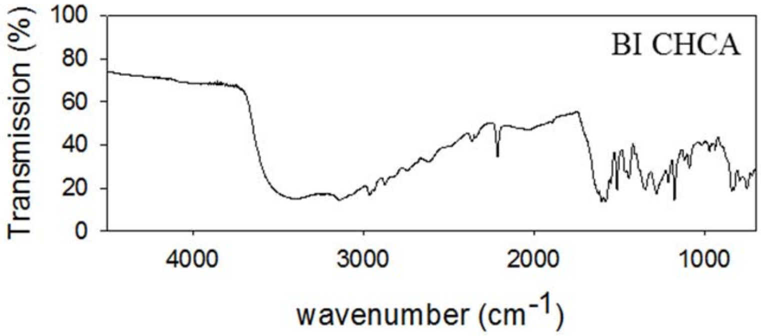
BI CHCA
Transmission (%)
100
80
60
40
20
0
4000
3000
2000
1000
wavenumber (cm-1)

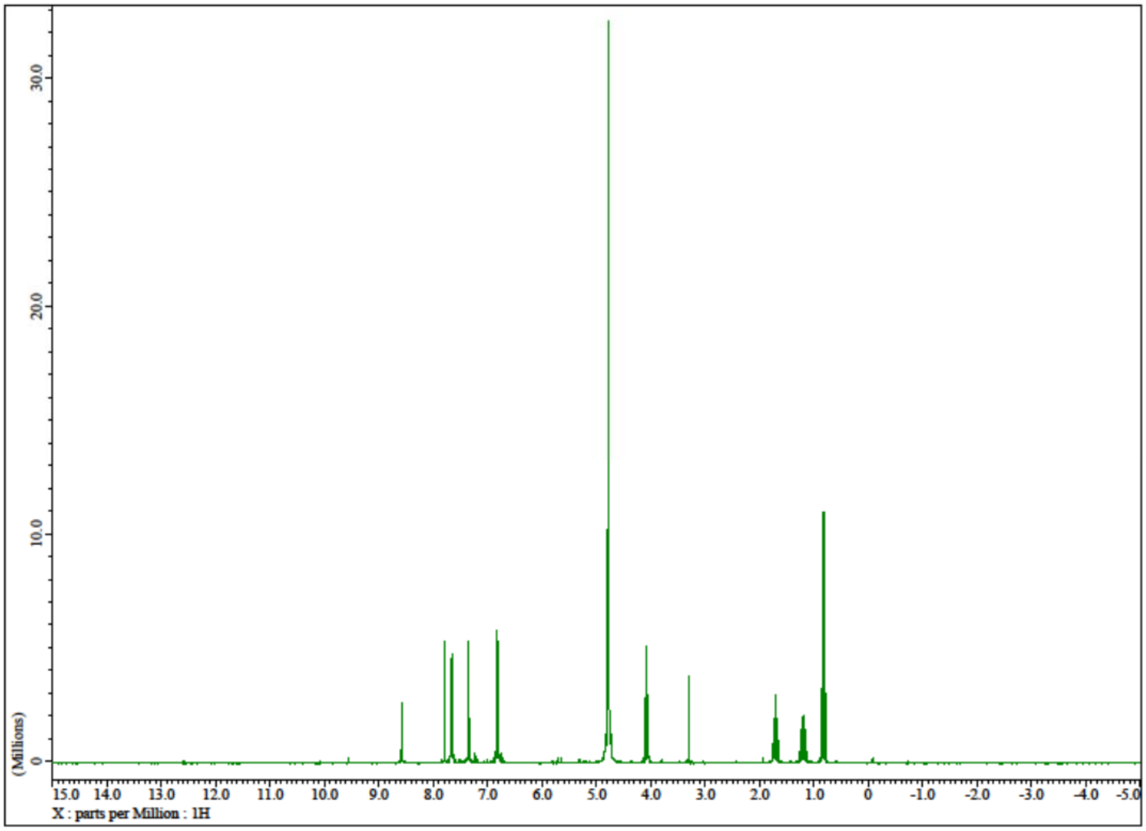
(Millions)
30.0
20.0
10.0
0
15.0
14.0
13.0
12.0
11.0
10.0
9.0
8.0
7.0
6.0
5.0
4.0
3.0
2.0
1.0
0
-1.0
-2.0
-3.0
-4.0
-5.0
X : parts per Million : 1H

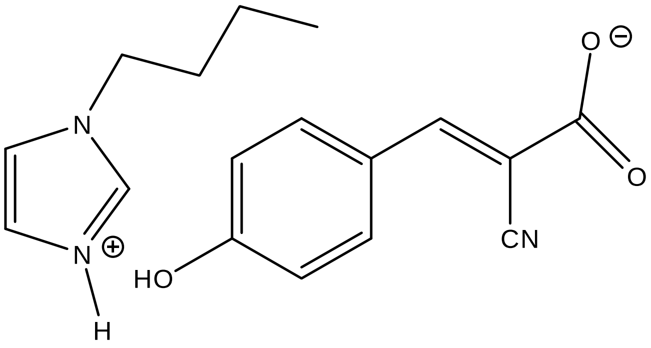
N
N
H
HO
O
O
CN

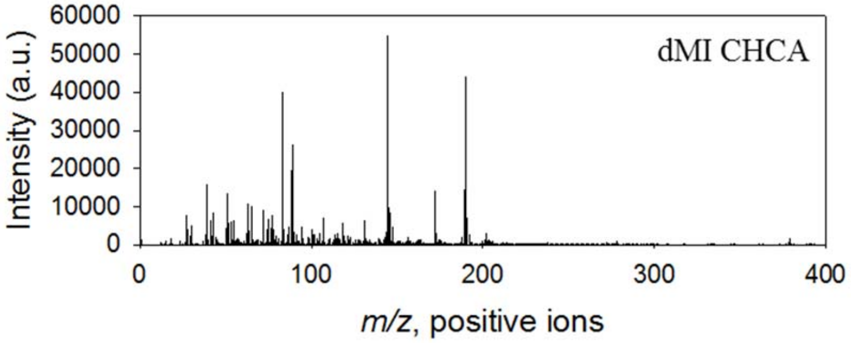
60000
50000
40000
30000
20000
10000
0
Intensity (a.u.)
dMI CHCA
0
100
200
300
400
m/z, positive ions

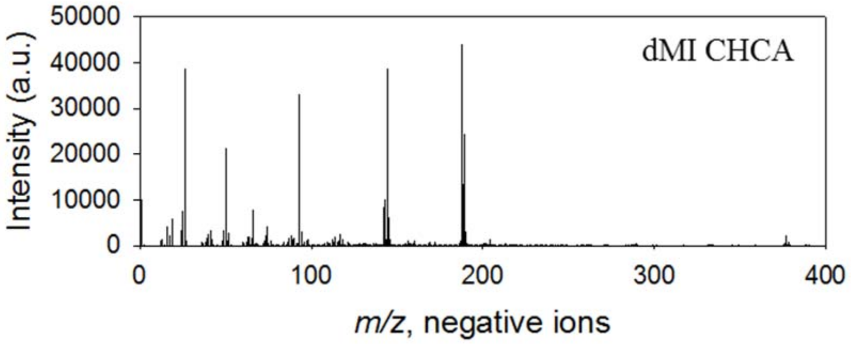
50000
40000
30000
20000
10000
0
Intensity (a.u.)
dMI CHCA
0
100
200
300
400
m/z, negative ions

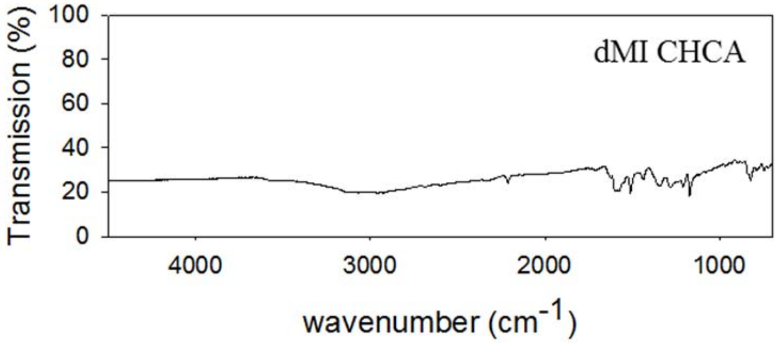
100
80
60
40
20
0
Transmission (%)
dMI CHCA
4000
3000
2000
1000
wavenumber (cm-1)

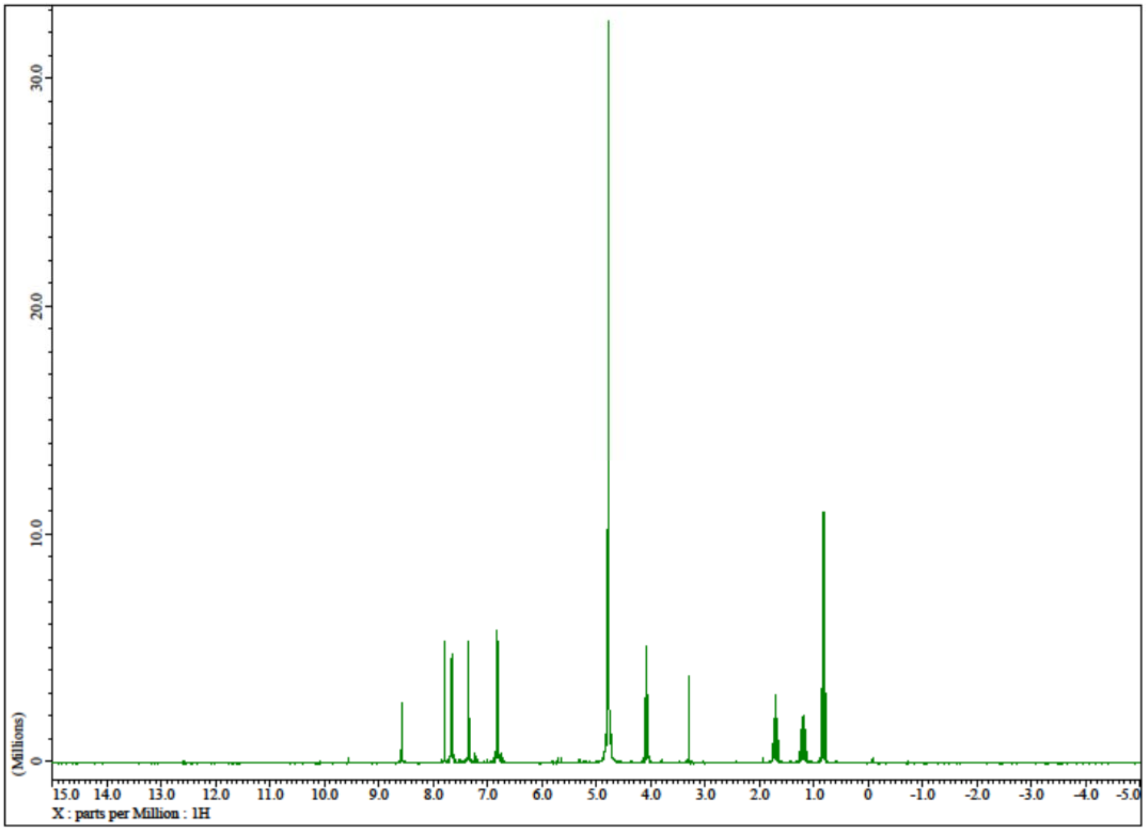
(Millions)
0
10.0
20.0
30.0
15.0 14.0 13.0 12.0 11.0 10.0 9.0 8.0 7.0 6.0 5.0 4.0 3.0 2.0 1.0 0 -1.0 -2.0 -3.0 -4.0 -5.0
X : parts per Million : 1H

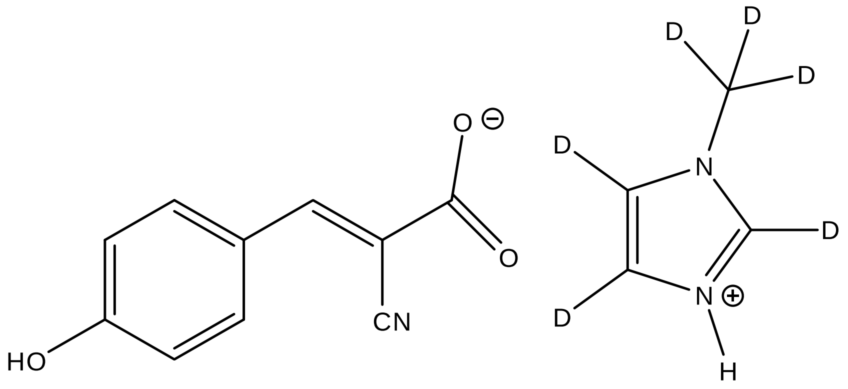
HO
CN
O
O
D
D
D
D
N
D
N
H
D

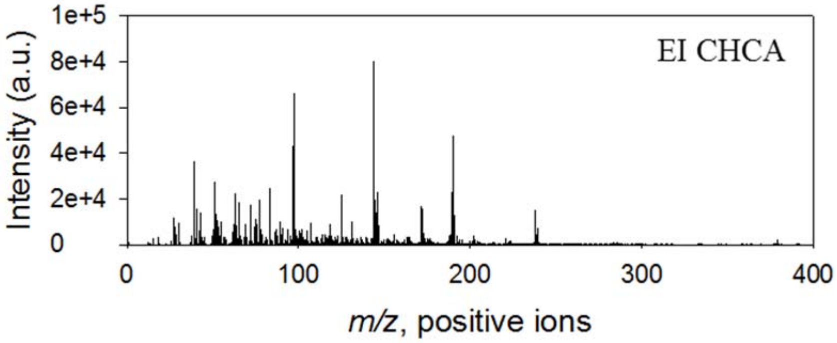
EI CHCA
Intensity (a.u.)
1e+5
8e+4
6e+4
4e+4
2e+4
0
0
100
200
300
400
m/z, positive ions

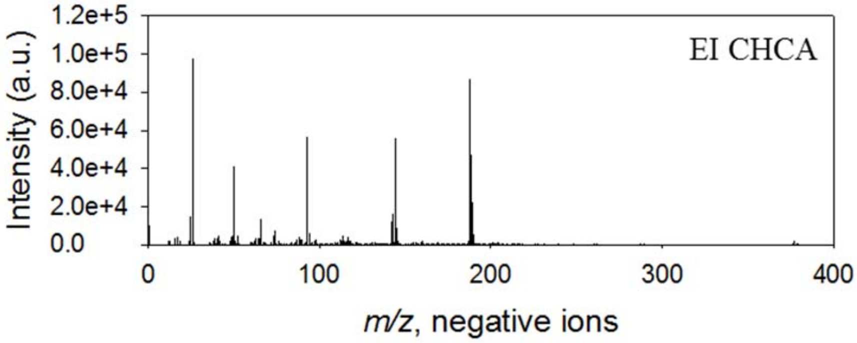
EI CHCA
Intensity (a.u.)
1.2e+5
1.0e+5
8.0e+4
6.0e+4
4.0e+4
2.0e+4
0.0
0
100
200
300
400
m/z, negative ions

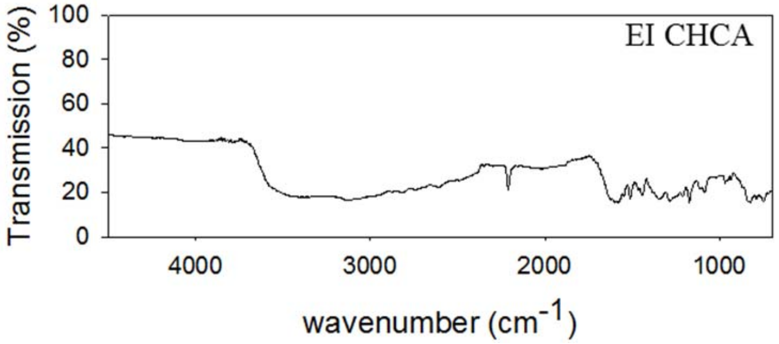
EI CHCA
Transmission (%)
100
80
60
40
20
0
4000
3000
2000
1000
wavenumber (cm-1)

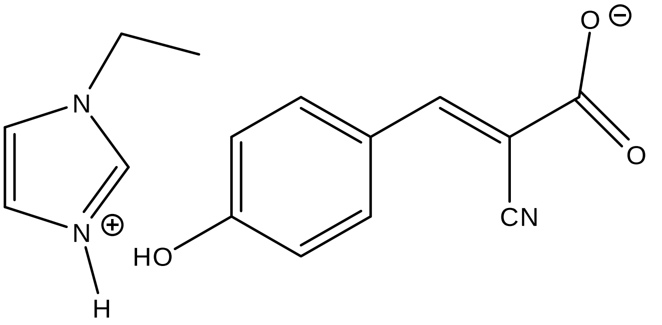
N
N⊕
H
HO
CN
O⊖
O

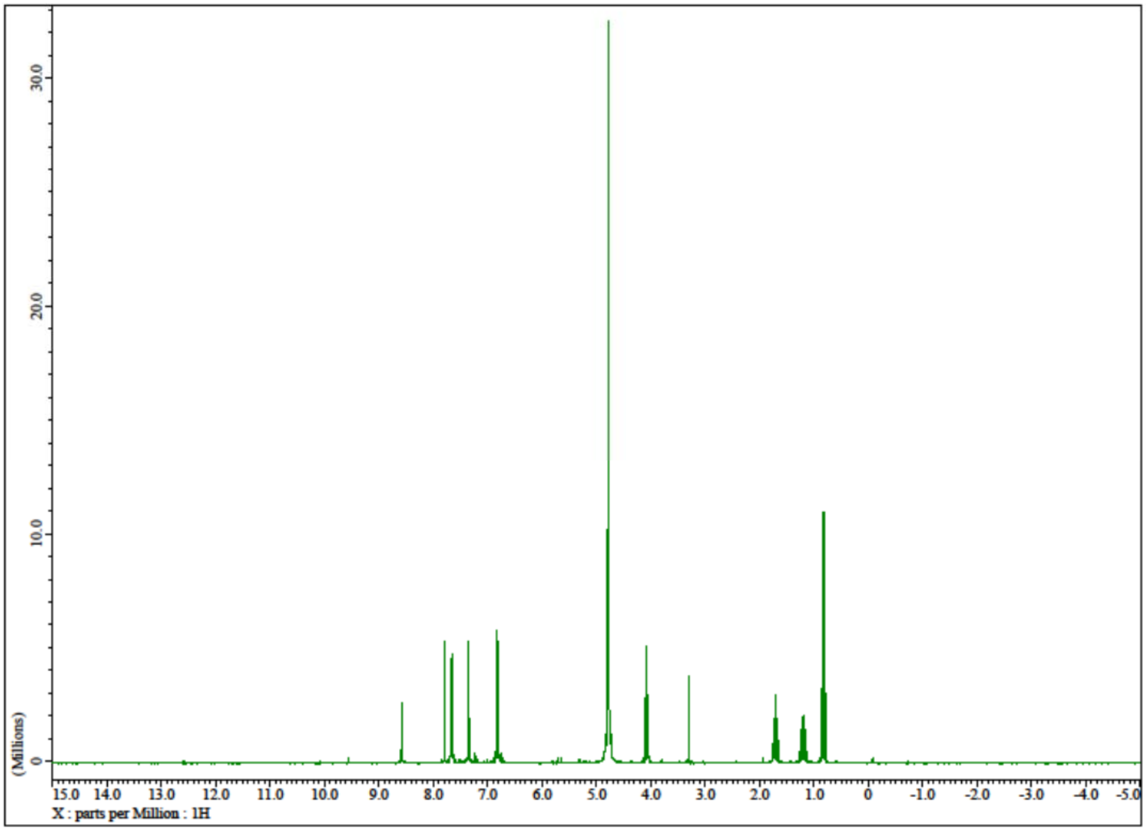
(Millions)
30.0
20.0
10.0
0
15.0 14.0 13.0 12.0 11.0 10.0 9.0 8.0 7.0 6.0 5.0 4.0 3.0 2.0 1.0 0 -1.0 -2.0 -3.0 -4.0 -5.0
X : parts per Million : 1H

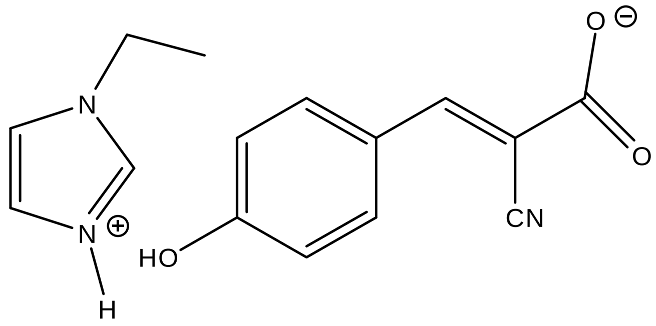
N
N
H
HO
O
O
CN

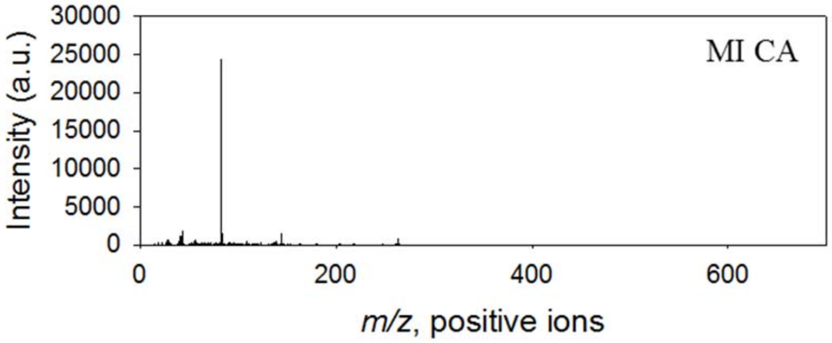
MI CA
Intensity (a.u.)
30000
25000
20000
15000
10000
5000
0
0
200
400
600
m/z, positive ions

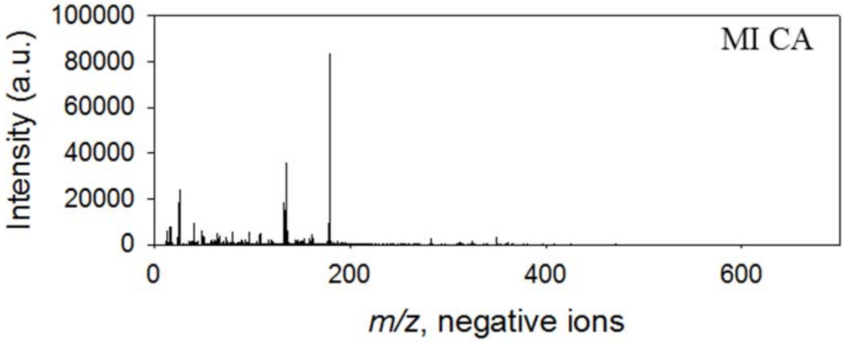
MI CA
Intensity (a.u.)
100000
80000
60000
40000
20000
0
0
200
400
600
m/z, negative ions

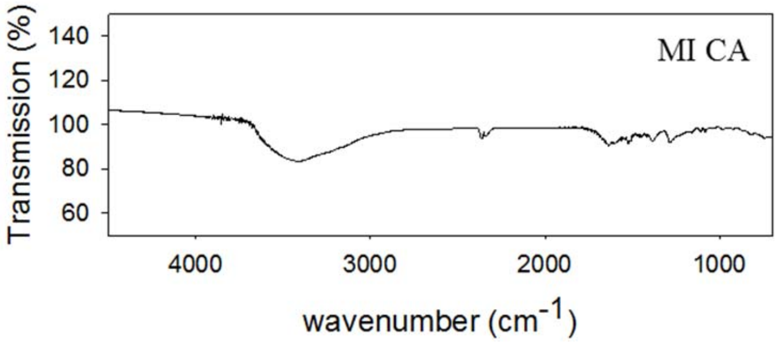
MI CA
Transmission (%)
140
120
100
80
60
4000
3000
2000
1000
wavenumber (cm-1)

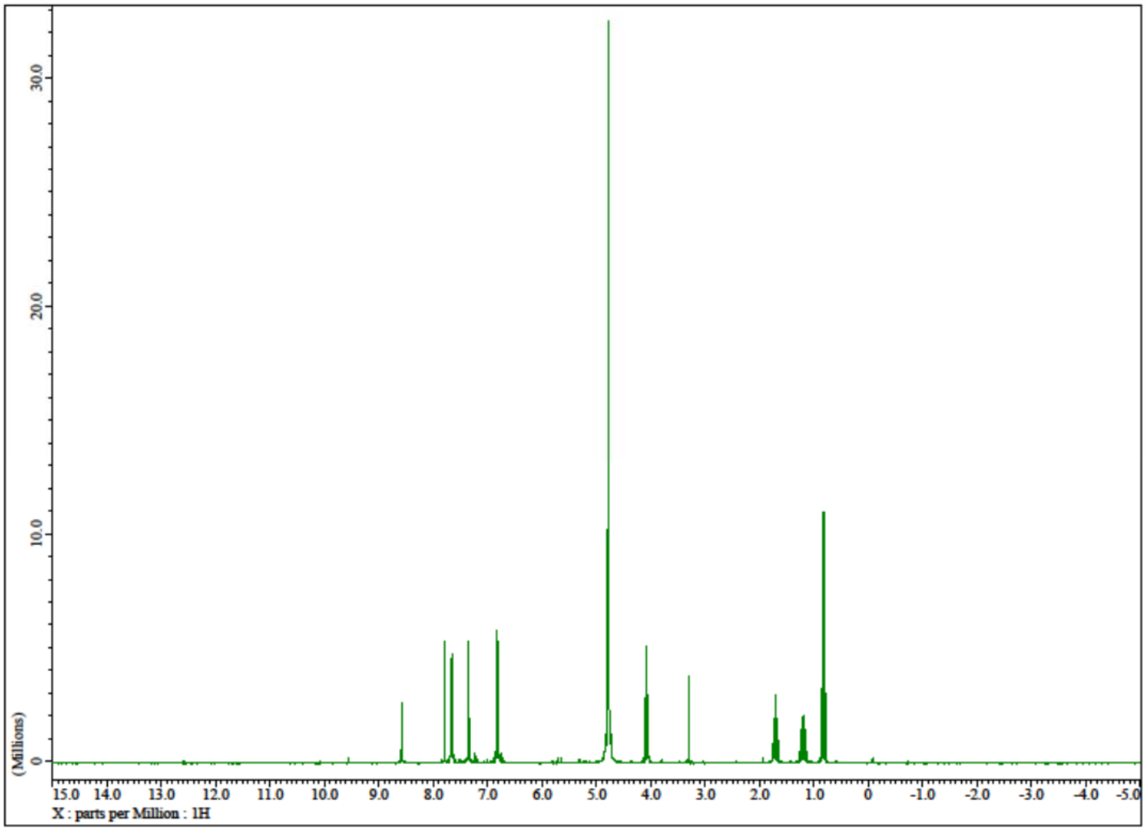
(Millions)
30.0
20.0
10.0
0
15.0
14.0
13.0
12.0
11.0
10.0
9.0
8.0
7.0
6.0
5.0
4.0
3.0
2.0
1.0
0
-1.0
-2.0
-3.0
-4.0
-5.0
X : parts per Million : 1H

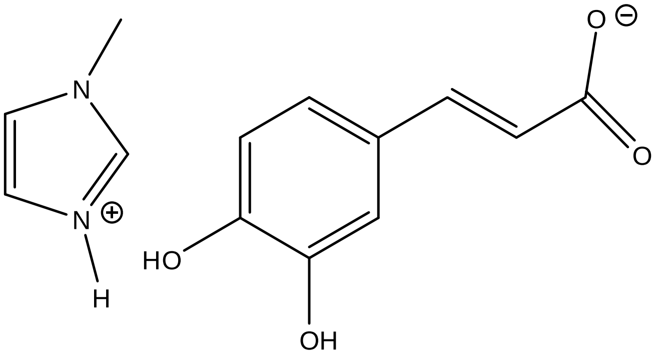
N
N
H
HO
OH
O
O

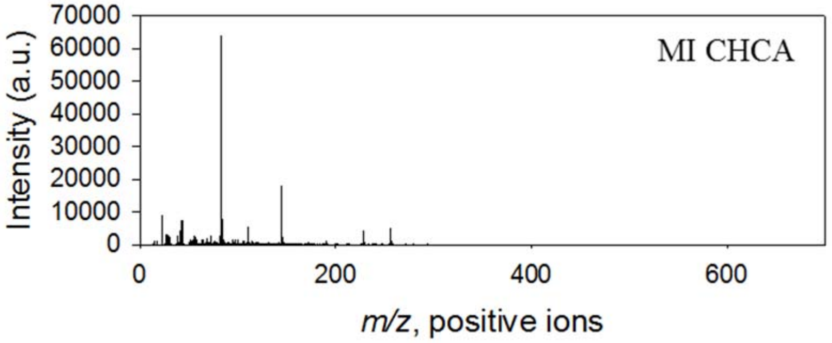
MI CHCA
Intensity (a.u.)
70000
60000
50000
40000
30000
20000
10000
0
0
200
400
600
m/z, positive ions

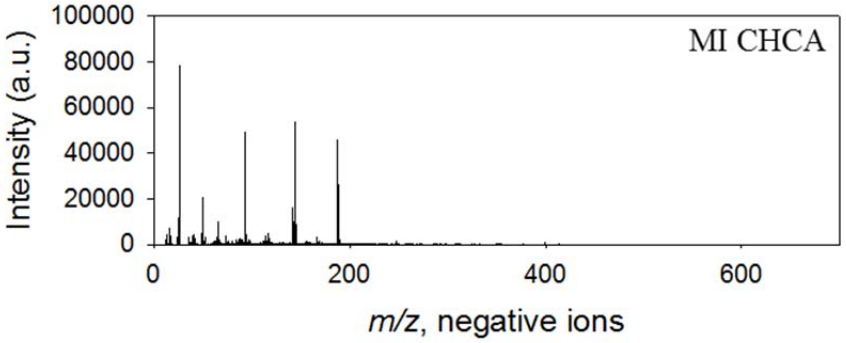
MI CHCA
Intensity (a.u.)
100000
80000
60000
40000
20000
0
0
200
400
600
m/z, negative ions

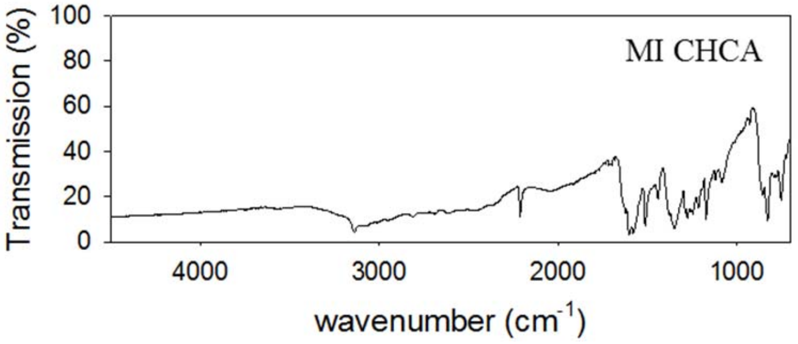
MI CHCA
Transmission (%)
100
80
60
40
20
0
4000
3000
2000
1000
wavenumber (cm-1)

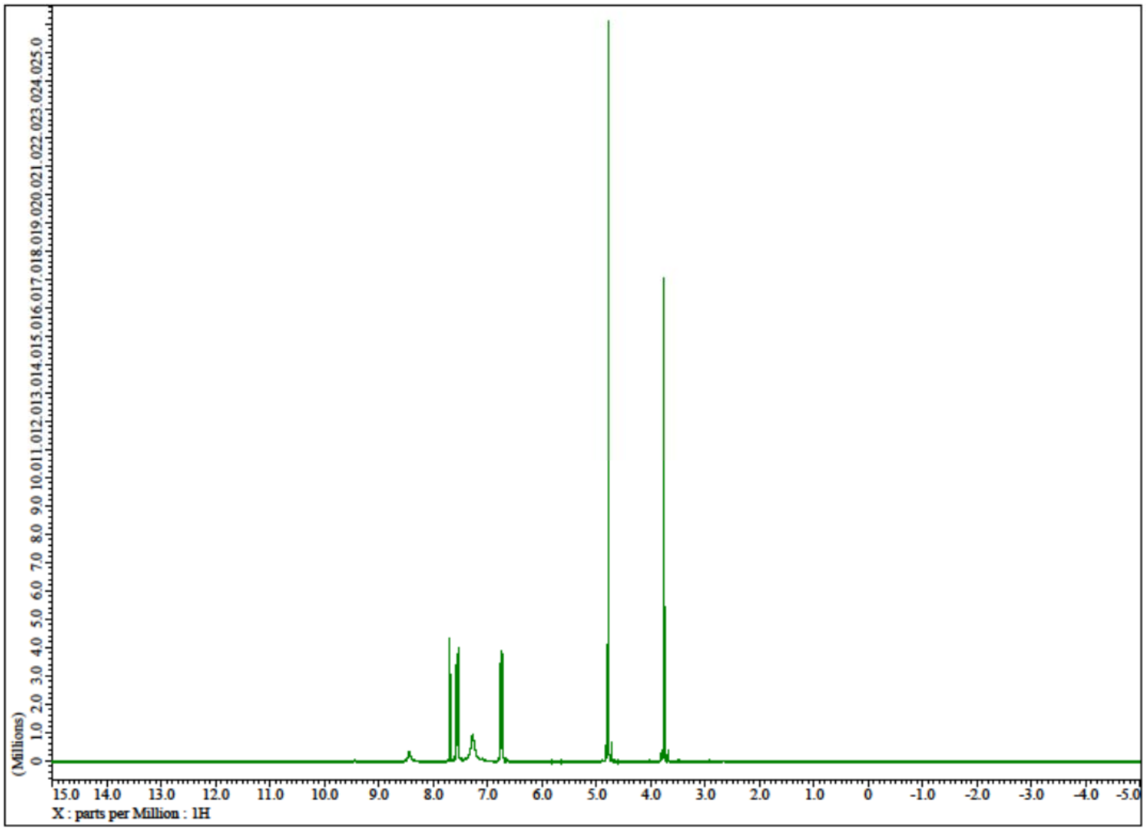
(Millions)
0
1.0
2.0
3.0
4.0
5.0
6.0
7.0
8.0
9.0
10.0
11.0
12.0
13.0
14.0
15.0
16.0
17.0
18.0
19.0
20.0
21.0
22.0
23.0
24.0
25.0
15.0 14.0 13.0 12.0 11.0 10.0 9.0 8.0 7.0 6.0 5.0 4.0 3.0 2.0 1.0 0 -1.0 -2.0 -3.0 -4.0 -5.0
X : parts per Million : 1H

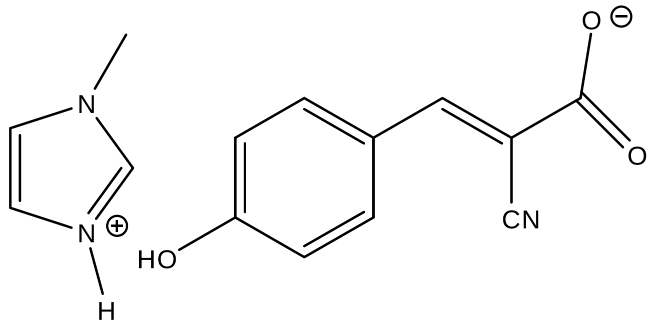
N
N⊕
H
HO
O⊖
O
CN

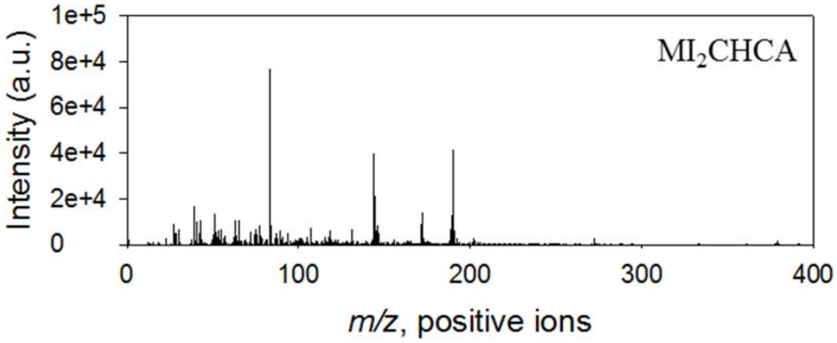
MI$_2$CHCA
Intensity (a.u.)
1e+5
8e+4
6e+4
4e+4
2e+4
0
0
100
200
300
400
m/z, positive ions

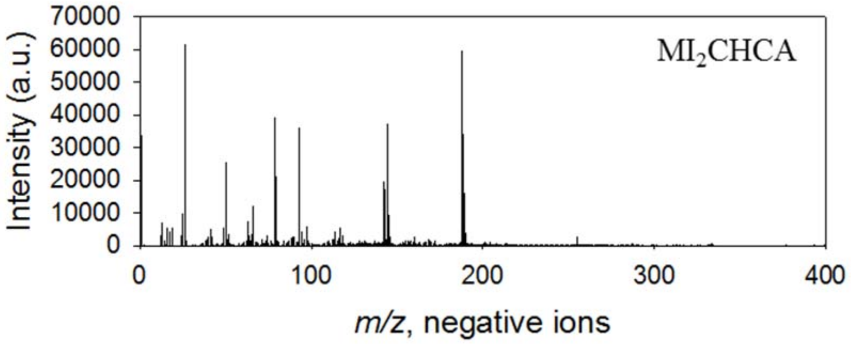
MI$_2$CHCA
Intensity (a.u.)
70000
60000
50000
40000
30000
20000
10000
0
0
100
200
300
400
m/z, negative ions

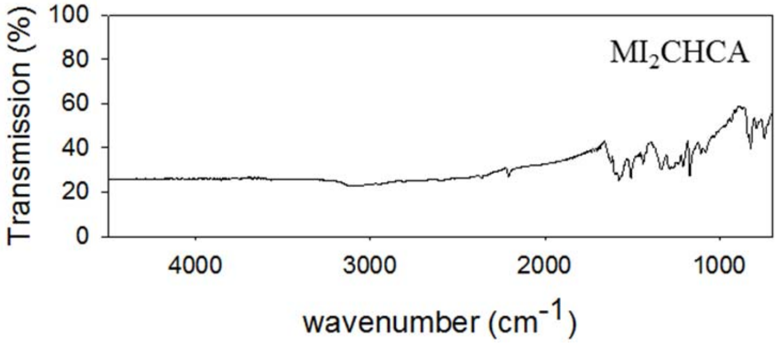
MI$_2$CHCA
Transmission (%)
100
80
60
40
20
0
4000
3000
2000
1000
wavenumber (cm^{-1})

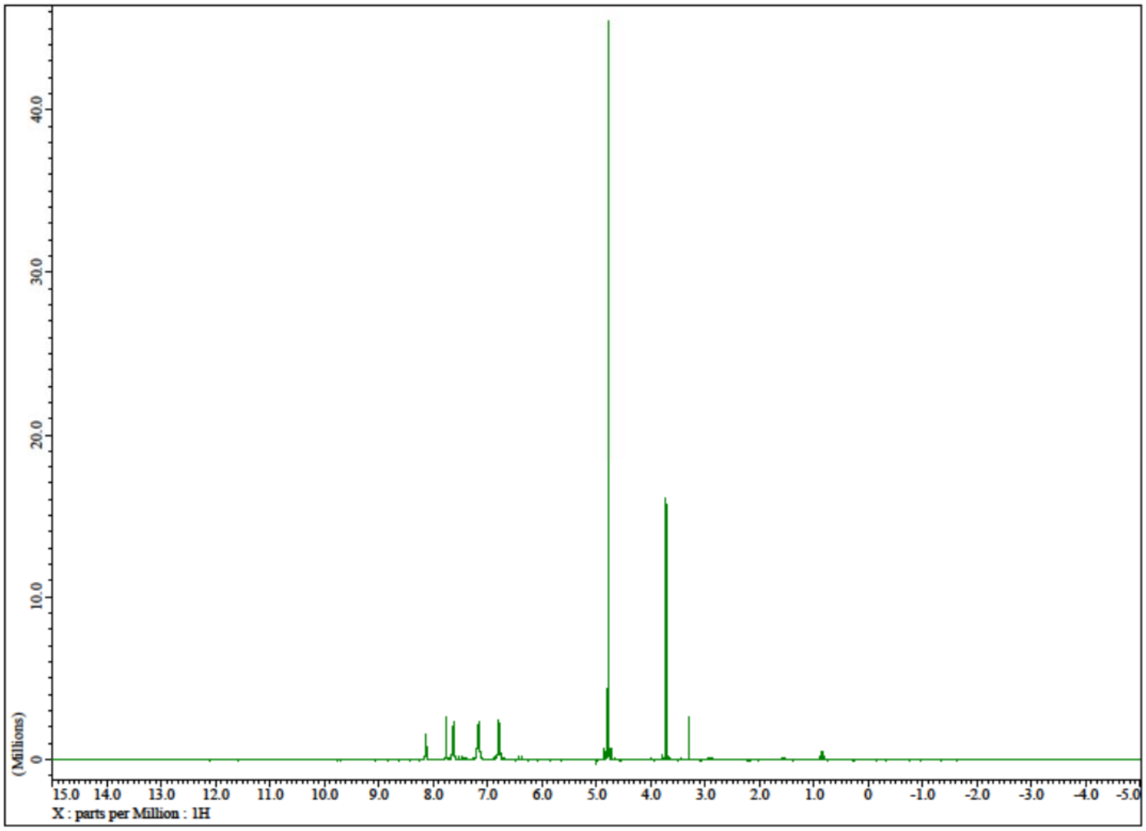
(Millions)
0
10.0
20.0
30.0
40.0
15.0 14.0 13.0 12.0 11.0 10.0 9.0 8.0 7.0 6.0 5.0 4.0 3.0 2.0 1.0 0 -1.0 -2.0 -3.0 -4.0 -5.0
X : parts per Million : 1H

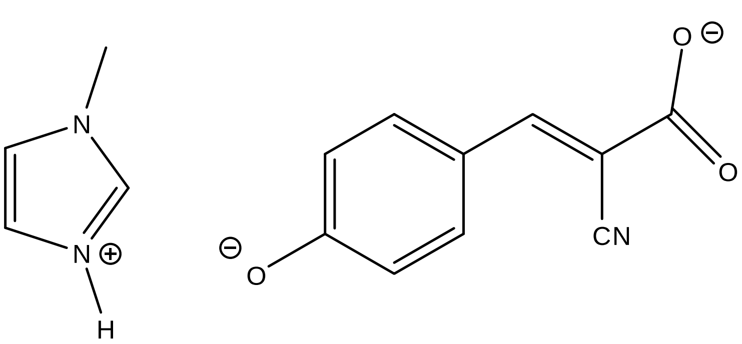
N
N ⊕
H
⊖ O
O ⊖
O
CN
N
N ⊕
H

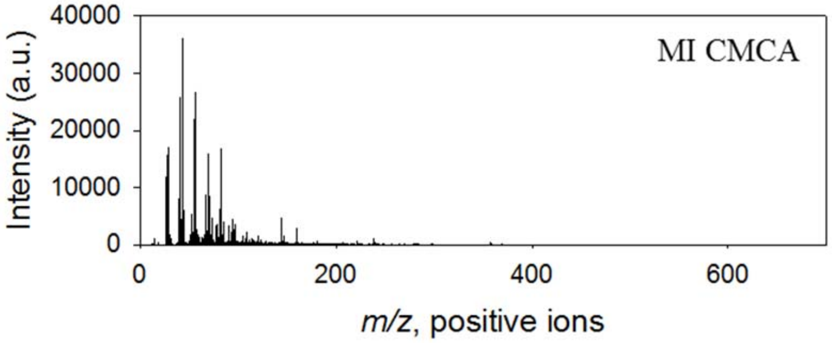
MI CMCA
Intensity (a.u.)
40000
30000
20000
10000
0
0
200
400
600
m/z, positive ions

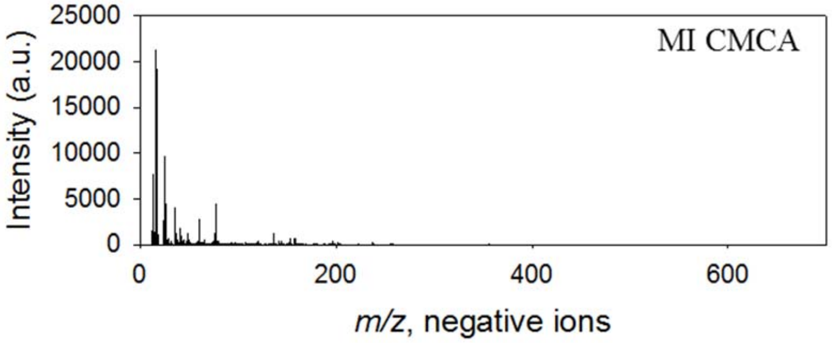
MI CMCA
Intensity (a.u.)
25000
20000
15000
10000
5000
0
0
200
400
600
m/z, negative ions

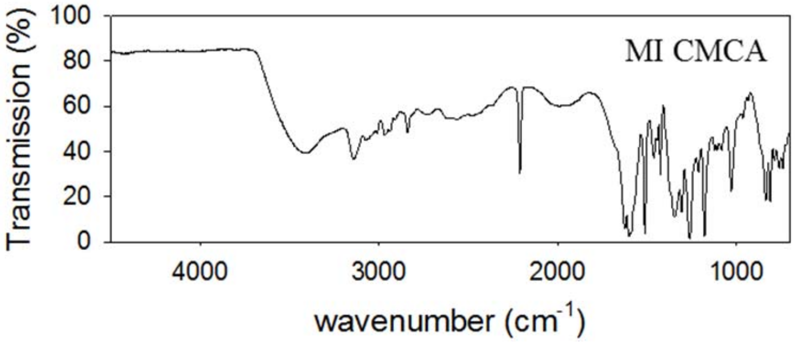
MI CMCA
Transmission (%)
100
80
60
40
20
0
4000
3000
2000
1000
wavenumber (cm^{-1})

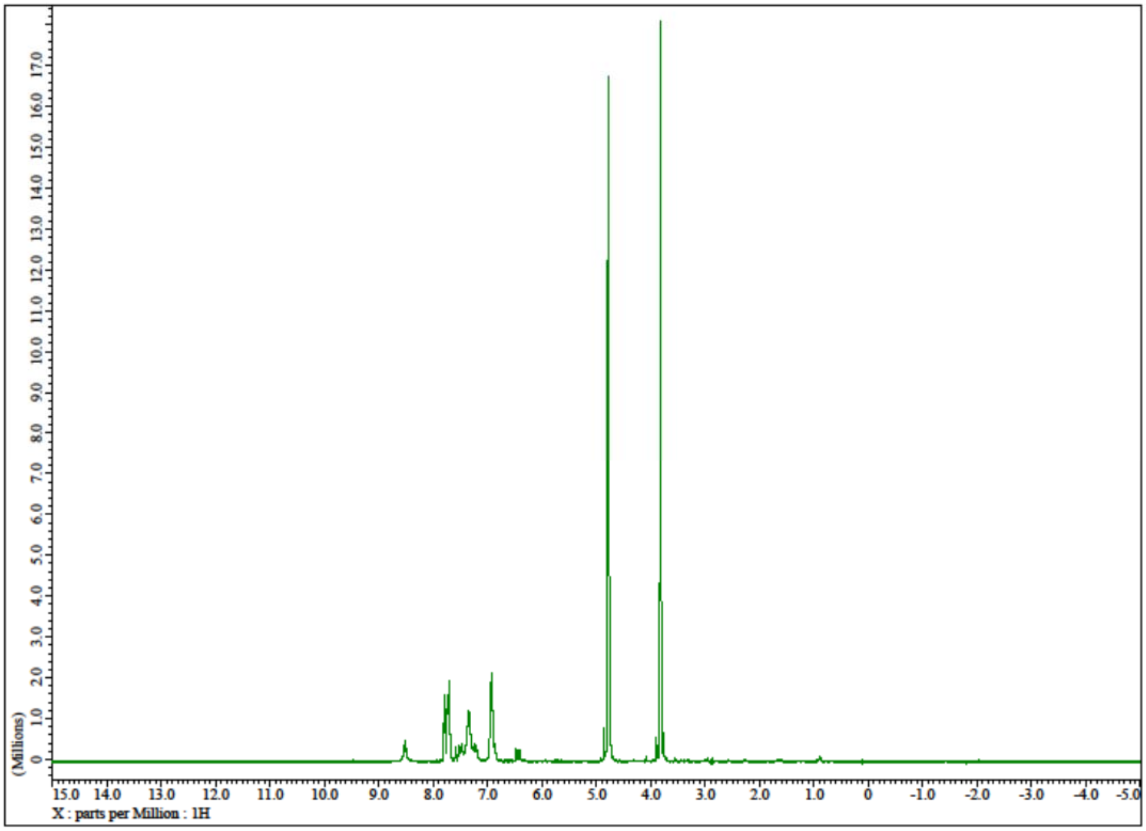
(Millions)
0
1.0
2.0
3.0
4.0
5.0
6.0
7.0
8.0
9.0
10.0
11.0
12.0
13.0
14.0
15.0
16.0
17.0
15.0 14.0 13.0 12.0 11.0 10.0 9.0 8.0 7.0 6.0 5.0 4.0 3.0 2.0 1.0 0 -1.0 -2.0 -3.0 -4.0 -5.0
X : parts per Million : 1H

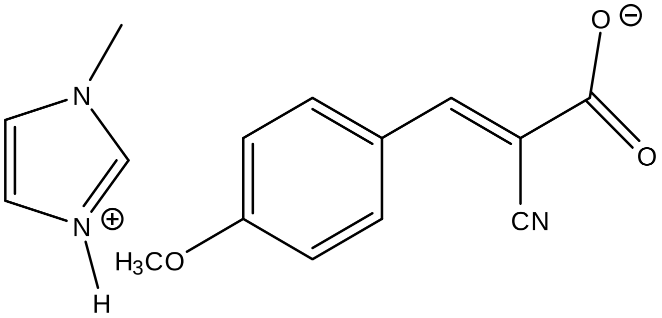
N
N
H
H3CO
O
O
CN

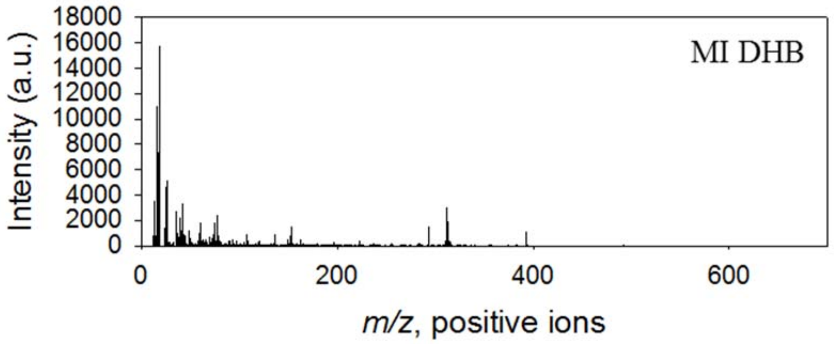
MI DHB
Intensity (a.u.)
18000
16000
14000
12000
10000
8000
6000
4000
2000
0
0
200
400
600
m/z, positive ions

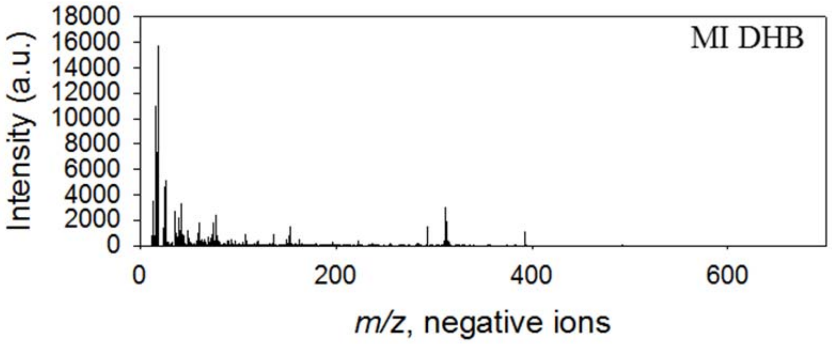
MI DHB
Intensity (a.u.)
18000
16000
14000
12000
10000
8000
6000
4000
2000
0
0
200
400
600
m/z, negative ions

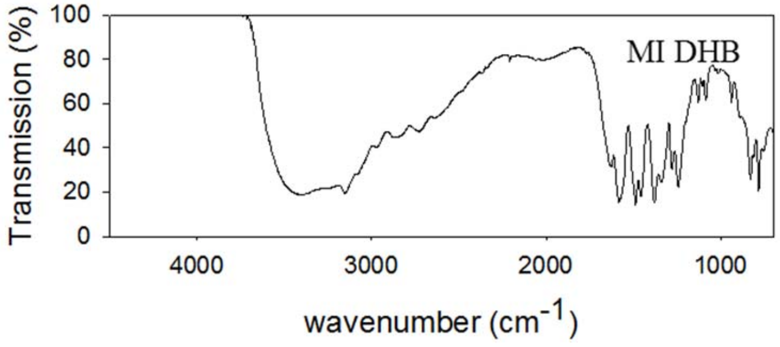
MI DHB
Transmission (%)
100
80
60
40
20
0
4000
3000
2000
1000
wavenumber (cm-1)

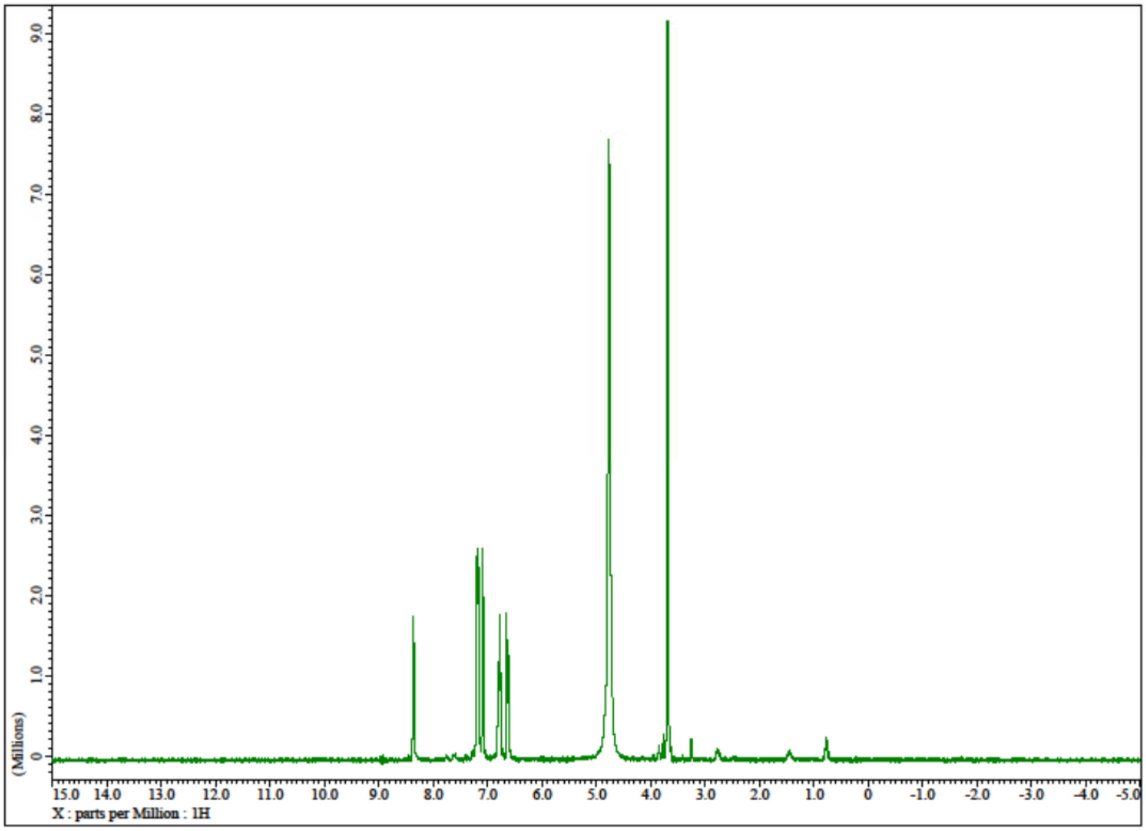
(Millions)
9.0
8.0
7.0
6.0
5.0
4.0
3.0
2.0
1.0
0
15.0 14.0 13.0 12.0 11.0 10.0 9.0 8.0 7.0 6.0 5.0 4.0 3.0 2.0 1.0 0 -1.0 -2.0 -3.0 -4.0 -5.0
X : parts per Million : 1H

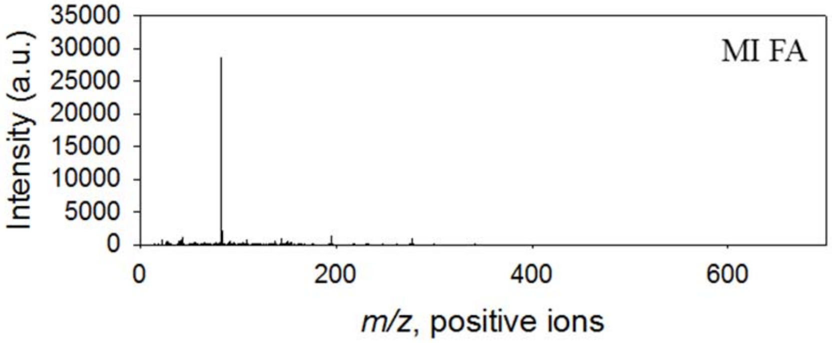
MI FA
Intensity (a.u.)
0
5000
10000
15000
20000
25000
30000
35000
0
200
400
600
m/z, positive ions

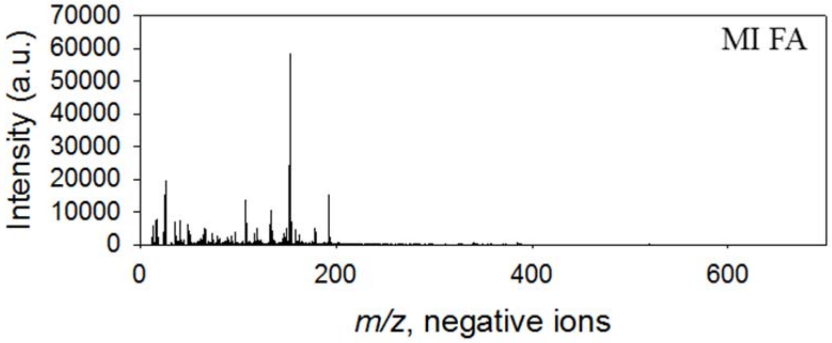
MI FA
Intensity (a.u.)
0
10000
20000
30000
40000
50000
60000
70000
0
200
400
600
m/z, negative ions

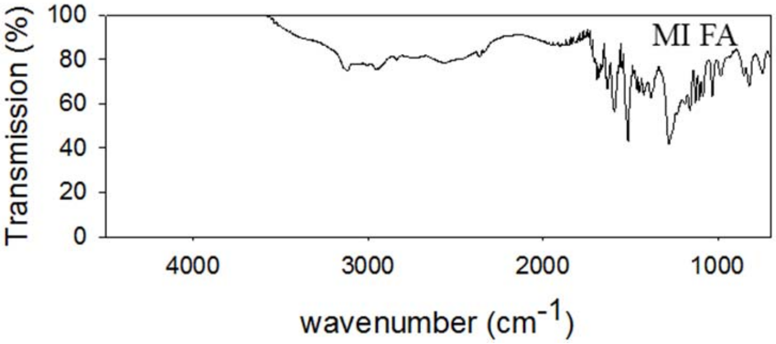
MI FA
Transmission (%)
0
20
40
60
80
100
4000
3000
2000
1000
wavenumber (cm-1)

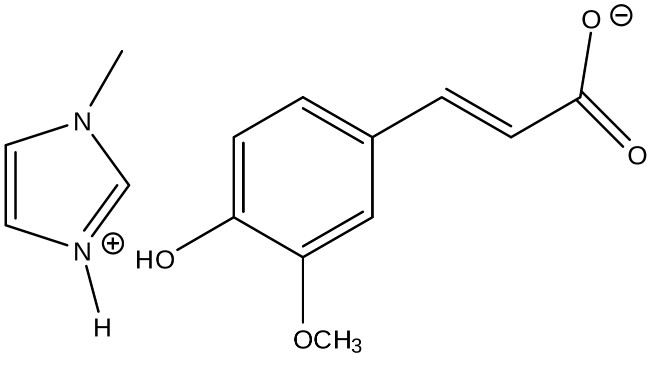
N
N
⊕
H
HO
OCH3
O ⊖
O

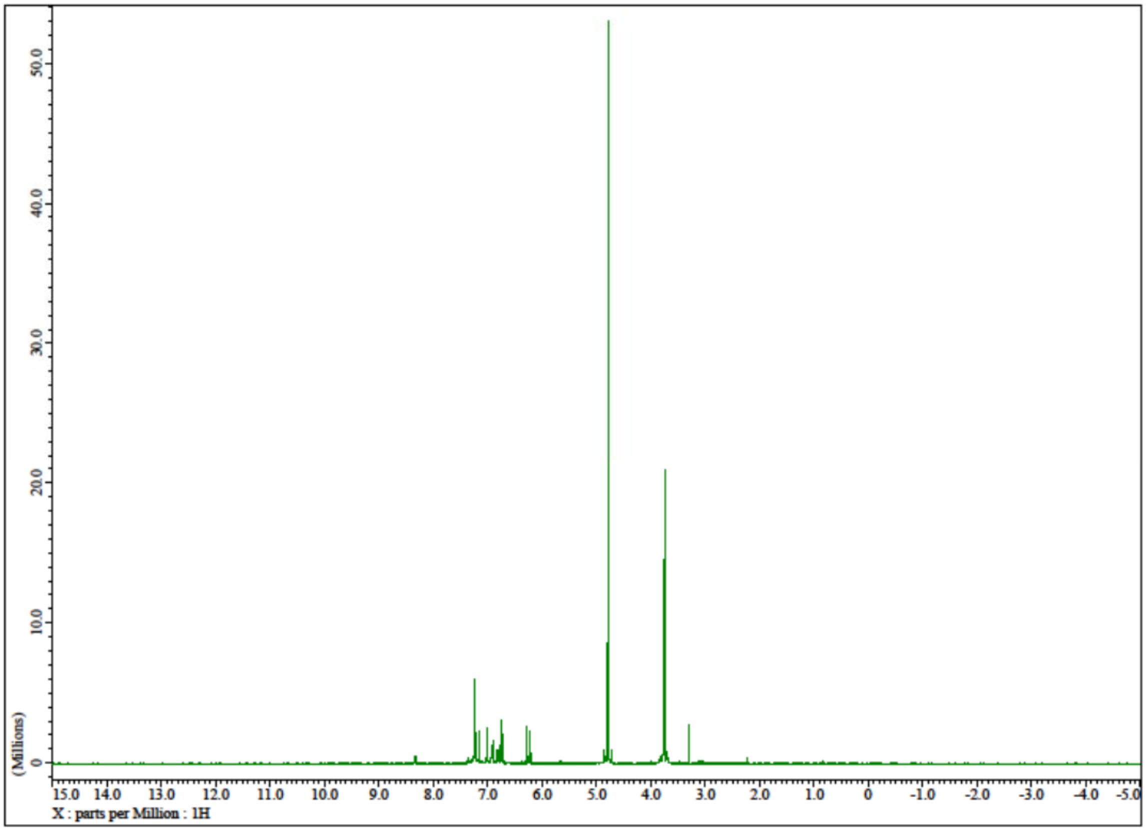

(Millions)
50.0
40.0
30.0
20.0
10.0
0
15.0 14.0 13.0 12.0 11.0 10.0 9.0 8.0 7.0 6.0 5.0 4.0 3.0 2.0 1.0 0 -1.0 -2.0 -3.0 -4.0 -5.0
X : parts per Million : 1H

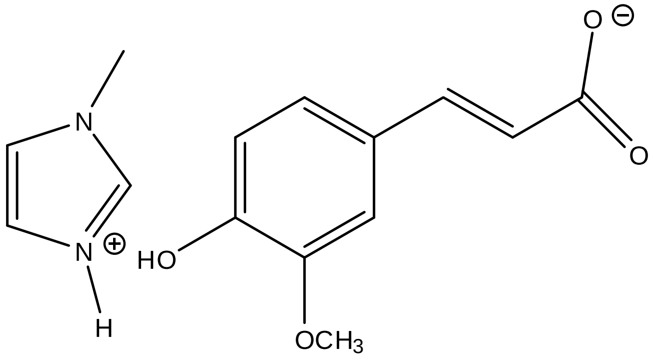

N
N⊕
H
HO
OCH3
O⊖
O

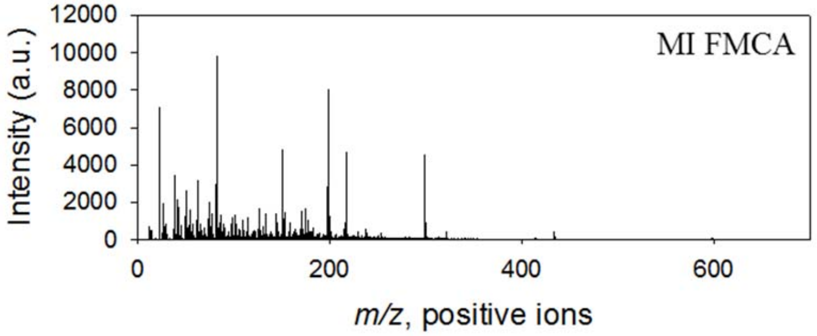
MI FMCA
Intensity (a.u.)
12000
10000
8000
6000
4000
2000
0
0
200
400
600
m/z, positive ions

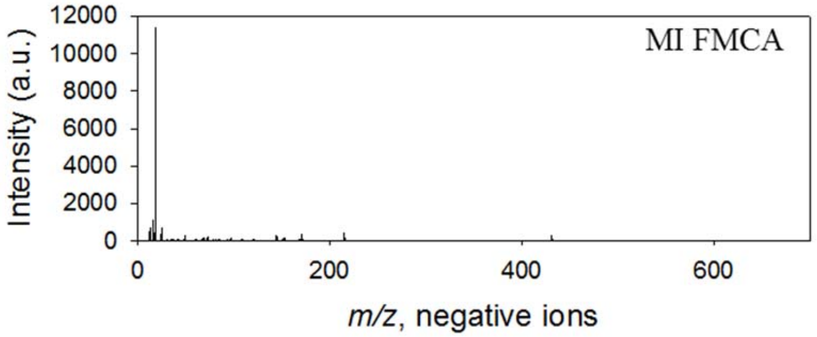
MI FMCA
Intensity (a.u.)
12000
10000
8000
6000
4000
2000
0
0
200
400
600
m/z, negative ions

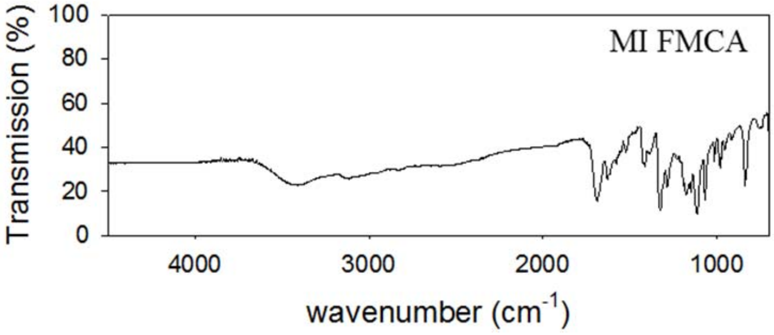
MI FMCA
Transmission (%)
100
80
60
40
20
0
4000
3000
2000
1000
wavenumber (cm-1)

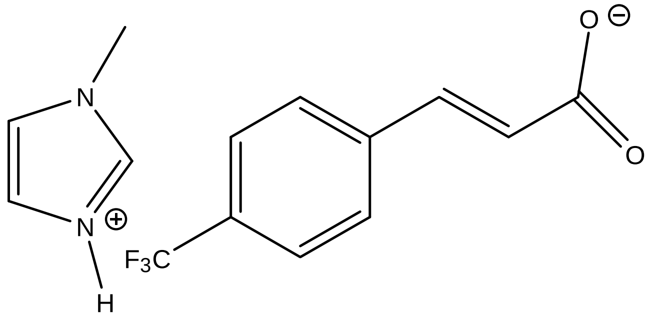
N
N⊕
H
F3C
O⊖
O

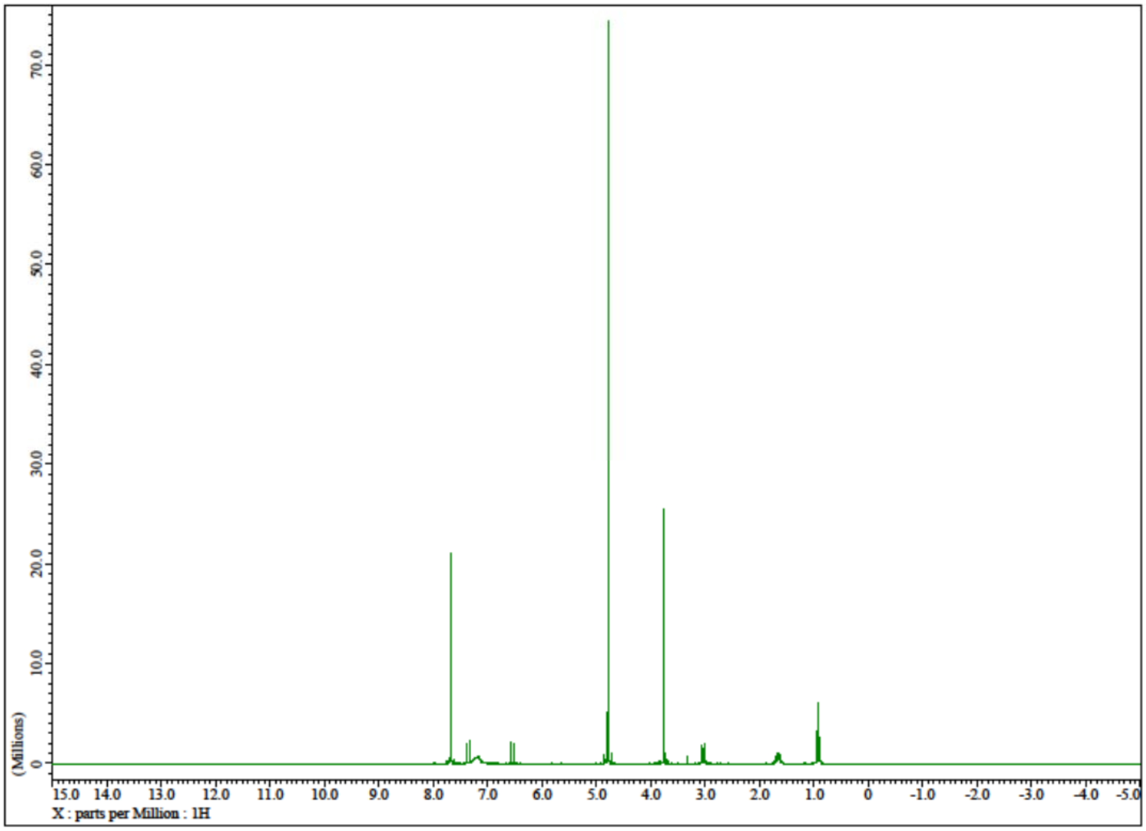
(Millions)
0
10.0
20.0
30.0
40.0
50.0
60.0
70.0
15.0
14.0
13.0
12.0
11.0
10.0
9.0
8.0
7.0
6.0
5.0
4.0
3.0
2.0
1.0
0
-1.0
-2.0
-3.0
-4.0
-5.0
X : parts per Million : 1H

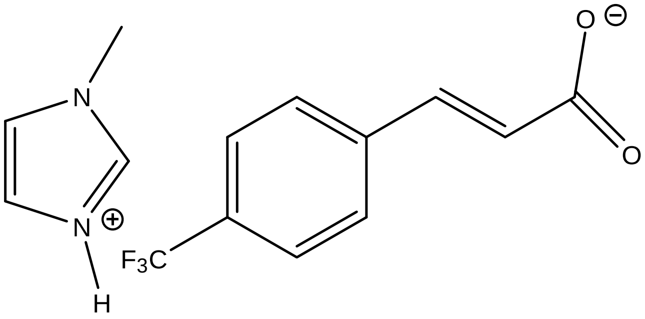
N
N
⊕
H
F3C
O
⊖
O

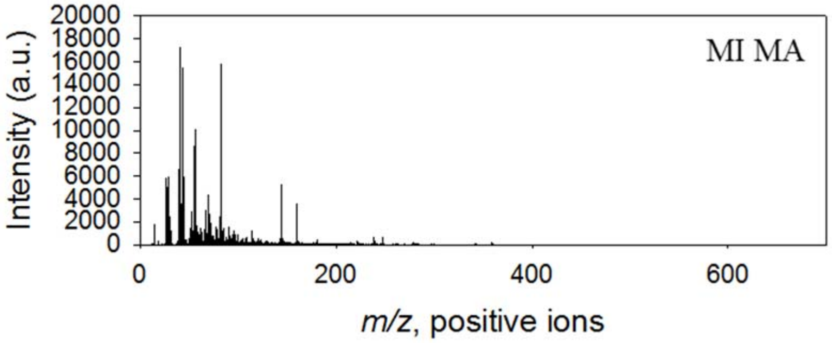
MI MA
Intensity (a.u.)
20000
18000
16000
14000
12000
10000
8000
6000
4000
2000
0
0
200
400
600
m/z, positive ions

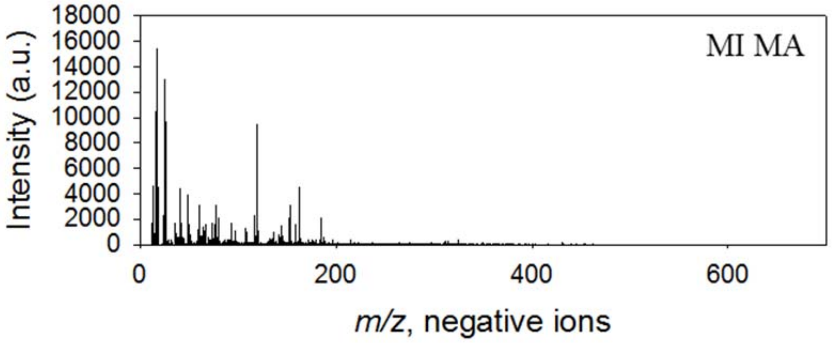
MI MA
Intensity (a.u.)
18000
16000
14000
12000
10000
8000
6000
4000
2000
0
0
200
400
600
m/z, negative ions

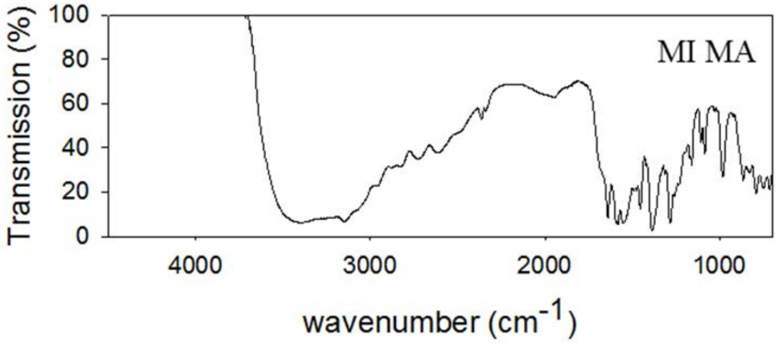
MI MA
Transmission (%)
100
80
60
40
20
0
4000
3000
2000
1000
wavenumber (cm-1)

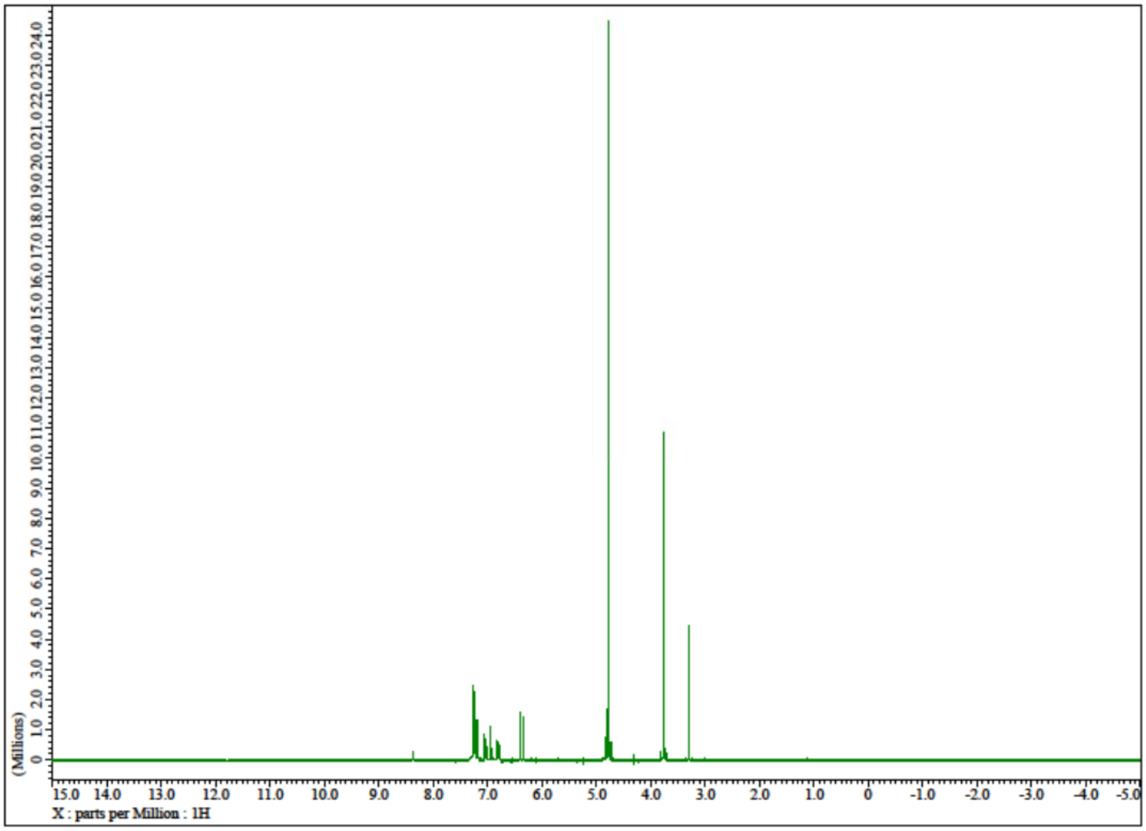
(Millions)
0
1.0
2.0
3.0
4.0
5.0
6.0
7.0
8.0
9.0
10.0
11.0
12.0
13.0
14.0
15.0
16.0
17.0
18.0
19.0
20.0
21.0
22.0
23.0
24.0
15.0
14.0
13.0
12.0
11.0
10.0
9.0
8.0
7.0
6.0
5.0
4.0
3.0
2.0
1.0
0
-1.0
-2.0
-3.0
-4.0
-5.0
X : parts per Million : 1H

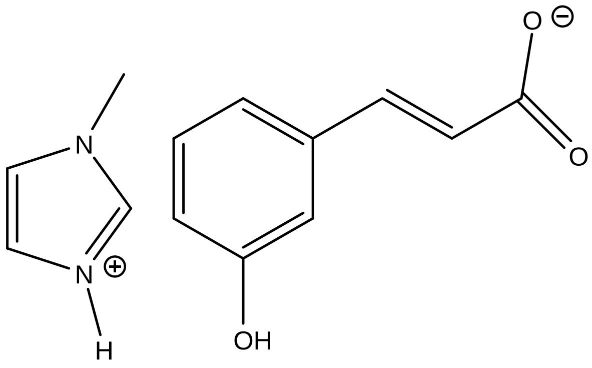
O
⊖
O
N
N
⊕
H
OH

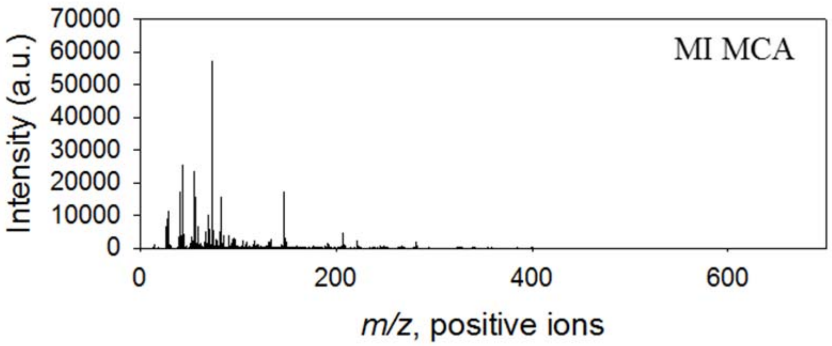
MI MCA
Intensity (a.u.)
70000
60000
50000
40000
30000
20000
10000
0
0
200
400
600
m/z, positive ions

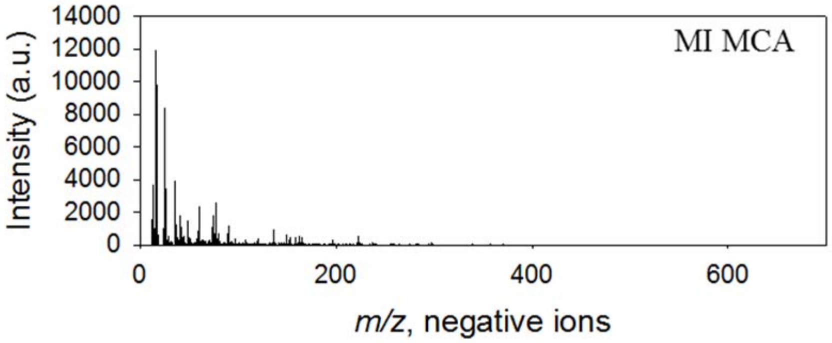
MI MCA
Intensity (a.u.)
14000
12000
10000
8000
6000
4000
2000
0
0
200
400
600
m/z, negative ions

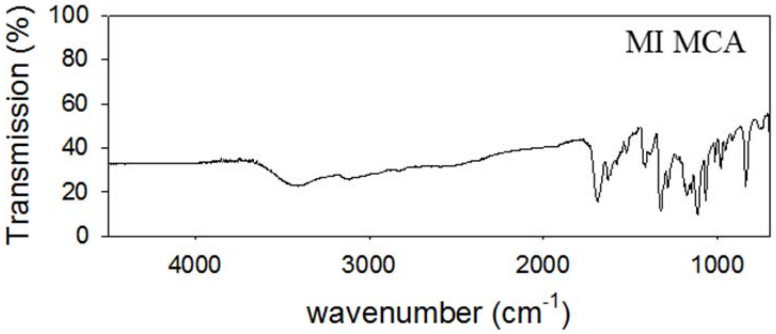
MI MCA
Transmission (%)
100
80
60
40
20
0
4000
3000
2000
1000
wavenumber (cm-1)

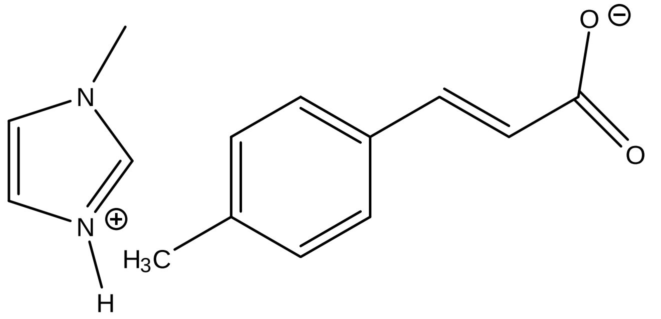
N
N
H
H3C
O
O

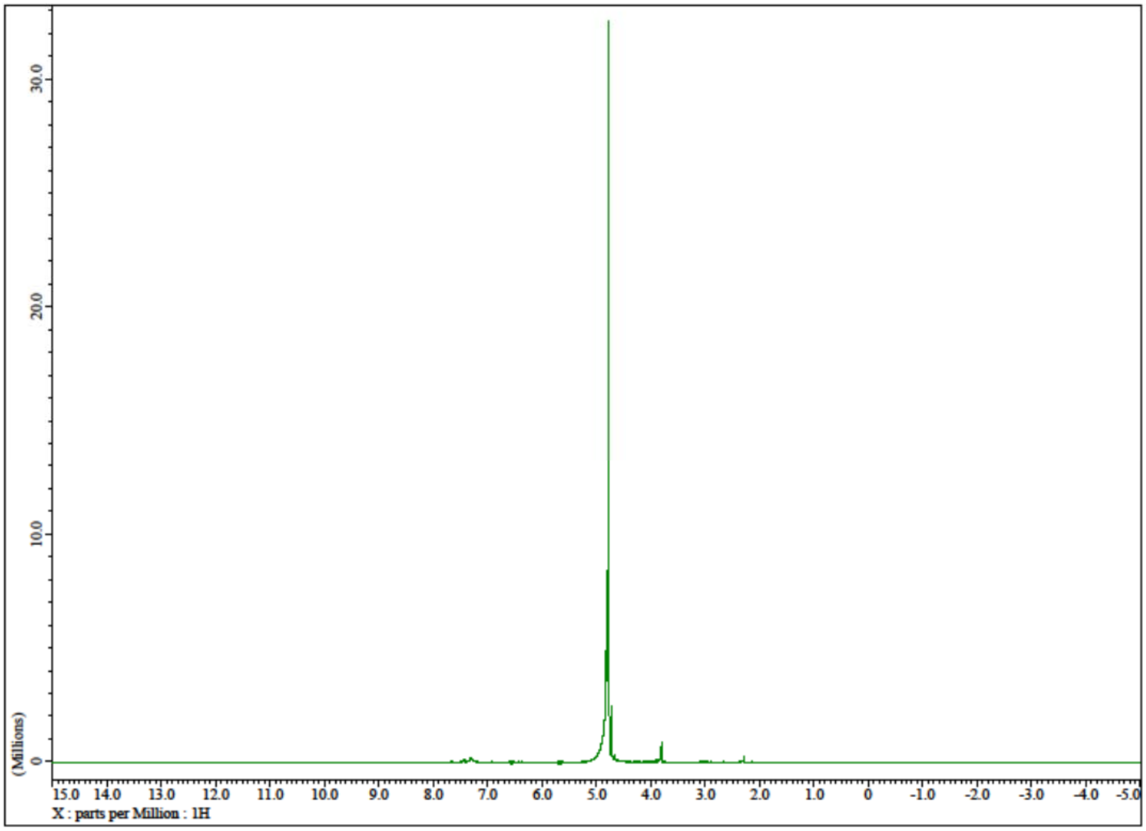
30.0
20.0
10.0
0
(Millions)
15.0 14.0 13.0 12.0 11.0 10.0 9.0 8.0 7.0 6.0 5.0 4.0 3.0 2.0 1.0 0 -1.0 -2.0 -3.0 -4.0 -5.0
X : parts per Million : 1H

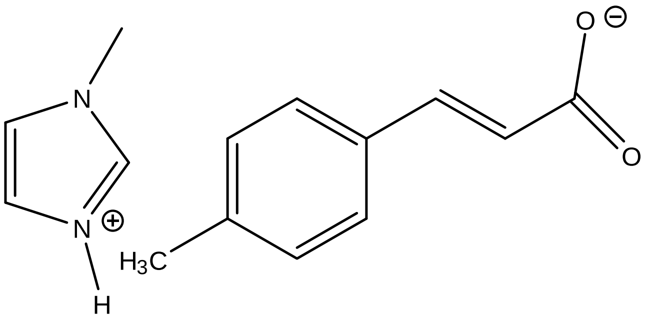
N
N
H
H3C
O
O

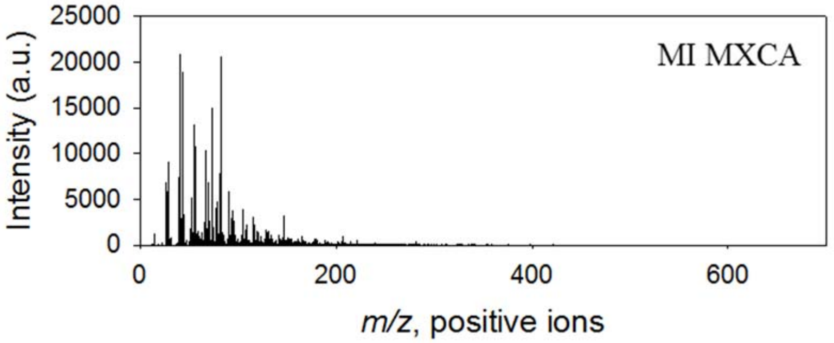
MI MXCA
Intensity (a.u.)
25000
20000
15000
10000
5000
0
0
200
400
600
m/z, positive ions

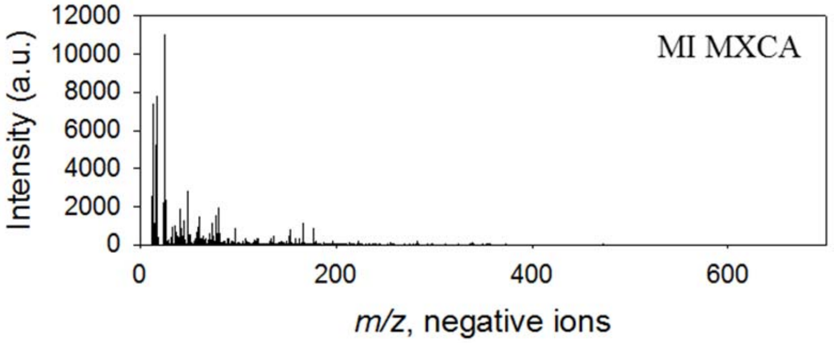
MI MXCA
Intensity (a.u.)
12000
10000
8000
6000
4000
2000
0
0
200
400
600
m/z, negative ions

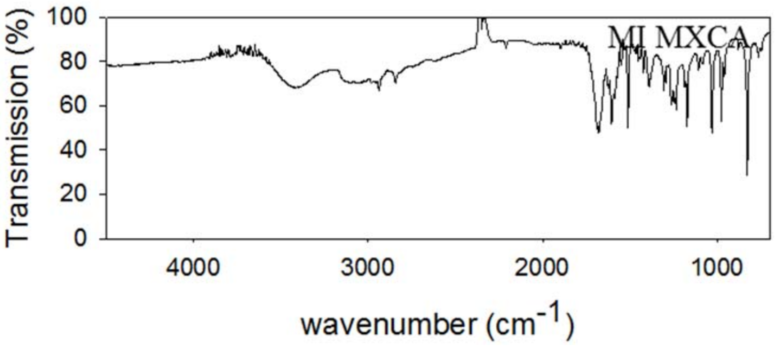
MI MXCA
Transmission (%)
100
80
60
40
20
0
4000
3000
2000
1000
wavenumber (cm-1)

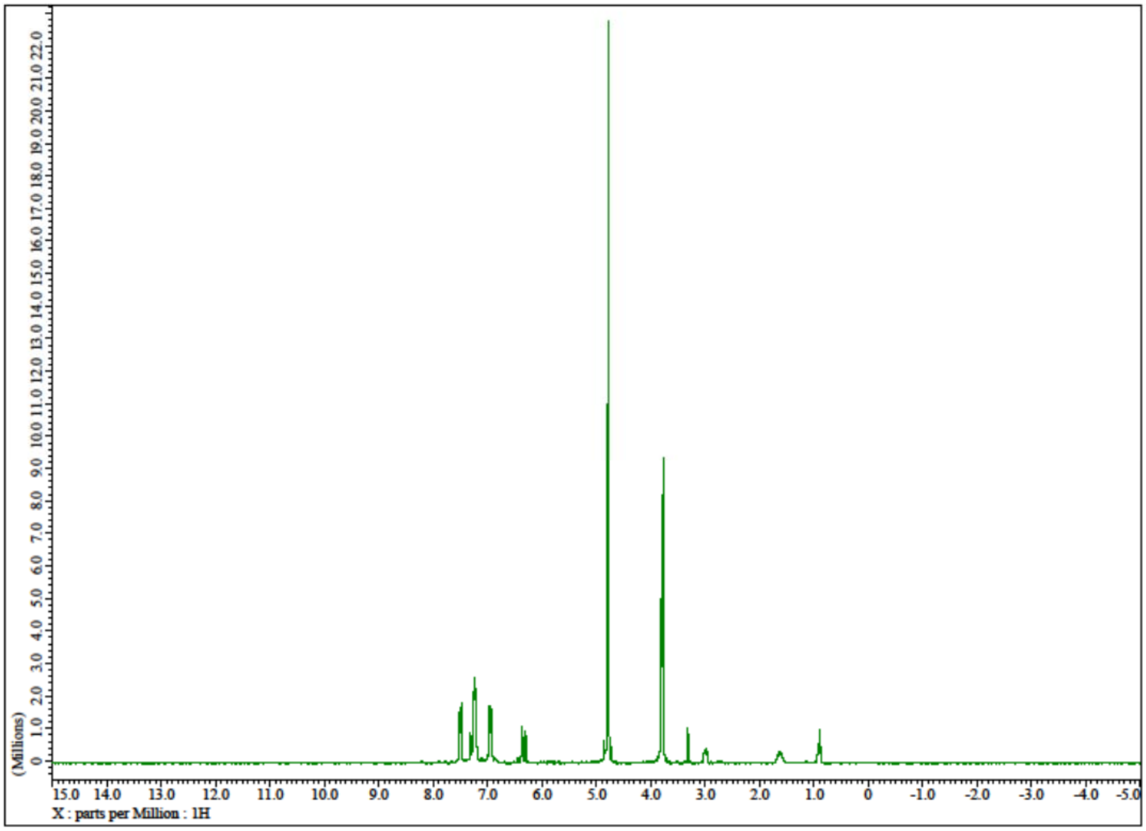
(Millions)
0
1.0
2.0
3.0
4.0
5.0
6.0
7.0
8.0
9.0
10.0
11.0
12.0
13.0
14.0
15.0
16.0
17.0
18.0
19.0
20.0
21.0
22.0
15.0
14.0
13.0
12.0
11.0
10.0
9.0
8.0
7.0
6.0
5.0
4.0
3.0
2.0
1.0
0
-1.0
-2.0
-3.0
-4.0
-5.0
X : parts per Million : 1H

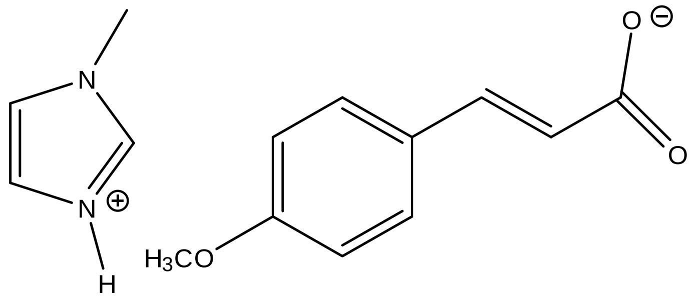
N
N
⊕
H
H3CO
O
⊖
O

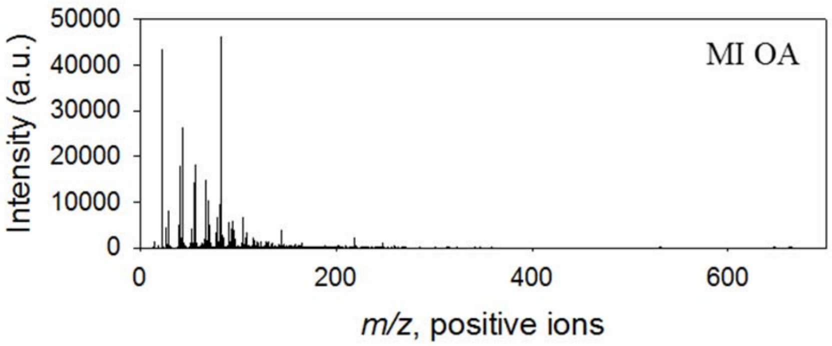
MI OA
Intensity (a.u.)
50000
40000
30000
20000
10000
0
0
200
400
600
m/z, positive ions

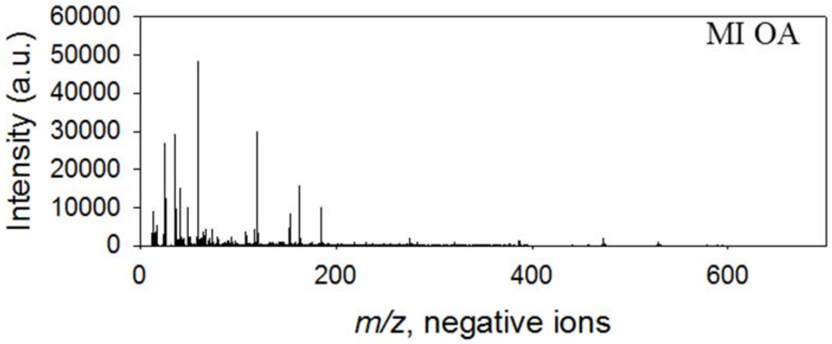
MI OA
Intensity (a.u.)
60000
50000
40000
30000
20000
10000
0
0
200
400
600
m/z, negative ions

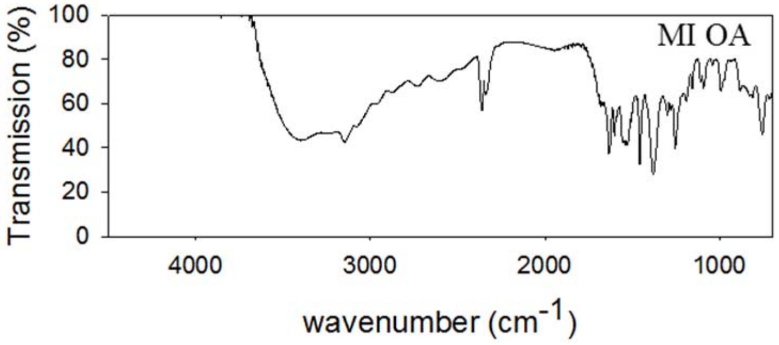
MI OA
Transmission (%)
100
80
60
40
20
0
4000
3000
2000
1000
wavenumber (cm-1)

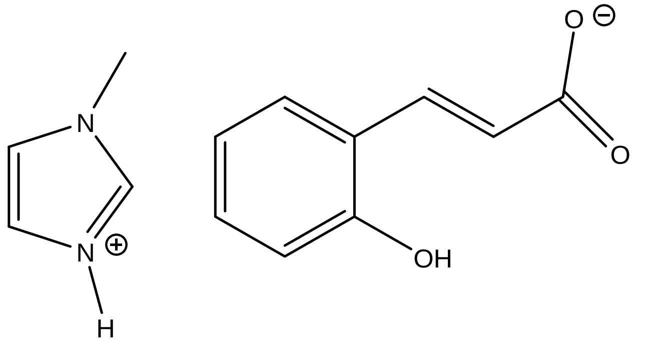
N
N⊕
H
O⊖
O
OH

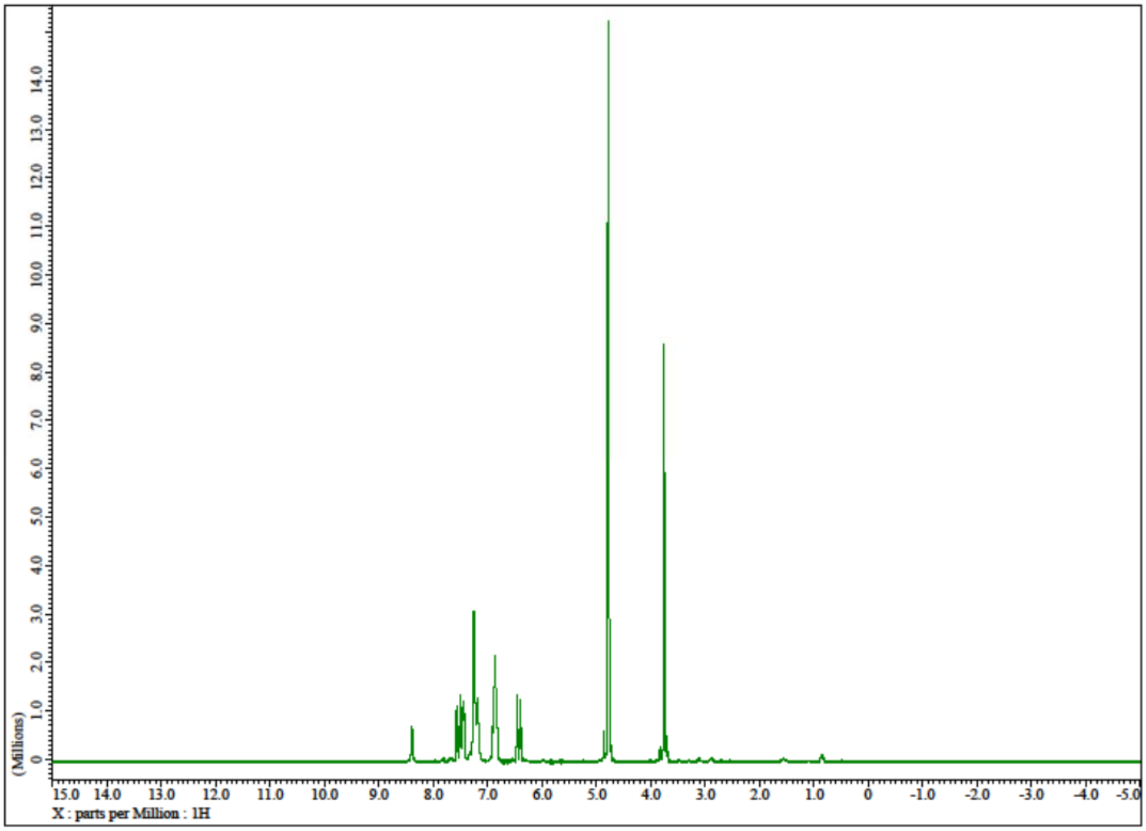
(Millions)
0
1.0
2.0
3.0
4.0
5.0
6.0
7.0
8.0
9.0
10.0
11.0
12.0
13.0
14.0
15.0
14.0
13.0
12.0
11.0
10.0
9.0
8.0
7.0
6.0
5.0
4.0
3.0
2.0
1.0
0
-1.0
-2.0
-3.0
-4.0
-5.0
X : parts per Million : 1H

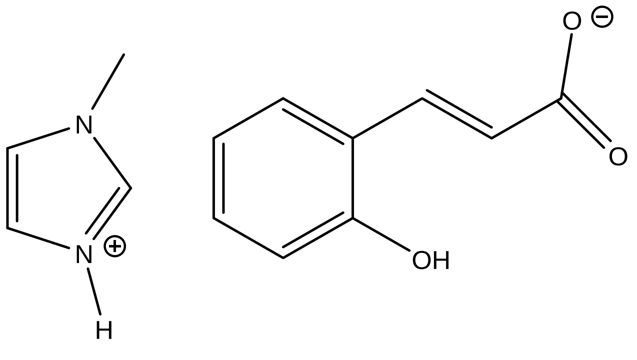
N
N⊕
H
O⊖
O
OH

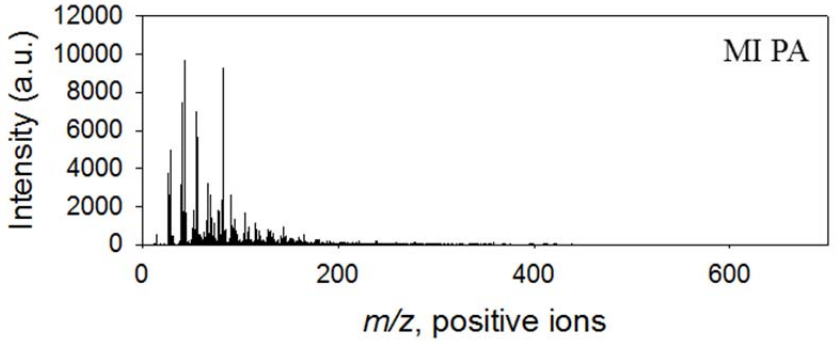
MI PA
Intensity (a.u.)
12000
10000
8000
6000
4000
2000
0
0
200
400
600
m/z, positive ions

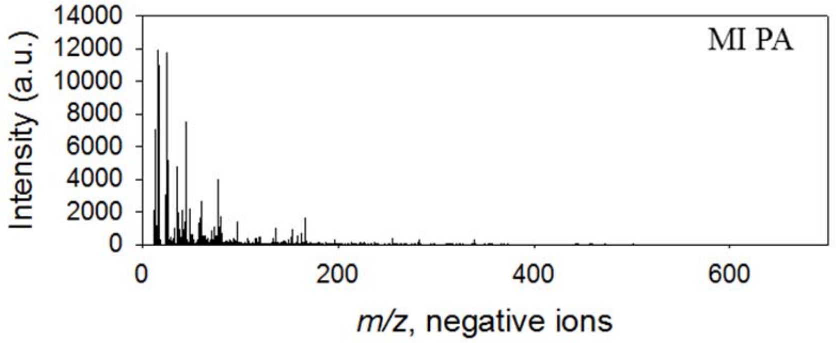
MI PA
Intensity (a.u.)
14000
12000
10000
8000
6000
4000
2000
0
0
200
400
600
m/z, negative ions

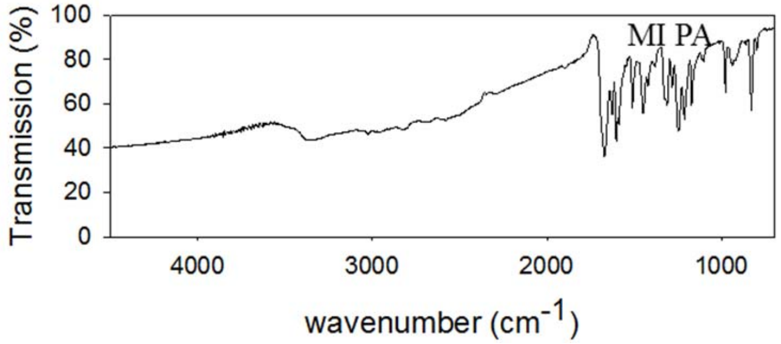
MI PA
Transmission (%)
100
80
60
40
20
0
4000
3000
2000
1000
wavenumber (cm-1)

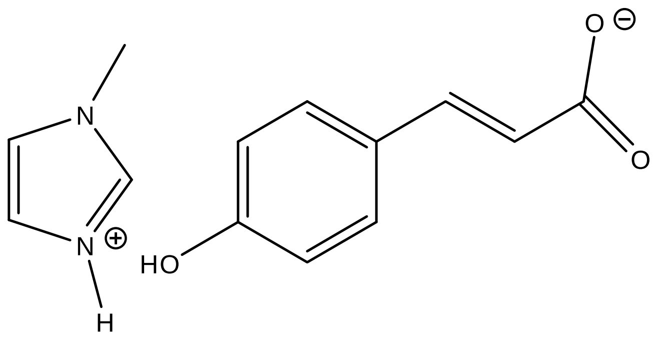
N
N
H
HO
O
O

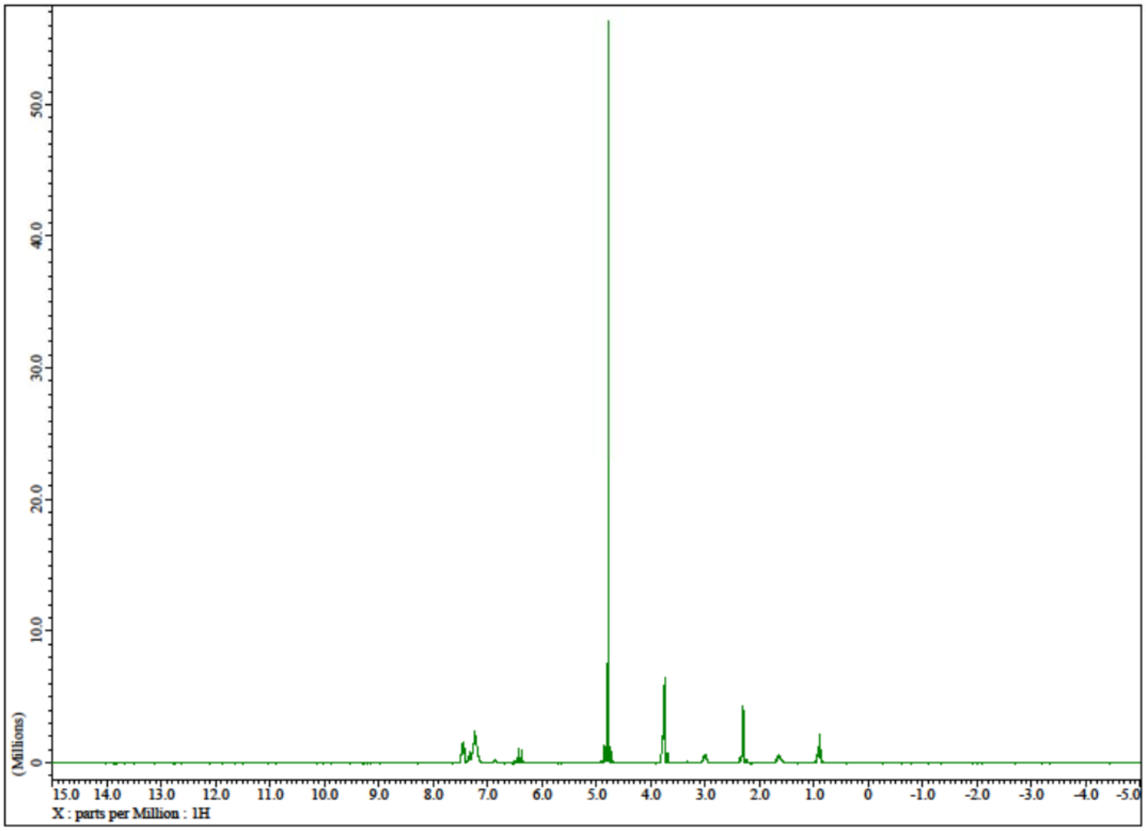
(Millions)
0
10.0
20.0
30.0
40.0
50.0
15.0
14.0
13.0
12.0
11.0
10.0
9.0
8.0
7.0
6.0
5.0
4.0
3.0
2.0
1.0
0
-1.0
-2.0
-3.0
-4.0
-5.0
X : parts per Million : 1H

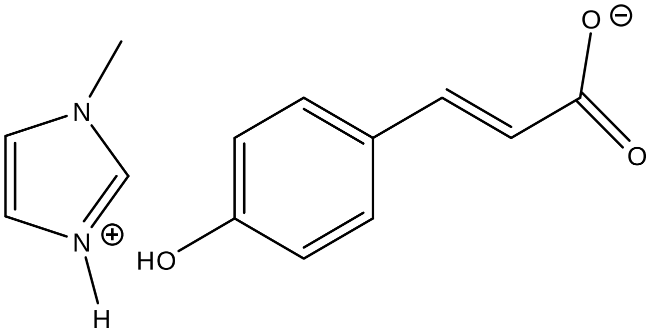
N
N⊕
H
HO
O⊖
O

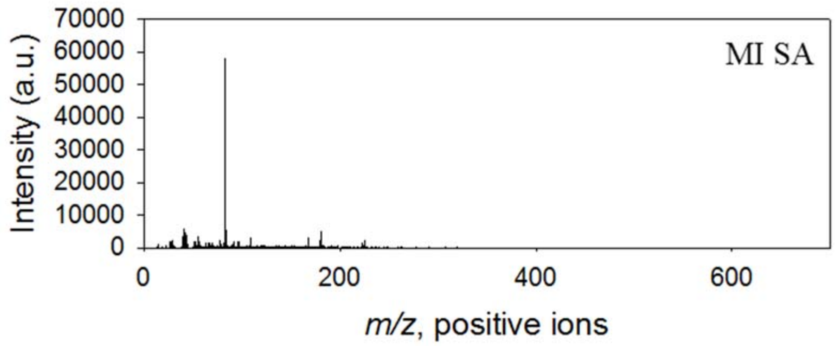
MI SA
Intensity (a.u.)
70000
60000
50000
40000
30000
20000
10000
0
0
200
400
600
m/z, positive ions

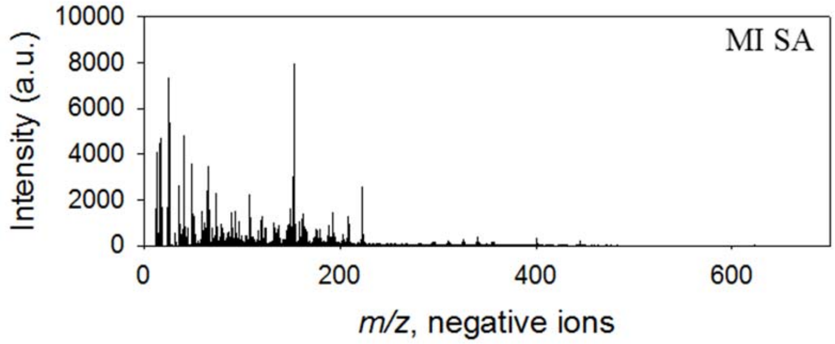
MI SA
Intensity (a.u.)
10000
8000
6000
4000
2000
0
0
200
400
600
m/z, negative ions

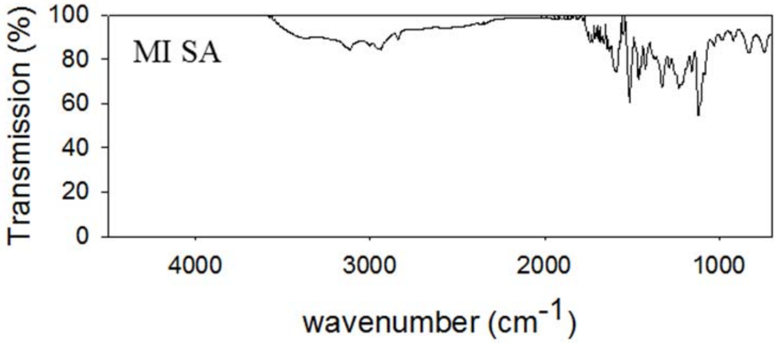
MI SA
Transmission (%)
100
80
60
40
20
0
4000
3000
2000
1000
wavenumber (cm-1)

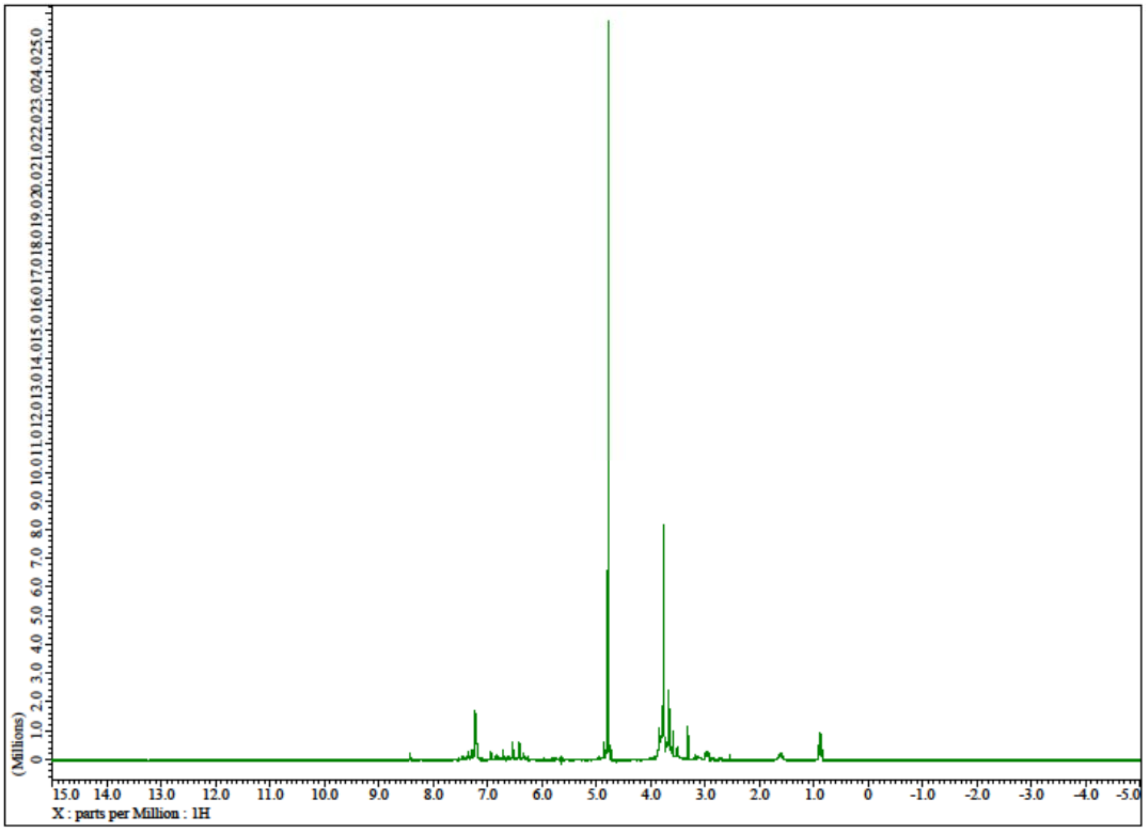
(Millions)
0
1.0
2.0
3.0
4.0
5.0
6.0
7.0
8.0
9.0
10.0
11.0
12.0
13.0
14.0
15.0
16.0
17.0
18.0
19.0
20.0
21.0
22.0
23.0
24.0
25.0
15.0
14.0
13.0
12.0
11.0
10.0
9.0
8.0
7.0
6.0
5.0
4.0
3.0
2.0
1.0
0
-1.0
-2.0
-3.0
-4.0
-5.0
X : parts per Million : 1H

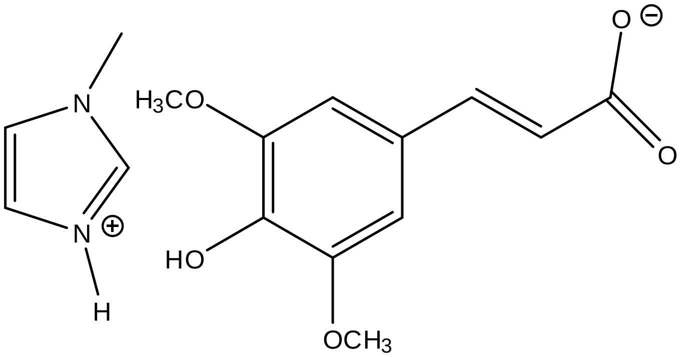
N
N
H
H$_3$CO
HO
OCH$_3$
O
O

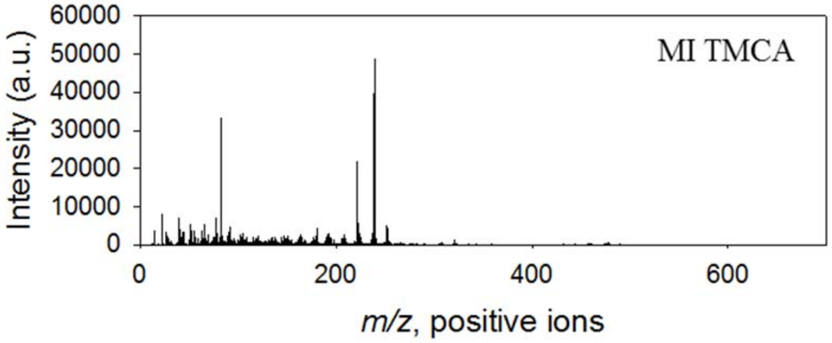
MI TMCA
Intensity (a.u.)
60000
50000
40000
30000
20000
10000
0
0
200
400
600
m/z, positive ions

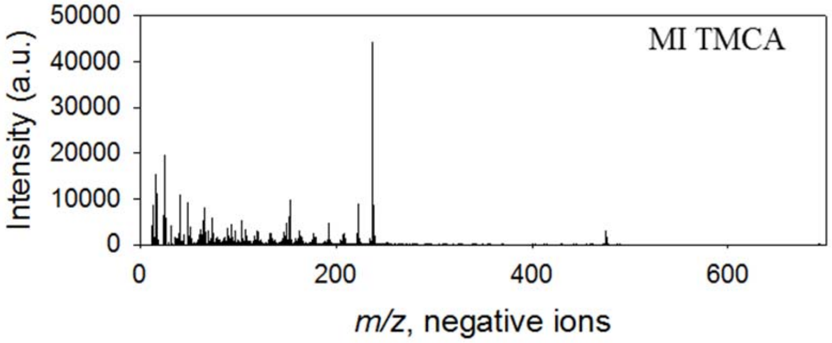
MI TMCA
Intensity (a.u.)
50000
40000
30000
20000
10000
0
0
200
400
600
m/z, negative ions

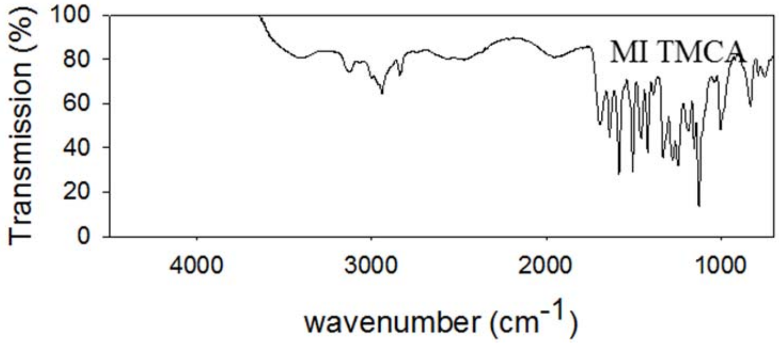
MI TMCA
Transmission (%)
100
80
60
40
20
0
4000
3000
2000
1000
wavenumber (cm-1)

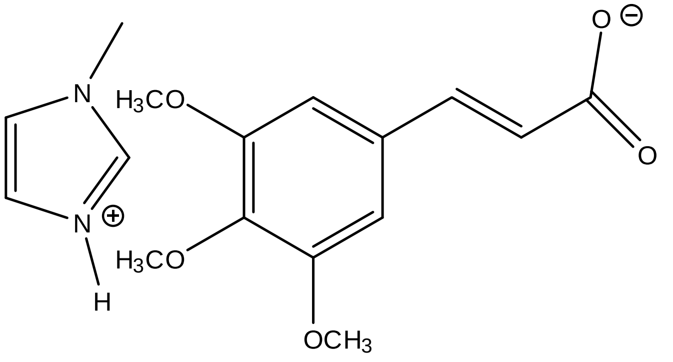
N
N
H
H3CO
H3CO
OCH3
O
O

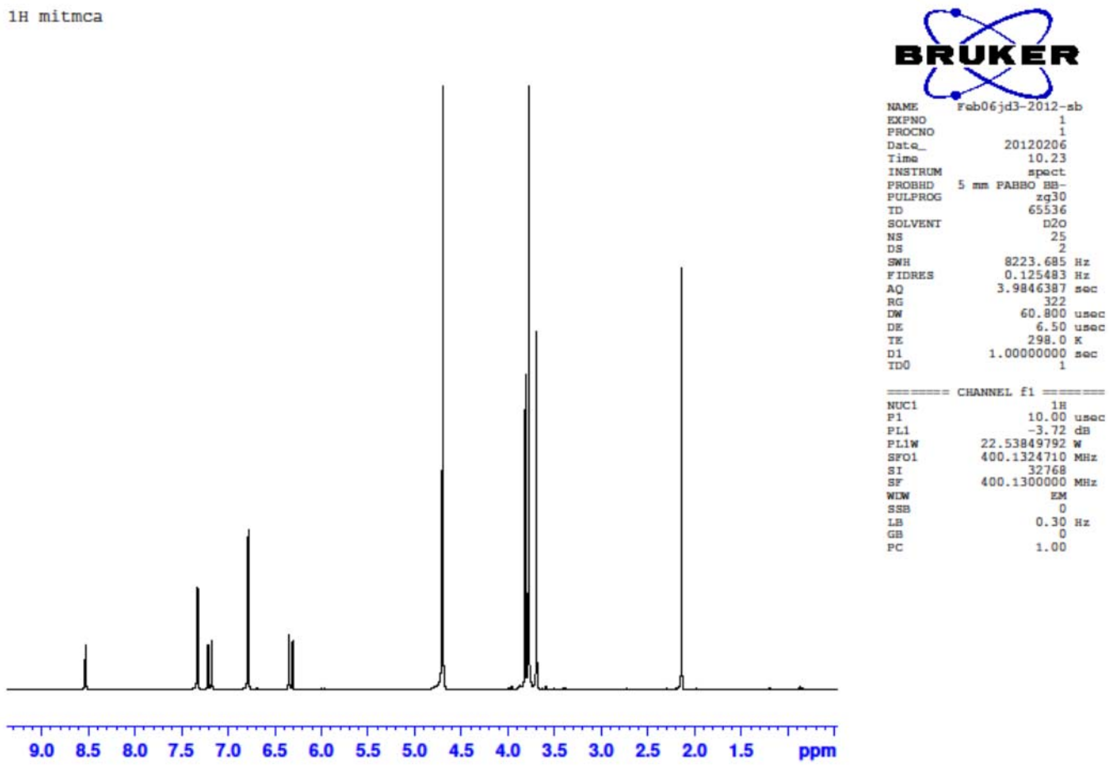

1H mitmca

```
NAME       Feb06jd3-2012-sb
EXPNO                     1
PROCNO                    1
Date_              20120206
Time                  10.23
INSTRUM               spect
PROBHD     5 mm PABBO BB-
PULPROG                zg30
TD                    65536
SOLVENT                 D2O
NS                       25
DS                        2
SWH                8223.685 Hz
FIDRES             0.125483 Hz
AQ                3.9846387 sec
RG                      322
DW                   60.800 usec
DE                     6.50 usec
TE                    298.0 K
D1               1.00000000 sec
TD0                       1

======== CHANNEL f1 ========
NUC1                     1H
P1                    10.00 usec
PL1                   -3.72 dB
PL1W            22.53849792 W
SFO1            400.1324710 MHz
SI                    32768
SF              400.1300000 MHz
WDW                      EM
SSB                       0
LB                     0.30 Hz
GB                        0
PC                     1.00
```

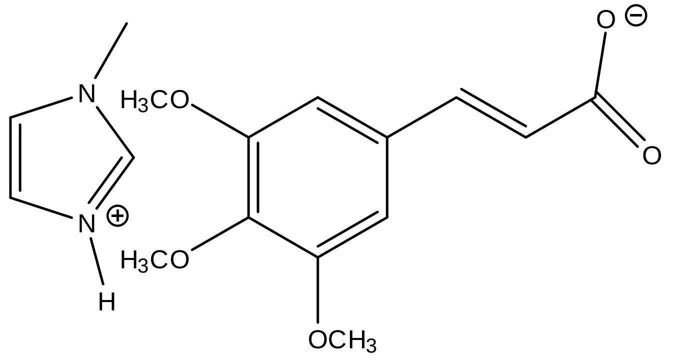

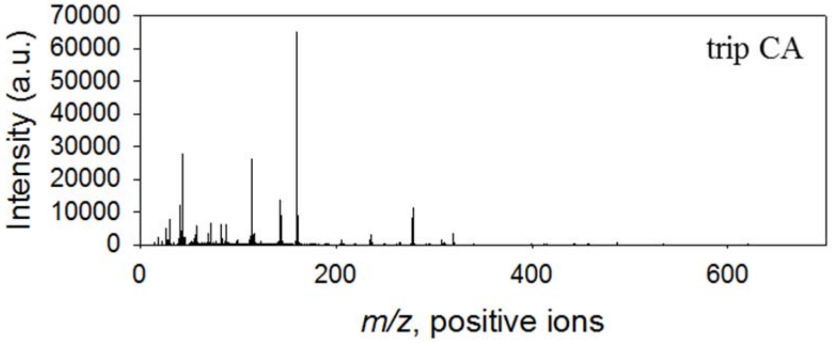
Intensity (a.u.)
70000
60000
50000
40000
30000
20000
10000
0
0
200
400
600
m/z, positive ions
trip CA

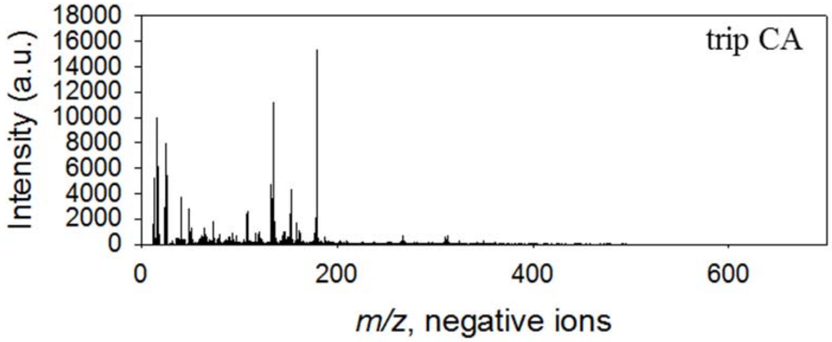
Intensity (a.u.)
18000
16000
14000
12000
10000
8000
6000
4000
2000
0
0
200
400
600
m/z, negative ions
trip CA

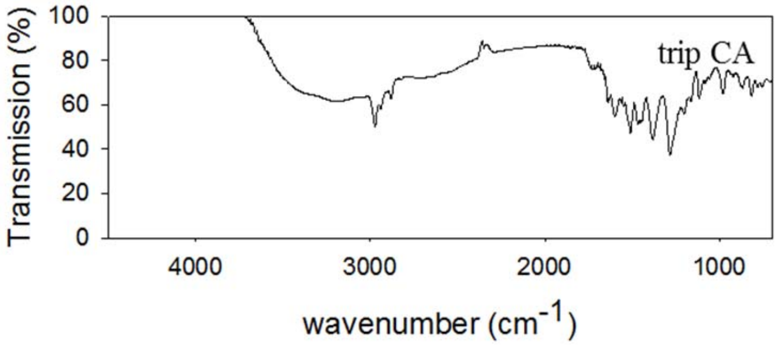
Transmission (%)
100
80
60
40
20
0
4000
3000
2000
1000
wavenumber (cm-1)
trip CA

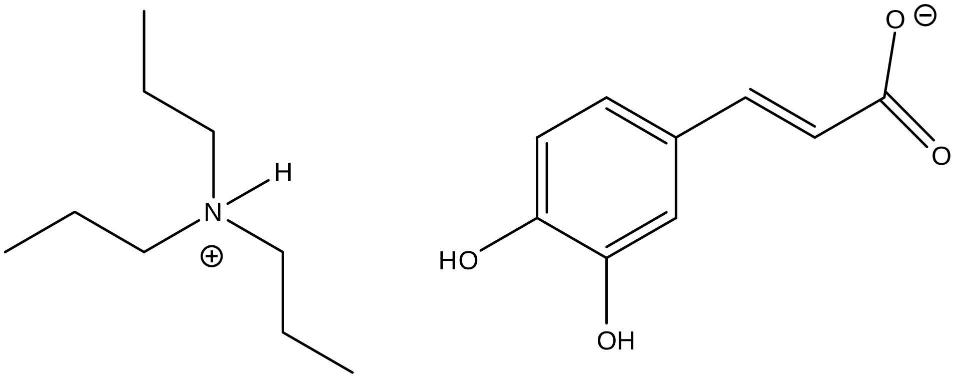
H
N
⊕
O ⊖
O
HO
OH

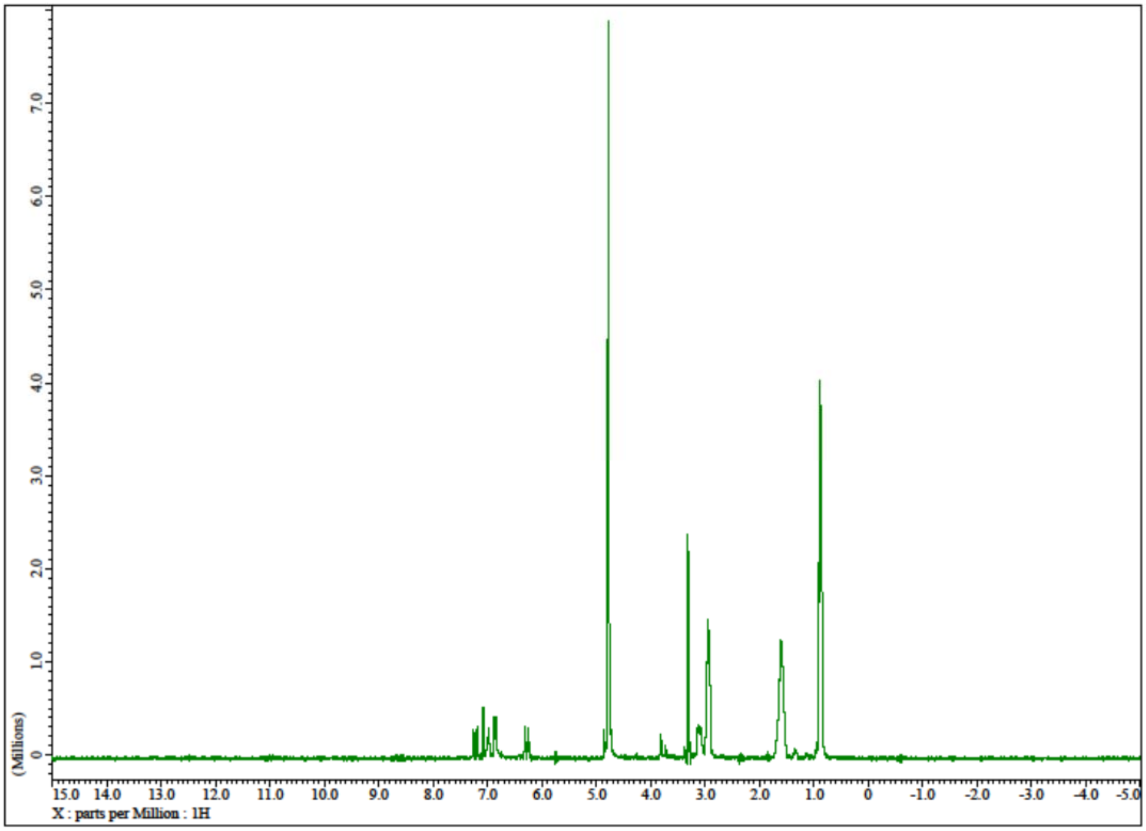
(Millions)
0
1.0
2.0
3.0
4.0
5.0
6.0
7.0
15.0
14.0
13.0
12.0
11.0
10.0
9.0
8.0
7.0
6.0
5.0
4.0
3.0
2.0
1.0
0
-1.0
-2.0
-3.0
-4.0
-5.0
X : parts per Million : 1H

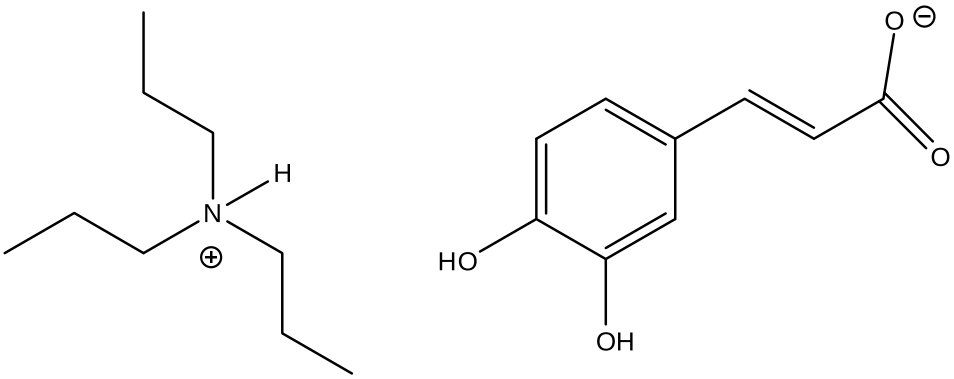
H
N
⊕
O ⊖
O
HO
OH

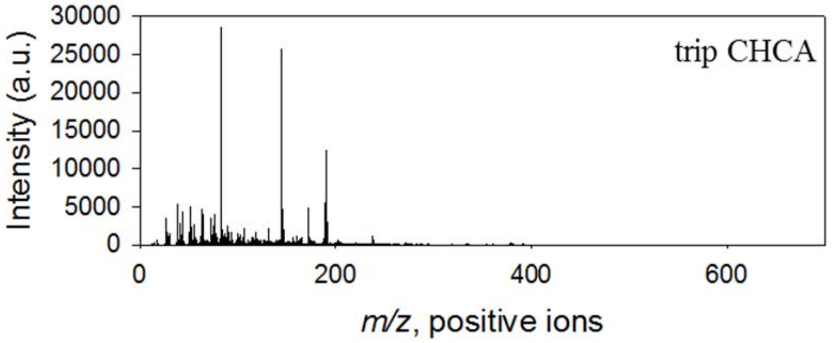
trip CHCA
Intensity (a.u.)
30000
25000
20000
15000
10000
5000
0
0
200
400
600
m/z, positive ions

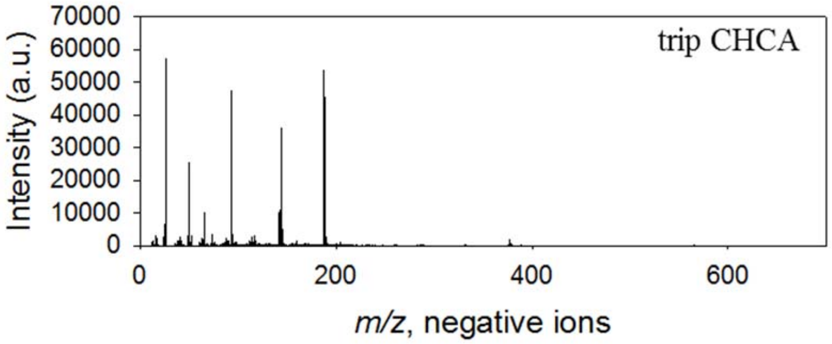
trip CHCA
Intensity (a.u.)
70000
60000
50000
40000
30000
20000
10000
0
0
200
400
600
m/z, negative ions

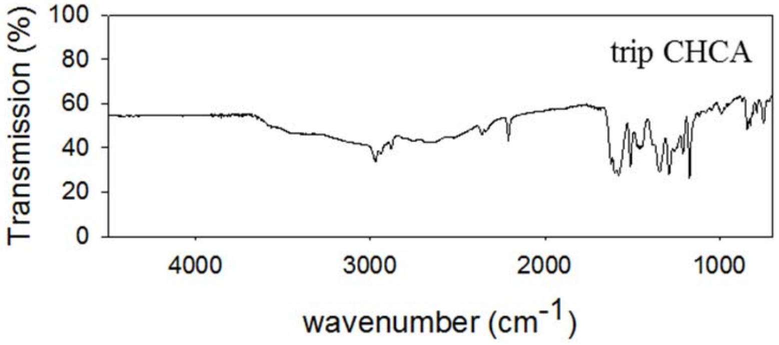
trip CHCA
Transmission (%)
100
80
60
40
20
0
4000
3000
2000
1000
wavenumber (cm-1)

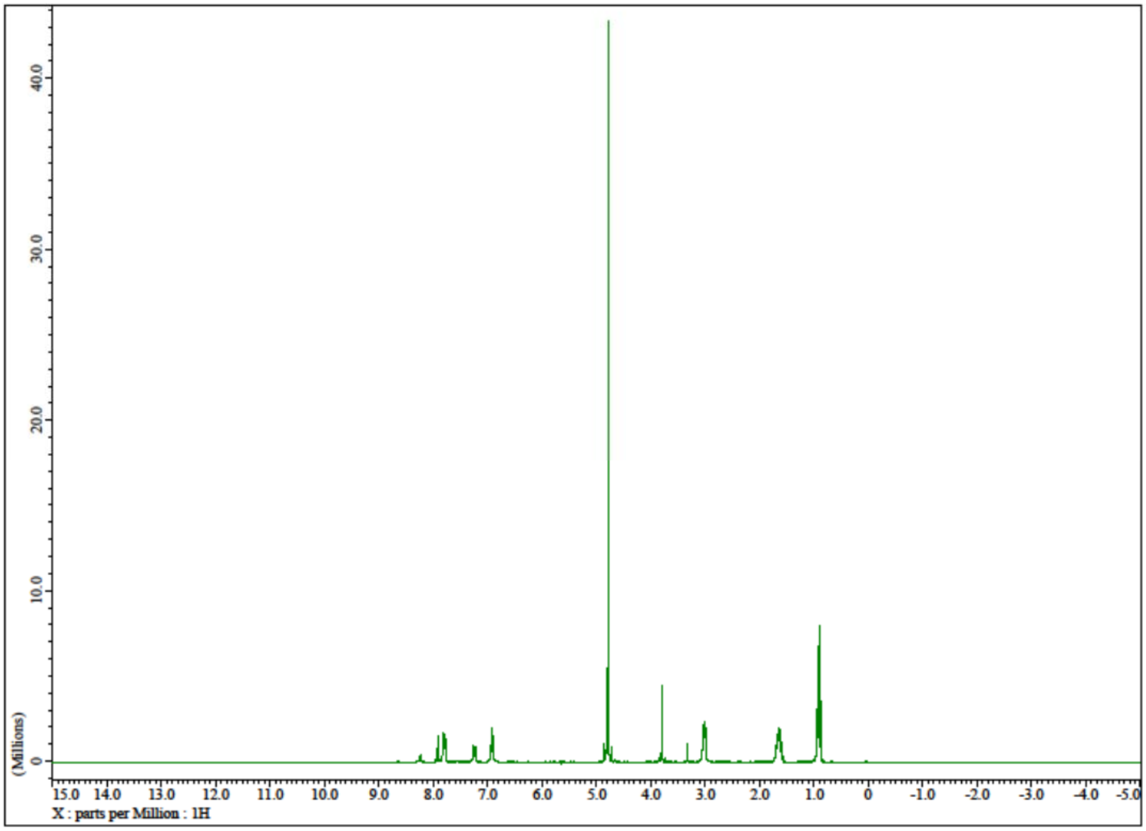
(Millions)
0
10.0
20.0
30.0
40.0
15.0 14.0 13.0 12.0 11.0 10.0 9.0 8.0 7.0 6.0 5.0 4.0 3.0 2.0 1.0 0 -1.0 -2.0 -3.0 -4.0 -5.0
X : parts per Million : 1H

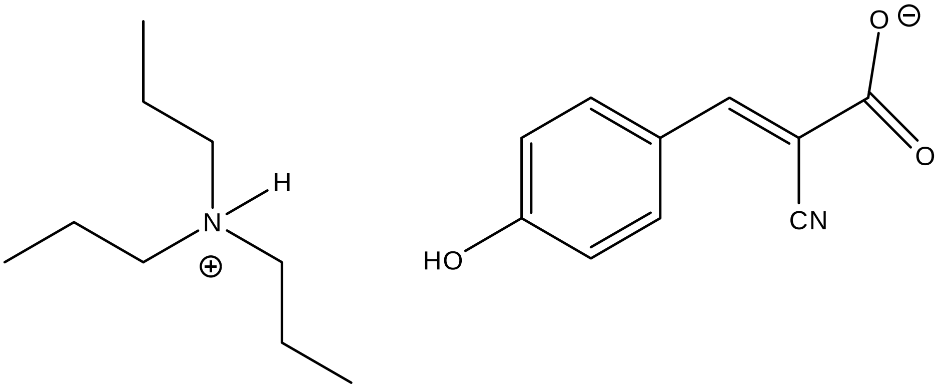
H
N
⊕
O ⊖
O
CN
HO

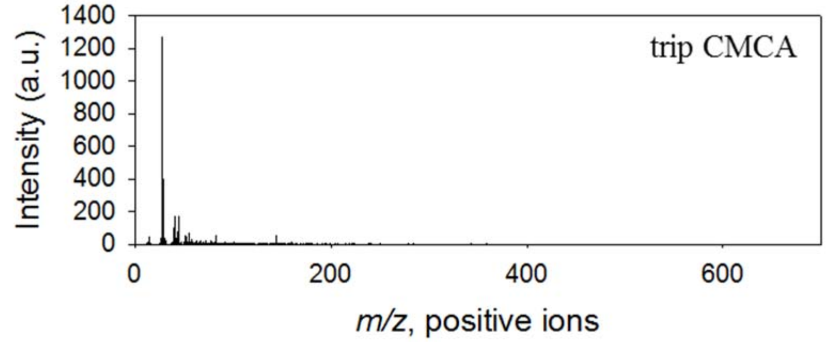
trip CMCA
Intensity (a.u.)
1400
1200
1000
800
600
400
200
0
0
200
400
600
m/z, positive ions

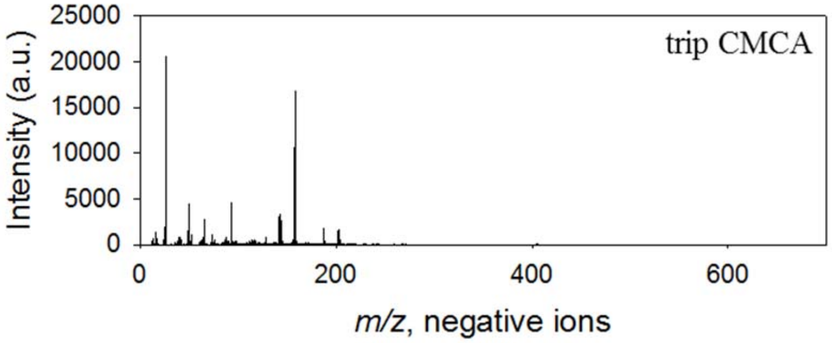
trip CMCA
Intensity (a.u.)
25000
20000
15000
10000
5000
0
0
200
400
600
m/z, negative ions

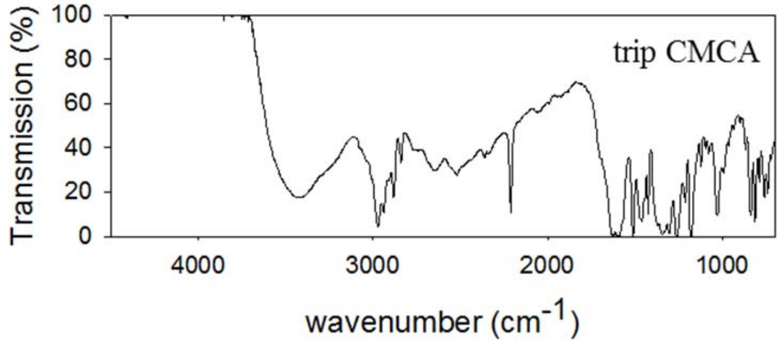
trip CMCA
Transmission (%)
100
80
60
40
20
0
4000
3000
2000
1000
wavenumber (cm-1)

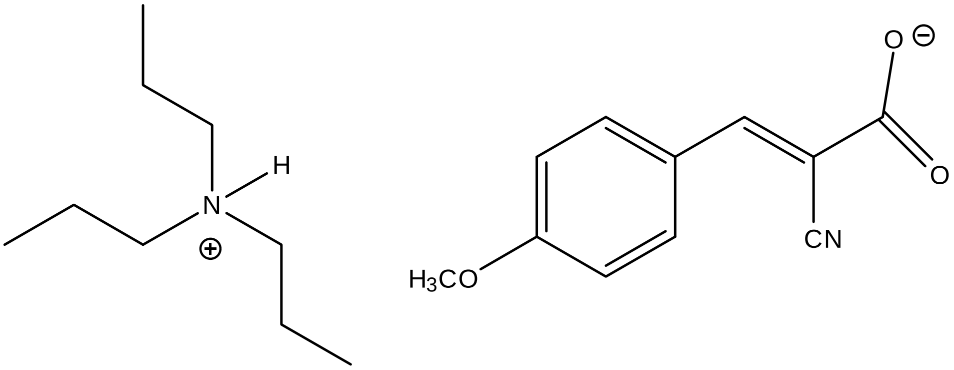
H
N
⊕
O ⊖
O
CN
H3CO

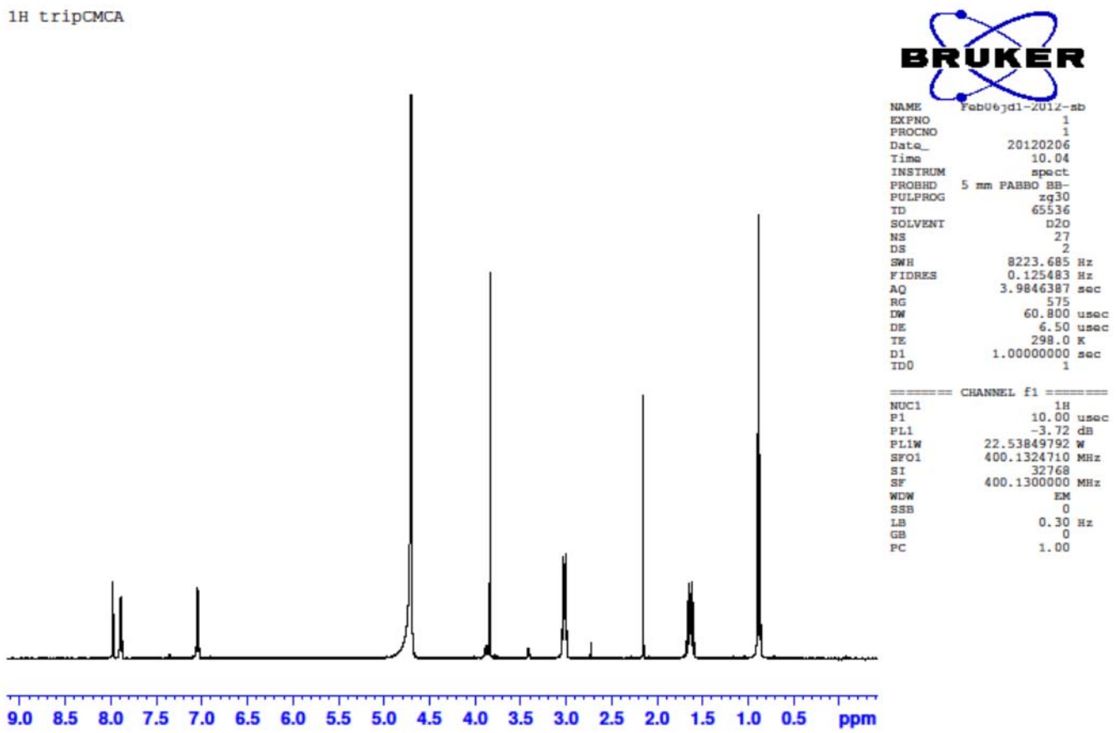

```
NAME      Feb06jd1-2012-sb
EXPNO                    1
PROCNO                   1
Date_             20120206
Time                 10.04
INSTRUM              spect
PROBHD    5 mm PABBO BB-
PULPROG               zg30
TD                   65536
SOLVENT                D2O
NS                      27
DS                       2
SWH               8223.685 Hz
FIDRES            0.125483 Hz
AQ               3.9846387 sec
RG                     575
DW                  60.800 usec
DE                    6.50 usec
TE                   298.0 K
D1              1.00000000 sec
TD0                      1

======= CHANNEL f1 =======
NUC1                    1H
P1                   10.00 usec
PL1                  -3.72 dB
PL1W           22.53849792 W
SFO1           400.1324710 MHz
SI                   32768
SF             400.1300000 MHz
WDW                     EM
SSB                      0
LB                    0.30 Hz
GB                       0
PC                    1.00
```

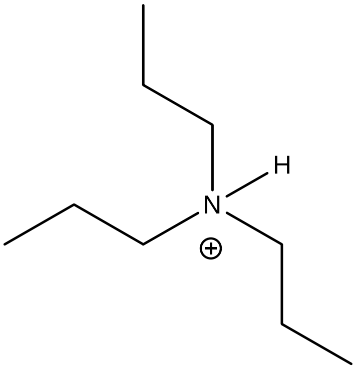

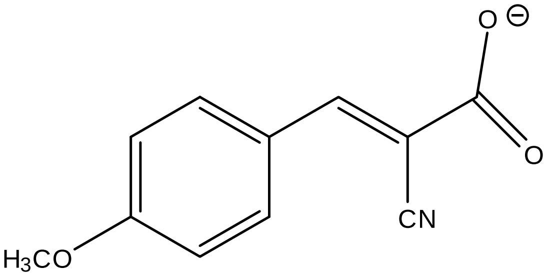

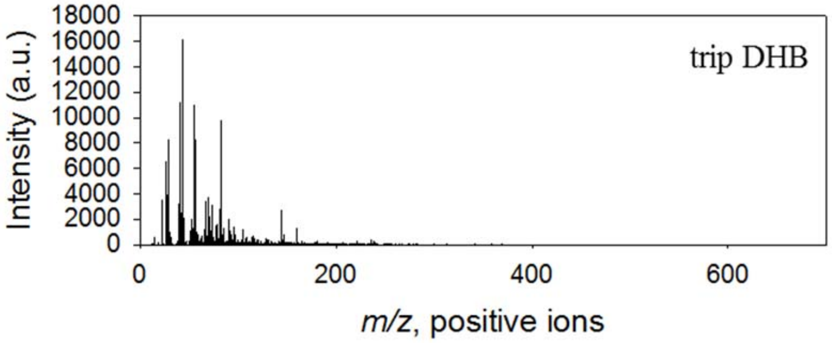
trip DHB
Intensity (a.u.)
18000
16000
14000
12000
10000
8000
6000
4000
2000
0
0
200
400
600
m/z, positive ions

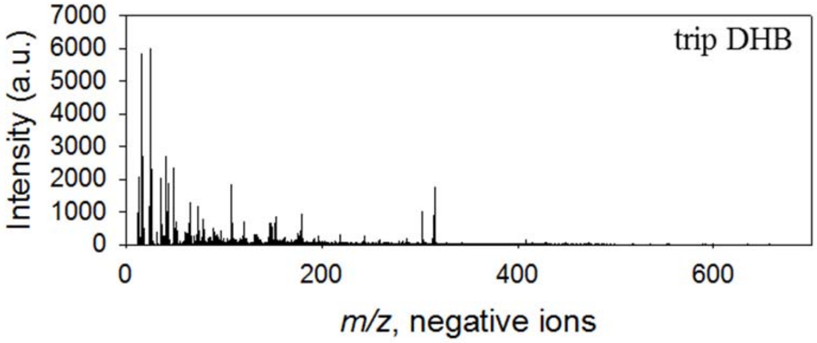
trip DHB
Intensity (a.u.)
7000
6000
5000
4000
3000
2000
1000
0
0
200
400
600
m/z, negative ions

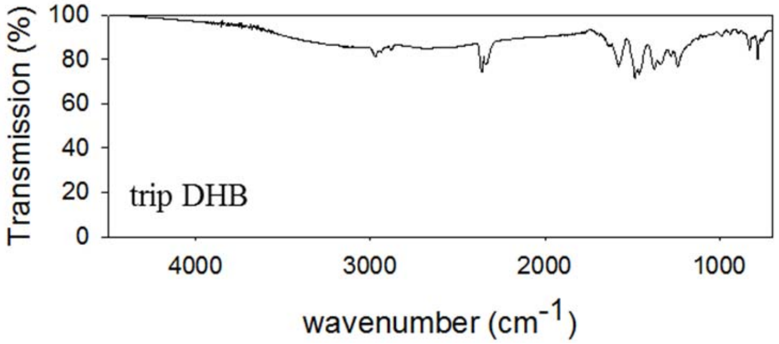
trip DHB
Transmission (%)
100
80
60
40
20
0
4000
3000
2000
1000
wavenumber (cm-1)

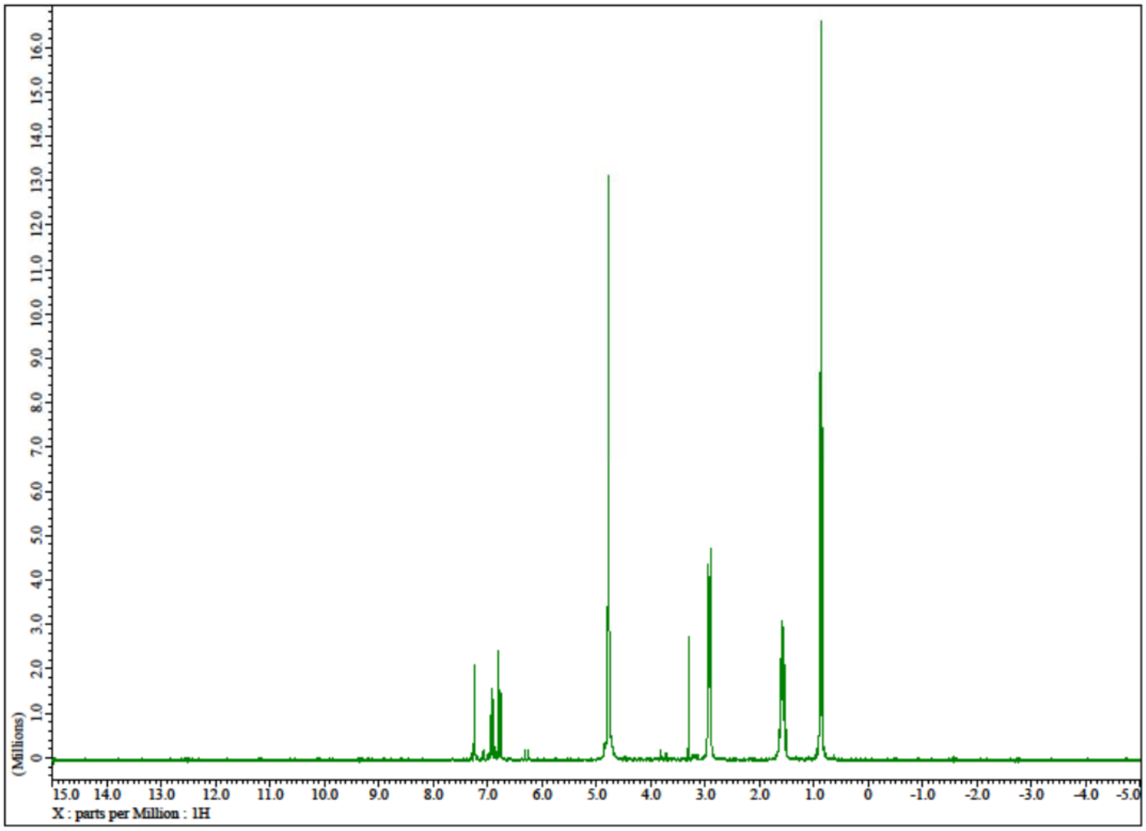(Millions)
16.0
15.0
14.0
13.0
12.0
11.0
10.0
9.0
8.0
7.0
6.0
5.0
4.0
3.0
2.0
1.0
0
15.0
14.0
13.0
12.0
11.0
10.0
9.0
8.0
7.0
6.0
5.0
4.0
3.0
2.0
1.0
0
-1.0
-2.0
-3.0
-4.0
-5.0
X : parts per Million : 1H

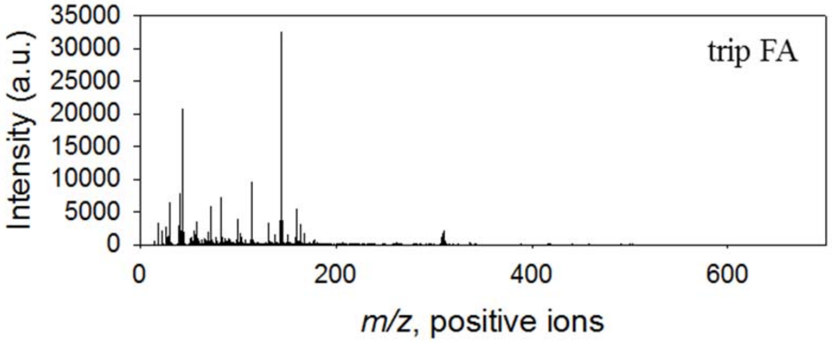
trip FA
Intensity (a.u.)
35000
30000
25000
20000
15000
10000
5000
0
0
200
400
600
m/z, positive ions

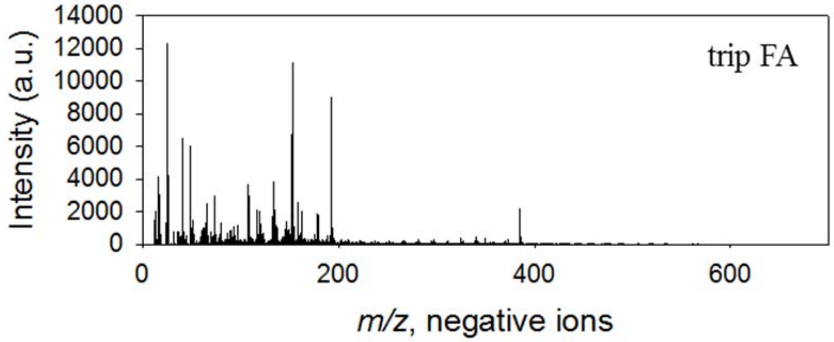
trip FA
Intensity (a.u.)
14000
12000
10000
8000
6000
4000
2000
0
0
200
400
600
m/z, negative ions

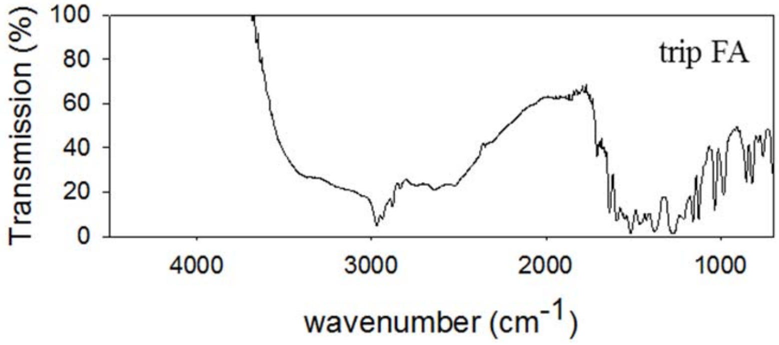
trip FA
Transmission (%)
100
80
60
40
20
0
4000
3000
2000
1000
wavenumber (cm-1)

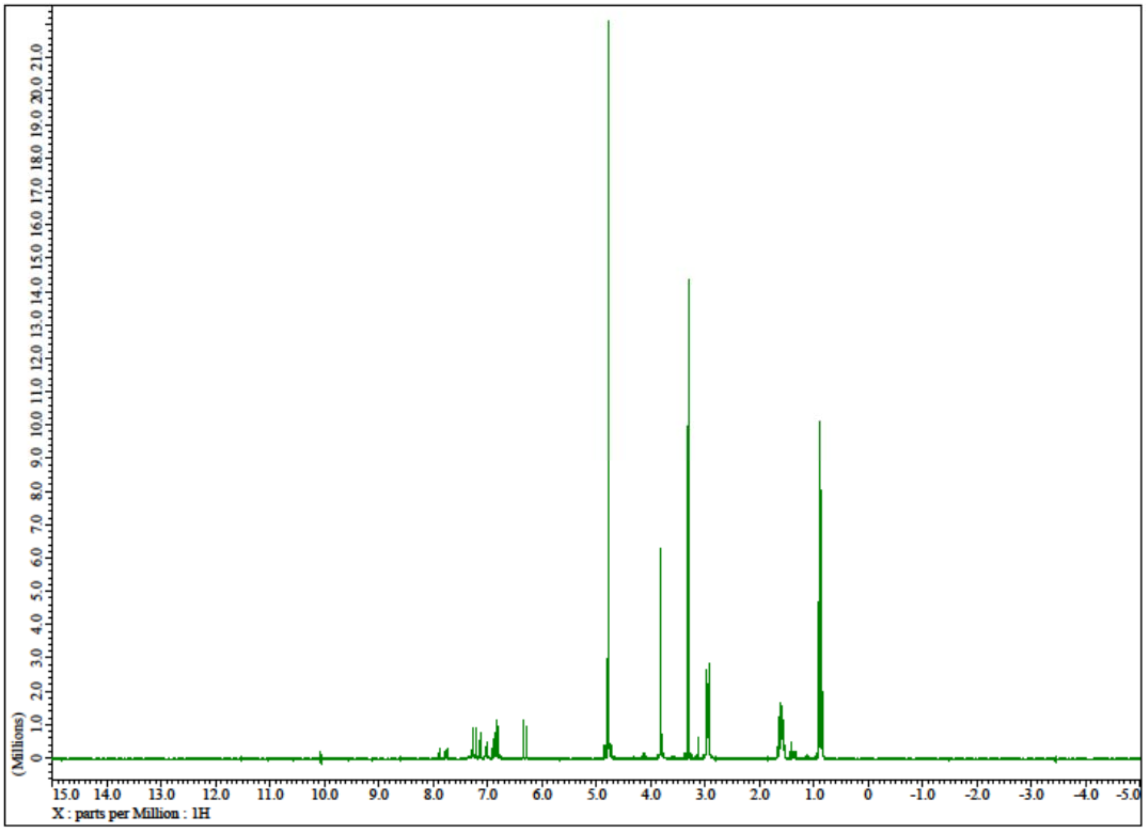
(Millions)
0
1.0
2.0
3.0
4.0
5.0
6.0
7.0
8.0
9.0
10.0
11.0
12.0
13.0
14.0
15.0
16.0
17.0
18.0
19.0
20.0
21.0
15.0
14.0
13.0
12.0
11.0
10.0
9.0
8.0
7.0
6.0
5.0
4.0
3.0
2.0
1.0
0
-1.0
-2.0
-3.0
-4.0
-5.0
X : parts per Million : 1H

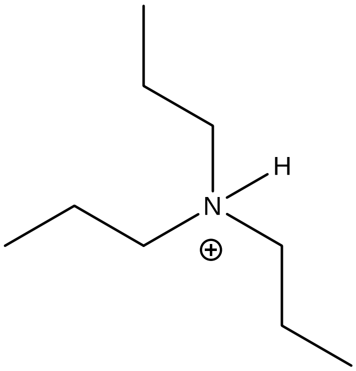
H
N
⊕

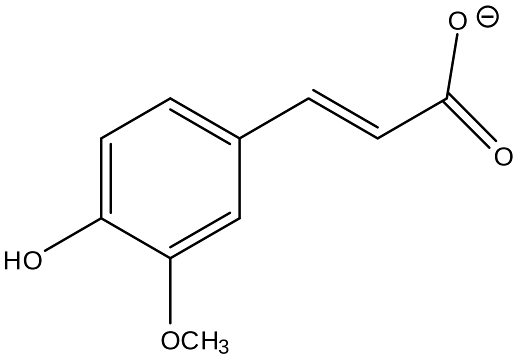
O ⊖
O
HO
OCH3

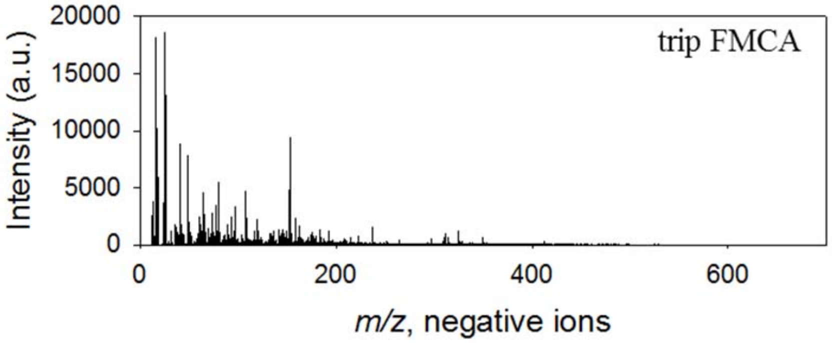

trip FMCA
Intensity (a.u.)
20000
15000
10000
5000
0
0
200
400
600
m/z, negative ions

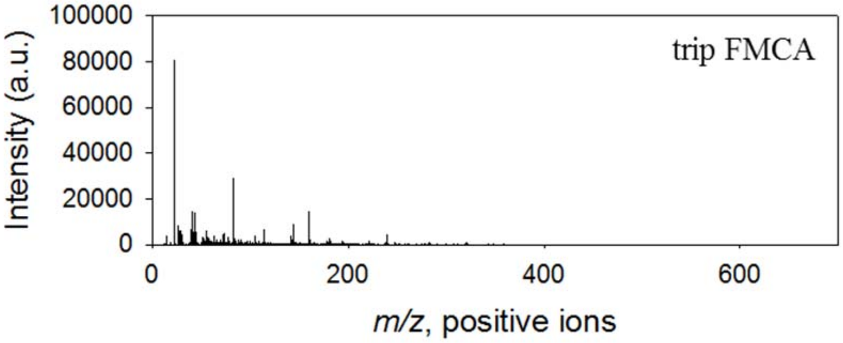

trip FMCA
Intensity (a.u.)
100000
80000
60000
40000
20000
0
0
200
400
600
m/z, positive ions

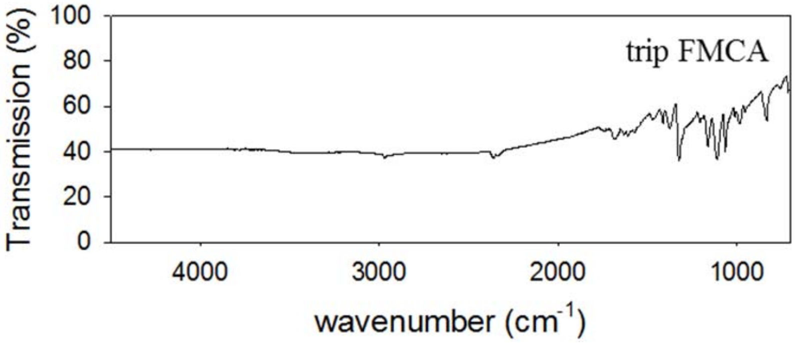

trip FMCA
Transmission (%)
100
80
60
40
20
0
4000
3000
2000
1000
wavenumber (cm-1)

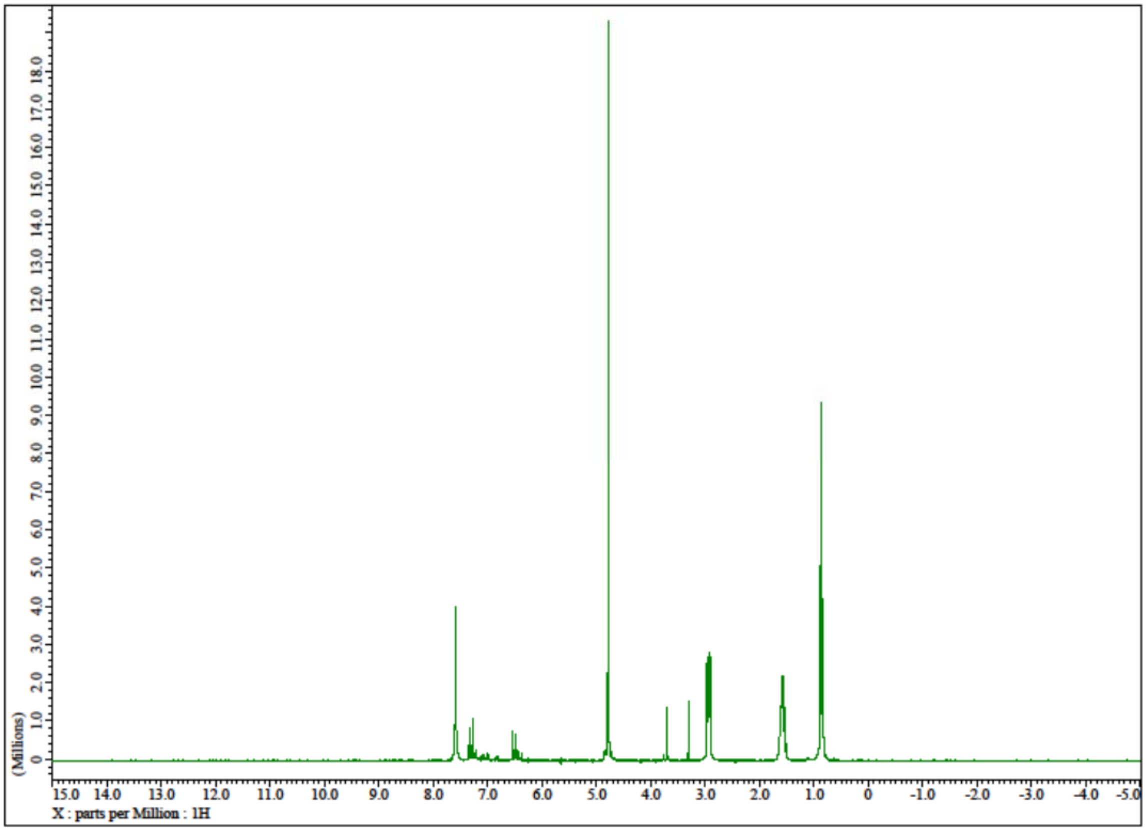
(Millions)
0
1.0
2.0
3.0
4.0
5.0
6.0
7.0
8.0
9.0
10.0
11.0
12.0
13.0
14.0
15.0
16.0
17.0
18.0
15.0
14.0
13.0
12.0
11.0
10.0
9.0
8.0
7.0
6.0
5.0
4.0
3.0
2.0
1.0
0
-1.0
-2.0
-3.0
-4.0
-5.0
X : parts per Million : 1H

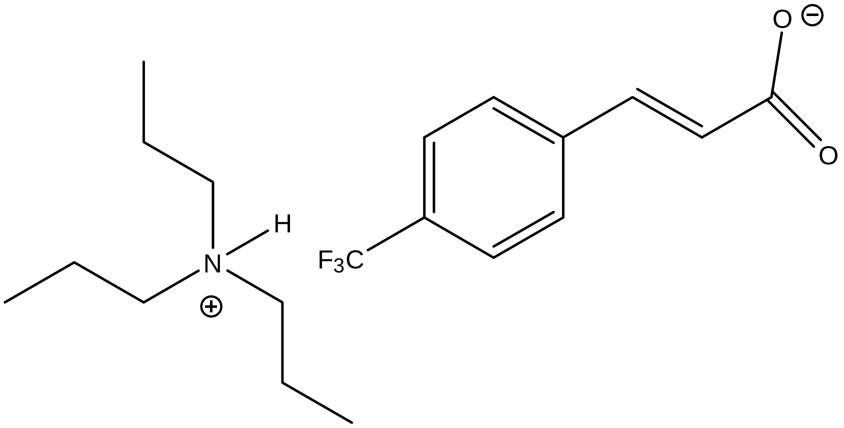
O ⊖
O
H
N
⊕
F3C

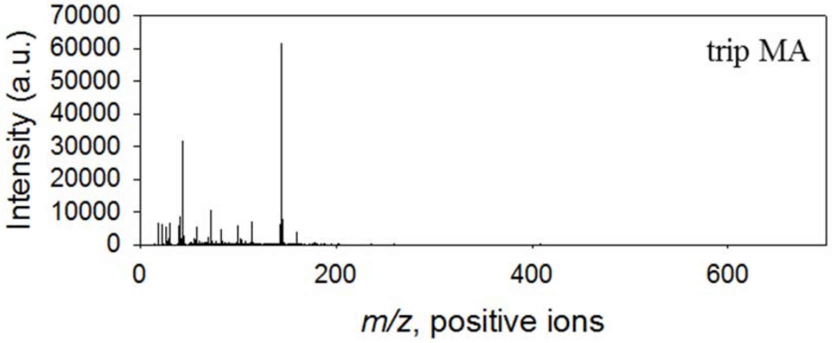
trip MA
Intensity (a.u.)
70000
60000
50000
40000
30000
20000
10000
0
0
200
400
600
m/z, positive ions

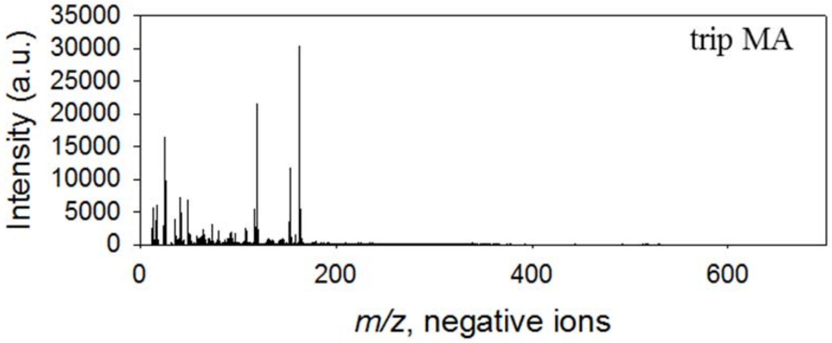
trip MA
Intensity (a.u.)
35000
30000
25000
20000
15000
10000
5000
0
0
200
400
600
m/z, negative ions

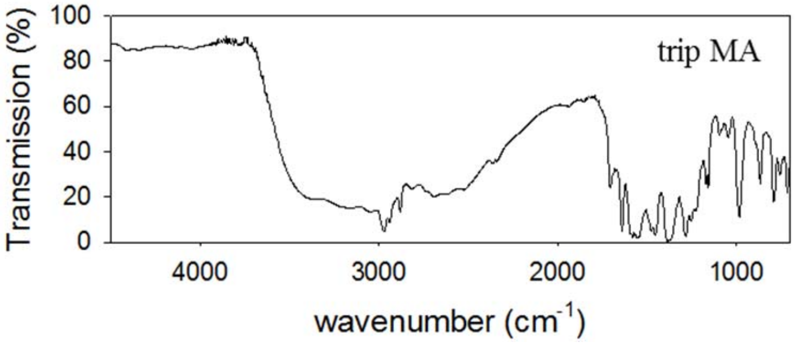
trip MA
Transmission (%)
100
80
60
40
20
0
4000
3000
2000
1000
wavenumber (cm^{-1})

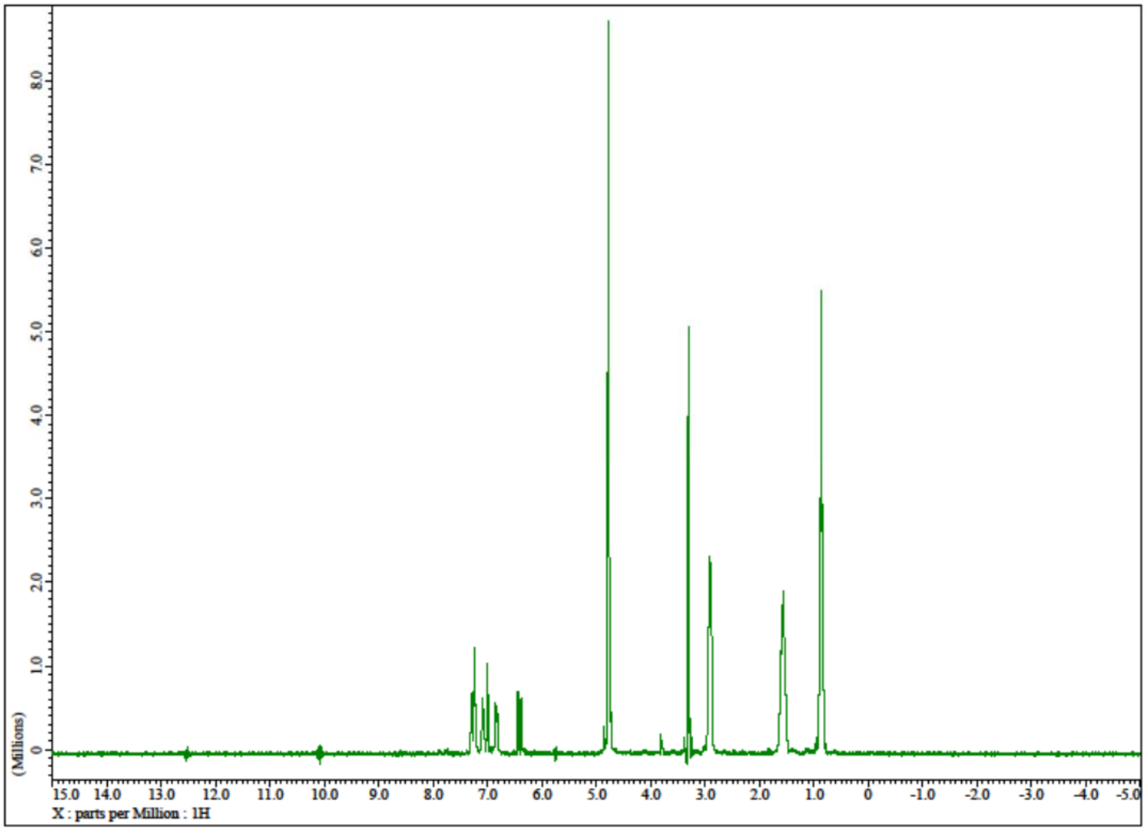
(Millions)
0
1.0
2.0
3.0
4.0
5.0
6.0
7.0
8.0
15.0
14.0
13.0
12.0
11.0
10.0
9.0
8.0
7.0
6.0
5.0
4.0
3.0
2.0
1.0
0
-1.0
-2.0
-3.0
-4.0
-5.0
X : parts per Million : 1H

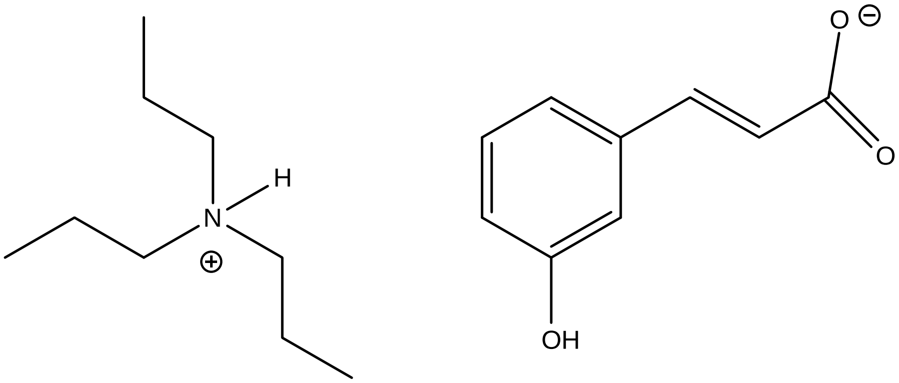
N
H
⊕
O
⊖
O
OH

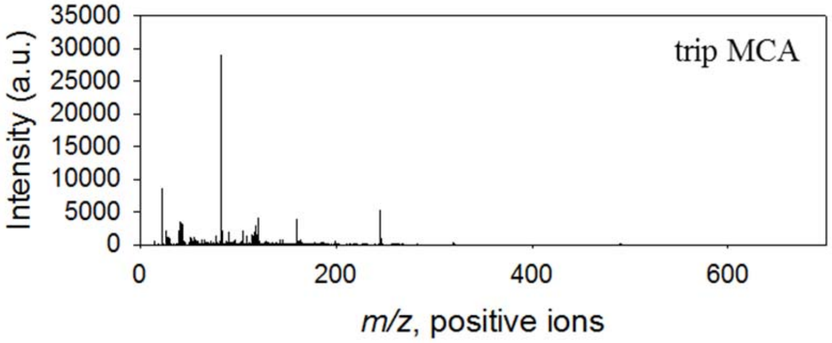

Intensity (a.u.)
35000
30000
25000
20000
15000
10000
5000
0
0
200
400
600
m/z, positive ions
trip MCA

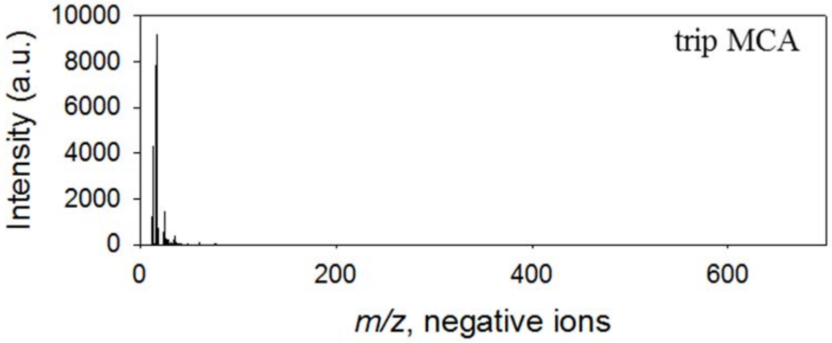

Intensity (a.u.)
10000
8000
6000
4000
2000
0
0
200
400
600
m/z, negative ions
trip MCA

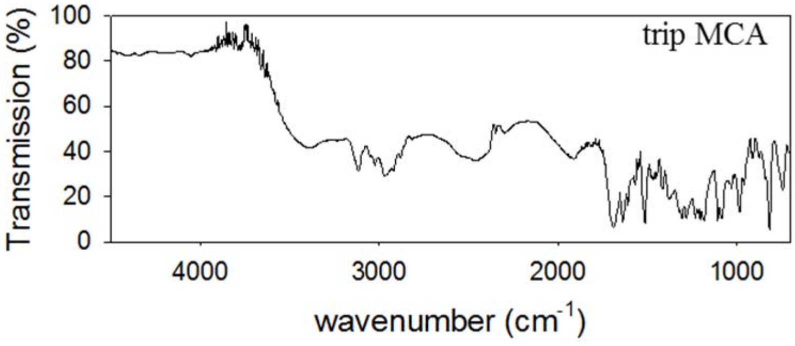

Transmission (%)
100
80
60
40
20
0
4000
3000
2000
1000
wavenumber (cm-1)
trip MCA

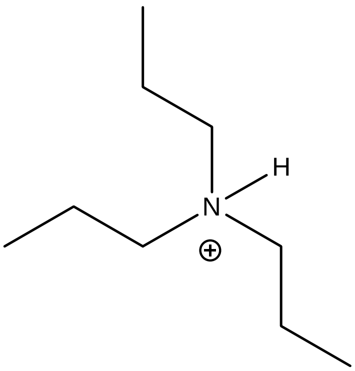

H
N
⊕

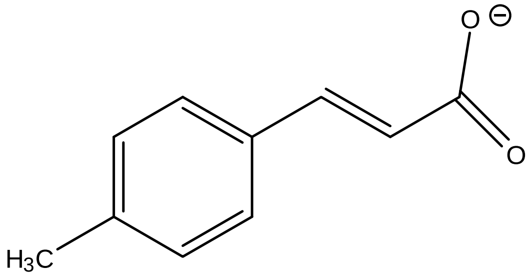

O ⊖
O
H3C

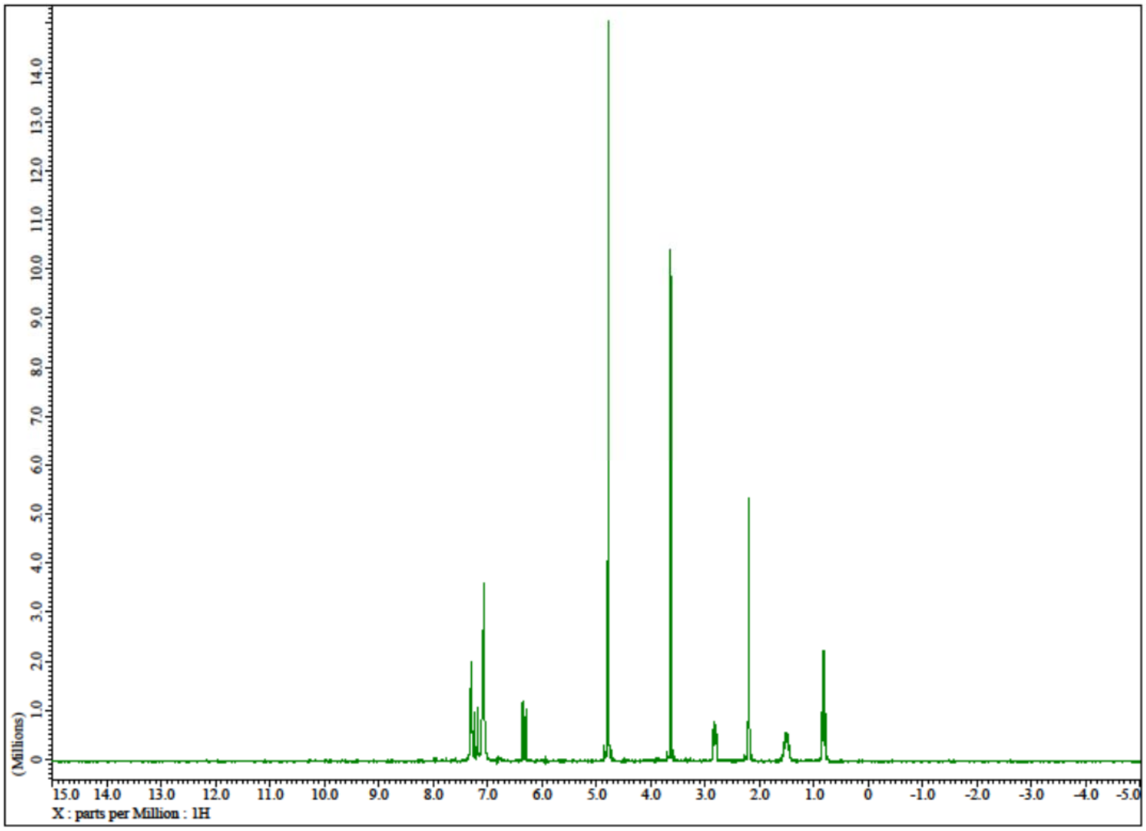
(Millions)
14.0
13.0
12.0
11.0
10.0
9.0
8.0
7.0
6.0
5.0
4.0
3.0
2.0
1.0
0
15.0 14.0 13.0 12.0 11.0 10.0 9.0 8.0 7.0 6.0 5.0 4.0 3.0 2.0 1.0 0 -1.0 -2.0 -3.0 -4.0 -5.0
X : parts per Million : 1H

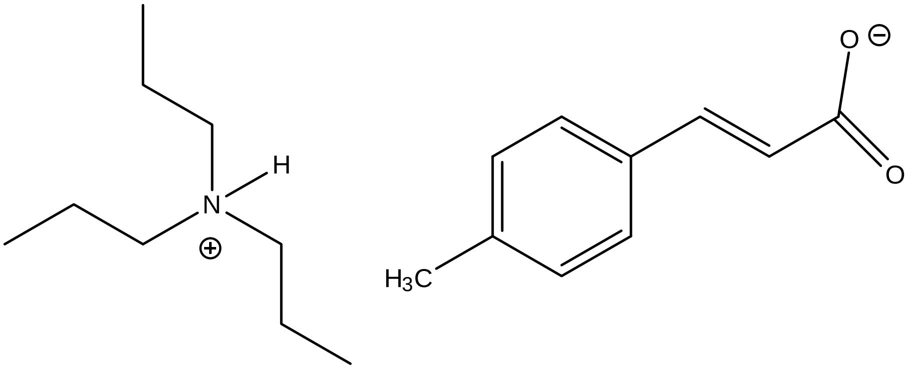
H
N
⊕
O ⊖
O
H3C

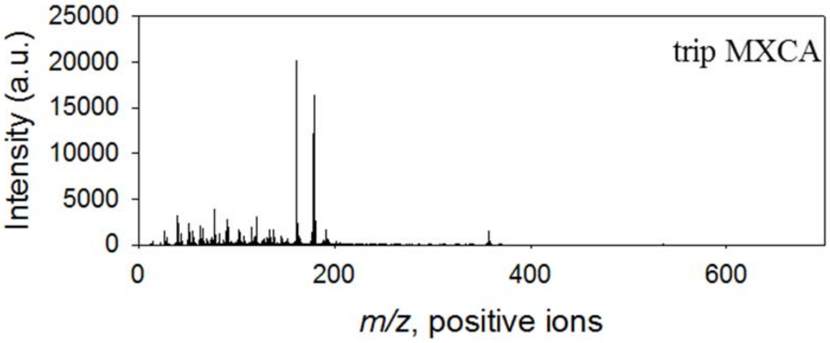
trip MXCA
Intensity (a.u.)
25000
20000
15000
10000
5000
0
0
200
400
600
m/z, positive ions

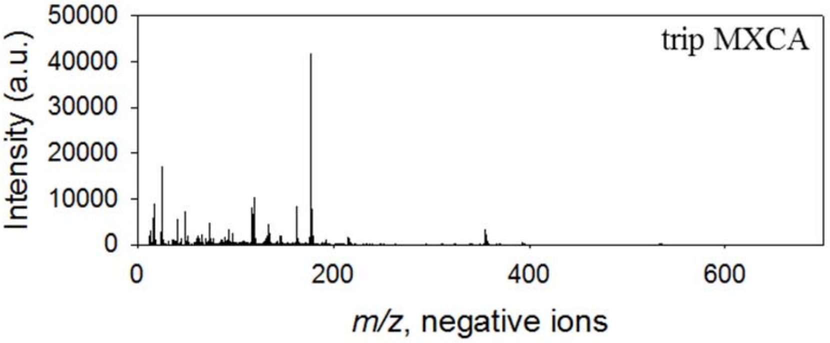
trip MXCA
Intensity (a.u.)
50000
40000
30000
20000
10000
0
0
200
400
600
m/z, negative ions

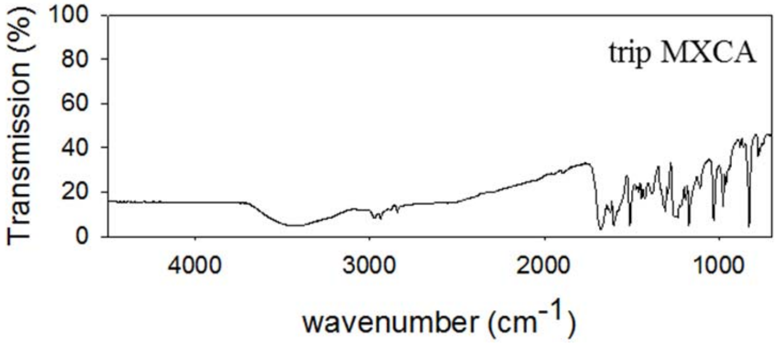
trip MXCA
Transmission (%)
100
80
60
40
20
0
4000
3000
2000
1000
wavenumber (cm-1)

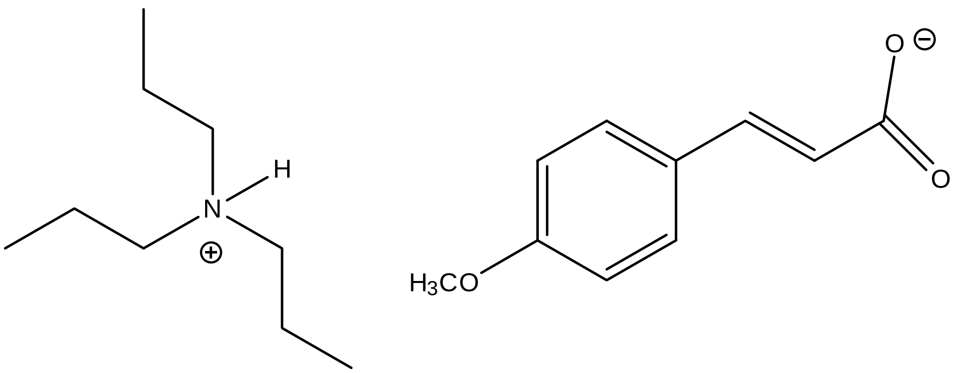
H
N
⊕
O ⊖
O
H3CO

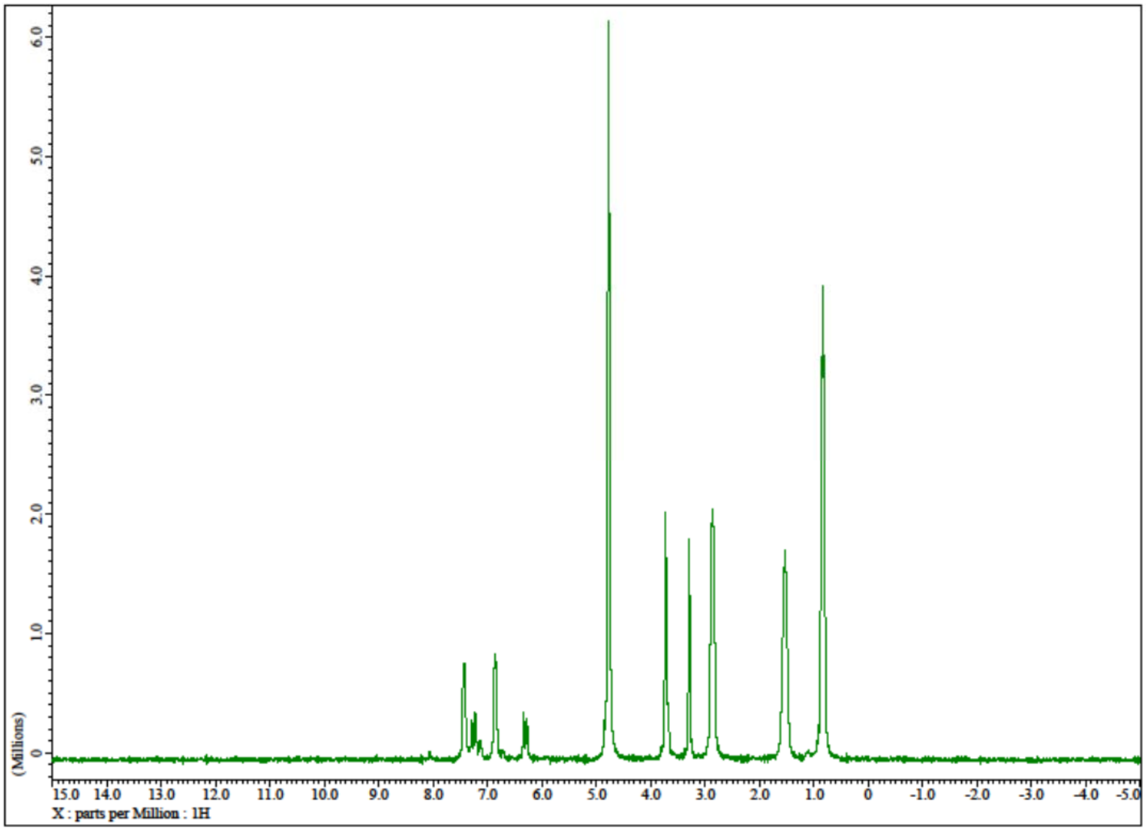
(Millions)
6.0
5.0
4.0
3.0
2.0
1.0
0
15.0 14.0 13.0 12.0 11.0 10.0 9.0 8.0 7.0 6.0 5.0 4.0 3.0 2.0 1.0 0 -1.0 -2.0 -3.0 -4.0 -5.0
X : parts per Million : 1H

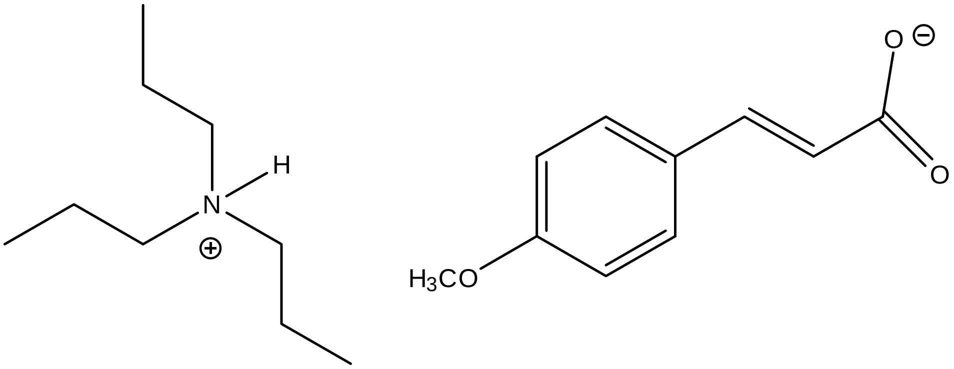
H
N
⊕
H3CO
O ⊖
O

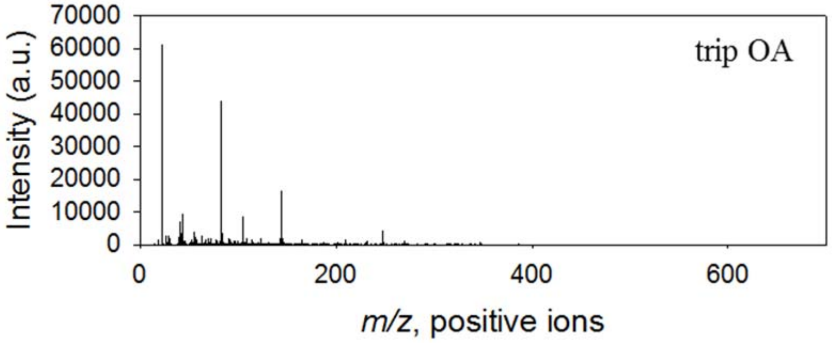
trip OA
Intensity (a.u.)
70000
60000
50000
40000
30000
20000
10000
0
0
200
400
600
m/z, positive ions

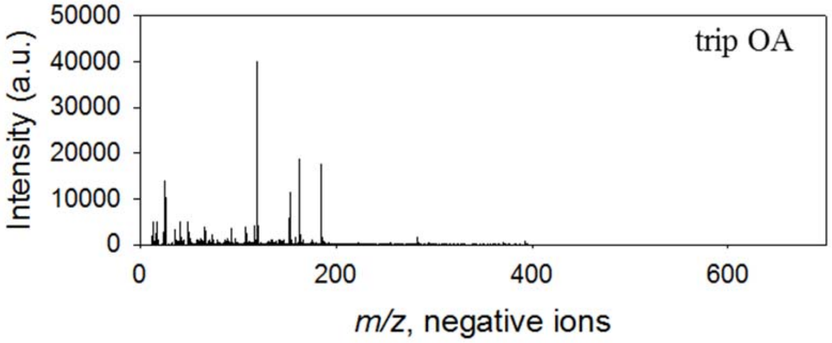
trip OA
Intensity (a.u.)
50000
40000
30000
20000
10000
0
0
200
400
600
m/z, negative ions

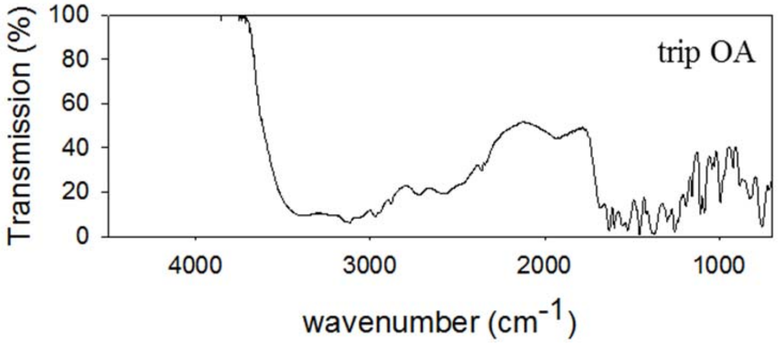
trip OA
Transmission (%)
100
80
60
40
20
0
4000
3000
2000
1000
wavenumber (cm-1)

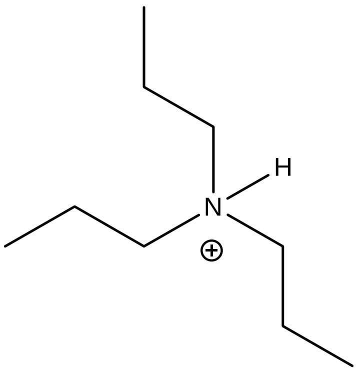
H
N
⊕

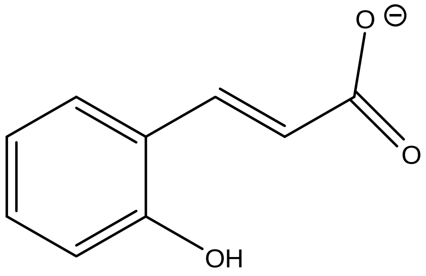
O ⊖
O
OH

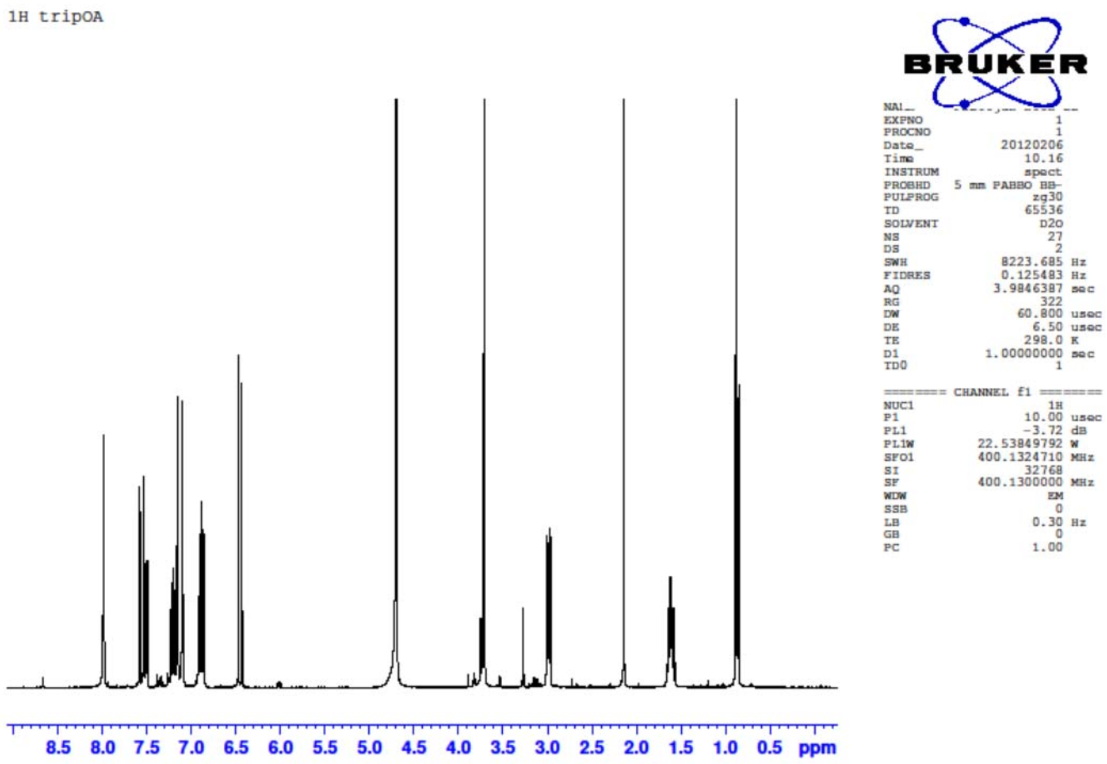

1H tripOA

```
NA[illegible]
EXPNO                    1
PROCNO                   1
Date_             20120206
Time                 10.16
INSTRUM              spect
PROBHD   5 mm PABBO BB-
PULPROG               zg30
TD                   65536
SOLVENT                D2O
NS                      27
DS                       2
SWH               8223.685 Hz
FIDRES            0.125483 Hz
AQ               3.9846387 sec
RG                     322
DW                  60.800 usec
DE                    6.50 usec
TE                   298.0 K
D1              1.00000000 sec
TD0                      1

======== CHANNEL f1 ========
NUC1                    1H
P1                   10.00 usec
PL1                  -3.72 dB
PL1W           22.53849792 W
SFO1           400.1324710 MHz
SI                   32768
SF             400.1300000 MHz
WDW                     EM
SSB                      0
LB                    0.30 Hz
GB                       0
PC                    1.00
```

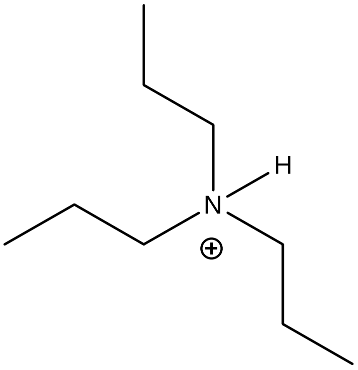

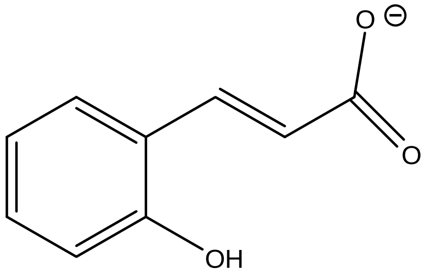

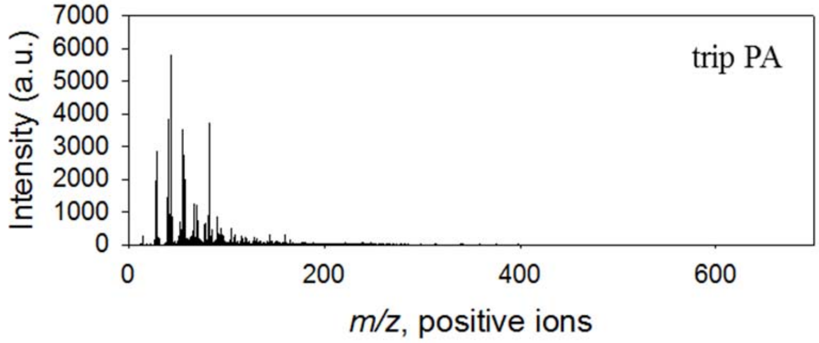
trip PA
Intensity (a.u.)
7000
6000
5000
4000
3000
2000
1000
0
0
200
400
600
m/z, positive ions

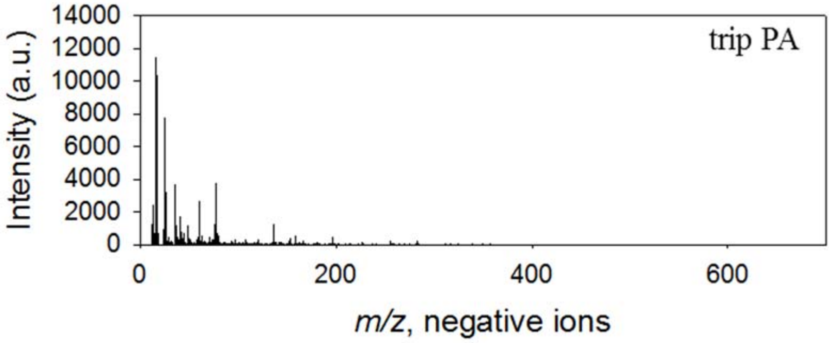
trip PA
Intensity (a.u.)
14000
12000
10000
8000
6000
4000
2000
0
0
200
400
600
m/z, negative ions

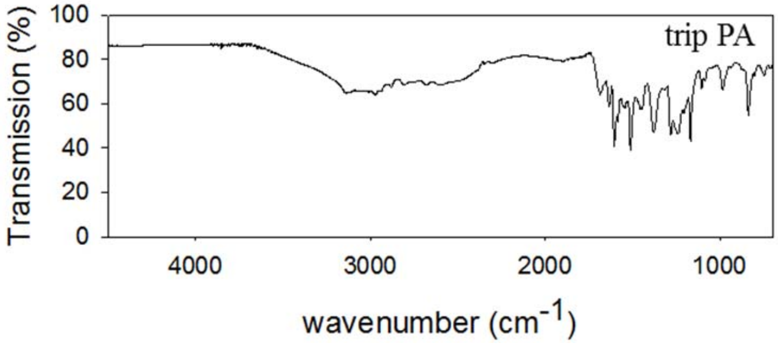
trip PA
Transmission (%)
100
80
60
40
20
0
4000
3000
2000
1000
wavenumber (cm-1)

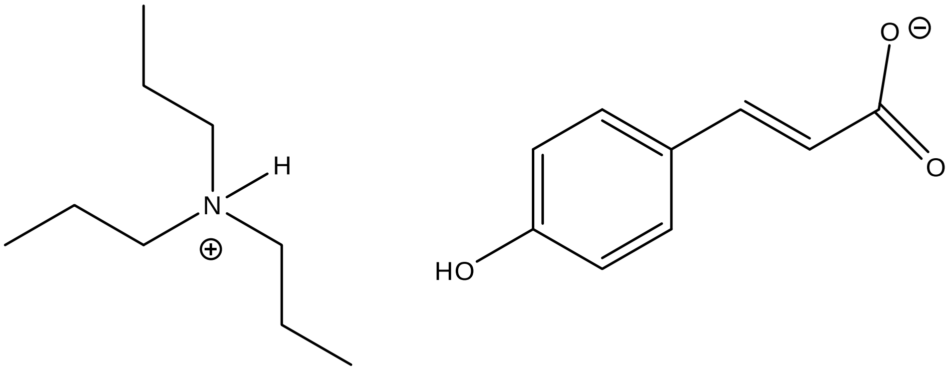
H
N
⊕
HO
O ⊖
O

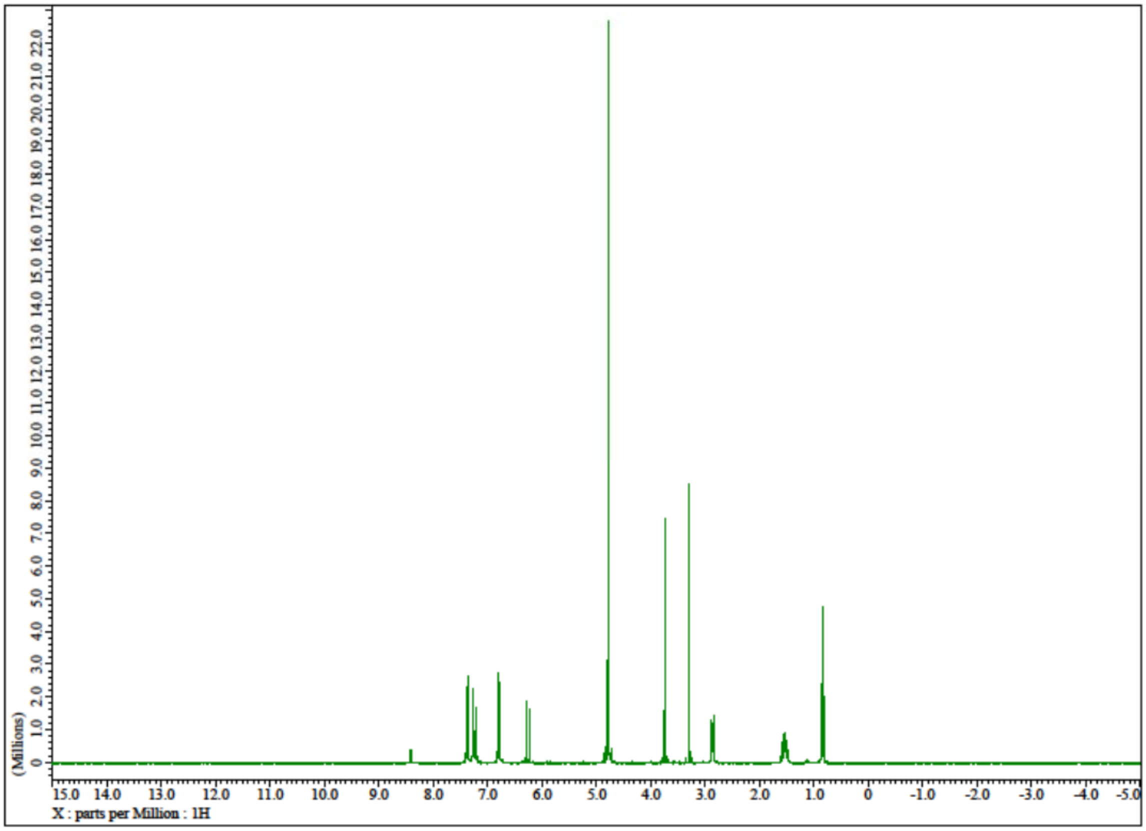
(Millions)
0
1.0
2.0
3.0
4.0
5.0
6.0
7.0
8.0
9.0
10.0
11.0
12.0
13.0
14.0
15.0
16.0
17.0
18.0
19.0
20.0
21.0
22.0
15.0
14.0
13.0
12.0
11.0
10.0
9.0
8.0
7.0
6.0
5.0
4.0
3.0
2.0
1.0
0
-1.0
-2.0
-3.0
-4.0
-5.0
X : parts per Million : 1H

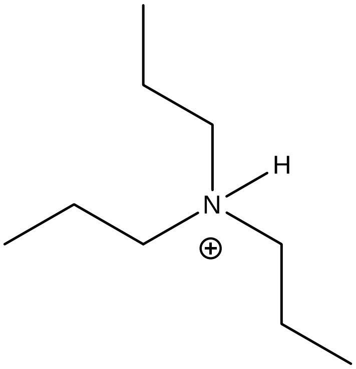
H
N
⊕

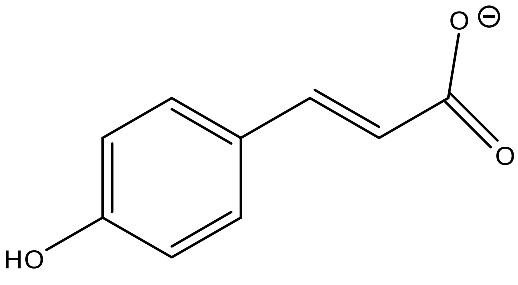
O ⊖
O
HO

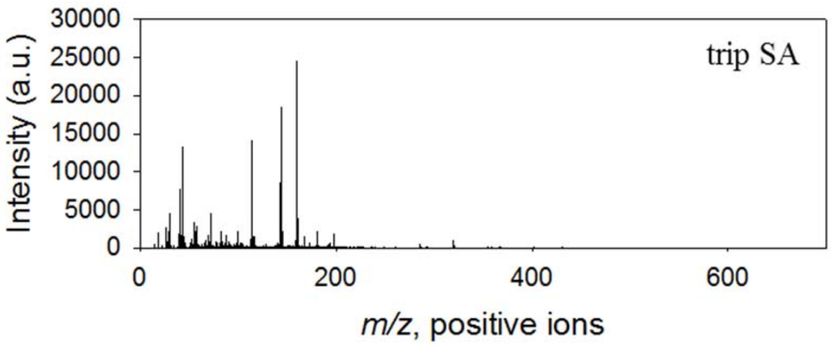
trip SA
Intensity (a.u.)
30000
25000
20000
15000
10000
5000
0
0
200
400
600
m/z, positive ions

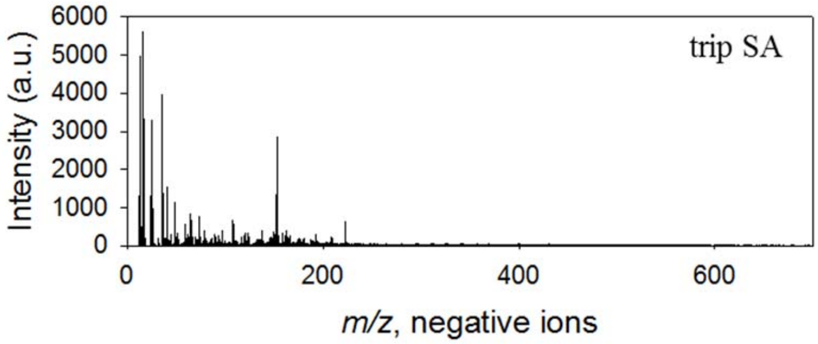
trip SA
Intensity (a.u.)
6000
5000
4000
3000
2000
1000
0
0
200
400
600
m/z, negative ions

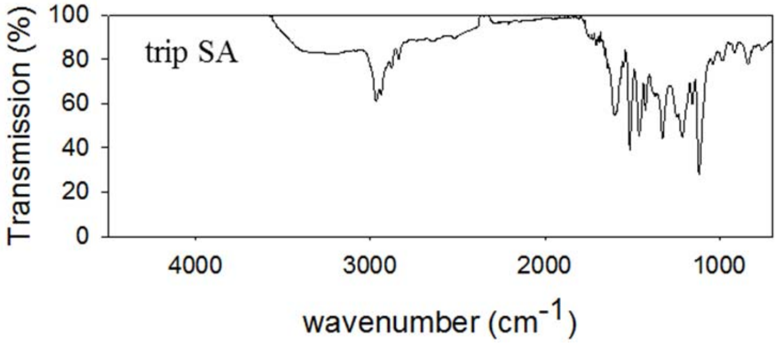
trip SA
Transmission (%)
100
80
60
40
20
0
4000
3000
2000
1000
wavenumber (cm-1)

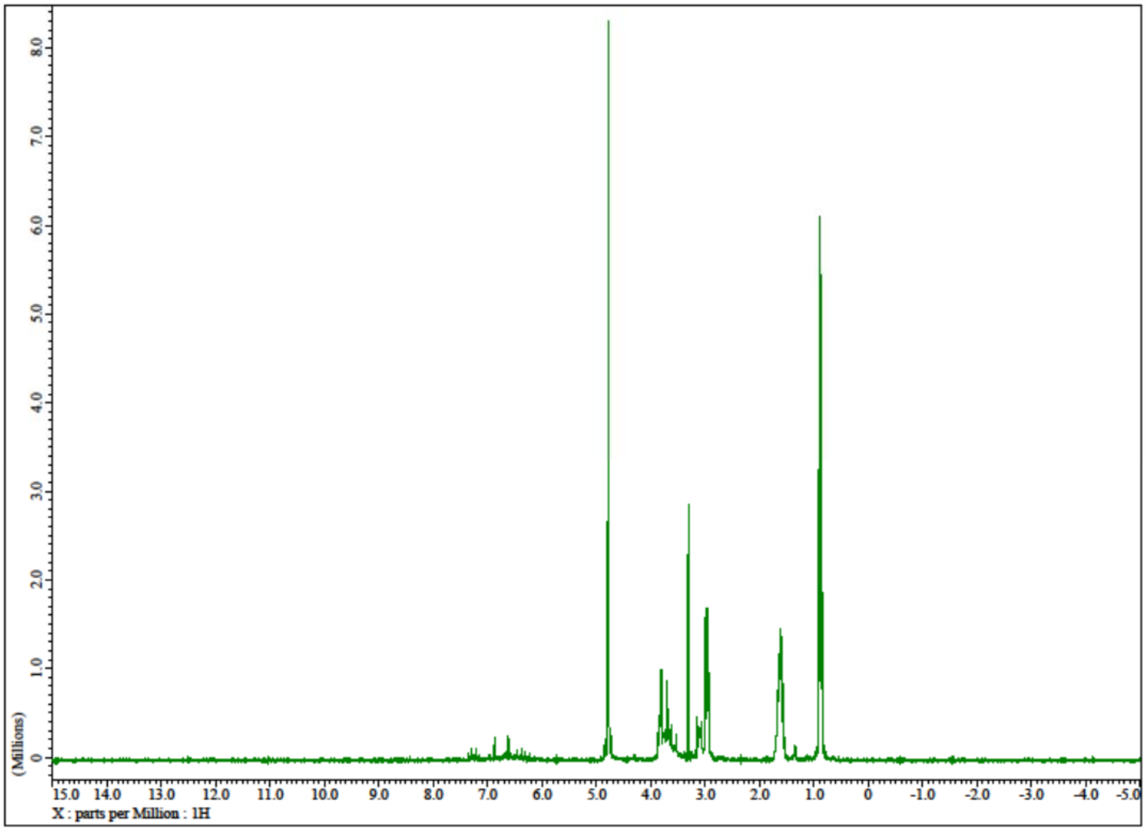
(Millions)
0
1.0
2.0
3.0
4.0
5.0
6.0
7.0
8.0
15.0 14.0 13.0 12.0 11.0 10.0 9.0 8.0 7.0 6.0 5.0 4.0 3.0 2.0 1.0 0 -1.0 -2.0 -3.0 -4.0 -5.0
X : parts per Million : 1H

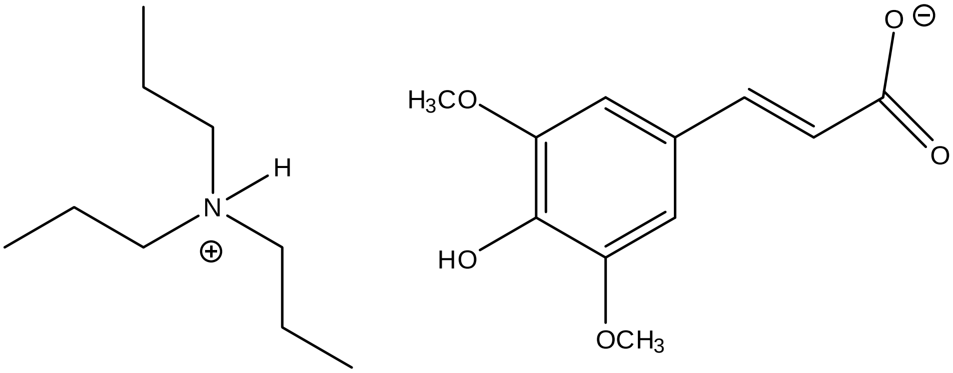
N
H
⊕
H3CO
HO
OCH3
O ⊖
O

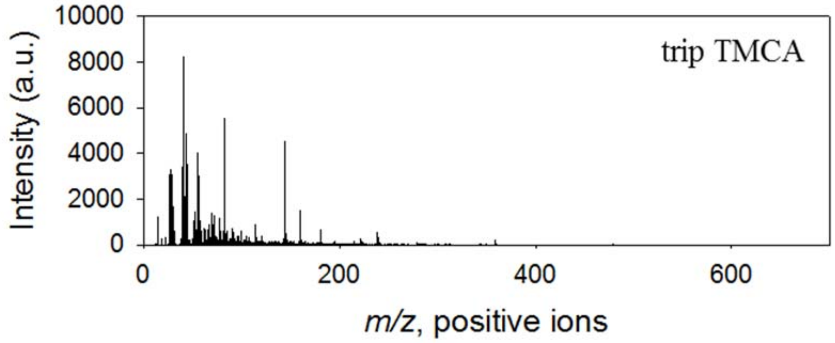
trip TMCA
Intensity (a.u.)
10000
8000
6000
4000
2000
0
0
200
400
600
m/z, positive ions

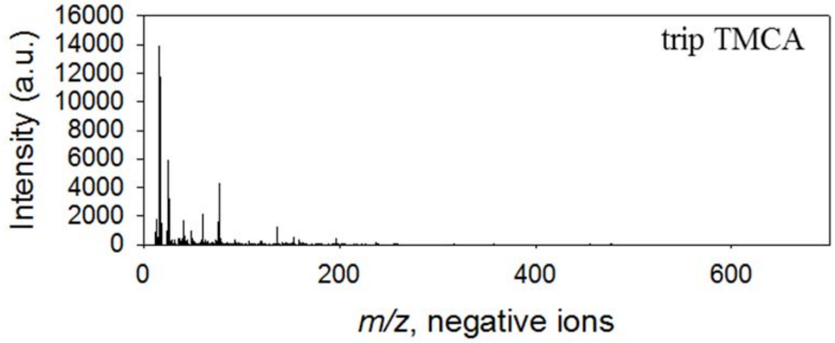
trip TMCA
Intensity (a.u.)
16000
14000
12000
10000
8000
6000
4000
2000
0
0
200
400
600
m/z, negative ions

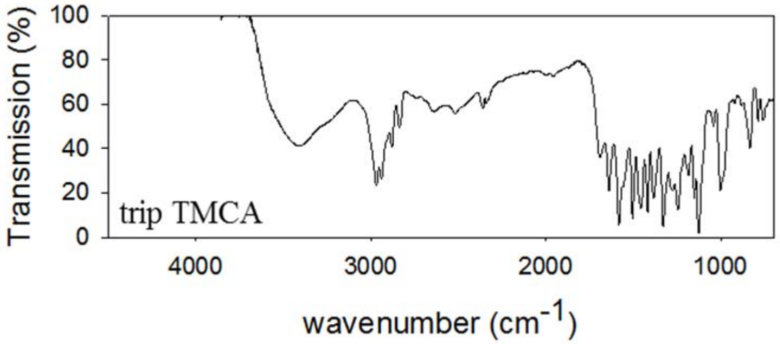
trip TMCA
Transmission (%)
100
80
60
40
20
0
4000
3000
2000
1000
wavenumber (cm-1)

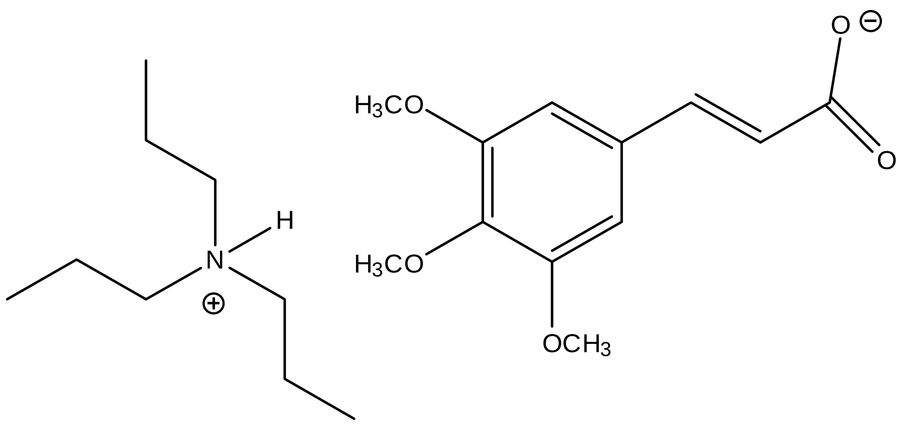
H
N
⊕
H3CO
H3CO
OCH3
O
O ⊖

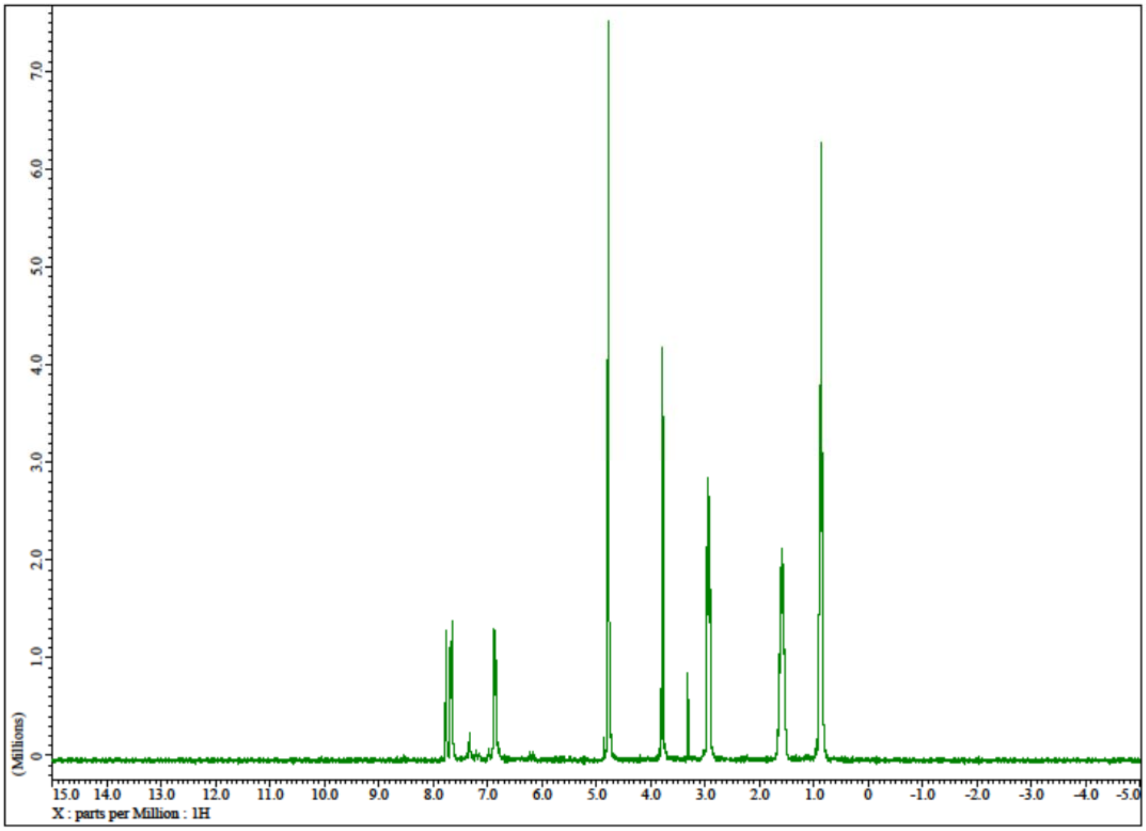
(Millions)
0
1.0
2.0
3.0
4.0
5.0
6.0
7.0
15.0 14.0 13.0 12.0 11.0 10.0 9.0 8.0 7.0 6.0 5.0 4.0 3.0 2.0 1.0 0 -1.0 -2.0 -3.0 -4.0 -5.0
X : parts per Million : 1H

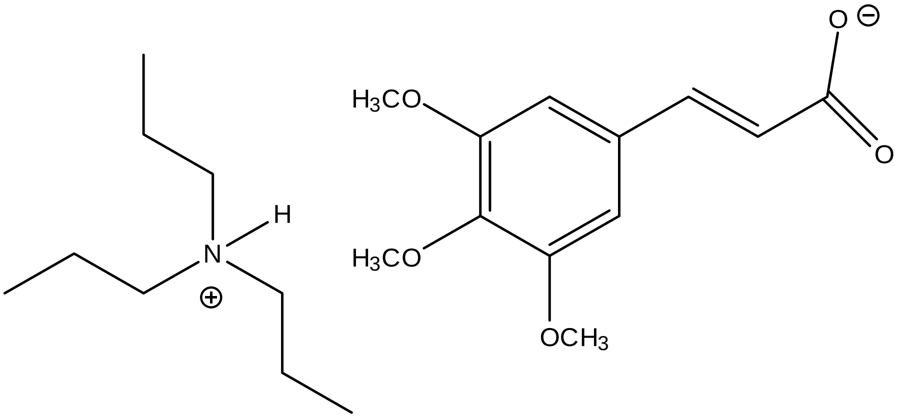
H
N
⊕
H3CO
H3CO
OCH3
O ⊖
O

Appendix 4

Complete Matrix and Analyte Spectra

Complete spectra of all ionic liquid and analyte spectra are in Appendix 4. They are arranged in the following manner. First by analyte, and then by alphabetical abbreviation of anion. The neat analyte spectra are always first. The order of the analytes is given below:

DPPC

d62 DPPC

d75 DPPC

DPPE

Cholesterol

Bradykinin

Leucine Enkephalin

PS

PPG

PDMPO

PEO

PMMA

PI

Angiotensin I

Insulin

Cytochrome c

GRFH

β endorphin

Bradykinin (2-7)

Bradykinin (2-9)

Lys-(Des-Arg9) bradykinin

Lys-(Des-Arg9-Leu8) bradykinin

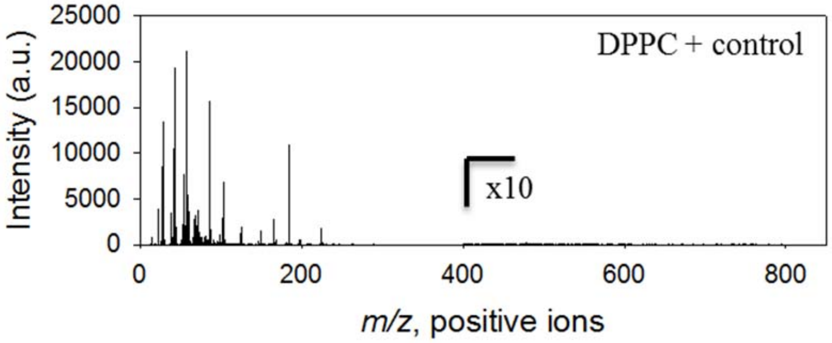
25000
20000
15000
10000
5000
0
Intensity (a.u.)
DPPC + control
x10
0
200
400
600
800
m/z, positive ions

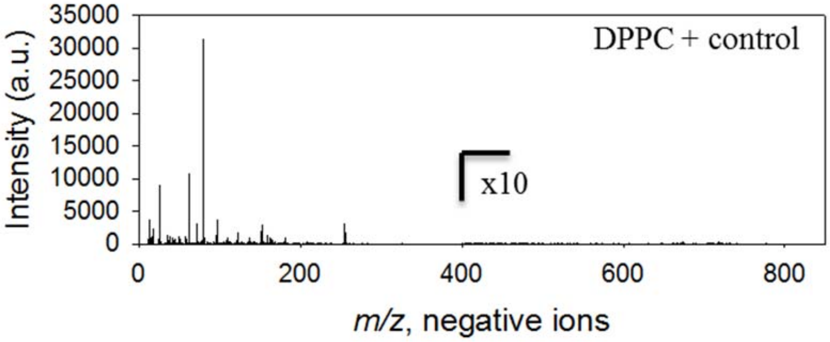
35000
30000
25000
20000
15000
10000
5000
0
Intensity (a.u.)
DPPC + control
x10
0
200
400
600
800
m/z, negative ions

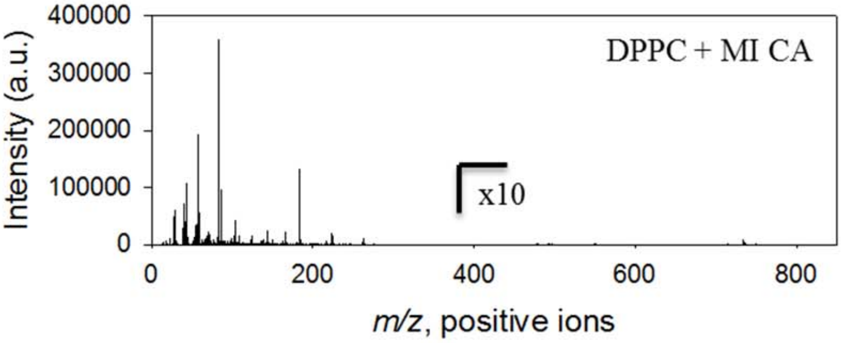
Intensity (a.u.)
400000
300000
200000
100000
0
DPPC + MI CA
x10
0
200
400
600
800
m/z, positive ions

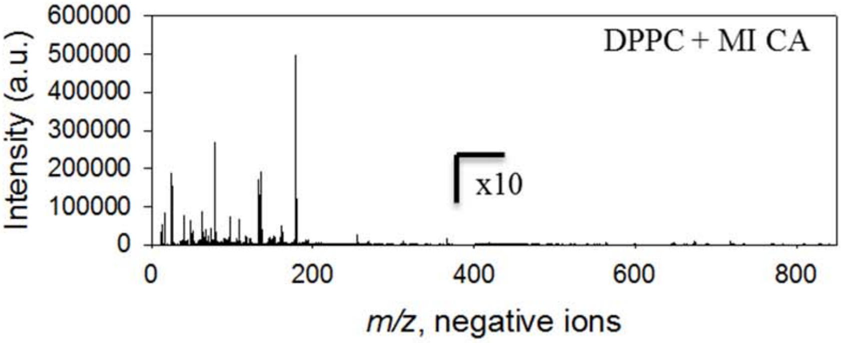
Intensity (a.u.)
600000
500000
400000
300000
200000
100000
0
DPPC + MI CA
x10
0
200
400
600
800
m/z, negative ions

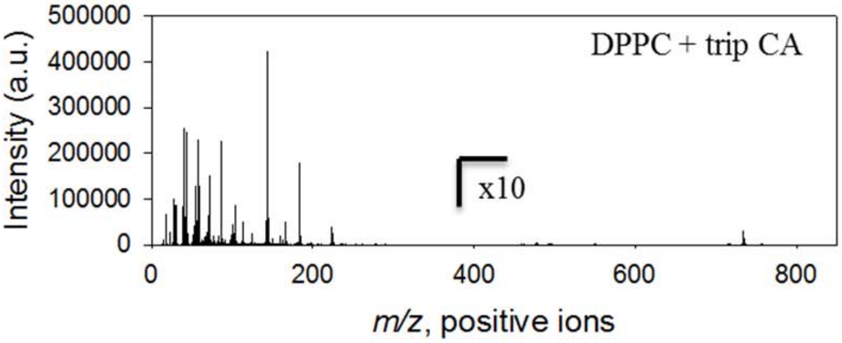
Intensity (a.u.)
500000
400000
300000
200000
100000
0
DPPC + trip CA
x10
0
200
400
600
800
m/z, positive ions

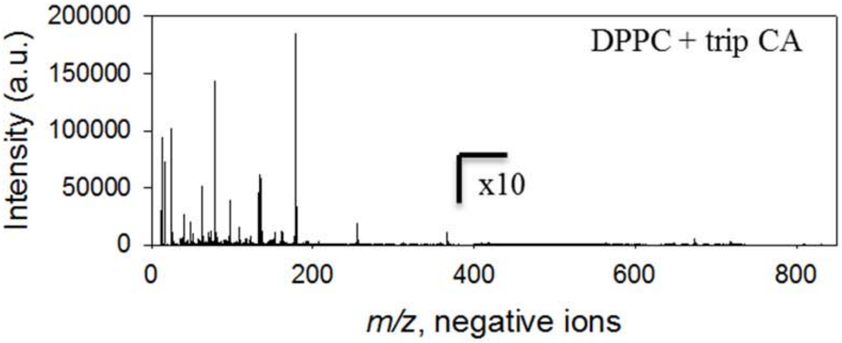
Intensity (a.u.)
200000
150000
100000
50000
0
DPPC + trip CA
x10
0
200
400
600
800
m/z, negative ions

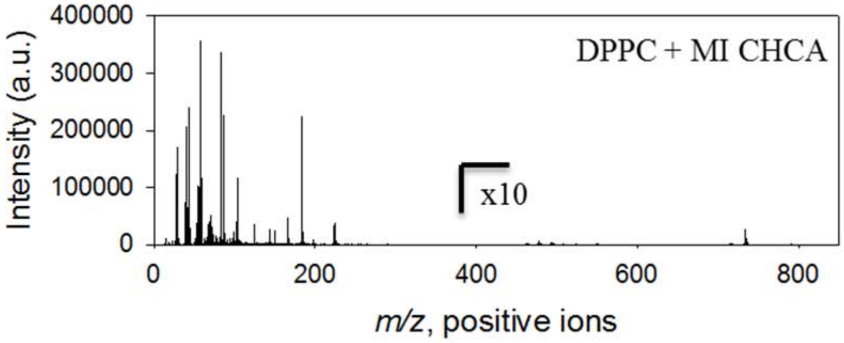
DPPC + MI CHCA
x10
Intensity (a.u.)
400000
300000
200000
100000
0
0
200
400
600
800
m/z, positive ions

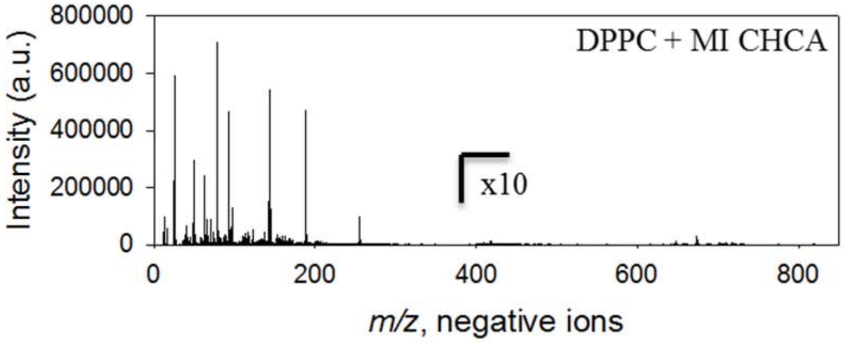
DPPC + MI CHCA
x10
Intensity (a.u.)
800000
600000
400000
200000
0
0
200
400
600
800
m/z, negative ions

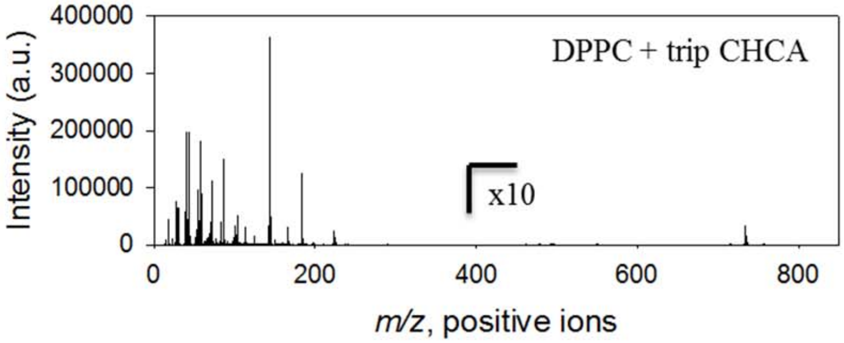
DPPC + trip CHCA
x10
Intensity (a.u.)
400000
300000
200000
100000
0
0
200
400
600
800
m/z, positive ions

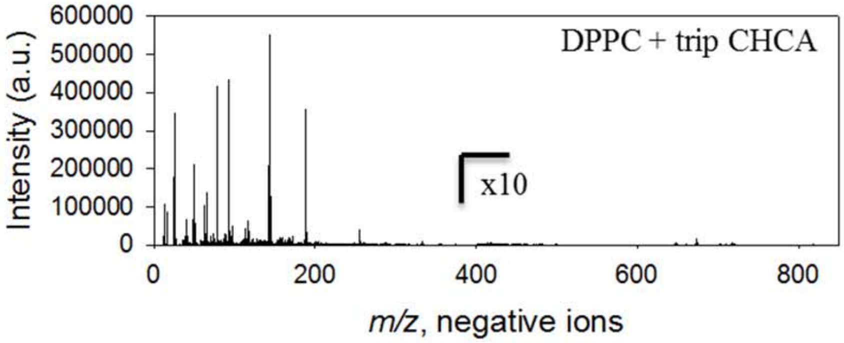
DPPC + trip CHCA
x10
Intensity (a.u.)
600000
500000
400000
300000
200000
100000
0
0
200
400
600
800
m/z, negative ions

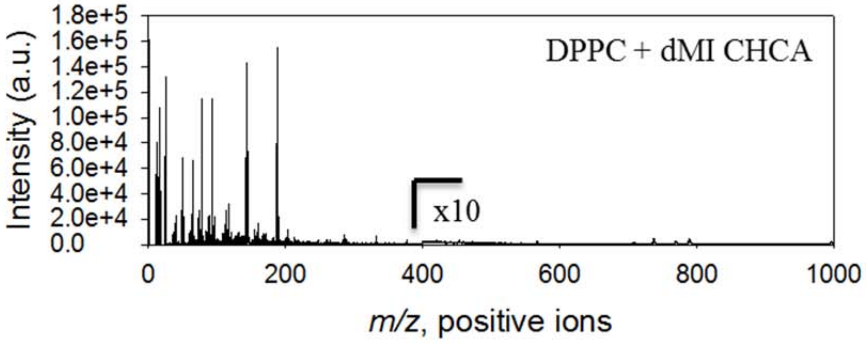
DPPC + dMI CHCA
Intensity (a.u.)
1.8e+5
1.6e+5
1.4e+5
1.2e+5
1.0e+5
8.0e+4
6.0e+4
4.0e+4
2.0e+4
0.0
x10
0
200
400
600
800
1000
m/z, positive ions

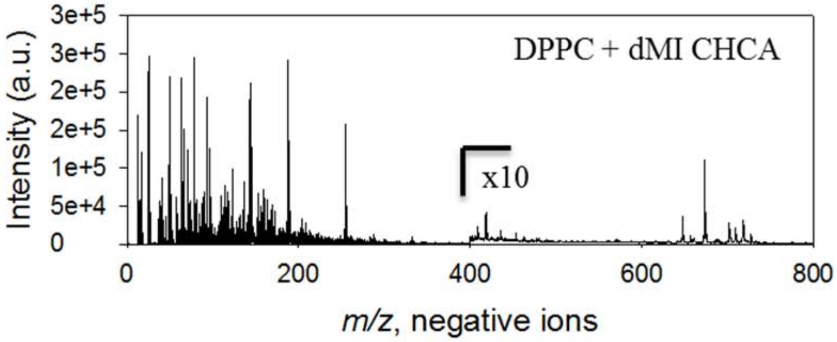
DPPC + dMI CHCA
Intensity (a.u.)
3e+5
3e+5
2e+5
2e+5
1e+5
5e+4
0
x10
0
200
400
600
800
m/z, negative ions

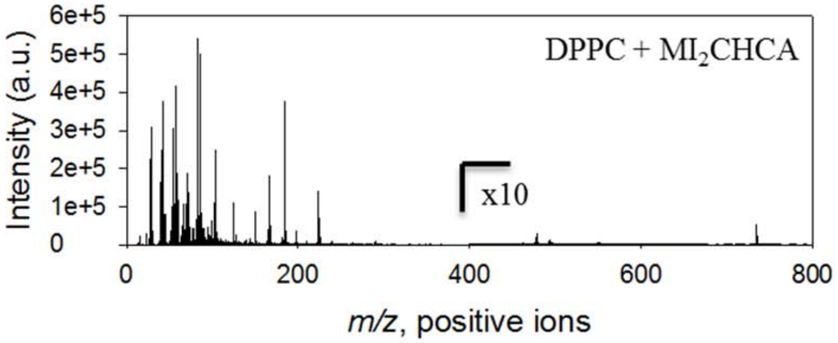
DPPC + MI_2CHCA
Intensity (a.u.)
6e+5
5e+5
4e+5
3e+5
2e+5
1e+5
0
x10
0
200
400
600
800
m/z, positive ions

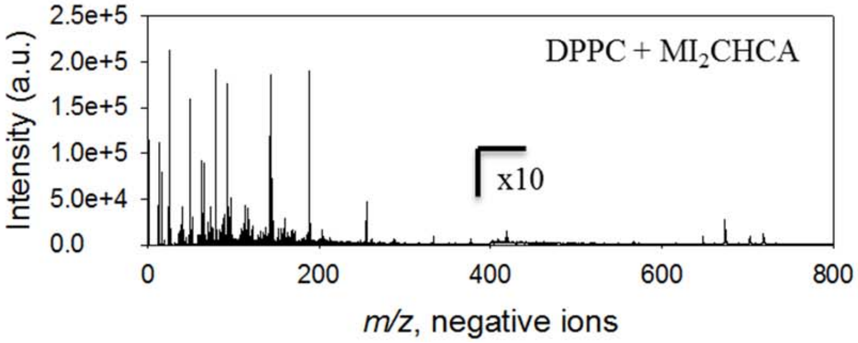
DPPC + MI_2CHCA
Intensity (a.u.)
2.5e+5
2.0e+5
1.5e+5
1.0e+5
5.0e+4
0.0
x10
0
200
400
600
800
m/z, negative ions

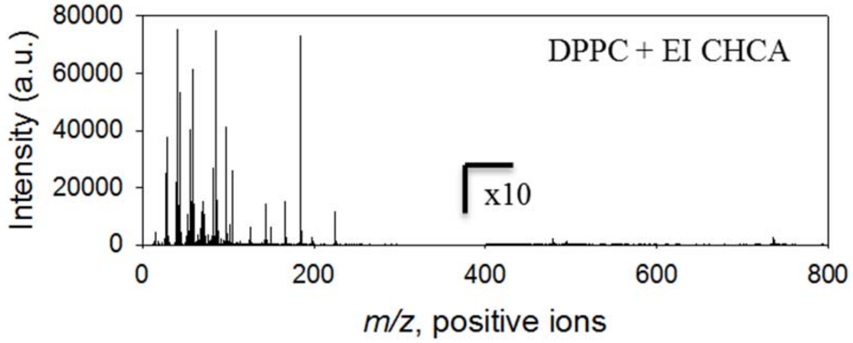
DPPC + EI CHCA
x10
Intensity (a.u.)
80000
60000
40000
20000
0
0
200
400
600
800
m/z, positive ions

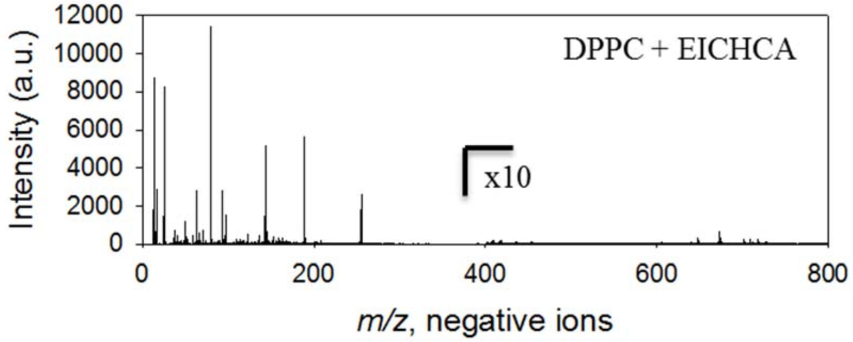
DPPC + EICHCA
x10
Intensity (a.u.)
12000
10000
8000
6000
4000
2000
0
0
200
400
600
800
m/z, negative ions

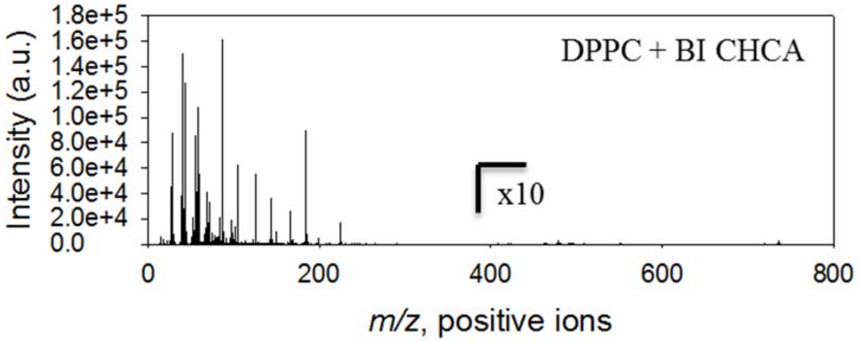
DPPC + BI CHCA
x10
Intensity (a.u.)
1.8e+5
1.6e+5
1.4e+5
1.2e+5
1.0e+5
8.0e+4
6.0e+4
4.0e+4
2.0e+4
0.0
0
200
400
600
800
m/z, positive ions

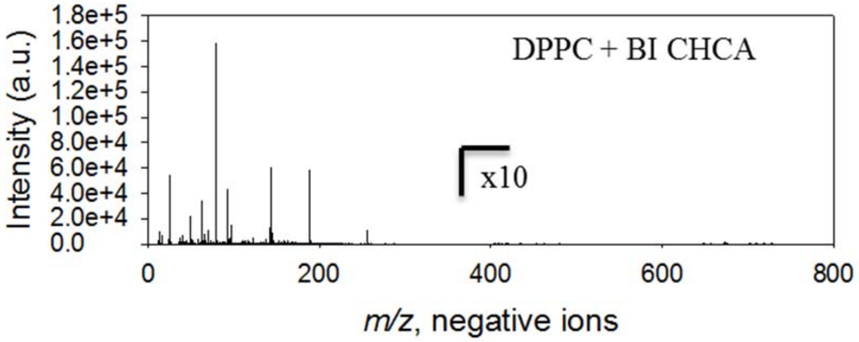
DPPC + BI CHCA
x10
Intensity (a.u.)
1.8e+5
1.6e+5
1.4e+5
1.2e+5
1.0e+5
8.0e+4
6.0e+4
4.0e+4
2.0e+4
0.0
0
200
400
600
800
m/z, negative ions

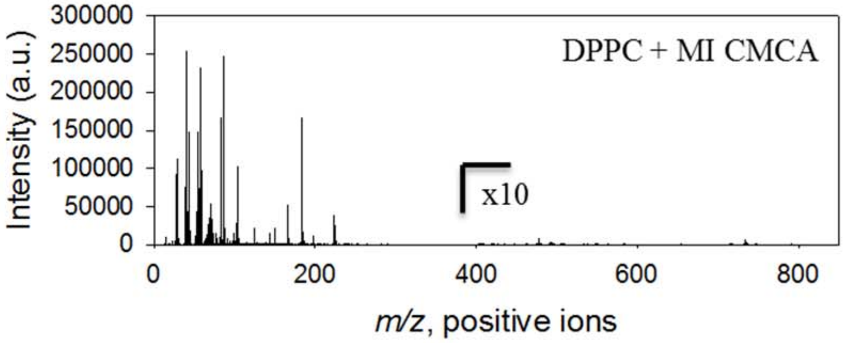
DPPC + MI CMCA
x10
Intensity (a.u.)
300000
250000
200000
150000
100000
50000
0
0
200
400
600
800
m/z, positive ions

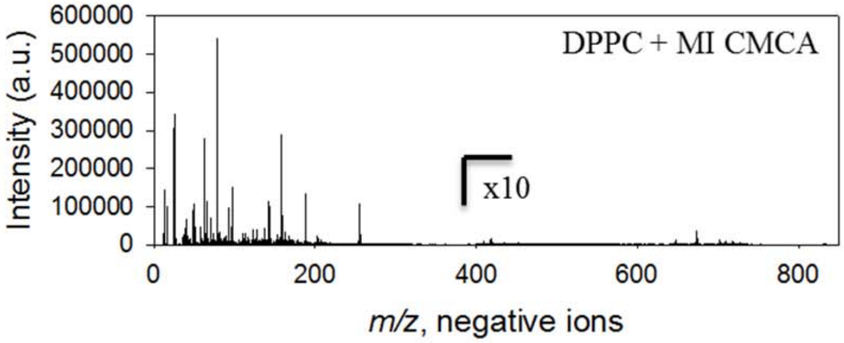
DPPC + MI CMCA
x10
Intensity (a.u.)
600000
500000
400000
300000
200000
100000
0
0
200
400
600
800
m/z, negative ions

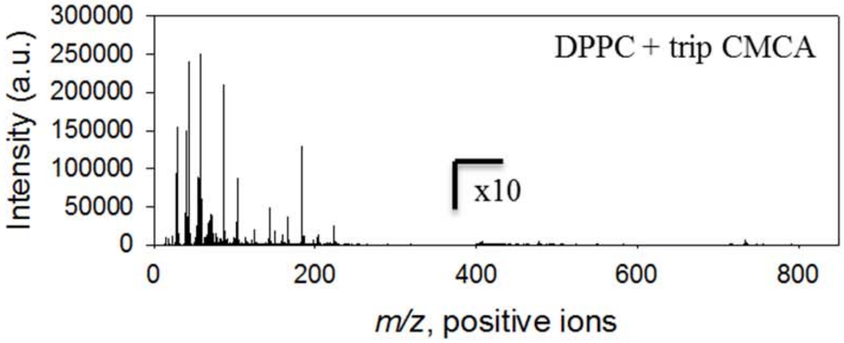
DPPC + trip CMCA
x10
Intensity (a.u.)
300000
250000
200000
150000
100000
50000
0
0
200
400
600
800
m/z, positive ions

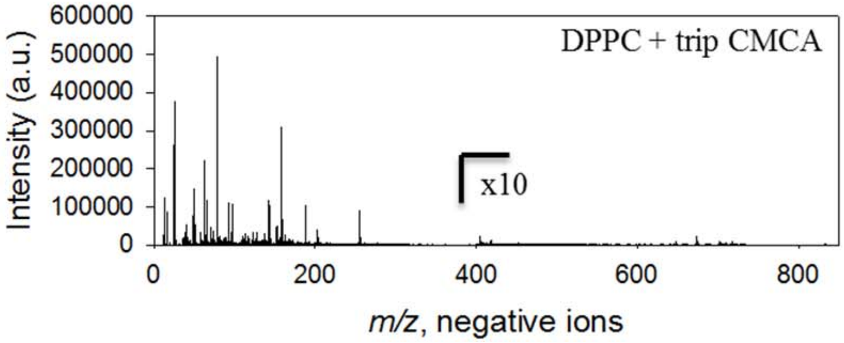
DPPC + trip CMCA
x10
Intensity (a.u.)
600000
500000
400000
300000
200000
100000
0
0
200
400
600
800
m/z, negative ions

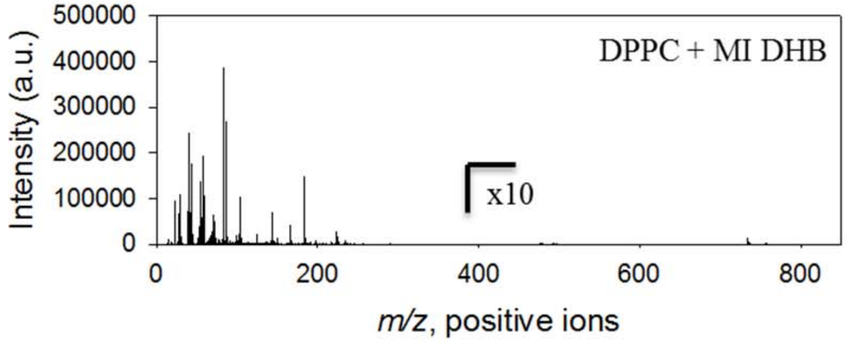
DPPC + MI DHB
x10
Intensity (a.u.)
500000
400000
300000
200000
100000
0
0
200
400
600
800
m/z, positive ions

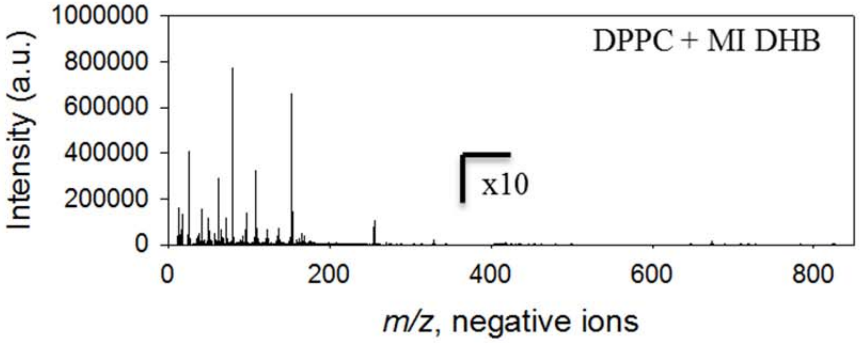
DPPC + MI DHB
x10
Intensity (a.u.)
1000000
800000
600000
400000
200000
0
0
200
400
600
800
m/z, negative ions

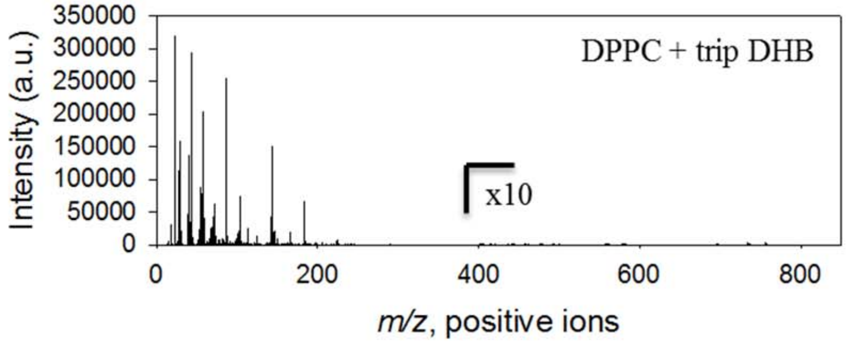
DPPC + trip DHB
x10
Intensity (a.u.)
350000
300000
250000
200000
150000
100000
50000
0
0
200
400
600
800
m/z, positive ions

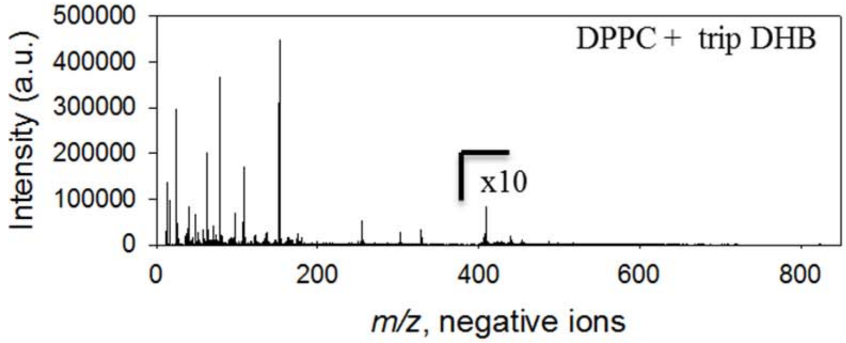
DPPC + trip DHB
x10
Intensity (a.u.)
500000
400000
300000
200000
100000
0
0
200
400
600
800
m/z, negative ions

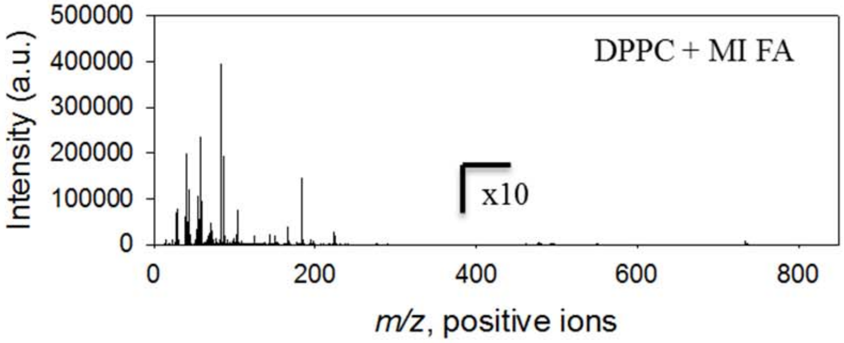
DPPC + MI FA
x10
Intensity (a.u.)
500000
400000
300000
200000
100000
0
0
200
400
600
800
m/z, positive ions

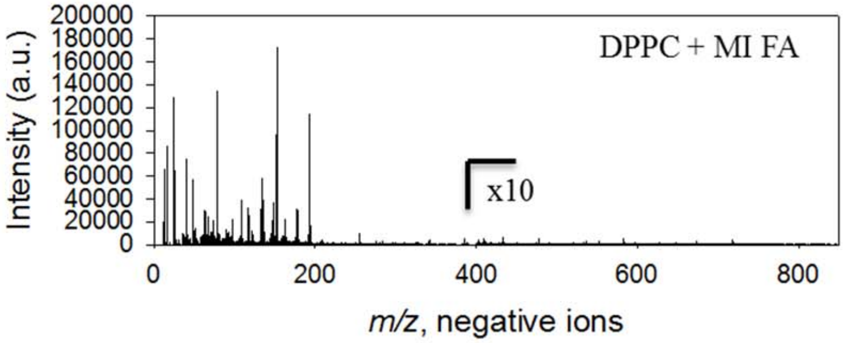
DPPC + MI FA
x10
Intensity (a.u.)
200000
180000
160000
140000
120000
100000
80000
60000
40000
20000
0
0
200
400
600
800
m/z, negative ions

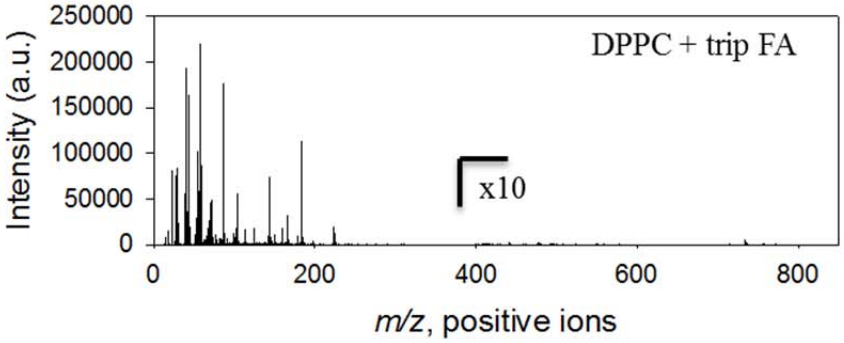
DPPC + trip FA
x10
Intensity (a.u.)
250000
200000
150000
100000
50000
0
0
200
400
600
800
m/z, positive ions

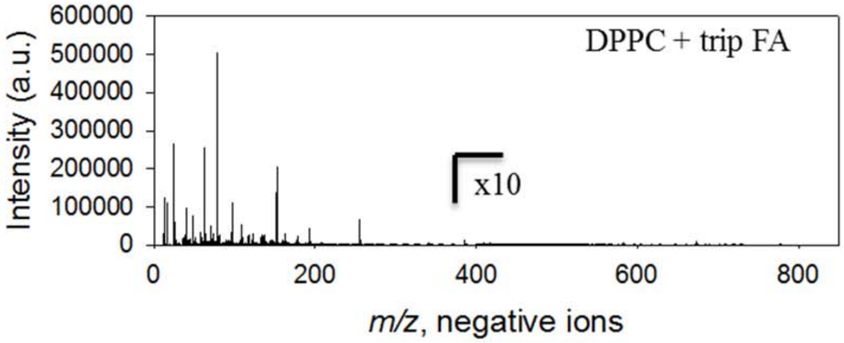
DPPC + trip FA
x10
Intensity (a.u.)
600000
500000
400000
300000
200000
100000
0
0
200
400
600
800
m/z, negative ions

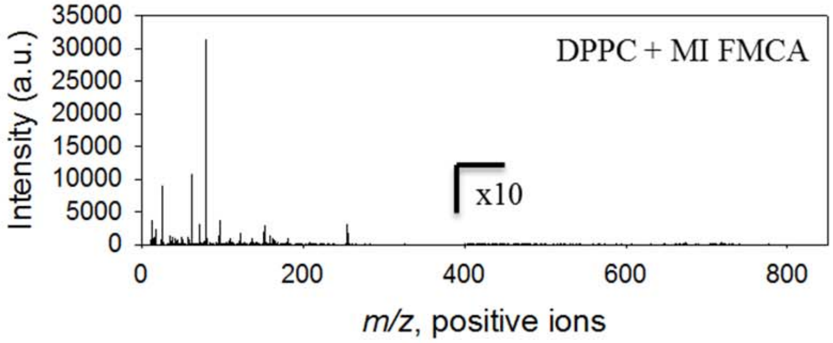
DPPC + MI FMCA
x10
Intensity (a.u.)
35000
30000
25000
20000
15000
10000
5000
0
0
200
400
600
800
m/z, positive ions

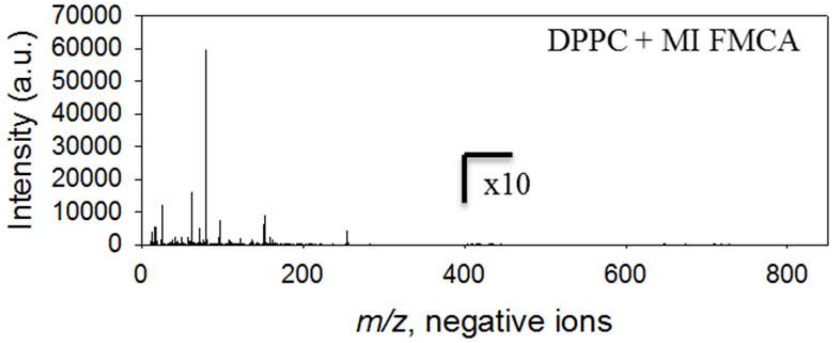
DPPC + MI FMCA
x10
Intensity (a.u.)
70000
60000
50000
40000
30000
20000
10000
0
0
200
400
600
800
m/z, negative ions

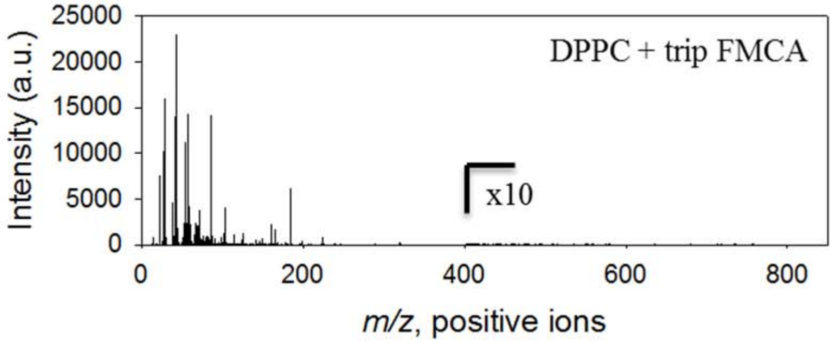
DPPC + trip FMCA
x10
Intensity (a.u.)
25000
20000
15000
10000
5000
0
0
200
400
600
800
m/z, positive ions

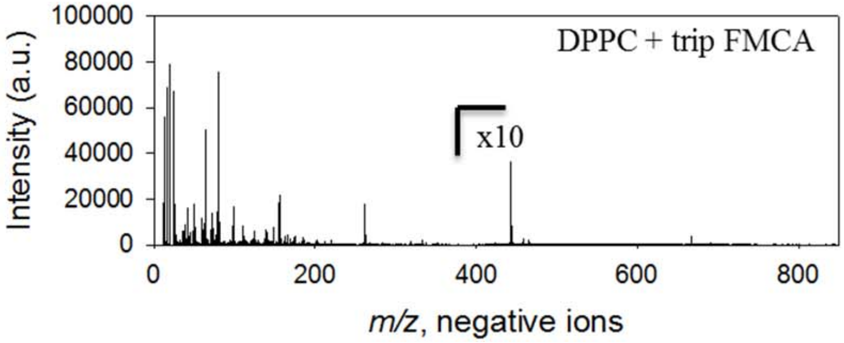
DPPC + trip FMCA
x10
Intensity (a.u.)
100000
80000
60000
40000
20000
0
0
200
400
600
800
m/z, negative ions

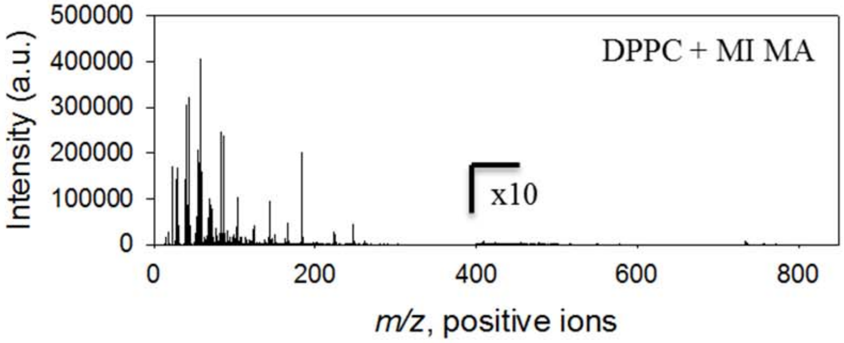
DPPC + MI MA
x10
Intensity (a.u.)
500000
400000
300000
200000
100000
0
0
200
400
600
800
m/z, positive ions

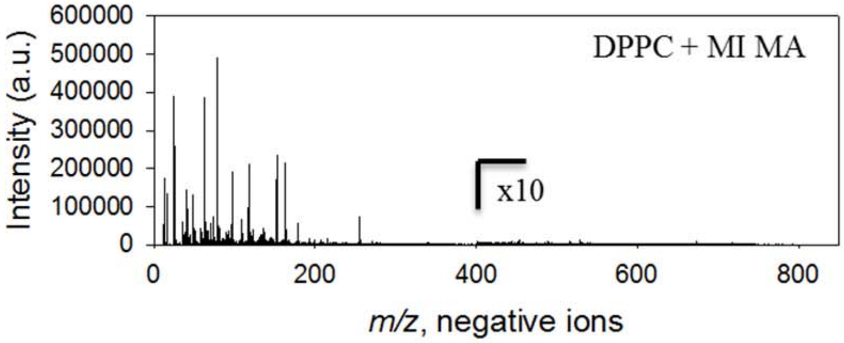
DPPC + MI MA
x10
Intensity (a.u.)
600000
500000
400000
300000
200000
100000
0
0
200
400
600
800
m/z, negative ions

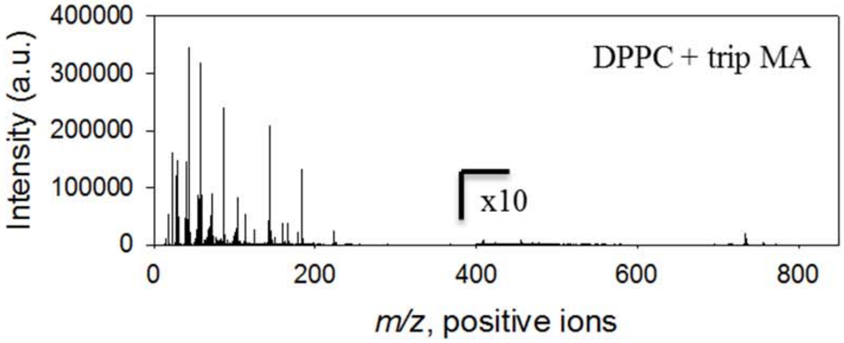
DPPC + trip MA
x10
Intensity (a.u.)
400000
300000
200000
100000
0
0
200
400
600
800
m/z, positive ions

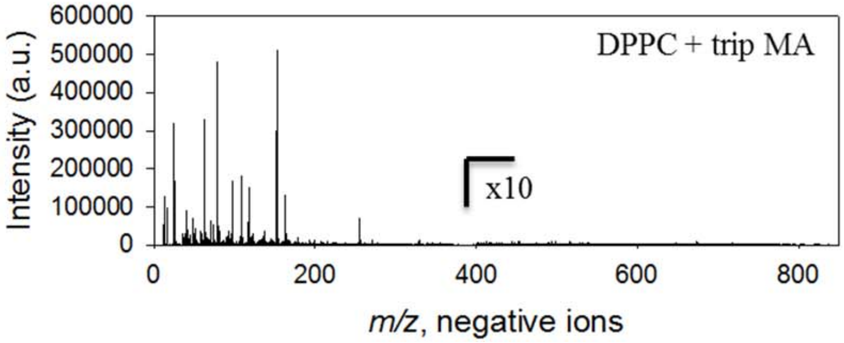
DPPC + trip MA
x10
Intensity (a.u.)
600000
500000
400000
300000
200000
100000
0
0
200
400
600
800
m/z, negative ions

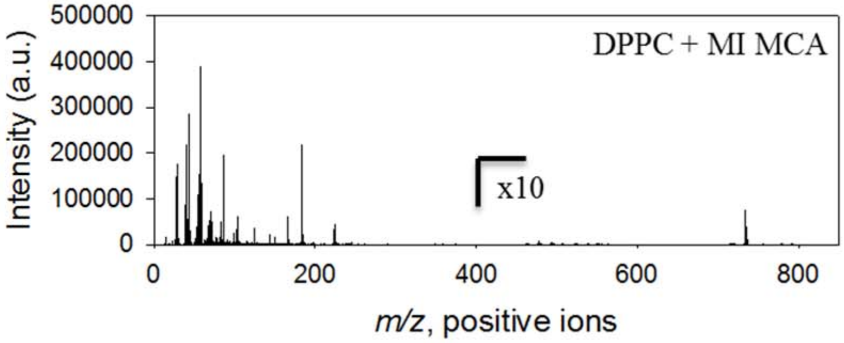
DPPC + MI MCA
x10
Intensity (a.u.)
500000
400000
300000
200000
100000
0
0
200
400
600
800
m/z, positive ions

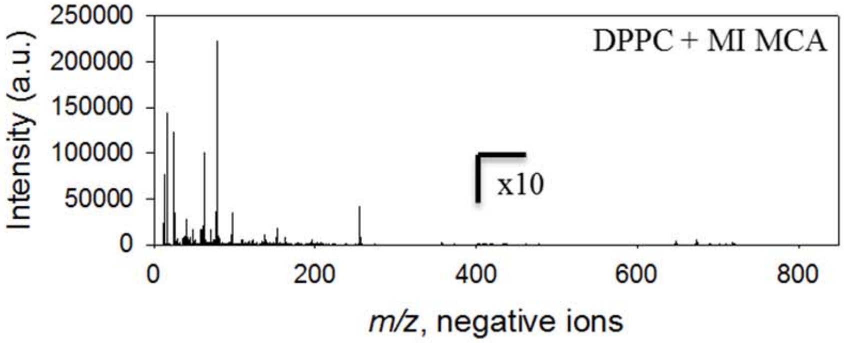
DPPC + MI MCA
x10
Intensity (a.u.)
250000
200000
150000
100000
50000
0
0
200
400
600
800
m/z, negative ions

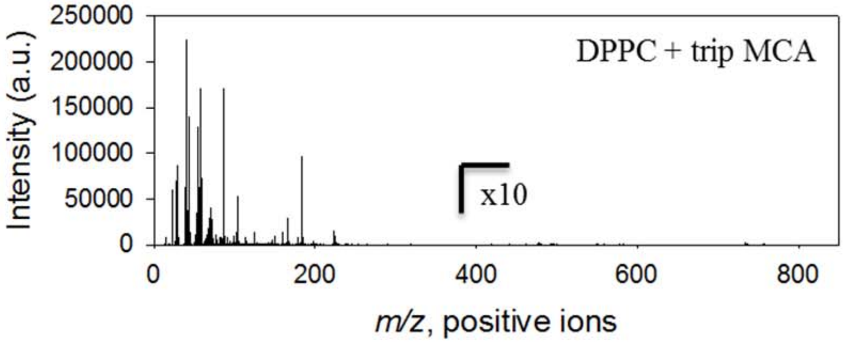
DPPC + trip MCA
x10
Intensity (a.u.)
250000
200000
150000
100000
50000
0
0
200
400
600
800
m/z, positive ions

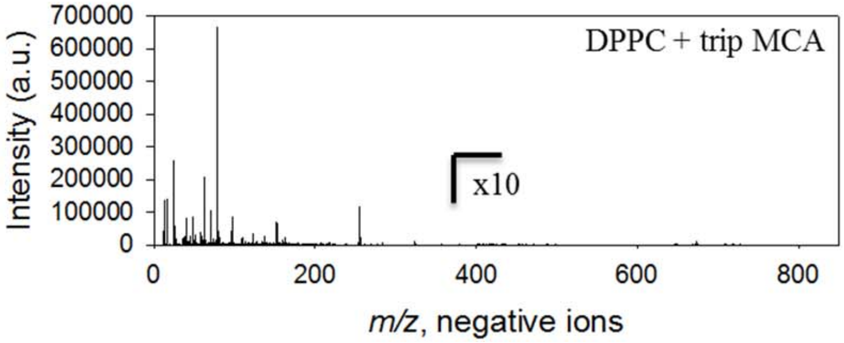
DPPC + trip MCA
x10
Intensity (a.u.)
700000
600000
500000
400000
300000
200000
100000
0
0
200
400
600
800
m/z, negative ions

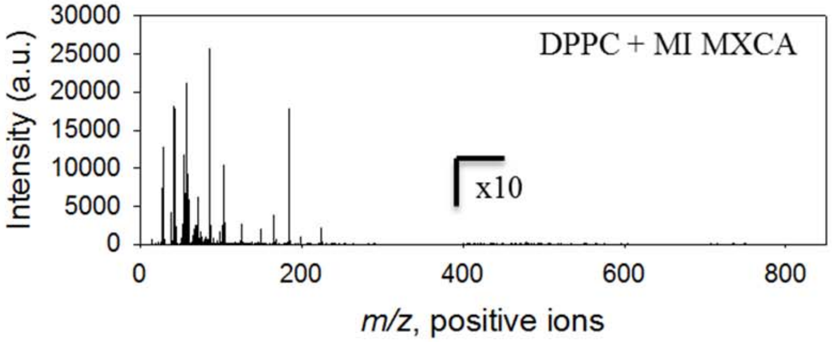
DPPC + MI MXCA
x10
Intensity (a.u.)
30000
25000
20000
15000
10000
5000
0
0
200
400
600
800
m/z, positive ions

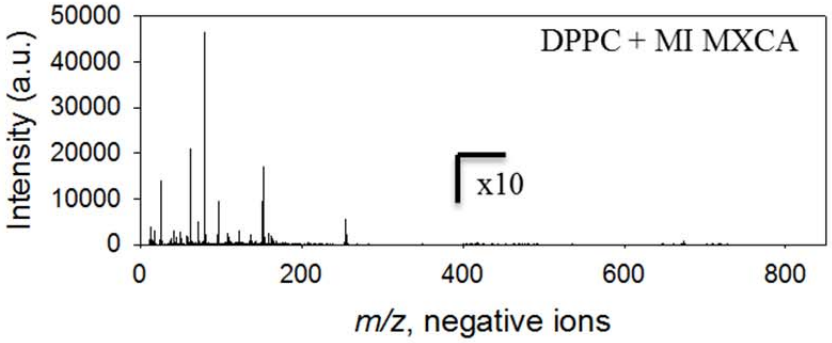
DPPC + MI MXCA
x10
Intensity (a.u.)
50000
40000
30000
20000
10000
0
0
200
400
600
800
m/z, negative ions

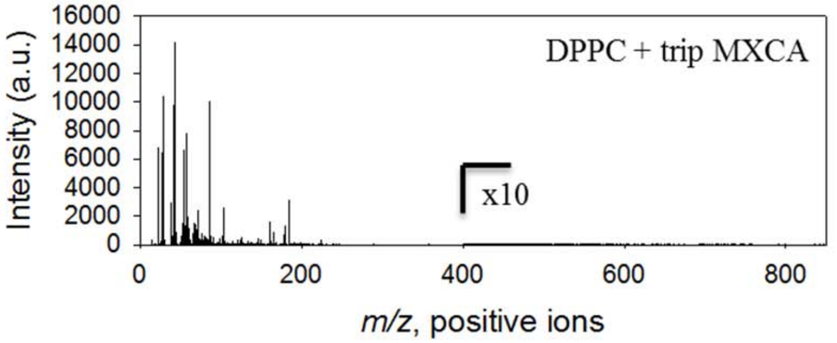
DPPC + trip MXCA
x10
Intensity (a.u.)
16000
14000
12000
10000
8000
6000
4000
2000
0
0
200
400
600
800
m/z, positive ions

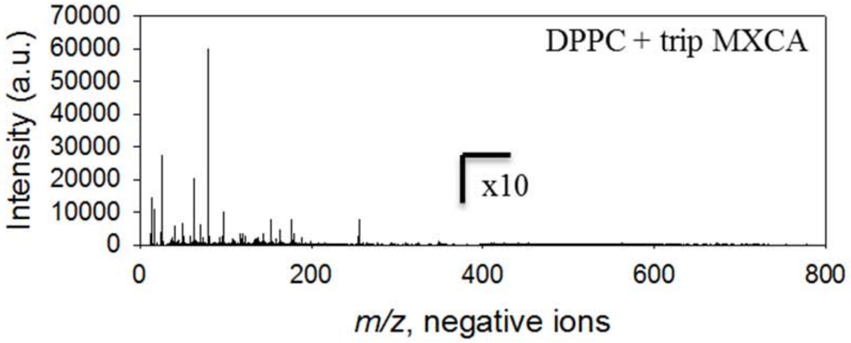
DPPC + trip MXCA
x10
Intensity (a.u.)
70000
60000
50000
40000
30000
20000
10000
0
0
200
400
600
800
m/z, negative ions

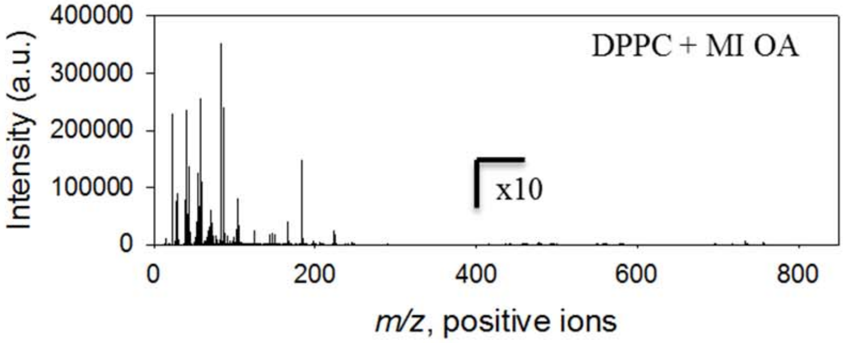
DPPC + MI OA
x10
Intensity (a.u.)
400000
300000
200000
100000
0
0
200
400
600
800
m/z, positive ions

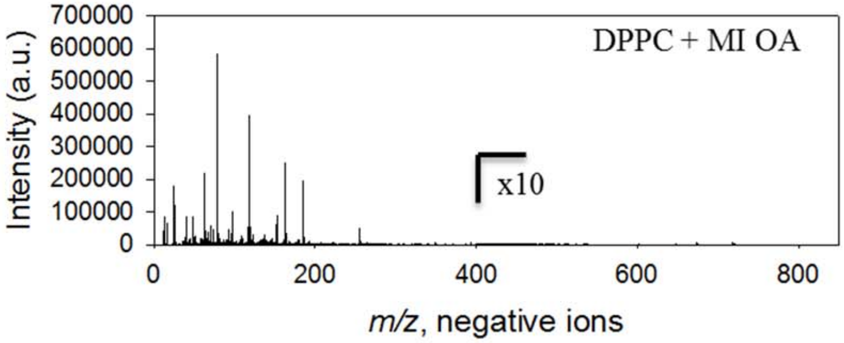
DPPC + MI OA
x10
Intensity (a.u.)
700000
600000
500000
400000
300000
200000
100000
0
0
200
400
600
800
m/z, negative ions

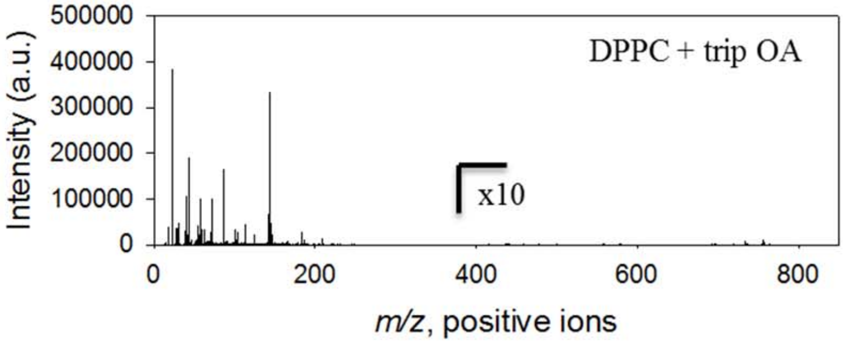
DPPC + trip OA
x10
Intensity (a.u.)
500000
400000
300000
200000
100000
0
0
200
400
600
800
m/z, positive ions

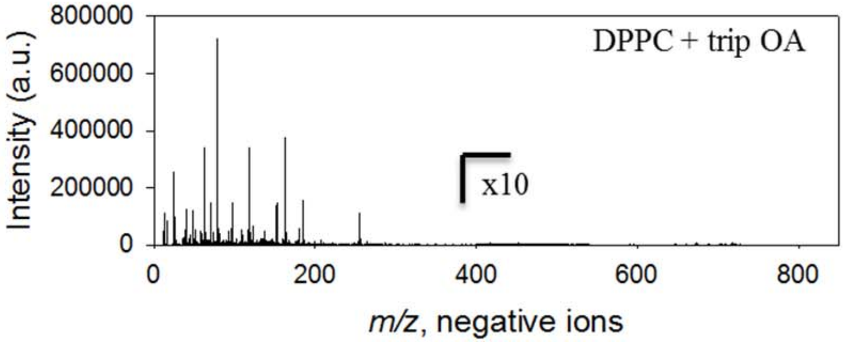
DPPC + trip OA
x10
Intensity (a.u.)
800000
600000
400000
200000
0
0
200
400
600
800
m/z, negative ions

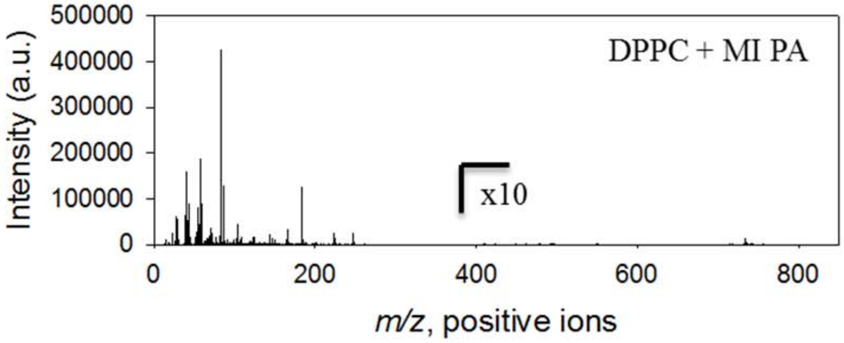
DPPC + MI PA
x10
Intensity (a.u.)
500000
400000
300000
200000
100000
0
0
200
400
600
800
m/z, positive ions

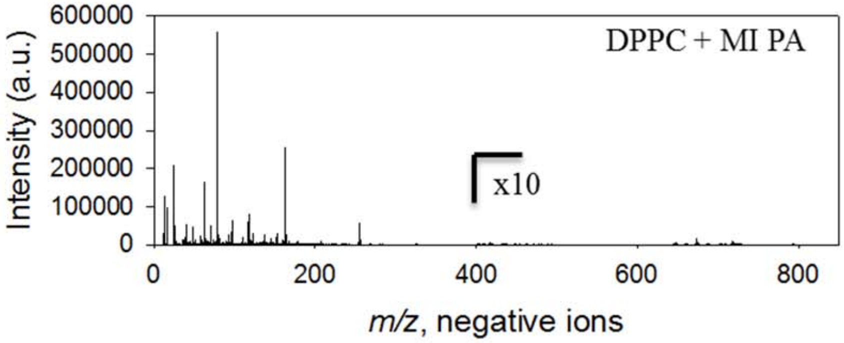
DPPC + MI PA
x10
Intensity (a.u.)
600000
500000
400000
300000
200000
100000
0
0
200
400
600
800
m/z, negative ions

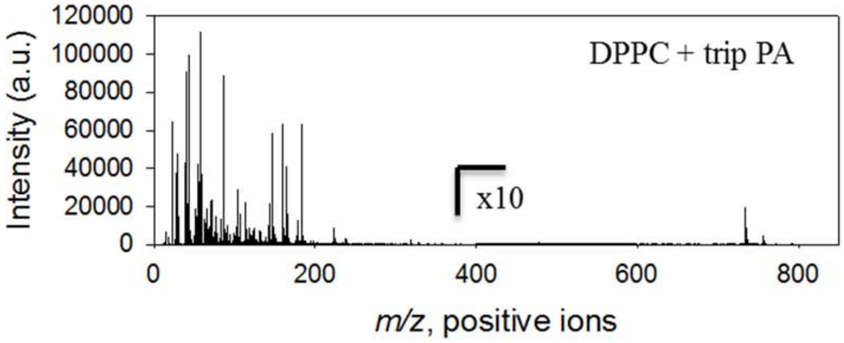
DPPC + trip PA
x10
Intensity (a.u.)
120000
100000
80000
60000
40000
20000
0
0
200
400
600
800
m/z, positive ions

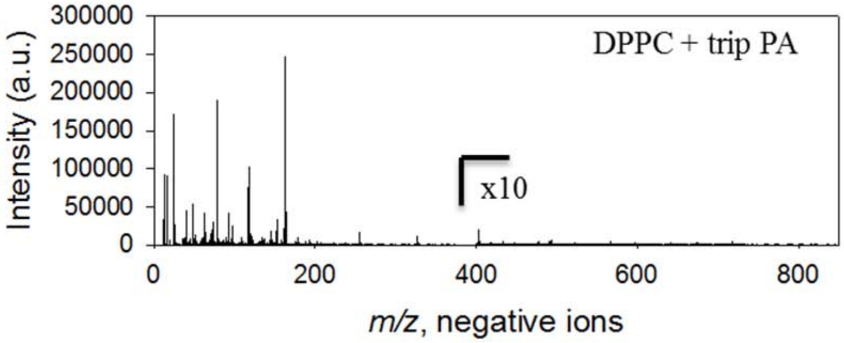
DPPC + trip PA
x10
Intensity (a.u.)
300000
250000
200000
150000
100000
50000
0
0
200
400
600
800
m/z, negative ions

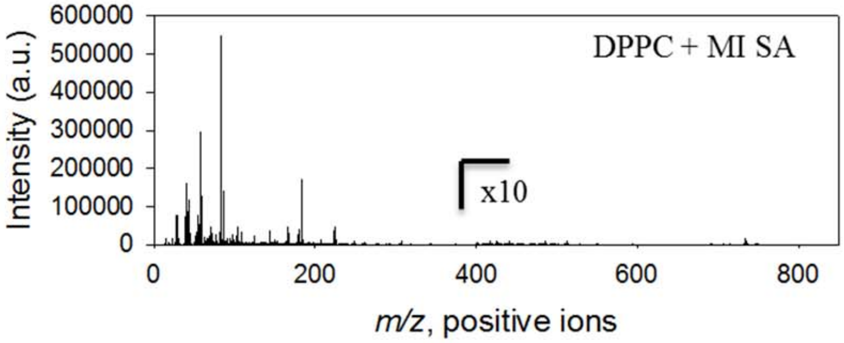
DPPC + MI SA
x10
Intensity (a.u.)
600000
500000
400000
300000
200000
100000
0
0
200
400
600
800
m/z, positive ions

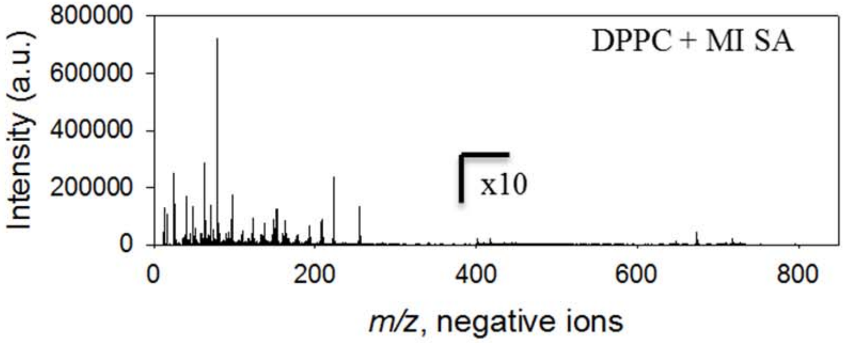
DPPC + MI SA
x10
Intensity (a.u.)
800000
600000
400000
200000
0
0
200
400
600
800
m/z, negative ions

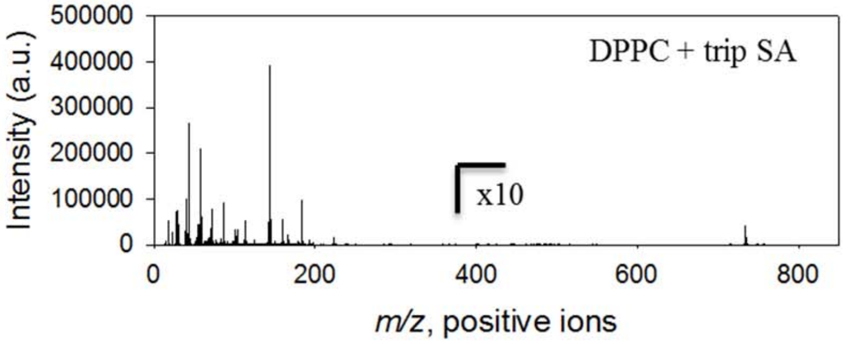
DPPC + trip SA
x10
Intensity (a.u.)
500000
400000
300000
200000
100000
0
0
200
400
600
800
m/z, positive ions

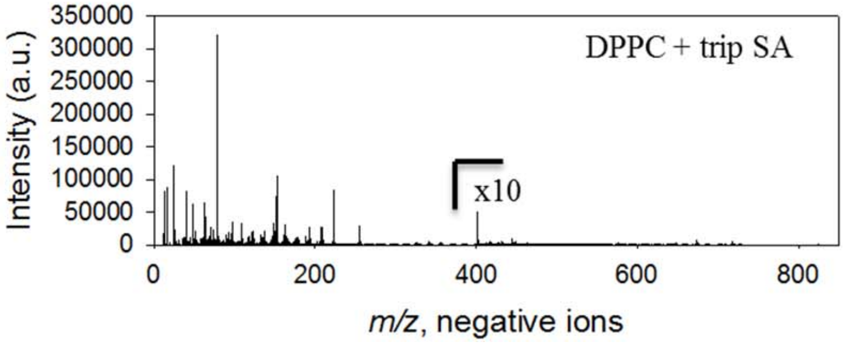
DPPC + trip SA
x10
Intensity (a.u.)
350000
300000
250000
200000
150000
100000
50000
0
0
200
400
600
800
m/z, negative ions

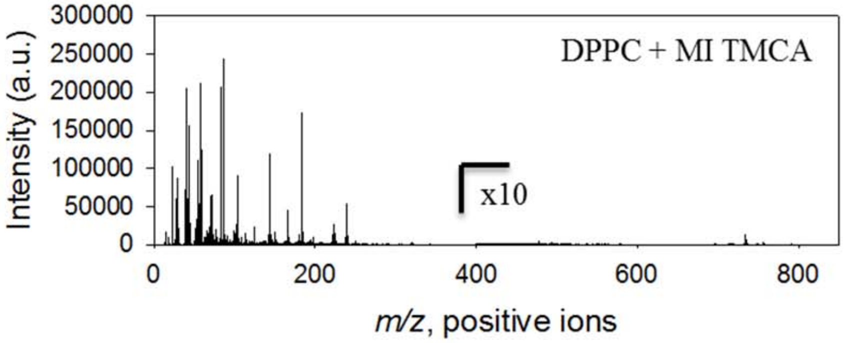
DPPC + MI TMCA
x10
Intensity (a.u.)
300000
250000
200000
150000
100000
50000
0
0
200
400
600
800
m/z, positive ions

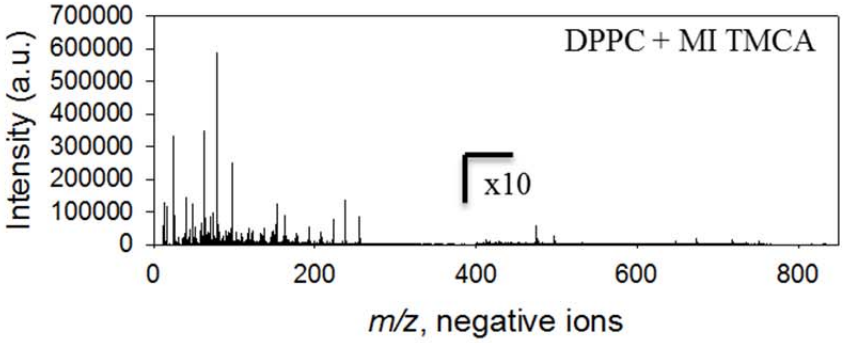
DPPC + MI TMCA
x10
Intensity (a.u.)
700000
600000
500000
400000
300000
200000
100000
0
0
200
400
600
800
m/z, negative ions

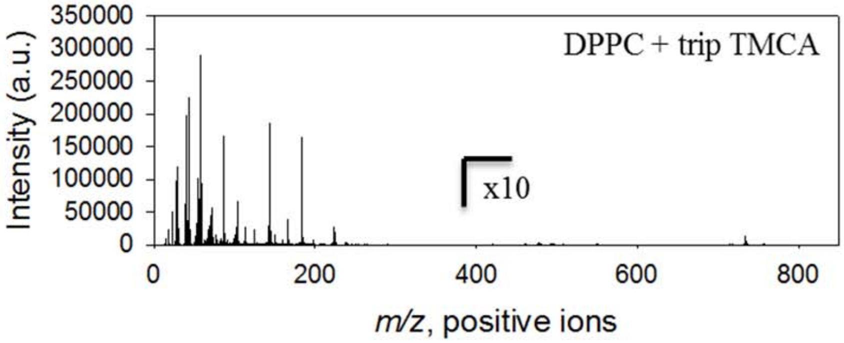
DPPC + trip TMCA
x10
Intensity (a.u.)
350000
300000
250000
200000
150000
100000
50000
0
0
200
400
600
800
m/z, positive ions

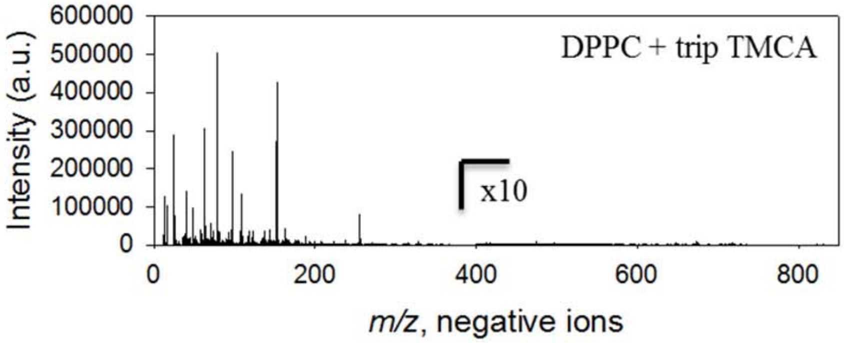
DPPC + trip TMCA
x10
Intensity (a.u.)
600000
500000
400000
300000
200000
100000
0
0
200
400
600
800
m/z, negative ions

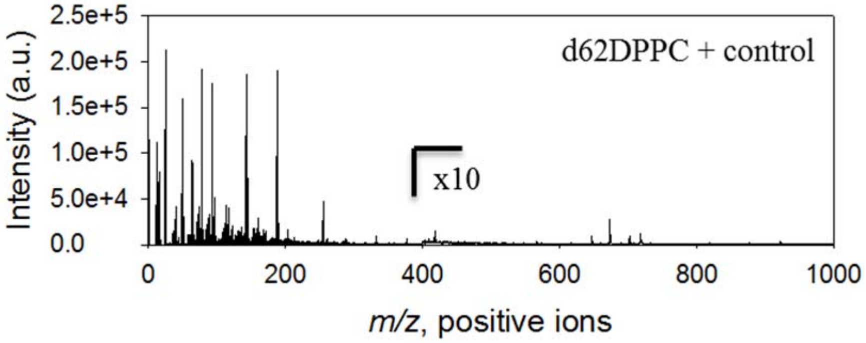

Intensity (a.u.)
2.5e+5
2.0e+5
1.5e+5
1.0e+5
5.0e+4
0.0
0
200
400
600
800
1000
m/z, positive ions
d62DPPC + control
x10

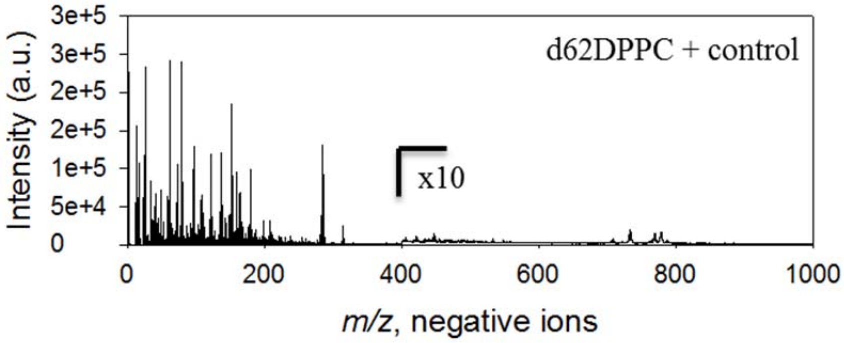

Intensity (a.u.)
3e+5
3e+5
2e+5
2e+5
1e+5
5e+4
0
0
200
400
600
800
1000
m/z, negative ions
d62DPPC + control
x10

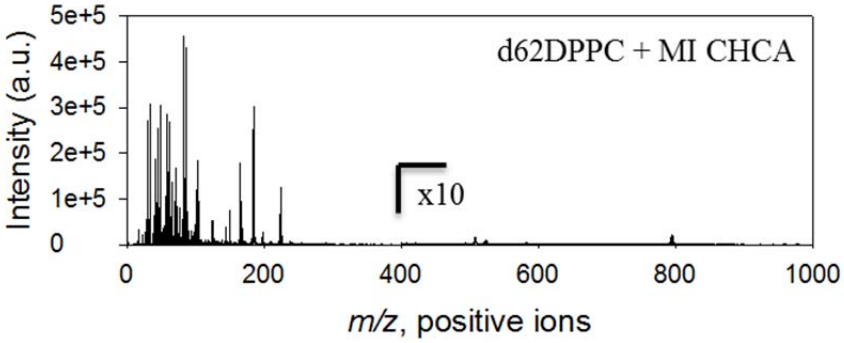
d62DPPC + MI CHCA
x10
Intensity (a.u.)
5e+5
4e+5
3e+5
2e+5
1e+5
0
0
200
400
600
800
1000
m/z, positive ions

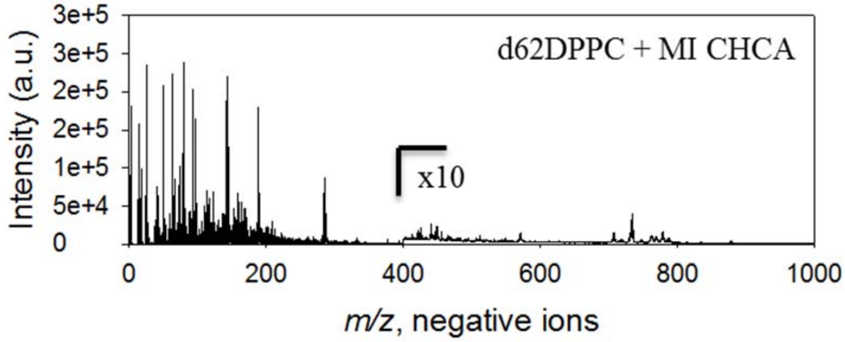
d62DPPC + MI CHCA
x10
Intensity (a.u.)
3e+5
3e+5
2e+5
2e+5
1e+5
5e+4
0
0
200
400
600
800
1000
m/z, negative ions

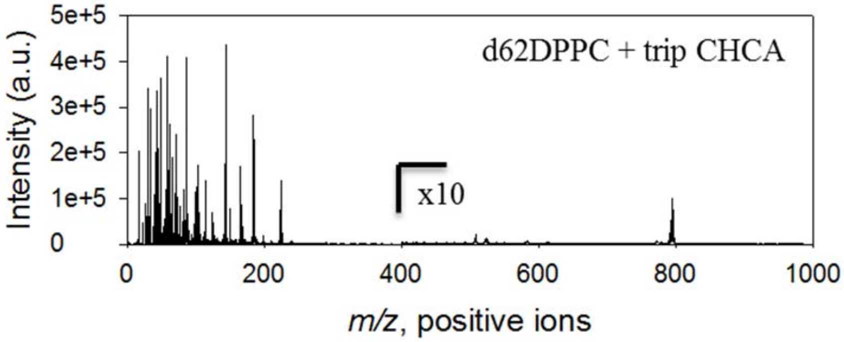
d62DPPC + trip CHCA
x10
Intensity (a.u.)
5e+5
4e+5
3e+5
2e+5
1e+5
0
0
200
400
600
800
1000
m/z, positive ions

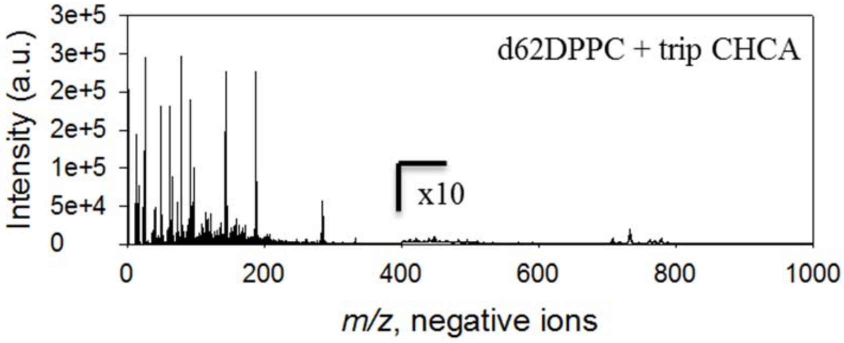
d62DPPC + trip CHCA
x10
Intensity (a.u.)
3e+5
3e+5
2e+5
2e+5
1e+5
5e+4
0
0
200
400
600
800
1000
m/z, negative ions

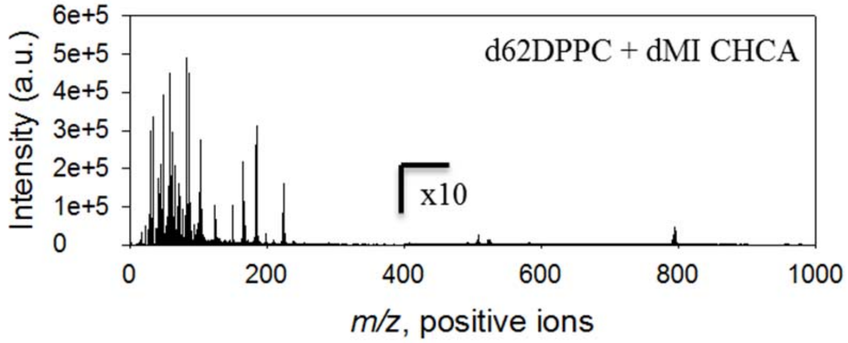
d62DPPC + dMI CHCA
x10
Intensity (a.u.)
6e+5
5e+5
4e+5
3e+5
2e+5
1e+5
0
0
200
400
600
800
1000
m/z, positive ions

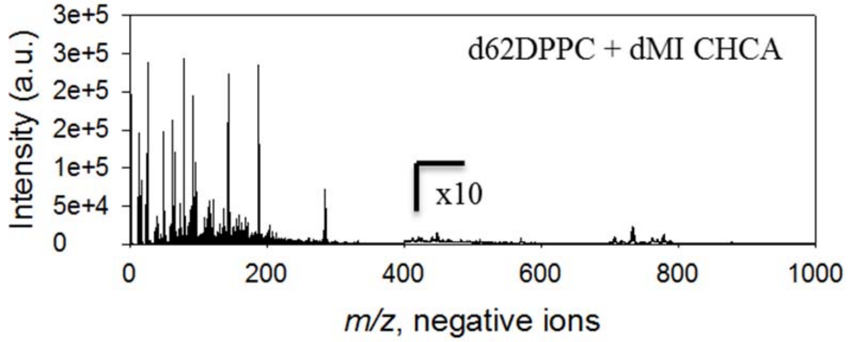
d62DPPC + dMI CHCA
x10
Intensity (a.u.)
3e+5
3e+5
2e+5
2e+5
1e+5
5e+4
0
0
200
400
600
800
1000
m/z, negative ions

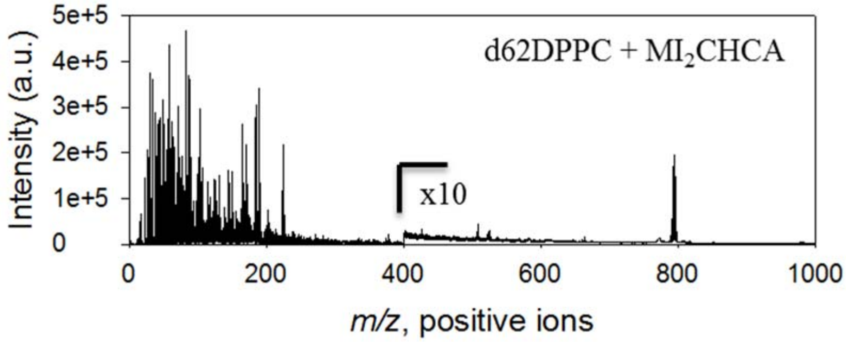
d62DPPC + MI2CHCA
x10
Intensity (a.u.)
5e+5
4e+5
3e+5
2e+5
1e+5
0
0
200
400
600
800
1000
m/z, positive ions

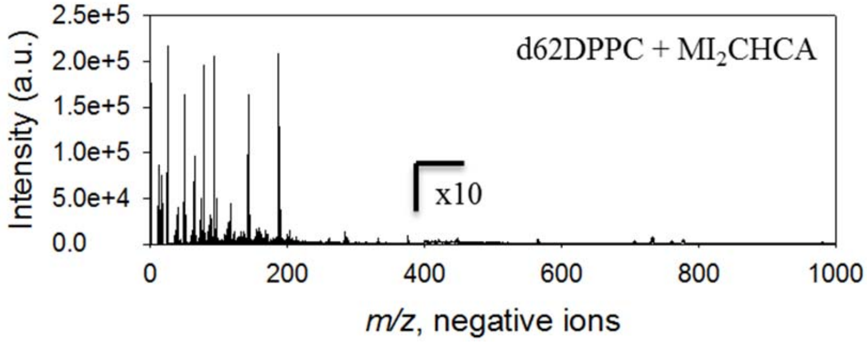
d62DPPC + MI2CHCA
x10
Intensity (a.u.)
2.5e+5
2.0e+5
1.5e+5
1.0e+5
5.0e+4
0.0
0
200
400
600
800
1000
m/z, negative ions

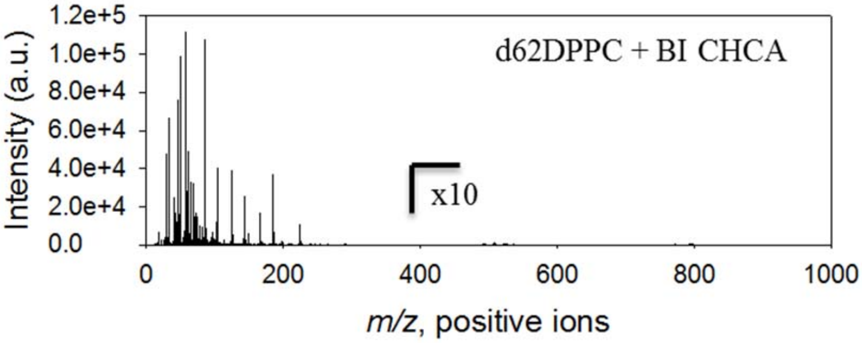
d62DPPC + BI CHCA
x10
Intensity (a.u.)
1.2e+5
1.0e+5
8.0e+4
6.0e+4
4.0e+4
2.0e+4
0.0
0
200
400
600
800
1000
m/z, positive ions

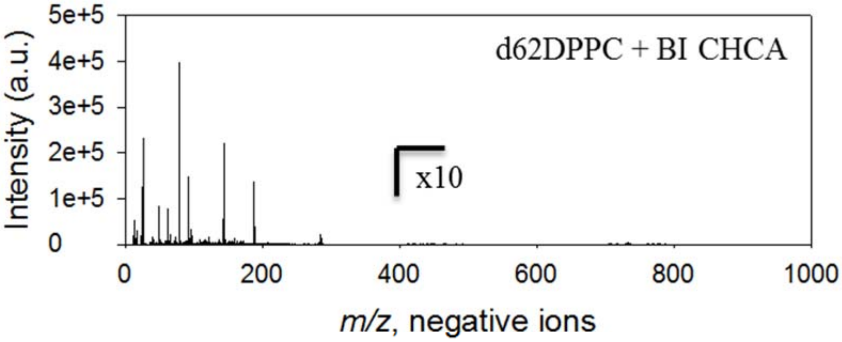
d62DPPC + BI CHCA
x10
Intensity (a.u.)
5e+5
4e+5
3e+5
2e+5
1e+5
0
0
200
400
600
800
1000
m/z, negative ions

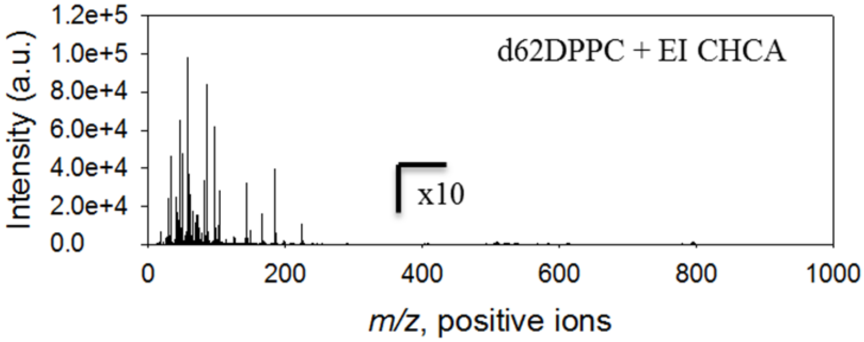
d62DPPC + EI CHCA
x10
Intensity (a.u.)
1.2e+5
1.0e+5
8.0e+4
6.0e+4
4.0e+4
2.0e+4
0.0
0
200
400
600
800
1000
m/z, positive ions

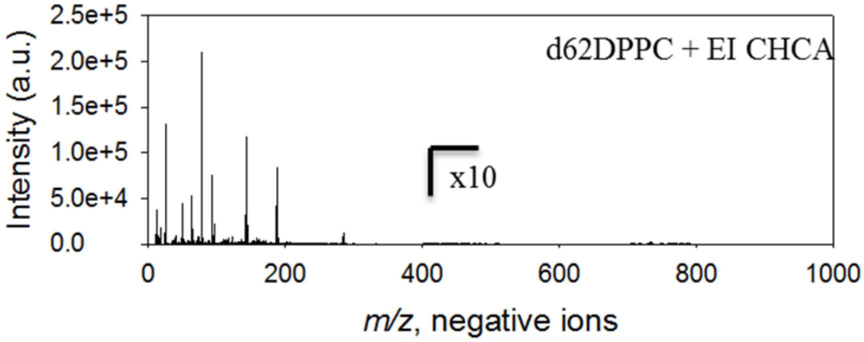
d62DPPC + EI CHCA
x10
Intensity (a.u.)
2.5e+5
2.0e+5
1.5e+5
1.0e+5
5.0e+4
0.0
0
200
400
600
800
1000
m/z, negative ions

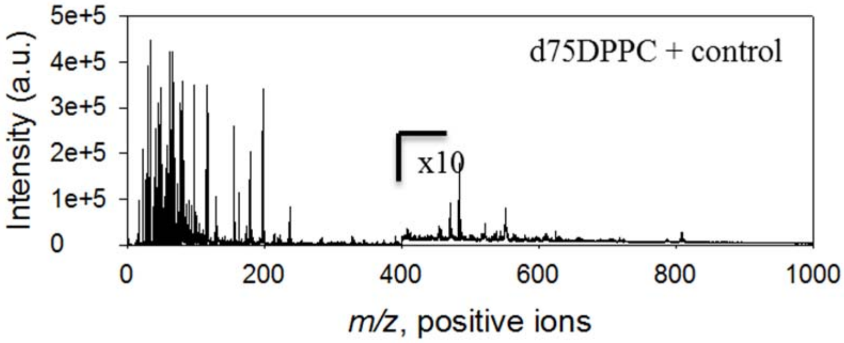
5e+5
4e+5
3e+5
2e+5
1e+5
0
Intensity (a.u.)
d75DPPC + control
x10
0
200
400
600
800
1000
m/z, positive ions

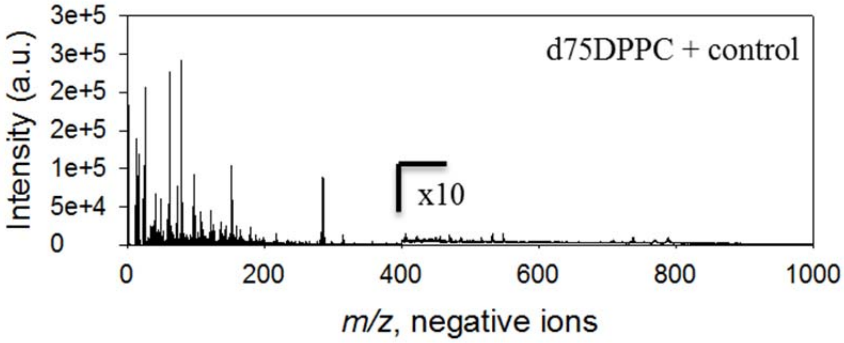
3e+5
3e+5
2e+5
2e+5
1e+5
5e+4
0
Intensity (a.u.)
d75DPPC + control
x10
0
200
400
600
800
1000
m/z, negative ions

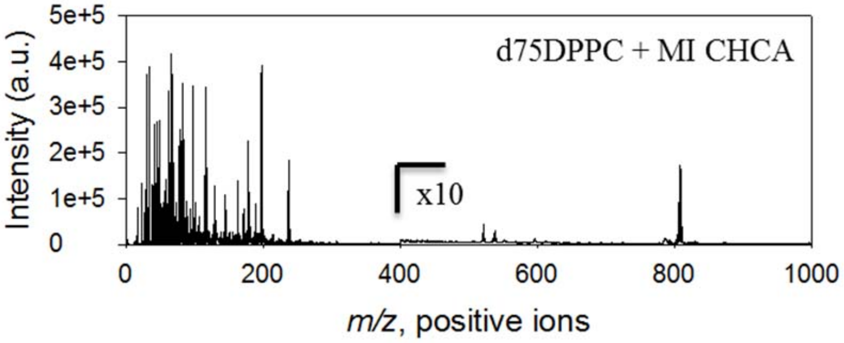
d75DPPC + MI CHCA
x10
Intensity (a.u.)
5e+5
4e+5
3e+5
2e+5
1e+5
0
0
200
400
600
800
1000
m/z, positive ions

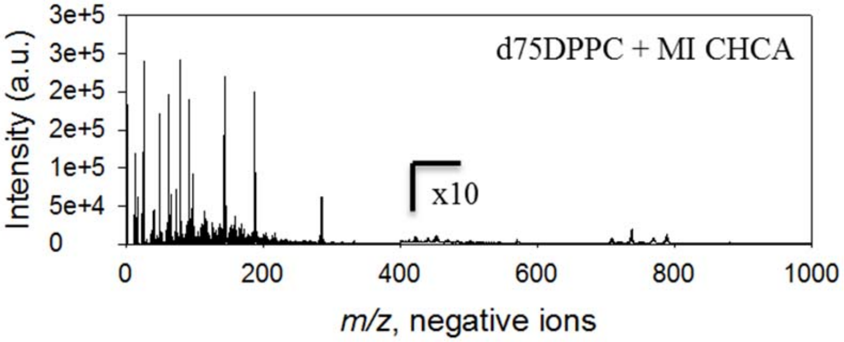
d75DPPC + MI CHCA
x10
Intensity (a.u.)
3e+5
3e+5
2e+5
2e+5
1e+5
5e+4
0
0
200
400
600
800
1000
m/z, negative ions

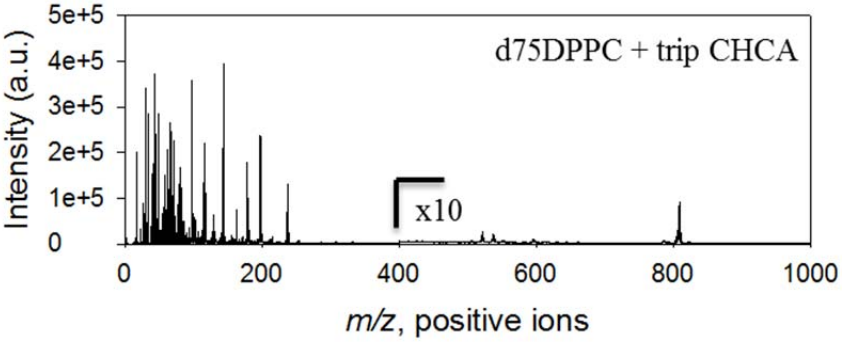
d75DPPC + trip CHCA
x10
Intensity (a.u.)
5e+5
4e+5
3e+5
2e+5
1e+5
0
0
200
400
600
800
1000
m/z, positive ions

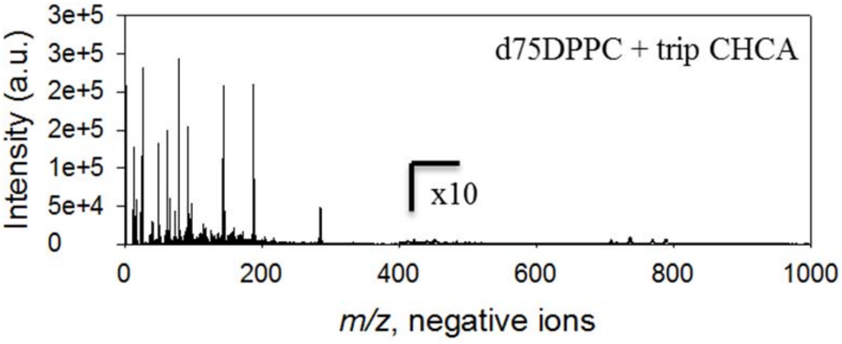
d75DPPC + trip CHCA
x10
Intensity (a.u.)
3e+5
3e+5
2e+5
2e+5
1e+5
5e+4
0
0
200
400
600
800
1000
m/z, negative ions

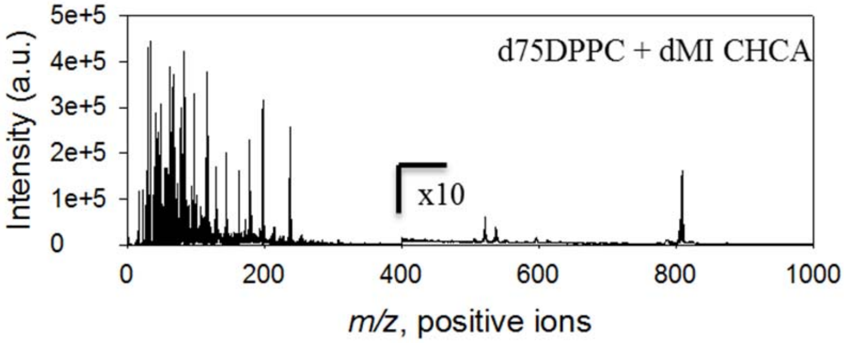
d75DPPC + dMI CHCA
x10
Intensity (a.u.)
5e+5
4e+5
3e+5
2e+5
1e+5
0
0
200
400
600
800
1000
m/z, positive ions

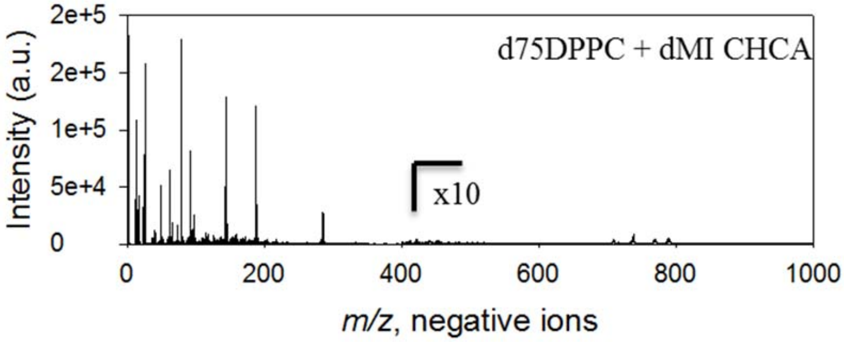
d75DPPC + dMI CHCA
x10
Intensity (a.u.)
2e+5
2e+5
1e+5
5e+4
0
0
200
400
600
800
1000
m/z, negative ions

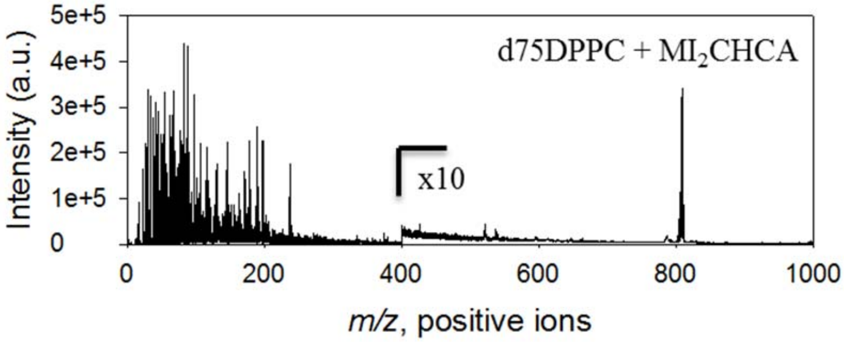
d75DPPC + MI$_2$CHCA
x10
Intensity (a.u.)
5e+5
4e+5
3e+5
2e+5
1e+5
0
0
200
400
600
800
1000
m/z, positive ions

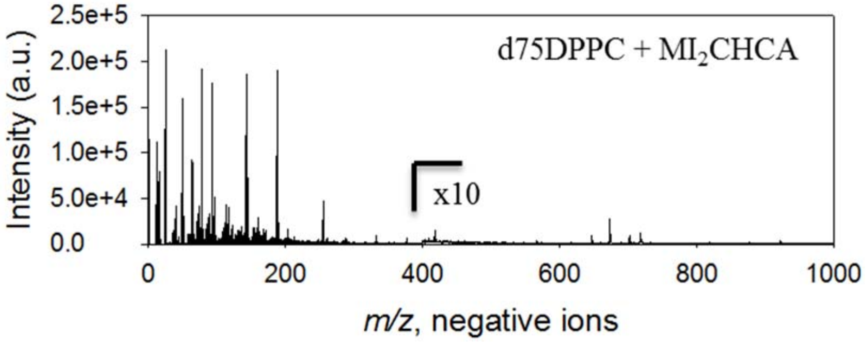
d75DPPC + MI$_2$CHCA
x10
Intensity (a.u.)
2.5e+5
2.0e+5
1.5e+5
1.0e+5
5.0e+4
0.0
0
200
400
600
800
1000
m/z, negative ions

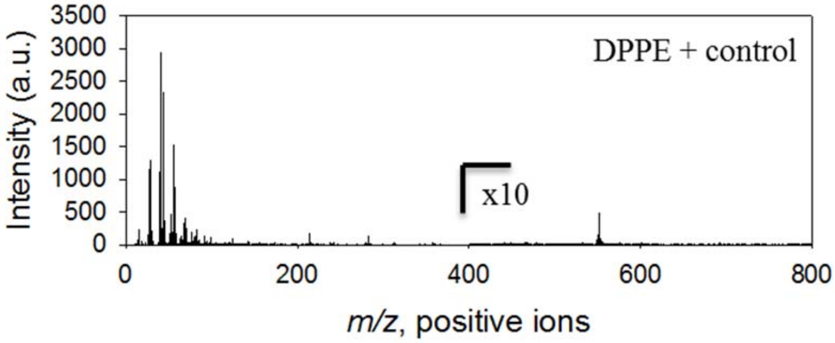

DPPE + control
x10
Intensity (a.u.)
3500
3000
2500
2000
1500
1000
500
0
0
200
400
600
800
m/z, positive ions

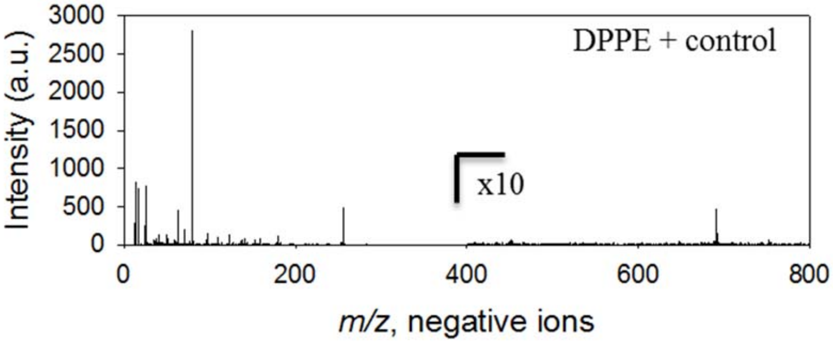

DPPE + control
x10
Intensity (a.u.)
3000
2500
2000
1500
1000
500
0
0
200
400
600
800
m/z, negative ions

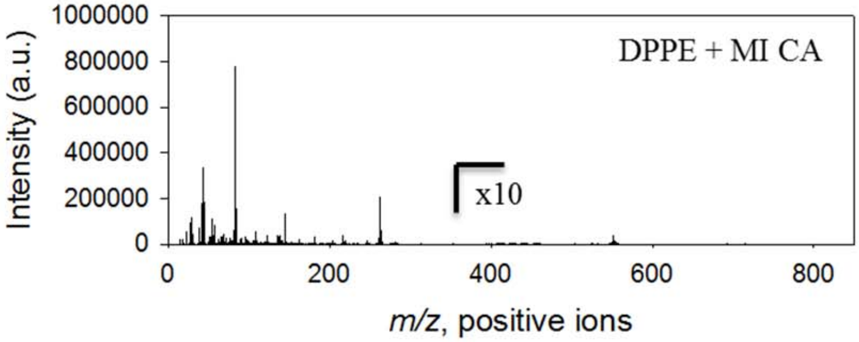
1000000
800000
600000
400000
200000
0
Intensity (a.u.)
DPPE + MI CA
x10
0
200
400
600
800
m/z, positive ions

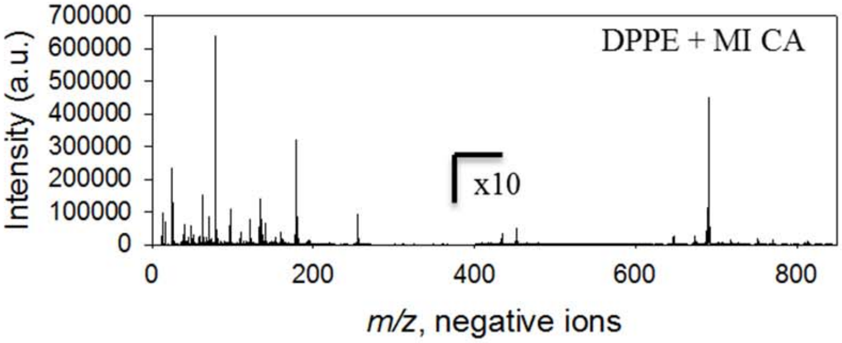
700000
600000
500000
400000
300000
200000
100000
0
Intensity (a.u.)
DPPE + MI CA
x10
0
200
400
600
800
m/z, negative ions

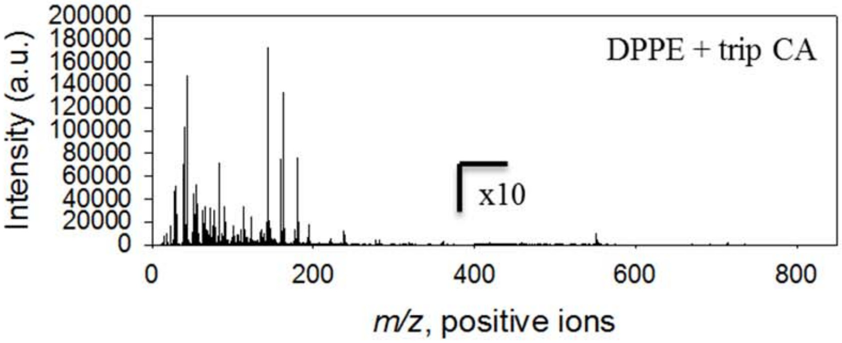
200000
180000
160000
140000
120000
100000
80000
60000
40000
20000
0
Intensity (a.u.)
DPPE + trip CA
x10
0
200
400
600
800
m/z, positive ions

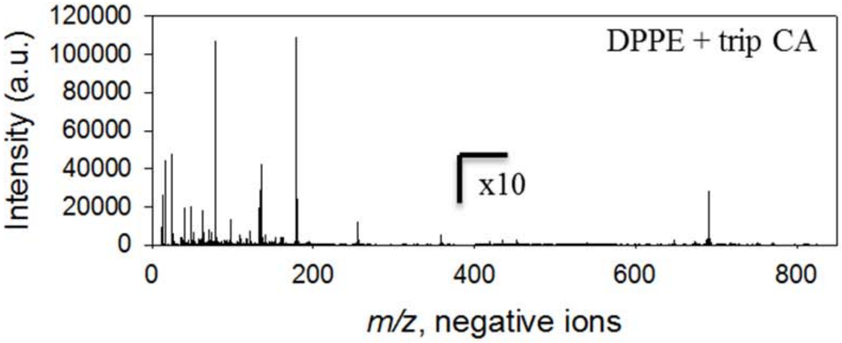
120000
100000
80000
60000
40000
20000
0
Intensity (a.u.)
DPPE + trip CA
x10
0
200
400
600
800
m/z, negative ions

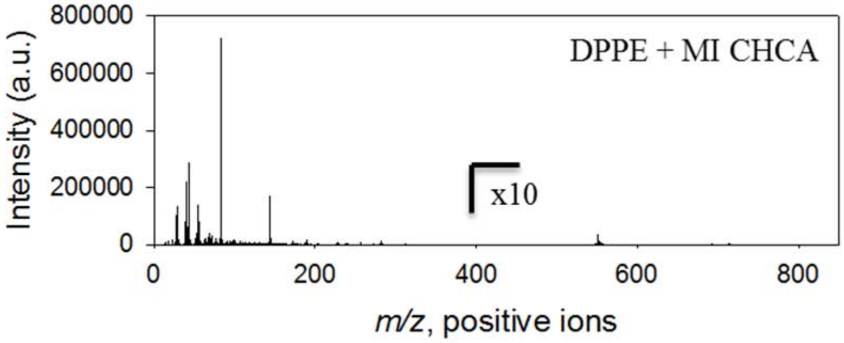
DPPE + MI CHCA
x10
Intensity (a.u.)
800000
600000
400000
200000
0
0
200
400
600
800
m/z, positive ions

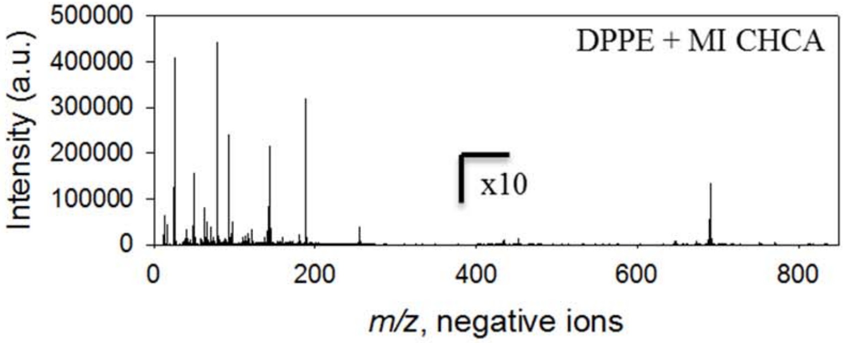
DPPE + MI CHCA
x10
Intensity (a.u.)
500000
400000
300000
200000
100000
0
0
200
400
600
800
m/z, negative ions

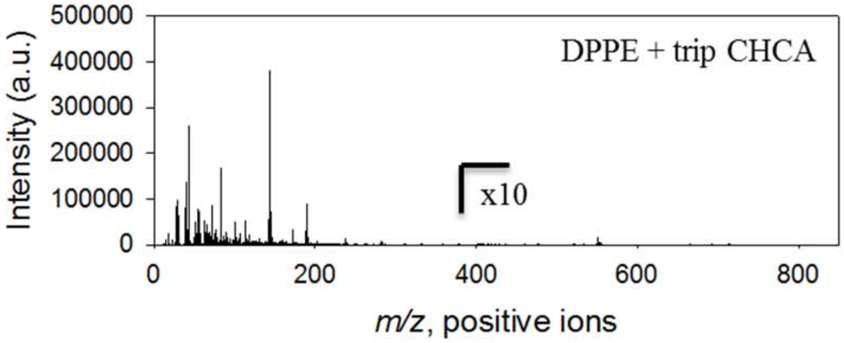
DPPE + trip CHCA
x10
Intensity (a.u.)
500000
400000
300000
200000
100000
0
0
200
400
600
800
m/z, positive ions

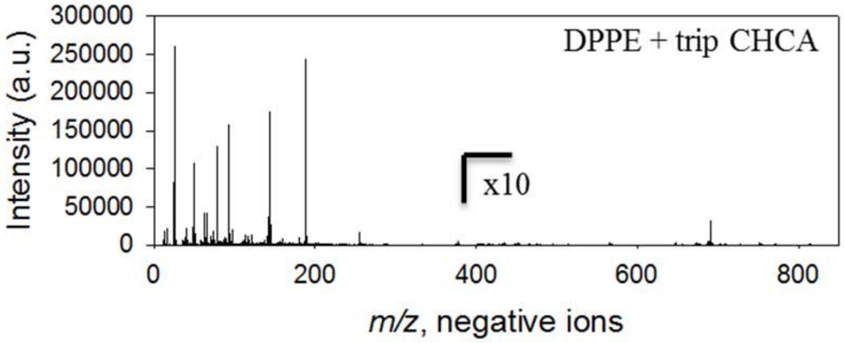
DPPE + trip CHCA
x10
Intensity (a.u.)
300000
250000
200000
150000
100000
50000
0
0
200
400
600
800
m/z, negative ions

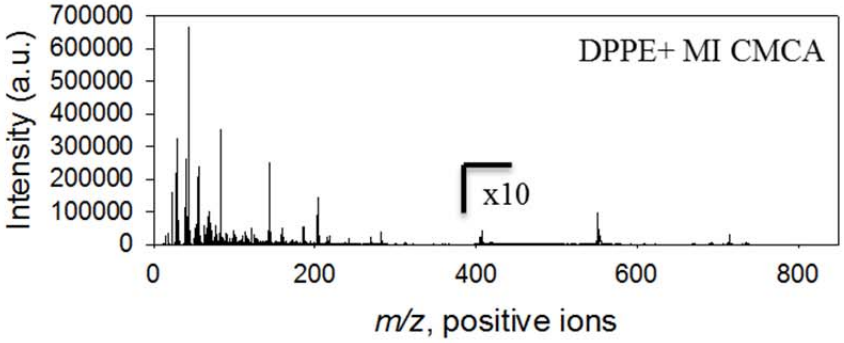
DPPE+ MI CMCA
Intensity (a.u.)
700000
600000
500000
400000
300000
200000
100000
0
x10
0
200
400
600
800
m/z, positive ions

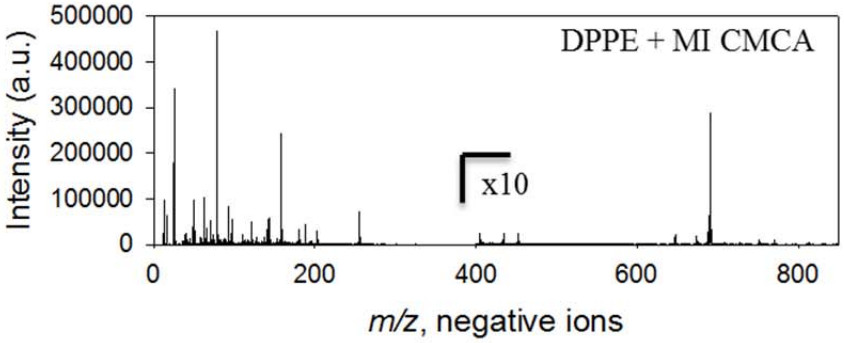
DPPE + MI CMCA
Intensity (a.u.)
500000
400000
300000
200000
100000
0
x10
0
200
400
600
800
m/z, negative ions

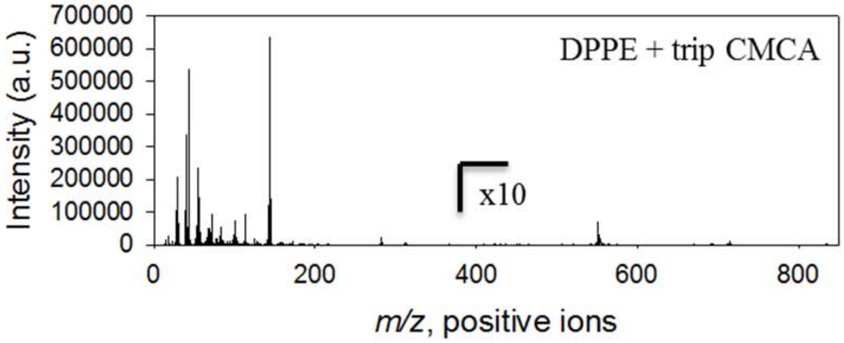
DPPE + trip CMCA
Intensity (a.u.)
700000
600000
500000
400000
300000
200000
100000
0
x10
0
200
400
600
800
m/z, positive ions

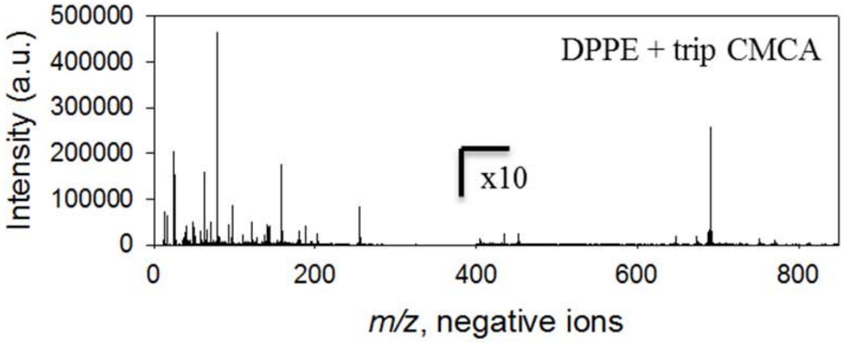
DPPE + trip CMCA
Intensity (a.u.)
500000
400000
300000
200000
100000
0
x10
0
200
400
600
800
m/z, negative ions

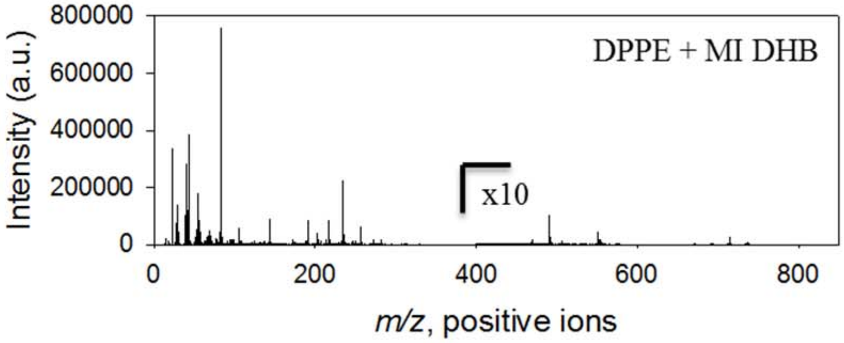
DPPE + MI DHB
x10
Intensity (a.u.)
800000
600000
400000
200000
0
0
200
400
600
800
m/z, positive ions

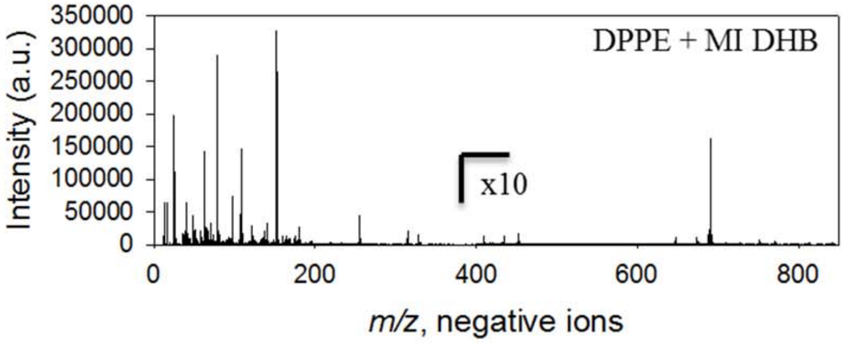
DPPE + MI DHB
x10
Intensity (a.u.)
350000
300000
250000
200000
150000
100000
50000
0
0
200
400
600
800
m/z, negative ions

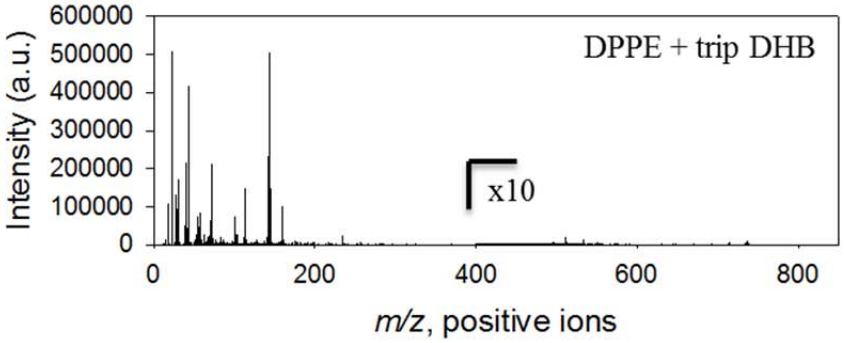
DPPE + trip DHB
x10
Intensity (a.u.)
600000
500000
400000
300000
200000
100000
0
0
200
400
600
800
m/z, positive ions

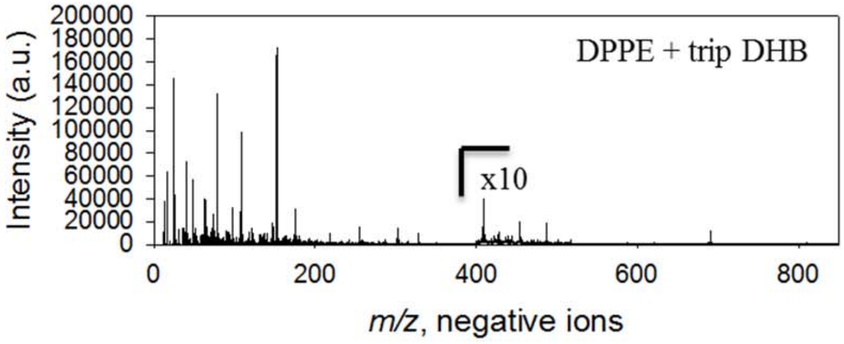
DPPE + trip DHB
x10
Intensity (a.u.)
200000
180000
160000
140000
120000
100000
80000
60000
40000
20000
0
0
200
400
600
800
m/z, negative ions

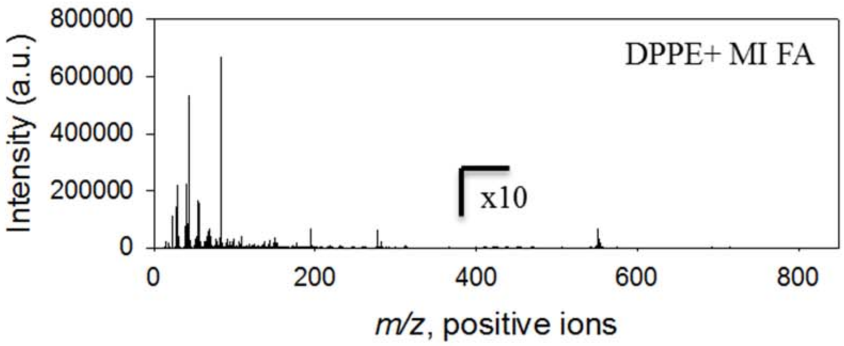
DPPE+ MI FA
x10
Intensity (a.u.)
800000
600000
400000
200000
0
0
200
400
600
800
m/z, positive ions

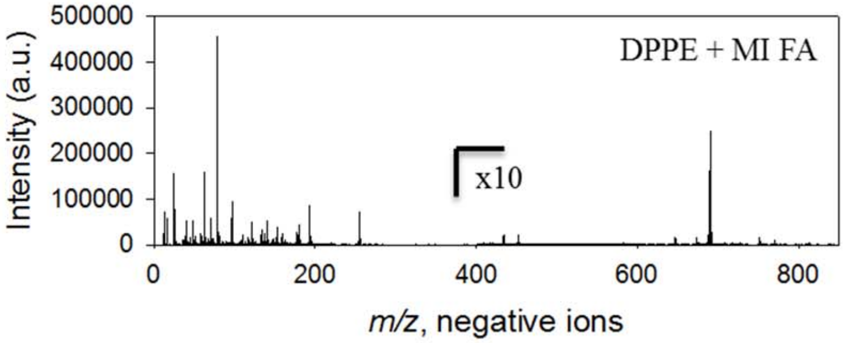
DPPE + MI FA
x10
Intensity (a.u.)
500000
400000
300000
200000
100000
0
0
200
400
600
800
m/z, negative ions

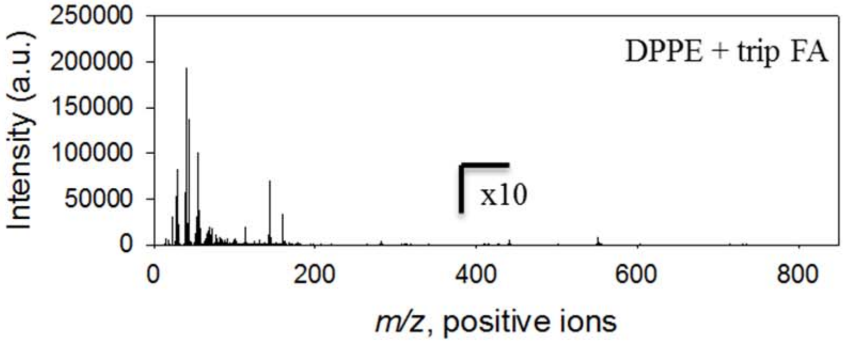
DPPE + trip FA
x10
Intensity (a.u.)
250000
200000
150000
100000
50000
0
0
200
400
600
800
m/z, positive ions

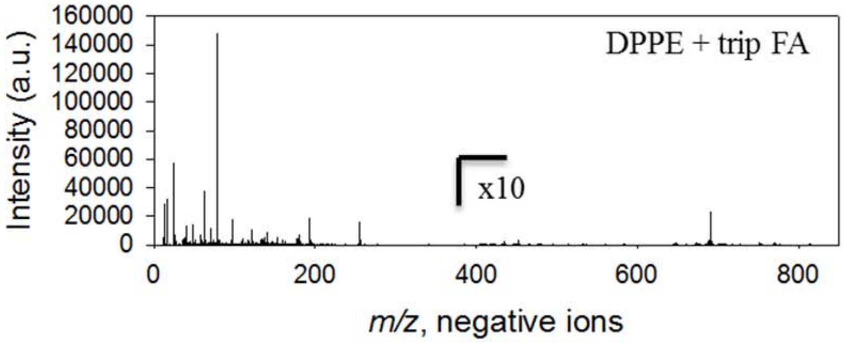
DPPE + trip FA
x10
Intensity (a.u.)
160000
140000
120000
100000
80000
60000
40000
20000
0
0
200
400
600
800
m/z, negative ions

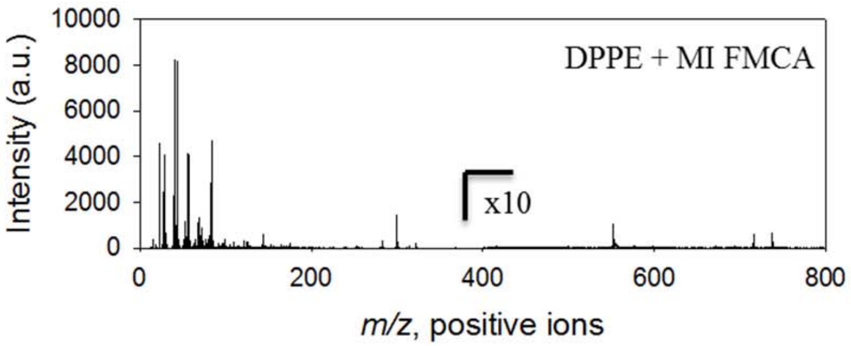
10000
8000
6000
4000
2000
0
Intensity (a.u.)
DPPE + MI FMCA
x10
0
200
400
600
800
m/z, positive ions

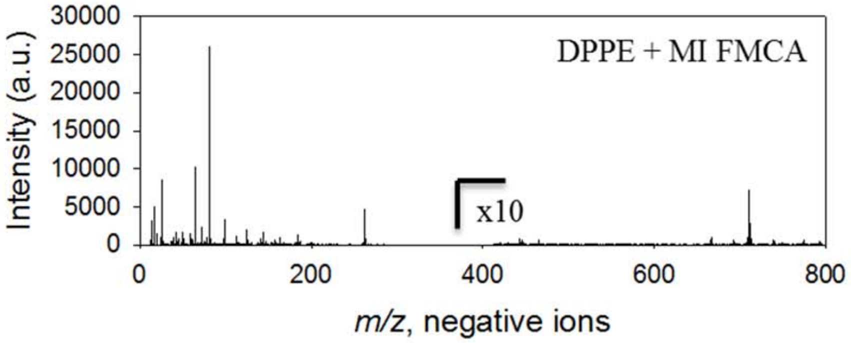
30000
25000
20000
15000
10000
5000
0
Intensity (a.u.)
DPPE + MI FMCA
x10
0
200
400
600
800
m/z, negative ions

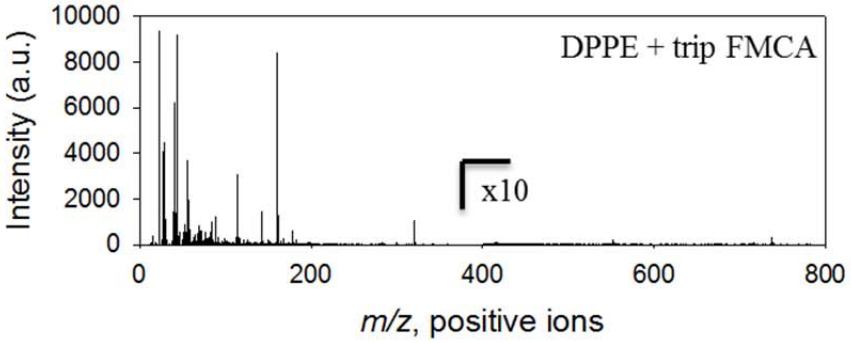
10000
8000
6000
4000
2000
0
Intensity (a.u.)
DPPE + trip FMCA
x10
0
200
400
600
800
m/z, positive ions

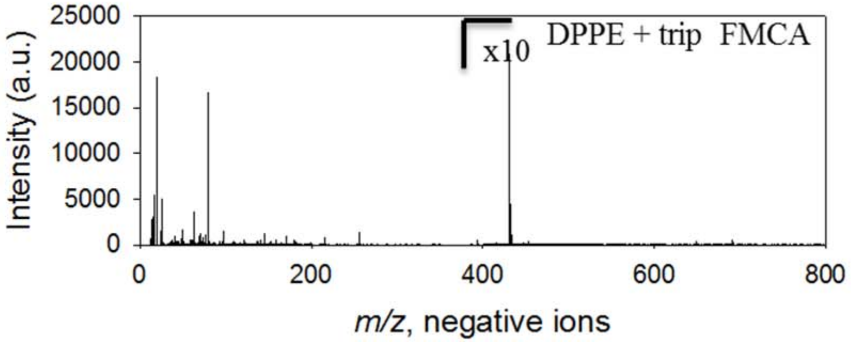
25000
20000
15000
10000
5000
0
Intensity (a.u.)
x10
DPPE + trip FMCA
0
200
400
600
800
m/z, negative ions

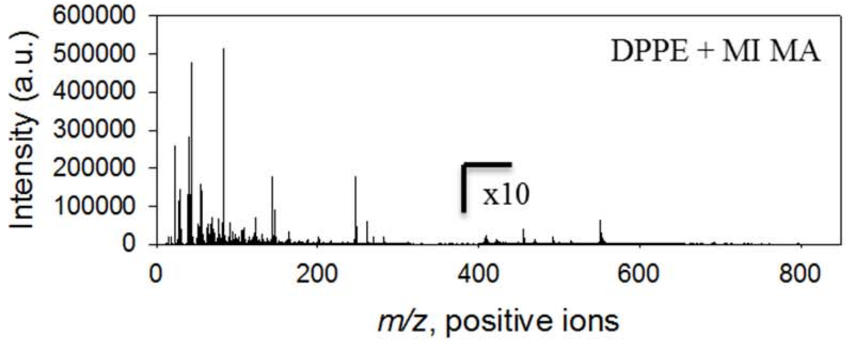
DPPE + MI MA
Intensity (a.u.)
600000
500000
400000
300000
200000
100000
0
x10
0
200
400
600
800
m/z, positive ions

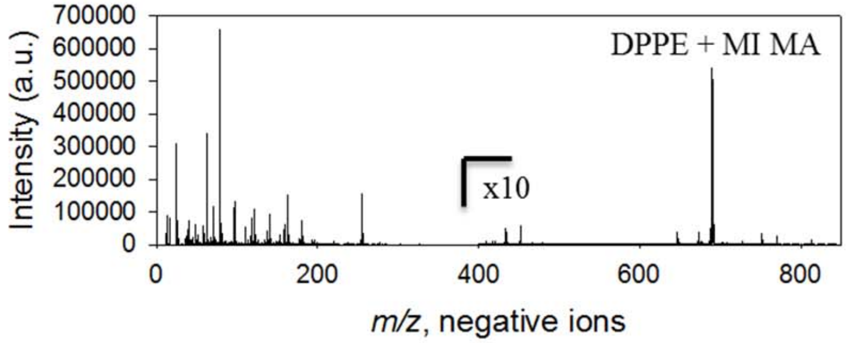
DPPE + MI MA
Intensity (a.u.)
700000
600000
500000
400000
300000
200000
100000
0
x10
0
200
400
600
800
m/z, negative ions

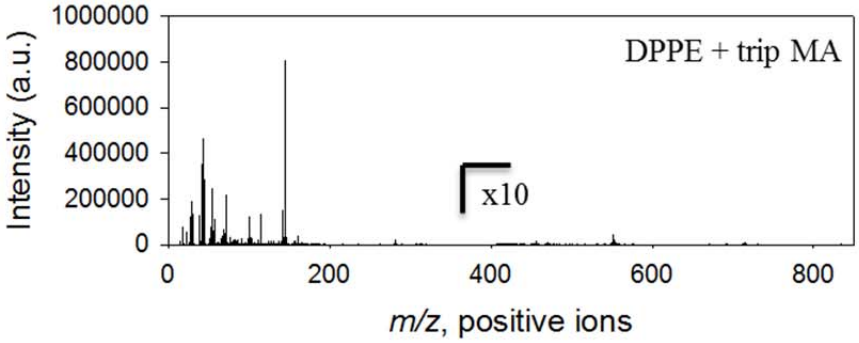
DPPE + trip MA
Intensity (a.u.)
1000000
800000
600000
400000
200000
0
x10
0
200
400
600
800
m/z, positive ions

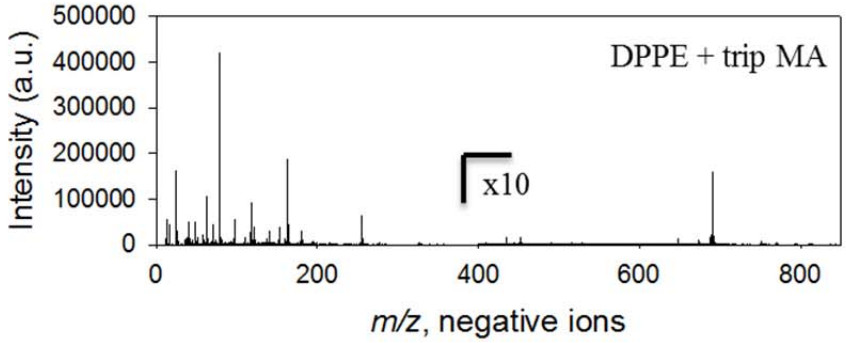
DPPE + trip MA
Intensity (a.u.)
500000
400000
300000
200000
100000
0
x10
0
200
400
600
800
m/z, negative ions

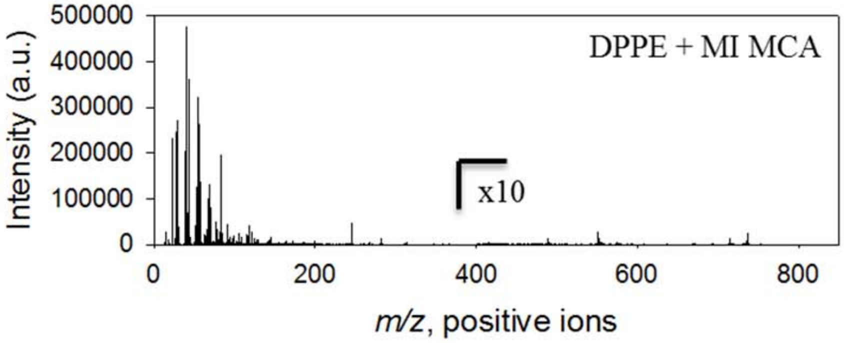
DPPE + MI MCA
x10
Intensity (a.u.)
500000
400000
300000
200000
100000
0
0
200
400
600
800
m/z, positive ions

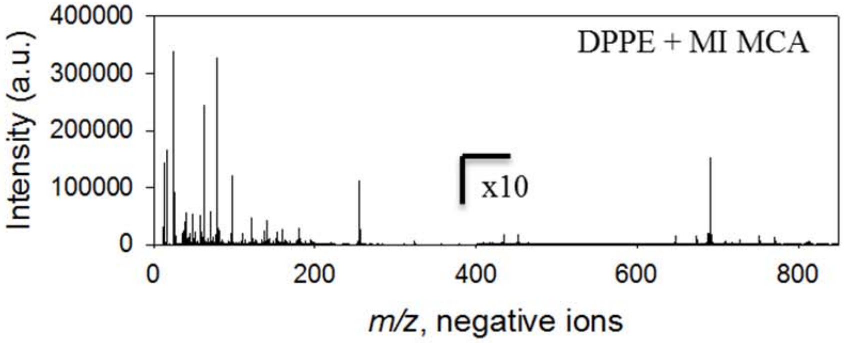
DPPE + MI MCA
x10
Intensity (a.u.)
400000
300000
200000
100000
0
0
200
400
600
800
m/z, negative ions

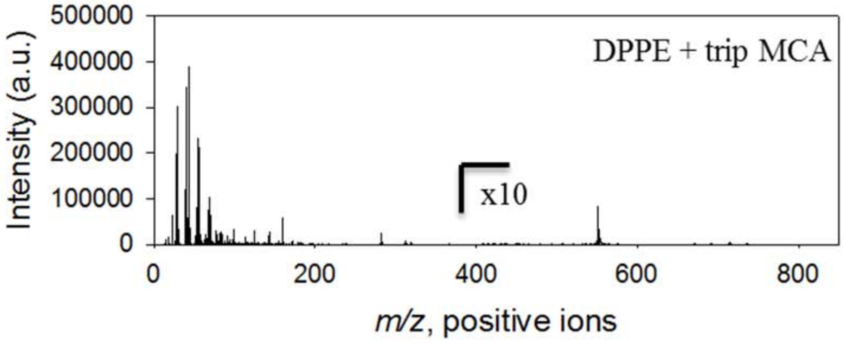
DPPE + trip MCA
x10
Intensity (a.u.)
500000
400000
300000
200000
100000
0
0
200
400
600
800
m/z, positive ions

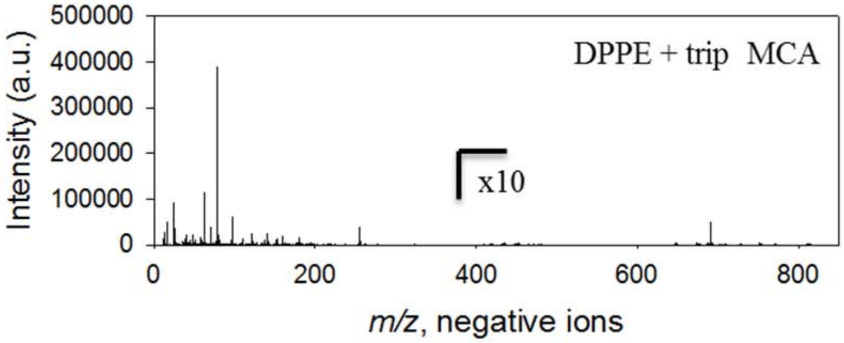
DPPE + trip MCA
x10
Intensity (a.u.)
500000
400000
300000
200000
100000
0
0
200
400
600
800
m/z, negative ions

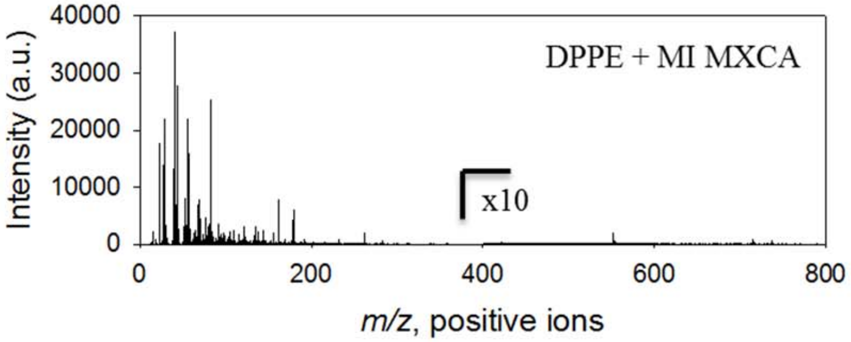
40000
30000
20000
10000
0
Intensity (a.u.)
DPPE + MI MXCA
x10
0
200
400
600
800
m/z, positive ions

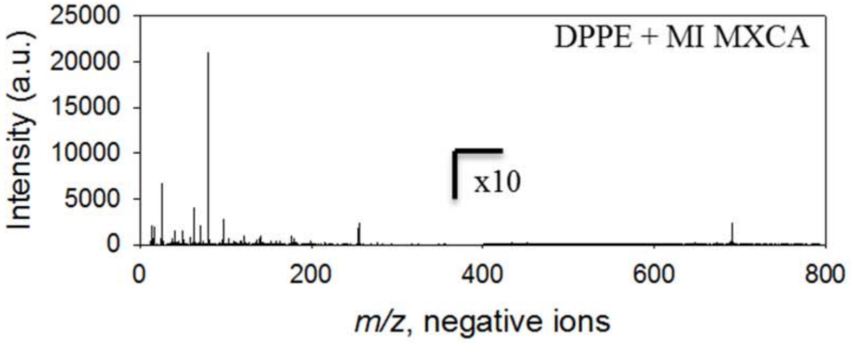
25000
20000
15000
10000
5000
0
Intensity (a.u.)
DPPE + MI MXCA
x10
0
200
400
600
800
m/z, negative ions

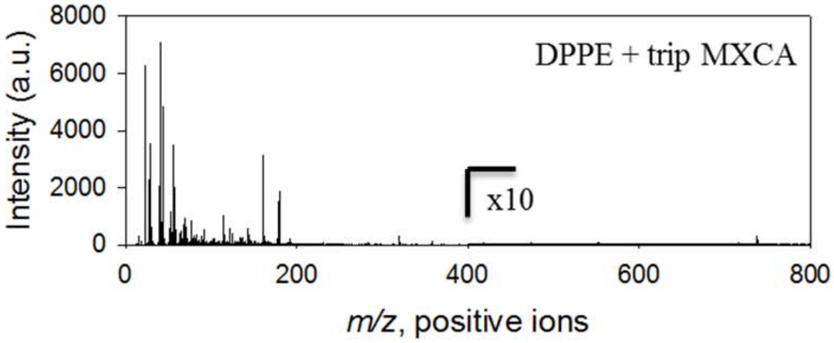
8000
6000
4000
2000
0
Intensity (a.u.)
DPPE + trip MXCA
x10
0
200
400
600
800
m/z, positive ions

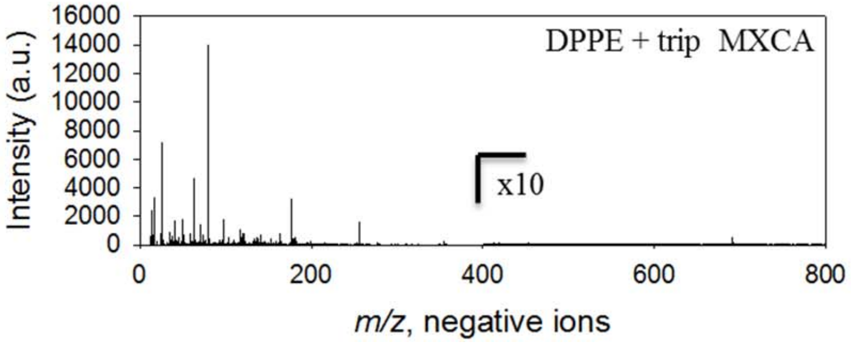
16000
14000
12000
10000
8000
6000
4000
2000
0
Intensity (a.u.)
DPPE + trip MXCA
x10
0
200
400
600
800
m/z, negative ions

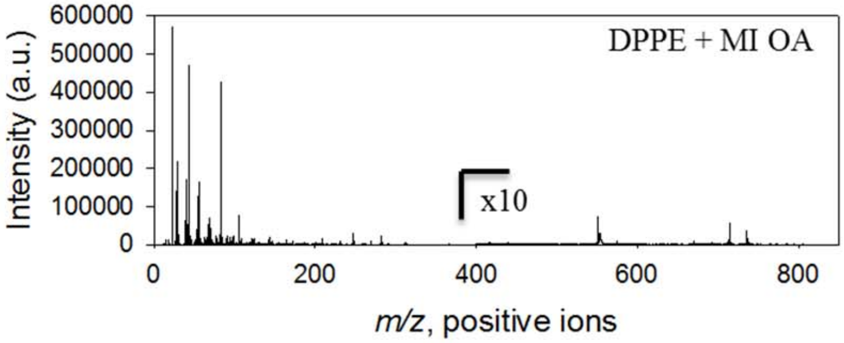

DPPE + MI OA
x10
Intensity (a.u.)
600000
500000
400000
300000
200000
100000
0
0
200
400
600
800
m/z, positive ions

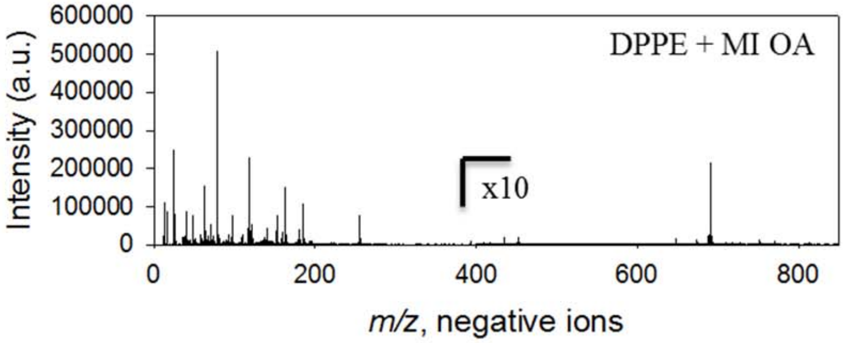

DPPE + MI OA
x10
Intensity (a.u.)
600000
500000
400000
300000
200000
100000
0
0
200
400
600
800
m/z, negative ions

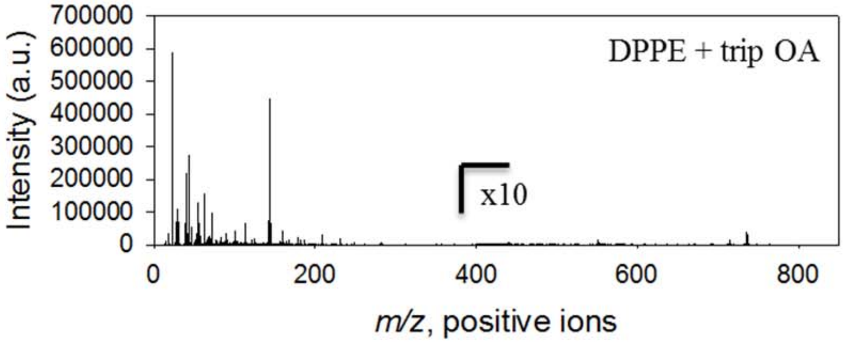

DPPE + trip OA
x10
Intensity (a.u.)
700000
600000
500000
400000
300000
200000
100000
0
0
200
400
600
800
m/z, positive ions

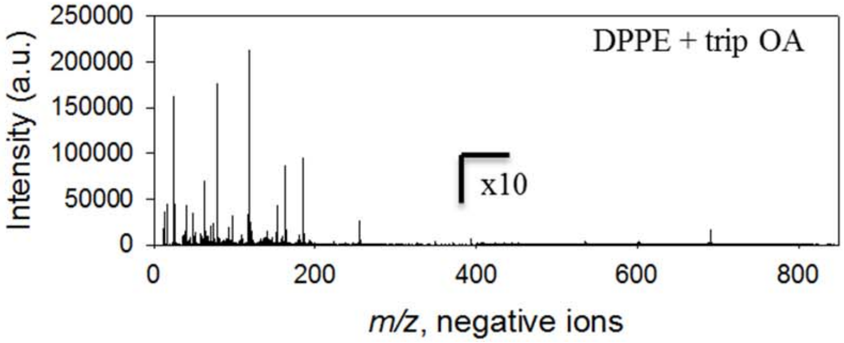

DPPE + trip OA
x10
Intensity (a.u.)
250000
200000
150000
100000
50000
0
0
200
400
600
800
m/z, negative ions

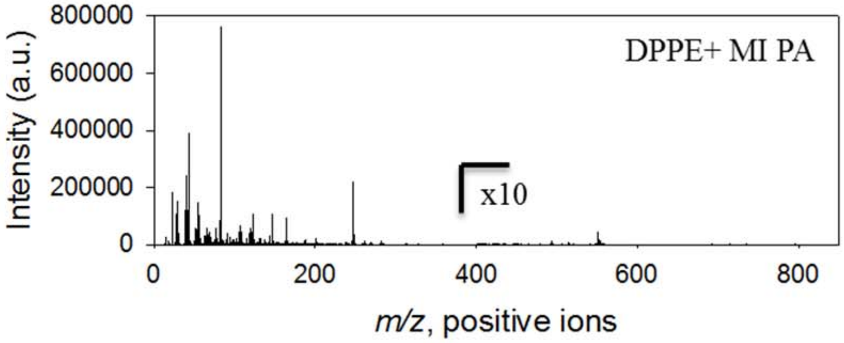
DPPE+ MI PA
x10
Intensity (a.u.)
800000
600000
400000
200000
0
0
200
400
600
800
m/z, positive ions

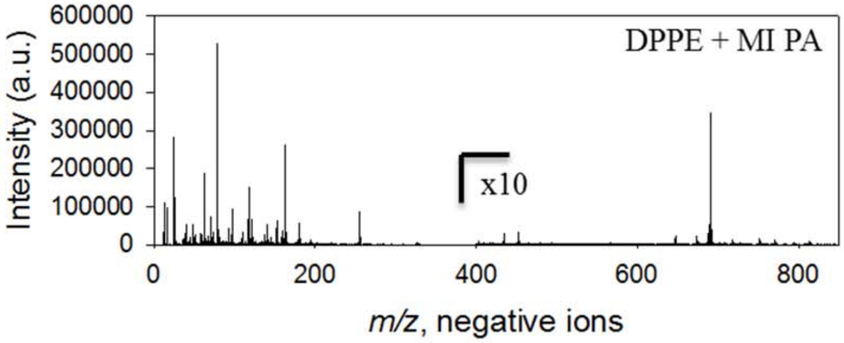
DPPE + MI PA
x10
Intensity (a.u.)
600000
500000
400000
300000
200000
100000
0
0
200
400
600
800
m/z, negative ions

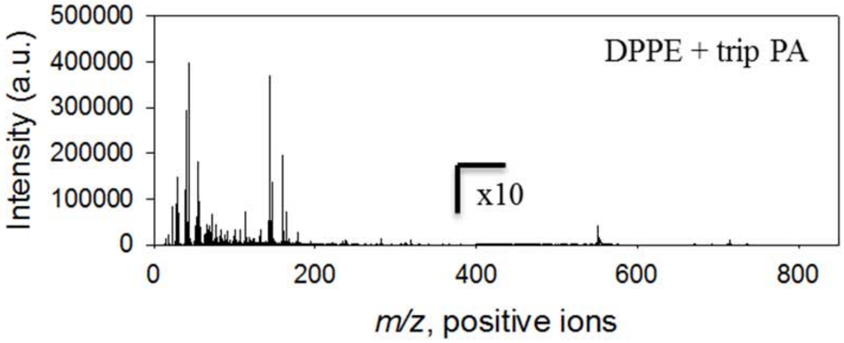
DPPE + trip PA
x10
Intensity (a.u.)
500000
400000
300000
200000
100000
0
0
200
400
600
800
m/z, positive ions

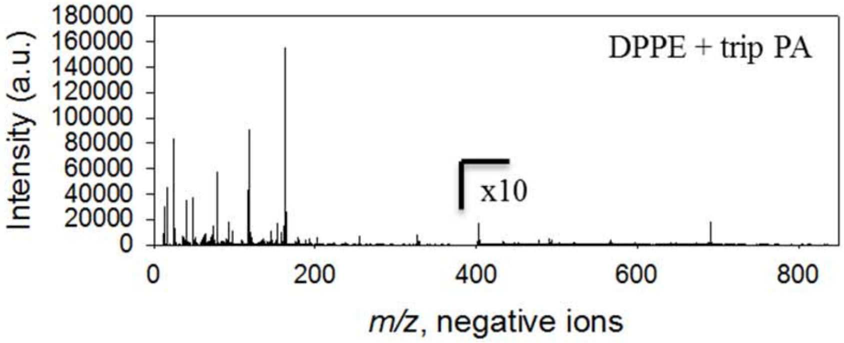
DPPE + trip PA
x10
Intensity (a.u.)
180000
160000
140000
120000
100000
80000
60000
40000
20000
0
0
200
400
600
800
m/z, negative ions

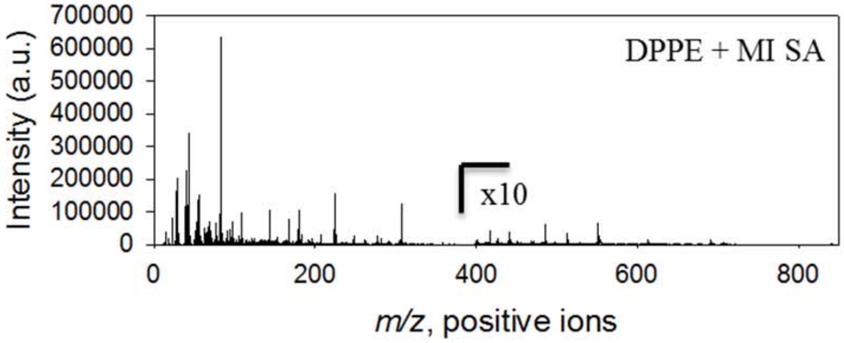
DPPE + MI SA
x10
Intensity (a.u.)
700000
600000
500000
400000
300000
200000
100000
0
0
200
400
600
800
m/z, positive ions

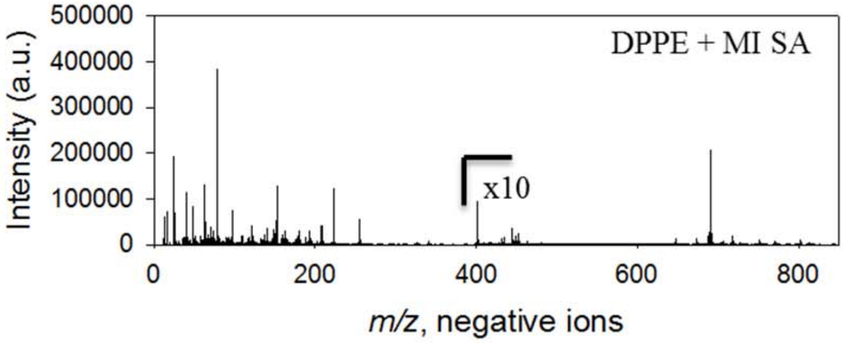
DPPE + MI SA
x10
Intensity (a.u.)
500000
400000
300000
200000
100000
0
0
200
400
600
800
m/z, negative ions

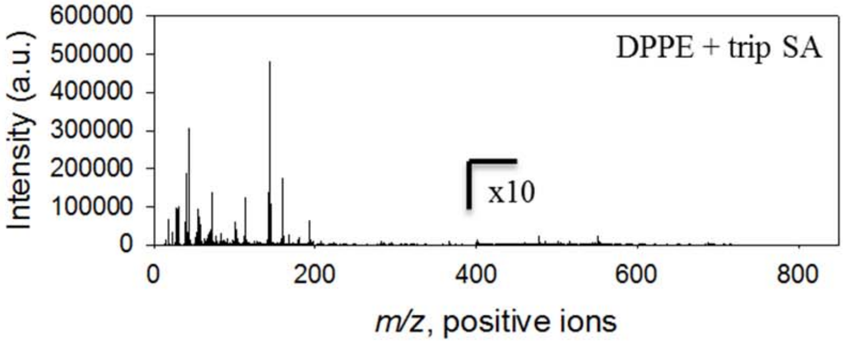
DPPE + trip SA
x10
Intensity (a.u.)
600000
500000
400000
300000
200000
100000
0
0
200
400
600
800
m/z, positive ions

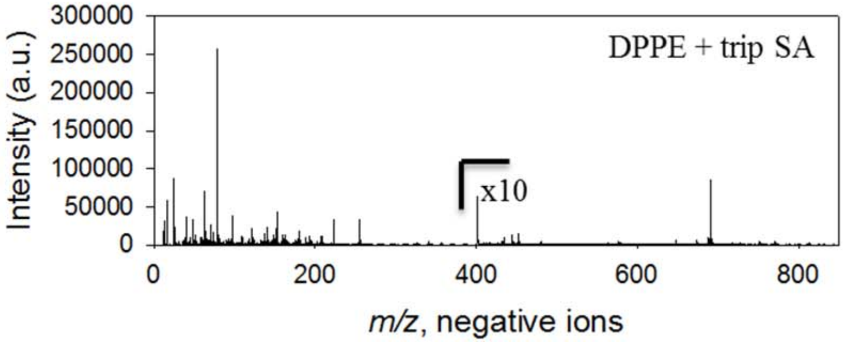
DPPE + trip SA
x10
Intensity (a.u.)
300000
250000
200000
150000
100000
50000
0
0
200
400
600
800
m/z, negative ions

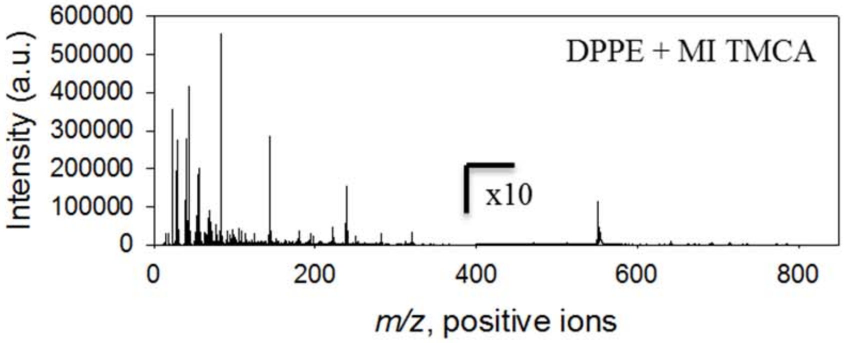
DPPE + MI TMCA
x10
Intensity (a.u.)
600000
500000
400000
300000
200000
100000
0
0
200
400
600
800
m/z, positive ions

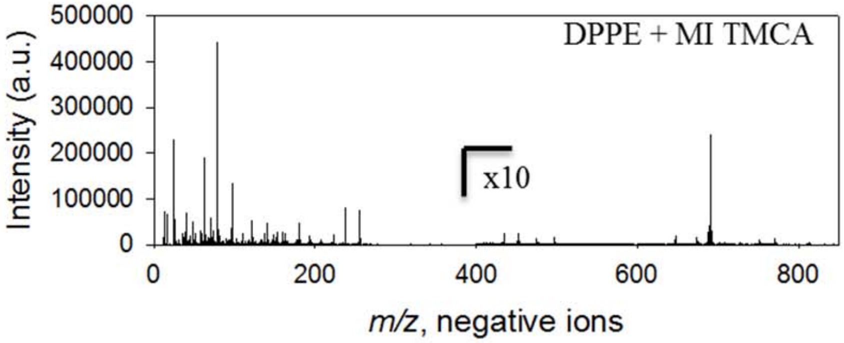
DPPE + MI TMCA
x10
Intensity (a.u.)
500000
400000
300000
200000
100000
0
0
200
400
600
800
m/z, negative ions

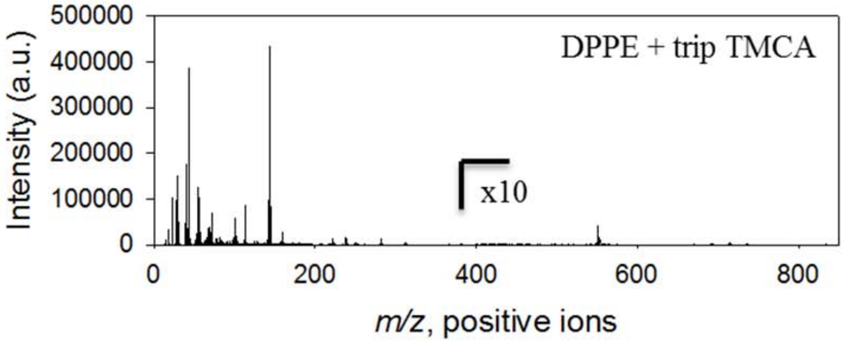
DPPE + trip TMCA
x10
Intensity (a.u.)
500000
400000
300000
200000
100000
0
0
200
400
600
800
m/z, positive ions

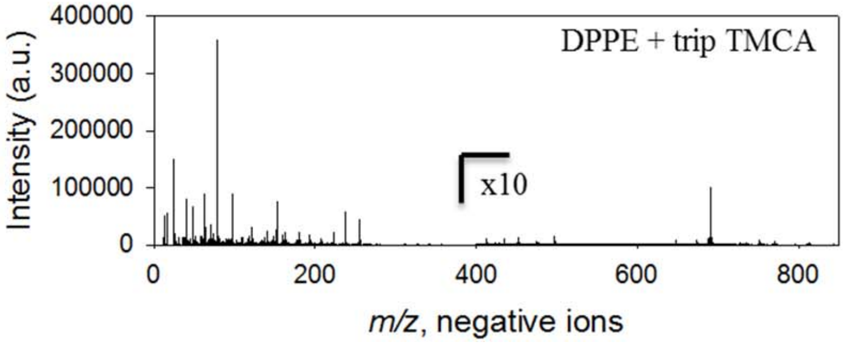
DPPE + trip TMCA
x10
Intensity (a.u.)
400000
300000
200000
100000
0
0
200
400
600
800
m/z, negative ions

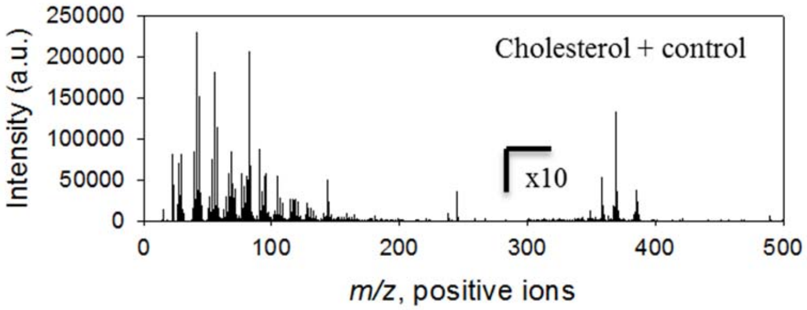
Cholesterol + control
x10
Intensity (a.u.)
250000
200000
150000
100000
50000
0
0
100
200
300
400
500
m/z, positive ions

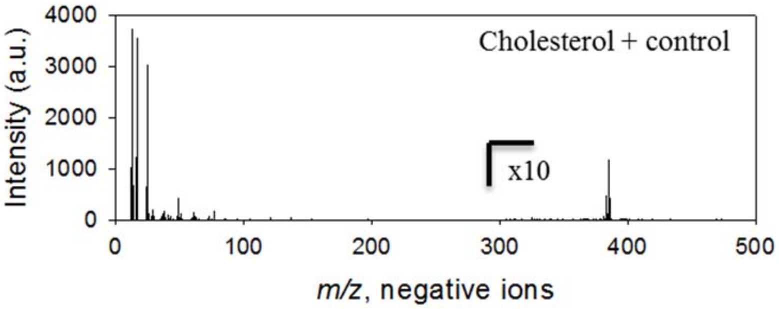
Cholesterol + control
x10
Intensity (a.u.)
4000
3000
2000
1000
0
0
100
200
300
400
500
m/z, negative ions

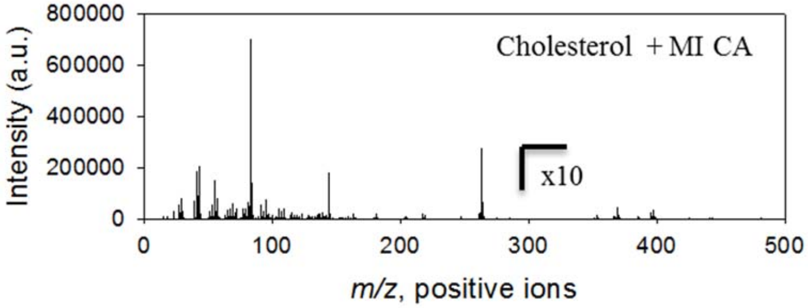
Cholesterol + MI CA
x10
Intensity (a.u.)
800000
600000
400000
200000
0
0
100
200
300
400
500
m/z, positive ions

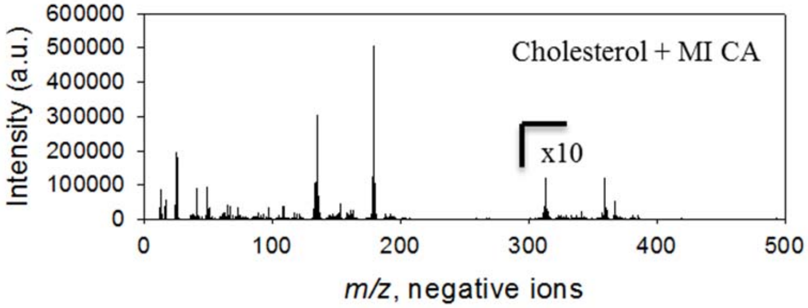
Cholesterol + MI CA
x10
Intensity (a.u.)
600000
500000
400000
300000
200000
100000
0
0
100
200
300
400
500
m/z, negative ions

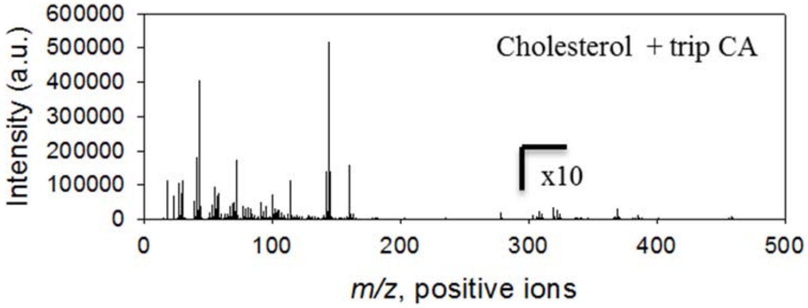
Cholesterol + trip CA
x10
Intensity (a.u.)
600000
500000
400000
300000
200000
100000
0
0
100
200
300
400
500
m/z, positive ions

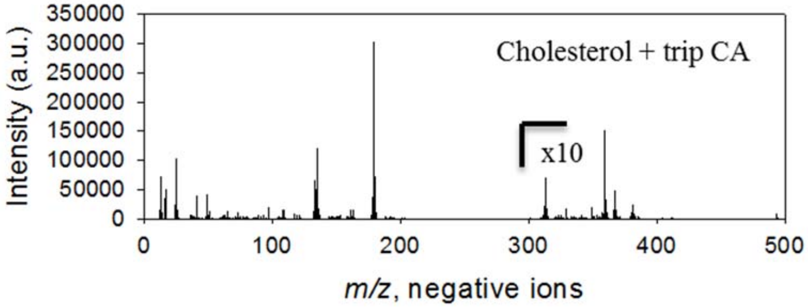
Cholesterol + trip CA
x10
Intensity (a.u.)
350000
300000
250000
200000
150000
100000
50000
0
0
100
200
300
400
500
m/z, negative ions

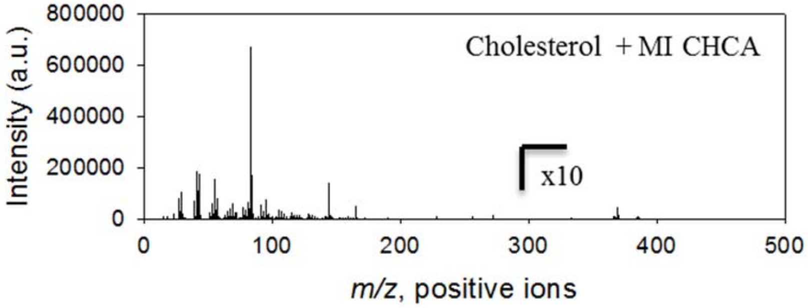
Cholesterol + MI CHCA
x10
Intensity (a.u.)
800000
600000
400000
200000
0
0
100
200
300
400
500
m/z, positive ions

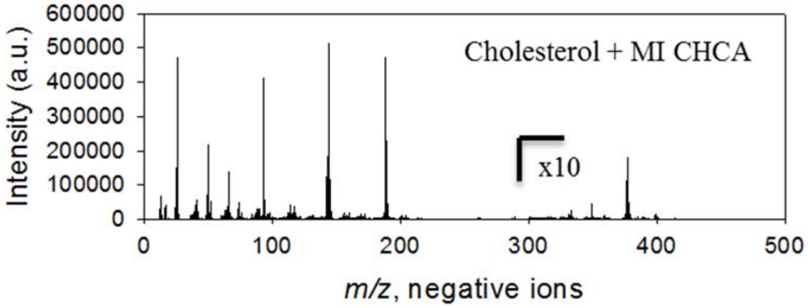
Cholesterol + MI CHCA
x10
Intensity (a.u.)
600000
500000
400000
300000
200000
100000
0
0
100
200
300
400
500
m/z, negative ions

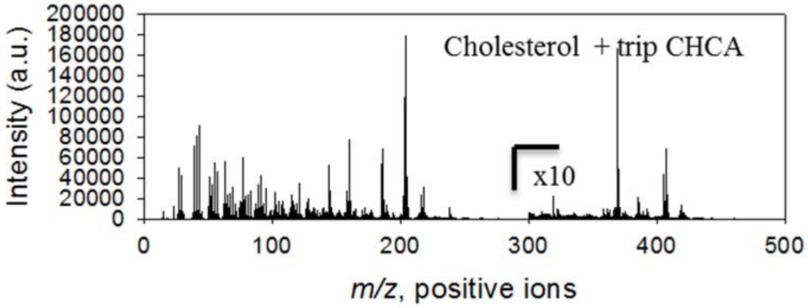
Cholesterol + trip CHCA
x10
Intensity (a.u.)
200000
180000
160000
140000
120000
100000
80000
60000
40000
20000
0
0
100
200
300
400
500
m/z, positive ions

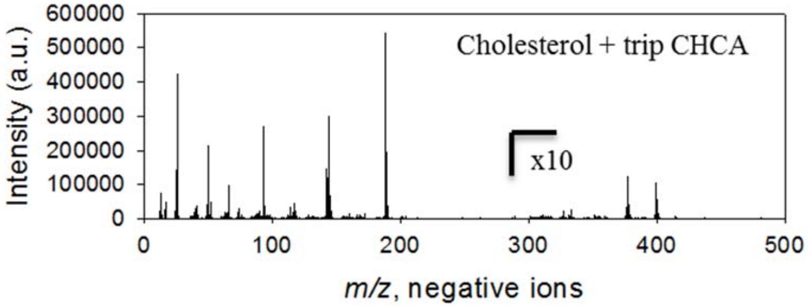
Cholesterol + trip CHCA
x10
Intensity (a.u.)
600000
500000
400000
300000
200000
100000
0
0
100
200
300
400
500
m/z, negative ions

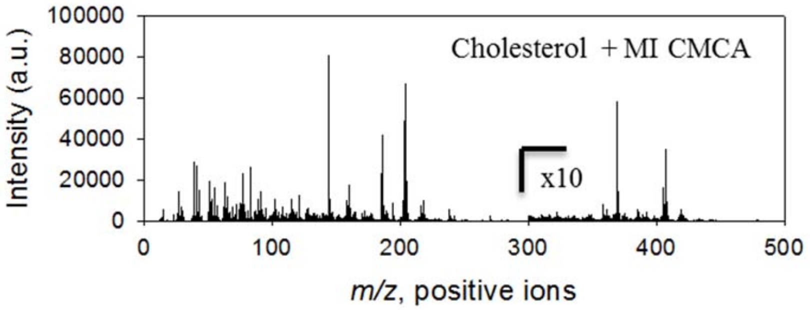
Cholesterol + MI CMCA
x10
Intensity (a.u.)
100000
80000
60000
40000
20000
0
0
100
200
300
400
500
m/z, positive ions

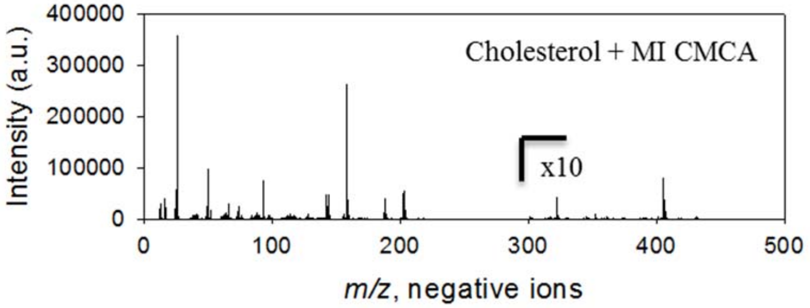
Cholesterol + MI CMCA
x10
Intensity (a.u.)
400000
300000
200000
100000
0
0
100
200
300
400
500
m/z, negative ions

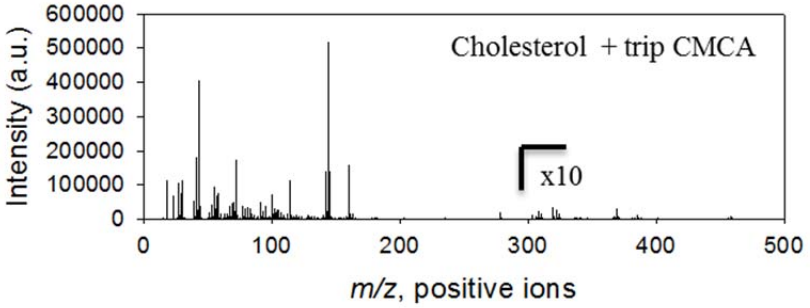
Cholesterol + trip CMCA
x10
Intensity (a.u.)
600000
500000
400000
300000
200000
100000
0
0
100
200
300
400
500
m/z, positive ions

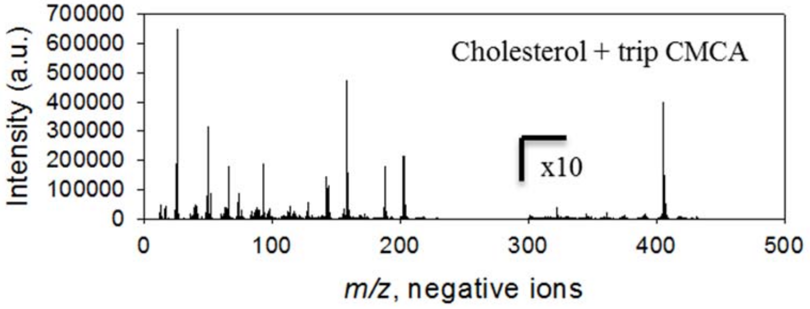
Cholesterol + trip CMCA
x10
Intensity (a.u.)
700000
600000
500000
400000
300000
200000
100000
0
0
100
200
300
400
500
m/z, negative ions

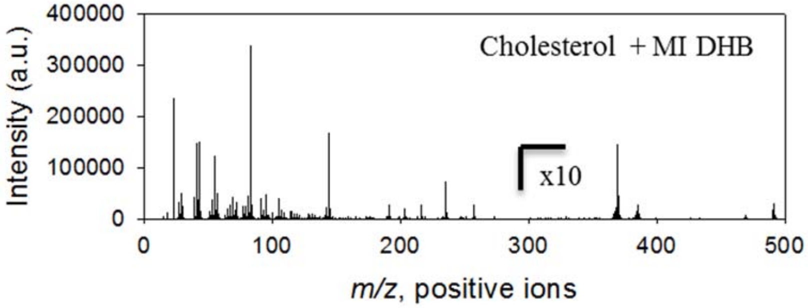
Cholesterol + MI DHB
x10
Intensity (a.u.)
400000
300000
200000
100000
0
0
100
200
300
400
500
m/z, positive ions

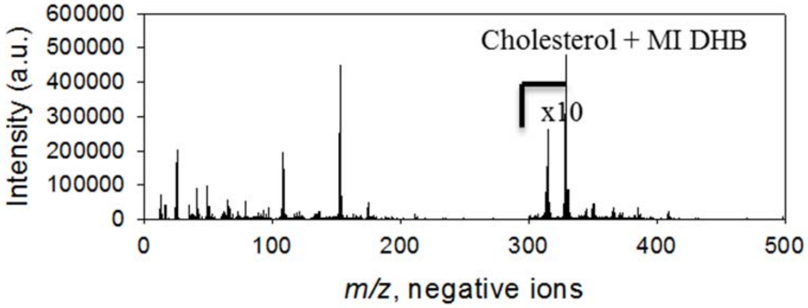
Cholesterol + MI DHB
x10
Intensity (a.u.)
600000
500000
400000
300000
200000
100000
0
0
100
200
300
400
500
m/z, negative ions

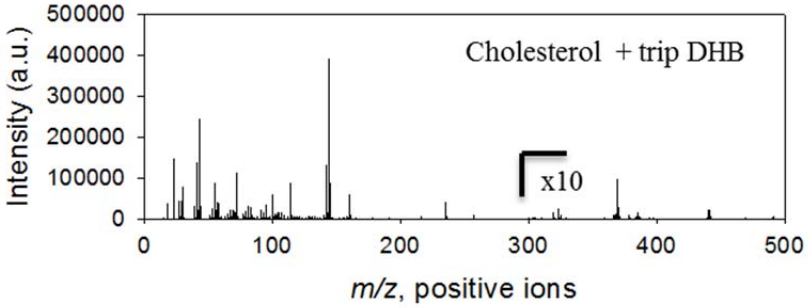
Cholesterol + trip DHB
x10
Intensity (a.u.)
500000
400000
300000
200000
100000
0
0
100
200
300
400
500
m/z, positive ions

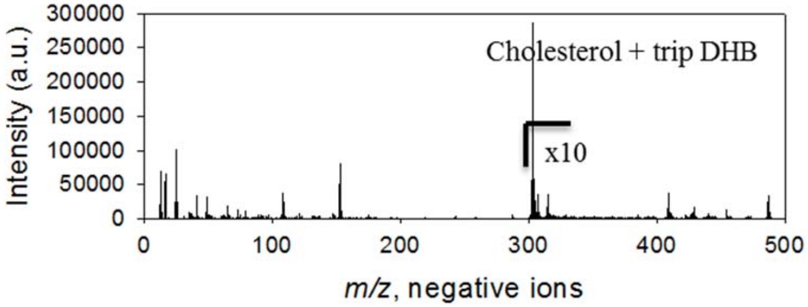
Cholesterol + trip DHB
x10
Intensity (a.u.)
300000
250000
200000
150000
100000
50000
0
0
100
200
300
400
500
m/z, negative ions

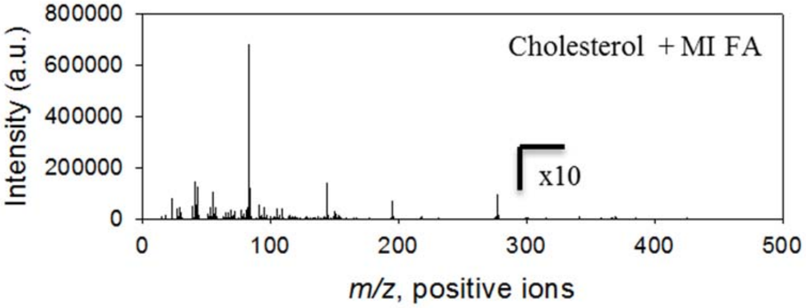
Intensity (a.u.)
800000
600000
400000
200000
0
Cholesterol + MI FA
x10
0
100
200
300
400
500
m/z, positive ions

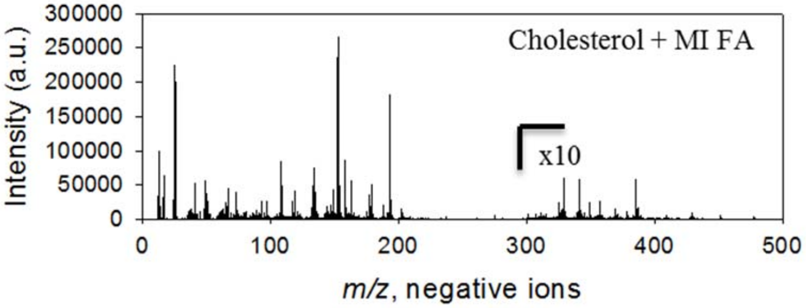
Intensity (a.u.)
300000
250000
200000
150000
100000
50000
0
Cholesterol + MI FA
x10
0
100
200
300
400
500
m/z, negative ions

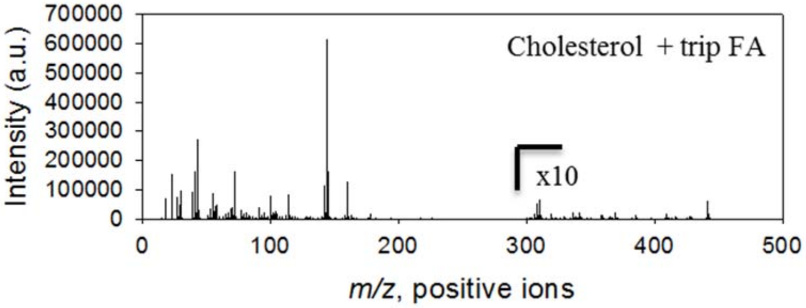
Intensity (a.u.)
700000
600000
500000
400000
300000
200000
100000
0
Cholesterol + trip FA
x10
0
100
200
300
400
500
m/z, positive ions

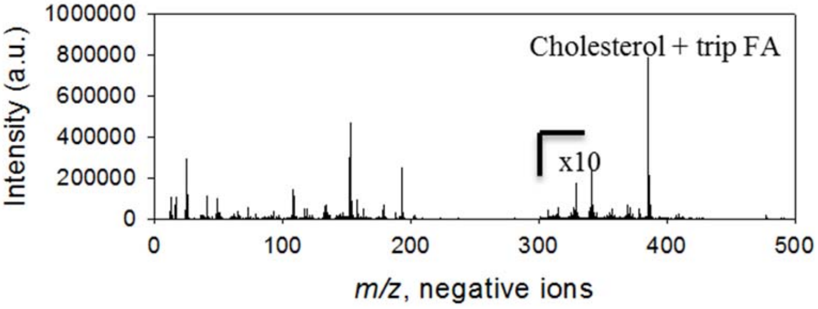
Intensity (a.u.)
1000000
800000
600000
400000
200000
0
Cholesterol + trip FA
x10
0
100
200
300
400
500
m/z, negative ions

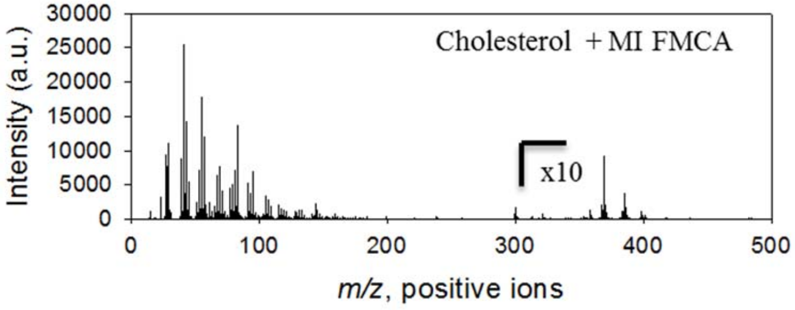
Cholesterol + MI FMCA
x10
Intensity (a.u.)
30000
25000
20000
15000
10000
5000
0
0
100
200
300
400
500
m/z, positive ions

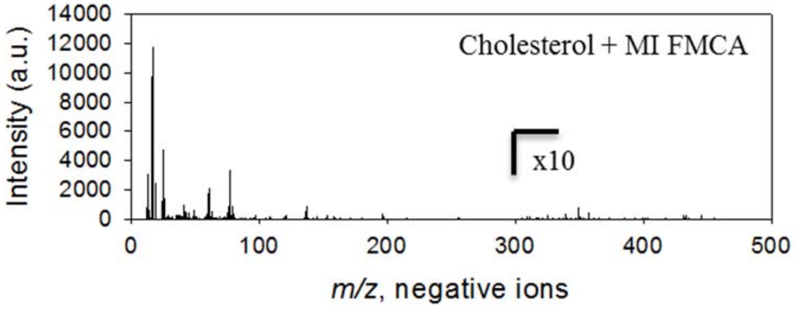
Cholesterol + MI FMCA
x10
Intensity (a.u.)
14000
12000
10000
8000
6000
4000
2000
0
0
100
200
300
400
500
m/z, negative ions

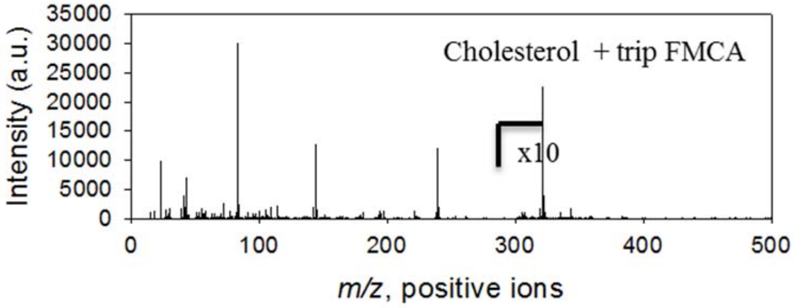
Cholesterol + trip FMCA
x10
Intensity (a.u.)
35000
30000
25000
20000
15000
10000
5000
0
0
100
200
300
400
500
m/z, positive ions

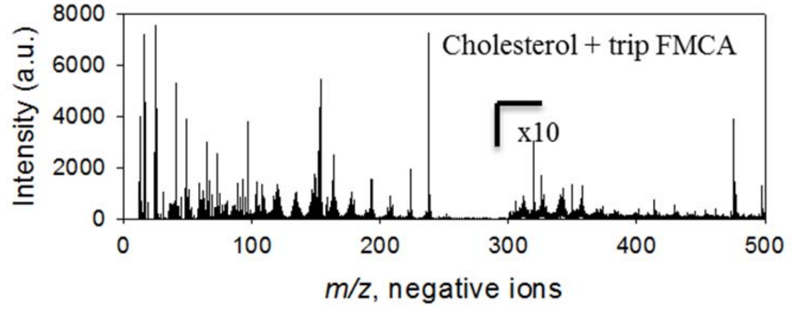
Cholesterol + trip FMCA
x10
Intensity (a.u.)
8000
6000
4000
2000
0
0
100
200
300
400
500
m/z, negative ions

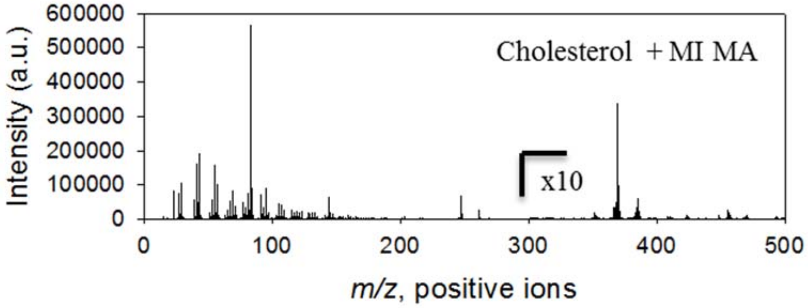
Intensity (a.u.)
600000
500000
400000
300000
200000
100000
0
Cholesterol + MI MA
x10
0
100
200
300
400
500
m/z, positive ions

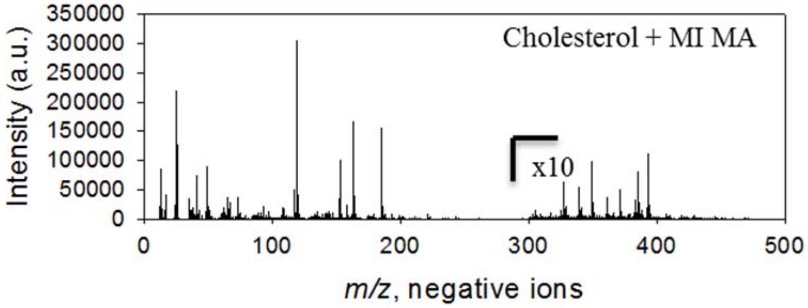
Intensity (a.u.)
350000
300000
250000
200000
150000
100000
50000
0
Cholesterol + MI MA
x10
0
100
200
300
400
500
m/z, negative ions

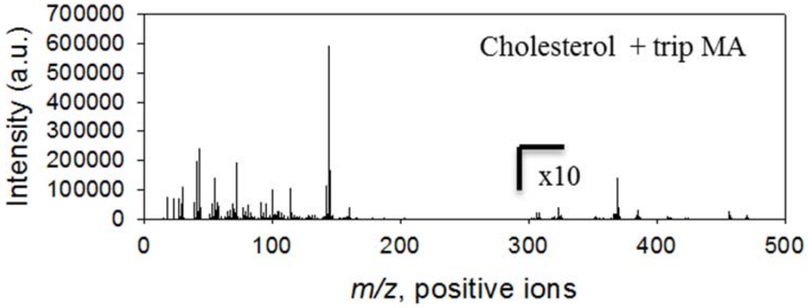
Intensity (a.u.)
700000
600000
500000
400000
300000
200000
100000
0
Cholesterol + trip MA
x10
0
100
200
300
400
500
m/z, positive ions

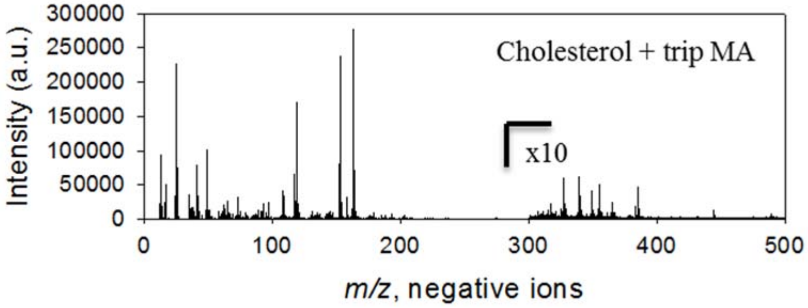
Intensity (a.u.)
300000
250000
200000
150000
100000
50000
0
Cholesterol + trip MA
x10
0
100
200
300
400
500
m/z, negative ions

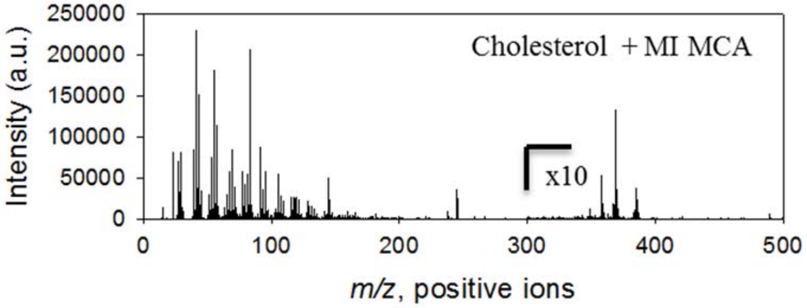
Cholesterol + MI MCA
x10
Intensity (a.u.)
250000
200000
150000
100000
50000
0
0
100
200
300
400
500
m/z, positive ions

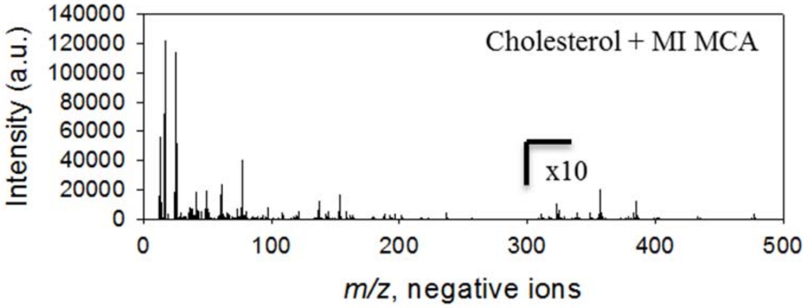
Cholesterol + MI MCA
x10
Intensity (a.u.)
140000
120000
100000
80000
60000
40000
20000
0
0
100
200
300
400
500
m/z, negative ions

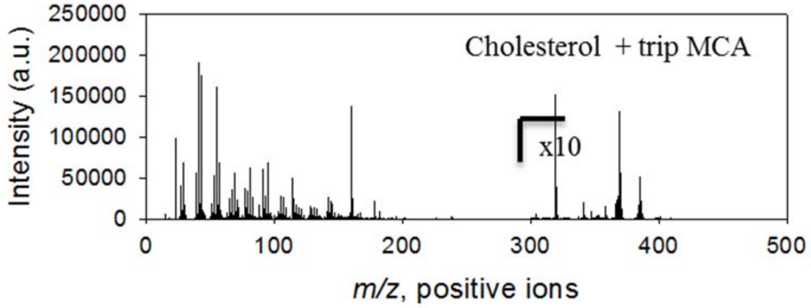
Cholesterol + trip MCA
x10
Intensity (a.u.)
250000
200000
150000
100000
50000
0
0
100
200
300
400
500
m/z, positive ions

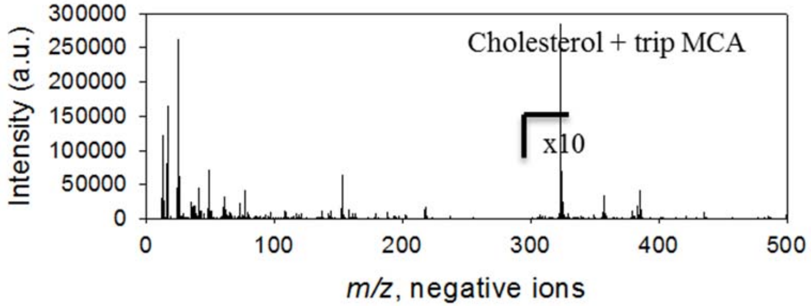
Cholesterol + trip MCA
x10
Intensity (a.u.)
300000
250000
200000
150000
100000
50000
0
0
100
200
300
400
500
m/z, negative ions

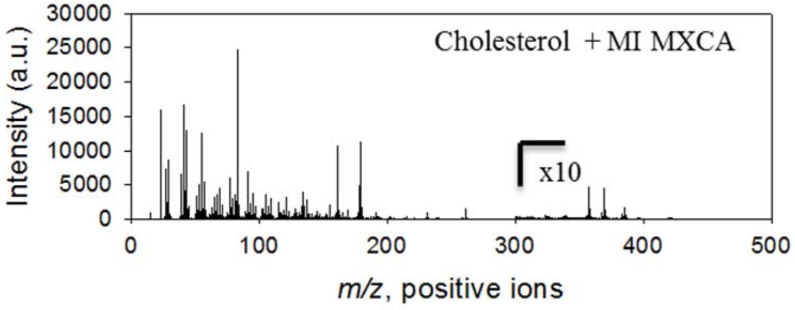
Cholesterol + MI MXCA
x10
Intensity (a.u.)
30000
25000
20000
15000
10000
5000
0
0
100
200
300
400
500
m/z, positive ions

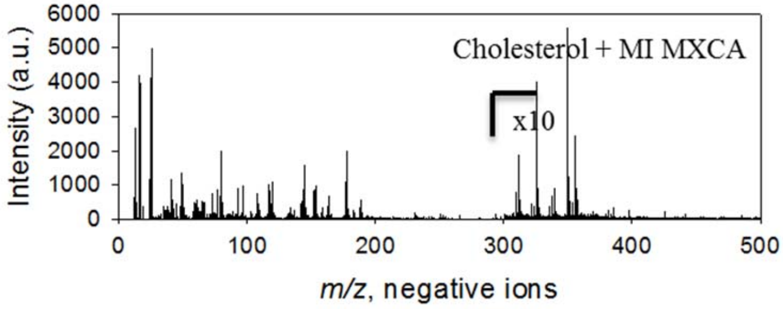
Cholesterol + MI MXCA
x10
Intensity (a.u.)
6000
5000
4000
3000
2000
1000
0
0
100
200
300
400
500
m/z, negative ions

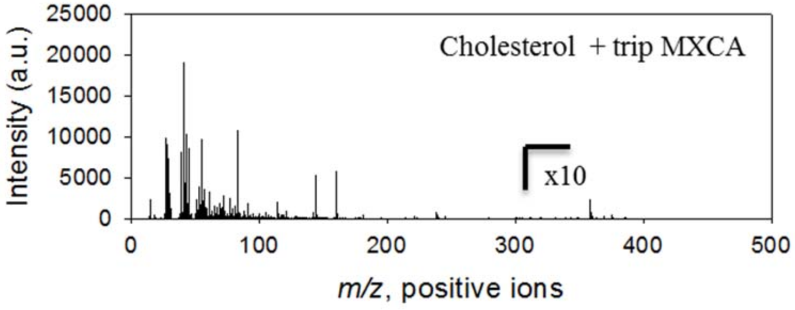
Cholesterol + trip MXCA
x10
Intensity (a.u.)
25000
20000
15000
10000
5000
0
0
100
200
300
400
500
m/z, positive ions

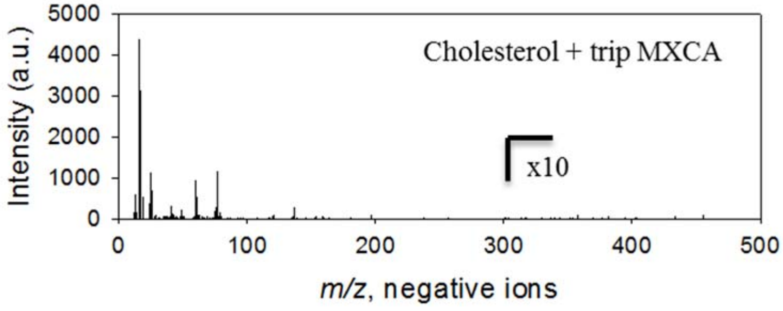
Cholesterol + trip MXCA
x10
Intensity (a.u.)
5000
4000
3000
2000
1000
0
0
100
200
300
400
500
m/z, negative ions

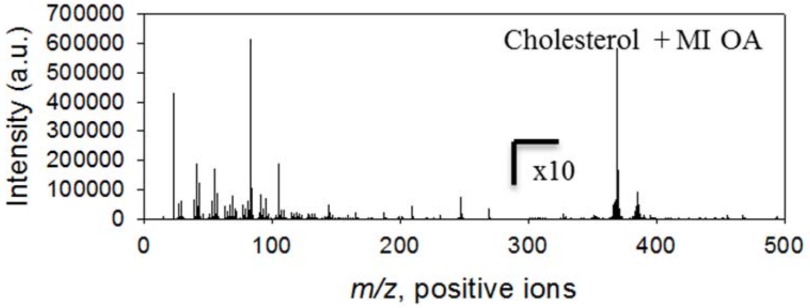
Cholesterol + MI OA
Intensity (a.u.)
700000
600000
500000
400000
300000
200000
100000
0
x10
0
100
200
300
400
500
m/z, positive ions

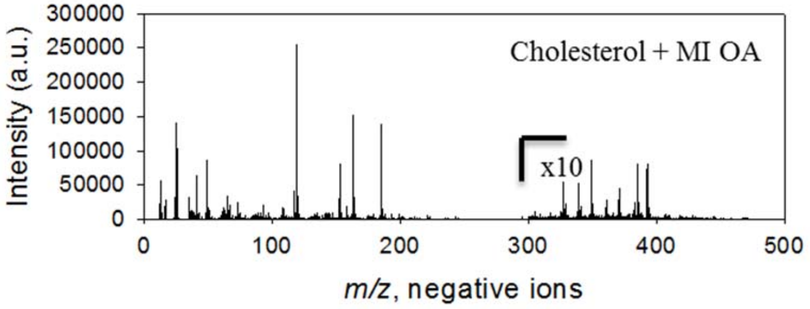
Cholesterol + MI OA
Intensity (a.u.)
300000
250000
200000
150000
100000
50000
0
x10
0
100
200
300
400
500
m/z, negative ions

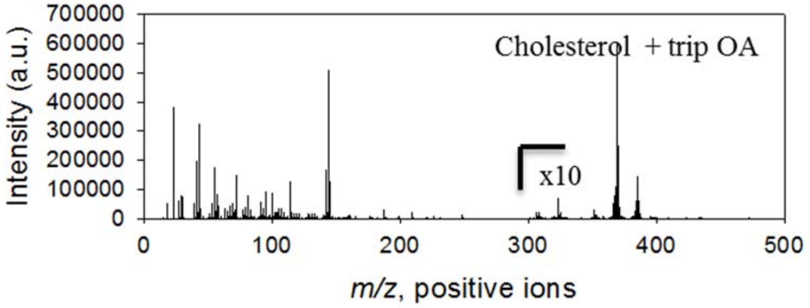
Cholesterol + trip OA
Intensity (a.u.)
700000
600000
500000
400000
300000
200000
100000
0
x10
0
100
200
300
400
500
m/z, positive ions

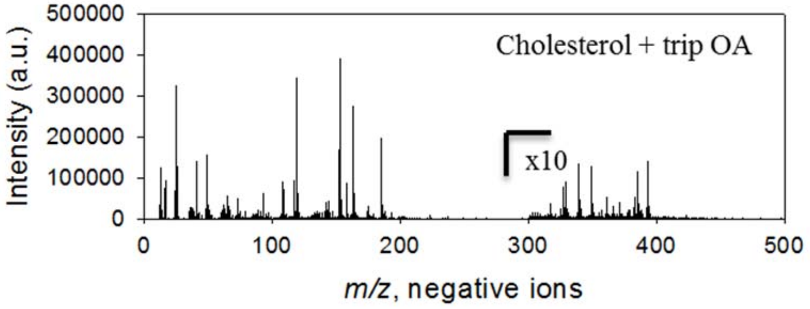
Cholesterol + trip OA
Intensity (a.u.)
500000
400000
300000
200000
100000
0
x10
0
100
200
300
400
500
m/z, negative ions

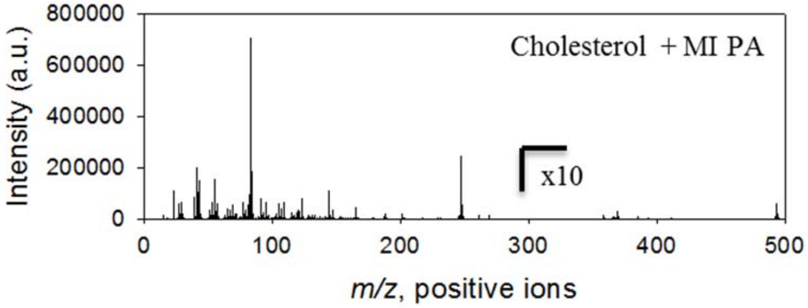
Cholesterol + MI PA
x10
Intensity (a.u.)
800000
600000
400000
200000
0
0
100
200
300
400
500
m/z, positive ions

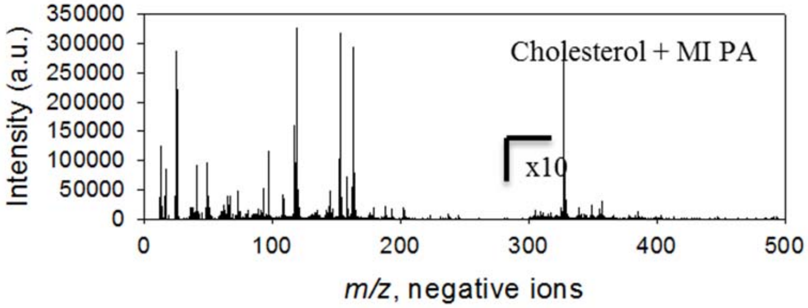
Cholesterol + MI PA
x10
Intensity (a.u.)
350000
300000
250000
200000
150000
100000
50000
0
0
100
200
300
400
500
m/z, negative ions

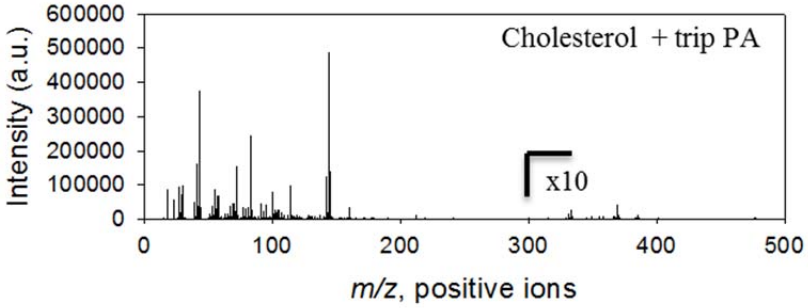
Cholesterol + trip PA
x10
Intensity (a.u.)
600000
500000
400000
300000
200000
100000
0
0
100
200
300
400
500
m/z, positive ions

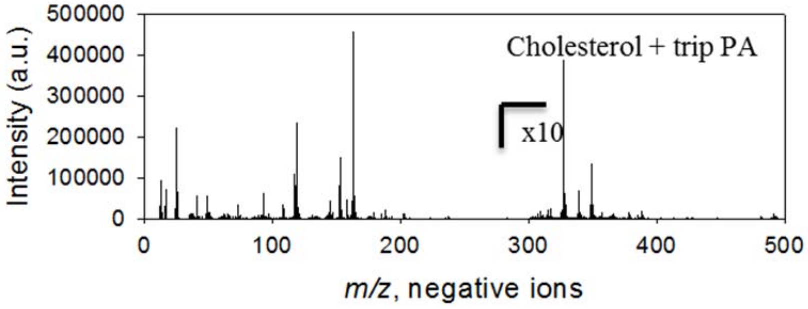
Cholesterol + trip PA
x10
Intensity (a.u.)
500000
400000
300000
200000
100000
0
0
100
200
300
400
500
m/z, negative ions

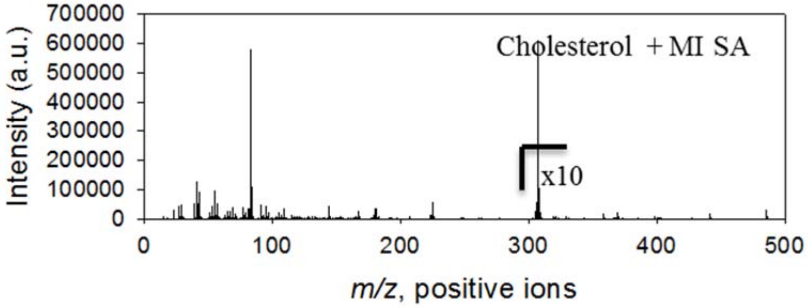
Cholesterol + MI SA
x10
Intensity (a.u.)
700000
600000
500000
400000
300000
200000
100000
0
0
100
200
300
400
500
m/z, positive ions

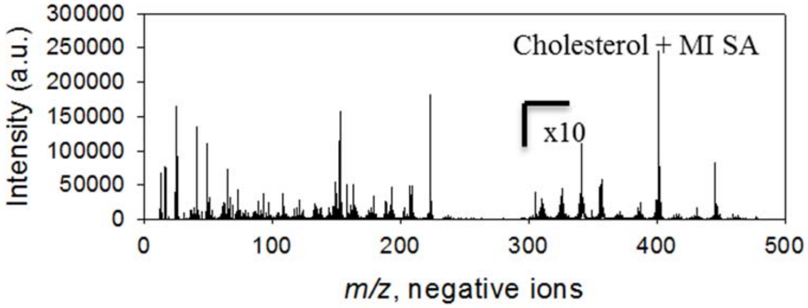
Cholesterol + MI SA
x10
Intensity (a.u.)
300000
250000
200000
150000
100000
50000
0
0
100
200
300
400
500
m/z, negative ions

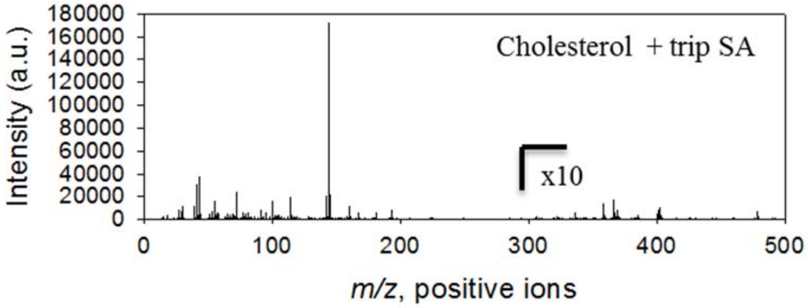
Cholesterol + trip SA
x10
Intensity (a.u.)
180000
160000
140000
120000
100000
80000
60000
40000
20000
0
0
100
200
300
400
500
m/z, positive ions

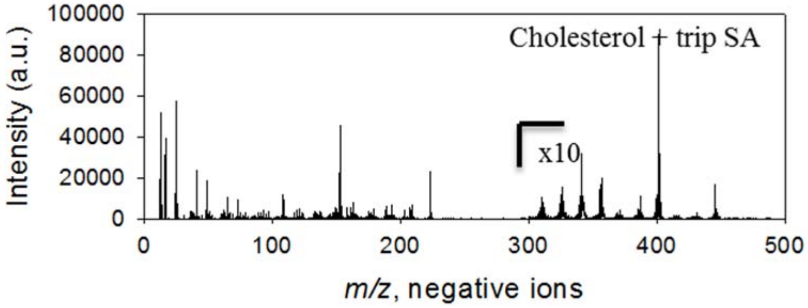
Cholesterol + trip SA
x10
Intensity (a.u.)
100000
80000
60000
40000
20000
0
0
100
200
300
400
500
m/z, negative ions

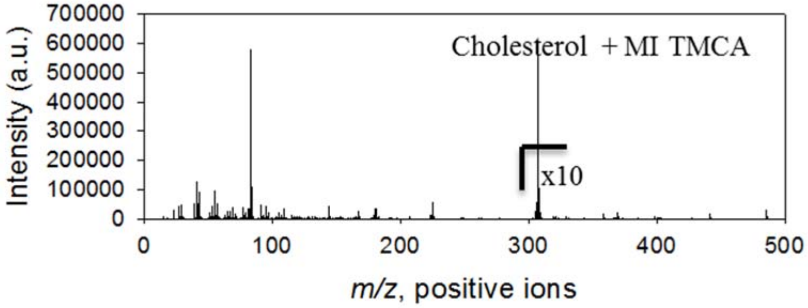
Cholesterol + MI TMCA
x10
Intensity (a.u.)
700000
600000
500000
400000
300000
200000
100000
0
0
100
200
300
400
500
m/z, positive ions

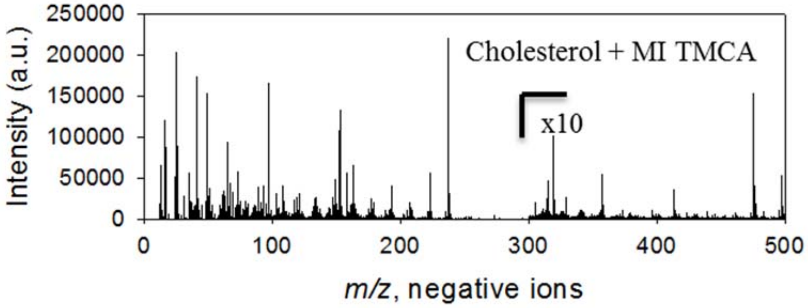
Cholesterol + MI TMCA
x10
Intensity (a.u.)
250000
200000
150000
100000
50000
0
0
100
200
300
400
500
m/z, negative ions

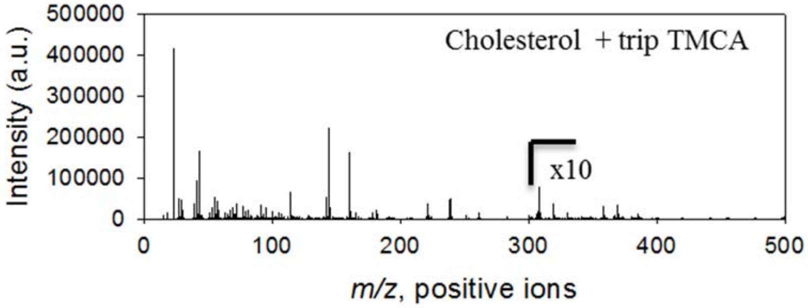
Cholesterol + trip TMCA
x10
Intensity (a.u.)
500000
400000
300000
200000
100000
0
0
100
200
300
400
500
m/z, positive ions

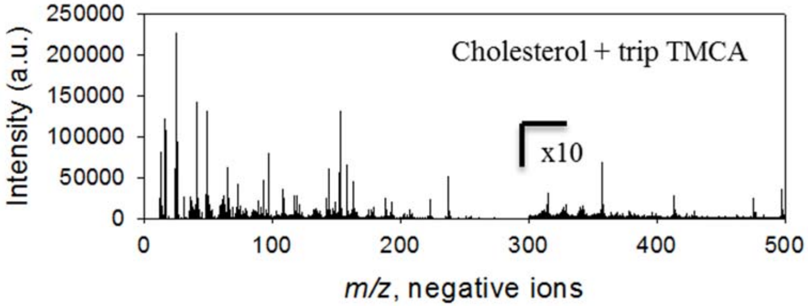
Cholesterol + trip TMCA
x10
Intensity (a.u.)
250000
200000
150000
100000
50000
0
0
100
200
300
400
500
m/z, negative ions

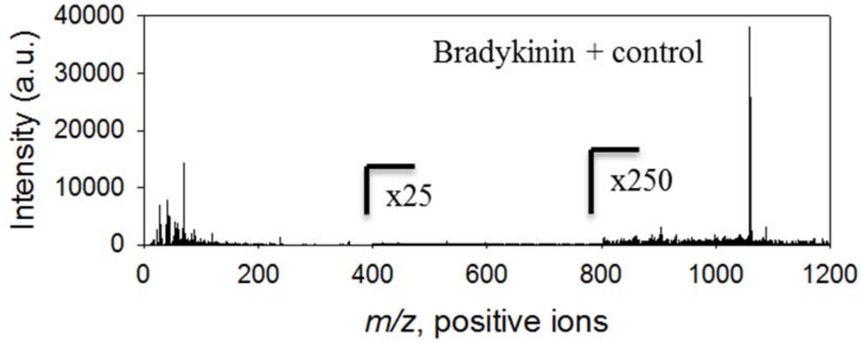
Bradykinin + control
x25
x250
Intensity (a.u.)
40000
30000
20000
10000
0
0
200
400
600
800
1000
1200
m/z, positive ions

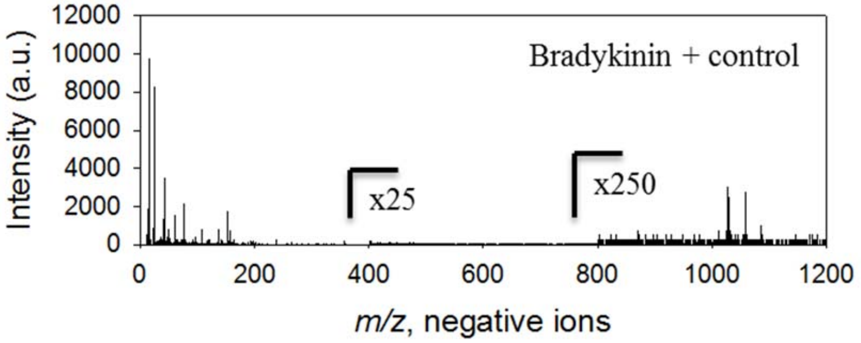
Bradykinin + control
x25
x250
Intensity (a.u.)
12000
10000
8000
6000
4000
2000
0
0
200
400
600
800
1000
1200
m/z, negative ions

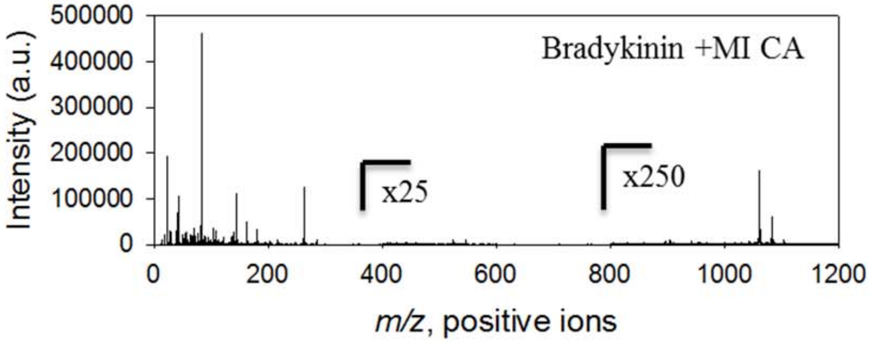
Bradykinin +MI CA
x25
x250
Intensity (a.u.)
500000
400000
300000
200000
100000
0
0
200
400
600
800
1000
1200
m/z, positive ions

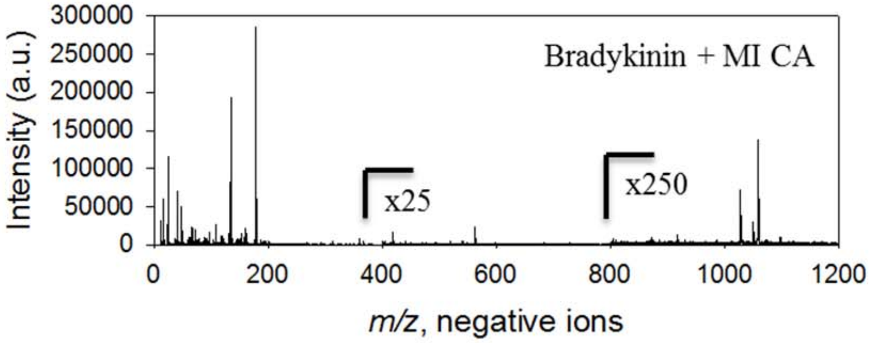
Bradykinin + MI CA
x25
x250
Intensity (a.u.)
300000
250000
200000
150000
100000
50000
0
0
200
400
600
800
1000
1200
m/z, negative ions

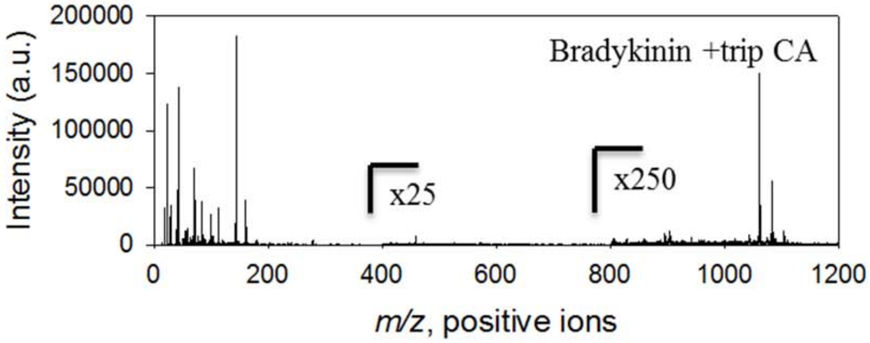
Bradykinin +trip CA
x25
x250
Intensity (a.u.)
200000
150000
100000
50000
0
0
200
400
600
800
1000
1200
m/z, positive ions

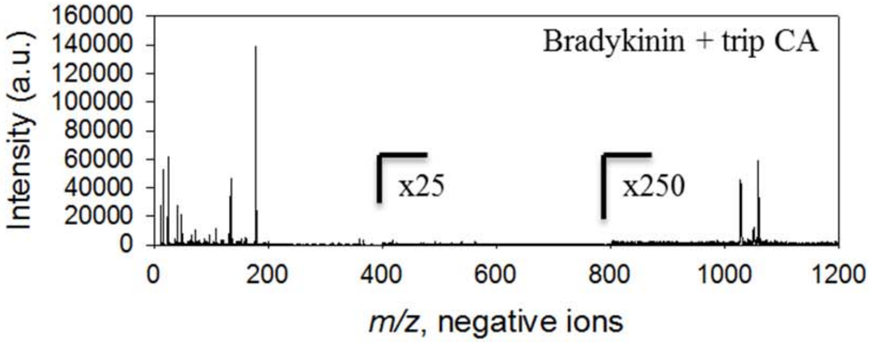
Bradykinin + trip CA
x25
x250
Intensity (a.u.)
160000
140000
120000
100000
80000
60000
40000
20000
0
0
200
400
600
800
1000
1200
m/z, negative ions

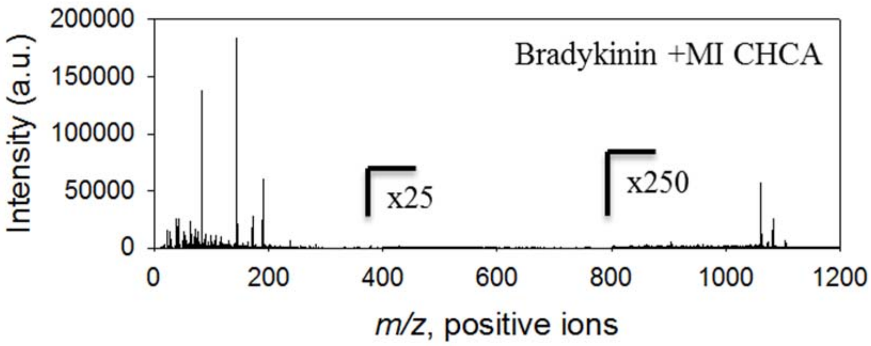
Bradykinin +MI CHCA
x25
x250
Intensity (a.u.)
0
50000
100000
150000
200000
0
200
400
600
800
1000
1200
m/z, positive ions

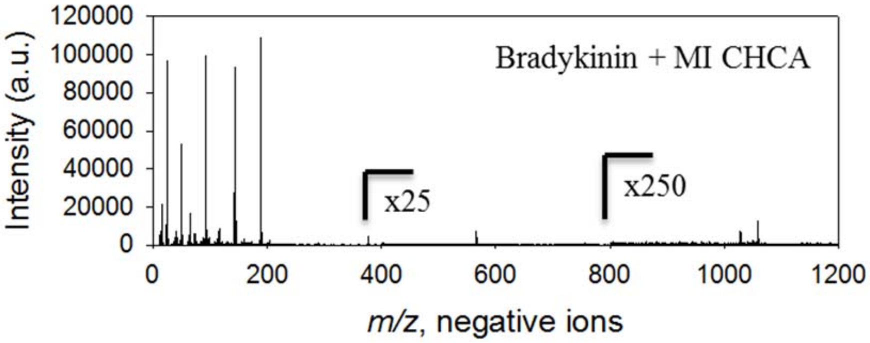
Bradykinin + MI CHCA
x25
x250
Intensity (a.u.)
0
20000
40000
60000
80000
100000
120000
0
200
400
600
800
1000
1200
m/z, negative ions

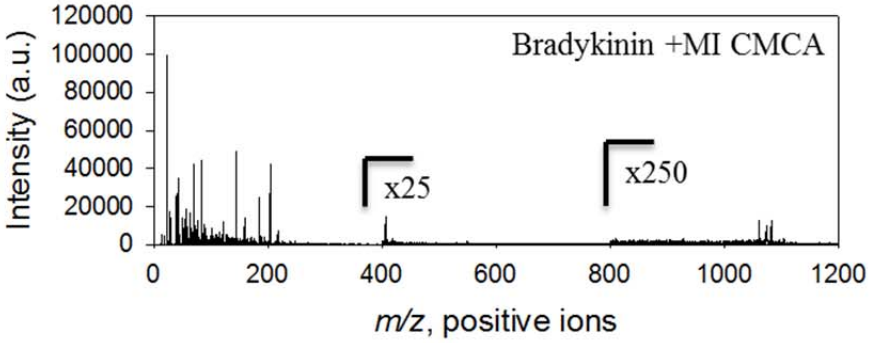
Bradykinin +MI CMCA
x25
x250
Intensity (a.u.)
120000
100000
80000
60000
40000
20000
0
0
200
400
600
800
1000
1200
m/z, positive ions

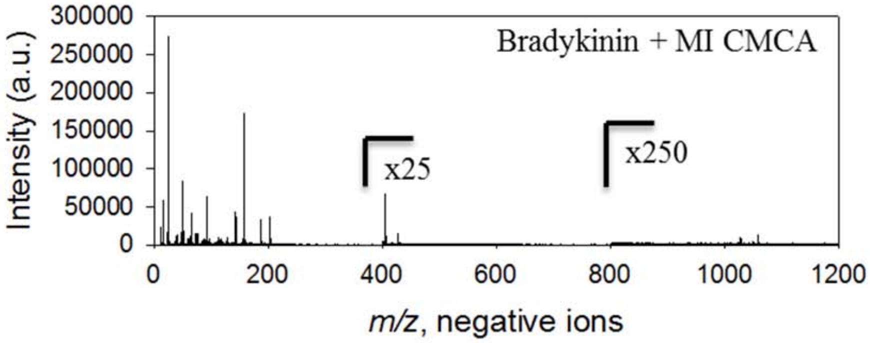
Bradykinin + MI CMCA
x25
x250
Intensity (a.u.)
300000
250000
200000
150000
100000
50000
0
0
200
400
600
800
1000
1200
m/z, negative ions

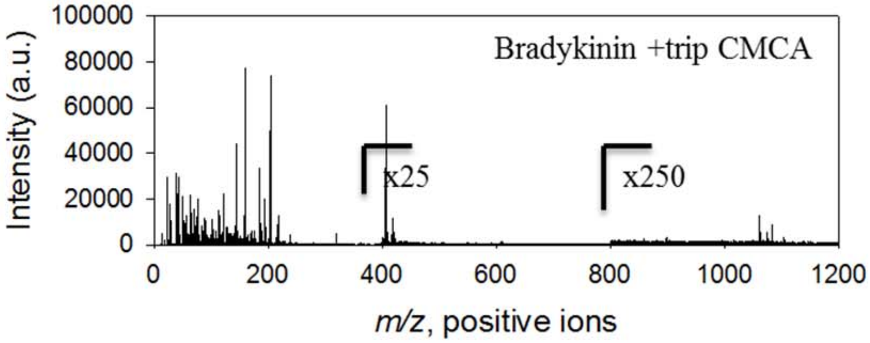
Bradykinin +trip CMCA
x25
x250
Intensity (a.u.)
100000
80000
60000
40000
20000
0
0
200
400
600
800
1000
1200
m/z, positive ions

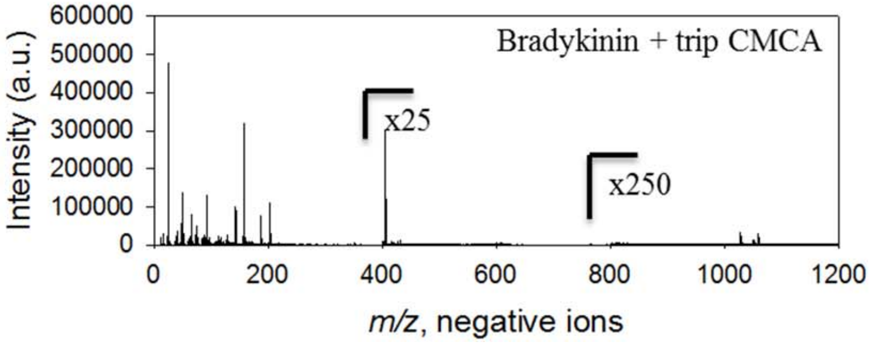
Bradykinin + trip CMCA
x25
x250
Intensity (a.u.)
600000
500000
400000
300000
200000
100000
0
0
200
400
600
800
1000
1200
m/z, negative ions

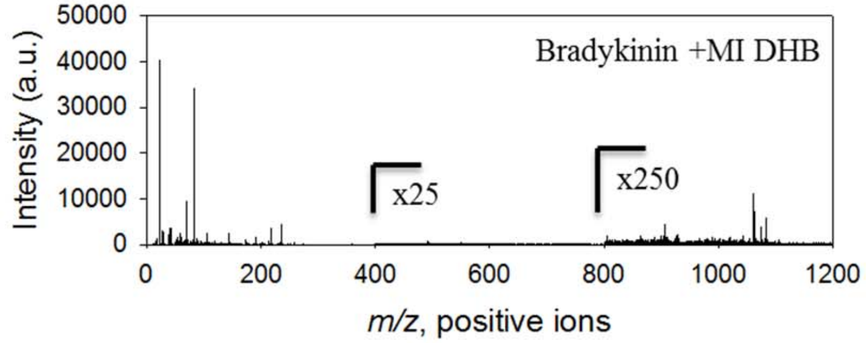
Bradykinin +MI DHB
x25
x250
Intensity (a.u.)
50000
40000
30000
20000
10000
0
0
200
400
600
800
1000
1200
m/z, positive ions

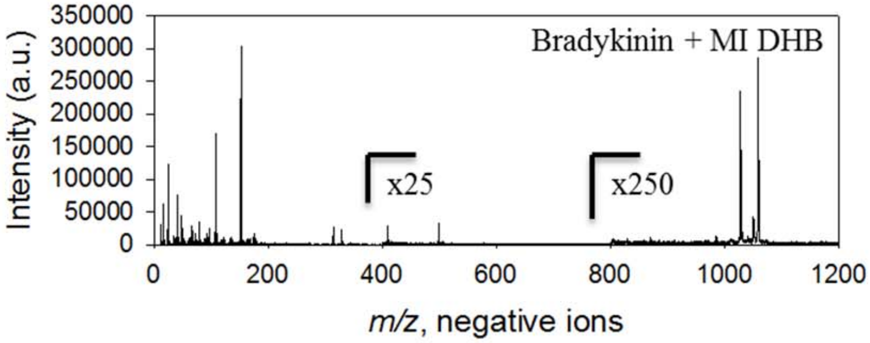
Bradykinin + MI DHB
x25
x250
Intensity (a.u.)
350000
300000
250000
200000
150000
100000
50000
0
0
200
400
600
800
1000
1200
m/z, negative ions

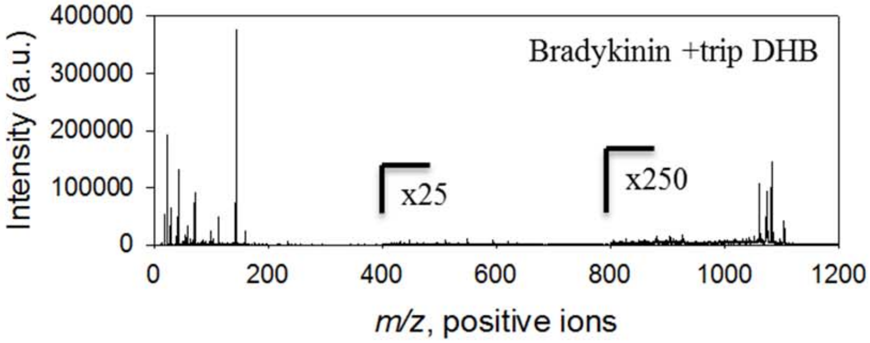
Bradykinin +trip DHB
x25
x250
Intensity (a.u.)
400000
300000
200000
100000
0
0
200
400
600
800
1000
1200
m/z, positive ions

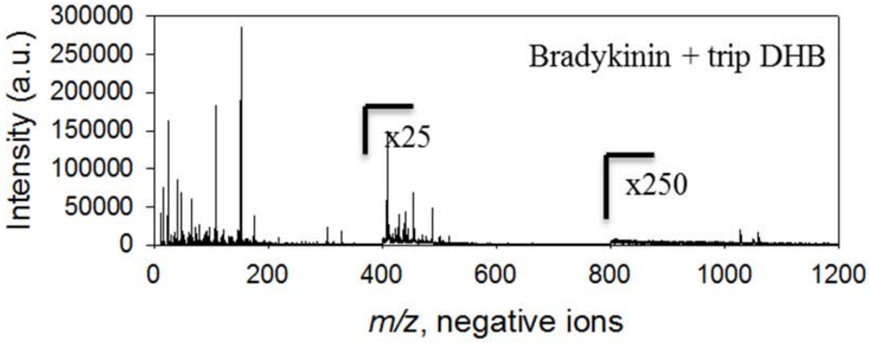
Bradykinin + trip DHB
x25
x250
Intensity (a.u.)
300000
250000
200000
150000
100000
50000
0
0
200
400
600
800
1000
1200
m/z, negative ions

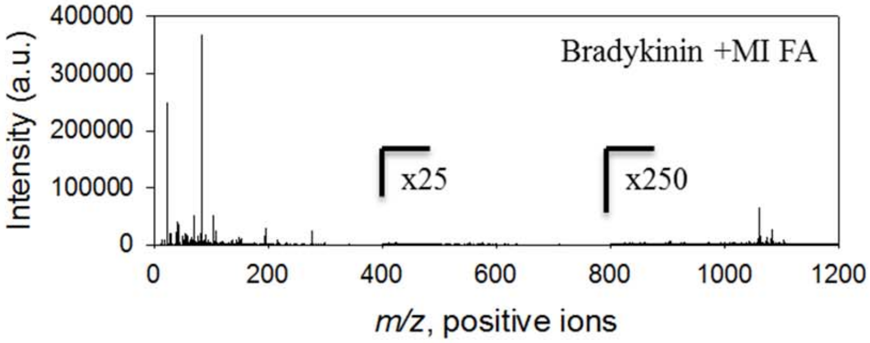
Bradykinin +MI FA
x25
x250
Intensity (a.u.)
400000
300000
200000
100000
0
0
200
400
600
800
1000
1200
m/z, positive ions

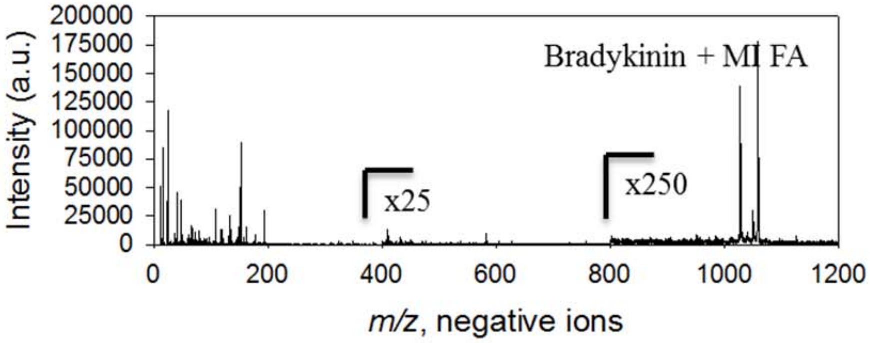
Bradykinin + MI FA
x25
x250
Intensity (a.u.)
200000
175000
150000
125000
100000
75000
50000
25000
0
0
200
400
600
800
1000
1200
m/z, negative ions

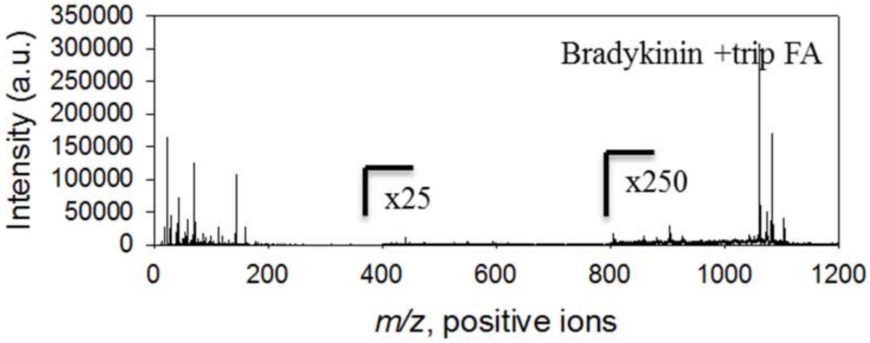
Bradykinin +trip FA
x25
x250
Intensity (a.u.)
350000
300000
250000
200000
150000
100000
50000
0
0
200
400
600
800
1000
1200
m/z, positive ions

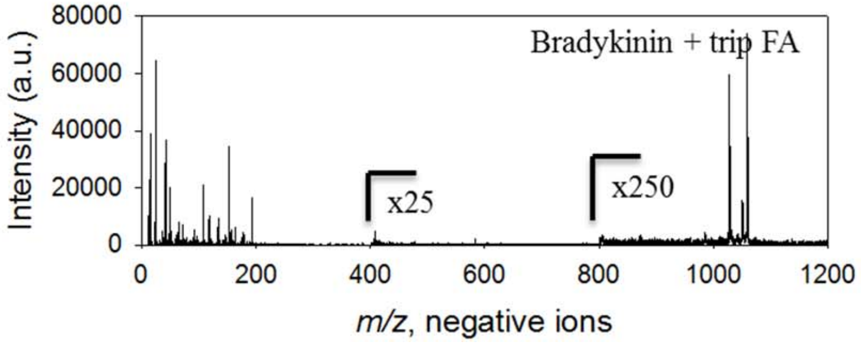
Bradykinin + trip FA
x25
x250
Intensity (a.u.)
80000
60000
40000
20000
0
0
200
400
600
800
1000
1200
m/z, negative ions

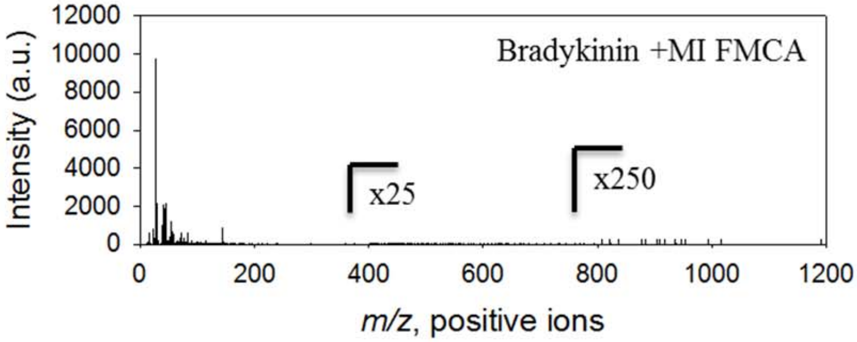
Bradykinin +MI FMCA
x25
x250
Intensity (a.u.)
12000
10000
8000
6000
4000
2000
0
0
200
400
600
800
1000
1200
m/z, positive ions

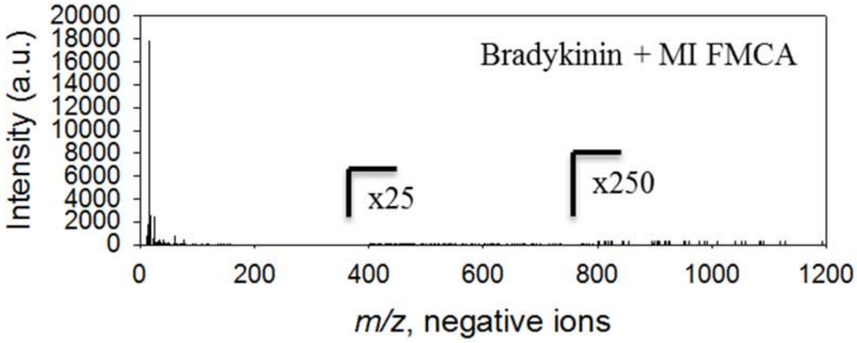
Bradykinin + MI FMCA
x25
x250
Intensity (a.u.)
20000
18000
16000
14000
12000
10000
8000
6000
4000
2000
0
0
200
400
600
800
1000
1200
m/z, negative ions

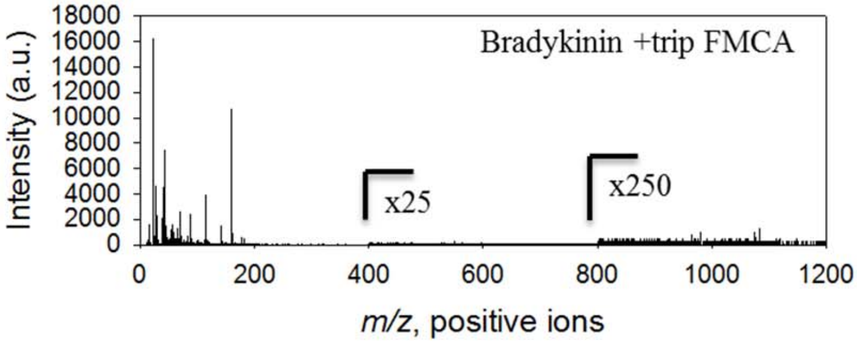
Bradykinin +trip FMCA
x25
x250
Intensity (a.u.)
18000
16000
14000
12000
10000
8000
6000
4000
2000
0
0
200
400
600
800
1000
1200
m/z, positive ions

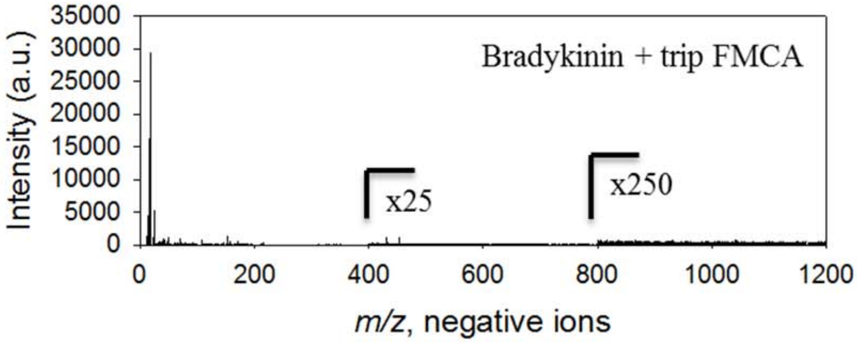
Bradykinin + trip FMCA
x25
x250
Intensity (a.u.)
35000
30000
25000
20000
15000
10000
5000
0
0
200
400
600
800
1000
1200
m/z, negative ions

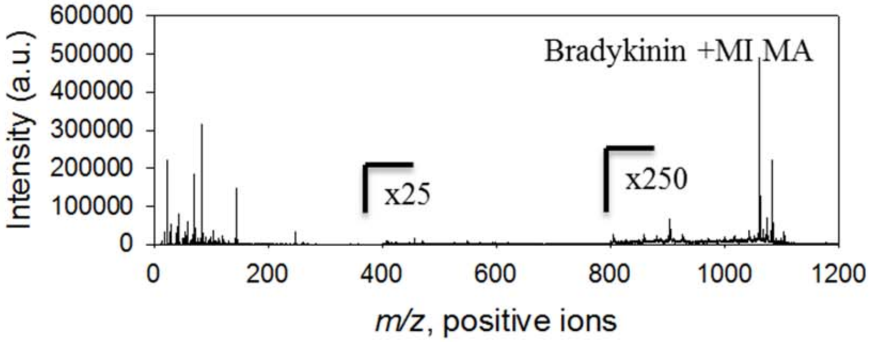
Bradykinin +MI MA
Intensity (a.u.)
600000
500000
400000
300000
200000
100000
0
x25
x250
0
200
400
600
800
1000
1200
m/z, positive ions

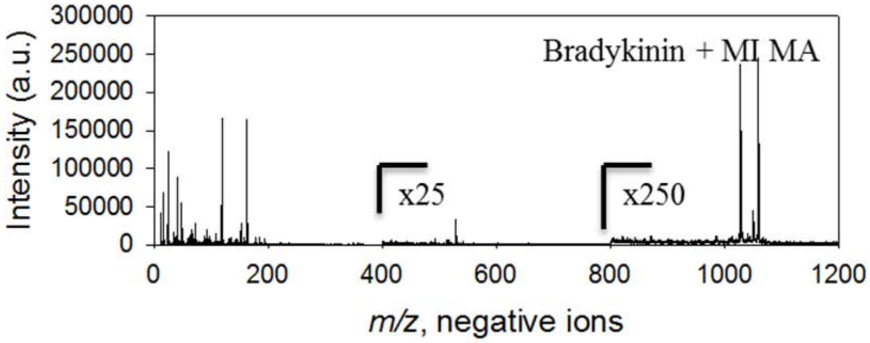
Bradykinin + MI MA
Intensity (a.u.)
300000
250000
200000
150000
100000
50000
0
x25
x250
0
200
400
600
800
1000
1200
m/z, negative ions

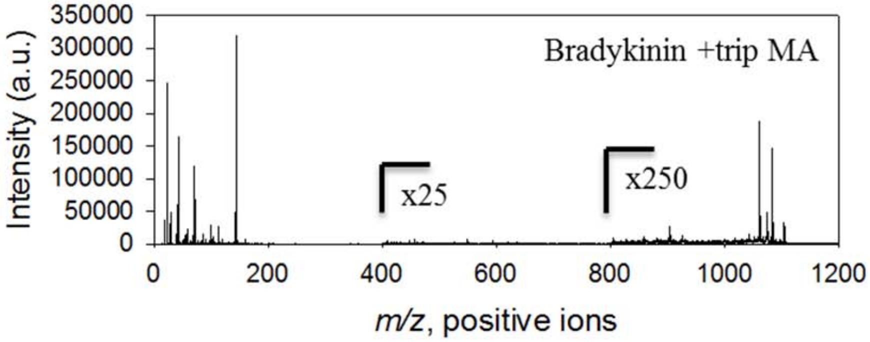
Bradykinin +trip MA
Intensity (a.u.)
350000
300000
250000
200000
150000
100000
50000
0
x25
x250
0
200
400
600
800
1000
1200
m/z, positive ions

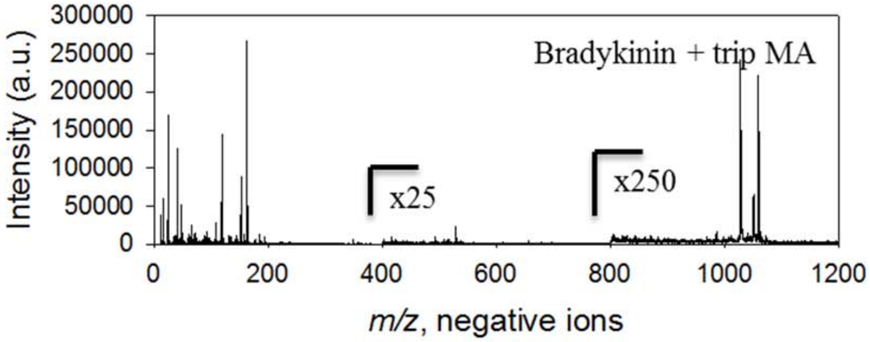
Bradykinin + trip MA
Intensity (a.u.)
300000
250000
200000
150000
100000
50000
0
x25
x250
0
200
400
600
800
1000
1200
m/z, negative ions

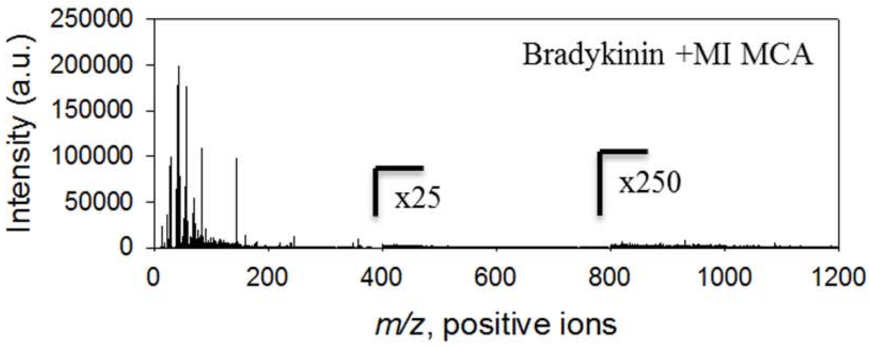
Bradykinin +MI MCA
x25
x250
Intensity (a.u.)
250000
200000
150000
100000
50000
0
0
200
400
600
800
1000
1200
m/z, positive ions

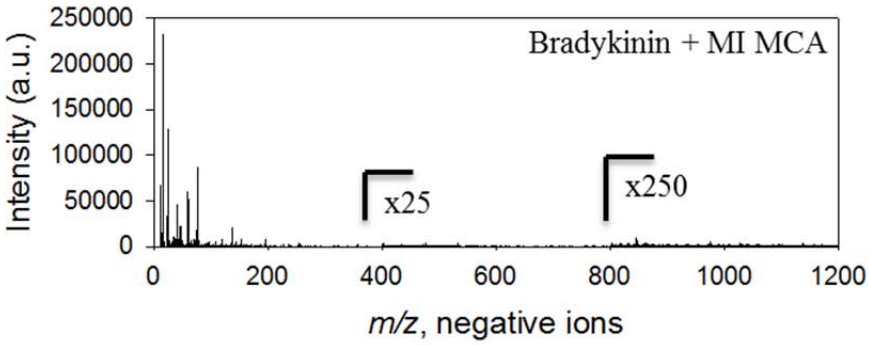
Bradykinin + MI MCA
x25
x250
Intensity (a.u.)
250000
200000
150000
100000
50000
0
0
200
400
600
800
1000
1200
m/z, negative ions

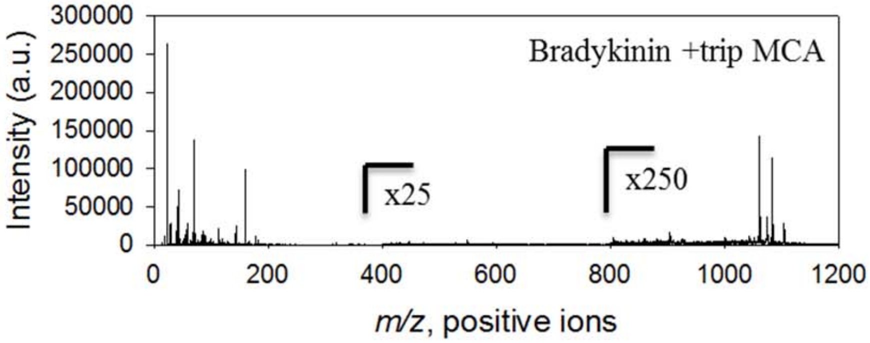
Bradykinin +trip MCA
x25
x250
Intensity (a.u.)
300000
250000
200000
150000
100000
50000
0
0
200
400
600
800
1000
1200
m/z, positive ions

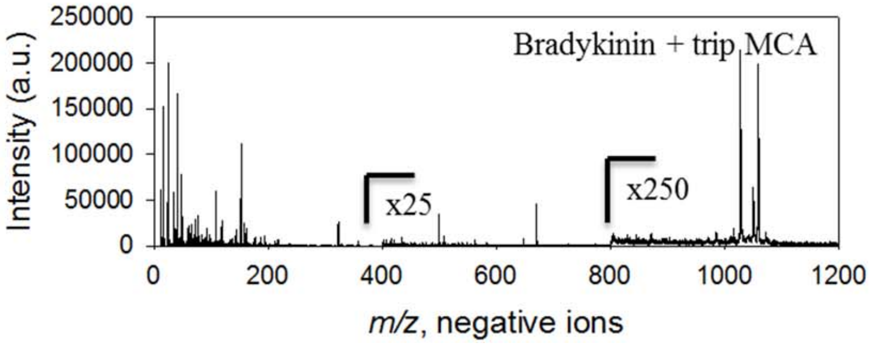
Bradykinin + trip MCA
x25
x250
Intensity (a.u.)
250000
200000
150000
100000
50000
0
0
200
400
600
800
1000
1200
m/z, negative ions

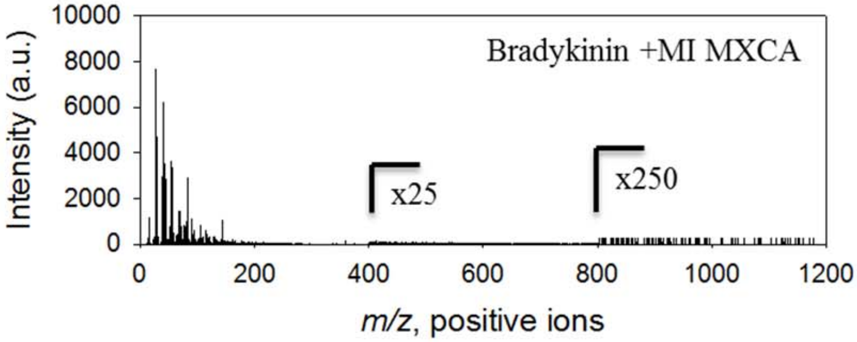
Bradykinin +MI MXCA
x25
x250
Intensity (a.u.)
10000
8000
6000
4000
2000
0
0
200
400
600
800
1000
1200
m/z, positive ions

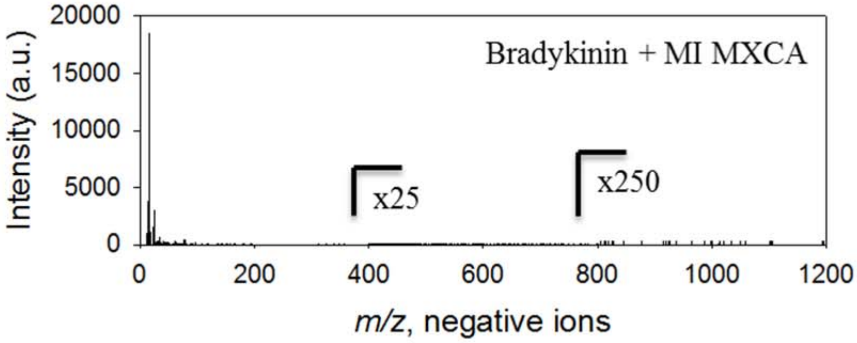
Bradykinin + MI MXCA
x25
x250
Intensity (a.u.)
20000
15000
10000
5000
0
0
200
400
600
800
1000
1200
m/z, negative ions

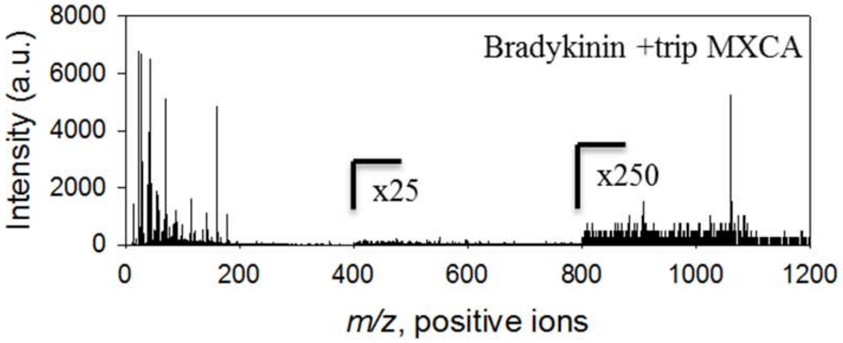
Bradykinin +trip MXCA
x25
x250
Intensity (a.u.)
8000
6000
4000
2000
0
0
200
400
600
800
1000
1200
m/z, positive ions

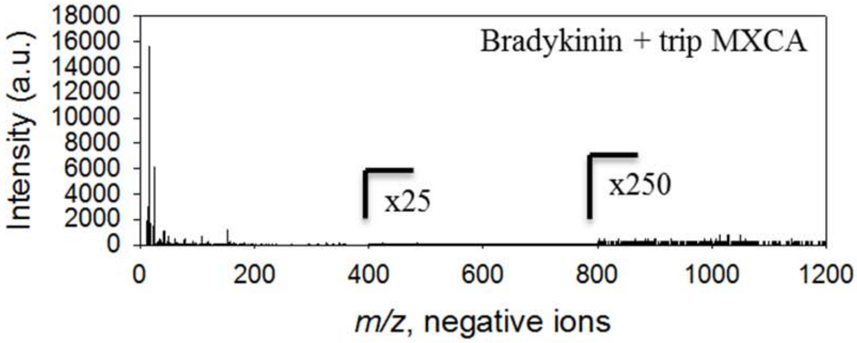
Bradykinin + trip MXCA
x25
x250
Intensity (a.u.)
18000
16000
14000
12000
10000
8000
6000
4000
2000
0
0
200
400
600
800
1000
1200
m/z, negative ions

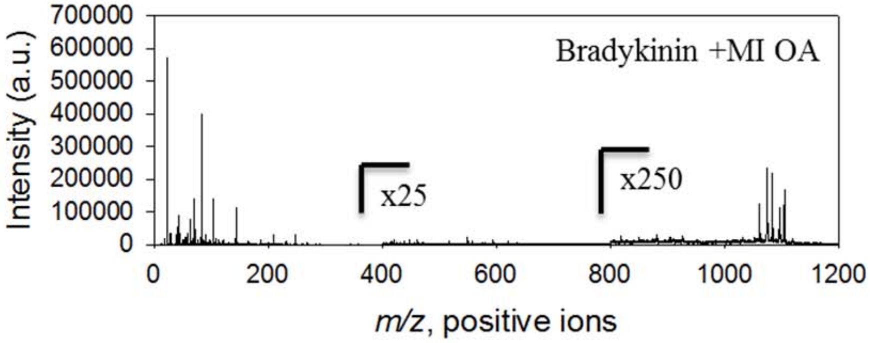
Bradykinin +MI OA
x25
x250
Intensity (a.u.)
700000
600000
500000
400000
300000
200000
100000
0
0
200
400
600
800
1000
1200
m/z, positive ions

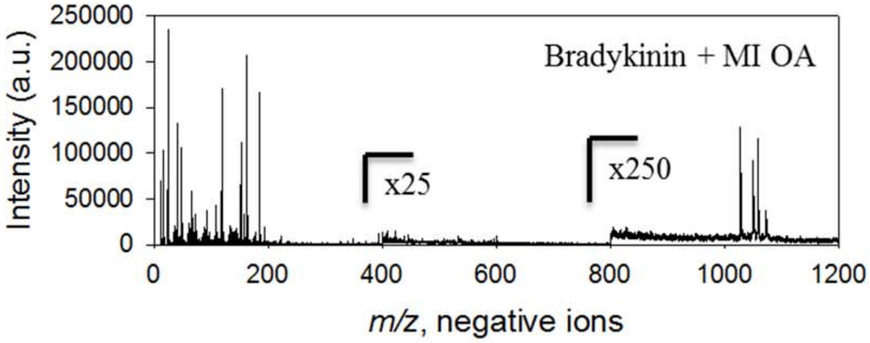
Bradykinin + MI OA
x25
x250
Intensity (a.u.)
250000
200000
150000
100000
50000
0
0
200
400
600
800
1000
1200
m/z, negative ions

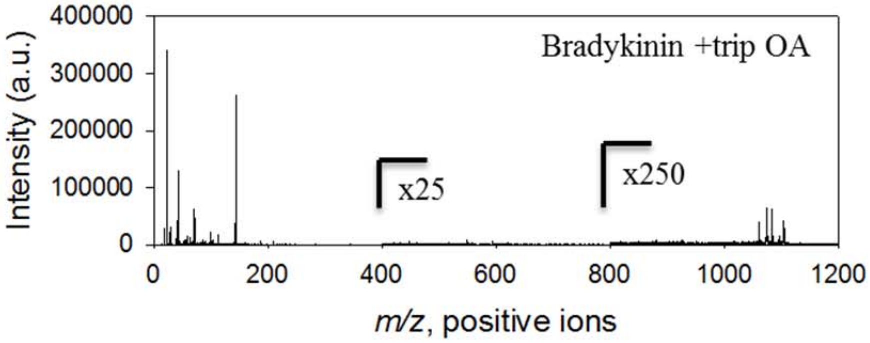
Bradykinin +trip OA
x25
x250
Intensity (a.u.)
400000
300000
200000
100000
0
0
200
400
600
800
1000
1200
m/z, positive ions

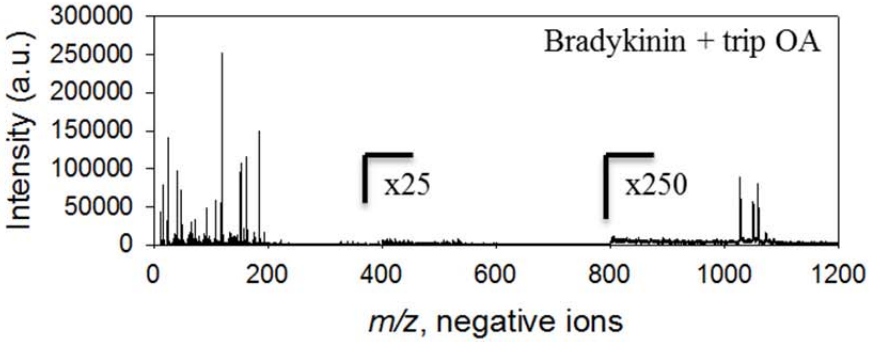
Bradykinin + trip OA
x25
x250
Intensity (a.u.)
300000
250000
200000
150000
100000
50000
0
0
200
400
600
800
1000
1200
m/z, negative ions

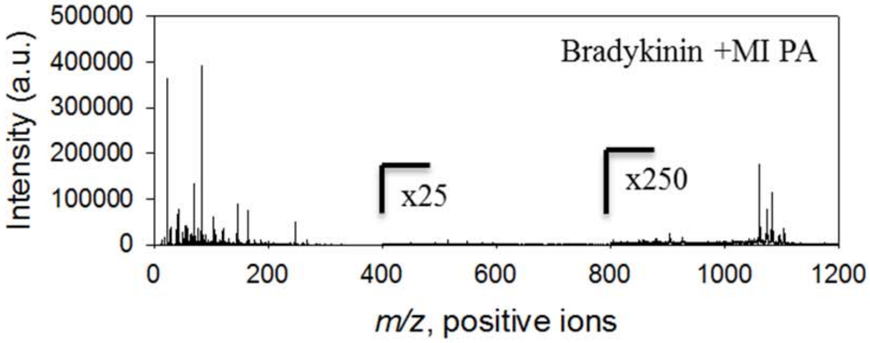
Bradykinin +MI PA
x25
x250
Intensity (a.u.)
500000
400000
300000
200000
100000
0
0
200
400
600
800
1000
1200
m/z, positive ions

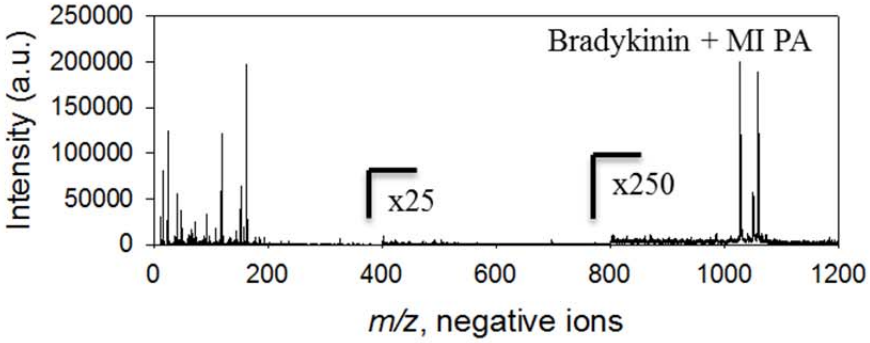
Bradykinin + MI PA
x25
x250
Intensity (a.u.)
250000
200000
150000
100000
50000
0
0
200
400
600
800
1000
1200
m/z, negative ions

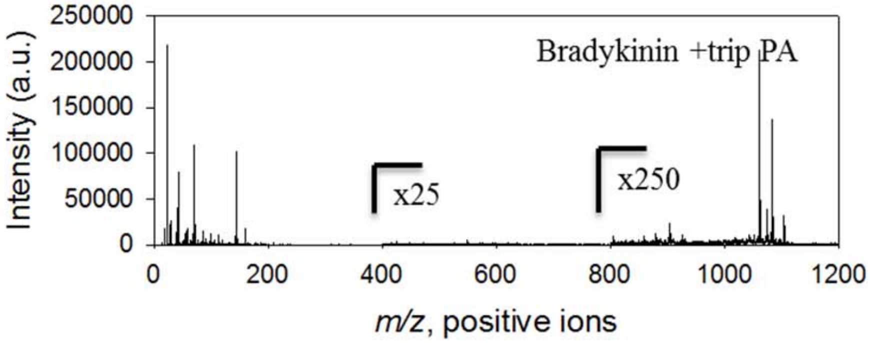
Bradykinin +trip PA
x25
x250
Intensity (a.u.)
250000
200000
150000
100000
50000
0
0
200
400
600
800
1000
1200
m/z, positive ions

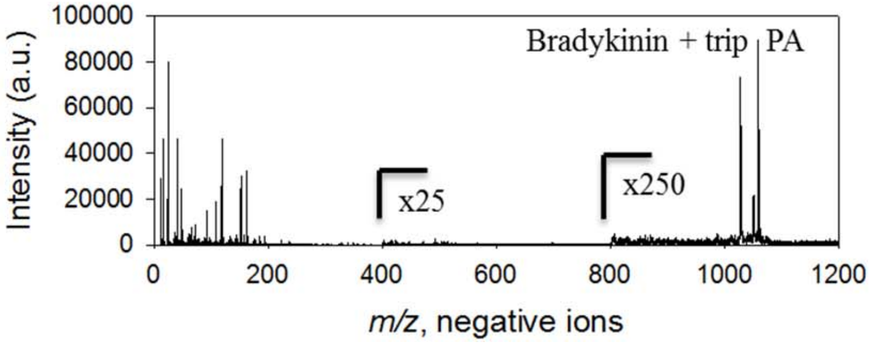
Bradykinin + trip PA
x25
x250
Intensity (a.u.)
100000
80000
60000
40000
20000
0
0
200
400
600
800
1000
1200
m/z, negative ions

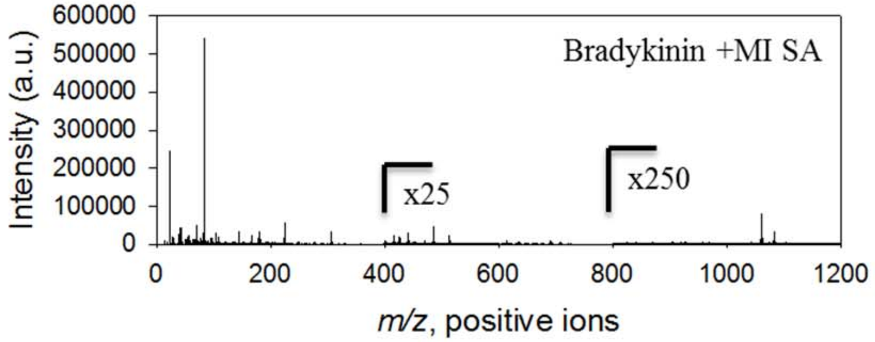
Bradykinin +MI SA
x25
x250
Intensity (a.u.)
600000
500000
400000
300000
200000
100000
0
0
200
400
600
800
1000
1200
m/z, positive ions

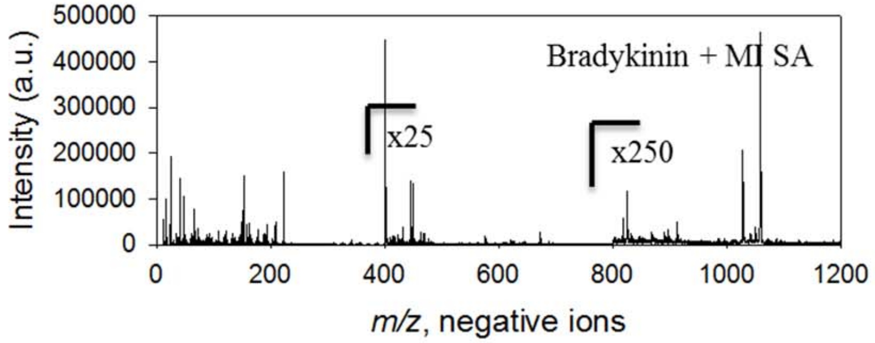
Bradykinin + MI SA
x25
x250
Intensity (a.u.)
500000
400000
300000
200000
100000
0
0
200
400
600
800
1000
1200
m/z, negative ions

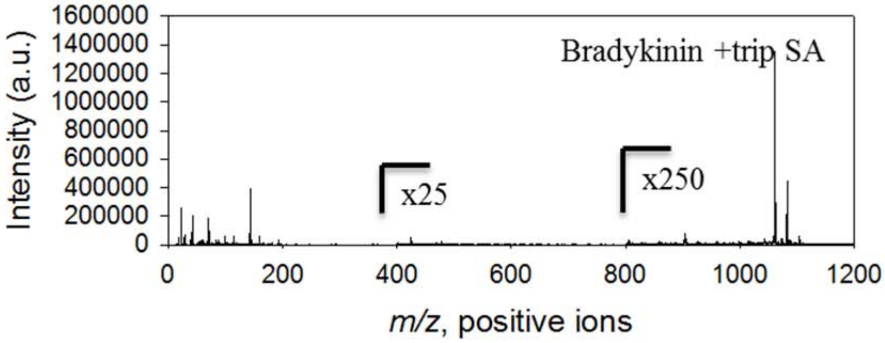
Bradykinin +trip SA
x25
x250
Intensity (a.u.)
1600000
1400000
1200000
1000000
800000
600000
400000
200000
0
0
200
400
600
800
1000
1200
m/z, positive ions

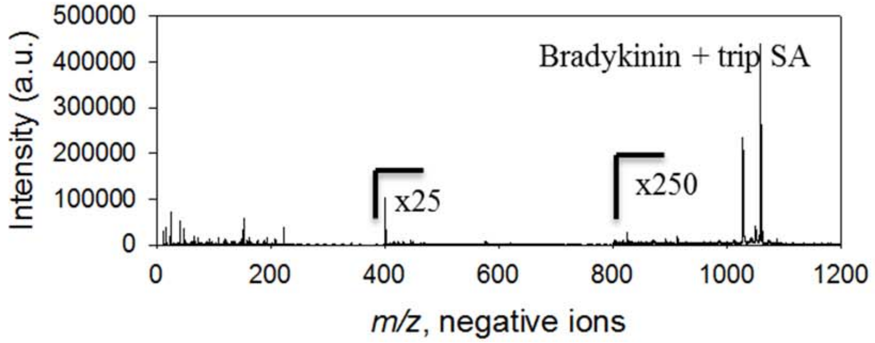
Bradykinin + trip SA
x25
x250
Intensity (a.u.)
500000
400000
300000
200000
100000
0
0
200
400
600
800
1000
1200
m/z, negative ions

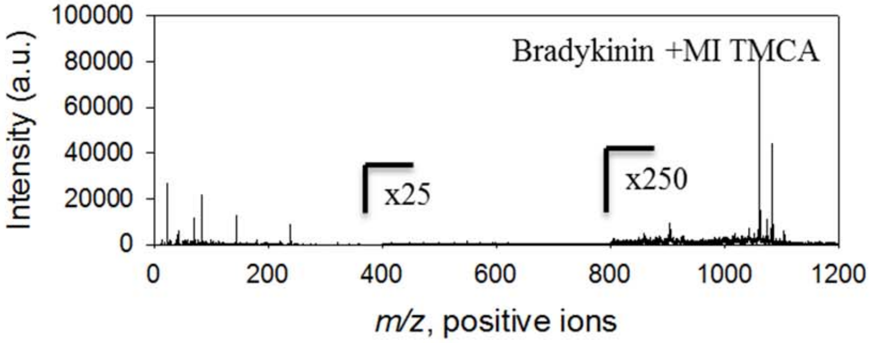
Bradykinin +MI TMCA
Intensity (a.u.)
100000
80000
60000
40000
20000
0
x25
x250
0
200
400
600
800
1000
1200
m/z, positive ions

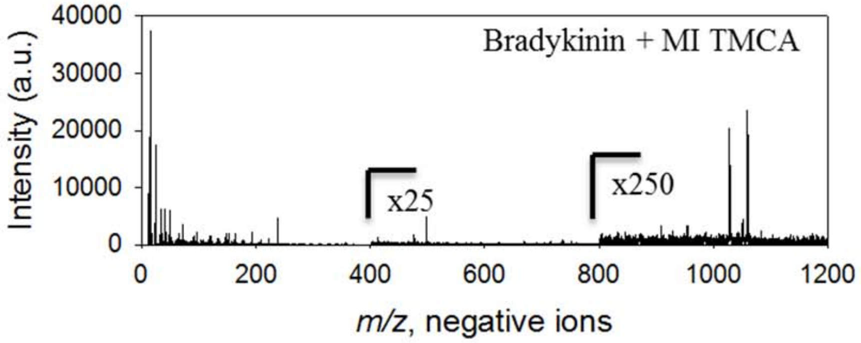
Bradykinin + MI TMCA
Intensity (a.u.)
40000
30000
20000
10000
0
x25
x250
0
200
400
600
800
1000
1200
m/z, negative ions

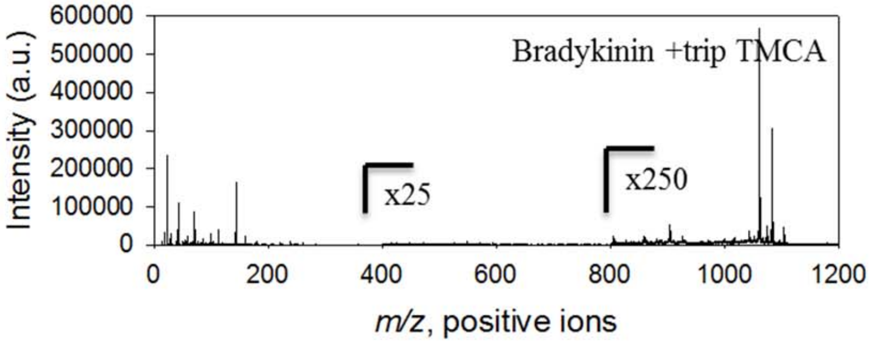
Bradykinin +trip TMCA
Intensity (a.u.)
600000
500000
400000
300000
200000
100000
0
x25
x250
0
200
400
600
800
1000
1200
m/z, positive ions

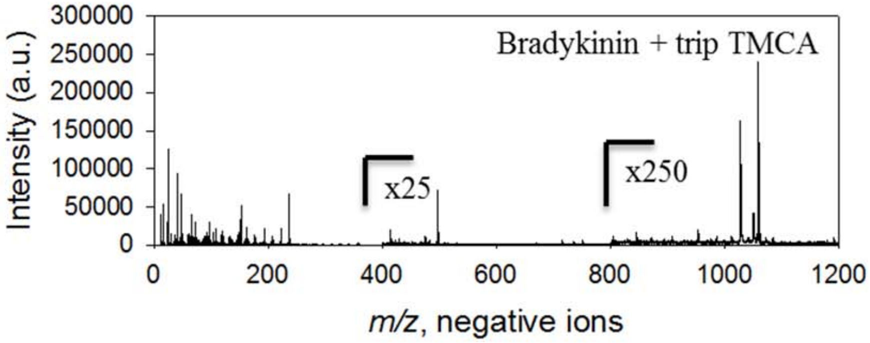
Bradykinin + trip TMCA
Intensity (a.u.)
300000
250000
200000
150000
100000
50000
0
x25
x250
0
200
400
600
800
1000
1200
m/z, negative ions

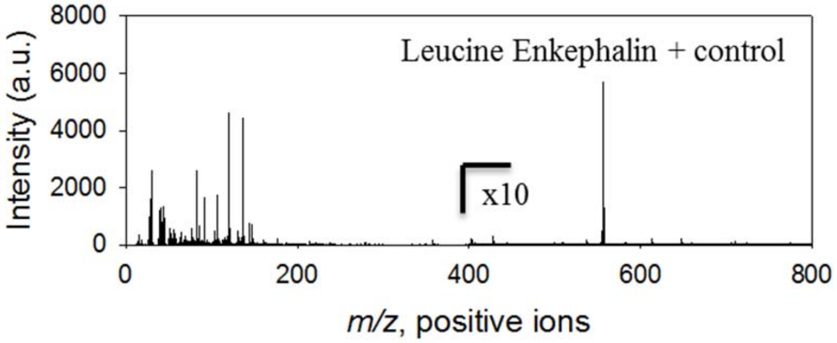
Leucine Enkephalin + control
x10
Intensity (a.u.)
8000
6000
4000
2000
0
0
200
400
600
800
m/z, positive ions

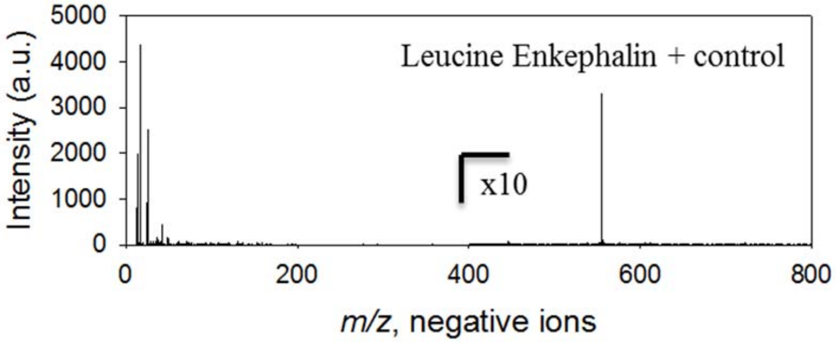
Leucine Enkephalin + control
x10
Intensity (a.u.)
5000
4000
3000
2000
1000
0
0
200
400
600
800
m/z, negative ions

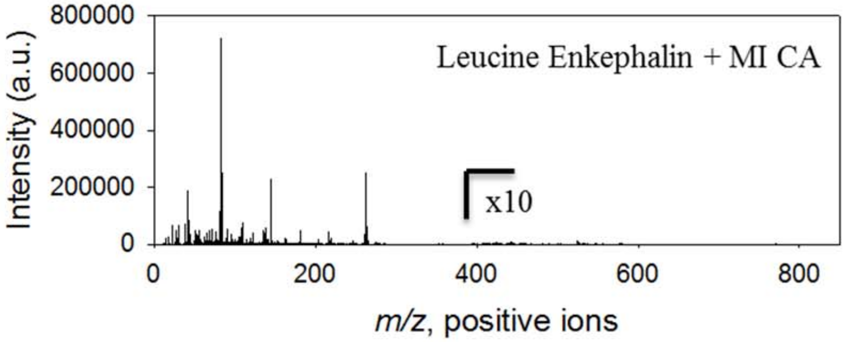
800000
600000
400000
200000
0
Intensity (a.u.)
Leucine Enkephalin + MI CA
x10
0
200
400
600
800
m/z, positive ions

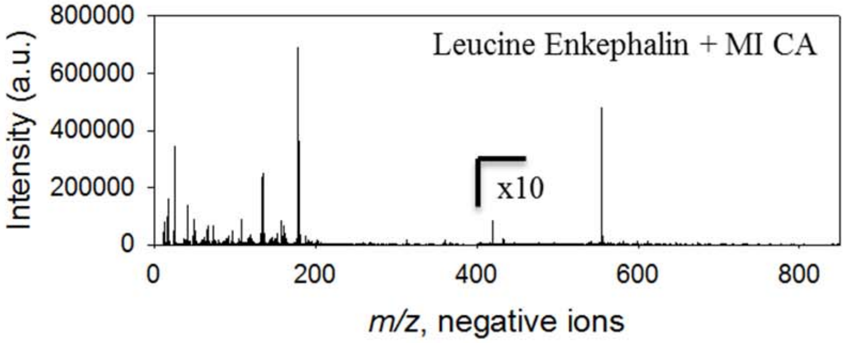
800000
600000
400000
200000
0
Intensity (a.u.)
Leucine Enkephalin + MI CA
x10
0
200
400
600
800
m/z, negative ions

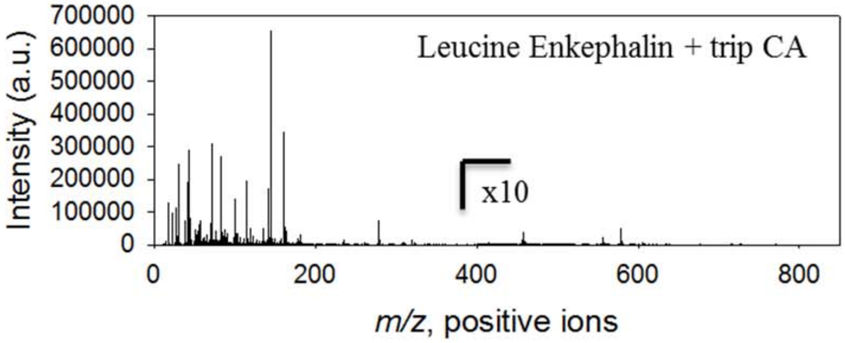
700000
600000
500000
400000
300000
200000
100000
0
Intensity (a.u.)
Leucine Enkephalin + trip CA
x10
0
200
400
600
800
m/z, positive ions

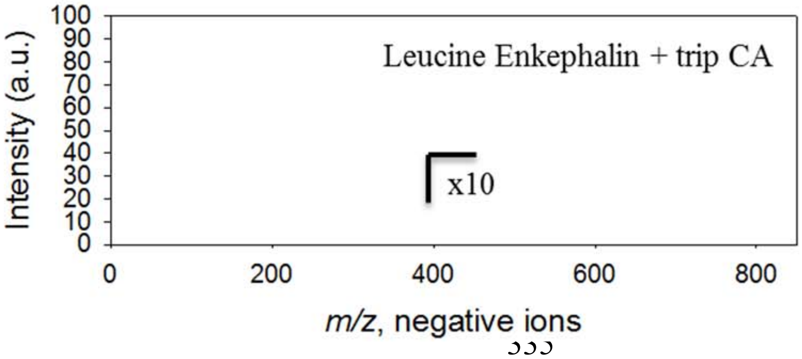
100
90
80
70
60
50
40
30
20
10
0
Intensity (a.u.)
Leucine Enkephalin + trip CA
x10
0
200
400
600
800
m/z, negative ions

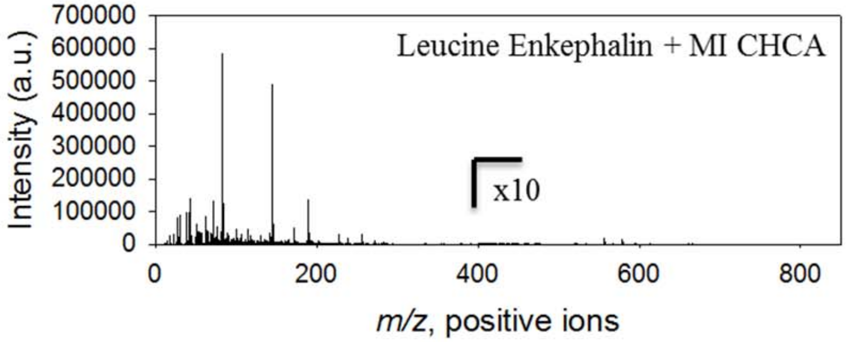
Leucine Enkephalin + MI CHCA
Intensity (a.u.)
700000
600000
500000
400000
300000
200000
100000
0
x10
0
200
400
600
800
m/z, positive ions

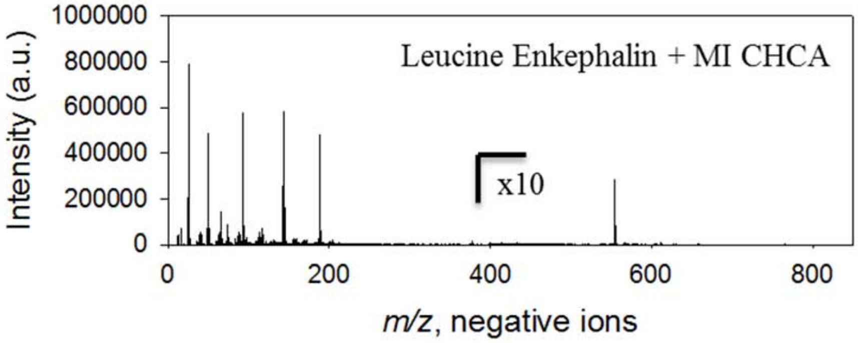
Leucine Enkephalin + MI CHCA
Intensity (a.u.)
1000000
800000
600000
400000
200000
0
x10
0
200
400
600
800
m/z, negative ions

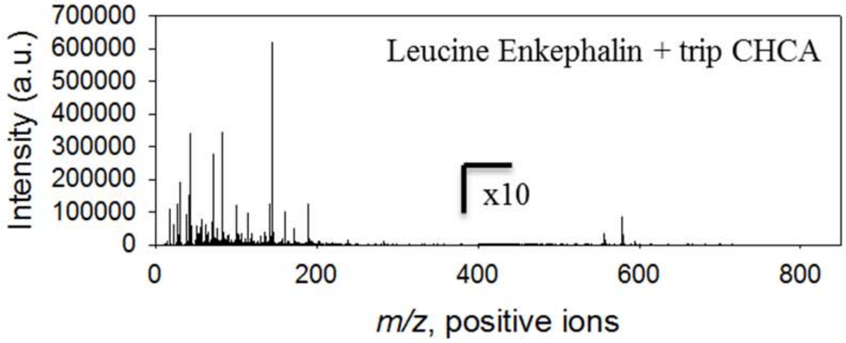
Leucine Enkephalin + trip CHCA
Intensity (a.u.)
700000
600000
500000
400000
300000
200000
100000
0
x10
0
200
400
600
800
m/z, positive ions

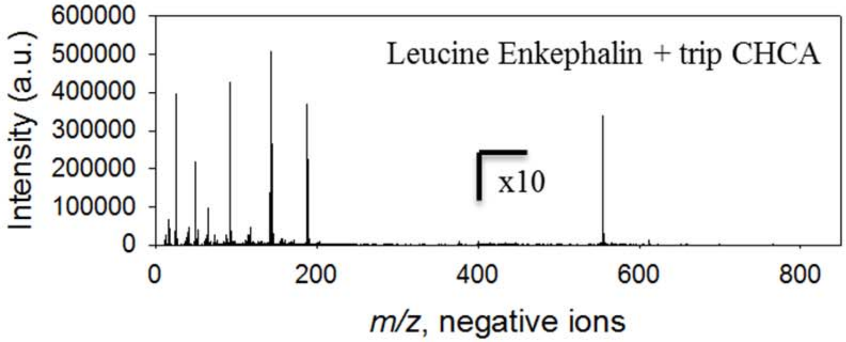
Leucine Enkephalin + trip CHCA
Intensity (a.u.)
600000
500000
400000
300000
200000
100000
0
x10
0
200
400
600
800
m/z, negative ions

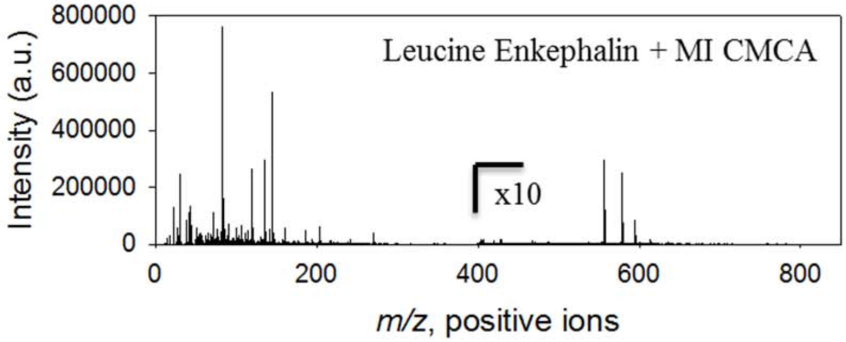
Leucine Enkephalin + MI CMCA
x10
Intensity (a.u.)
800000
600000
400000
200000
0
0
200
400
600
800
m/z, positive ions

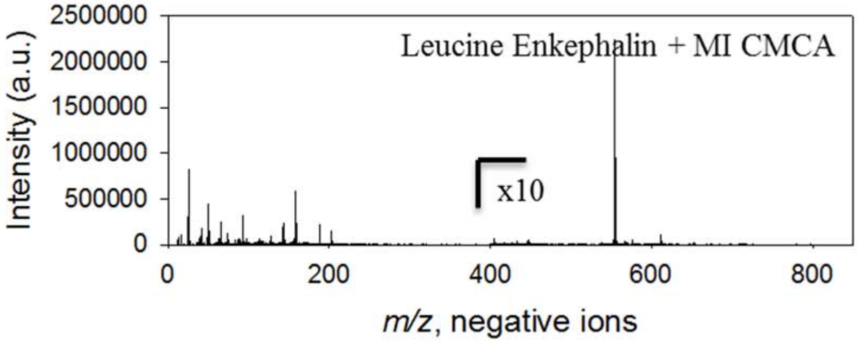
Leucine Enkephalin + MI CMCA
x10
Intensity (a.u.)
2500000
2000000
1500000
1000000
500000
0
0
200
400
600
800
m/z, negative ions

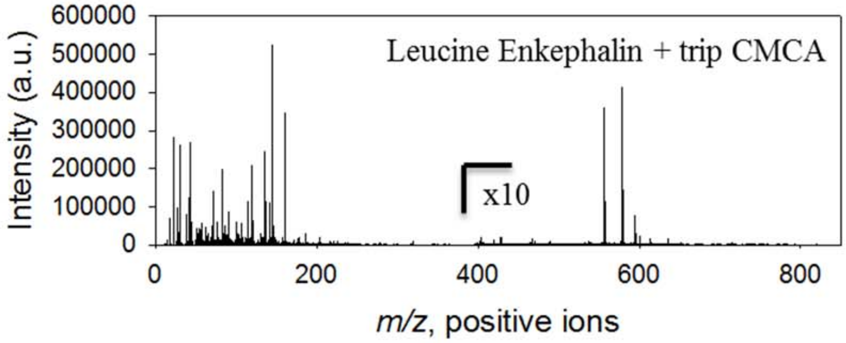
Leucine Enkephalin + trip CMCA
x10
Intensity (a.u.)
600000
500000
400000
300000
200000
100000
0
0
200
400
600
800
m/z, positive ions

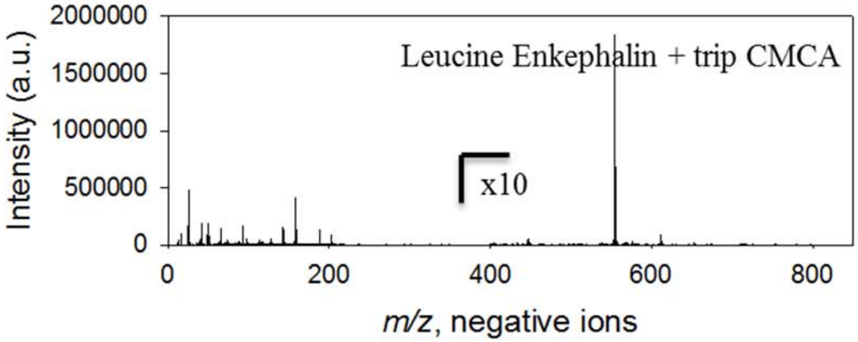
Leucine Enkephalin + trip CMCA
x10
Intensity (a.u.)
2000000
1500000
1000000
500000
0
0
200
400
600
800
m/z, negative ions

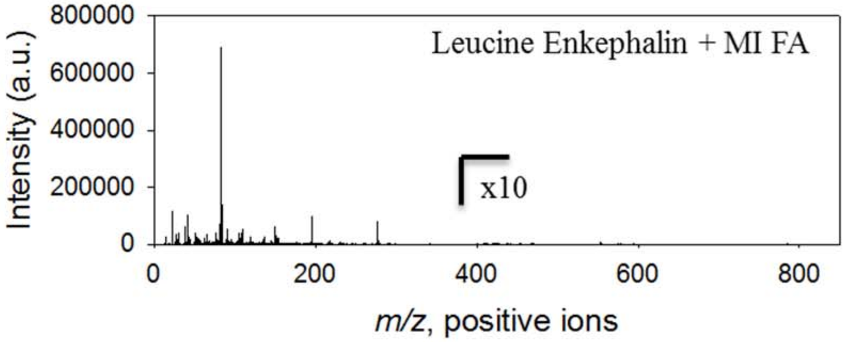
800000
600000
400000
200000
0
Intensity (a.u.)
Leucine Enkephalin + MI FA
x10
0
200
400
600
800
m/z, positive ions

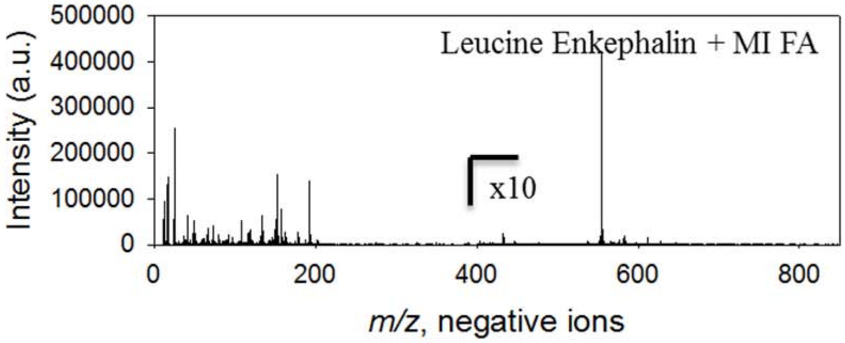
500000
400000
300000
200000
100000
0
Intensity (a.u.)
Leucine Enkephalin + MI FA
x10
0
200
400
600
800
m/z, negative ions

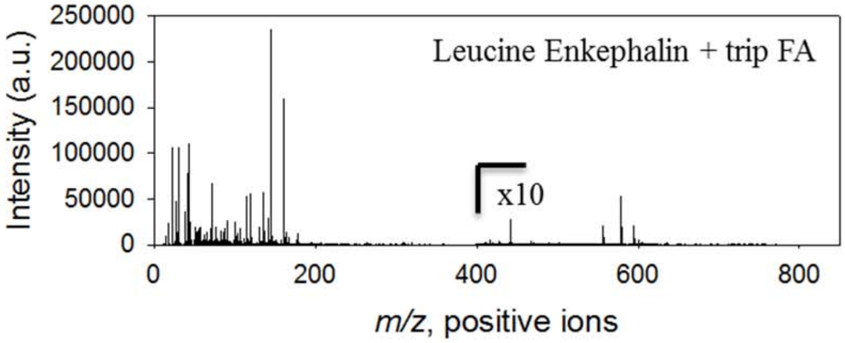
250000
200000
150000
100000
50000
0
Intensity (a.u.)
Leucine Enkephalin + trip FA
x10
0
200
400
600
800
m/z, positive ions

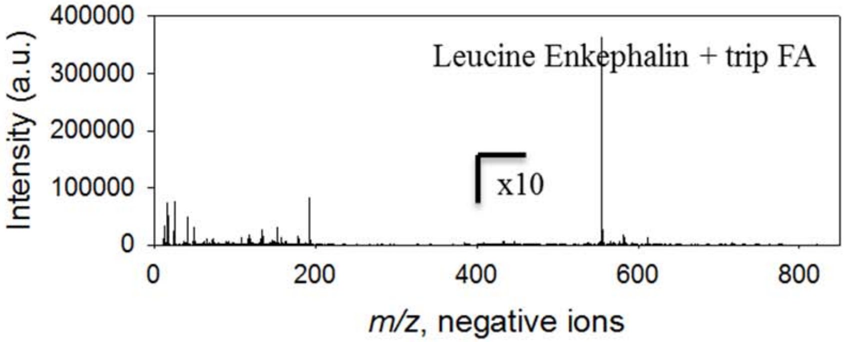
400000
300000
200000
100000
0
Intensity (a.u.)
Leucine Enkephalin + trip FA
x10
0
200
400
600
800
m/z, negative ions

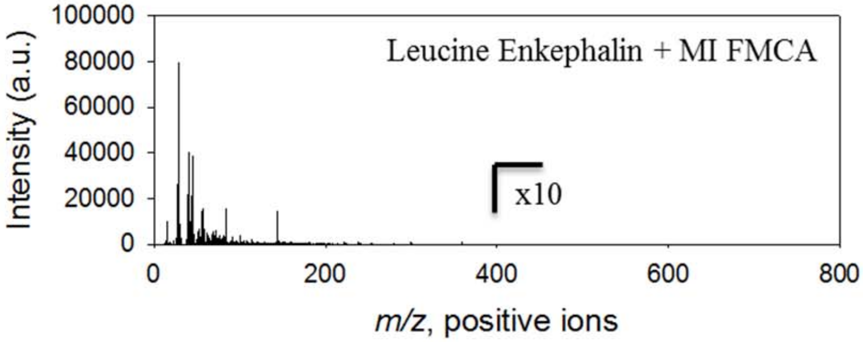
Leucine Enkephalin + MI FMCA
x10
Intensity (a.u.)
100000
80000
60000
40000
20000
0
0
200
400
600
800
m/z, positive ions

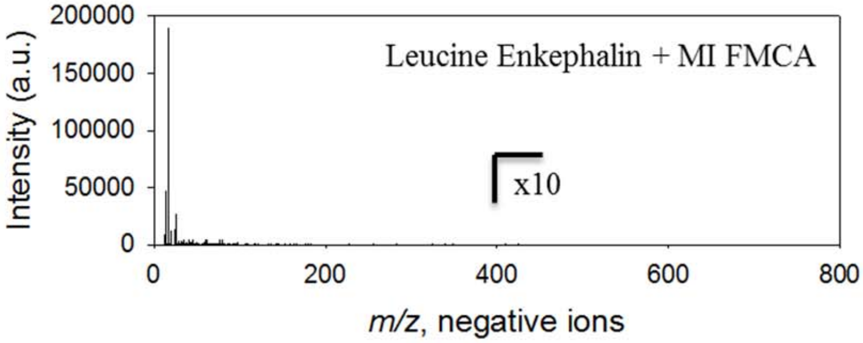
Leucine Enkephalin + MI FMCA
x10
Intensity (a.u.)
200000
150000
100000
50000
0
0
200
400
600
800
m/z, negative ions

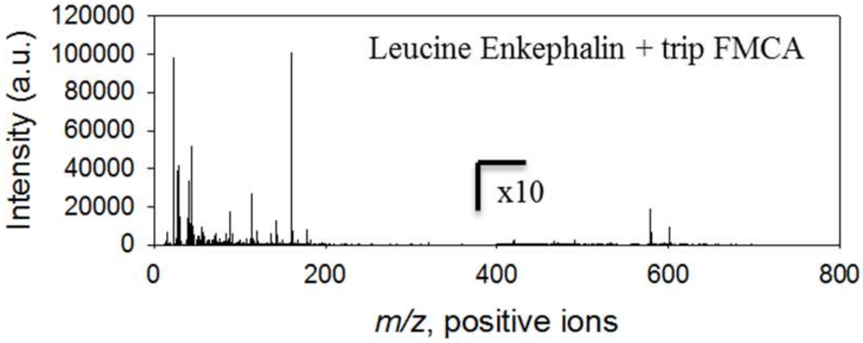
Leucine Enkephalin + trip FMCA
x10
Intensity (a.u.)
120000
100000
80000
60000
40000
20000
0
0
200
400
600
800
m/z, positive ions

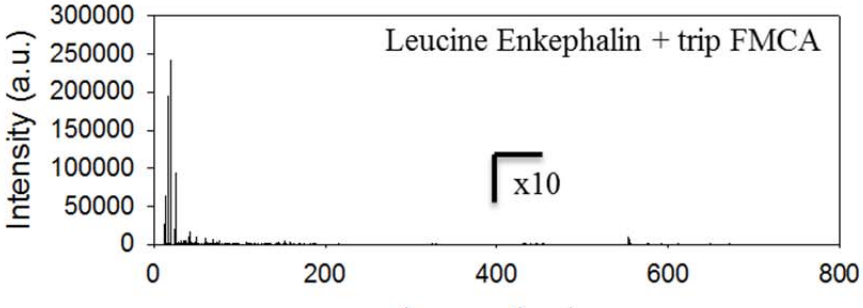
Leucine Enkephalin + trip FMCA
x10
Intensity (a.u.)
300000
250000
200000
150000
100000
50000
0
0
200
400
600
800
m/z, negative ions

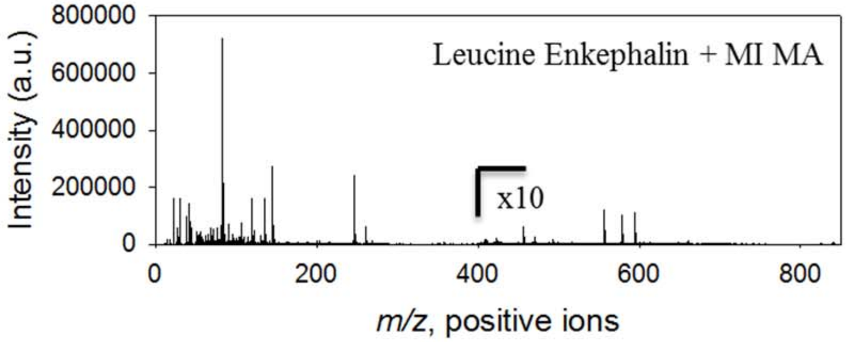
Leucine Enkephalin + MI MA
x10
Intensity (a.u.)
800000
600000
400000
200000
0
0
200
400
600
800
m/z, positive ions

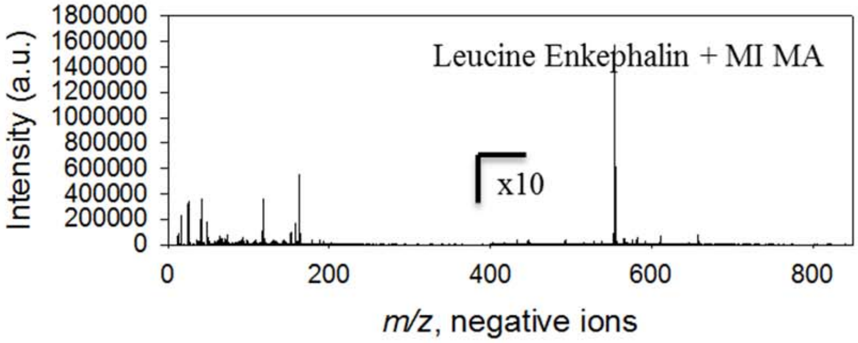
Leucine Enkephalin + MI MA
x10
Intensity (a.u.)
1800000
1600000
1400000
1200000
1000000
800000
600000
400000
200000
0
0
200
400
600
800
m/z, negative ions

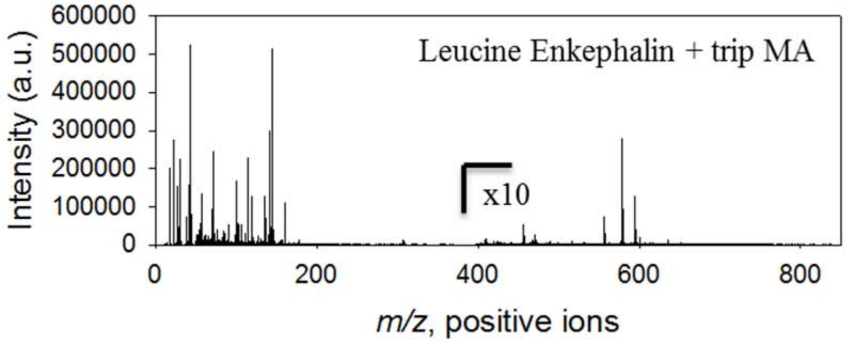
Leucine Enkephalin + trip MA
x10
Intensity (a.u.)
600000
500000
400000
300000
200000
100000
0
0
200
400
600
800
m/z, positive ions

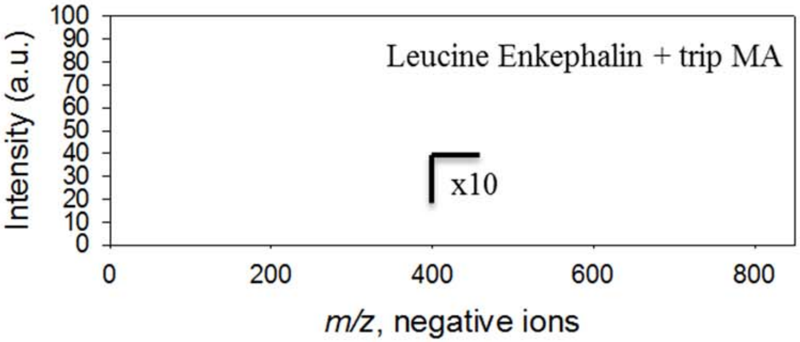
Leucine Enkephalin + trip MA
x10
Intensity (a.u.)
100
90
80
70
60
50
40
30
20
10
0
0
200
400
600
800
m/z, negative ions

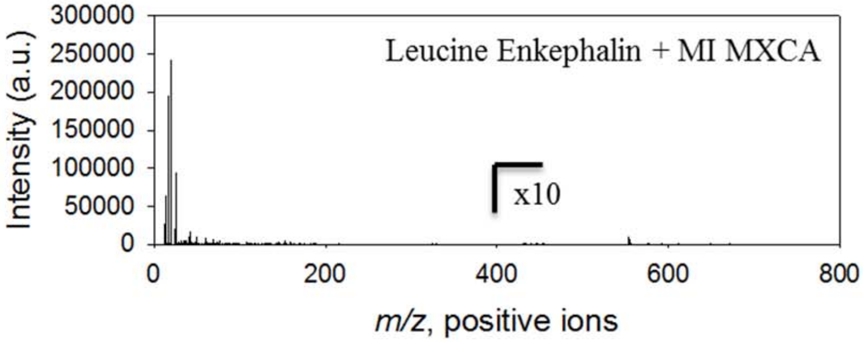
Leucine Enkephalin + MI MXCA
x10
Intensity (a.u.)
300000
250000
200000
150000
100000
50000
0
0
200
400
600
800
m/z, positive ions

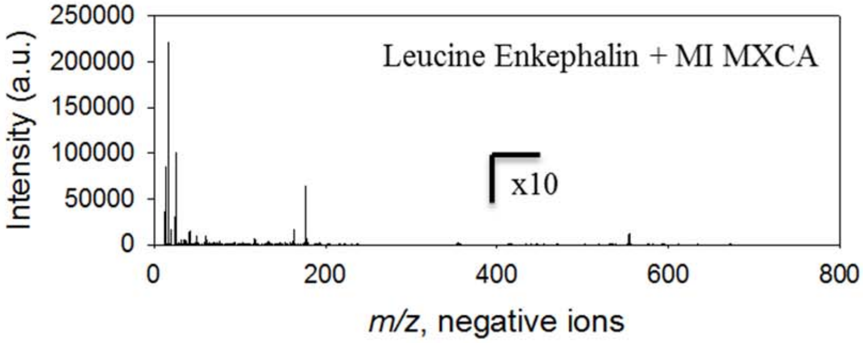
Leucine Enkephalin + MI MXCA
x10
Intensity (a.u.)
250000
200000
150000
100000
50000
0
0
200
400
600
800
m/z, negative ions

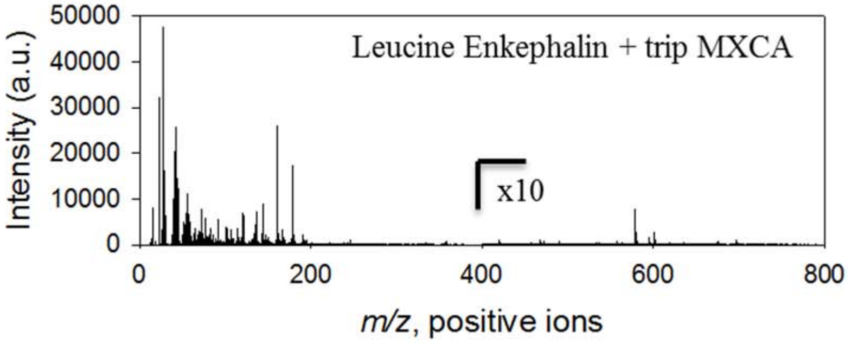
Leucine Enkephalin + trip MXCA
x10
Intensity (a.u.)
50000
40000
30000
20000
10000
0
0
200
400
600
800
m/z, positive ions

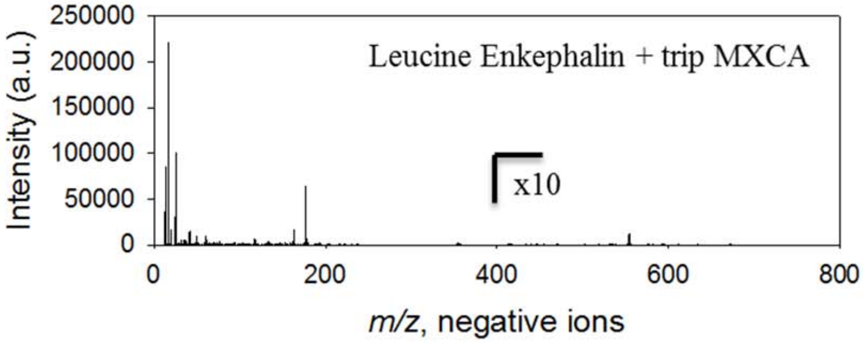
Leucine Enkephalin + trip MXCA
x10
Intensity (a.u.)
250000
200000
150000
100000
50000
0
0
200
400
600
800
m/z, negative ions

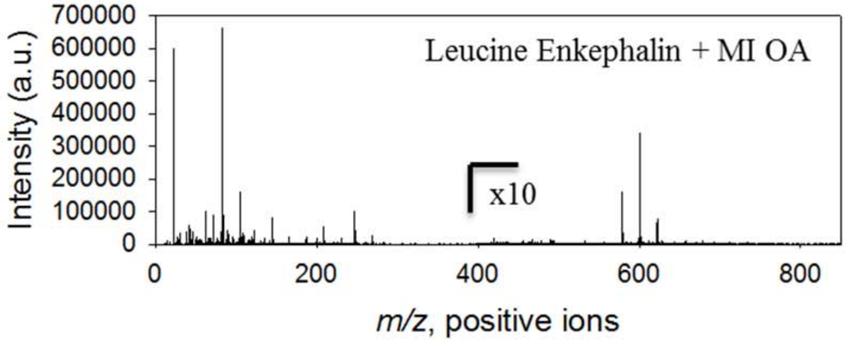
Leucine Enkephalin + MI OA
x10
Intensity (a.u.)
700000
600000
500000
400000
300000
200000
100000
0
0
200
400
600
800
m/z, positive ions

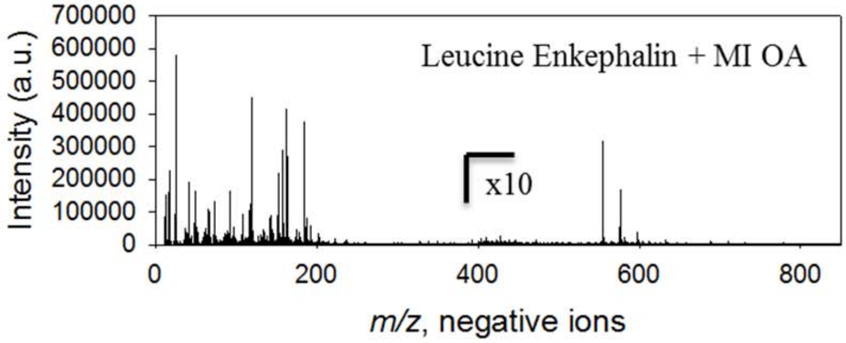
Leucine Enkephalin + MI OA
x10
Intensity (a.u.)
700000
600000
500000
400000
300000
200000
100000
0
0
200
400
600
800
m/z, negative ions

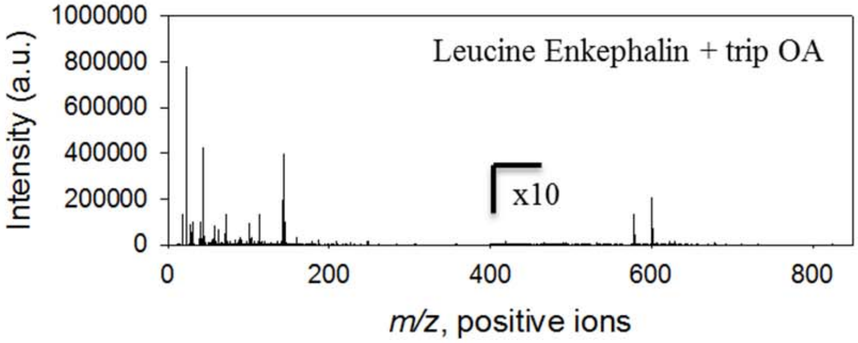
Leucine Enkephalin + trip OA
x10
Intensity (a.u.)
1000000
800000
600000
400000
200000
0
0
200
400
600
800
m/z, positive ions

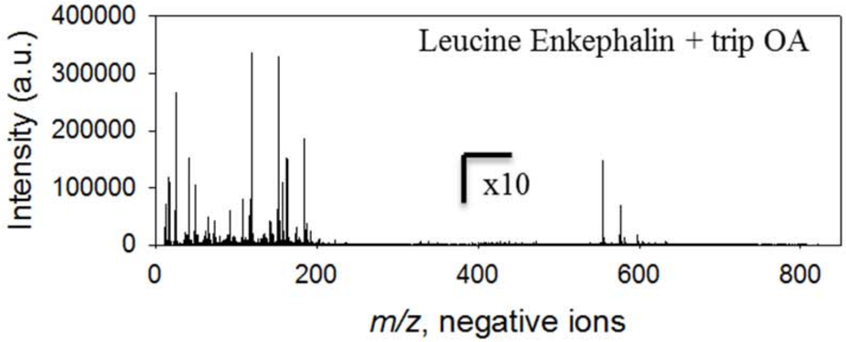
Leucine Enkephalin + trip OA
x10
Intensity (a.u.)
400000
300000
200000
100000
0
0
200
400
600
800
m/z, negative ions

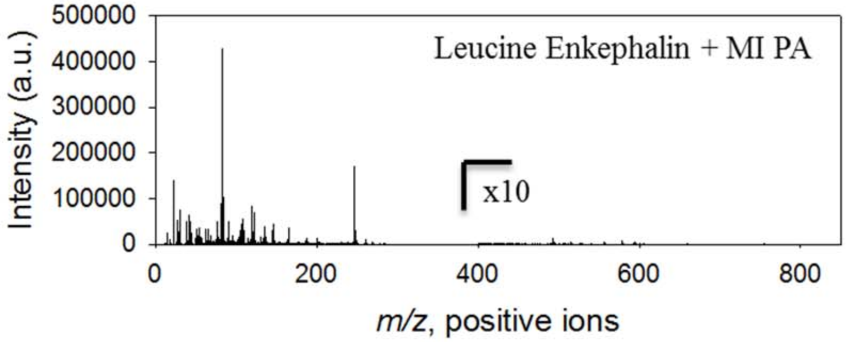
500000
400000
300000
200000
100000
0
Intensity (a.u.)
Leucine Enkephalin + MI PA
x10
0
200
400
600
800
m/z, positive ions

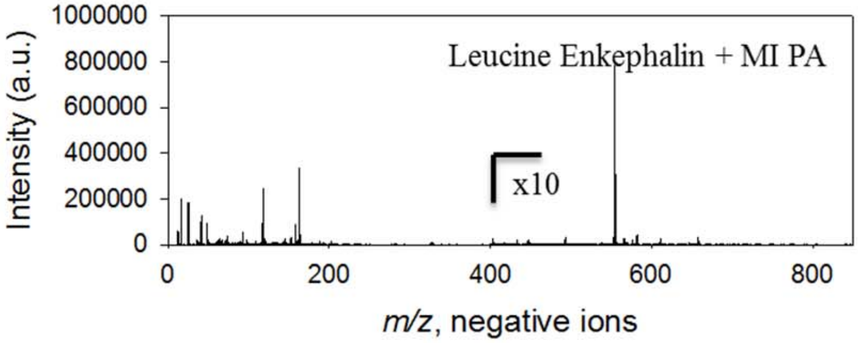
1000000
800000
600000
400000
200000
0
Intensity (a.u.)
Leucine Enkephalin + MI PA
x10
0
200
400
600
800
m/z, negative ions

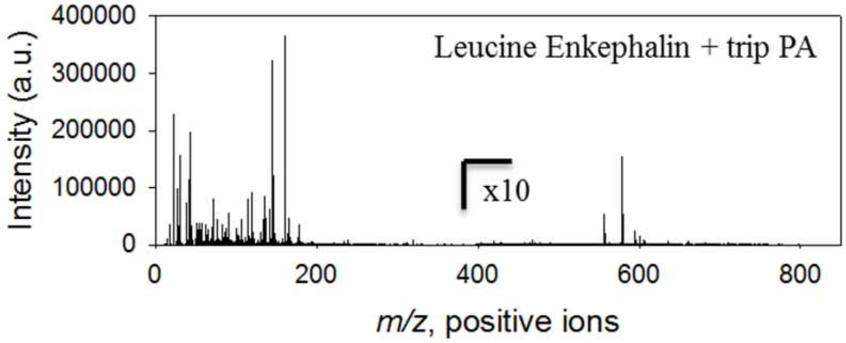
400000
300000
200000
100000
0
Intensity (a.u.)
Leucine Enkephalin + trip PA
x10
0
200
400
600
800
m/z, positive ions

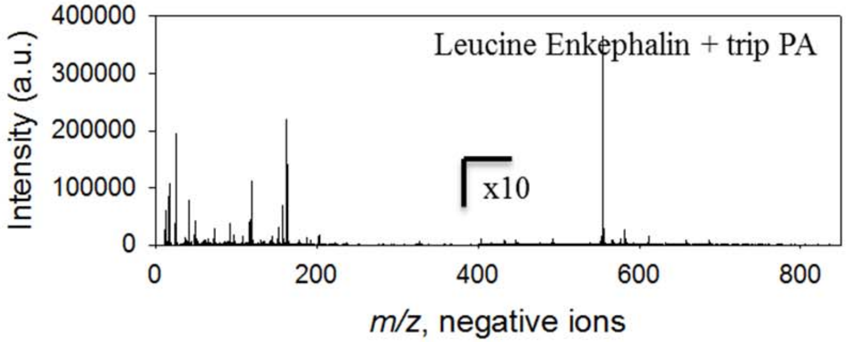
400000
300000
200000
100000
0
Intensity (a.u.)
Leucine Enkephalin + trip PA
x10
0
200
400
600
800
m/z, negative ions

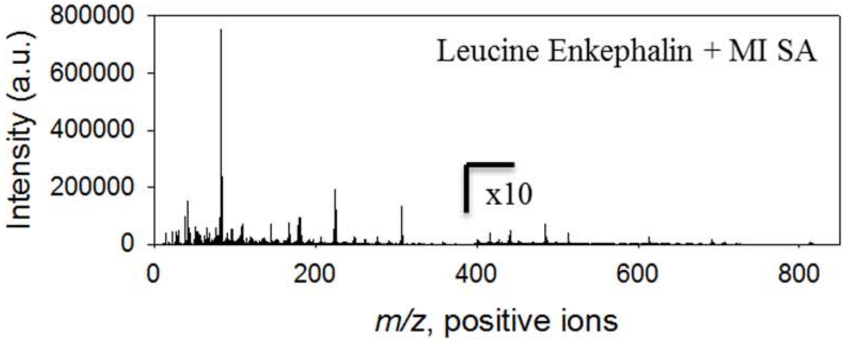
Leucine Enkephalin + MI SA
x10
Intensity (a.u.)
800000
600000
400000
200000
0
0
200
400
600
800
m/z, positive ions

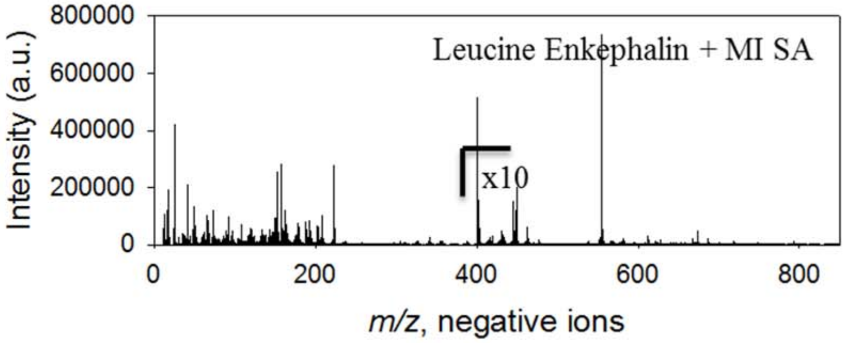
Leucine Enkephalin + MI SA
x10
Intensity (a.u.)
800000
600000
400000
200000
0
0
200
400
600
800
m/z, negative ions

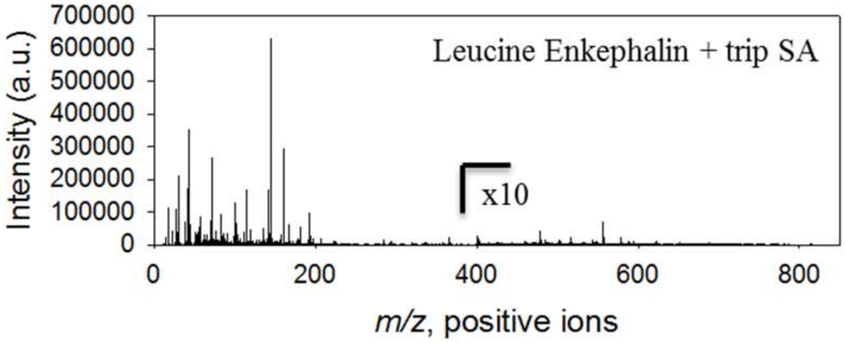
Leucine Enkephalin + trip SA
x10
Intensity (a.u.)
700000
600000
500000
400000
300000
200000
100000
0
0
200
400
600
800
m/z, positive ions

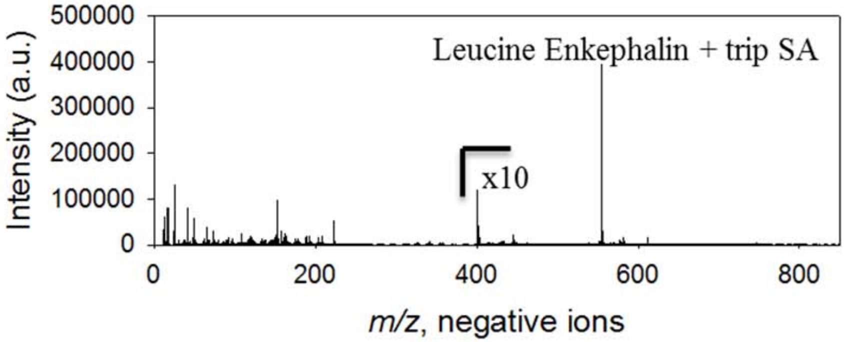
Leucine Enkephalin + trip SA
x10
Intensity (a.u.)
500000
400000
300000
200000
100000
0
0
200
400
600
800
m/z, negative ions

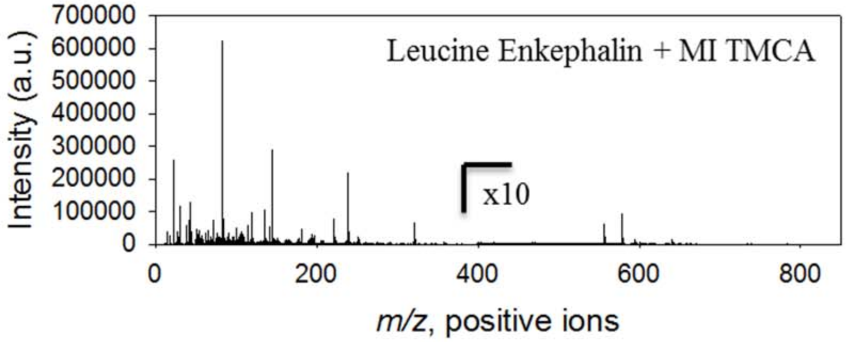
Leucine Enkephalin + MI TMCA
x10
Intensity (a.u.)
700000
600000
500000
400000
300000
200000
100000
0
0
200
400
600
800
m/z, positive ions

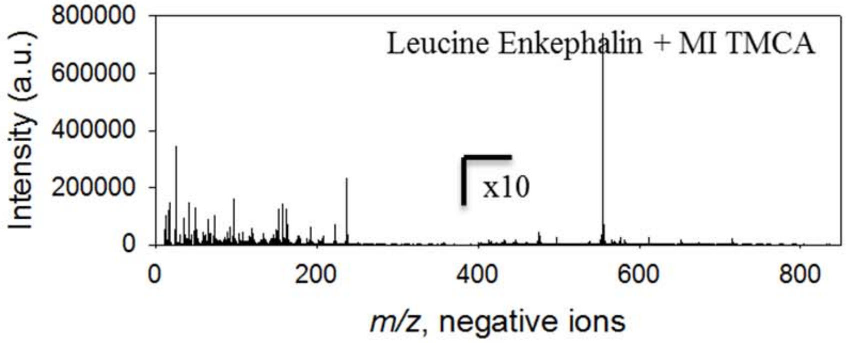
Leucine Enkephalin + MI TMCA
x10
Intensity (a.u.)
800000
600000
400000
200000
0
0
200
400
600
800
m/z, negative ions

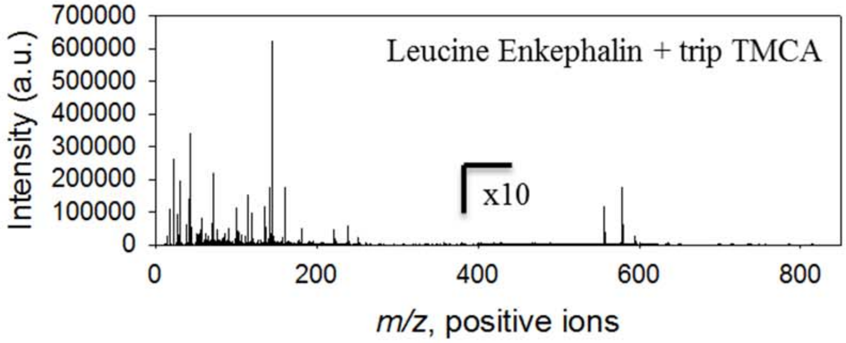
Leucine Enkephalin + trip TMCA
x10
Intensity (a.u.)
700000
600000
500000
400000
300000
200000
100000
0
0
200
400
600
800
m/z, positive ions

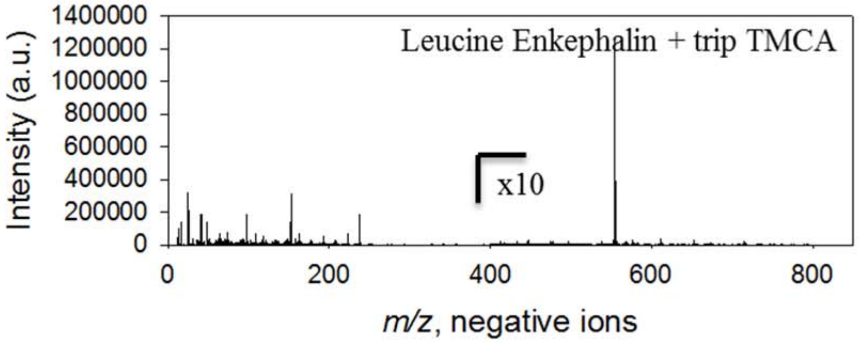
Leucine Enkephalin + trip TMCA
x10
Intensity (a.u.)
1400000
1200000
1000000
800000
600000
400000
200000
0
0
200
400
600
800
m/z, negative ions

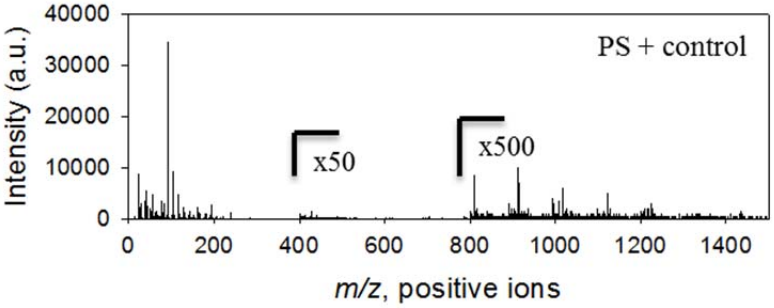

PS + control
Intensity (a.u.)
40000
30000
20000
10000
0
x50
x500
0
200
400
600
800
1000
1200
1400
m/z, positive ions

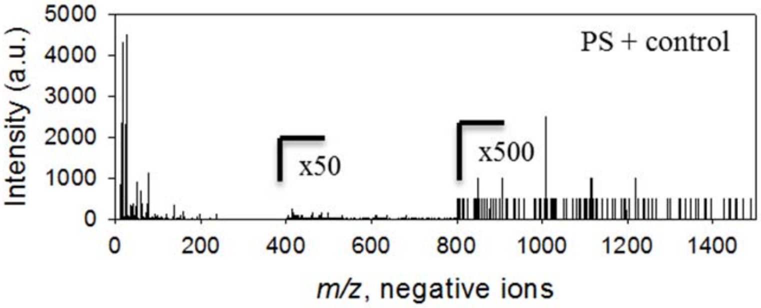

PS + control
Intensity (a.u.)
5000
4000
3000
2000
1000
0
x50
x500
0
200
400
600
800
1000
1200
1400
m/z, negative ions

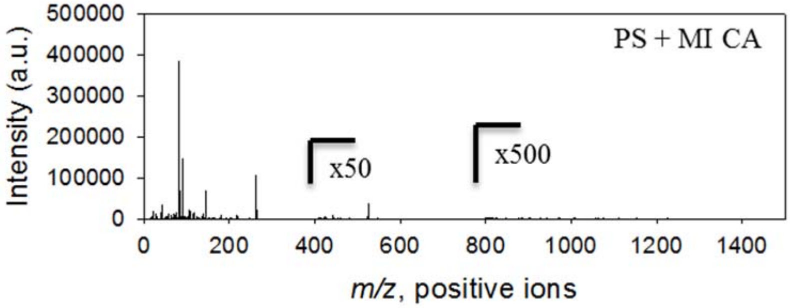

PS + MI CA
Intensity (a.u.)
500000
400000
300000
200000
100000
0
x50
x500
0
200
400
600
800
1000
1200
1400
m/z, positive ions

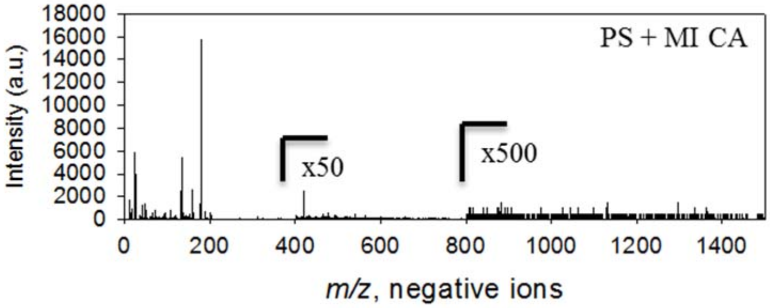

PS + MI CA
Intensity (a.u.)
18000
16000
14000
12000
10000
8000
6000
4000
2000
0
x50
x500
0
200
400
600
800
1000
1200
1400
m/z, negative ions

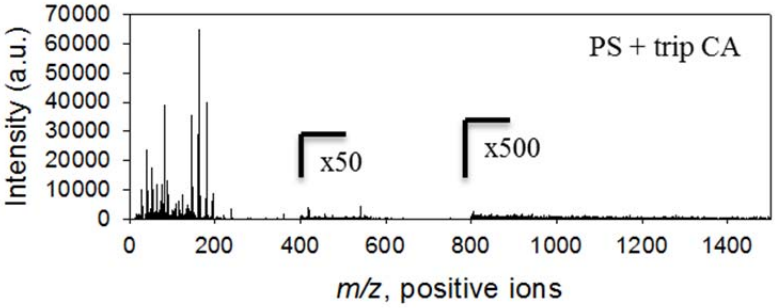

PS + trip CA
Intensity (a.u.)
70000
60000
50000
40000
30000
20000
10000
0
x50
x500
0
200
400
600
800
1000
1200
1400
m/z, positive ions

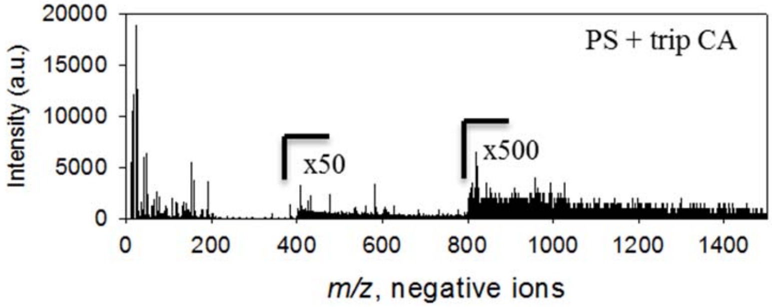

PS + trip CA
Intensity (a.u.)
20000
15000
10000
5000
0
x50
x500
0
200
400
600
800
1000
1200
1400
m/z, negative ions

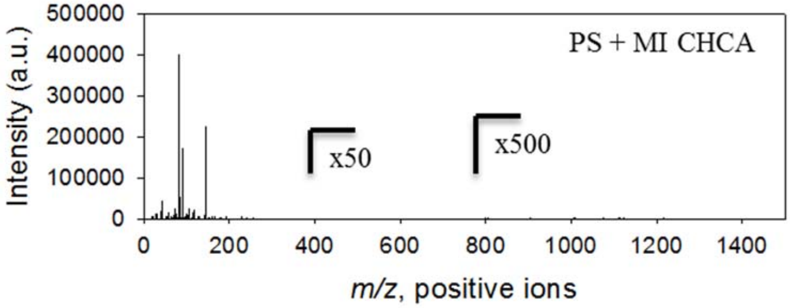
PS + MI CHCA
x50
x500
Intensity (a.u.)
500000
400000
300000
200000
100000
0
0
200
400
600
800
1000
1200
1400
m/z, positive ions

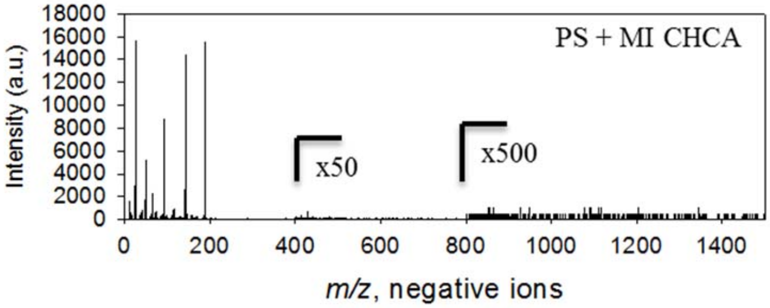
PS + MI CHCA
x50
x500
Intensity (a.u.)
18000
16000
14000
12000
10000
8000
6000
4000
2000
0
0
200
400
600
800
1000
1200
1400
m/z, negative ions

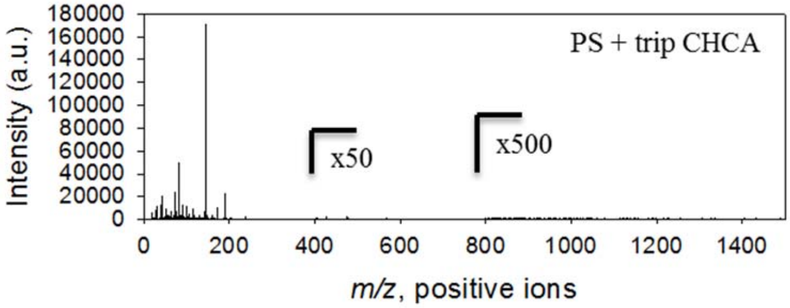
PS + trip CHCA
x50
x500
Intensity (a.u.)
180000
160000
140000
120000
100000
80000
60000
40000
20000
0
0
200
400
600
800
1000
1200
1400
m/z, positive ions

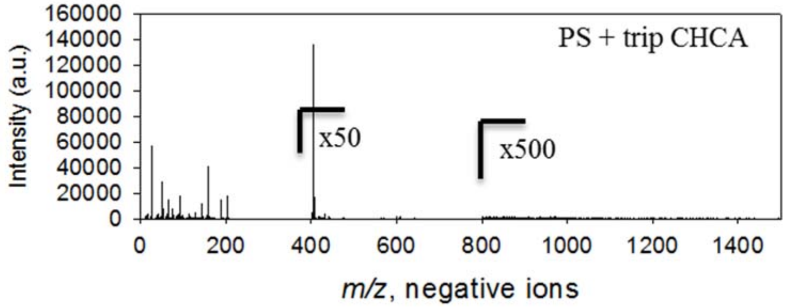
PS + trip CHCA
x50
x500
Intensity (a.u.)
160000
140000
120000
100000
80000
60000
40000
20000
0
0
200
400
600
800
1000
1200
1400
m/z, negative ions

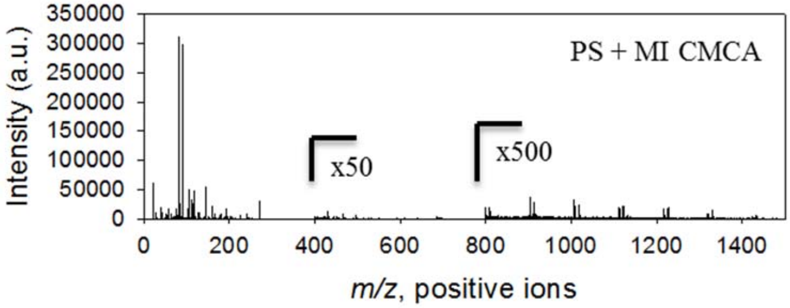
PS + MI CMCA
x50
x500
Intensity (a.u.)
350000
300000
250000
200000
150000
100000
50000
0
0
200
400
600
800
1000
1200
1400
m/z, positive ions

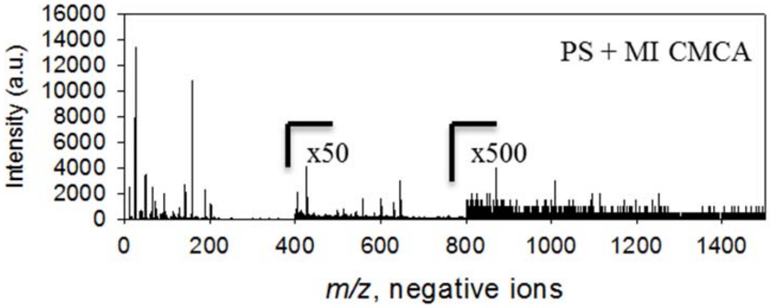
PS + MI CMCA
x50
x500
Intensity (a.u.)
16000
14000
12000
10000
8000
6000
4000
2000
0
0
200
400
600
800
1000
1200
1400
m/z, negative ions

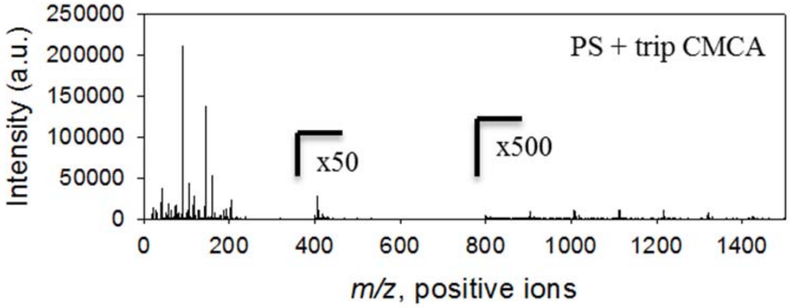
PS + trip CMCA
x50
x500
Intensity (a.u.)
250000
200000
150000
100000
50000
0
0
200
400
600
800
1000
1200
1400
m/z, positive ions

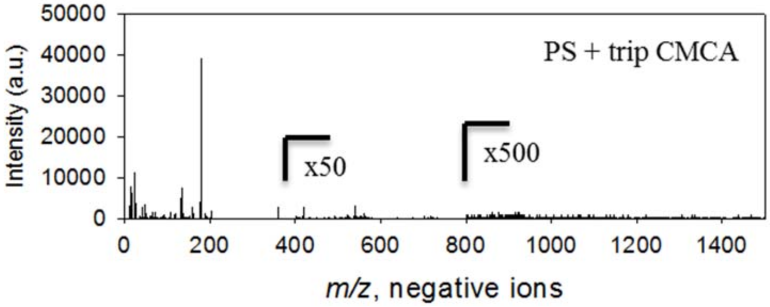
PS + trip CMCA
x50
x500
Intensity (a.u.)
50000
40000
30000
20000
10000
0
0
200
400
600
800
1000
1200
1400
m/z, negative ions

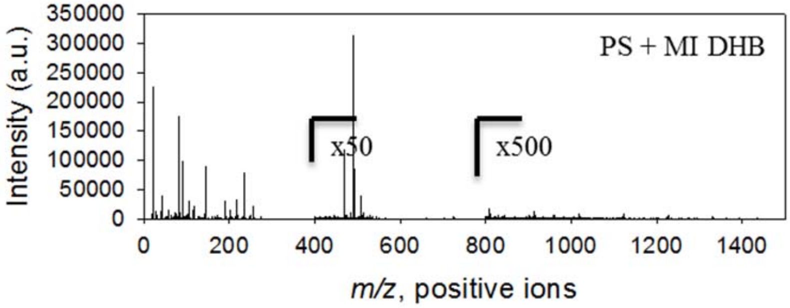
Intensity (a.u.)
350000
300000
250000
200000
150000
100000
50000
0
0
200
400
600
800
1000
1200
1400
m/z, positive ions
PS + MI DHB
x50
x500

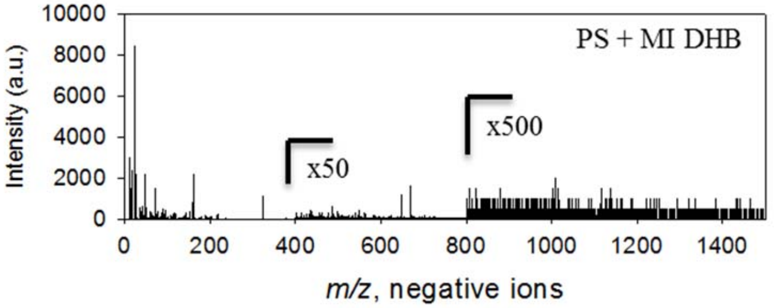
Intensity (a.u.)
10000
8000
6000
4000
2000
0
0
200
400
600
800
1000
1200
1400
m/z, negative ions
PS + MI DHB
x50
x500

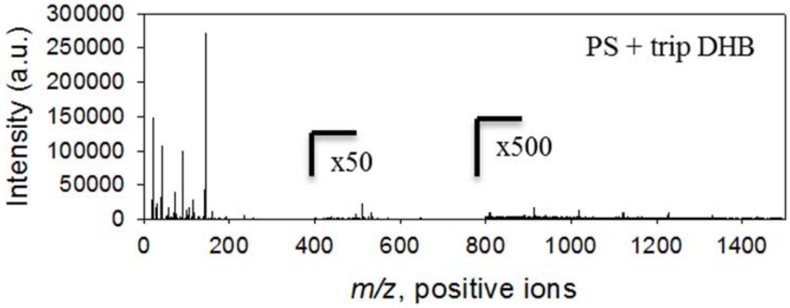
Intensity (a.u.)
300000
250000
200000
150000
100000
50000
0
0
200
400
600
800
1000
1200
1400
m/z, positive ions
PS + trip DHB
x50
x500

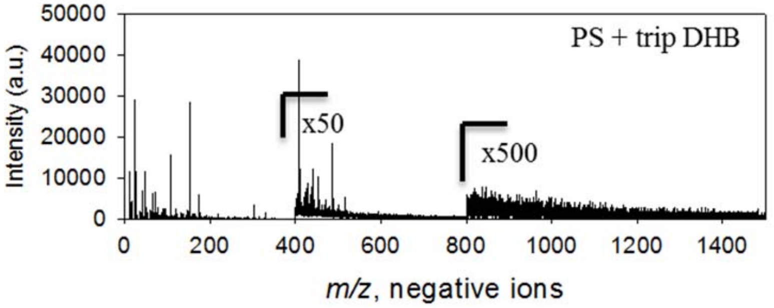
Intensity (a.u.)
50000
40000
30000
20000
10000
0
0
200
400
600
800
1000
1200
1400
m/z, negative ions
PS + trip DHB
x50
x500

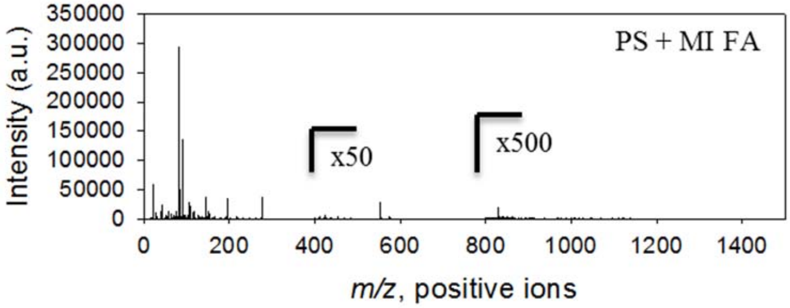
Intensity (a.u.)
350000
300000
250000
200000
150000
100000
50000
0
PS + MI FA
x50
x500
0
200
400
600
800
1000
1200
1400
m/z, positive ions

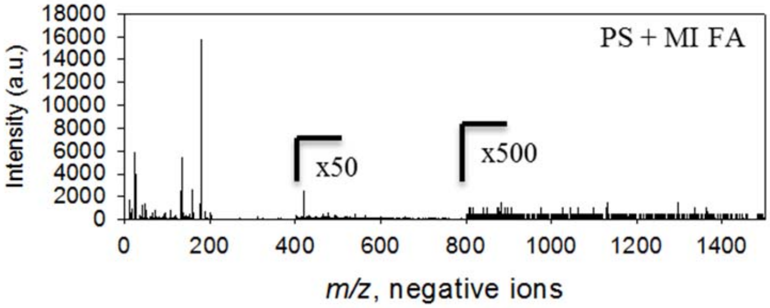
Intensity (a.u.)
18000
16000
14000
12000
10000
8000
6000
4000
2000
0
PS + MI FA
x50
x500
0
200
400
600
800
1000
1200
1400
m/z, negative ions

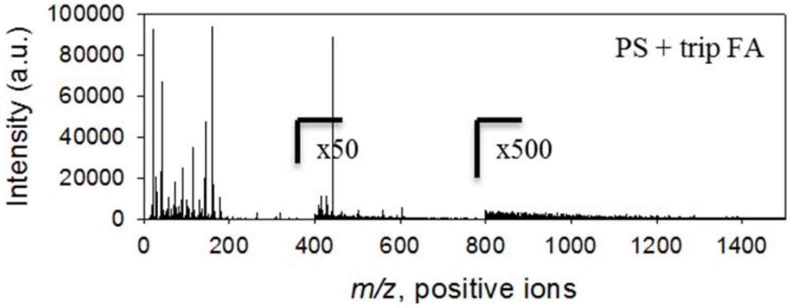
Intensity (a.u.)
100000
80000
60000
40000
20000
0
PS + trip FA
x50
x500
0
200
400
600
800
1000
1200
1400
m/z, positive ions

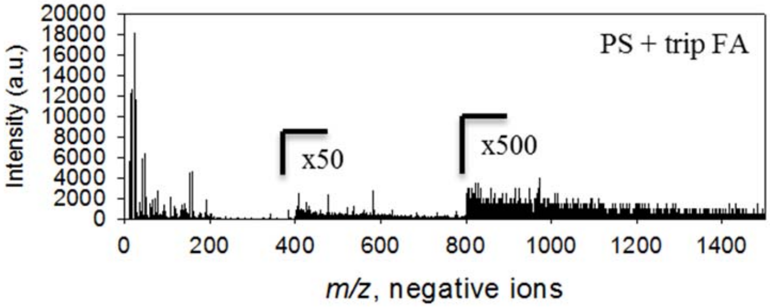
Intensity (a.u.)
20000
18000
16000
14000
12000
10000
8000
6000
4000
2000
0
PS + trip FA
x50
x500
0
200
400
600
800
1000
1200
1400
m/z, negative ions

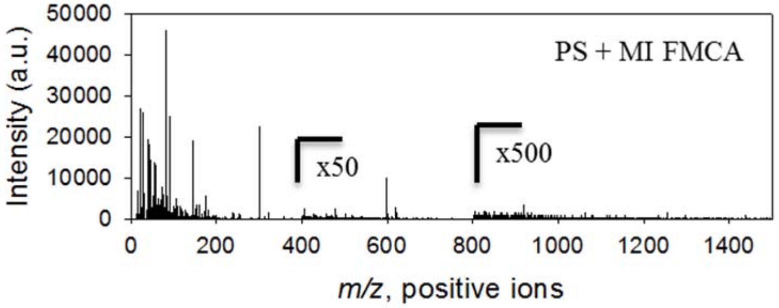
PS + MI FMCA
x50
x500
Intensity (a.u.)
50000
40000
30000
20000
10000
0
0
200
400
600
800
1000
1200
1400
m/z, positive ions

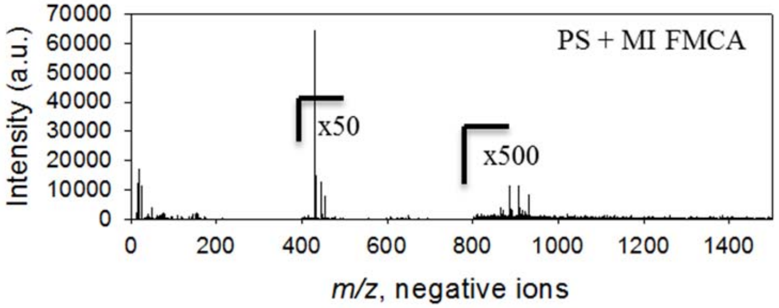
PS + MI FMCA
x50
x500
Intensity (a.u.)
70000
60000
50000
40000
30000
20000
10000
0
0
200
400
600
800
1000
1200
1400
m/z, negative ions

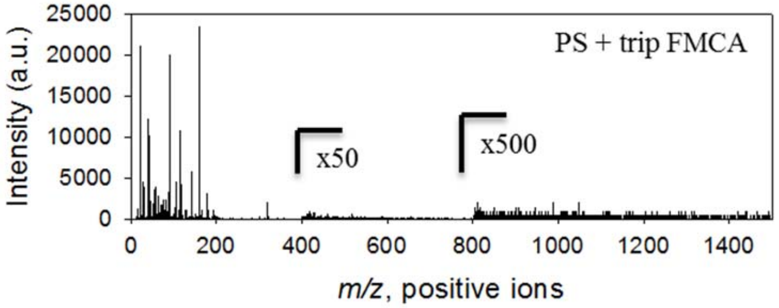
PS + trip FMCA
x50
x500
Intensity (a.u.)
25000
20000
15000
10000
5000
0
0
200
400
600
800
1000
1200
1400
m/z, positive ions

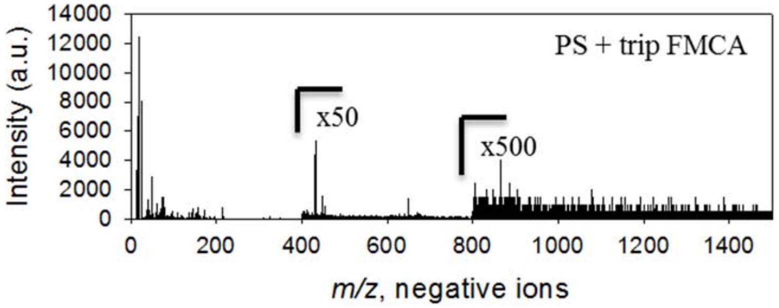
PS + trip FMCA
x50
x500
Intensity (a.u.)
14000
12000
10000
8000
6000
4000
2000
0
0
200
400
600
800
1000
1200
1400
m/z, negative ions

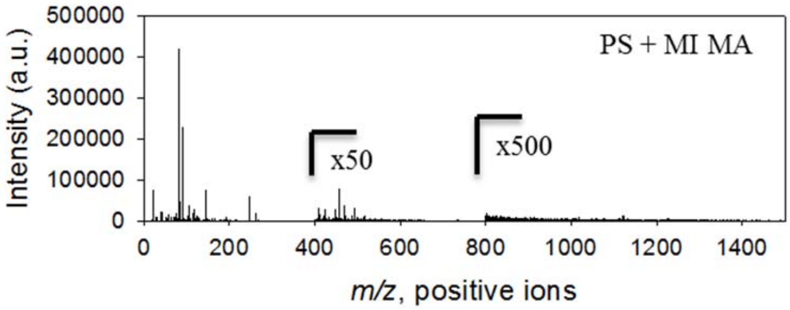
500000
400000
300000
200000
100000
0
Intensity (a.u.)
PS + MI MA
x50
x500
0
200
400
600
800
1000
1200
1400
m/z, positive ions

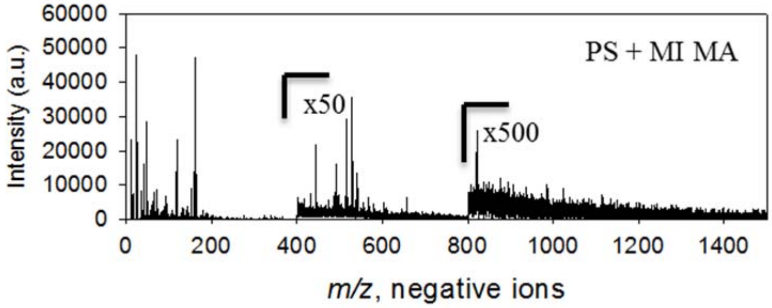
60000
50000
40000
30000
20000
10000
0
Intensity (a.u.)
PS + MI MA
x50
x500
0
200
400
600
800
1000
1200
1400
m/z, negative ions

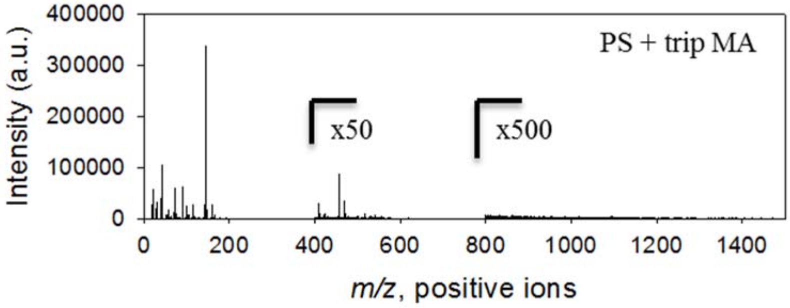
400000
300000
200000
100000
0
Intensity (a.u.)
PS + trip MA
x50
x500
0
200
400
600
800
1000
1200
1400
m/z, positive ions

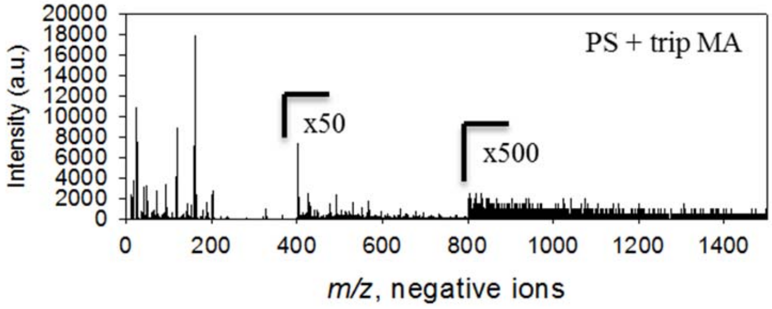
20000
18000
16000
14000
12000
10000
8000
6000
4000
2000
0
Intensity (a.u.)
PS + trip MA
x50
x500
0
200
400
600
800
1000
1200
1400
m/z, negative ions

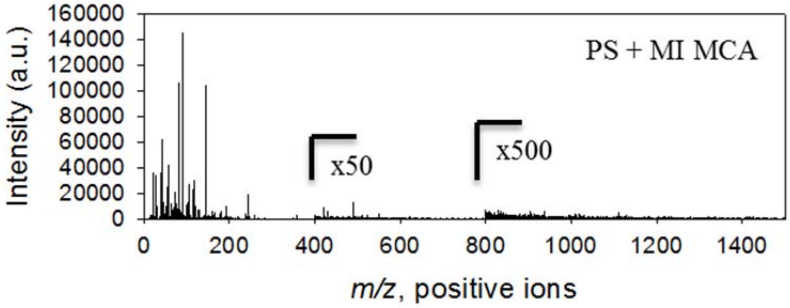
PS + MI MCA
x50
x500
Intensity (a.u.)
0
20000
40000
60000
80000
100000
120000
140000
160000
0
200
400
600
800
1000
1200
1400
m/z, positive ions

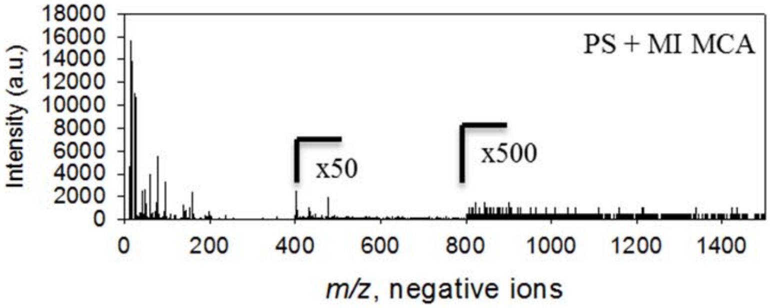
PS + MI MCA
x50
x500
Intensity (a.u.)
0
2000
4000
6000
8000
10000
12000
14000
16000
18000
0
200
400
600
800
1000
1200
1400
m/z, negative ions

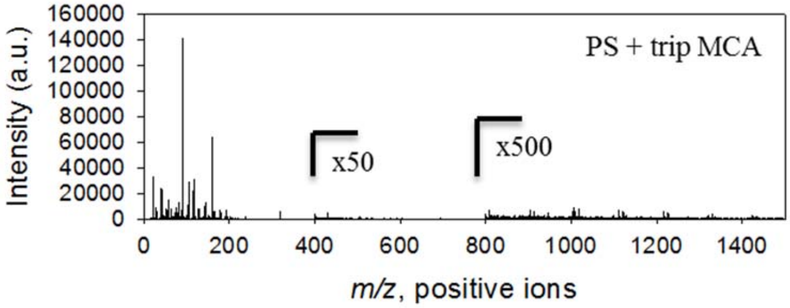
PS + trip MCA
x50
x500
Intensity (a.u.)
0
20000
40000
60000
80000
100000
120000
140000
160000
0
200
400
600
800
1000
1200
1400
m/z, positive ions

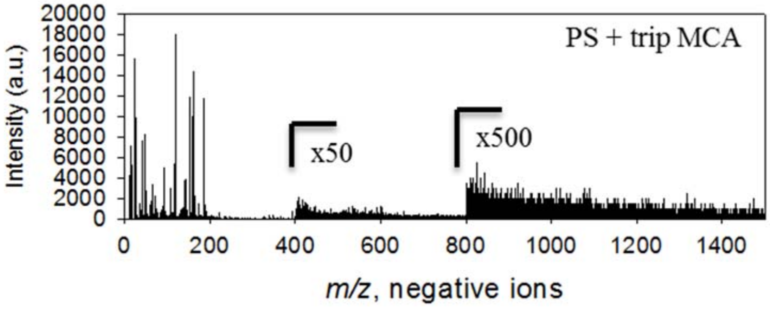
PS + trip MCA
x50
x500
Intensity (a.u.)
0
2000
4000
6000
8000
10000
12000
14000
16000
18000
20000
0
200
400
600
800
1000
1200
1400
m/z, negative ions

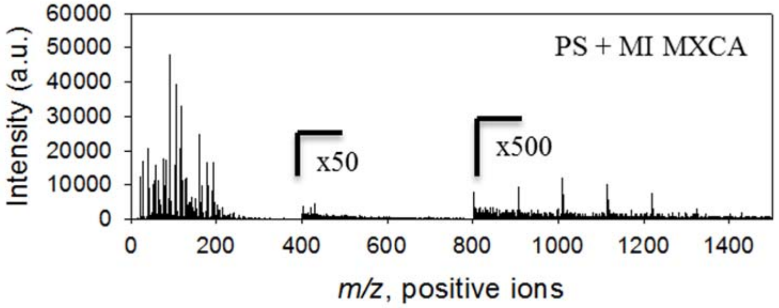
60000
50000
40000
30000
20000
10000
0
Intensity (a.u.)
PS + MI MXCA
x50
x500
0
200
400
600
800
1000
1200
1400
m/z, positive ions

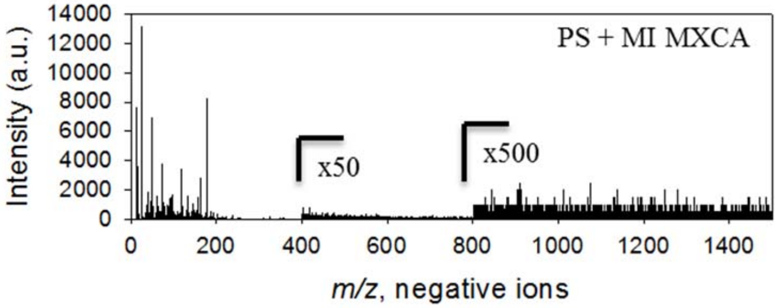
14000
12000
10000
8000
6000
4000
2000
0
Intensity (a.u.)
PS + MI MXCA
x50
x500
0
200
400
600
800
1000
1200
1400
m/z, negative ions

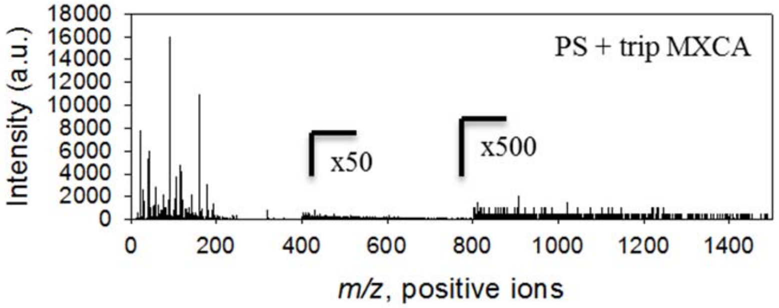
18000
16000
14000
12000
10000
8000
6000
4000
2000
0
Intensity (a.u.)
PS + trip MXCA
x50
x500
0
200
400
600
800
1000
1200
1400
m/z, positive ions

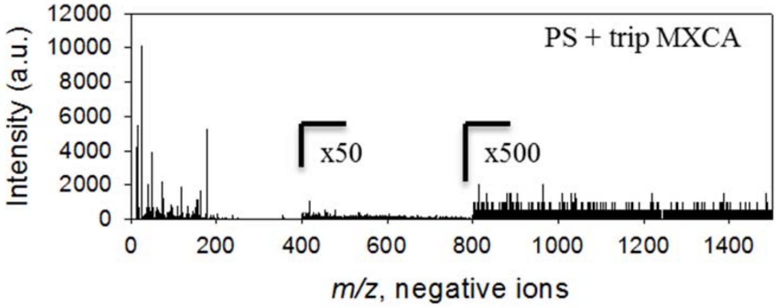
12000
10000
8000
6000
4000
2000
0
Intensity (a.u.)
PS + trip MXCA
x50
x500
0
200
400
600
800
1000
1200
1400
m/z, negative ions

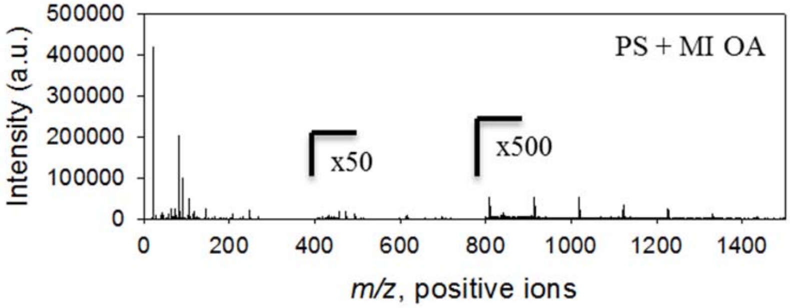
PS + MI OA
x50
x500
Intensity (a.u.)
500000
400000
300000
200000
100000
0
0
200
400
600
800
1000
1200
1400
m/z, positive ions

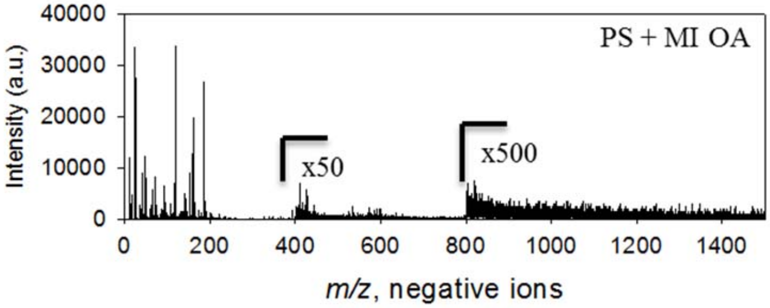
PS + MI OA
x50
x500
Intensity (a.u.)
40000
30000
20000
10000
0
0
200
400
600
800
1000
1200
1400
m/z, negative ions

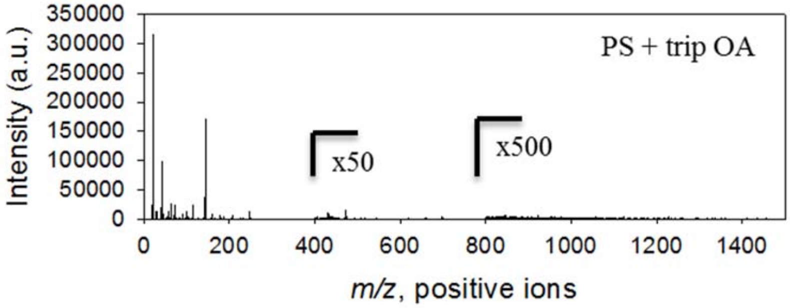
PS + trip OA
x50
x500
Intensity (a.u.)
350000
300000
250000
200000
150000
100000
50000
0
0
200
400
600
800
1000
1200
1400
m/z, positive ions

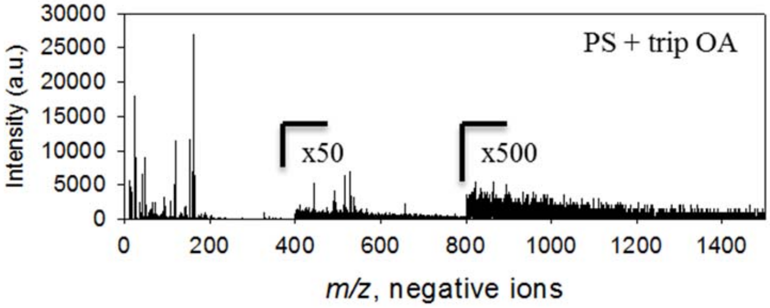
PS + trip OA
x50
x500
Intensity (a.u.)
30000
25000
20000
15000
10000
5000
0
0
200
400
600
800
1000
1200
1400
m/z, negative ions

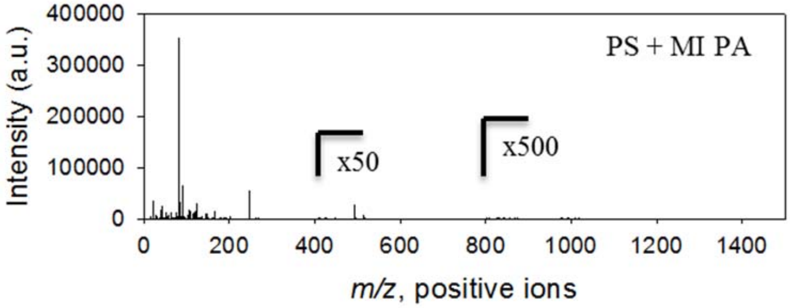
PS + MI PA
Intensity (a.u.)
400000
300000
200000
100000
0
x50
x500
0
200
400
600
800
1000
1200
1400
m/z, positive ions

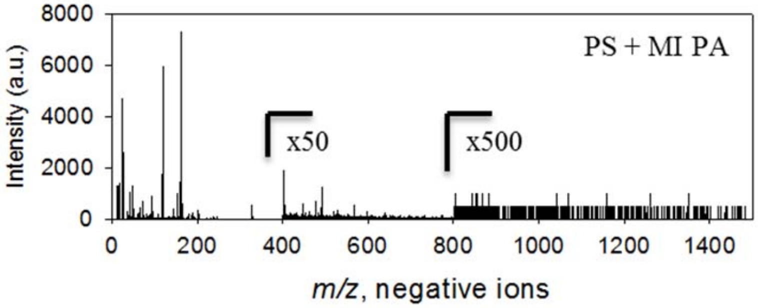
PS + MI PA
Intensity (a.u.)
8000
6000
4000
2000
0
x50
x500
0
200
400
600
800
1000
1200
1400
m/z, negative ions

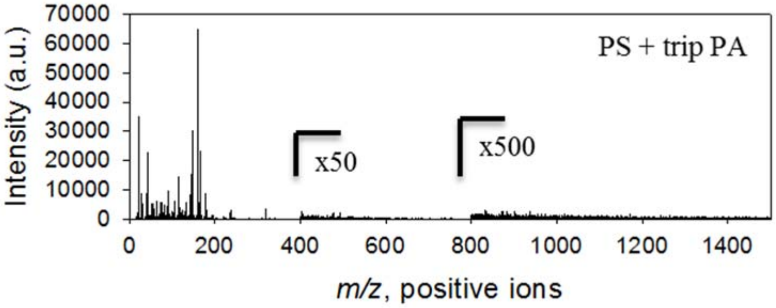
PS + trip PA
Intensity (a.u.)
70000
60000
50000
40000
30000
20000
10000
0
x50
x500
0
200
400
600
800
1000
1200
1400
m/z, positive ions

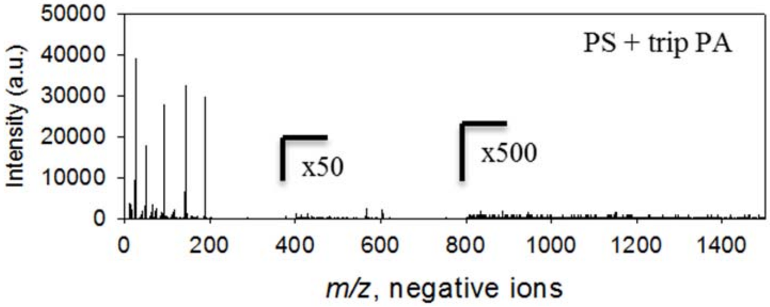
PS + trip PA
Intensity (a.u.)
50000
40000
30000
20000
10000
0
x50
x500
0
200
400
600
800
1000
1200
1400
m/z, negative ions

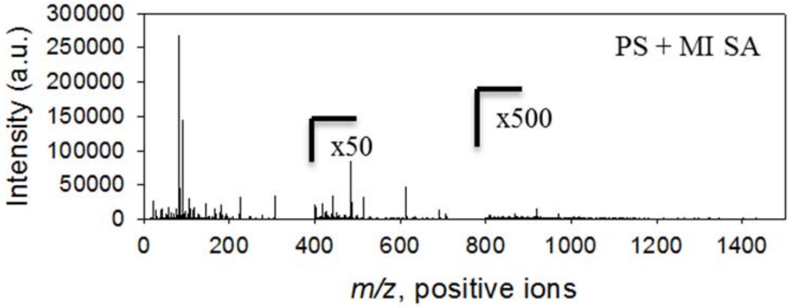
PS + MI SA
x50
x500
Intensity (a.u.)
300000
250000
200000
150000
100000
50000
0
0
200
400
600
800
1000
1200
1400
m/z, positive ions

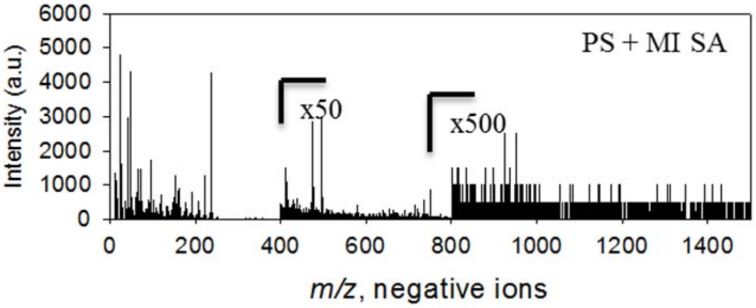
PS + MI SA
x50
x500
Intensity (a.u.)
6000
5000
4000
3000
2000
1000
0
0
200
400
600
800
1000
1200
1400
m/z, negative ions

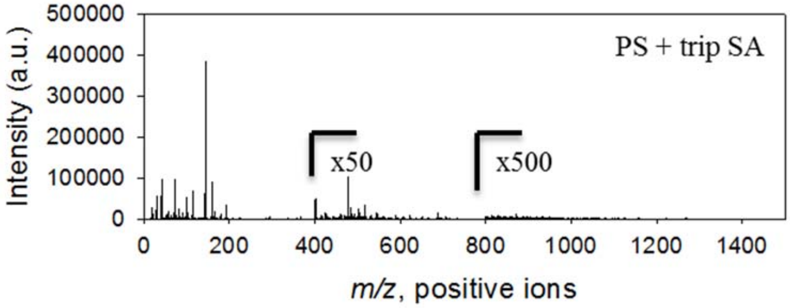
PS + trip SA
x50
x500
Intensity (a.u.)
500000
400000
300000
200000
100000
0
0
200
400
600
800
1000
1200
1400
m/z, positive ions

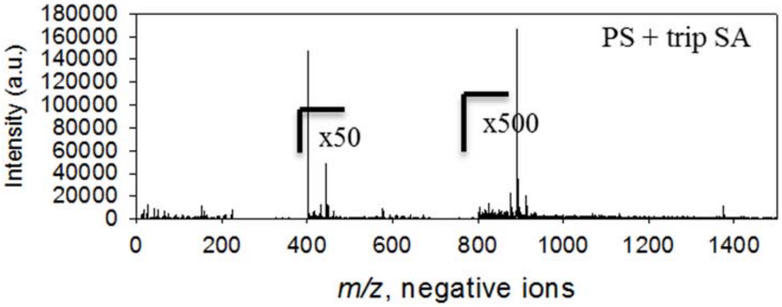
PS + trip SA
x50
x500
Intensity (a.u.)
180000
160000
140000
120000
100000
80000
60000
40000
20000
0
0
200
400
600
800
1000
1200
1400
m/z, negative ions

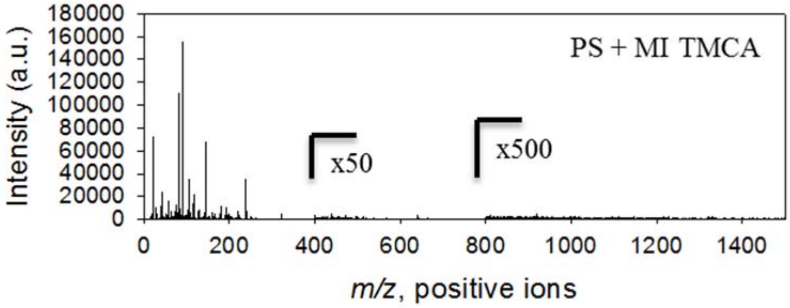
PS + MI TMCA
x50
x500
Intensity (a.u.)
180000
160000
140000
120000
100000
80000
60000
40000
20000
0
0
200
400
600
800
1000
1200
1400
m/z, positive ions

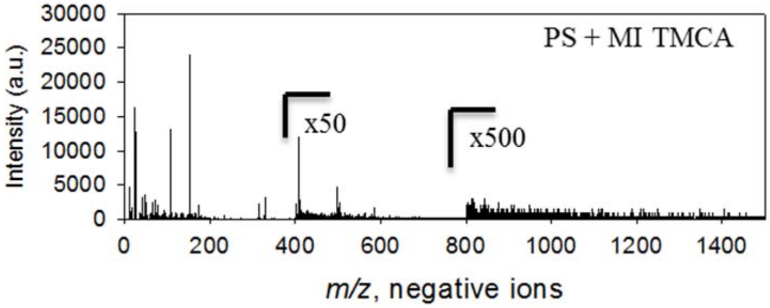
PS + MI TMCA
x50
x500
Intensity (a.u.)
30000
25000
20000
15000
10000
5000
0
0
200
400
600
800
1000
1200
1400
m/z, negative ions

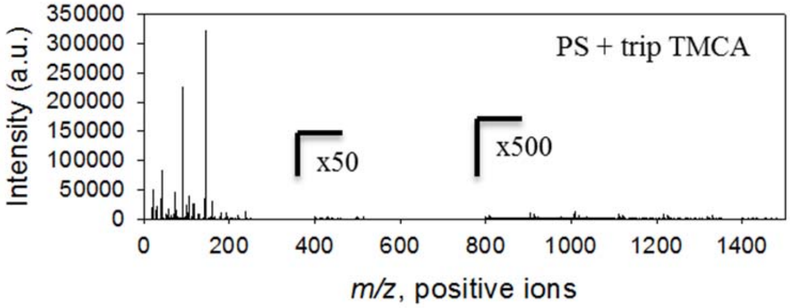
PS + trip TMCA
x50
x500
Intensity (a.u.)
350000
300000
250000
200000
150000
100000
50000
0
0
200
400
600
800
1000
1200
1400
m/z, positive ions

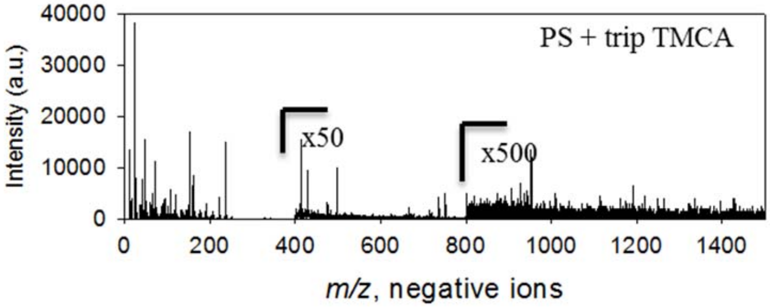
PS + trip TMCA
x50
x500
Intensity (a.u.)
40000
30000
20000
10000
0
0
200
400
600
800
1000
1200
1400
m/z, negative ions

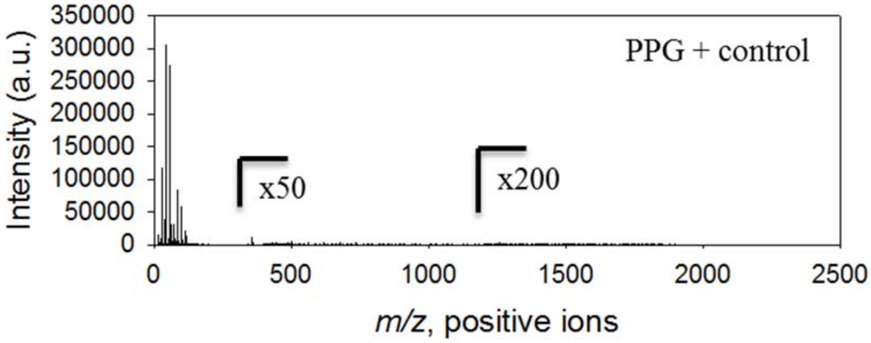
PPG + control
x50
x200
Intensity (a.u.)
350000
300000
250000
200000
150000
100000
50000
0
0
500
1000
1500
2000
2500
m/z, positive ions

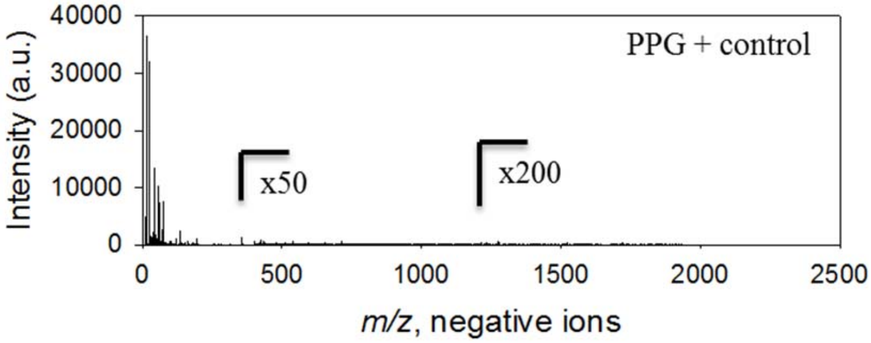
PPG + control
x50
x200
Intensity (a.u.)
40000
30000
20000
10000
0
0
500
1000
1500
2000
2500
m/z, negative ions

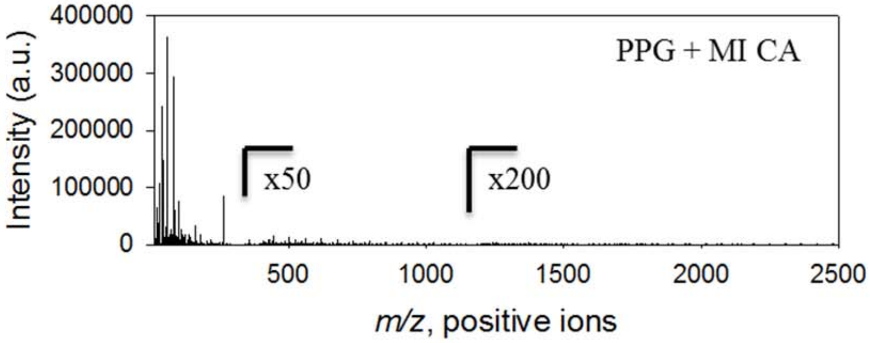
PPG + MI CA
x50
x200
Intensity (a.u.)
400000
300000
200000
100000
0
500
1000
1500
2000
2500
m/z, positive ions

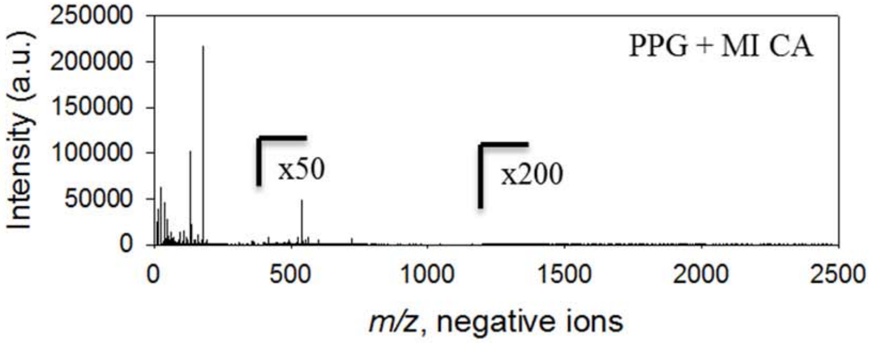
PPG + MI CA
x50
x200
Intensity (a.u.)
250000
200000
150000
100000
50000
0
0
500
1000
1500
2000
2500
m/z, negative ions

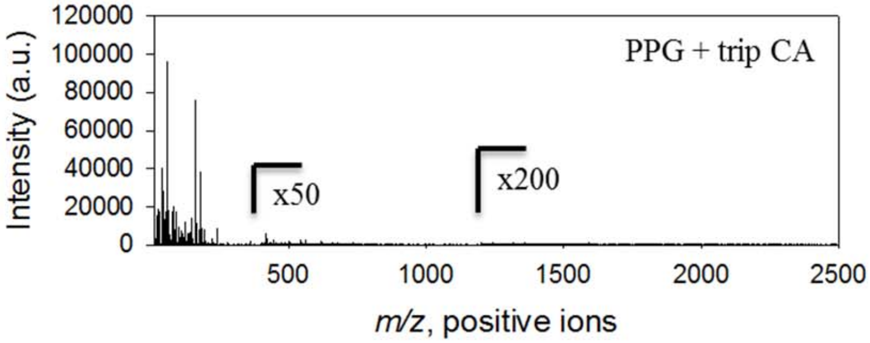
PPG + trip CA
x50
x200
Intensity (a.u.)
120000
100000
80000
60000
40000
20000
0
500
1000
1500
2000
2500
m/z, positive ions

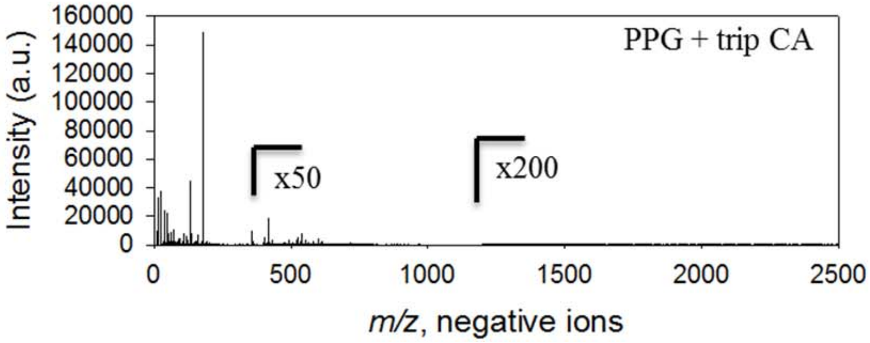
PPG + trip CA
x50
x200
Intensity (a.u.)
160000
140000
120000
100000
80000
60000
40000
20000
0
0
500
1000
1500
2000
2500
m/z, negative ions

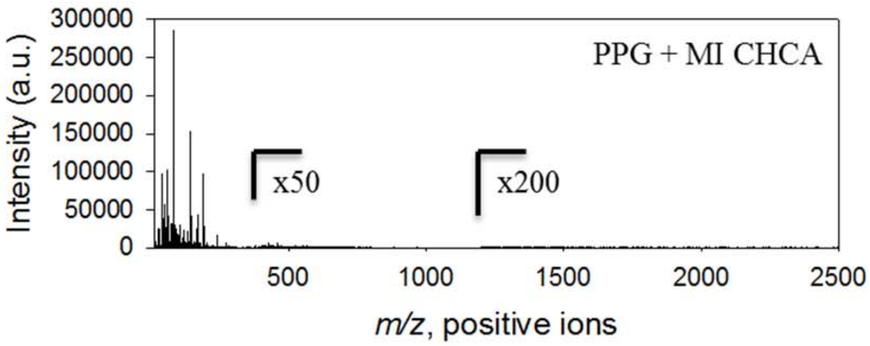
PPG + MI CHCA
x50
x200
Intensity (a.u.)
300000
250000
200000
150000
100000
50000
0
500
1000
1500
2000
2500
m/z, positive ions

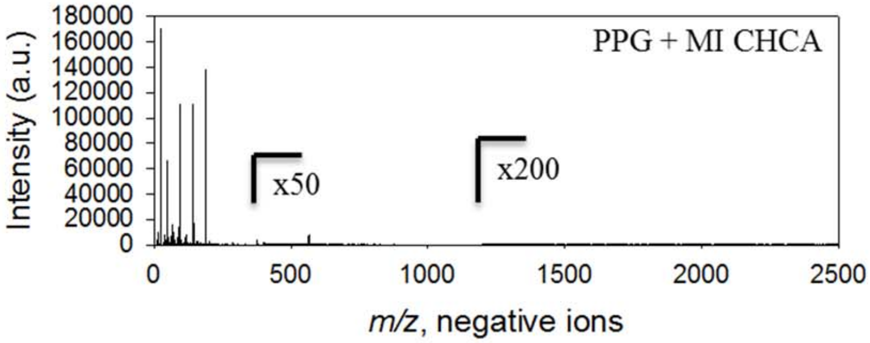
PPG + MI CHCA
x50
x200
Intensity (a.u.)
180000
160000
140000
120000
100000
80000
60000
40000
20000
0
0
500
1000
1500
2000
2500
m/z, negative ions

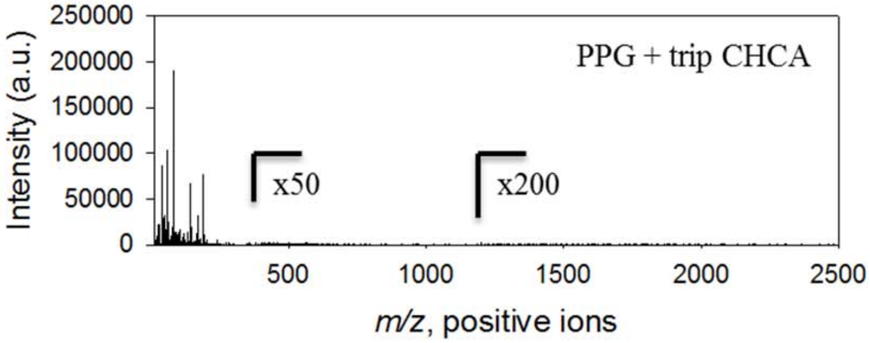
PPG + trip CHCA
x50
x200
Intensity (a.u.)
250000
200000
150000
100000
50000
0
500
1000
1500
2000
2500
m/z, positive ions

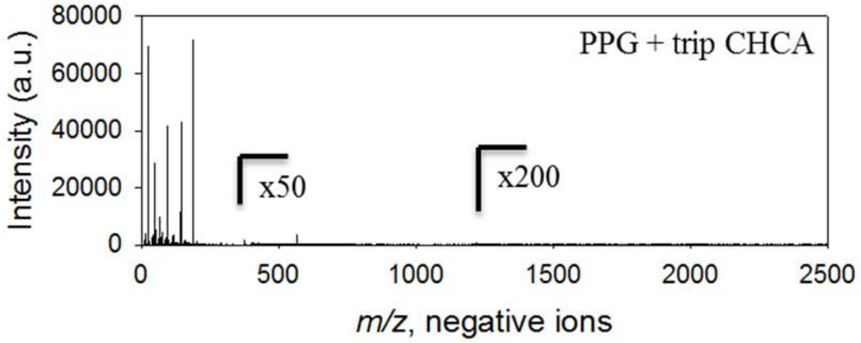
PPG + trip CHCA
x50
x200
Intensity (a.u.)
80000
60000
40000
20000
0
0
500
1000
1500
2000
2500
m/z, negative ions

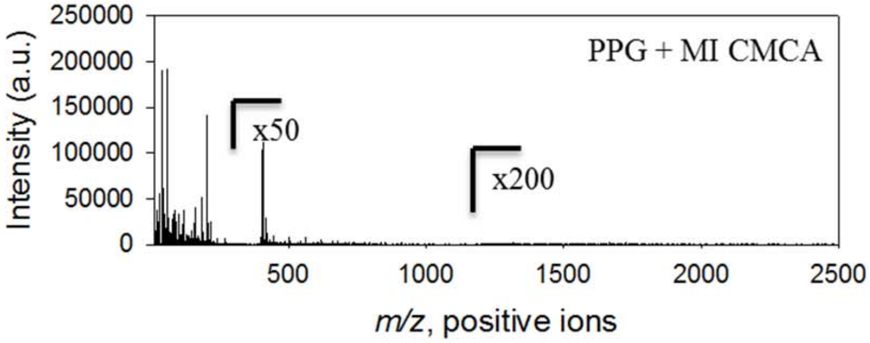
PPG + MI CMCA
x50
x200
Intensity (a.u.)
250000
200000
150000
100000
50000
0
500
1000
1500
2000
2500
m/z, positive ions

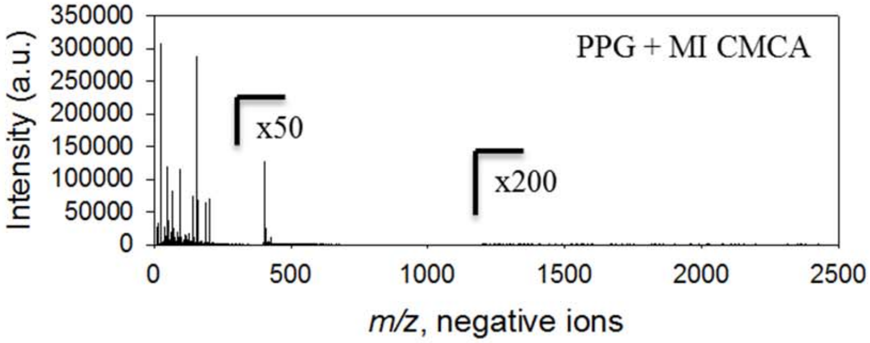
PPG + MI CMCA
x50
x200
Intensity (a.u.)
350000
300000
250000
200000
150000
100000
50000
0
0
500
1000
1500
2000
2500
m/z, negative ions

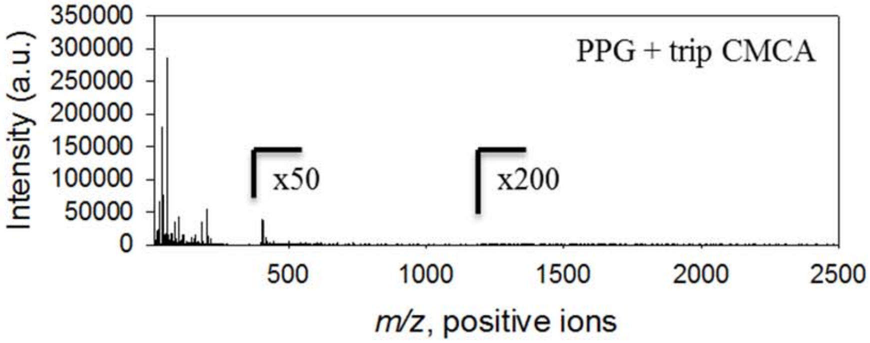
PPG + trip CMCA
x50
x200
Intensity (a.u.)
350000
300000
250000
200000
150000
100000
50000
0
500
1000
1500
2000
2500
m/z, positive ions

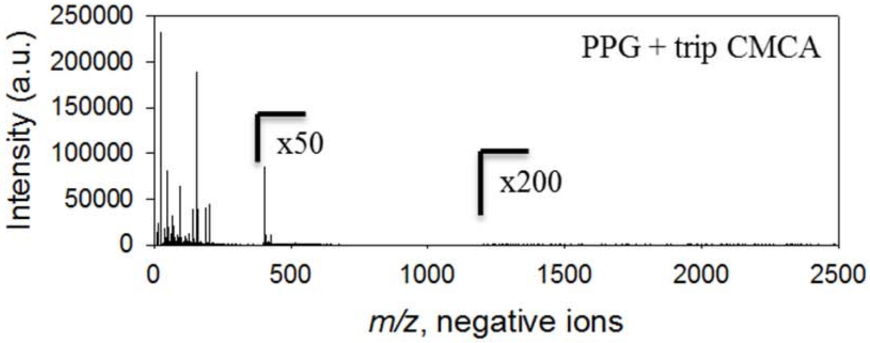
PPG + trip CMCA
x50
x200
Intensity (a.u.)
250000
200000
150000
100000
50000
0
0
500
1000
1500
2000
2500
m/z, negative ions

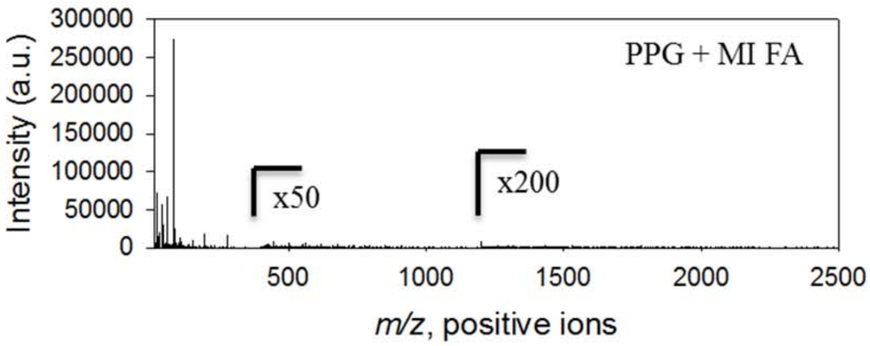
PPG + MI FA
x50
x200
Intensity (a.u.)
300000
250000
200000
150000
100000
50000
0
500
1000
1500
2000
2500
m/z, positive ions

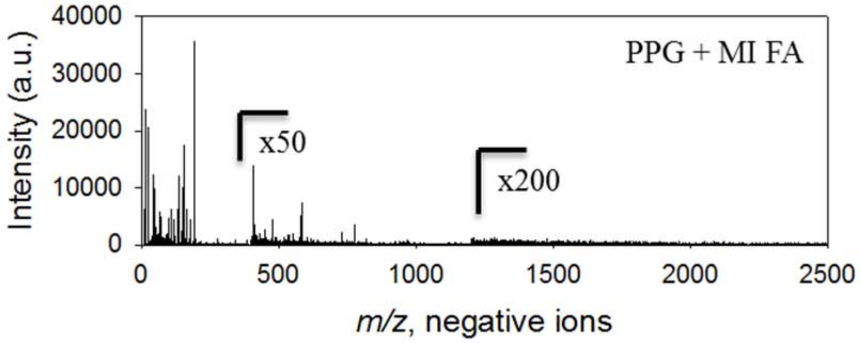
PPG + MI FA
x50
x200
Intensity (a.u.)
40000
30000
20000
10000
0
0
500
1000
1500
2000
2500
m/z, negative ions

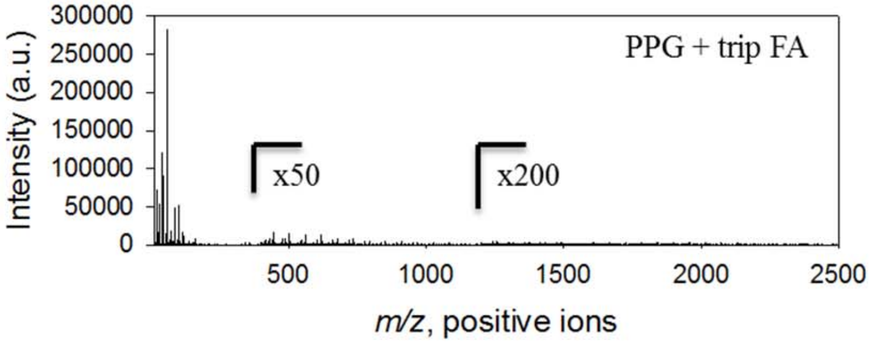
PPG + trip FA
x50
x200
Intensity (a.u.)
300000
250000
200000
150000
100000
50000
0
500
1000
1500
2000
2500
m/z, positive ions

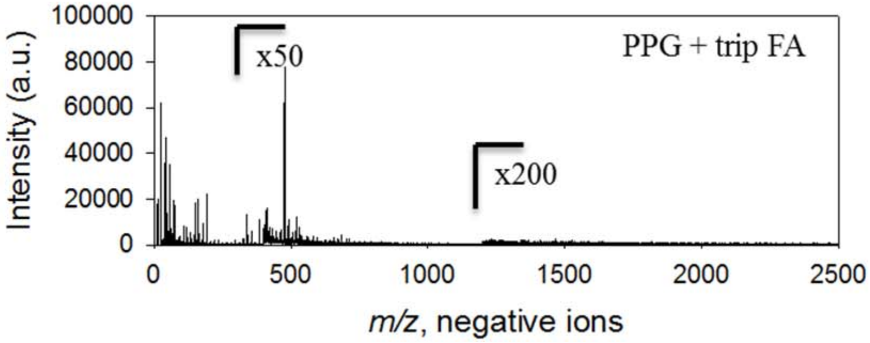
PPG + trip FA
x50
x200
Intensity (a.u.)
100000
80000
60000
40000
20000
0
0
500
1000
1500
2000
2500
m/z, negative ions

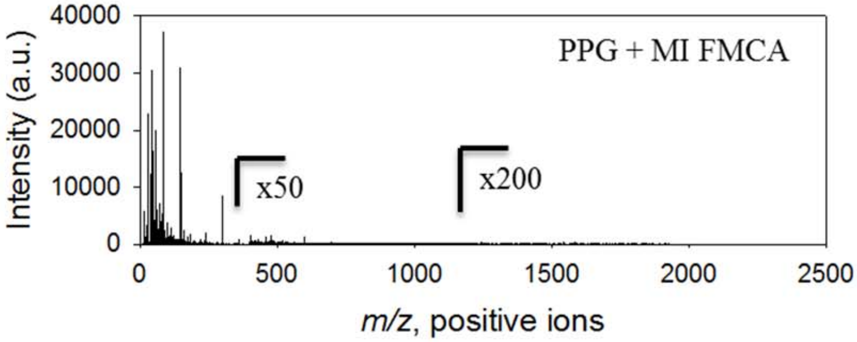
PPG + MI FMCA
x50
x200
Intensity (a.u.)
40000
30000
20000
10000
0
0
500
1000
1500
2000
2500
m/z, positive ions

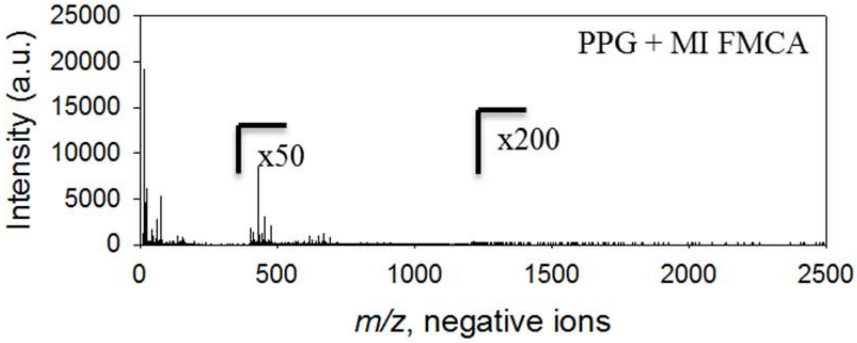
PPG + MI FMCA
x50
x200
Intensity (a.u.)
25000
20000
15000
10000
5000
0
0
500
1000
1500
2000
2500
m/z, negative ions

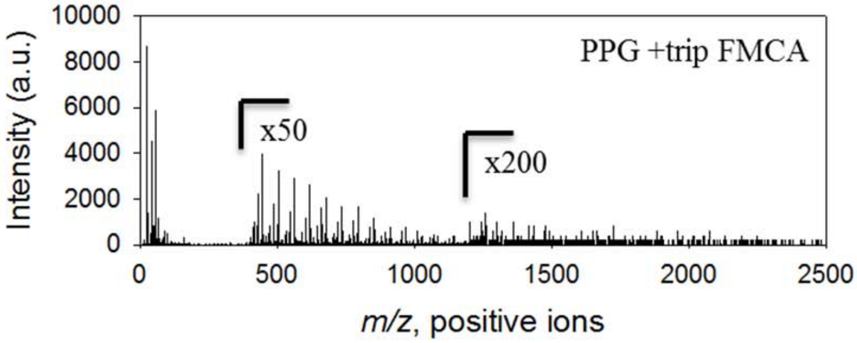
PPG +trip FMCA
x50
x200
Intensity (a.u.)
10000
8000
6000
4000
2000
0
0
500
1000
1500
2000
2500
m/z, positive ions

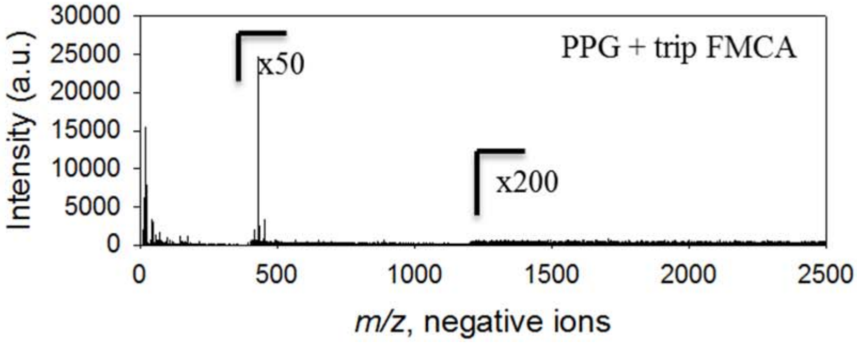
PPG + trip FMCA
x50
x200
Intensity (a.u.)
30000
25000
20000
15000
10000
5000
0
0
500
1000
1500
2000
2500
m/z, negative ions

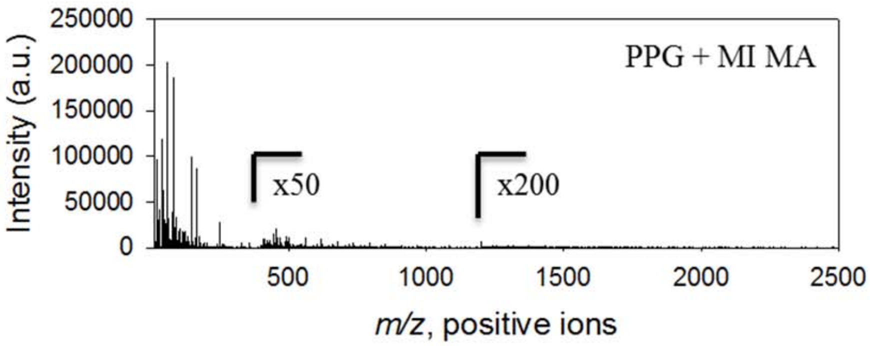
PPG + MI MA
x50
x200
Intensity (a.u.)
250000
200000
150000
100000
50000
0
500
1000
1500
2000
2500
m/z, positive ions

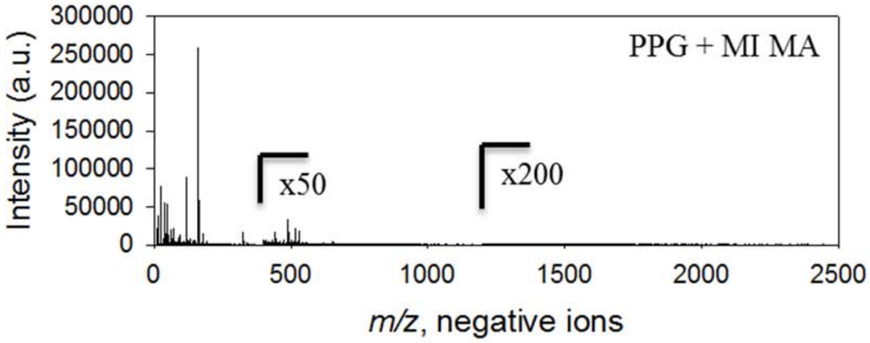
PPG + MI MA
x50
x200
Intensity (a.u.)
300000
250000
200000
150000
100000
50000
0
0
500
1000
1500
2000
2500
m/z, negative ions

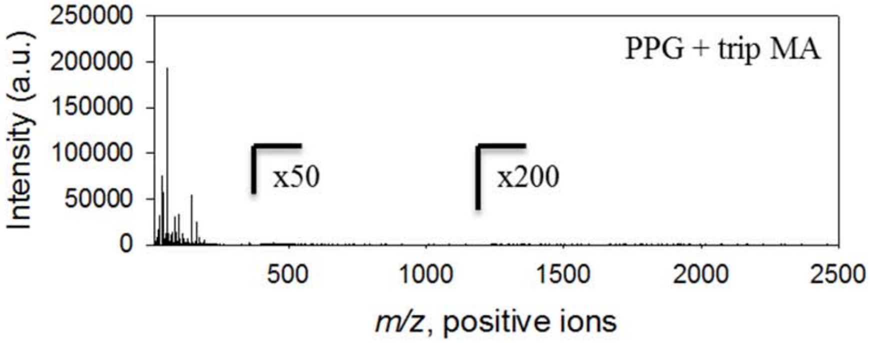
PPG + trip MA
x50
x200
Intensity (a.u.)
250000
200000
150000
100000
50000
0
500
1000
1500
2000
2500
m/z, positive ions

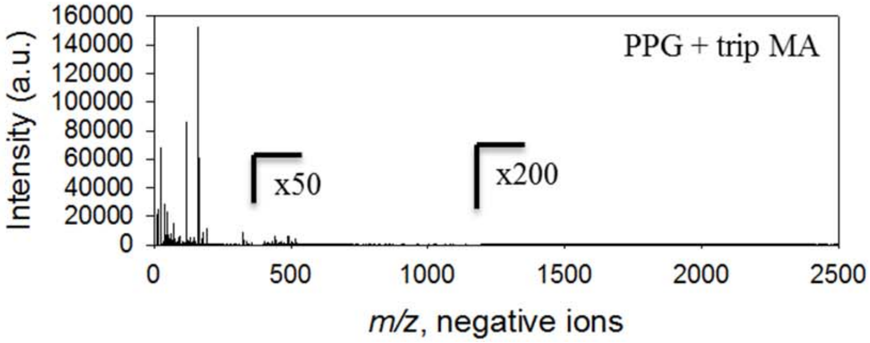
PPG + trip MA
x50
x200
Intensity (a.u.)
160000
140000
120000
100000
80000
60000
40000
20000
0
0
500
1000
1500
2000
2500
m/z, negative ions

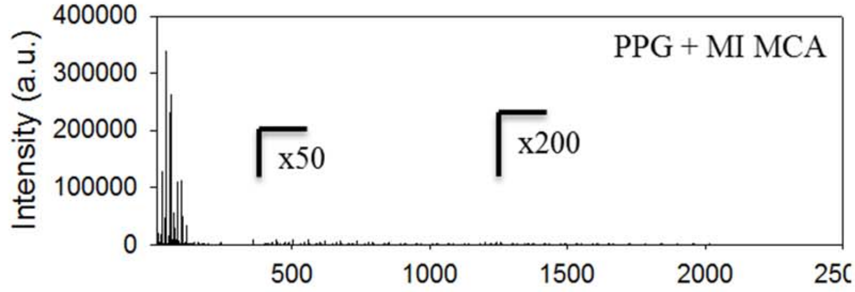
PPG + MI MCA
x50
x200
Intensity (a.u.)
400000
300000
200000
100000
0
500
1000
1500
2000
25

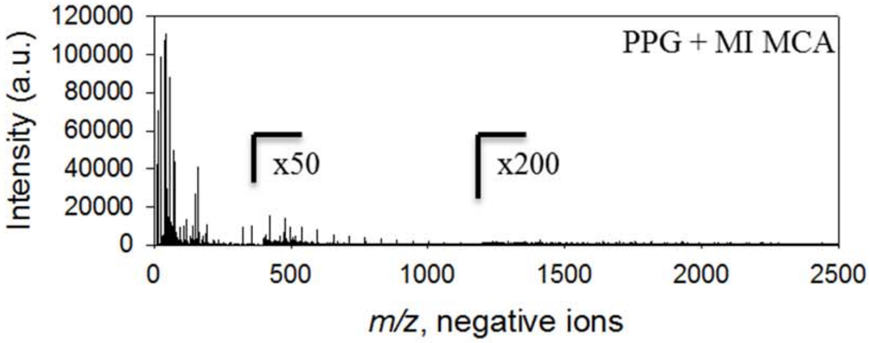
PPG + MI MCA
x50
x200
Intensity (a.u.)
120000
100000
80000
60000
40000
20000
0
0
500
1000
1500
2000
2500
m/z, negative ions

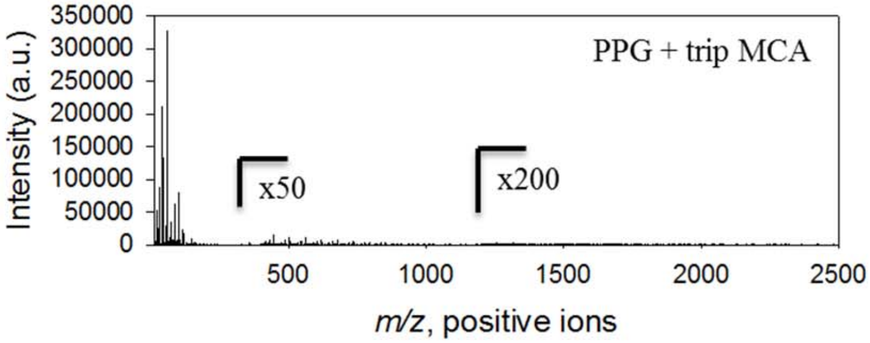
PPG + trip MCA
x50
x200
Intensity (a.u.)
350000
300000
250000
200000
150000
100000
50000
0
500
1000
1500
2000
2500
m/z, positive ions

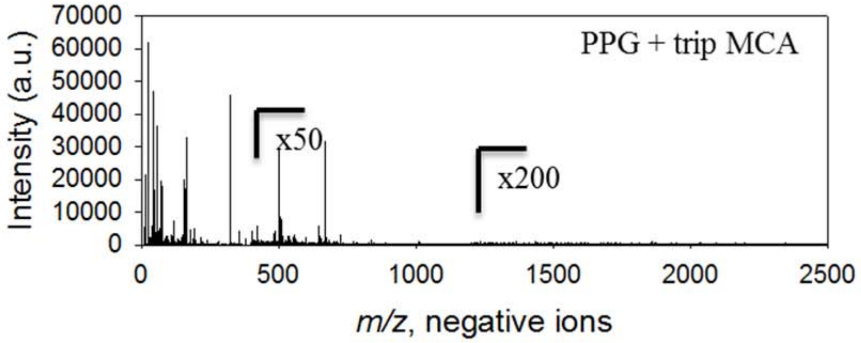
PPG + trip MCA
x50
x200
Intensity (a.u.)
70000
60000
50000
40000
30000
20000
10000
0
0
500
1000
1500
2000
2500
m/z, negative ions

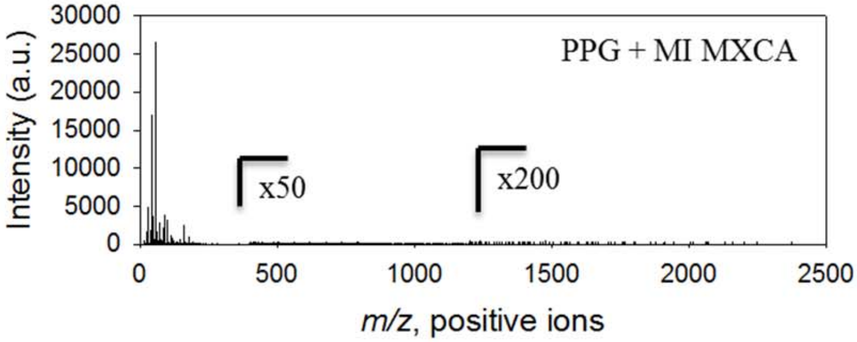
PPG + MI MXCA
x50
x200
Intensity (a.u.)
30000
25000
20000
15000
10000
5000
0
0
500
1000
1500
2000
2500
m/z, positive ions

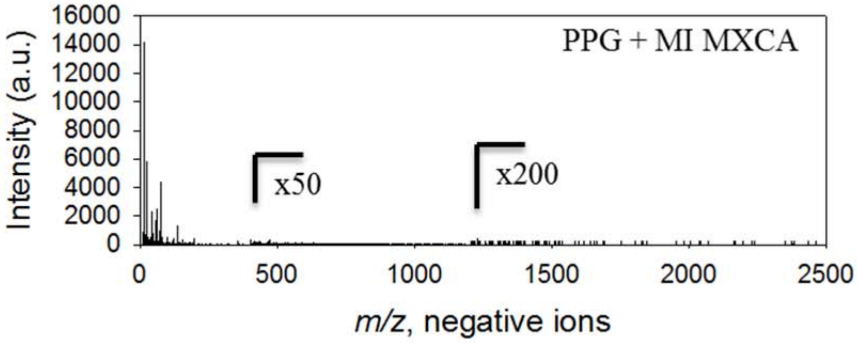
PPG + MI MXCA
x50
x200
Intensity (a.u.)
16000
14000
12000
10000
8000
6000
4000
2000
0
0
500
1000
1500
2000
2500
m/z, negative ions

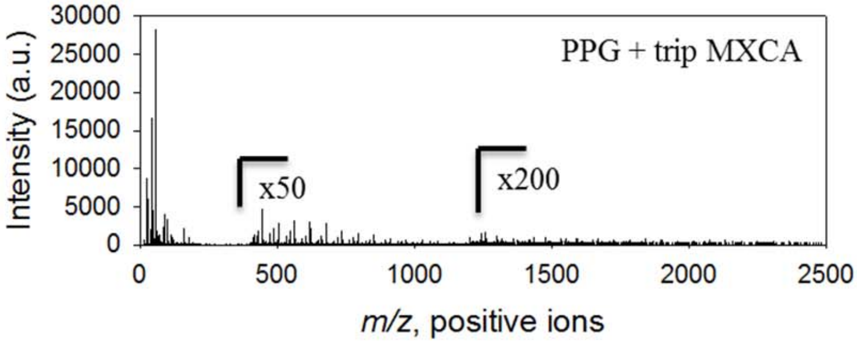
PPG + trip MXCA
x50
x200
Intensity (a.u.)
30000
25000
20000
15000
10000
5000
0
0
500
1000
1500
2000
2500
m/z, positive ions

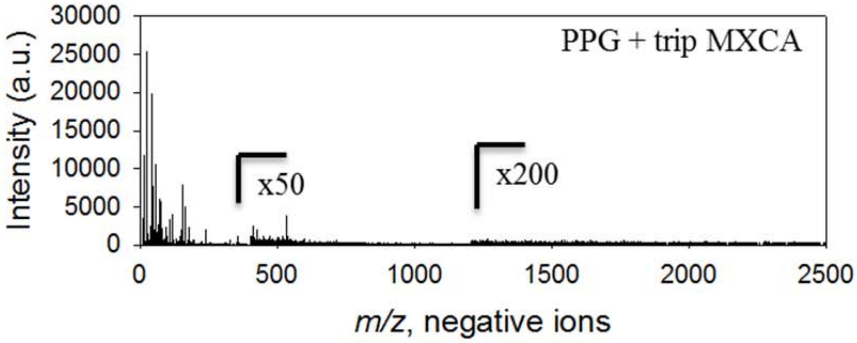
PPG + trip MXCA
x50
x200
Intensity (a.u.)
30000
25000
20000
15000
10000
5000
0
0
500
1000
1500
2000
2500
m/z, negative ions

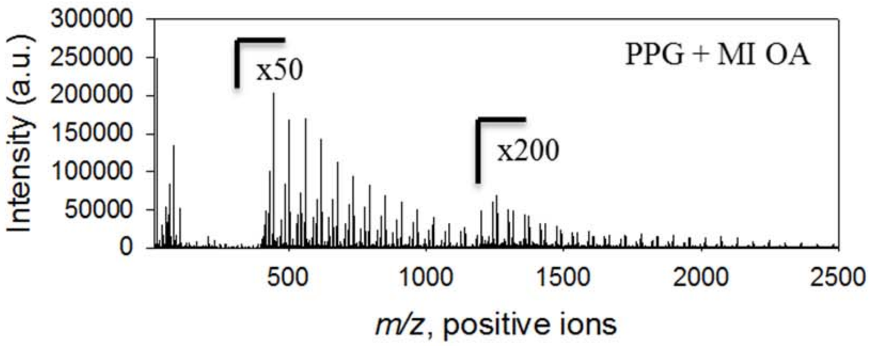
PPG + MI OA
x50
x200
Intensity (a.u.)
300000
250000
200000
150000
100000
50000
0
500
1000
1500
2000
2500
m/z, positive ions

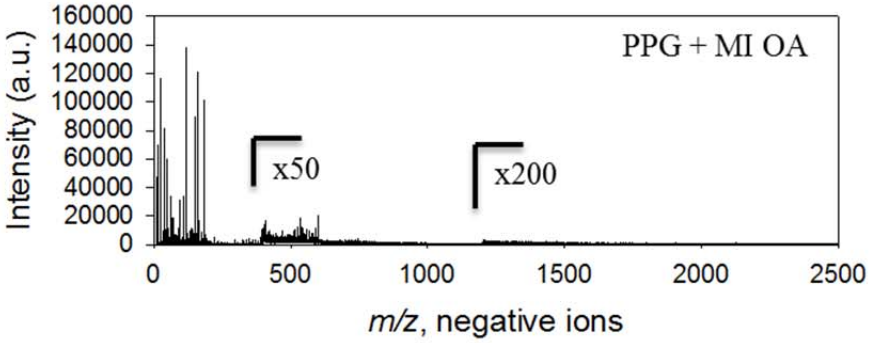
PPG + MI OA
x50
x200
Intensity (a.u.)
160000
140000
120000
100000
80000
60000
40000
20000
0
0
500
1000
1500
2000
2500
m/z, negative ions

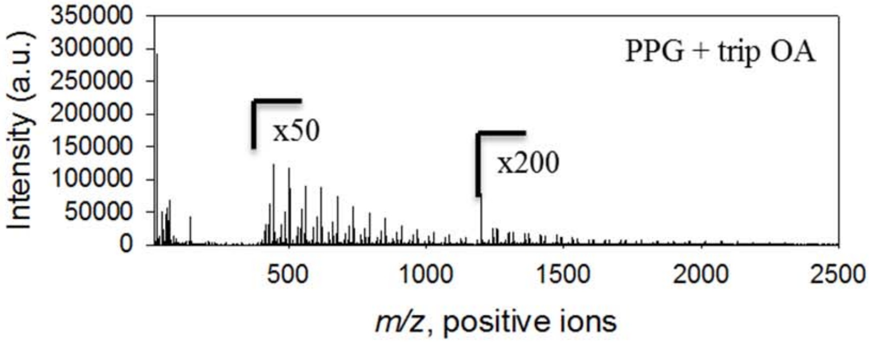
PPG + trip OA
x50
x200
Intensity (a.u.)
350000
300000
250000
200000
150000
100000
50000
0
500
1000
1500
2000
2500
m/z, positive ions

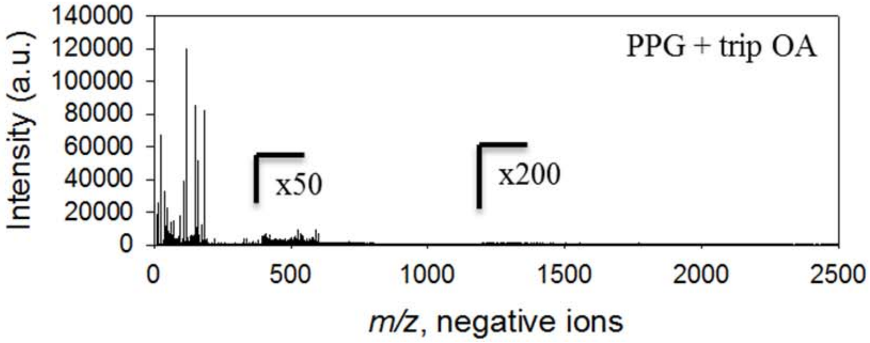
PPG + trip OA
x50
x200
Intensity (a.u.)
140000
120000
100000
80000
60000
40000
20000
0
0
500
1000
1500
2000
2500
m/z, negative ions

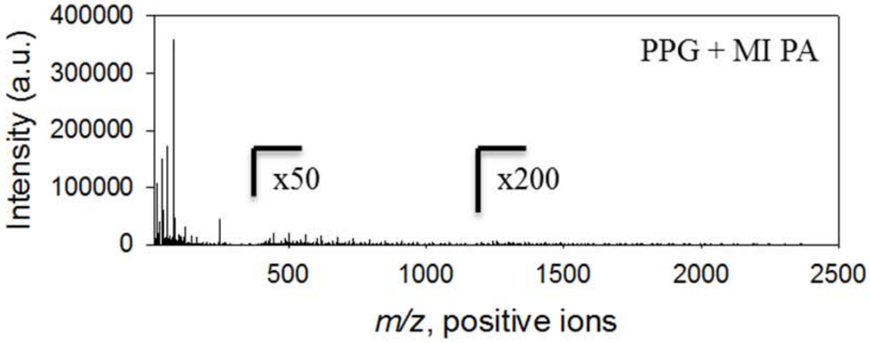
PPG + MI PA
Intensity (a.u.)
400000
300000
200000
100000
0
x50
x200
500
1000
1500
2000
2500
m/z, positive ions

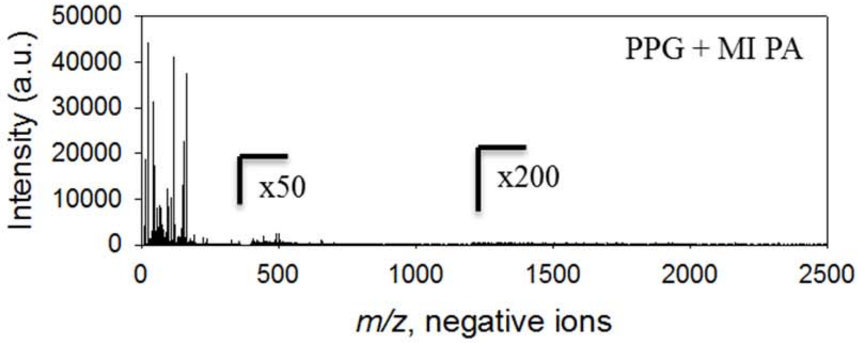
PPG + MI PA
Intensity (a.u.)
50000
40000
30000
20000
10000
0
x50
x200
0
500
1000
1500
2000
2500
m/z, negative ions

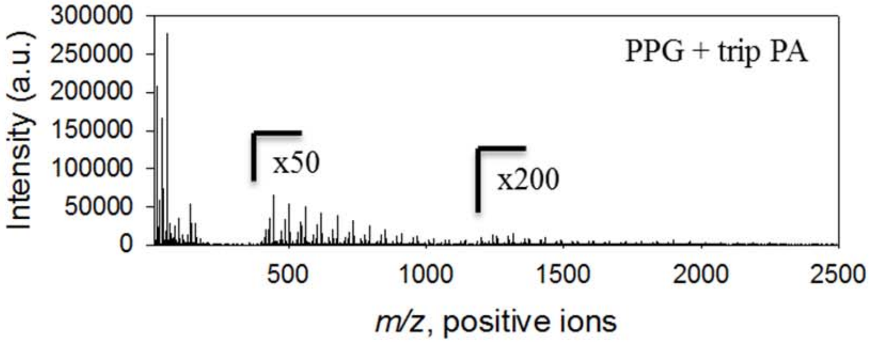
PPG + trip PA
Intensity (a.u.)
300000
250000
200000
150000
100000
50000
0
x50
x200
500
1000
1500
2000
2500
m/z, positive ions

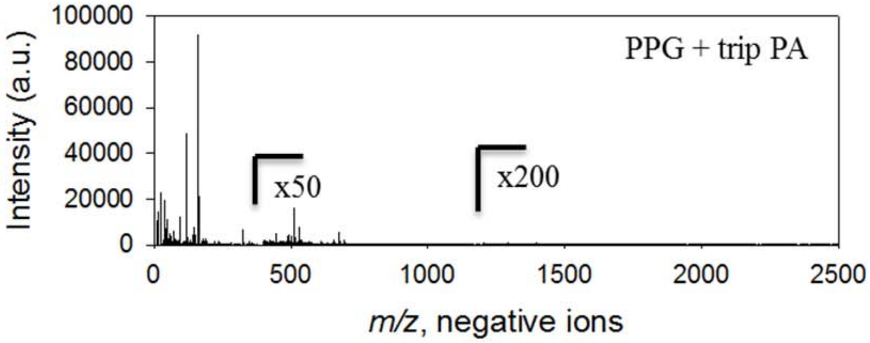
PPG + trip PA
Intensity (a.u.)
100000
80000
60000
40000
20000
0
x50
x200
0
500
1000
1500
2000
2500
m/z, negative ions

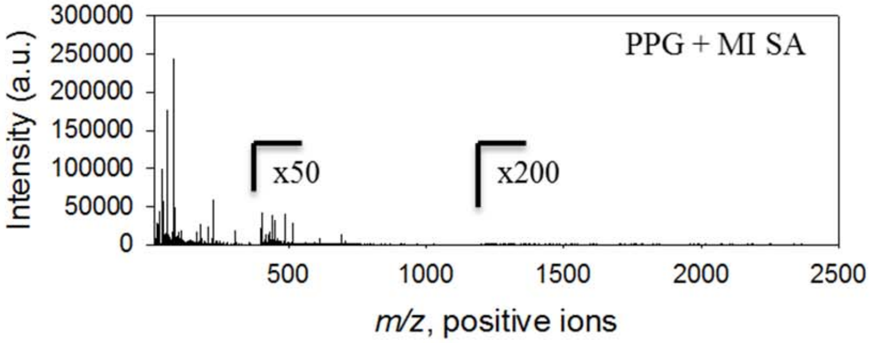
PPG + MI SA
x50
x200
Intensity (a.u.)
300000
250000
200000
150000
100000
50000
0
500
1000
1500
2000
2500
m/z, positive ions

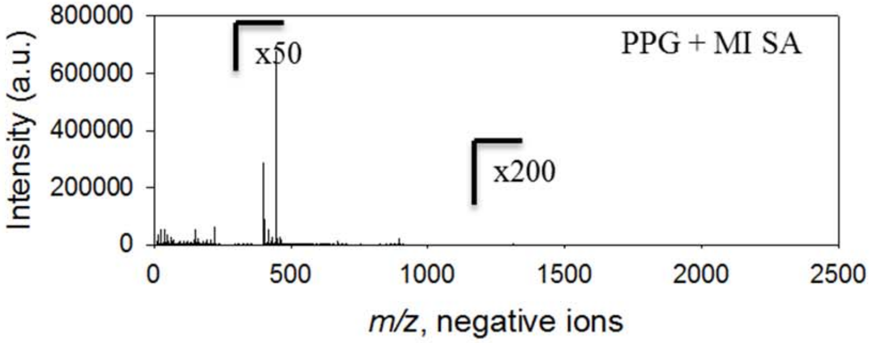
PPG + MI SA
x50
x200
Intensity (a.u.)
800000
600000
400000
200000
0
0
500
1000
1500
2000
2500
m/z, negative ions

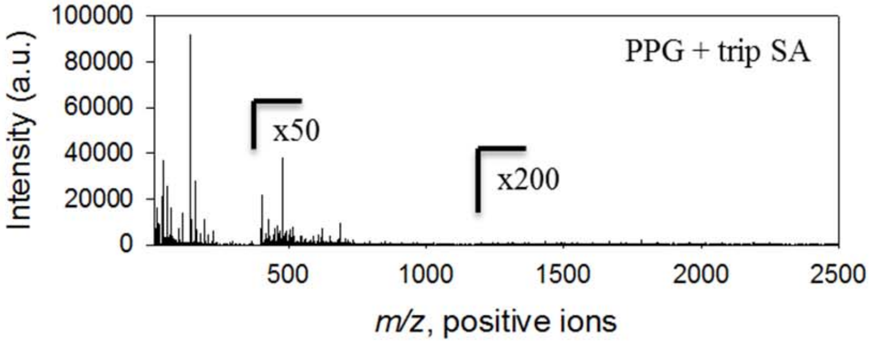
PPG + trip SA
x50
x200
Intensity (a.u.)
100000
80000
60000
40000
20000
0
500
1000
1500
2000
2500
m/z, positive ions

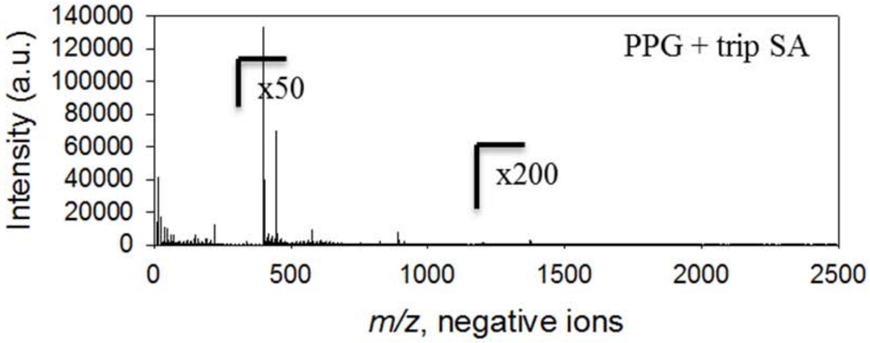
PPG + trip SA
x50
x200
Intensity (a.u.)
140000
120000
100000
80000
60000
40000
20000
0
0
500
1000
1500
2000
2500
m/z, negative ions

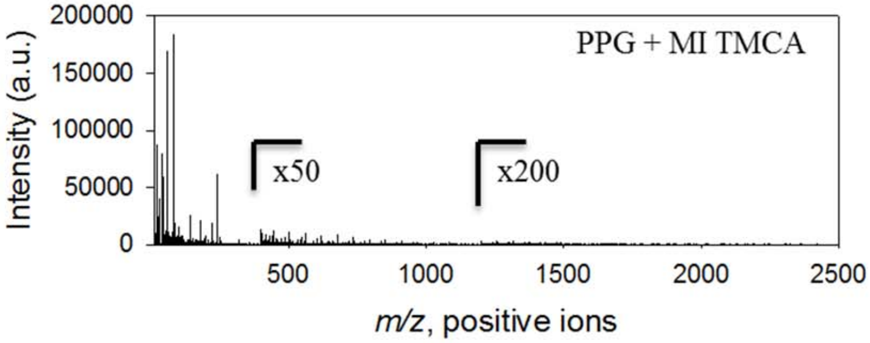

Intensity (a.u.)
200000
150000
100000
50000
0
PPG + MI TMCA
x50
x200
500
1000
1500
2000
2500
m/z, positive ions

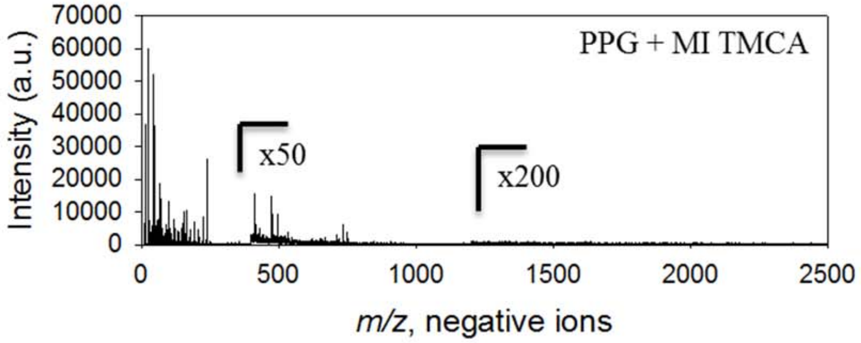

Intensity (a.u.)
70000
60000
50000
40000
30000
20000
10000
0
PPG + MI TMCA
x50
x200
0
500
1000
1500
2000
2500
m/z, negative ions

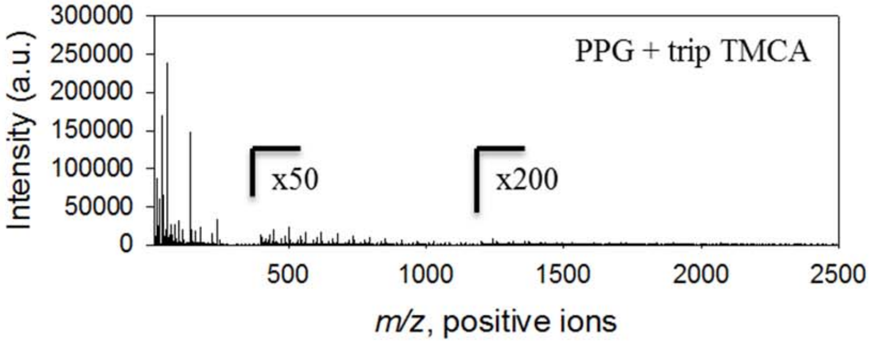

Intensity (a.u.)
300000
250000
200000
150000
100000
50000
0
PPG + trip TMCA
x50
x200
500
1000
1500
2000
2500
m/z, positive ions

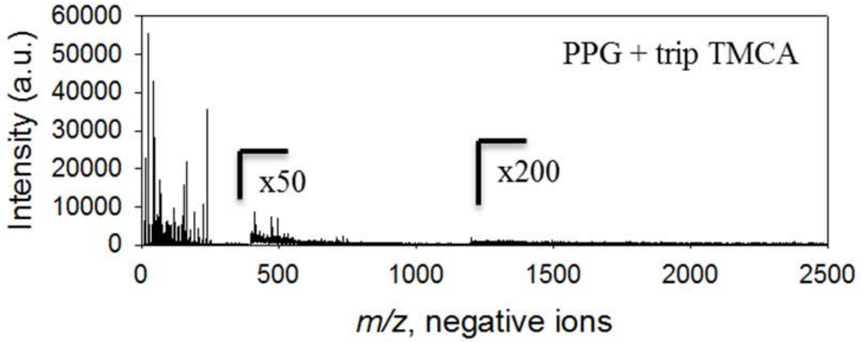

Intensity (a.u.)
60000
50000
40000
30000
20000
10000
0
PPG + trip TMCA
x50
x200
0
500
1000
1500
2000
2500
m/z, negative ions

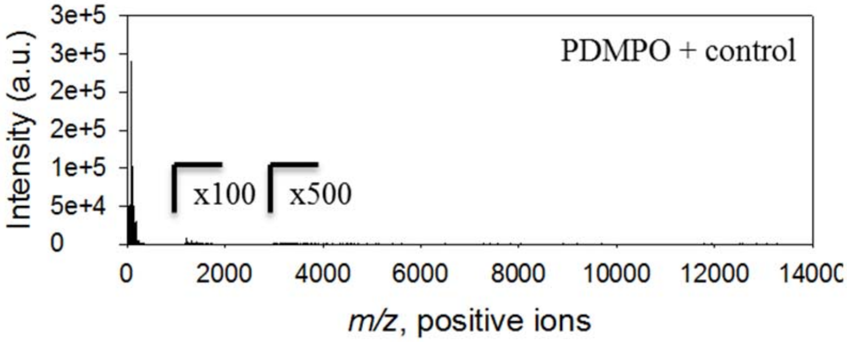
3e+5
3e+5
2e+5
2e+5
1e+5
5e+4
0
Intensity (a.u.)
PDMPO + control
x100
x500
0
2000
4000
6000
8000
10000
12000
1400
m/z, positive ions

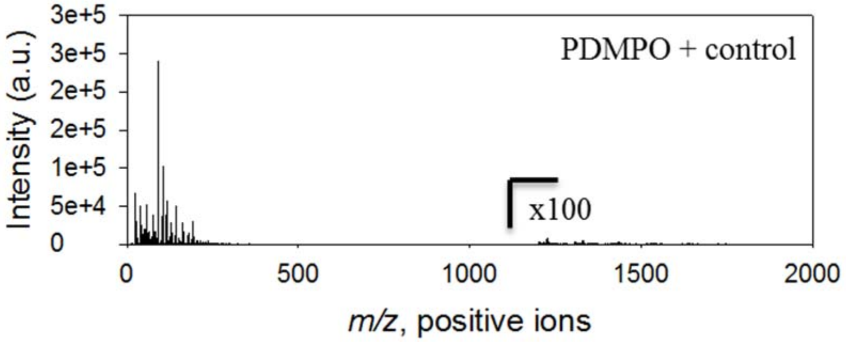
3e+5
3e+5
2e+5
2e+5
1e+5
5e+4
0
Intensity (a.u.)
PDMPO + control
x100
0
500
1000
1500
2000
m/z, positive ions

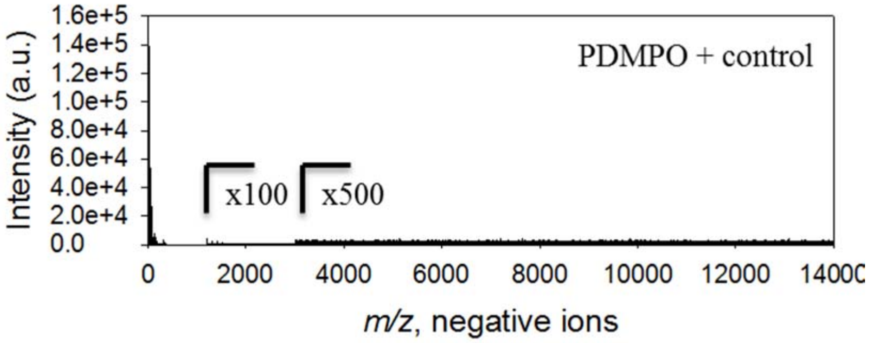
1.6e+5
1.4e+5
1.2e+5
1.0e+5
8.0e+4
6.0e+4
4.0e+4
2.0e+4
0.0
Intensity (a.u.)
PDMPO + control
x100
x500
0
2000
4000
6000
8000
10000
12000
1400
m/z, negative ions

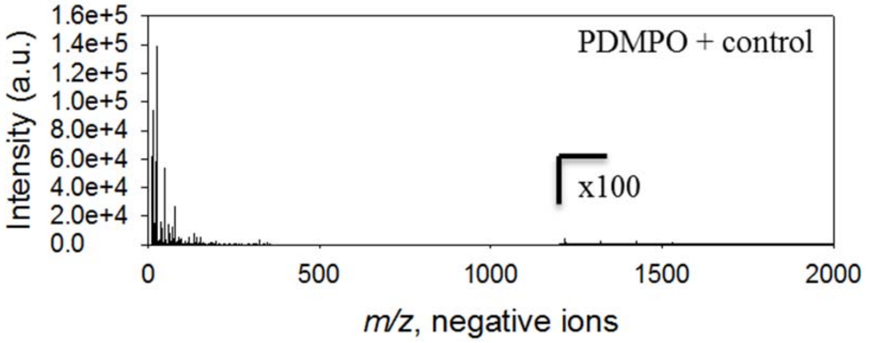
1.6e+5
1.4e+5
1.2e+5
1.0e+5
8.0e+4
6.0e+4
4.0e+4
2.0e+4
0.0
Intensity (a.u.)
PDMPO + control
x100
0
500
1000
1500
2000
m/z, negative ions

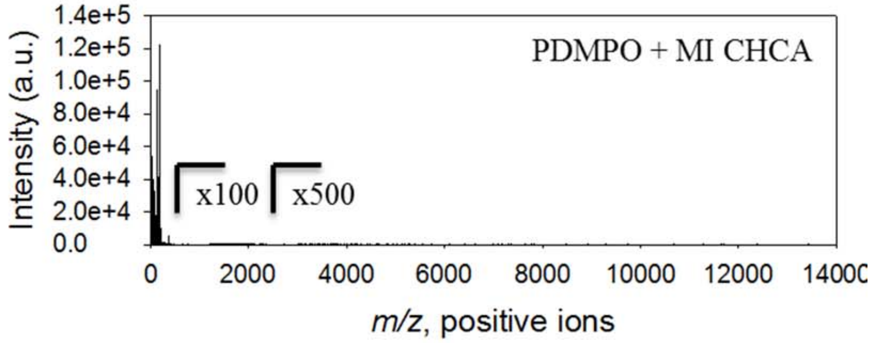
PDMPO + MI CHCA
Intensity (a.u.)
1.4e+5
1.2e+5
1.0e+5
8.0e+4
6.0e+4
4.0e+4
2.0e+4
0.0
x100
x500
0
2000
4000
6000
8000
10000
12000
14000
m/z, positive ions

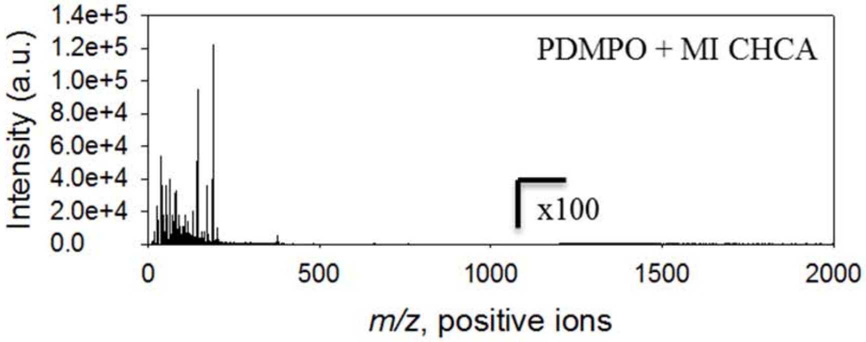
PDMPO + MI CHCA
Intensity (a.u.)
1.4e+5
1.2e+5
1.0e+5
8.0e+4
6.0e+4
4.0e+4
2.0e+4
0.0
x100
0
500
1000
1500
2000
m/z, positive ions

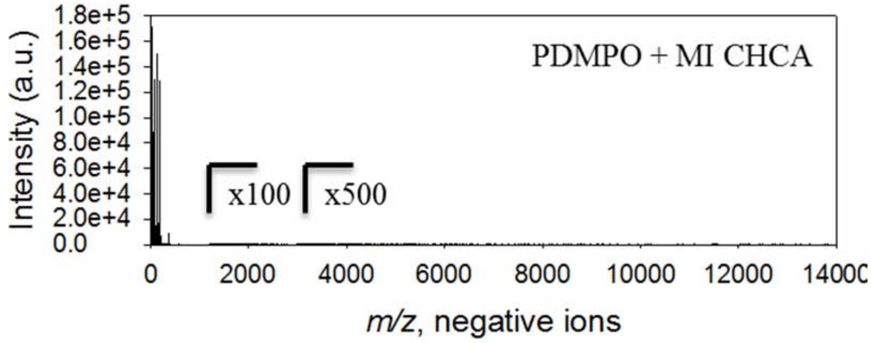
PDMPO + MI CHCA
Intensity (a.u.)
1.8e+5
1.6e+5
1.4e+5
1.2e+5
1.0e+5
8.0e+4
6.0e+4
4.0e+4
2.0e+4
0.0
x100
x500
0
2000
4000
6000
8000
10000
12000
14000
m/z, negative ions

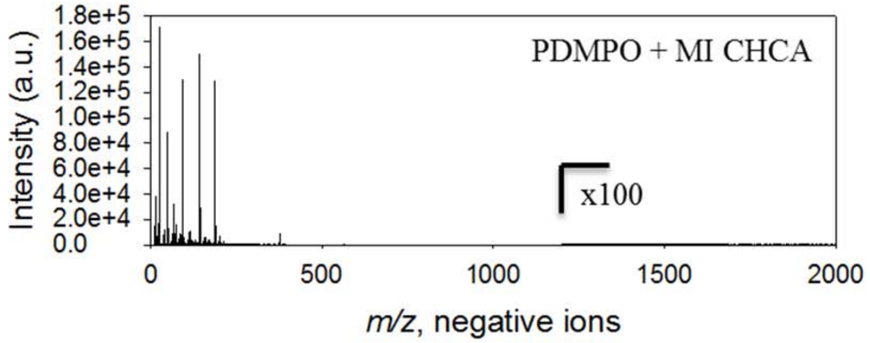
PDMPO + MI CHCA
Intensity (a.u.)
1.8e+5
1.6e+5
1.4e+5
1.2e+5
1.0e+5
8.0e+4
6.0e+4
4.0e+4
2.0e+4
0.0
x100
0
500
1000
1500
2000
m/z, negative ions

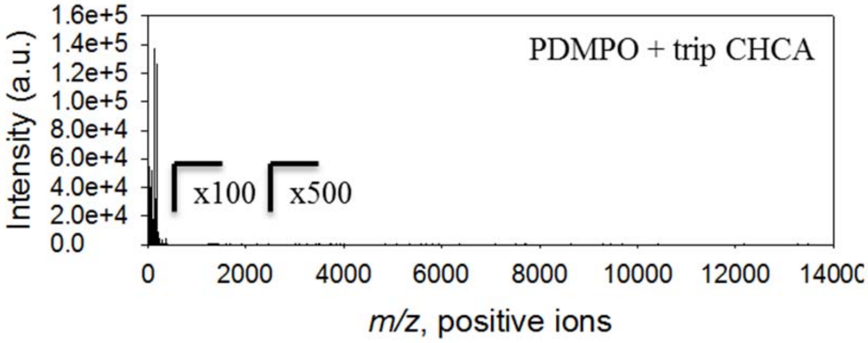
PDMPO + trip CHCA
x100
x500
Intensity (a.u.)
1.6e+5
1.4e+5
1.2e+5
1.0e+5
8.0e+4
6.0e+4
4.0e+4
2.0e+4
0.0
0
2000
4000
6000
8000
10000
12000
1400C
m/z, positive ions

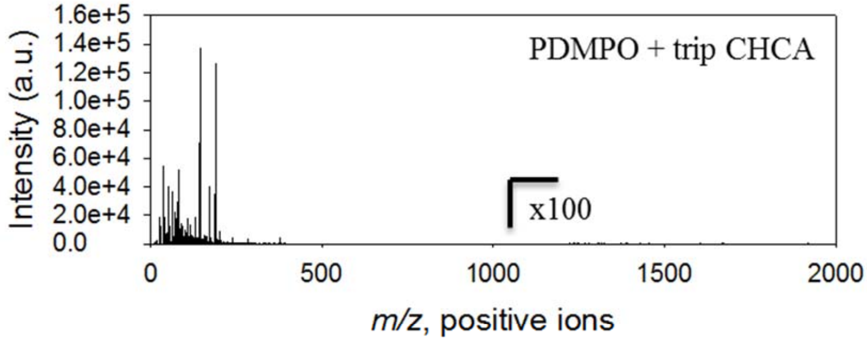
PDMPO + trip CHCA
x100
Intensity (a.u.)
1.6e+5
1.4e+5
1.2e+5
1.0e+5
8.0e+4
6.0e+4
4.0e+4
2.0e+4
0.0
0
500
1000
1500
2000
m/z, positive ions

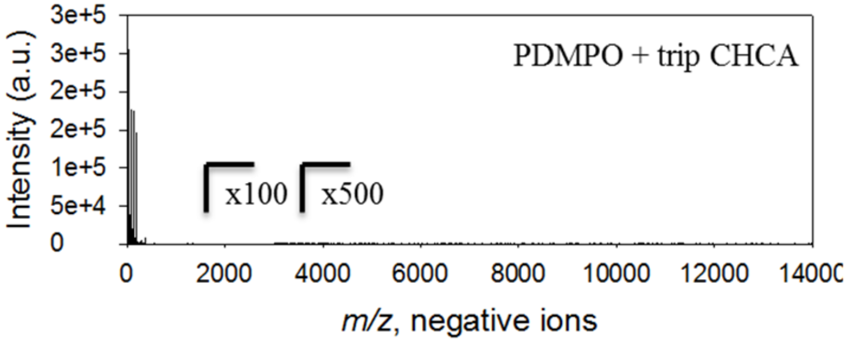
PDMPO + trip CHCA
x100
x500
Intensity (a.u.)
3e+5
3e+5
2e+5
2e+5
1e+5
5e+4
0
0
2000
4000
6000
8000
10000
12000
1400C
m/z, negative ions

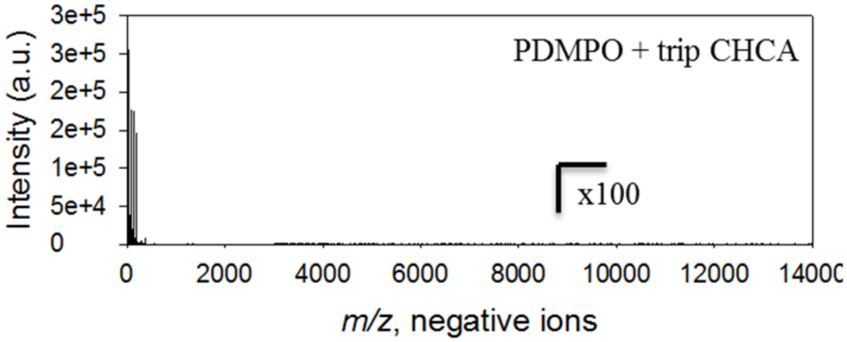
PDMPO + trip CHCA
x100
Intensity (a.u.)
3e+5
3e+5
2e+5
2e+5
1e+5
5e+4
0
0
2000
4000
6000
8000
10000
12000
1400C
m/z, negative ions

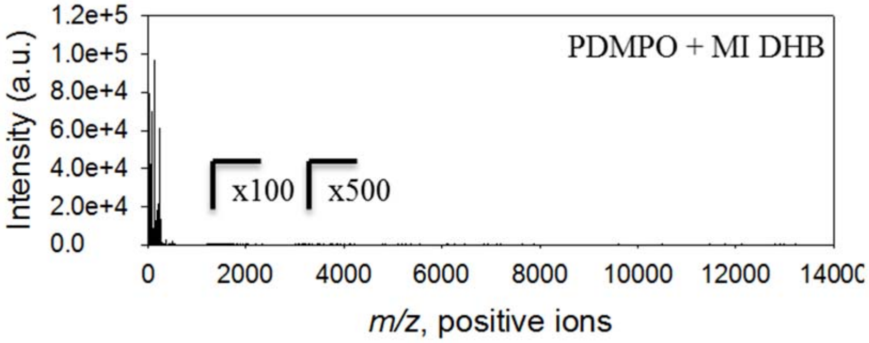
PDMPO + MI DHB
x100
x500
Intensity (a.u.)
1.2e+5
1.0e+5
8.0e+4
6.0e+4
4.0e+4
2.0e+4
0.0
0
2000
4000
6000
8000
10000
12000
1400C
m/z, positive ions

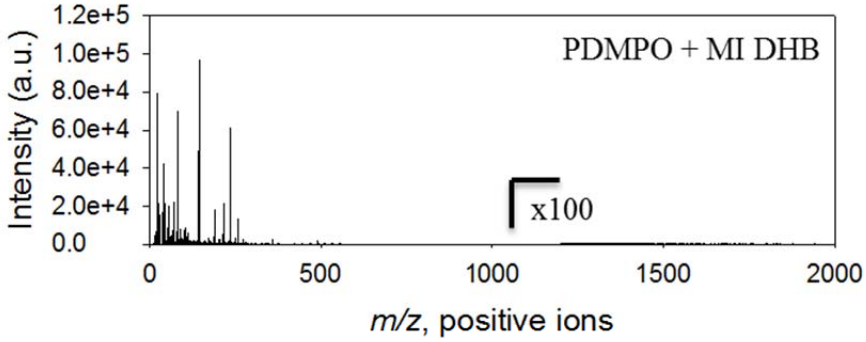
PDMPO + MI DHB
x100
Intensity (a.u.)
1.2e+5
1.0e+5
8.0e+4
6.0e+4
4.0e+4
2.0e+4
0.0
0
500
1000
1500
2000
m/z, positive ions

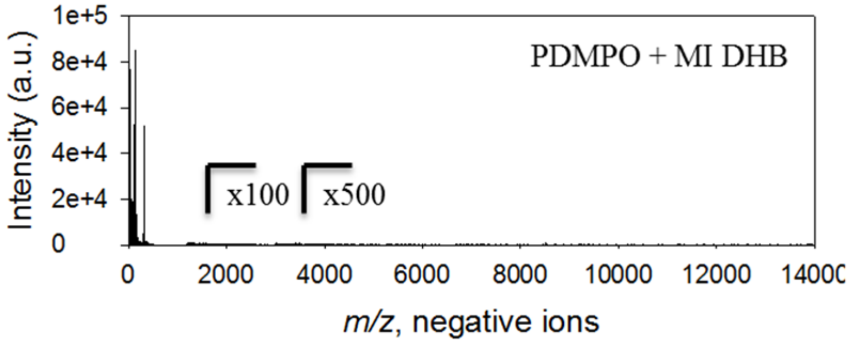
PDMPO + MI DHB
x100
x500
Intensity (a.u.)
1e+5
8e+4
6e+4
4e+4
2e+4
0
0
2000
4000
6000
8000
10000
12000
1400C
m/z, negative ions

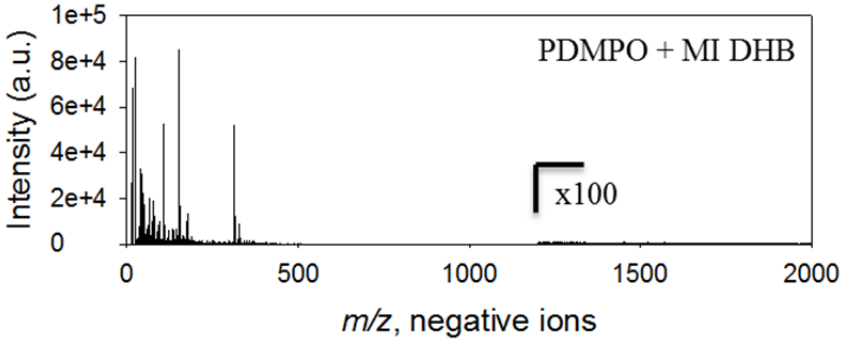
PDMPO + MI DHB
x100
Intensity (a.u.)
1e+5
8e+4
6e+4
4e+4
2e+4
0
0
500
1000
1500
2000
m/z, negative ions

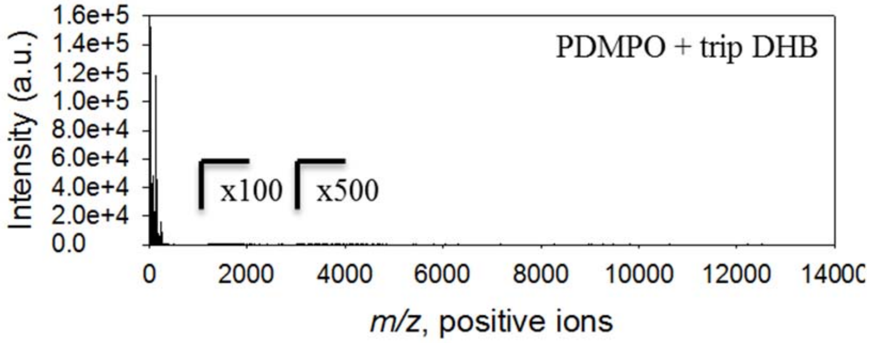
PDMPO + trip DHB
x100
x500
Intensity (a.u.)
1.6e+5
1.4e+5
1.2e+5
1.0e+5
8.0e+4
6.0e+4
4.0e+4
2.0e+4
0.0
0
2000
4000
6000
8000
10000
12000
14000
m/z, positive ions

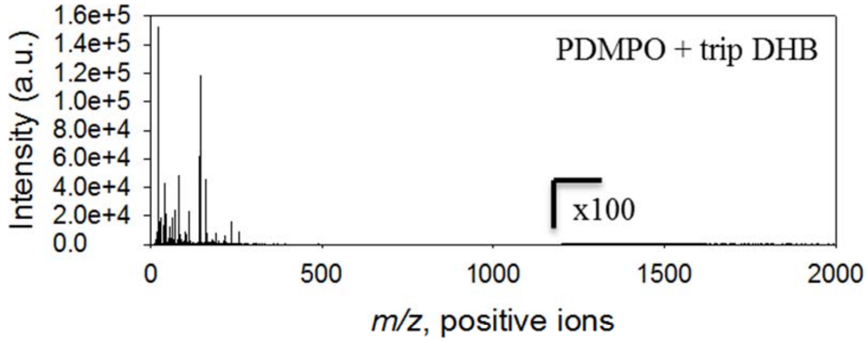
PDMPO + trip DHB
x100
Intensity (a.u.)
1.6e+5
1.4e+5
1.2e+5
1.0e+5
8.0e+4
6.0e+4
4.0e+4
2.0e+4
0.0
0
500
1000
1500
2000
m/z, positive ions

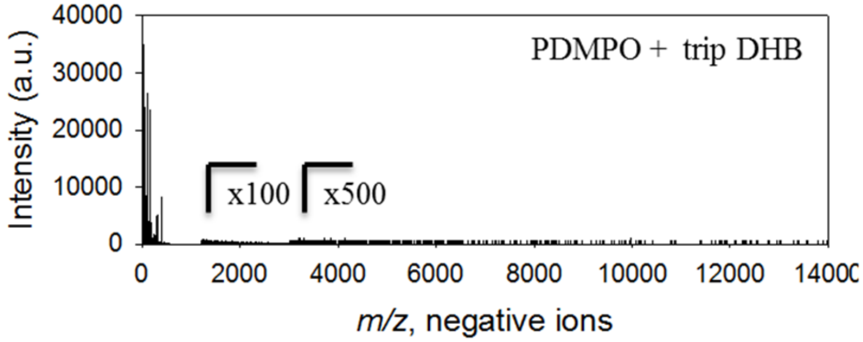
PDMPO + trip DHB
x100
x500
Intensity (a.u.)
40000
30000
20000
10000
0
0
2000
4000
6000
8000
10000
12000
14000
m/z, negative ions

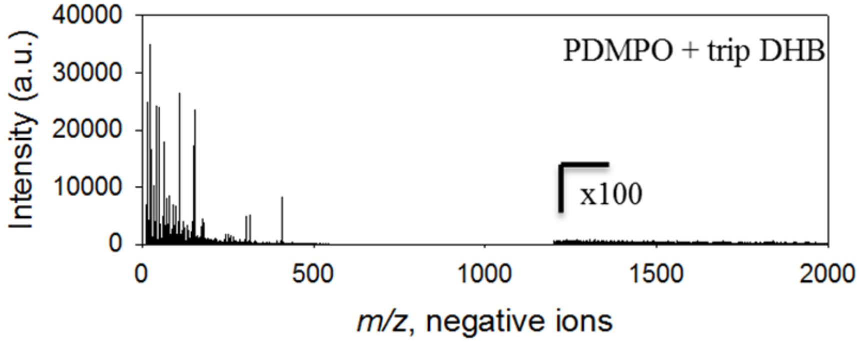
PDMPO + trip DHB
x100
Intensity (a.u.)
40000
30000
20000
10000
0
0
500
1000
1500
2000
m/z, negative ions

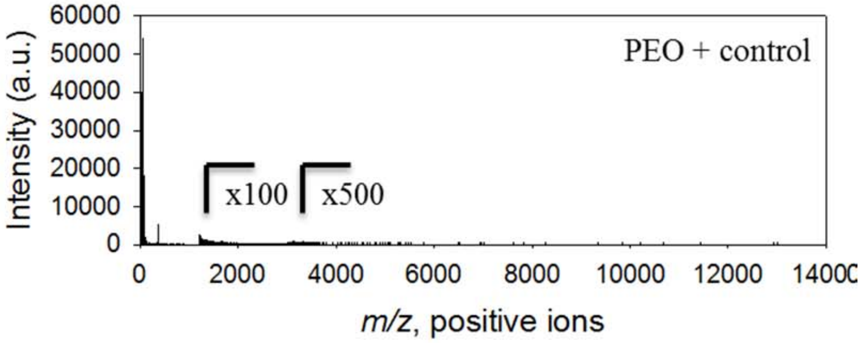
PEO + control
x100
x500
Intensity (a.u.)
60000
50000
40000
30000
20000
10000
0
0
2000
4000
6000
8000
10000
12000
1400
m/z, positive ions

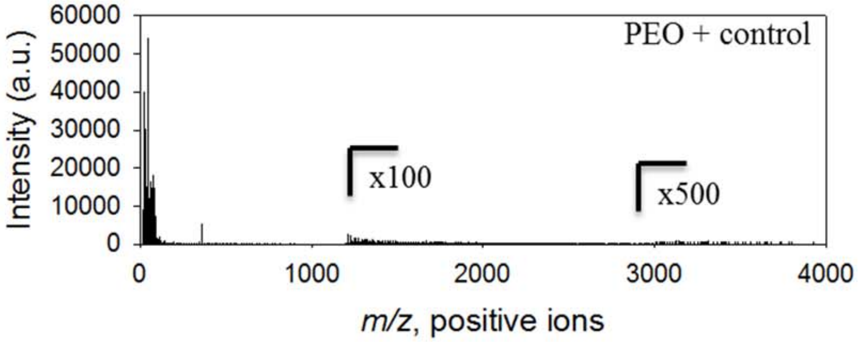
PEO + control
x100
x500
Intensity (a.u.)
60000
50000
40000
30000
20000
10000
0
0
1000
2000
3000
4000
m/z, positive ions

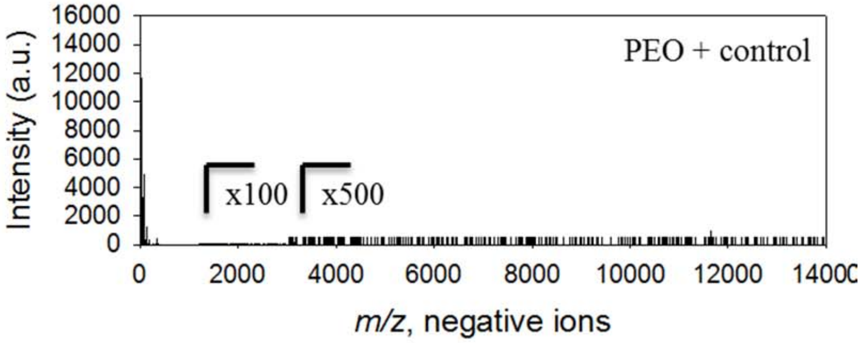
PEO + control
x100
x500
Intensity (a.u.)
16000
14000
12000
10000
8000
6000
4000
2000
0
0
2000
4000
6000
8000
10000
12000
1400
m/z, negative ions

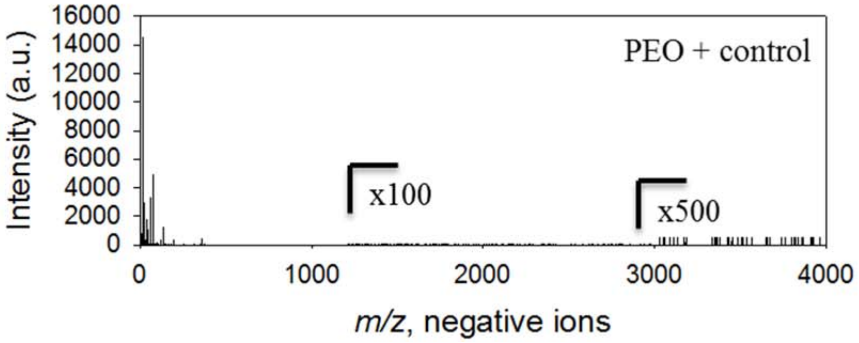
PEO + control
x100
x500
Intensity (a.u.)
16000
14000
12000
10000
8000
6000
4000
2000
0
0
1000
2000
3000
4000
m/z, negative ions

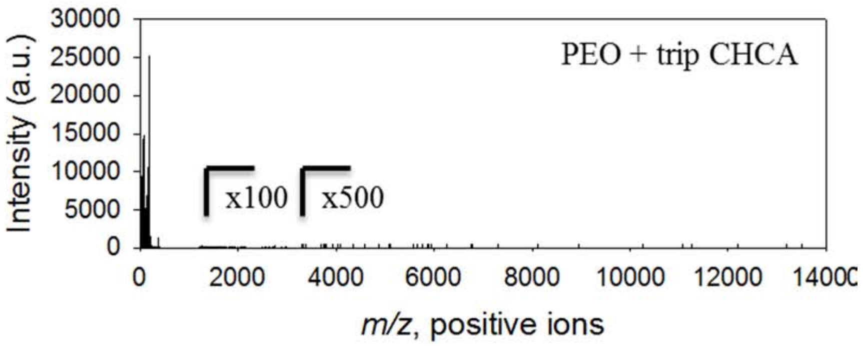
PEO + trip CHCA
x100
x500
Intensity (a.u.)
30000
25000
20000
15000
10000
5000
0
0
2000
4000
6000
8000
10000
12000
14000
m/z, positive ions

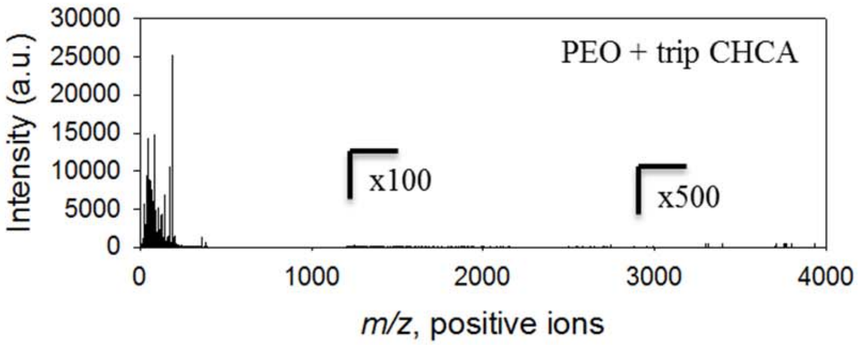
PEO + trip CHCA
x100
x500
Intensity (a.u.)
30000
25000
20000
15000
10000
5000
0
0
1000
2000
3000
4000
m/z, positive ions

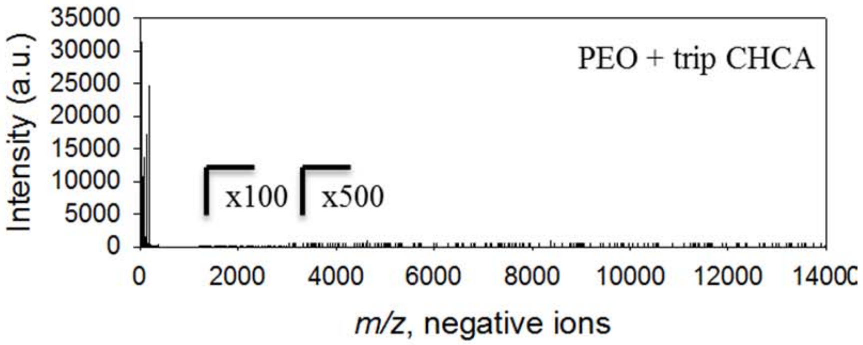
PEO + trip CHCA
x100
x500
Intensity (a.u.)
35000
30000
25000
20000
15000
10000
5000
0
0
2000
4000
6000
8000
10000
12000
14000
m/z, negative ions

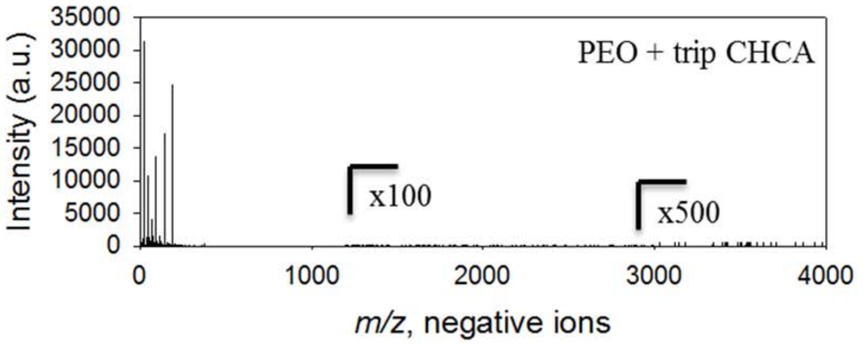
PEO + trip CHCA
x100
x500
Intensity (a.u.)
35000
30000
25000
20000
15000
10000
5000
0
0
1000
2000
3000
4000
m/z, negative ions

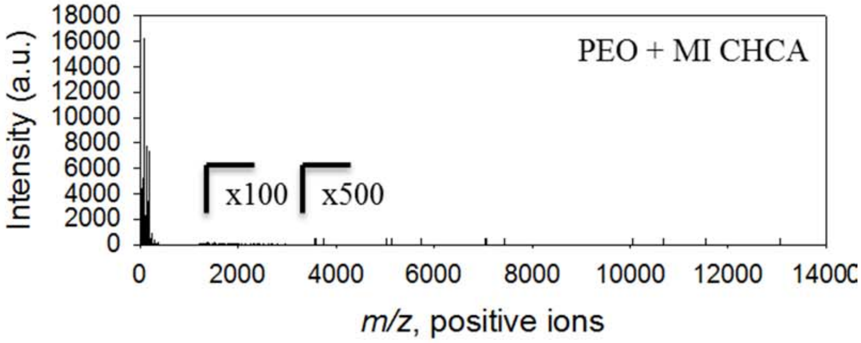
PEO + MI CHCA
x100
x500
Intensity (a.u.)
18000
16000
14000
12000
10000
8000
6000
4000
2000
0
0
2000
4000
6000
8000
10000
12000
14000
m/z, positive ions

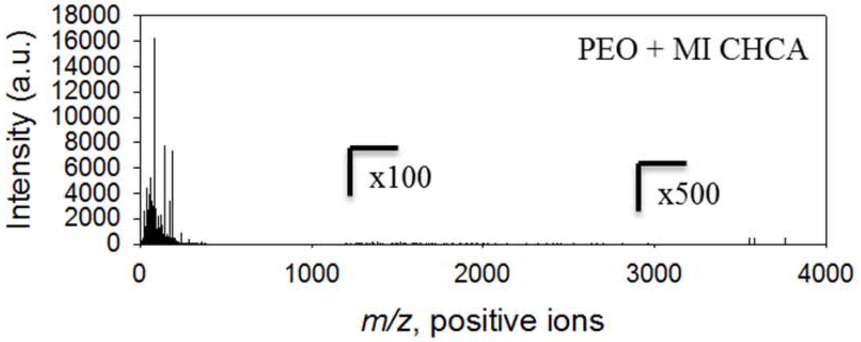
PEO + MI CHCA
x100
x500
Intensity (a.u.)
18000
16000
14000
12000
10000
8000
6000
4000
2000
0
0
1000
2000
3000
4000
m/z, positive ions

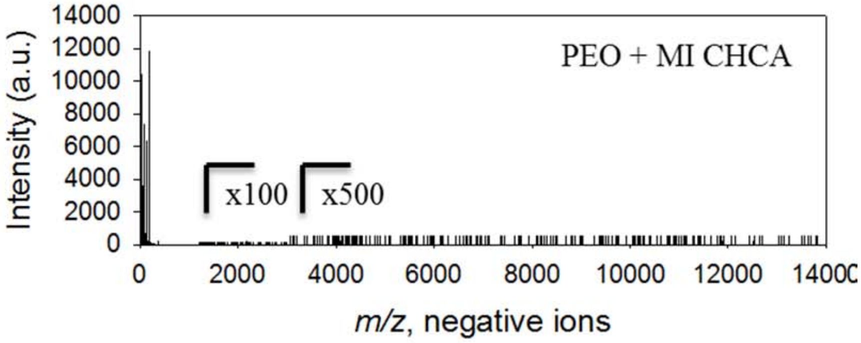
PEO + MI CHCA
x100
x500
Intensity (a.u.)
14000
12000
10000
8000
6000
4000
2000
0
0
2000
4000
6000
8000
10000
12000
14000
m/z, negative ions

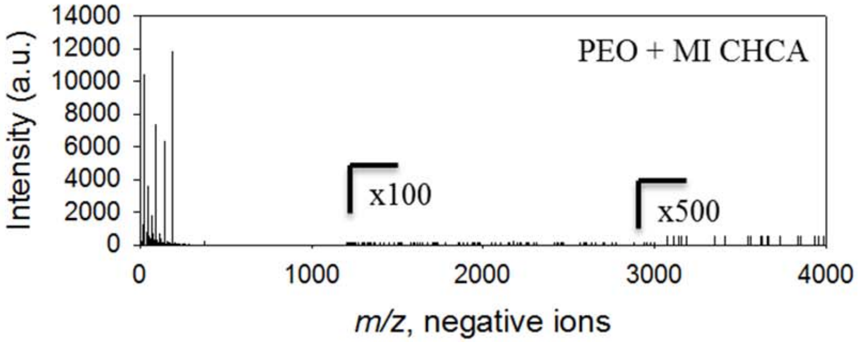
PEO + MI CHCA
x100
x500
Intensity (a.u.)
14000
12000
10000
8000
6000
4000
2000
0
0
1000
2000
3000
4000
m/z, negative ions

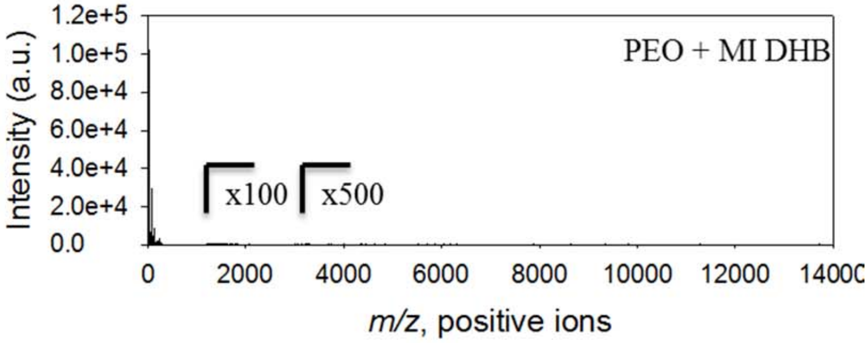
PEO + MI DHB
x100
x500
Intensity (a.u.)
1.2e+5
1.0e+5
8.0e+4
6.0e+4
4.0e+4
2.0e+4
0.0
0
2000
4000
6000
8000
10000
12000
1400
m/z, positive ions

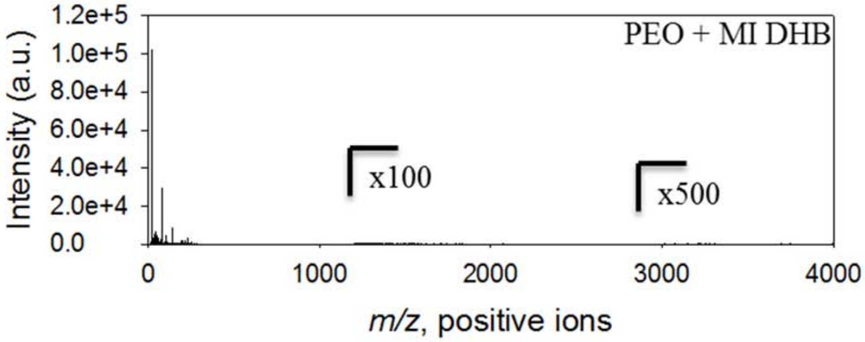
PEO + MI DHB
x100
x500
Intensity (a.u.)
1.2e+5
1.0e+5
8.0e+4
6.0e+4
4.0e+4
2.0e+4
0.0
0
1000
2000
3000
4000
m/z, positive ions

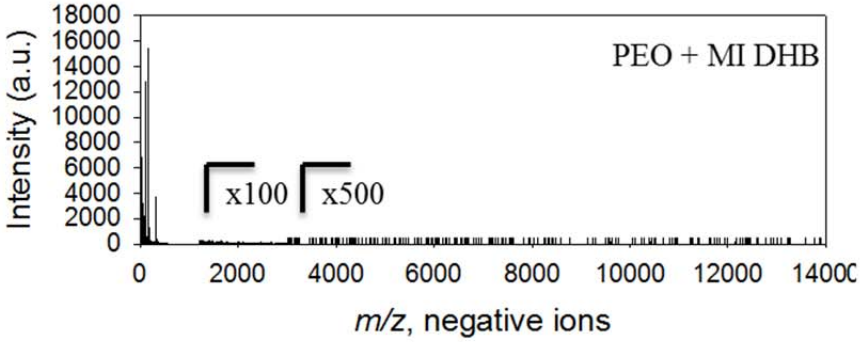
PEO + MI DHB
x100
x500
Intensity (a.u.)
18000
16000
14000
12000
10000
8000
6000
4000
2000
0
0
2000
4000
6000
8000
10000
12000
1400
m/z, negative ions

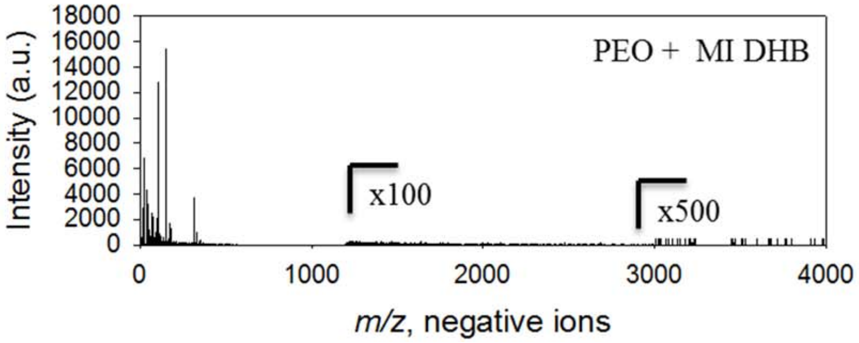
PEO + MI DHB
x100
x500
Intensity (a.u.)
18000
16000
14000
12000
10000
8000
6000
4000
2000
0
0
1000
2000
3000
4000
m/z, negative ions

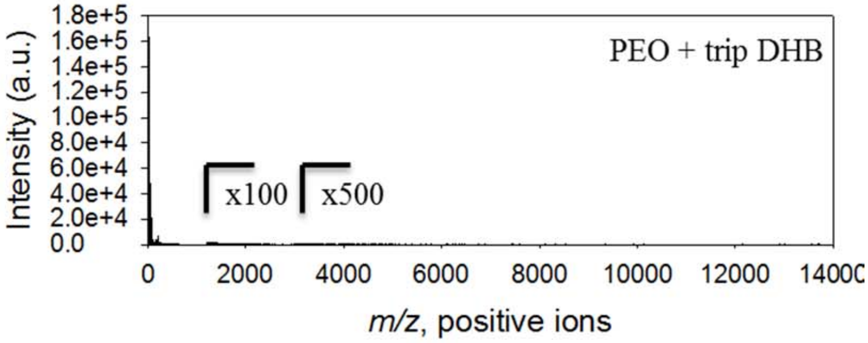
PEO + trip DHB
x100
x500
Intensity (a.u.)
1.8e+5
1.6e+5
1.4e+5
1.2e+5
1.0e+5
8.0e+4
6.0e+4
4.0e+4
2.0e+4
0.0
0
2000
4000
6000
8000
10000
12000
14000
m/z, positive ions

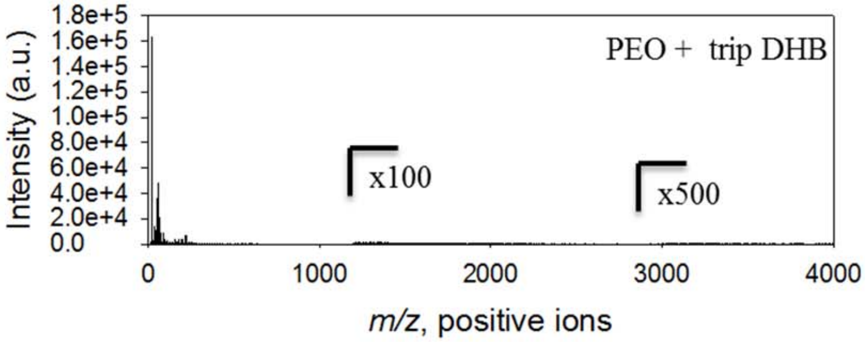
PEO + trip DHB
x100
x500
Intensity (a.u.)
1.8e+5
1.6e+5
1.4e+5
1.2e+5
1.0e+5
8.0e+4
6.0e+4
4.0e+4
2.0e+4
0.0
0
1000
2000
3000
4000
m/z, positive ions

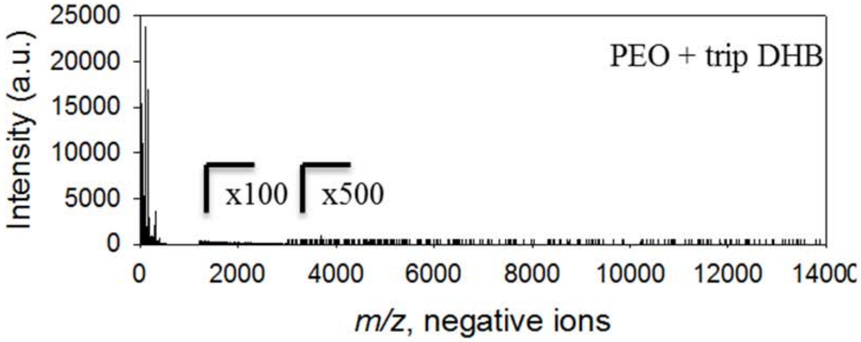
PEO + trip DHB
x100
x500
Intensity (a.u.)
25000
20000
15000
10000
5000
0
0
2000
4000
6000
8000
10000
12000
14000
m/z, negative ions

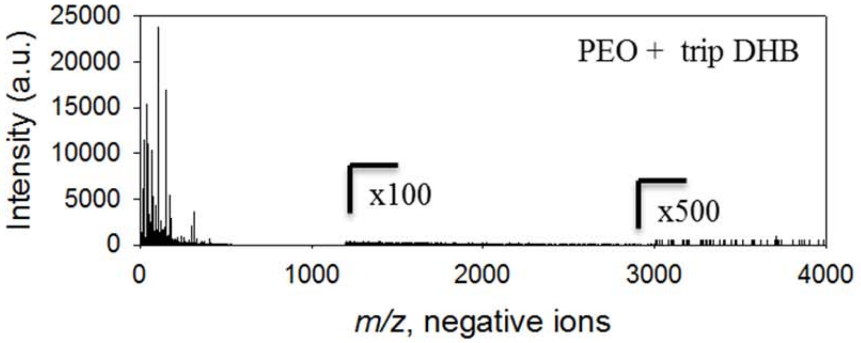
PEO + trip DHB
x100
x500
Intensity (a.u.)
25000
20000
15000
10000
5000
0
0
1000
2000
3000
4000
m/z, negative ions

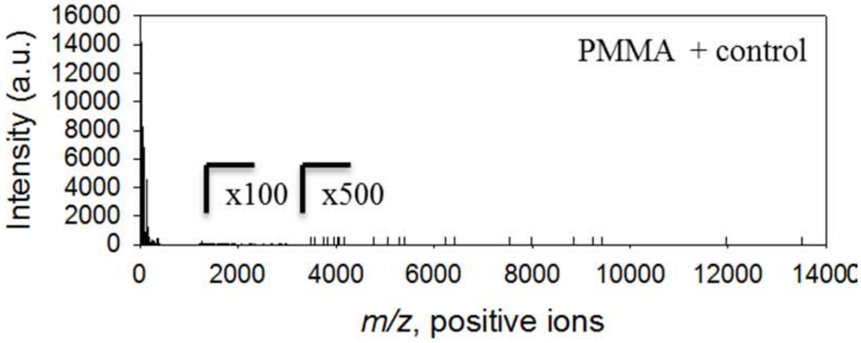
PMMA + control
Intensity (a.u.)
16000
14000
12000
10000
8000
6000
4000
2000
0
x100
x500
0
2000
4000
6000
8000
10000
12000
14000
m/z, positive ions

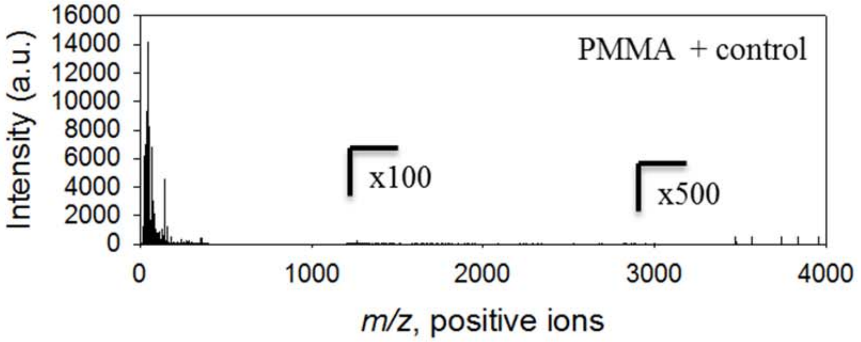
PMMA + control
Intensity (a.u.)
16000
14000
12000
10000
8000
6000
4000
2000
0
x100
x500
0
1000
2000
3000
4000
m/z, positive ions

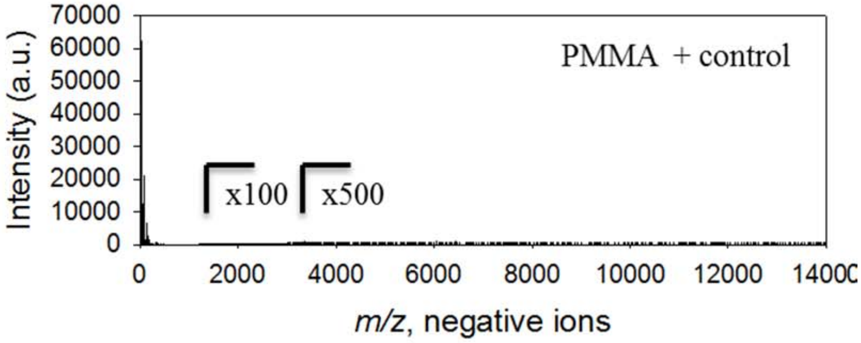
PMMA + control
Intensity (a.u.)
70000
60000
50000
40000
30000
20000
10000
0
x100
x500
0
2000
4000
6000
8000
10000
12000
14000
m/z, negative ions

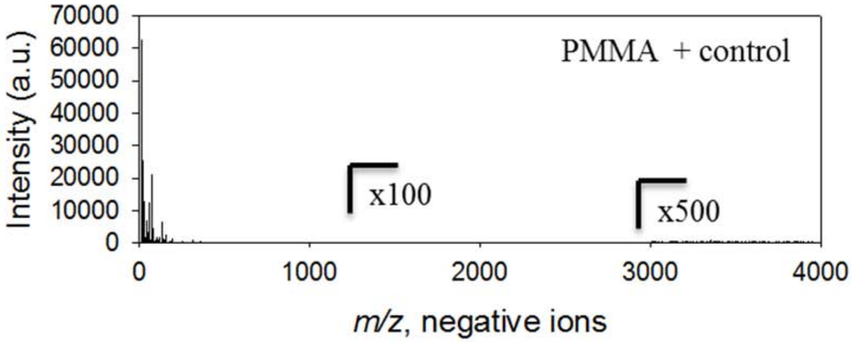
PMMA + control
Intensity (a.u.)
70000
60000
50000
40000
30000
20000
10000
0
x100
x500
0
1000
2000
3000
4000
m/z, negative ions

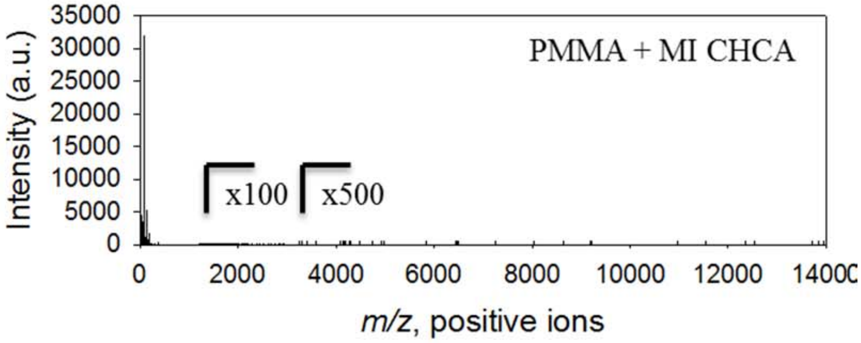
PMMA + MI CHCA
x100
x500
Intensity (a.u.)
35000
30000
25000
20000
15000
10000
5000
0
0
2000
4000
6000
8000
10000
12000
14000
m/z, positive ions

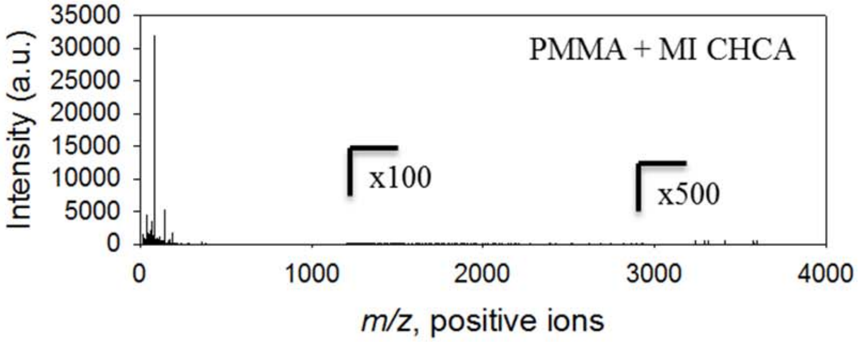
PMMA + MI CHCA
x100
x500
Intensity (a.u.)
35000
30000
25000
20000
15000
10000
5000
0
0
1000
2000
3000
4000
m/z, positive ions

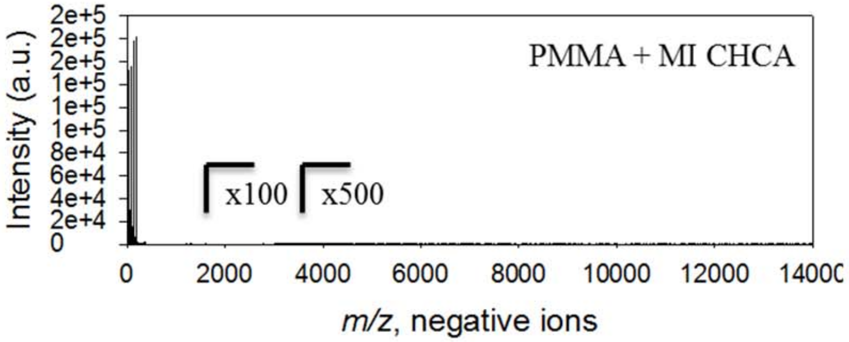
PMMA + MI CHCA
x100
x500
Intensity (a.u.)
2e+5
2e+5
2e+5
1e+5
1e+5
1e+5
8e+4
6e+4
4e+4
2e+4
0
0
2000
4000
6000
8000
10000
12000
14000
m/z, negative ions

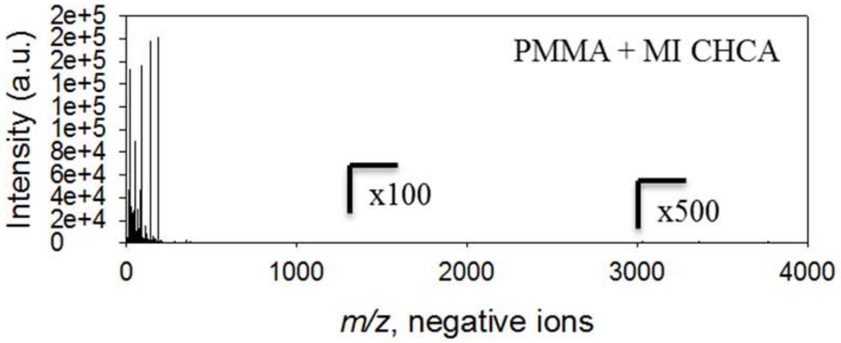
PMMA + MI CHCA
x100
x500
Intensity (a.u.)
2e+5
2e+5
2e+5
1e+5
1e+5
1e+5
8e+4
6e+4
4e+4
2e+4
0
0
1000
2000
3000
4000
m/z, negative ions

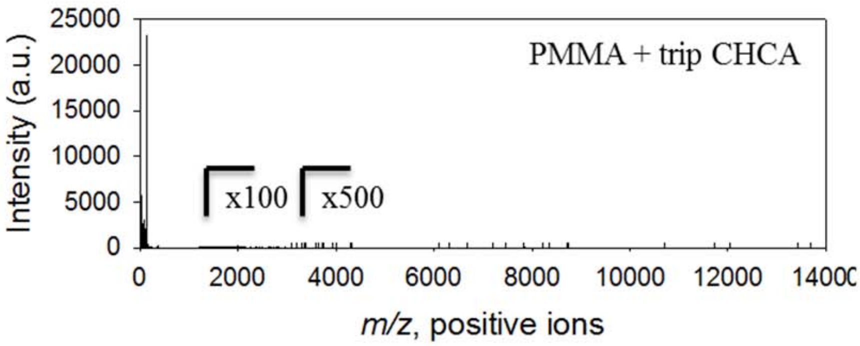
PMMA + trip CHCA
Intensity (a.u.)
25000
20000
15000
10000
5000
0
x100
x500
0
2000
4000
6000
8000
10000
12000
14000
m/z, positive ions

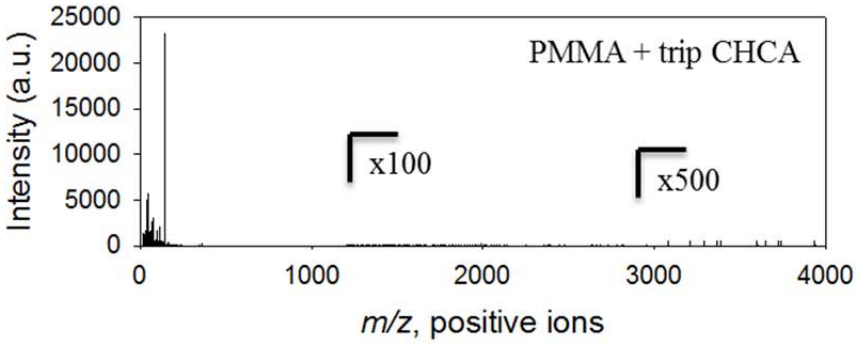
PMMA + trip CHCA
Intensity (a.u.)
25000
20000
15000
10000
5000
0
x100
x500
0
1000
2000
3000
4000
m/z, positive ions

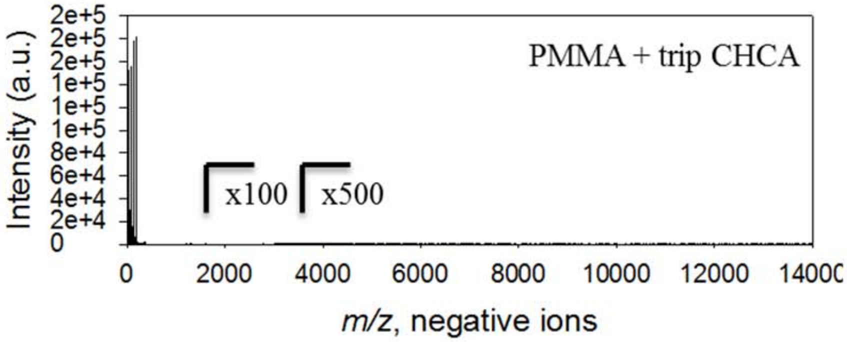
PMMA + trip CHCA
Intensity (a.u.)
2e+5
2e+5
2e+5
1e+5
1e+5
1e+5
8e+4
6e+4
4e+4
2e+4
0
x100
x500
0
2000
4000
6000
8000
10000
12000
14000
m/z, negative ions

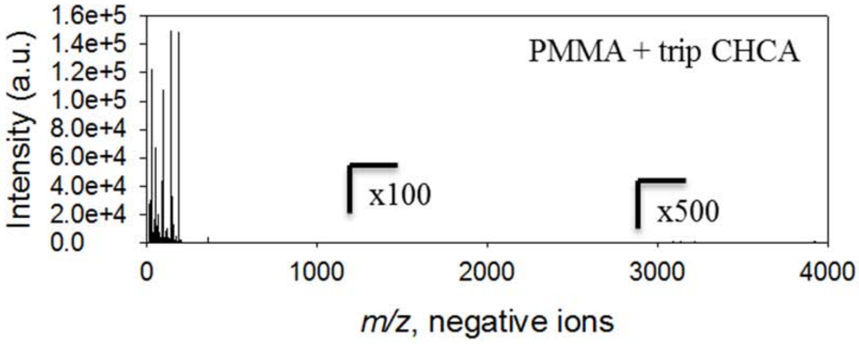
PMMA + trip CHCA
Intensity (a.u.)
1.6e+5
1.4e+5
1.2e+5
1.0e+5
8.0e+4
6.0e+4
4.0e+4
2.0e+4
0.0
x100
x500
0
1000
2000
3000
4000
m/z, negative ions

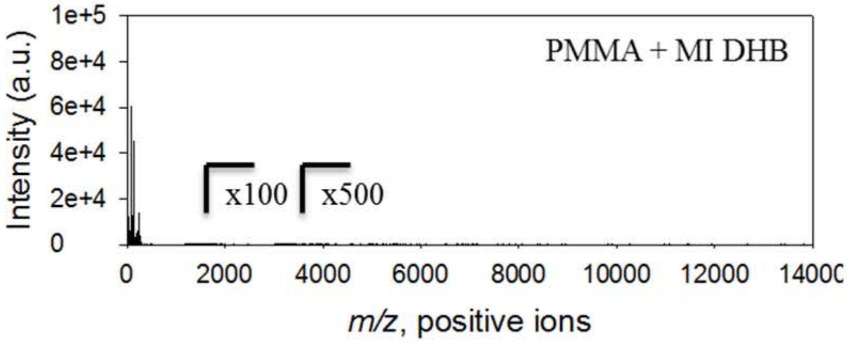
PMMA + MI DHB
x100
x500
Intensity (a.u.)
1e+5
8e+4
6e+4
4e+4
2e+4
0
0
2000
4000
6000
8000
10000
12000
1400
m/z, positive ions

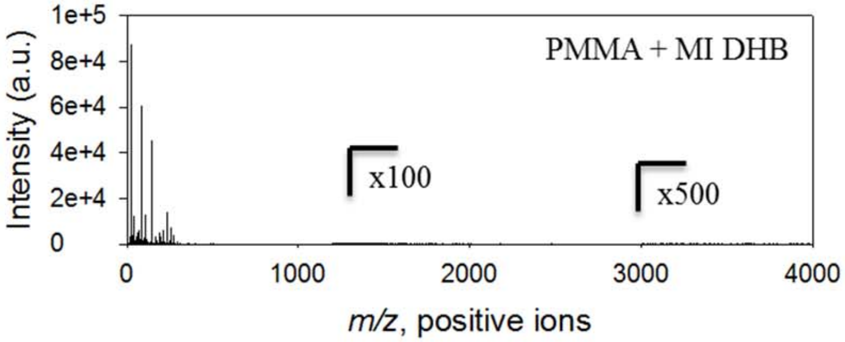
PMMA + MI DHB
x100
x500
Intensity (a.u.)
1e+5
8e+4
6e+4
4e+4
2e+4
0
0
1000
2000
3000
4000
m/z, positive ions

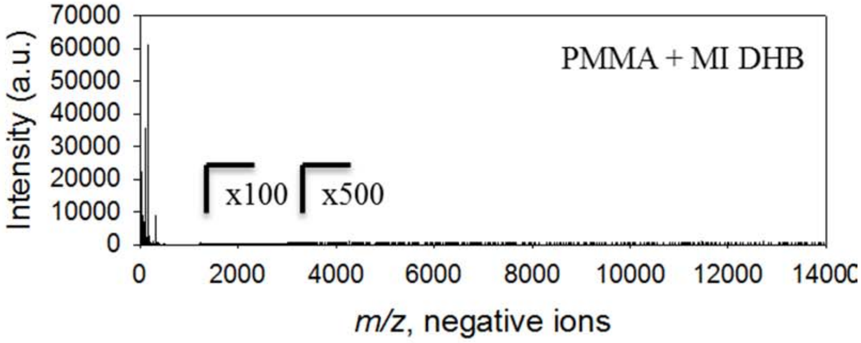
PMMA + MI DHB
x100
x500
Intensity (a.u.)
70000
60000
50000
40000
30000
20000
10000
0
0
2000
4000
6000
8000
10000
12000
1400
m/z, negative ions

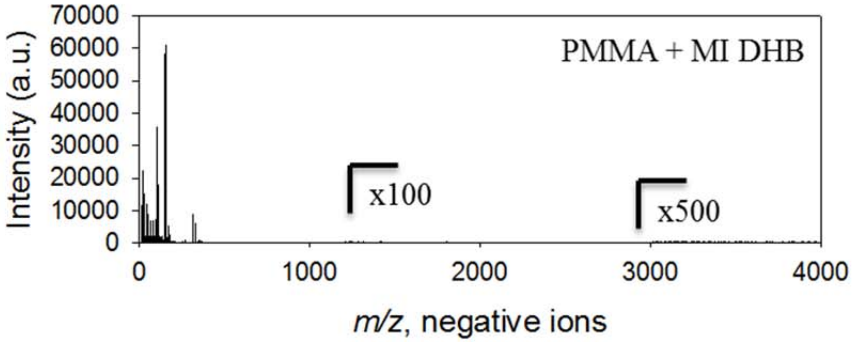
PMMA + MI DHB
x100
x500
Intensity (a.u.)
70000
60000
50000
40000
30000
20000
10000
0
0
1000
2000
3000
4000
m/z, negative ions

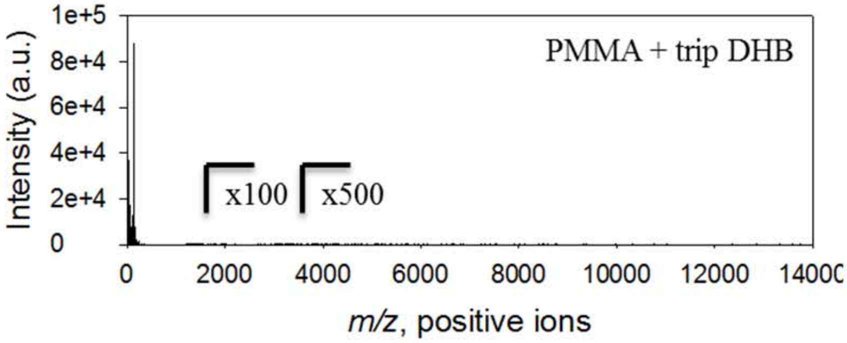
PMMA + trip DHB
x100
x500
Intensity (a.u.)
1e+5
8e+4
6e+4
4e+4
2e+4
0
0
2000
4000
6000
8000
10000
12000
14000
m/z, positive ions

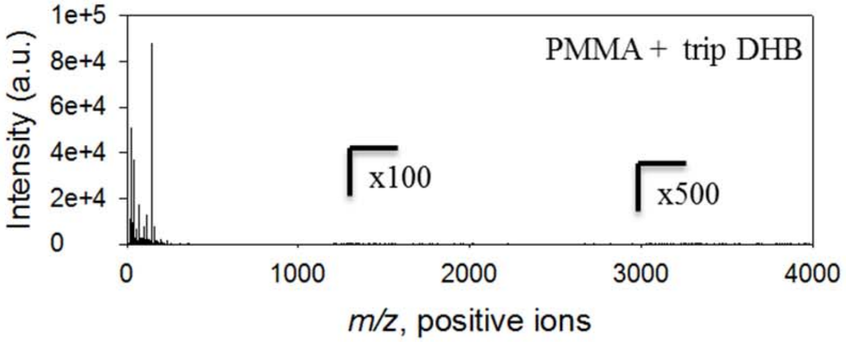
PMMA + trip DHB
x100
x500
Intensity (a.u.)
1e+5
8e+4
6e+4
4e+4
2e+4
0
0
1000
2000
3000
4000
m/z, positive ions

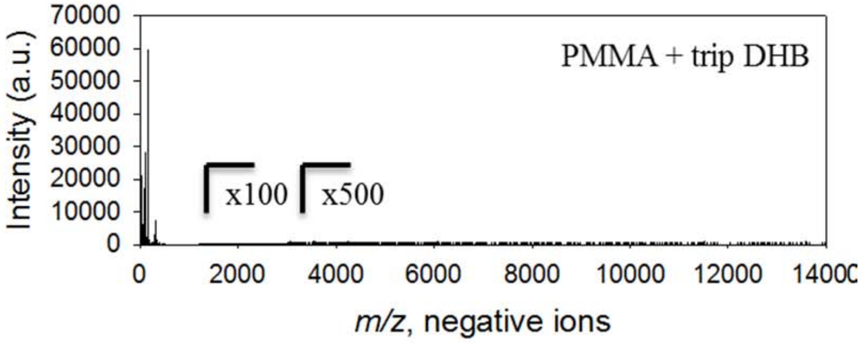
PMMA + trip DHB
x100
x500
Intensity (a.u.)
70000
60000
50000
40000
30000
20000
10000
0
0
2000
4000
6000
8000
10000
12000
14000
m/z, negative ions

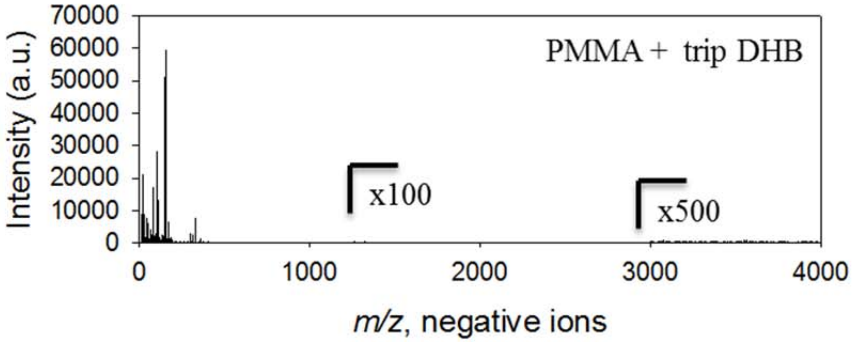
PMMA + trip DHB
x100
x500
Intensity (a.u.)
70000
60000
50000
40000
30000
20000
10000
0
0
1000
2000
3000
4000
m/z, negative ions

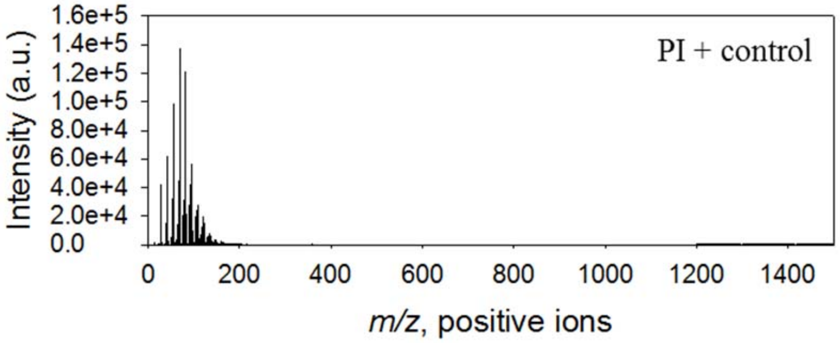
PI + control
Intensity (a.u.)
1.6e+5
1.4e+5
1.2e+5
1.0e+5
8.0e+4
6.0e+4
4.0e+4
2.0e+4
0.0
0
200
400
600
800
1000
1200
1400
m/z, positive ions

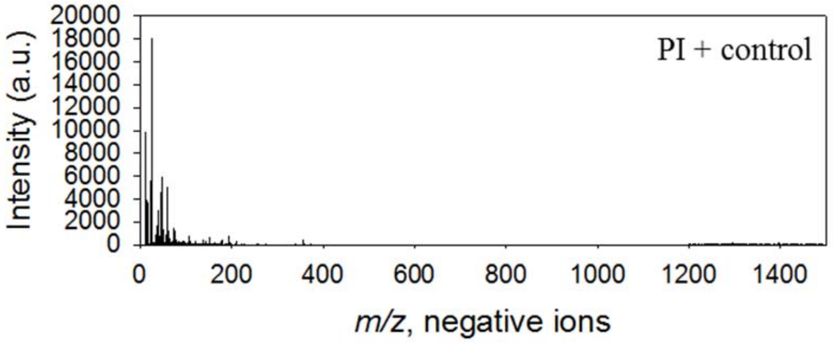
PI + control
Intensity (a.u.)
20000
18000
16000
14000
12000
10000
8000
6000
4000
2000
0
0
200
400
600
800
1000
1200
1400
m/z, negative ions

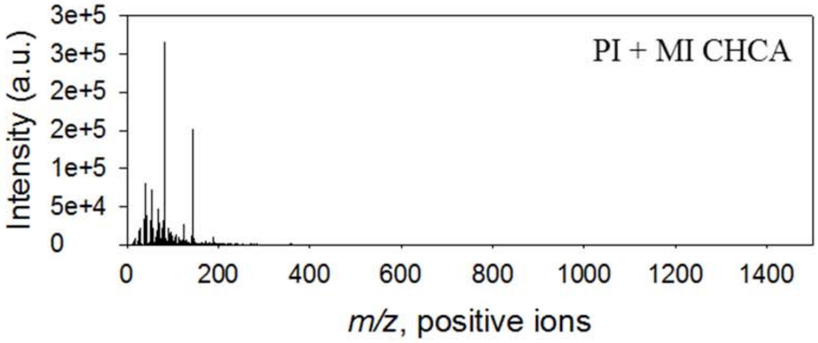
PI + MI CHCA
Intensity (a.u.)
3e+5
3e+5
2e+5
2e+5
1e+5
5e+4
0
0
200
400
600
800
1000
1200
1400
m/z, positive ions

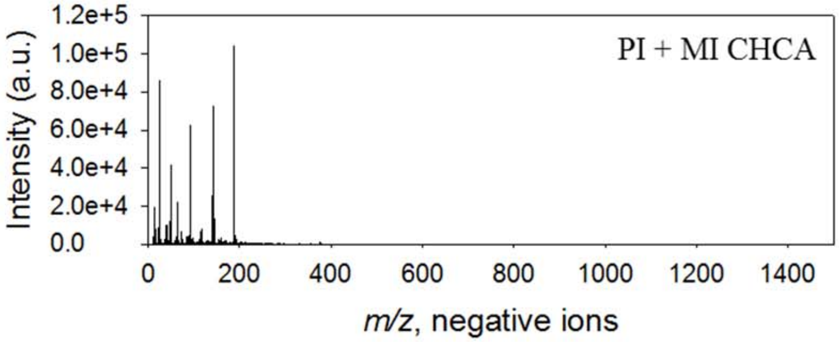
PI + MI CHCA
Intensity (a.u.)
1.2e+5
1.0e+5
8.0e+4
6.0e+4
4.0e+4
2.0e+4
0.0
0
200
400
600
800
1000
1200
1400
m/z, negative ions

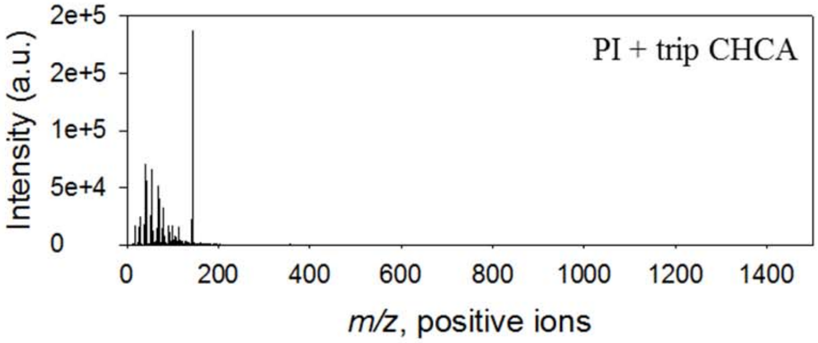
PI + trip CHCA
Intensity (a.u.)
2e+5
2e+5
1e+5
5e+4
0
0
200
400
600
800
1000
1200
1400
m/z, positive ions

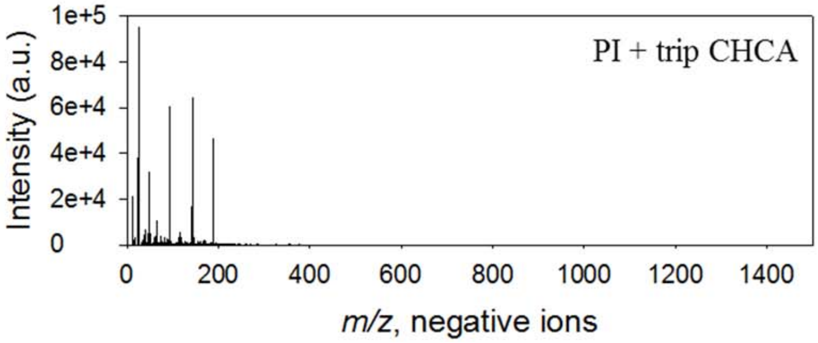
PI + trip CHCA
Intensity (a.u.)
1e+5
8e+4
6e+4
4e+4
2e+4
0
0
200
400
600
800
1000
1200
1400
m/z, negative ions

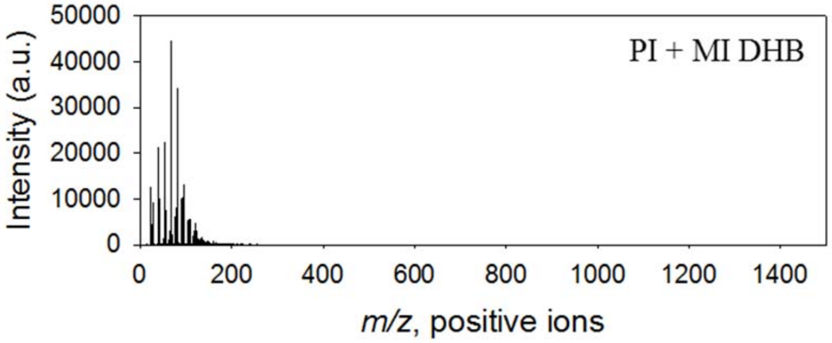
PI + MI DHB
Intensity (a.u.)
50000
40000
30000
20000
10000
0
0
200
400
600
800
1000
1200
1400
m/z, positive ions

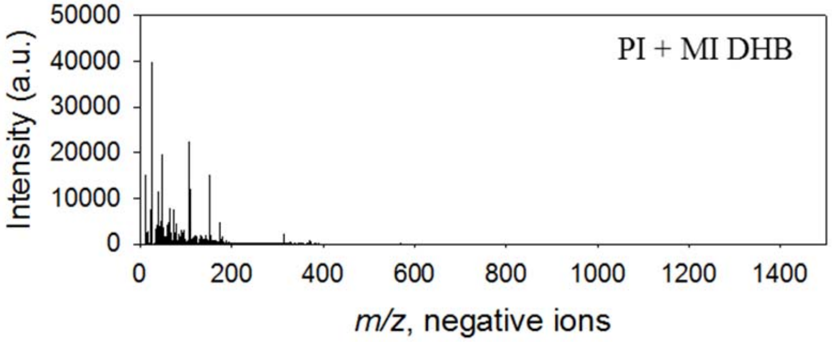
PI + MI DHB
Intensity (a.u.)
50000
40000
30000
20000
10000
0
0
200
400
600
800
1000
1200
1400
m/z, negative ions

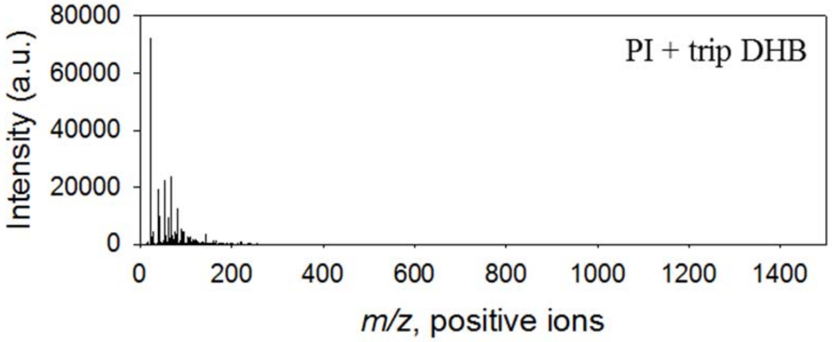
PI + trip DHB
Intensity (a.u.)
80000
60000
40000
20000
0
0
200
400
600
800
1000
1200
1400
m/z, positive ions

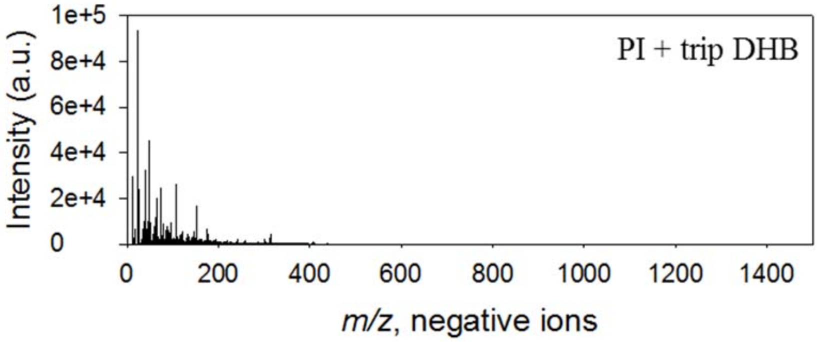
PI + trip DHB
Intensity (a.u.)
1e+5
8e+4
6e+4
4e+4
2e+4
0
0
200
400
600
800
1000
1200
1400
m/z, negative ions

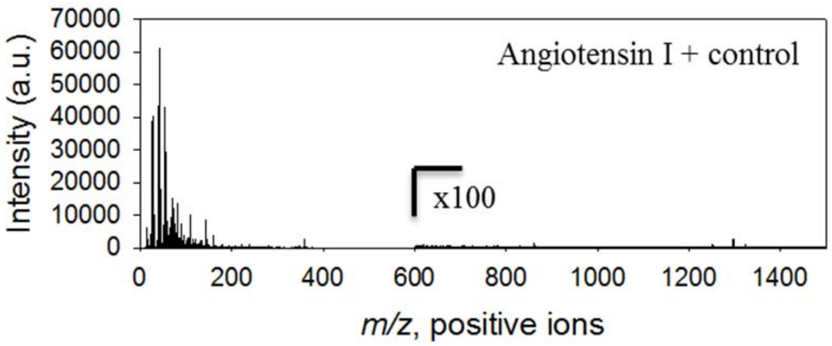
70000
60000
50000
40000
30000
20000
10000
0
Intensity (a.u.)
Angiotensin I + control
x100
0
200
400
600
800
1000
1200
1400
m/z, positive ions

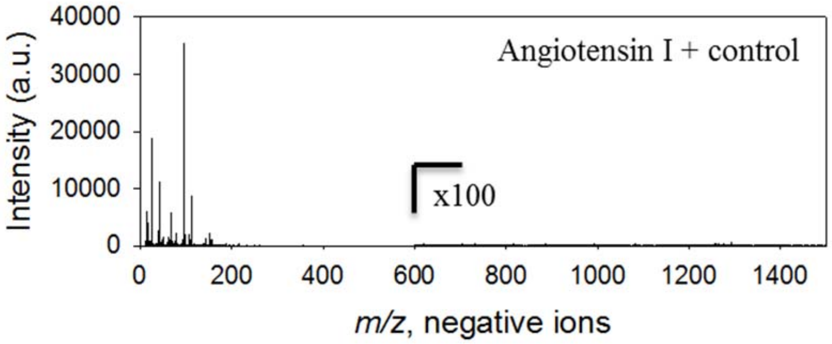
40000
30000
20000
10000
0
Intensity (a.u.)
Angiotensin I + control
x100
0
200
400
600
800
1000
1200
1400
m/z, negative ions

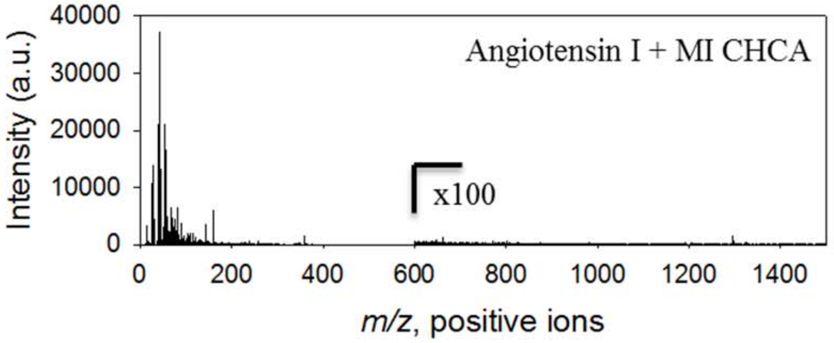
Angiotensin I + MI CHCA
x100
Intensity (a.u.)
40000
30000
20000
10000
0
0
200
400
600
800
1000
1200
1400
m/z, positive ions

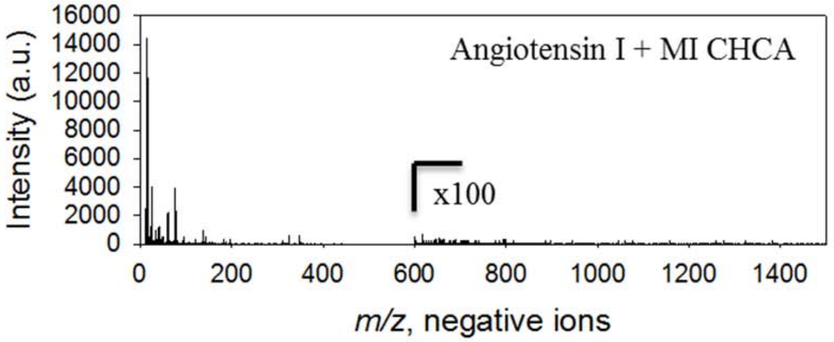
Angiotensin I + MI CHCA
x100
Intensity (a.u.)
16000
14000
12000
10000
8000
6000
4000
2000
0
0
200
400
600
800
1000
1200
1400
m/z, negative ions

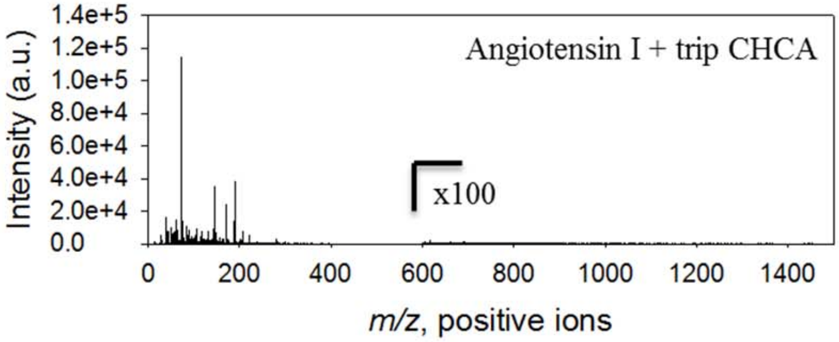
Angiotensin I + trip CHCA
x100
Intensity (a.u.)
1.4e+5
1.2e+5
1.0e+5
8.0e+4
6.0e+4
4.0e+4
2.0e+4
0.0
0
200
400
600
800
1000
1200
1400
m/z, positive ions

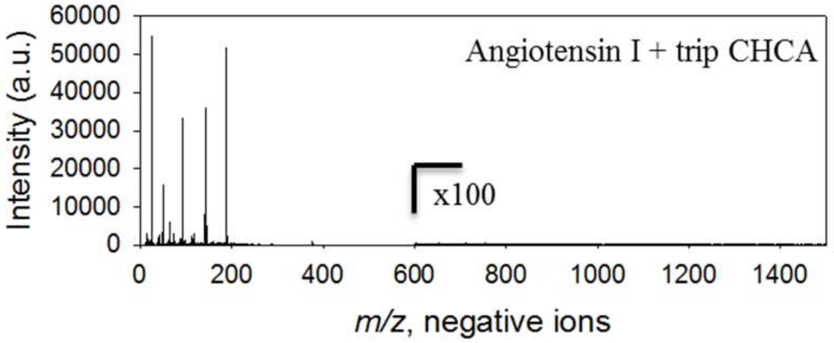
Angiotensin I + trip CHCA
x100
Intensity (a.u.)
60000
50000
40000
30000
20000
10000
0
0
200
400
600
800
1000
1200
1400
m/z, negative ions

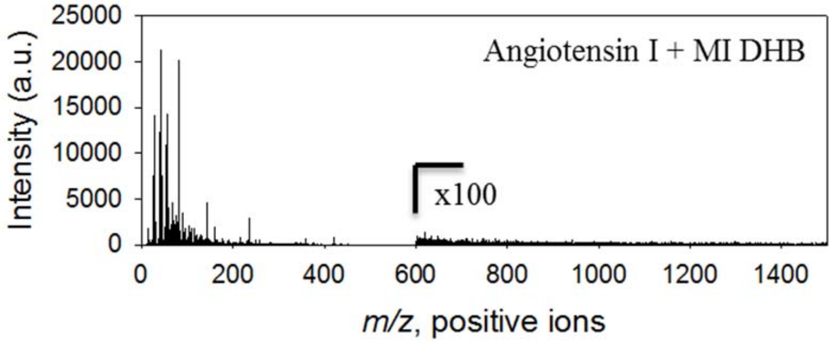
Angiotensin I + MI DHB
x100
Intensity (a.u.)
25000
20000
15000
10000
5000
0
0
200
400
600
800
1000
1200
1400
m/z, positive ions

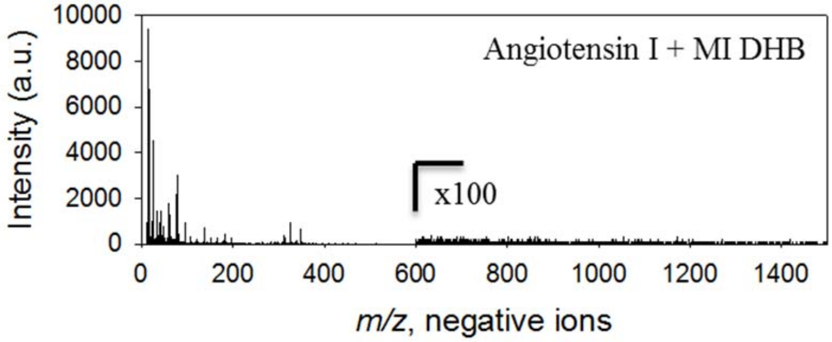
Angiotensin I + MI DHB
x100
Intensity (a.u.)
10000
8000
6000
4000
2000
0
0
200
400
600
800
1000
1200
1400
m/z, negative ions

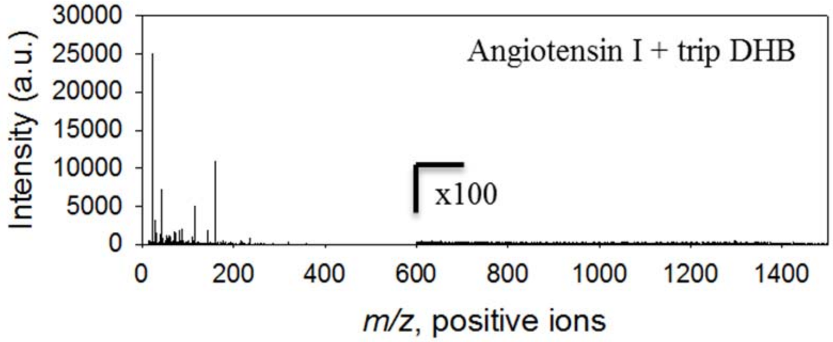
Angiotensin I + trip DHB
x100
Intensity (a.u.)
30000
25000
20000
15000
10000
5000
0
0
200
400
600
800
1000
1200
1400
m/z, positive ions

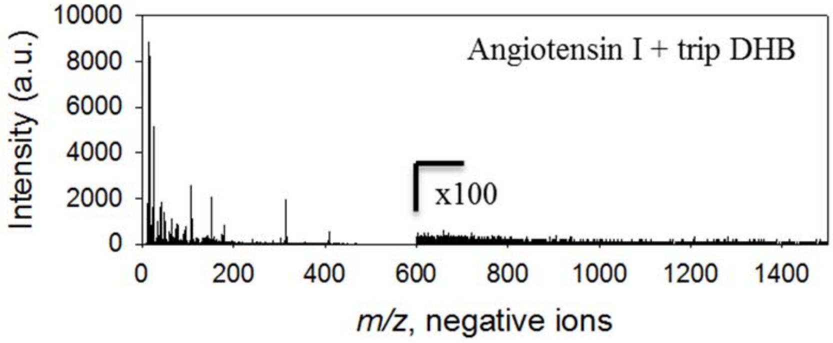
Angiotensin I + trip DHB
x100
Intensity (a.u.)
10000
8000
6000
4000
2000
0
0
200
400
600
800
1000
1200
1400
m/z, negative ions

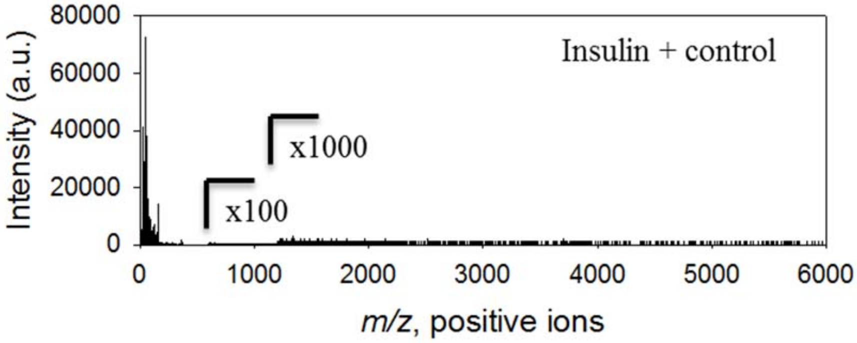
Insulin + control
x1000
x100
Intensity (a.u.)
80000
60000
40000
20000
0
0
1000
2000
3000
4000
5000
6000
m/z, positive ions

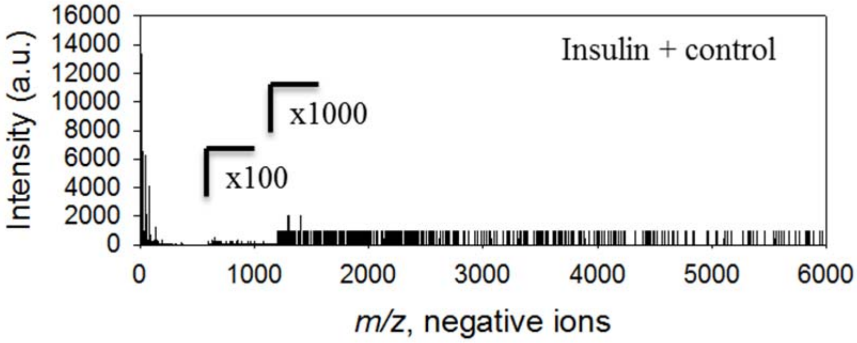
Insulin + control
x1000
x100
Intensity (a.u.)
16000
14000
12000
10000
8000
6000
4000
2000
0
0
1000
2000
3000
4000
5000
6000
m/z, negative ions

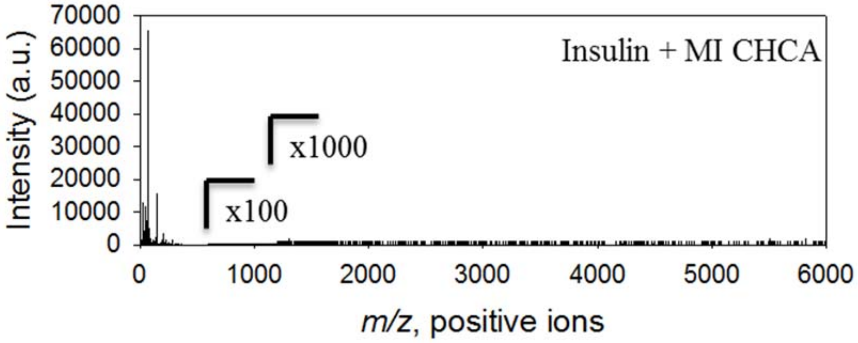
Insulin + MI CHCA
x1000
x100
Intensity (a.u.)
70000
60000
50000
40000
30000
20000
10000
0
0
1000
2000
3000
4000
5000
6000
m/z, positive ions

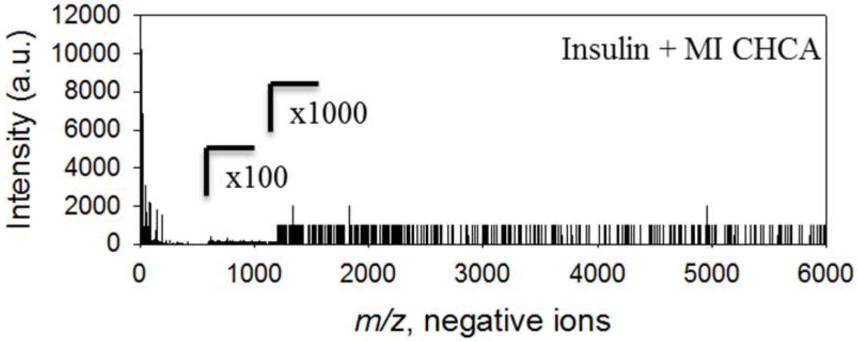
Insulin + MI CHCA
x1000
x100
Intensity (a.u.)
12000
10000
8000
6000
4000
2000
0
0
1000
2000
3000
4000
5000
6000
m/z, negative ions

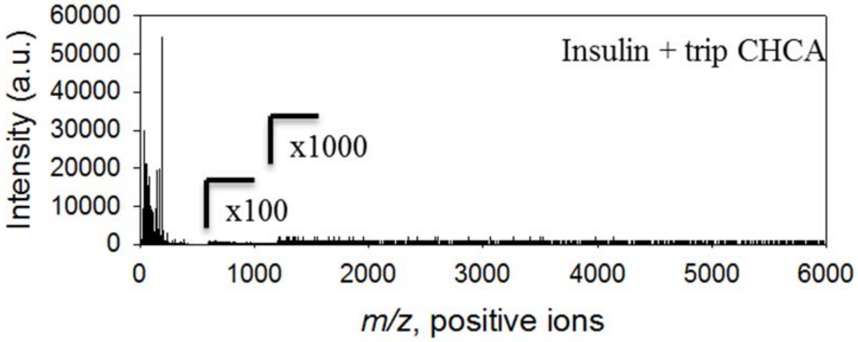
Insulin + trip CHCA
x1000
x100
Intensity (a.u.)
60000
50000
40000
30000
20000
10000
0
0
1000
2000
3000
4000
5000
6000
m/z, positive ions

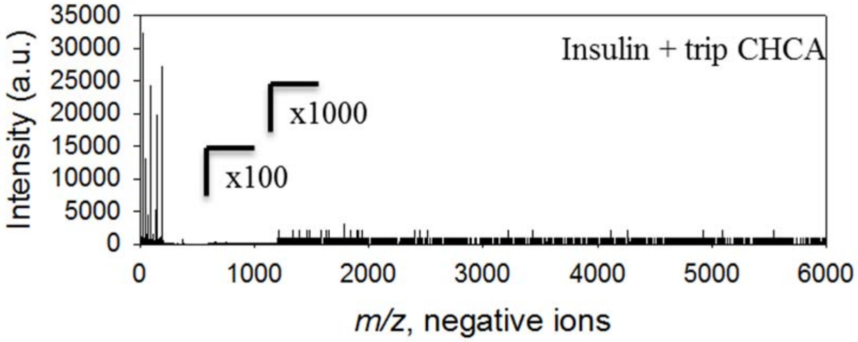
Insulin + trip CHCA
x1000
x100
Intensity (a.u.)
35000
30000
25000
20000
15000
10000
5000
0
0
1000
2000
3000
4000
5000
6000
m/z, negative ions

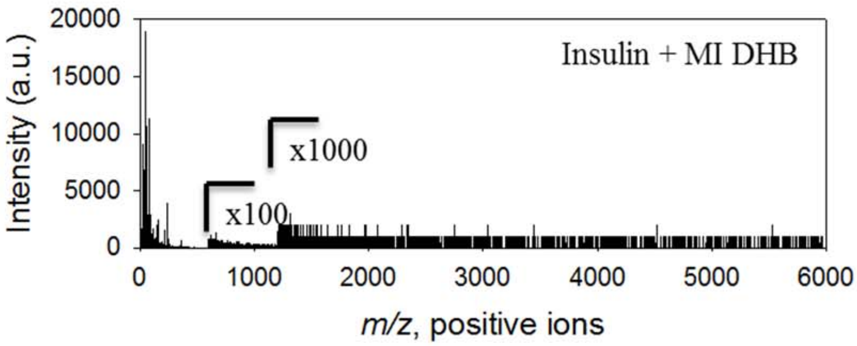
Insulin + MI DHB
x1000
x100
Intensity (a.u.)
20000
15000
10000
5000
0
0
1000
2000
3000
4000
5000
6000
m/z, positive ions

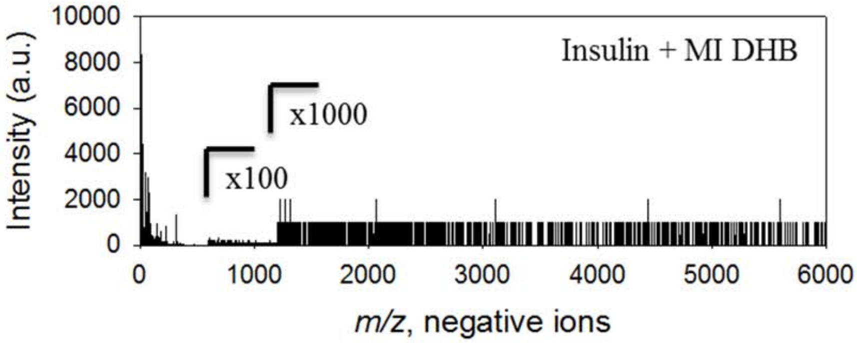
Insulin + MI DHB
x1000
x100
Intensity (a.u.)
10000
8000
6000
4000
2000
0
0
1000
2000
3000
4000
5000
6000
m/z, negative ions

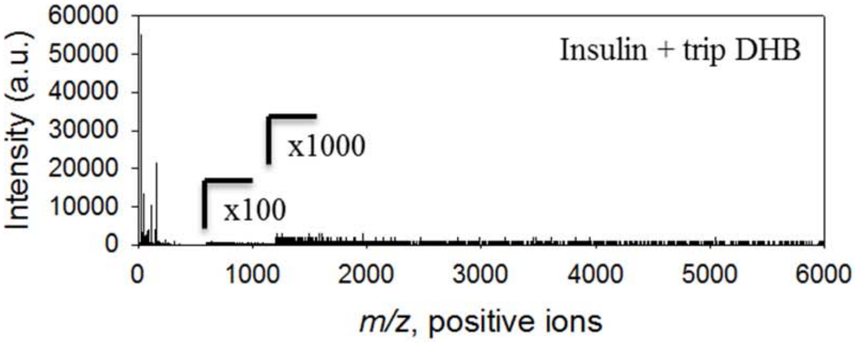
Insulin + trip DHB
x1000
x100
Intensity (a.u.)
60000
50000
40000
30000
20000
10000
0
0
1000
2000
3000
4000
5000
6000
m/z, positive ions

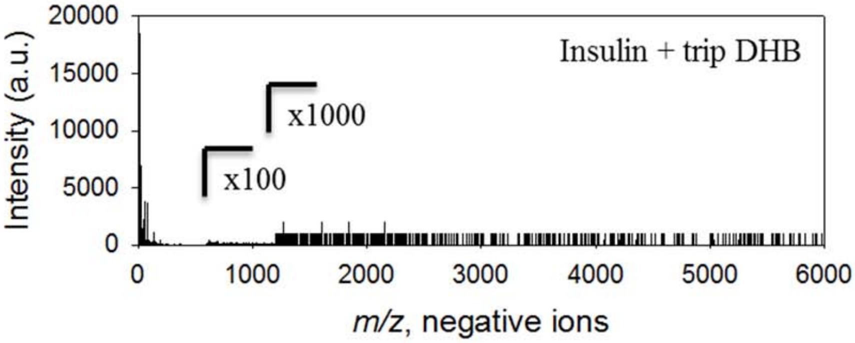
Insulin + trip DHB
x1000
x100
Intensity (a.u.)
20000
15000
10000
5000
0
0
1000
2000
3000
4000
5000
6000
m/z, negative ions

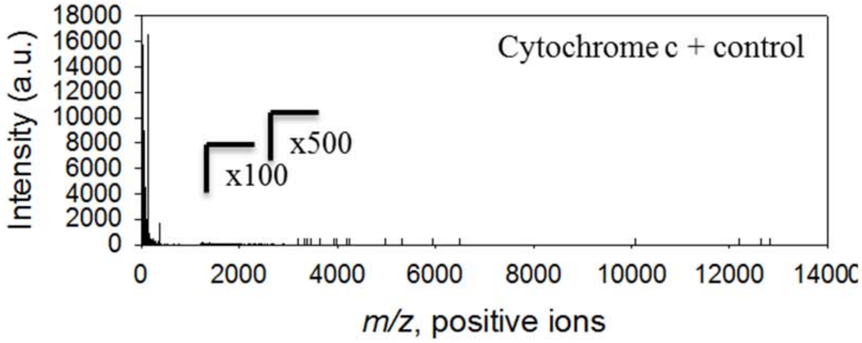
Intensity (a.u.)
18000
16000
14000
12000
10000
8000
6000
4000
2000
0
Cytochrome c + control
x100
x500
0
2000
4000
6000
8000
10000
12000
14000
m/z, positive ions

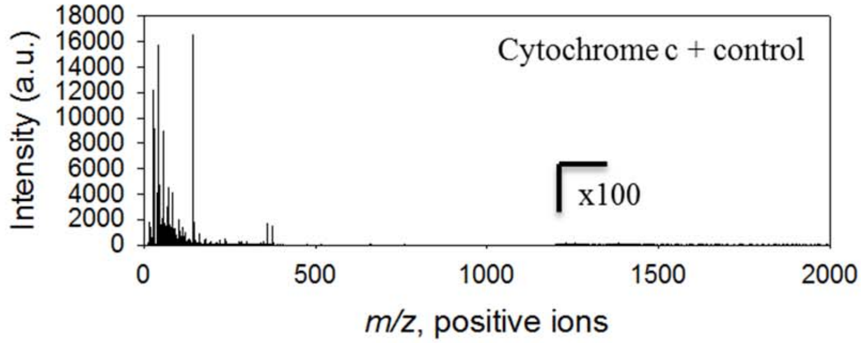
Intensity (a.u.)
18000
16000
14000
12000
10000
8000
6000
4000
2000
0
Cytochrome c + control
x100
0
500
1000
1500
2000
m/z, positive ions

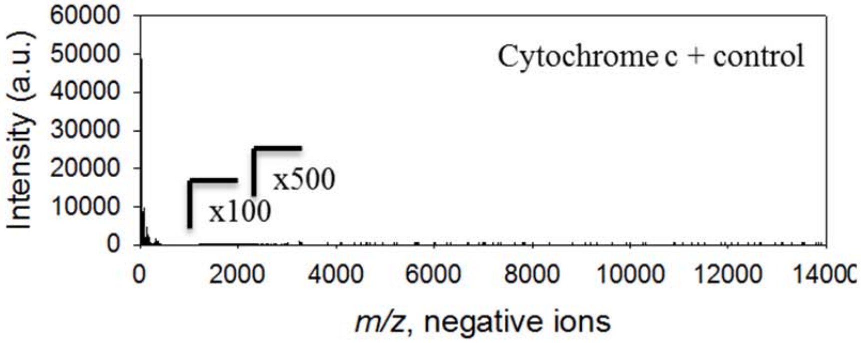
Intensity (a.u.)
60000
50000
40000
30000
20000
10000
0
Cytochrome c + control
x100
x500
0
2000
4000
6000
8000
10000
12000
14000
m/z, negative ions

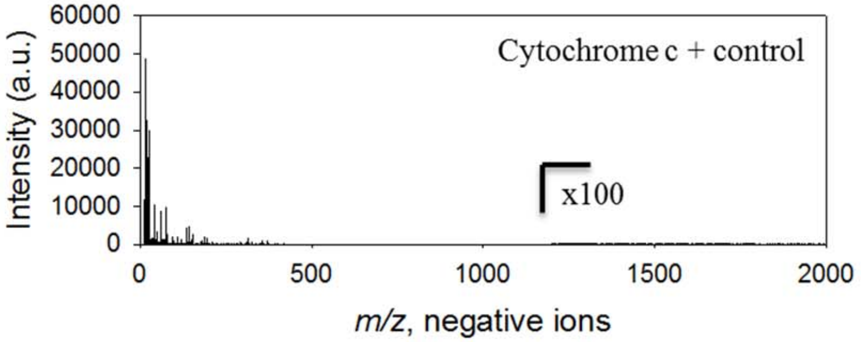
Intensity (a.u.)
60000
50000
40000
30000
20000
10000
0
Cytochrome c + control
x100
0
500
1000
1500
2000
m/z, negative ions

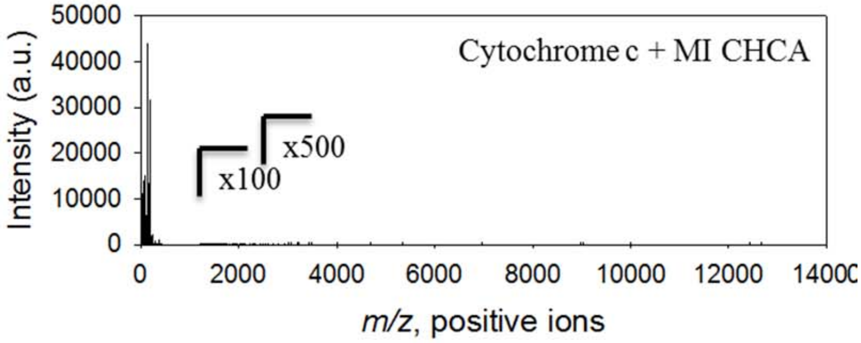
Cytochrome c + MI CHCA
x100
x500
Intensity (a.u.)
50000
40000
30000
20000
10000
0
0
2000
4000
6000
8000
10000
12000
14000
m/z, positive ions

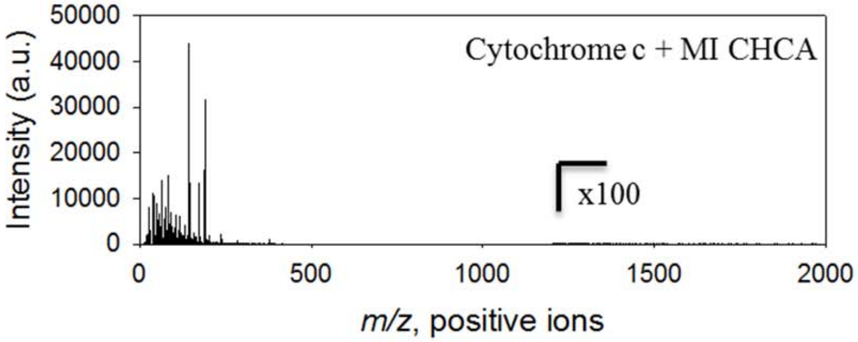
Cytochrome c + MI CHCA
x100
Intensity (a.u.)
50000
40000
30000
20000
10000
0
0
500
1000
1500
2000
m/z, positive ions

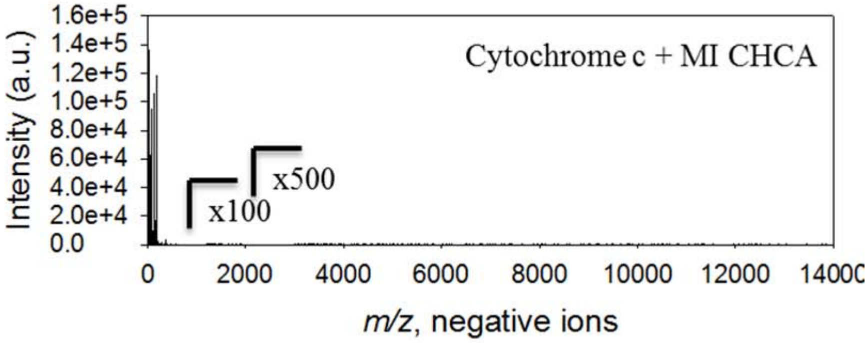
Cytochrome c + MI CHCA
x100
x500
Intensity (a.u.)
1.6e+5
1.4e+5
1.2e+5
1.0e+5
8.0e+4
6.0e+4
4.0e+4
2.0e+4
0.0
0
2000
4000
6000
8000
10000
12000
14000
m/z, negative ions

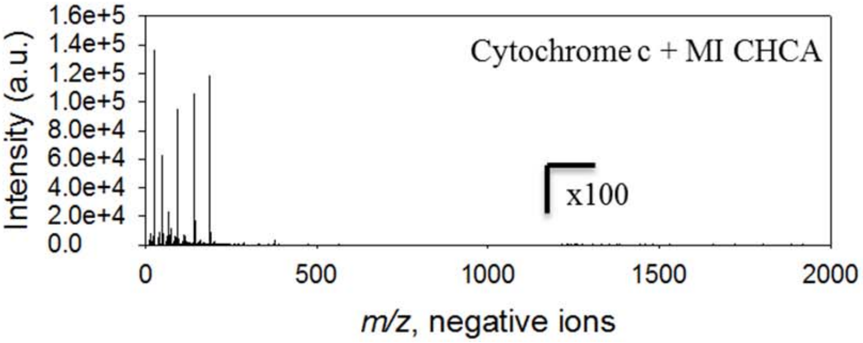
Cytochrome c + MI CHCA
x100
Intensity (a.u.)
1.6e+5
1.4e+5
1.2e+5
1.0e+5
8.0e+4
6.0e+4
4.0e+4
2.0e+4
0.0
0
500
1000
1500
2000
m/z, negative ions

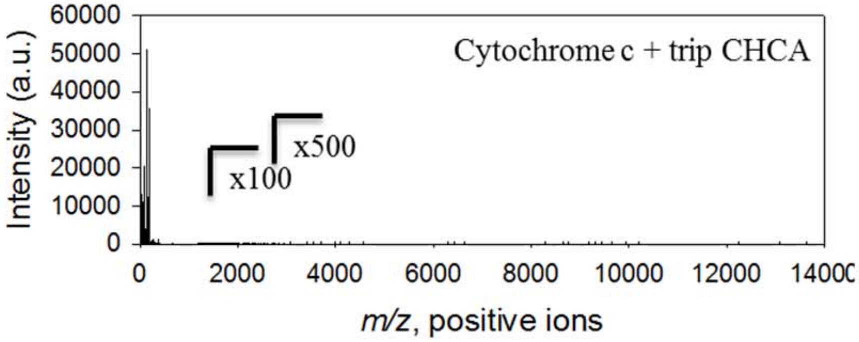
Cytochrome c + trip CHCA
x100
x500
Intensity (a.u.)
60000
50000
40000
30000
20000
10000
0
0
2000
4000
6000
8000
10000
12000
14000
m/z, positive ions

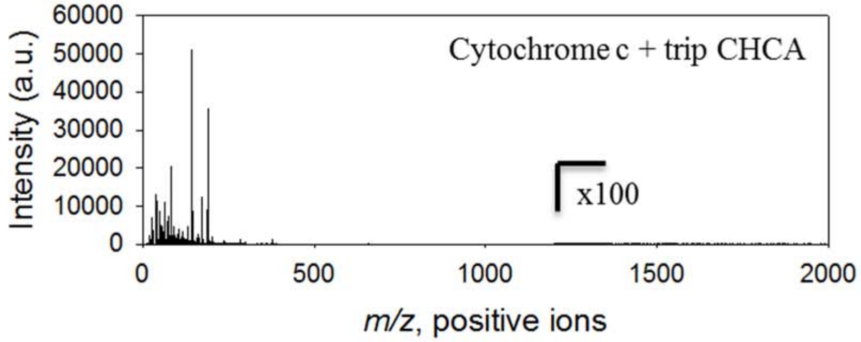
Cytochrome c + trip CHCA
x100
Intensity (a.u.)
60000
50000
40000
30000
20000
10000
0
0
500
1000
1500
2000
m/z, positive ions

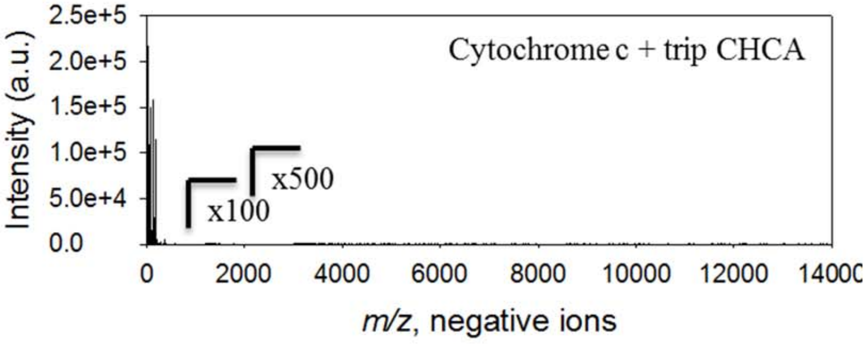
Cytochrome c + trip CHCA
x100
x500
Intensity (a.u.)
2.5e+5
2.0e+5
1.5e+5
1.0e+5
5.0e+4
0.0
0
2000
4000
6000
8000
10000
12000
14000
m/z, negative ions

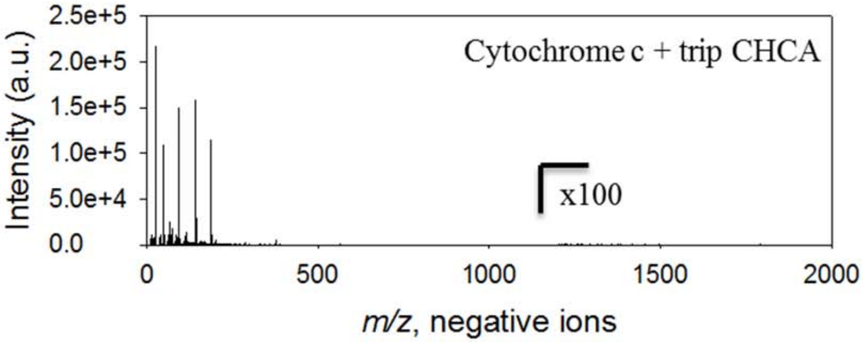
Cytochrome c + trip CHCA
x100
Intensity (a.u.)
2.5e+5
2.0e+5
1.5e+5
1.0e+5
5.0e+4
0.0
0
500
1000
1500
2000
m/z, negative ions

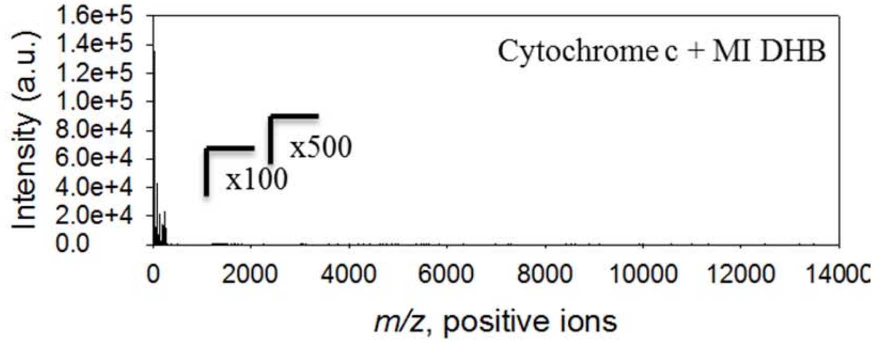
Cytochrome c + MI DHB
x100
x500
Intensity (a.u.)
1.6e+5
1.4e+5
1.2e+5
1.0e+5
8.0e+4
6.0e+4
4.0e+4
2.0e+4
0.0
0
2000
4000
6000
8000
10000
12000
1400C
m/z, positive ions

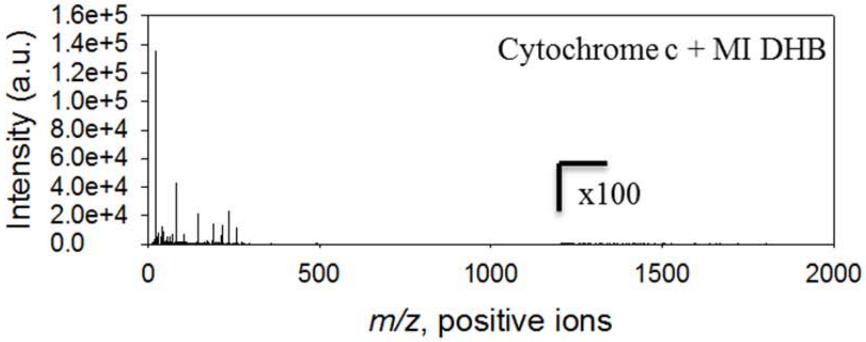
Cytochrome c + MI DHB
x100
Intensity (a.u.)
1.6e+5
1.4e+5
1.2e+5
1.0e+5
8.0e+4
6.0e+4
4.0e+4
2.0e+4
0.0
0
500
1000
1500
2000
m/z, positive ions

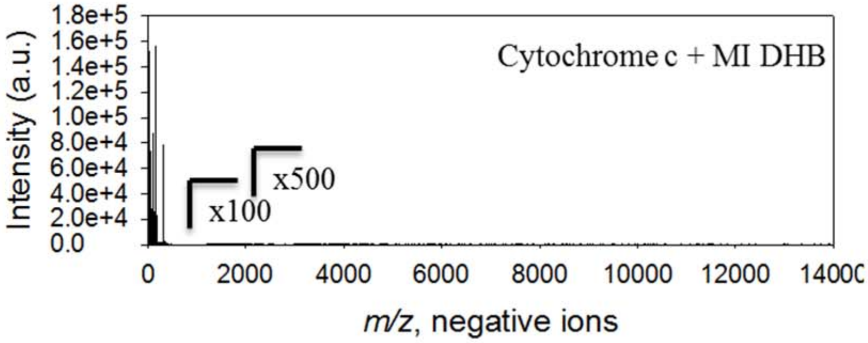
Cytochrome c + MI DHB
x100
x500
Intensity (a.u.)
1.8e+5
1.6e+5
1.4e+5
1.2e+5
1.0e+5
8.0e+4
6.0e+4
4.0e+4
2.0e+4
0.0
0
2000
4000
6000
8000
10000
12000
1400C
m/z, negative ions

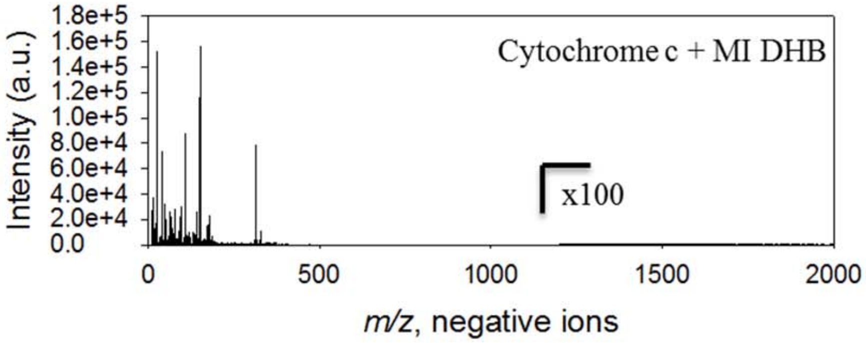
Cytochrome c + MI DHB
x100
Intensity (a.u.)
1.8e+5
1.6e+5
1.4e+5
1.2e+5
1.0e+5
8.0e+4
6.0e+4
4.0e+4
2.0e+4
0.0
0
500
1000
1500
2000
m/z, negative ions

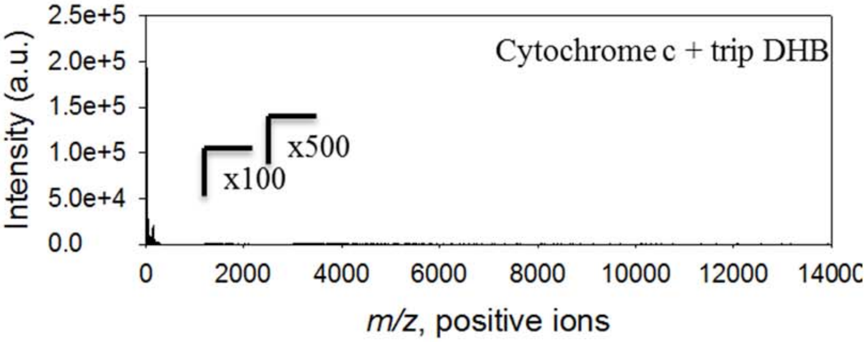
Cytochrome c + trip DHB
x100
x500
Intensity (a.u.)
2.5e+5
2.0e+5
1.5e+5
1.0e+5
5.0e+4
0.0
0
2000
4000
6000
8000
10000
12000
14000
m/z, positive ions

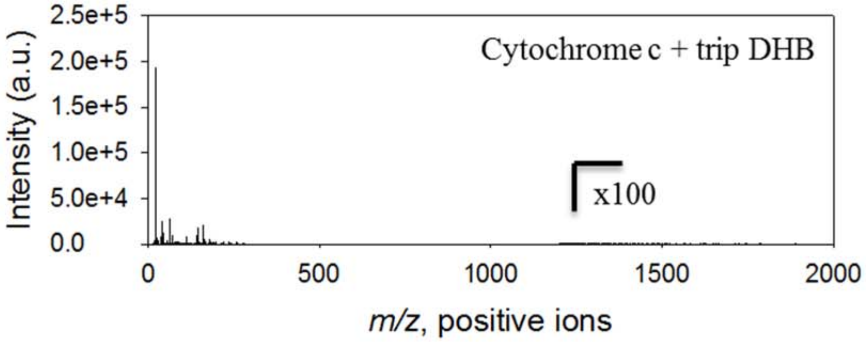
Cytochrome c + trip DHB
x100
Intensity (a.u.)
2.5e+5
2.0e+5
1.5e+5
1.0e+5
5.0e+4
0.0
0
500
1000
1500
2000
m/z, positive ions

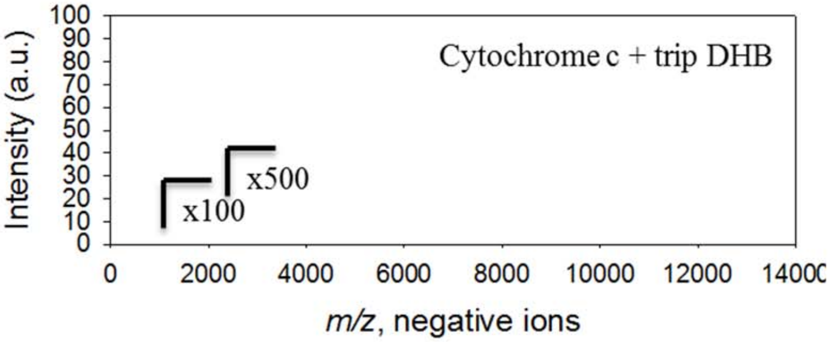
Cytochrome c + trip DHB
x100
x500
Intensity (a.u.)
100
90
80
70
60
50
40
30
20
10
0
0
2000
4000
6000
8000
10000
12000
14000
m/z, negative ions

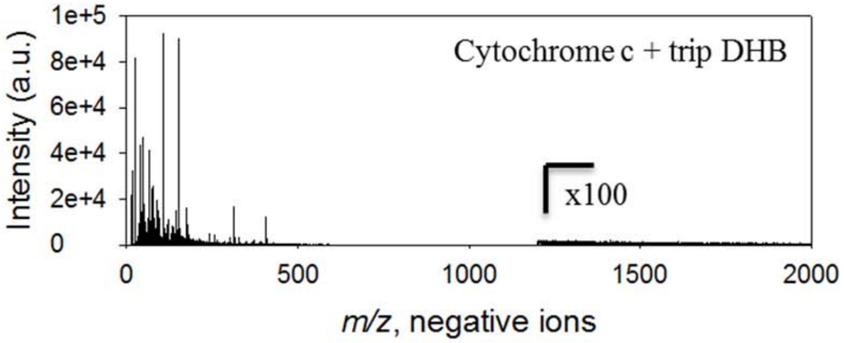
Cytochrome c + trip DHB
x100
Intensity (a.u.)
1e+5
8e+4
6e+4
4e+4
2e+4
0
0
500
1000
1500
2000
m/z, negative ions

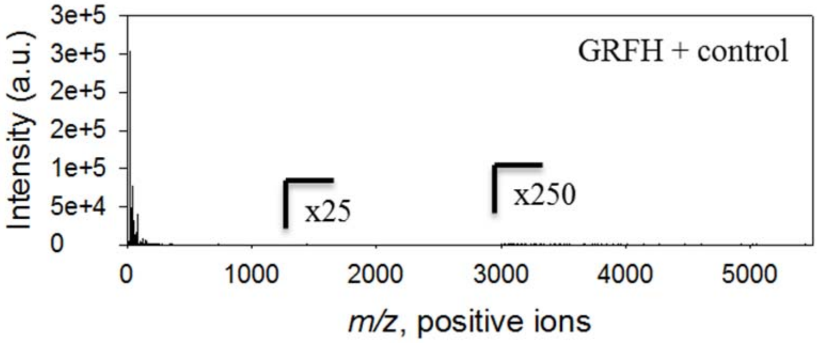
3e+5
3e+5
2e+5
2e+5
1e+5
5e+4
0
Intensity (a.u.)
GRFH + control
x25
x250
0
1000
2000
3000
4000
5000
m/z, positive ions

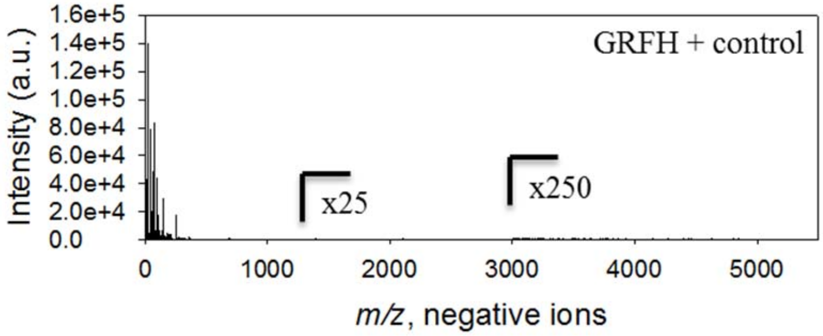
1.6e+5
1.4e+5
1.2e+5
1.0e+5
8.0e+4
6.0e+4
4.0e+4
2.0e+4
0.0
Intensity (a.u.)
GRFH + control
x25
x250
0
1000
2000
3000
4000
5000
m/z, negative ions

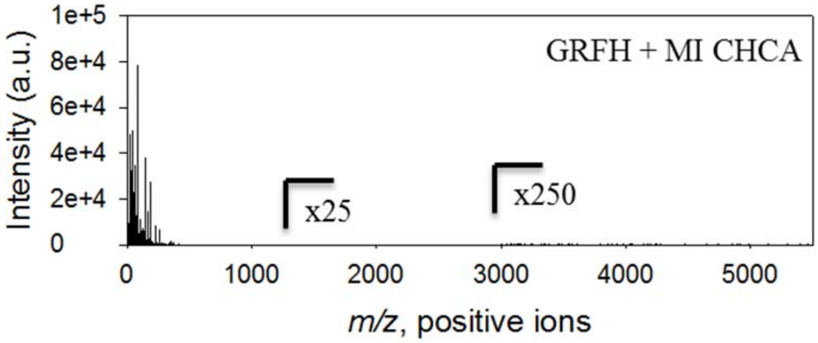
GRFH + MI CHCA
x25
x250
Intensity (a.u.)
1e+5
8e+4
6e+4
4e+4
2e+4
0
0
1000
2000
3000
4000
5000
m/z, positive ions

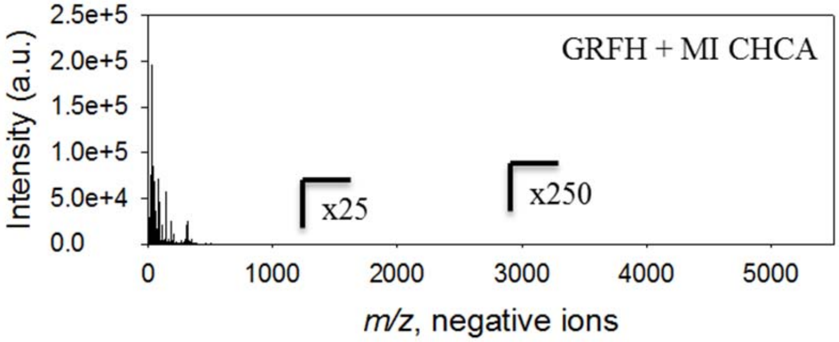
GRFH + MI CHCA
x25
x250
Intensity (a.u.)
2.5e+5
2.0e+5
1.5e+5
1.0e+5
5.0e+4
0.0
0
1000
2000
3000
4000
5000
m/z, negative ions

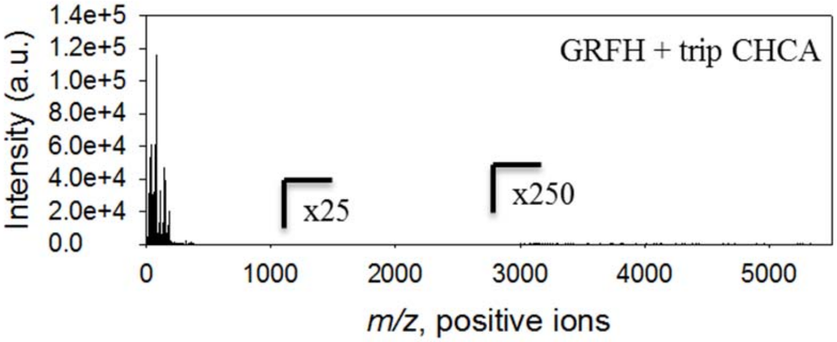
GRFH + trip CHCA
x25
x250
Intensity (a.u.)
1.4e+5
1.2e+5
1.0e+5
8.0e+4
6.0e+4
4.0e+4
2.0e+4
0.0
0
1000
2000
3000
4000
5000
m/z, positive ions

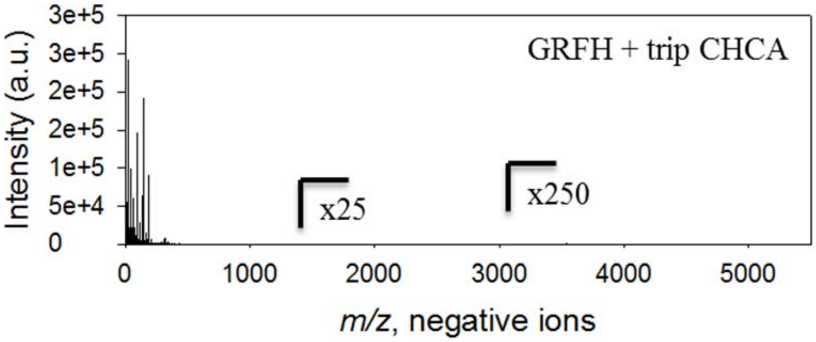
GRFH + trip CHCA
x25
x250
Intensity (a.u.)
3e+5
3e+5
2e+5
2e+5
1e+5
5e+4
0
0
1000
2000
3000
4000
5000
m/z, negative ions

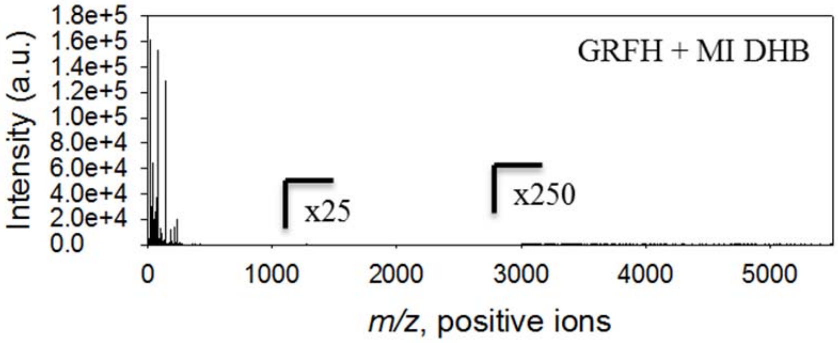
GRFH + MI DHB
x25
x250
Intensity (a.u.)
1.8e+5
1.6e+5
1.4e+5
1.2e+5
1.0e+5
8.0e+4
6.0e+4
4.0e+4
2.0e+4
0.0
0
1000
2000
3000
4000
5000
m/z, positive ions

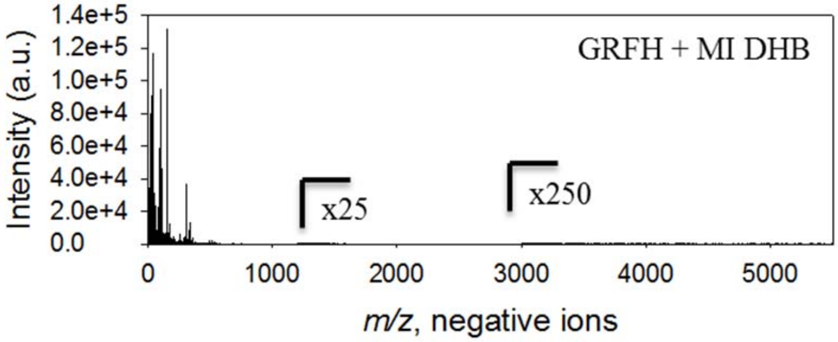
GRFH + MI DHB
x25
x250
Intensity (a.u.)
1.4e+5
1.2e+5
1.0e+5
8.0e+4
6.0e+4
4.0e+4
2.0e+4
0.0
0
1000
2000
3000
4000
5000
m/z, negative ions

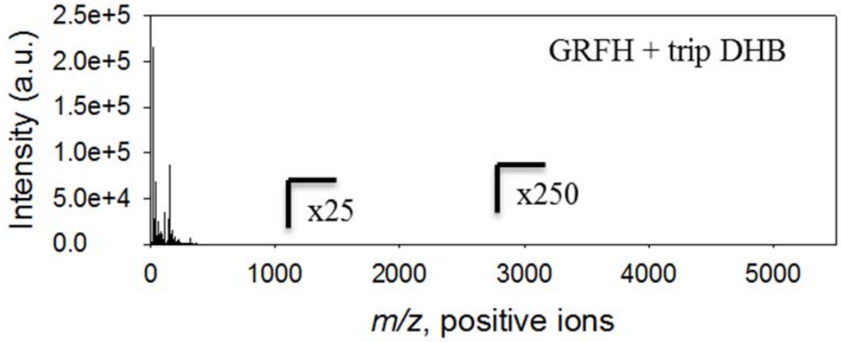
GRFH + trip DHB
x25
x250
Intensity (a.u.)
2.5e+5
2.0e+5
1.5e+5
1.0e+5
5.0e+4
0.0
0
1000
2000
3000
4000
5000
m/z, positive ions

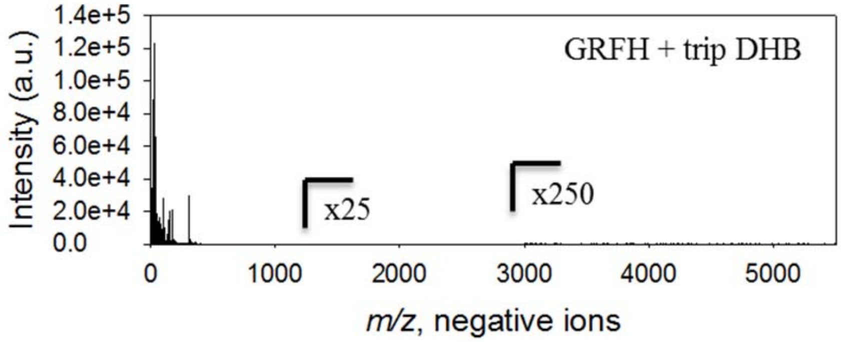
GRFH + trip DHB
x25
x250
Intensity (a.u.)
1.4e+5
1.2e+5
1.0e+5
8.0e+4
6.0e+4
4.0e+4
2.0e+4
0.0
0
1000
2000
3000
4000
5000
m/z, negative ions

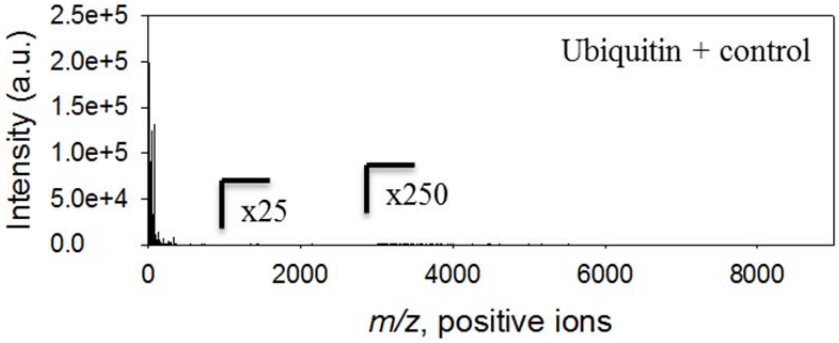
Ubiquitin + control
Intensity (a.u.)
2.5e+5
2.0e+5
1.5e+5
1.0e+5
5.0e+4
0.0
x25
x250
0
2000
4000
6000
8000
m/z, positive ions

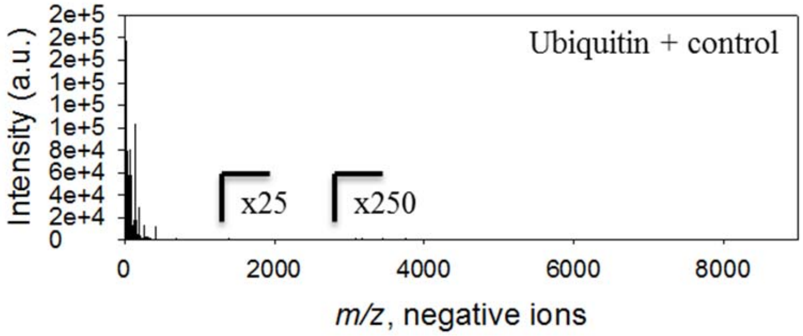
Ubiquitin + control
Intensity (a.u.)
2e+5
2e+5
2e+5
1e+5
1e+5
1e+5
8e+4
6e+4
4e+4
2e+4
0
x25
x250
0
2000
4000
6000
8000
m/z, negative ions

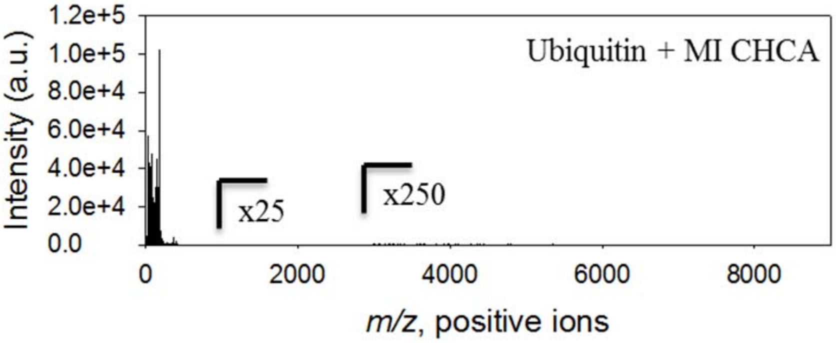
Ubiquitin + MI CHCA
x25
x250
Intensity (a.u.)
1.2e+5
1.0e+5
8.0e+4
6.0e+4
4.0e+4
2.0e+4
0.0
0
2000
4000
6000
8000
m/z, positive ions

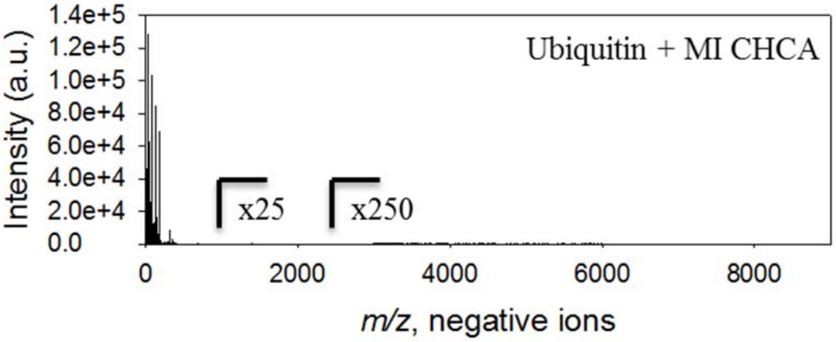
Ubiquitin + MI CHCA
x25
x250
Intensity (a.u.)
1.4e+5
1.2e+5
1.0e+5
8.0e+4
6.0e+4
4.0e+4
2.0e+4
0.0
0
2000
4000
6000
8000
m/z, negative ions

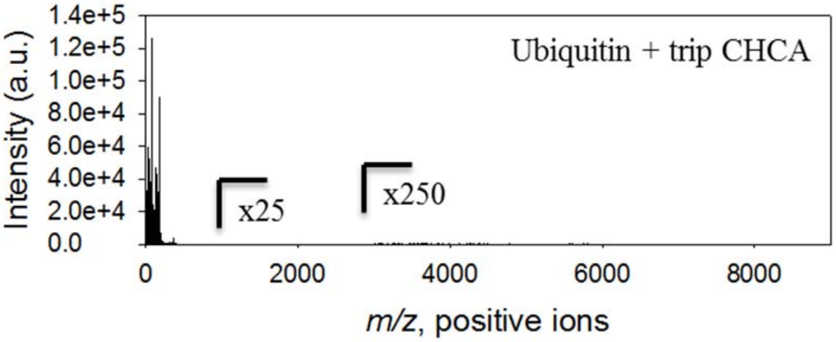
Ubiquitin + trip CHCA
x25
x250
Intensity (a.u.)
1.4e+5
1.2e+5
1.0e+5
8.0e+4
6.0e+4
4.0e+4
2.0e+4
0.0
0
2000
4000
6000
8000
m/z, positive ions

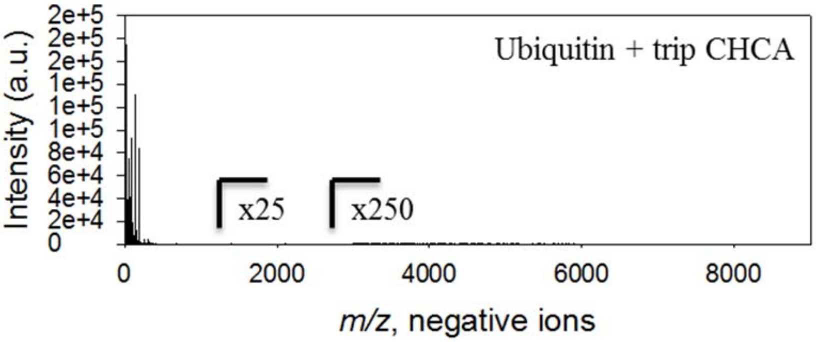
Ubiquitin + trip CHCA
x25
x250
Intensity (a.u.)
2e+5
2e+5
2e+5
1e+5
1e+5
1e+5
8e+4
6e+4
4e+4
2e+4
0
0
2000
4000
6000
8000
m/z, negative ions

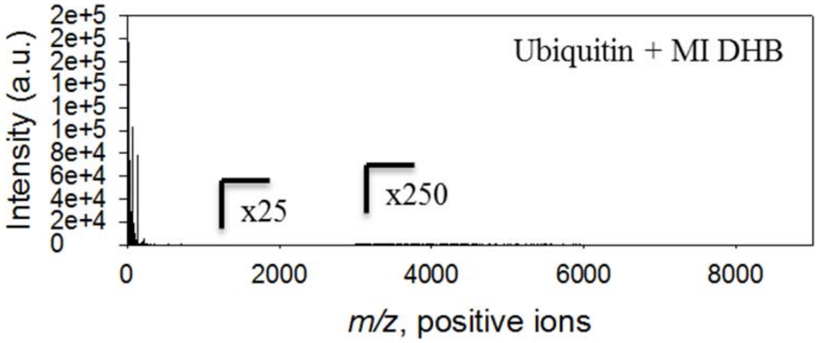
Ubiquitin + MI DHB
Intensity (a.u.)
2e+5
2e+5
2e+5
1e+5
1e+5
1e+5
8e+4
6e+4
4e+4
2e+4
0
x25
x250
0
2000
4000
6000
8000
m/z, positive ions

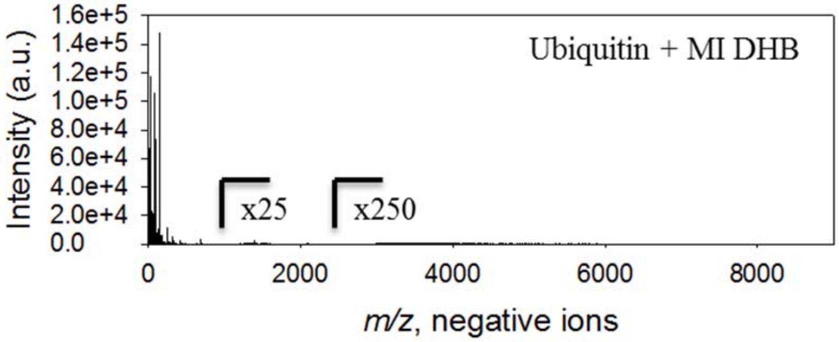
Ubiquitin + MI DHB
Intensity (a.u.)
1.6e+5
1.4e+5
1.2e+5
1.0e+5
8.0e+4
6.0e+4
4.0e+4
2.0e+4
0.0
x25
x250
0
2000
4000
6000
8000
m/z, negative ions

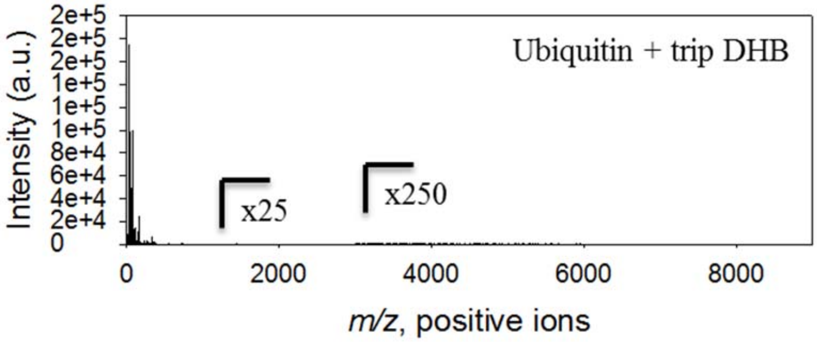
Ubiquitin + trip DHB
Intensity (a.u.)
2e+5
2e+5
2e+5
1e+5
1e+5
1e+5
8e+4
6e+4
4e+4
2e+4
0
x25
x250
0
2000
4000
6000
8000
m/z, positive ions

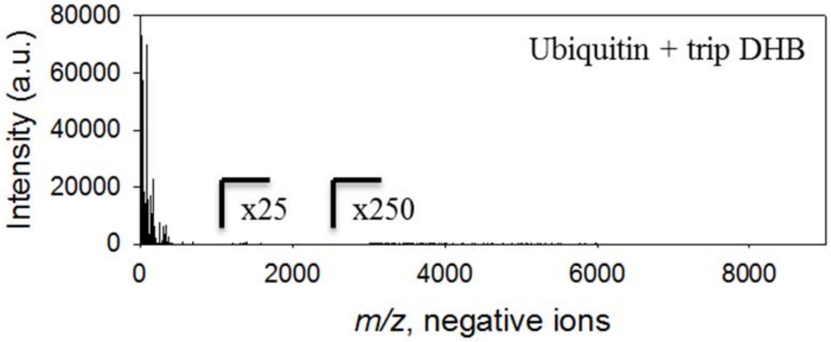
Ubiquitin + trip DHB
Intensity (a.u.)
80000
60000
40000
20000
0
x25
x250
0
2000
4000
6000
8000
m/z, negative ions

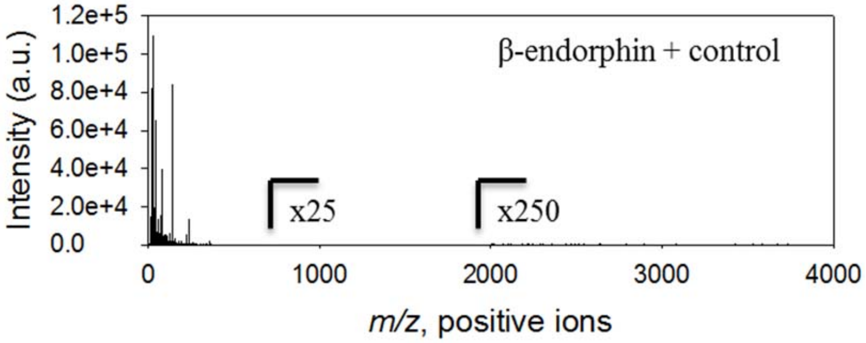
1.2e+5
1.0e+5
8.0e+4
6.0e+4
4.0e+4
2.0e+4
0.0
Intensity (a.u.)
β-endorphin + control
x25
x250
0
1000
2000
3000
4000
m/z, positive ions

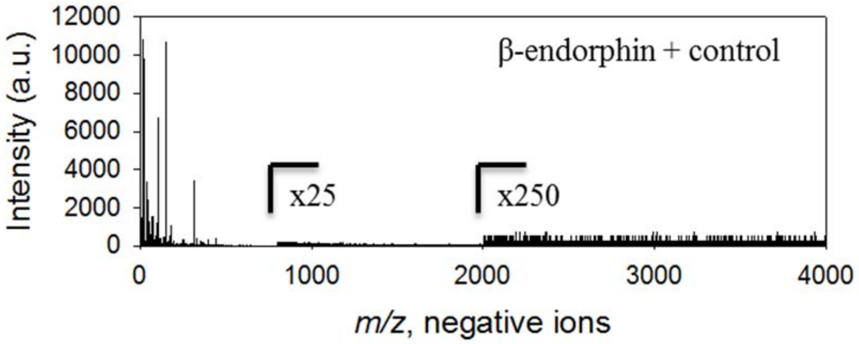
12000
10000
8000
6000
4000
2000
0
Intensity (a.u.)
β-endorphin + control
x25
x250
0
1000
2000
3000
4000
m/z, negative ions

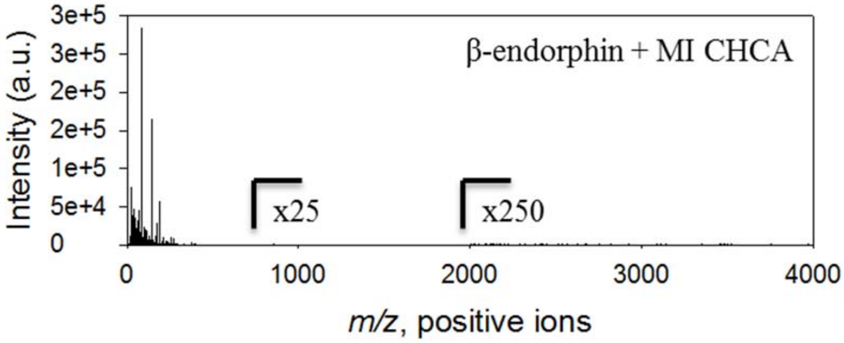
β-endorphin + MI CHCA
x25
x250
3e+5
3e+5
2e+5
2e+5
1e+5
5e+4
0
Intensity (a.u.)
0
1000
2000
3000
4000
m/z, positive ions

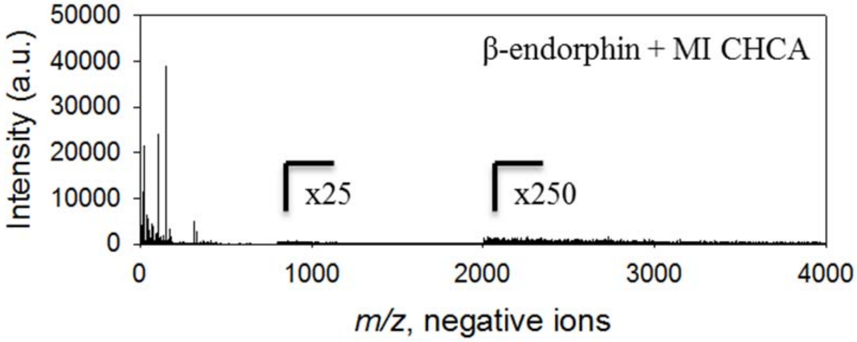
β-endorphin + MI CHCA
x25
x250
50000
40000
30000
20000
10000
0
Intensity (a.u.)
0
1000
2000
3000
4000
m/z, negative ions

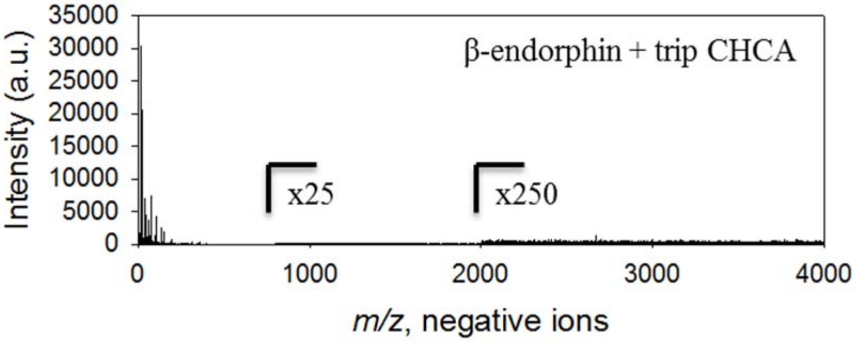
β-endorphin + trip CHCA
x25
x250
35000
30000
25000
20000
15000
10000
5000
0
Intensity (a.u.)
0
1000
2000
3000
4000
m/z, negative ions

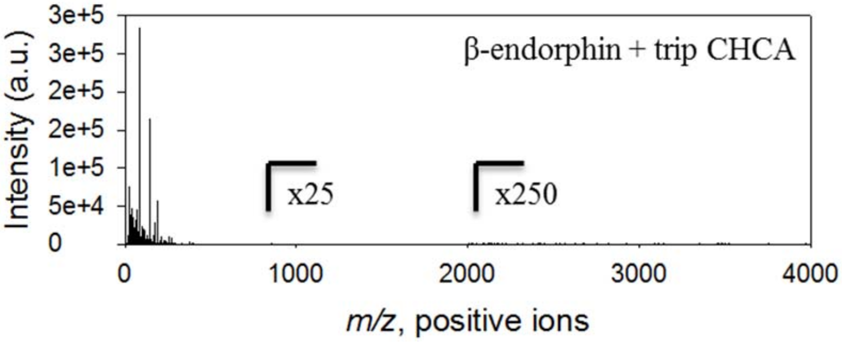
β-endorphin + trip CHCA
x25
x250
3e+5
3e+5
2e+5
2e+5
1e+5
5e+4
0
Intensity (a.u.)
0
1000
2000
3000
4000
m/z, positive ions

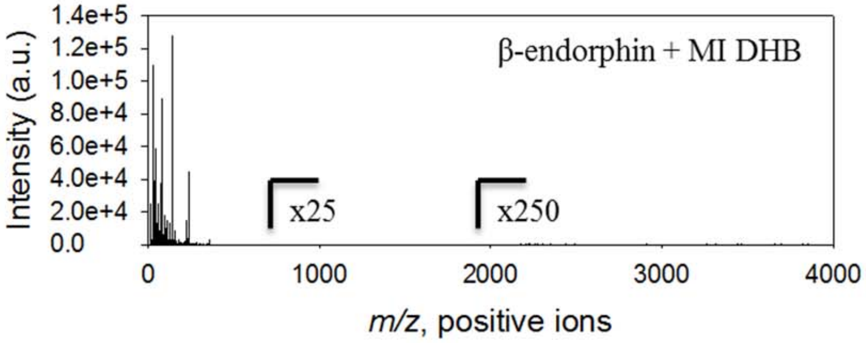
β-endorphin + MI DHB
x25
x250
Intensity (a.u.)
1.4e+5
1.2e+5
1.0e+5
8.0e+4
6.0e+4
4.0e+4
2.0e+4
0.0
0
1000
2000
3000
4000
m/z, positive ions

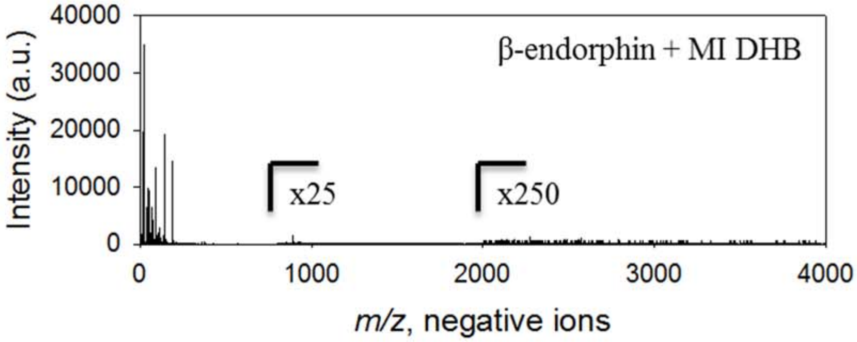
β-endorphin + MI DHB
x25
x250
Intensity (a.u.)
40000
30000
20000
10000
0
0
1000
2000
3000
4000
m/z, negative ions

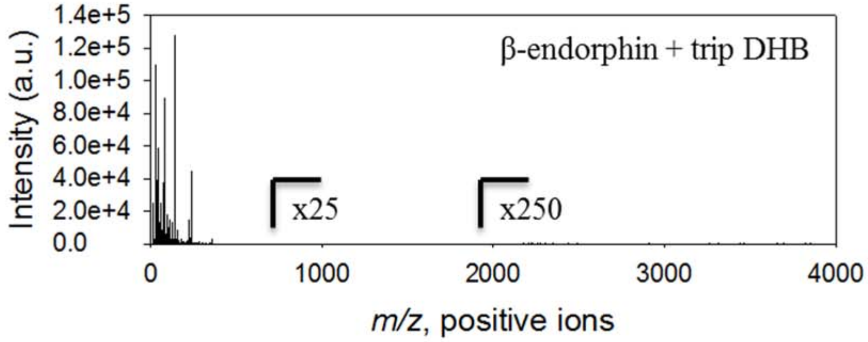
β-endorphin + trip DHB
x25
x250
Intensity (a.u.)
1.4e+5
1.2e+5
1.0e+5
8.0e+4
6.0e+4
4.0e+4
2.0e+4
0.0
0
1000
2000
3000
4000
m/z, positive ions

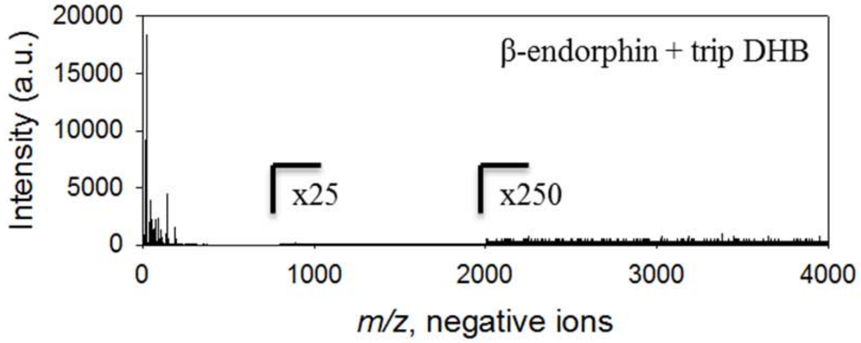
β-endorphin + trip DHB
x25
x250
Intensity (a.u.)
20000
15000
10000
5000
0
0
1000
2000
3000
4000
m/z, negative ions

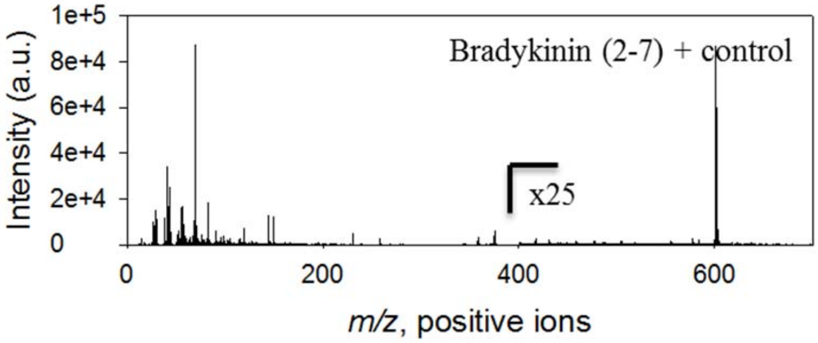
Bradykinin (2-7) + control
x25
Intensity (a.u.)
1e+5
8e+4
6e+4
4e+4
2e+4
0
0
200
400
600
m/z, positive ions

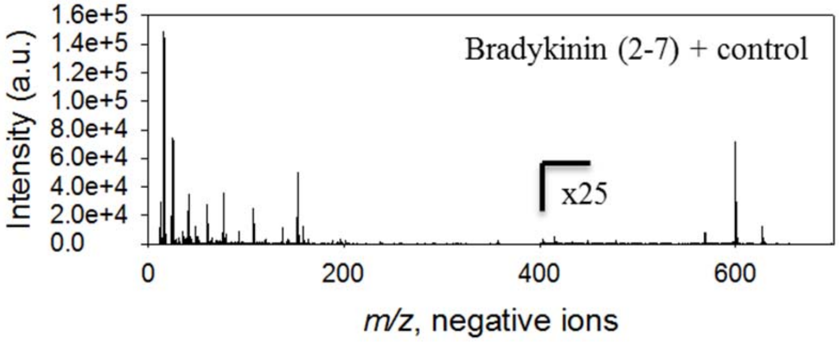
Bradykinin (2-7) + control
x25
Intensity (a.u.)
1.6e+5
1.4e+5
1.2e+5
1.0e+5
8.0e+4
6.0e+4
4.0e+4
2.0e+4
0.0
0
200
400
600
m/z, negative ions

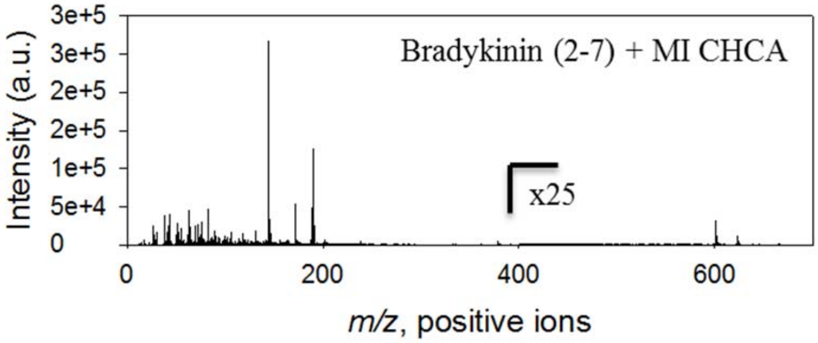
Bradykinin (2-7) + MI CHCA
x25
Intensity (a.u.)
3e+5
3e+5
2e+5
2e+5
1e+5
5e+4
0
0
200
400
600
m/z, positive ions

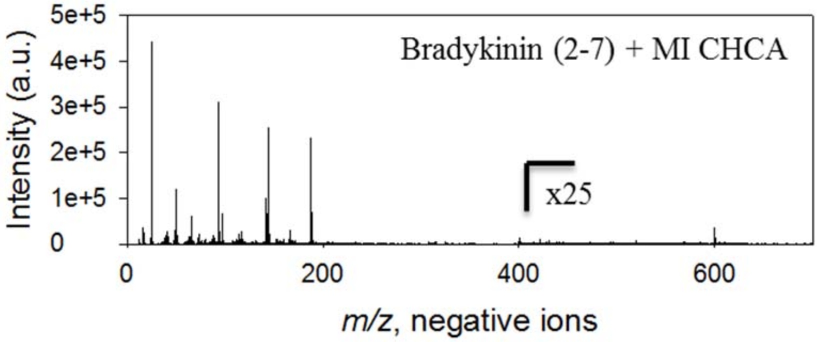
Bradykinin (2-7) + MI CHCA
x25
Intensity (a.u.)
5e+5
4e+5
3e+5
2e+5
1e+5
0
0
200
400
600
m/z, negative ions

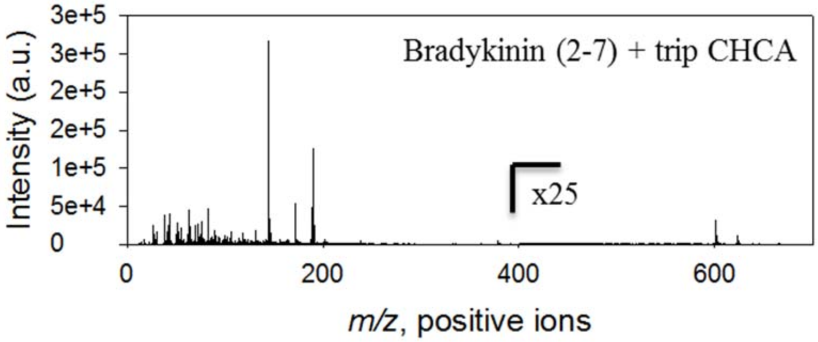
Bradykinin (2-7) + trip CHCA
x25
Intensity (a.u.)
3e+5
3e+5
2e+5
2e+5
1e+5
5e+4
0
0
200
400
600
m/z, positive ions

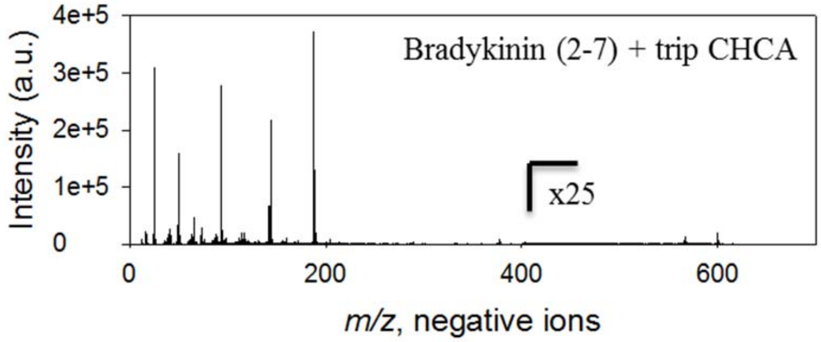
Bradykinin (2-7) + trip CHCA
x25
Intensity (a.u.)
4e+5
3e+5
2e+5
1e+5
0
0
200
400
600
m/z, negative ions

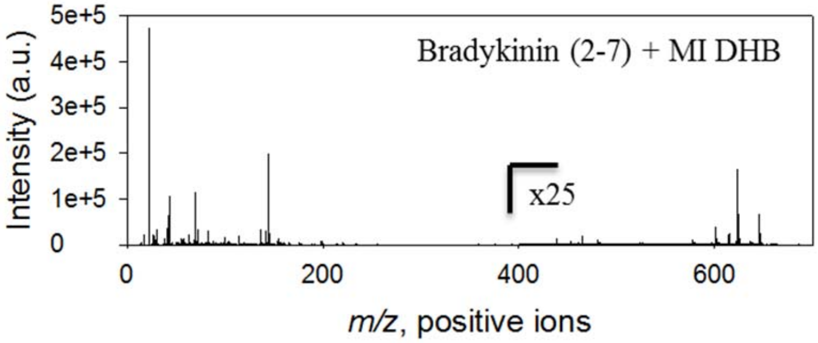
Bradykinin (2-7) + MI DHB
x25
Intensity (a.u.)
5e+5
4e+5
3e+5
2e+5
1e+5
0
0
200
400
600
m/z, positive ions

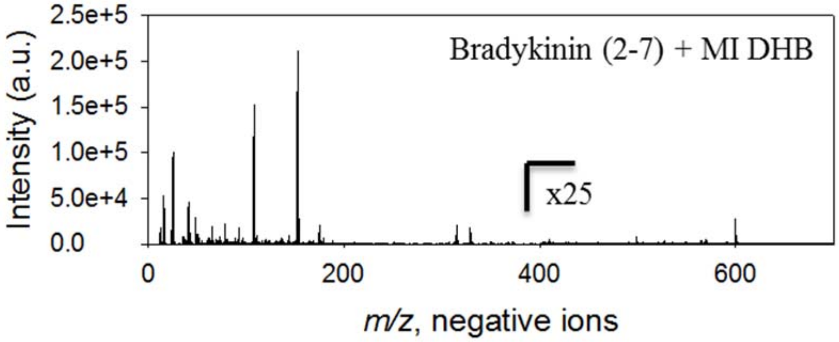
Bradykinin (2-7) + MI DHB
x25
Intensity (a.u.)
2.5e+5
2.0e+5
1.5e+5
1.0e+5
5.0e+4
0.0
0
200
400
600
m/z, negative ions

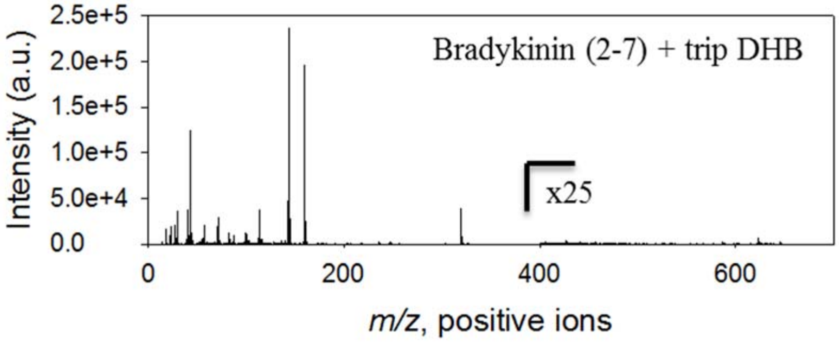
Bradykinin (2-7) + trip DHB
x25
Intensity (a.u.)
2.5e+5
2.0e+5
1.5e+5
1.0e+5
5.0e+4
0.0
0
200
400
600
m/z, positive ions

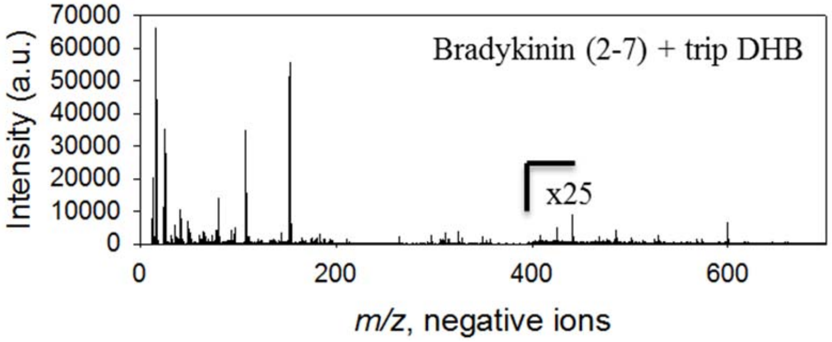
Bradykinin (2-7) + trip DHB
x25
Intensity (a.u.)
70000
60000
50000
40000
30000
20000
10000
0
0
200
400
600
m/z, negative ions

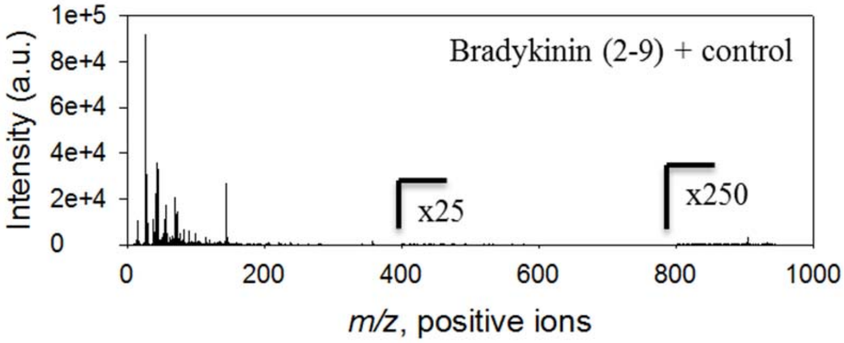
Intensity (a.u.)
1e+5
8e+4
6e+4
4e+4
2e+4
0
0
200
400
600
800
1000
m/z, positive ions
Bradykinin (2-9) + control
x25
x250

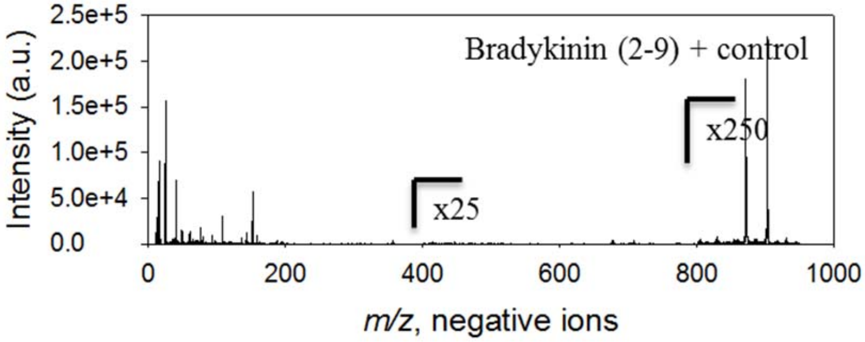
Intensity (a.u.)
2.5e+5
2.0e+5
1.5e+5
1.0e+5
5.0e+4
0.0
0
200
400
600
800
1000
m/z, negative ions
Bradykinin (2-9) + control
x25
x250

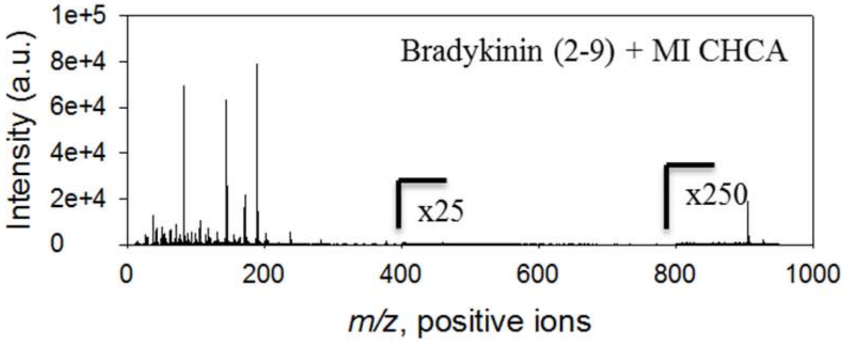
Bradykinin (2-9) + MI CHCA
Intensity (a.u.)
1e+5
8e+4
6e+4
4e+4
2e+4
0
x25
x250
0
200
400
600
800
1000
m/z, positive ions

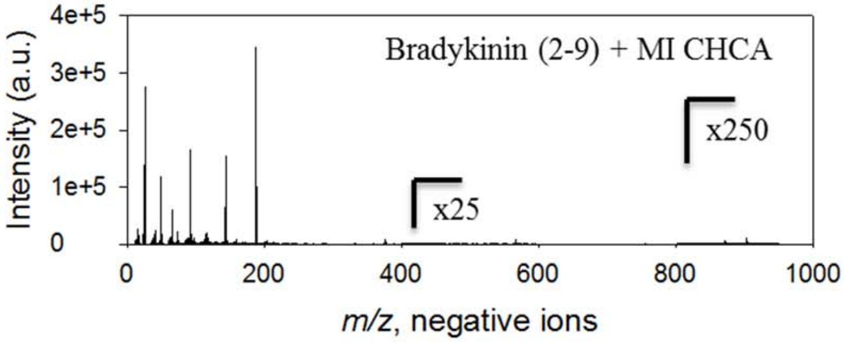
Bradykinin (2-9) + MI CHCA
Intensity (a.u.)
4e+5
3e+5
2e+5
1e+5
0
x25
x250
0
200
400
600
800
1000
m/z, negative ions

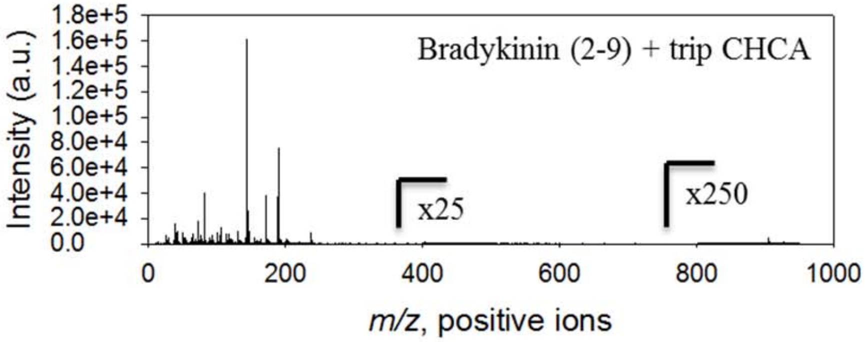
Bradykinin (2-9) + trip CHCA
Intensity (a.u.)
1.8e+5
1.6e+5
1.4e+5
1.2e+5
1.0e+5
8.0e+4
6.0e+4
4.0e+4
2.0e+4
0.0
x25
x250
0
200
400
600
800
1000
m/z, positive ions

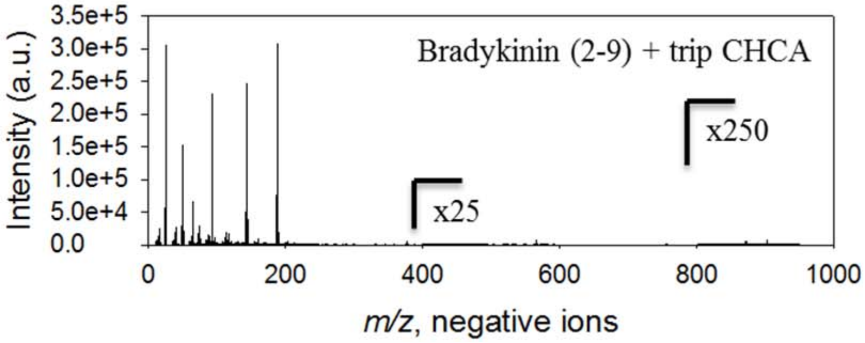
Bradykinin (2-9) + trip CHCA
Intensity (a.u.)
3.5e+5
3.0e+5
2.5e+5
2.0e+5
1.5e+5
1.0e+5
5.0e+4
0.0
x25
x250
0
200
400
600
800
1000
m/z, negative ions

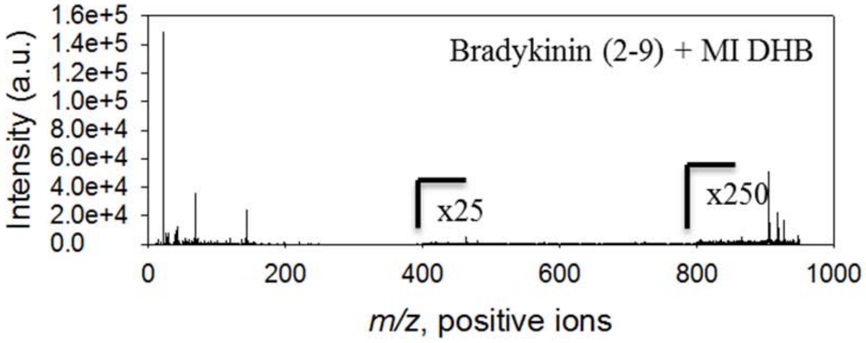
Bradykinin (2-9) + MI DHB
x25
x250
Intensity (a.u.)
1.6e+5
1.4e+5
1.2e+5
1.0e+5
8.0e+4
6.0e+4
4.0e+4
2.0e+4
0.0
0
200
400
600
800
1000
m/z, positive ions

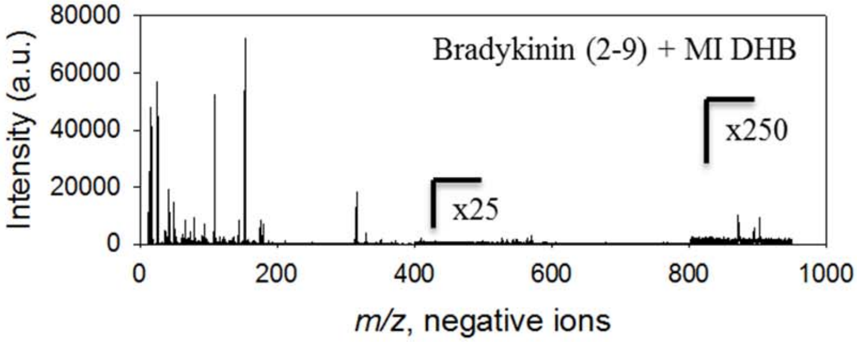
Bradykinin (2-9) + MI DHB
x25
x250
Intensity (a.u.)
80000
60000
40000
20000
0
0
200
400
600
800
1000
m/z, negative ions

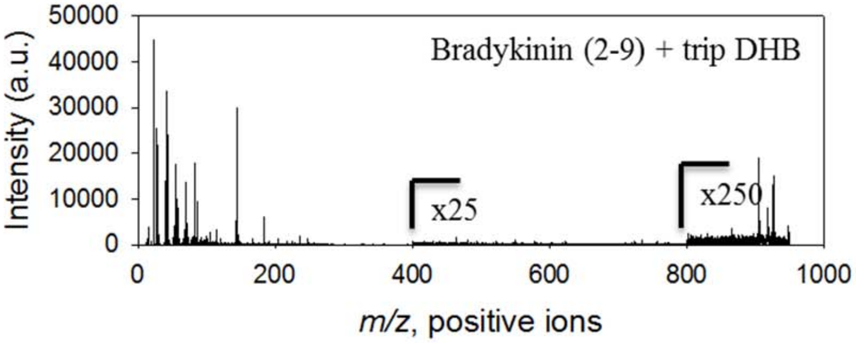
Bradykinin (2-9) + trip DHB
x25
x250
Intensity (a.u.)
50000
40000
30000
20000
10000
0
0
200
400
600
800
1000
m/z, positive ions

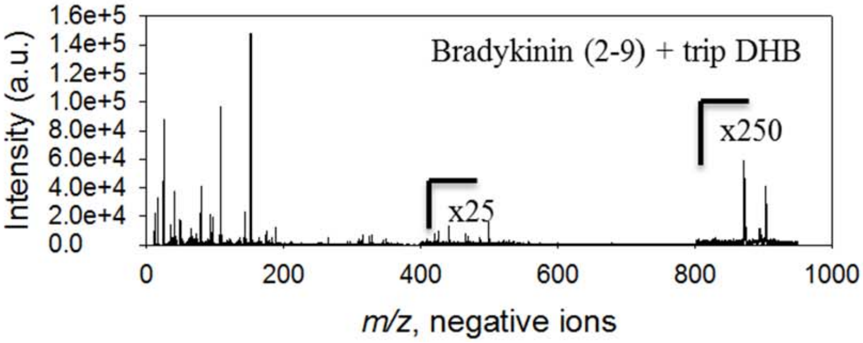
Bradykinin (2-9) + trip DHB
x25
x250
Intensity (a.u.)
1.6e+5
1.4e+5
1.2e+5
1.0e+5
8.0e+4
6.0e+4
4.0e+4
2.0e+4
0.0
0
200
400
600
800
1000
m/z, negative ions

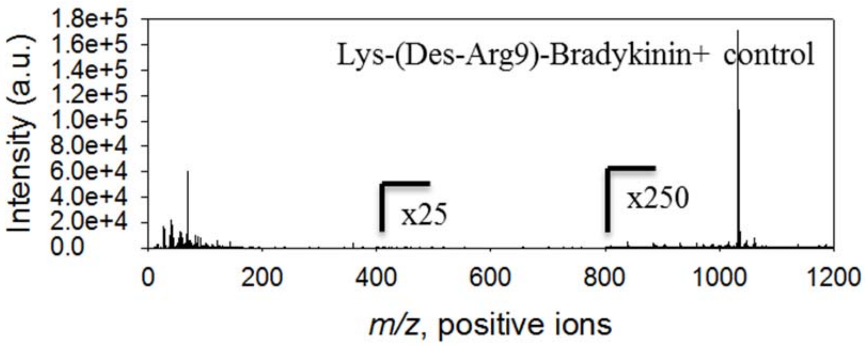
Lys-(Des-Arg9)-Bradykinin+ control
x25
x250
Intensity (a.u.)
1.8e+5
1.6e+5
1.4e+5
1.2e+5
1.0e+5
8.0e+4
6.0e+4
4.0e+4
2.0e+4
0.0
0
200
400
600
800
1000
1200
m/z, positive ions

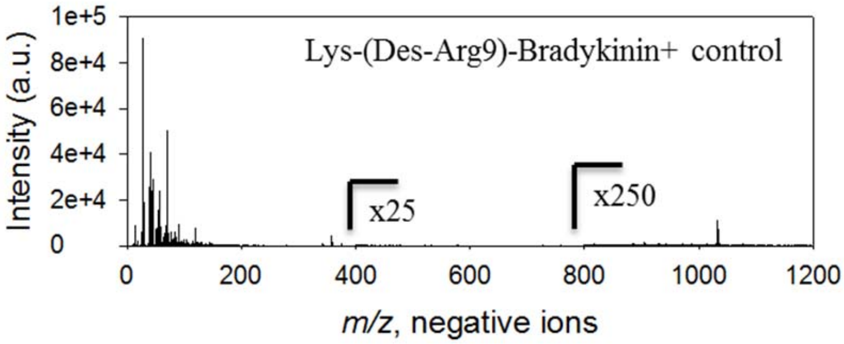
Lys-(Des-Arg9)-Bradykinin+ control
x25
x250
Intensity (a.u.)
1e+5
8e+4
6e+4
4e+4
2e+4
0
0
200
400
600
800
1000
1200
m/z, negative ions

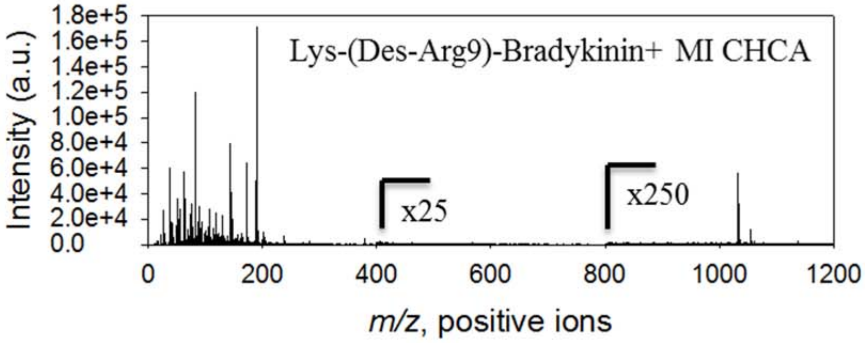
Lys-(Des-Arg9)-Bradykinin+ MI CHCA
x25
x250
Intensity (a.u.)
1.8e+5
1.6e+5
1.4e+5
1.2e+5
1.0e+5
8.0e+4
6.0e+4
4.0e+4
2.0e+4
0.0
0
200
400
600
800
1000
1200
m/z, positive ions

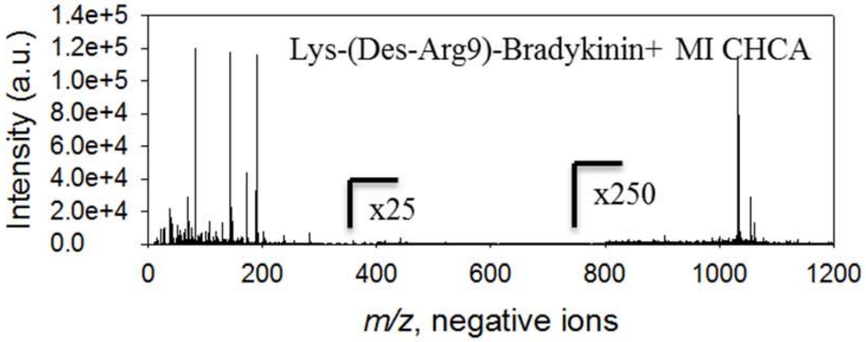
Lys-(Des-Arg9)-Bradykinin+ MI CHCA
x25
x250
Intensity (a.u.)
1.4e+5
1.2e+5
1.0e+5
8.0e+4
6.0e+4
4.0e+4
2.0e+4
0.0
0
200
400
600
800
1000
1200
m/z, negative ions

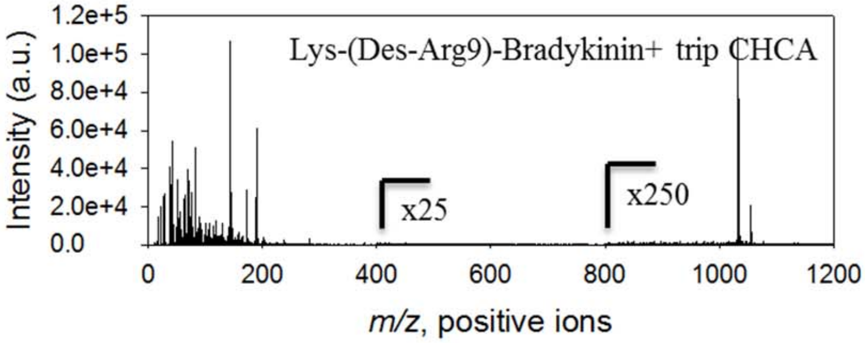
Lys-(Des-Arg9)-Bradykinin+ trip CHCA
x25
x250
Intensity (a.u.)
1.2e+5
1.0e+5
8.0e+4
6.0e+4
4.0e+4
2.0e+4
0.0
0
200
400
600
800
1000
1200
m/z, positive ions

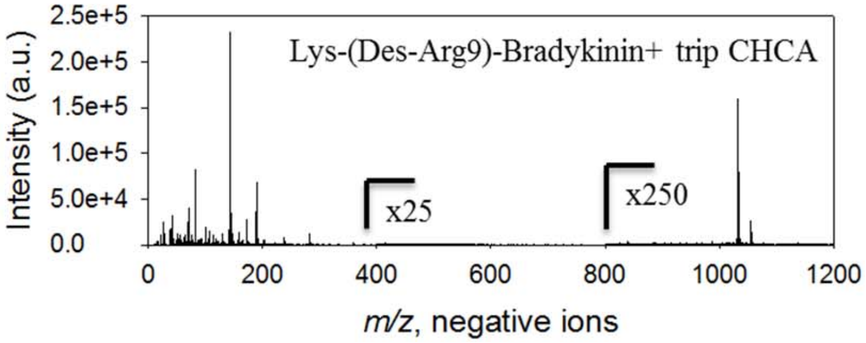
Lys-(Des-Arg9)-Bradykinin+ trip CHCA
x25
x250
Intensity (a.u.)
2.5e+5
2.0e+5
1.5e+5
1.0e+5
5.0e+4
0.0
0
200
400
600
800
1000
1200
m/z, negative ions

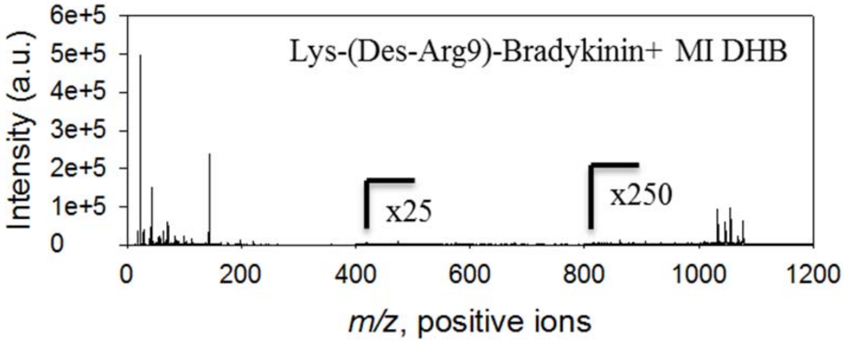
Lys-(Des-Arg9)-Bradykinin+ MI DHB
x25
x250
Intensity (a.u.)
6e+5
5e+5
4e+5
3e+5
2e+5
1e+5
0
0
200
400
600
800
1000
1200
m/z, positive ions

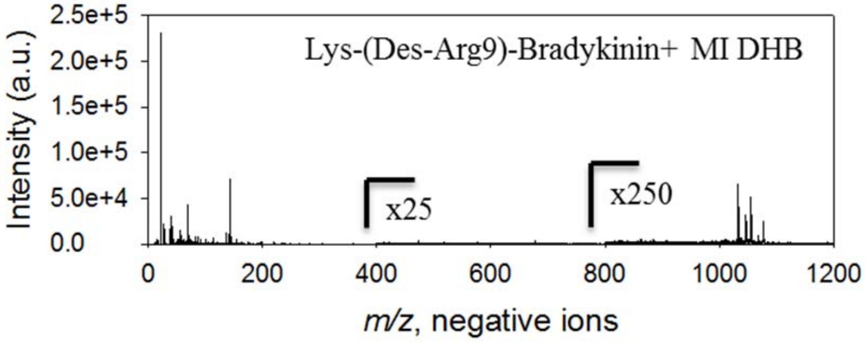
Lys-(Des-Arg9)-Bradykinin+ MI DHB
x25
x250
Intensity (a.u.)
2.5e+5
2.0e+5
1.5e+5
1.0e+5
5.0e+4
0.0
0
200
400
600
800
1000
1200
m/z, negative ions

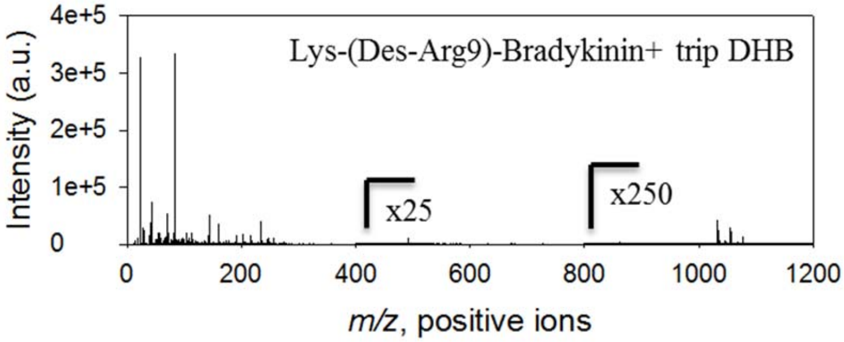
Lys-(Des-Arg9)-Bradykinin+ trip DHB
x25
x250
Intensity (a.u.)
4e+5
3e+5
2e+5
1e+5
0
0
200
400
600
800
1000
1200
m/z, positive ions

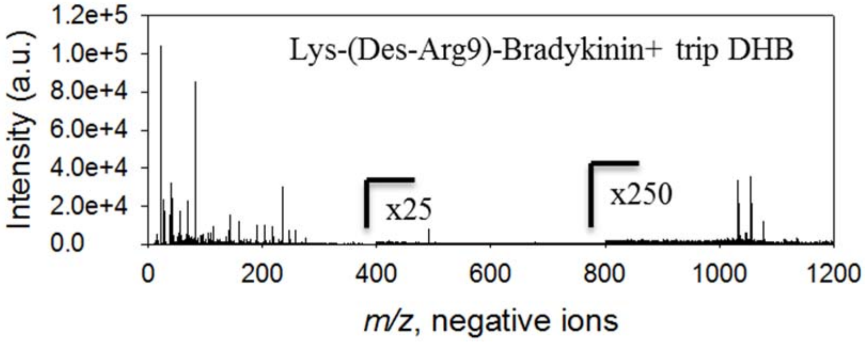
Lys-(Des-Arg9)-Bradykinin+ trip DHB
x25
x250
Intensity (a.u.)
1.2e+5
1.0e+5
8.0e+4
6.0e+4
4.0e+4
2.0e+4
0.0
0
200
400
600
800
1000
1200
m/z, negative ions

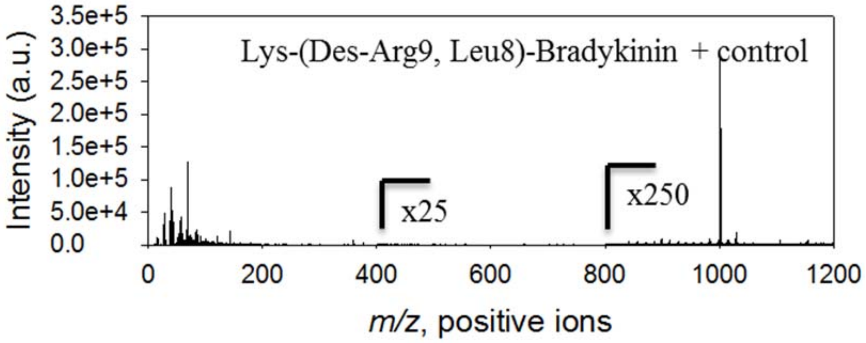
Lys-(Des-Arg9, Leu8)-Bradykinin + control
x25
x250
Intensity (a.u.)
3.5e+5
3.0e+5
2.5e+5
2.0e+5
1.5e+5
1.0e+5
5.0e+4
0.0
0
200
400
600
800
1000
1200
m/z, positive ions

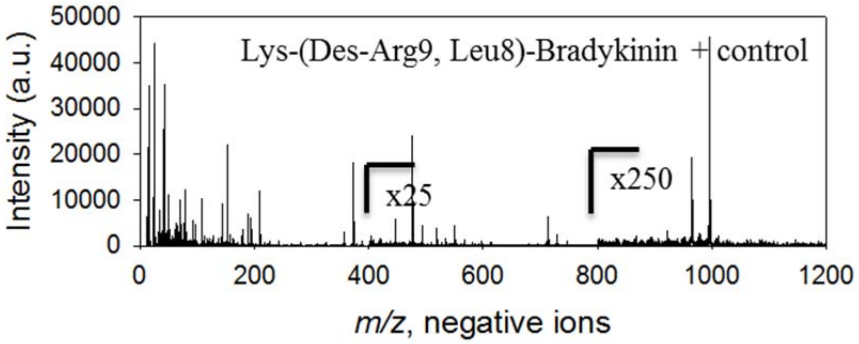
Lys-(Des-Arg9, Leu8)-Bradykinin + control
x25
x250
Intensity (a.u.)
50000
40000
30000
20000
10000
0
0
200
400
600
800
1000
1200
m/z, negative ions

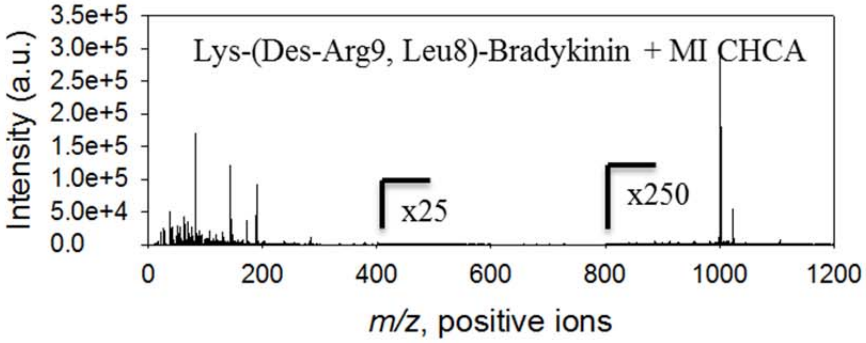
Lys-(Des-Arg9, Leu8)-Bradykinin + MI CHCA
x25
x250
Intensity (a.u.)
3.5e+5
3.0e+5
2.5e+5
2.0e+5
1.5e+5
1.0e+5
5.0e+4
0.0
0
200
400
600
800
1000
1200
m/z, positive ions

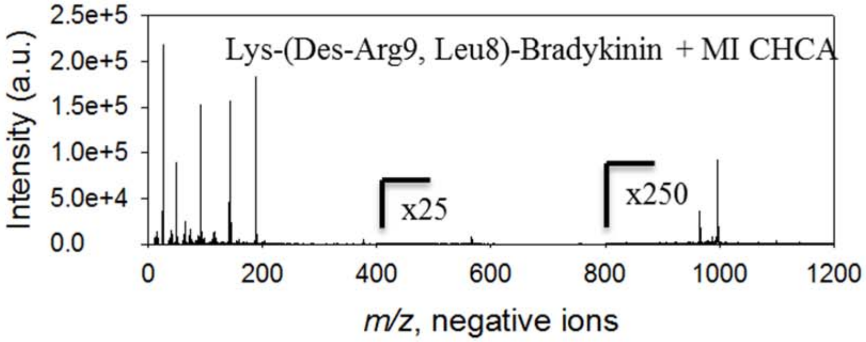
Lys-(Des-Arg9, Leu8)-Bradykinin + MI CHCA
x25
x250
Intensity (a.u.)
2.5e+5
2.0e+5
1.5e+5
1.0e+5
5.0e+4
0.0
0
200
400
600
800
1000
1200
m/z, negative ions

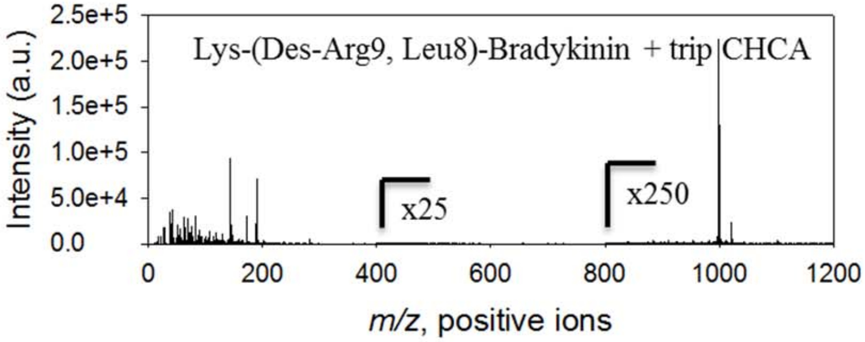
Lys-(Des-Arg9, Leu8)-Bradykinin + trip CHCA
x25
x250
Intensity (a.u.)
2.5e+5
2.0e+5
1.5e+5
1.0e+5
5.0e+4
0.0
0
200
400
600
800
1000
1200
m/z, positive ions

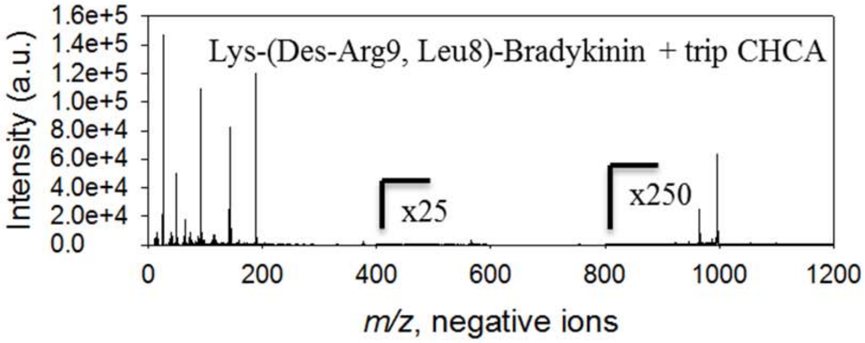
Lys-(Des-Arg9, Leu8)-Bradykinin + trip CHCA
x25
x250
Intensity (a.u.)
1.6e+5
1.4e+5
1.2e+5
1.0e+5
8.0e+4
6.0e+4
4.0e+4
2.0e+4
0.0
0
200
400
600
800
1000
1200
m/z, negative ions

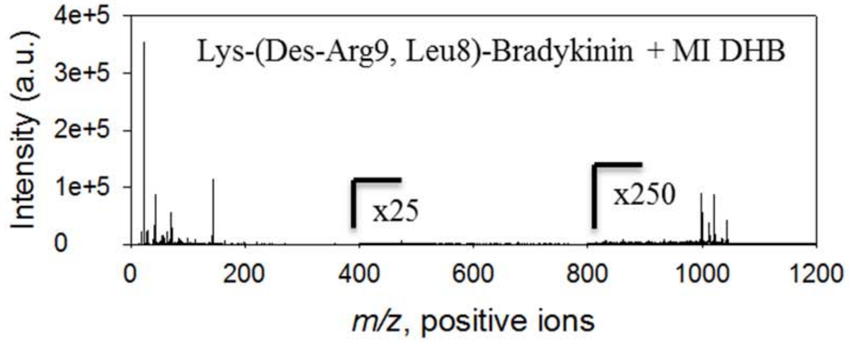
Lys-(Des-Arg9, Leu8)-Bradykinin + MI DHB
x25
x250
Intensity (a.u.)
4e+5
3e+5
2e+5
1e+5
0
0
200
400
600
800
1000
1200
m/z, positive ions

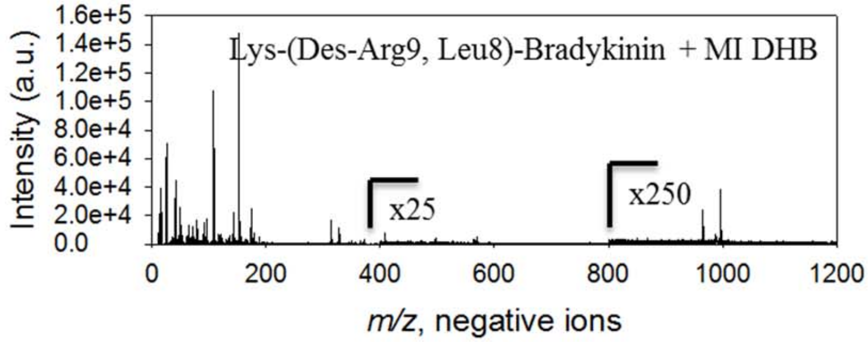
Lys-(Des-Arg9, Leu8)-Bradykinin + MI DHB
x25
x250
Intensity (a.u.)
1.6e+5
1.4e+5
1.2e+5
1.0e+5
8.0e+4
6.0e+4
4.0e+4
2.0e+4
0.0
0
200
400
600
800
1000
1200
m/z, negative ions

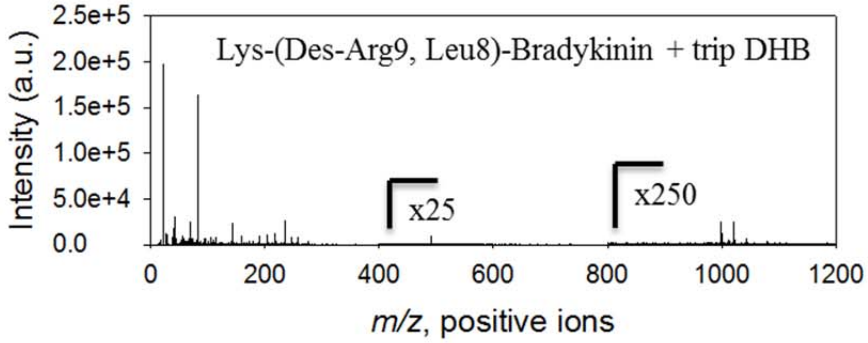
Lys-(Des-Arg9, Leu8)-Bradykinin + trip DHB
x25
x250
Intensity (a.u.)
2.5e+5
2.0e+5
1.5e+5
1.0e+5
5.0e+4
0.0
0
200
400
600
800
1000
1200
m/z, positive ions

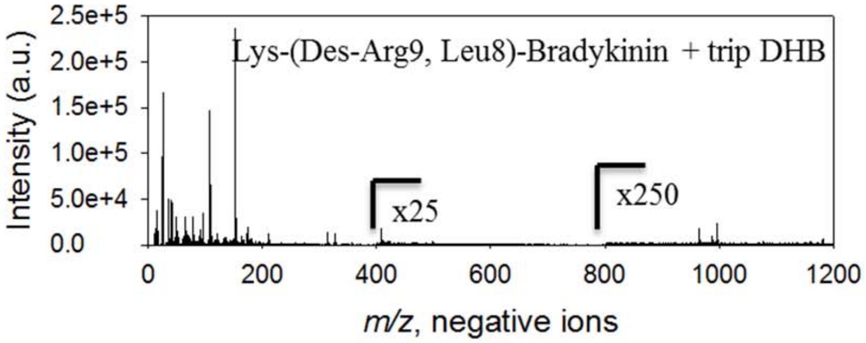
Lys-(Des-Arg9, Leu8)-Bradykinin + trip DHB
x25
x250
Intensity (a.u.)
2.5e+5
2.0e+5
1.5e+5
1.0e+5
5.0e+4
0.0
0
200
400
600
800
1000
1200
m/z, negative ions

Appendix 5

Fragment Ions of Deuterated Species

The deuteration of the d62DPPC and d75DPPC starting material was questioned as to its completeness. From the Avanti website there could be incomplete deuteration, due to the exchange on the alpha carbonyl positions.[1] However, we continue to believe that there is proton transfer happening to obtain the spectra observed.

First, it should be noted that the most important finding of the deuterated studies is that ever molecular ion has a gain of H^+. This H^+ is from the ionic liquid. Second, deuterium is exchanged with the ionic liquid, leading to $[\text{cation} + D]^+$ peaks observed (Chapter 6).

Third, the head group fragment ions show that deuterium is exchanging within these ions. Previous studies show that the $C_5H_{15}NPO_4^+$ ion is formed via the mechanism seen below in figure 1. However, in both d62DPPC and d75DPPC, the hydrogen thought to transfer remains a hydrogen and does not get deuterated. Whe the tail group is deuterated a rise in the $C_5H_{14}DNPO_4^+$ ion is seen. This suggests that the current mechanism is not correct and the the deuterium is labile on the tail group.

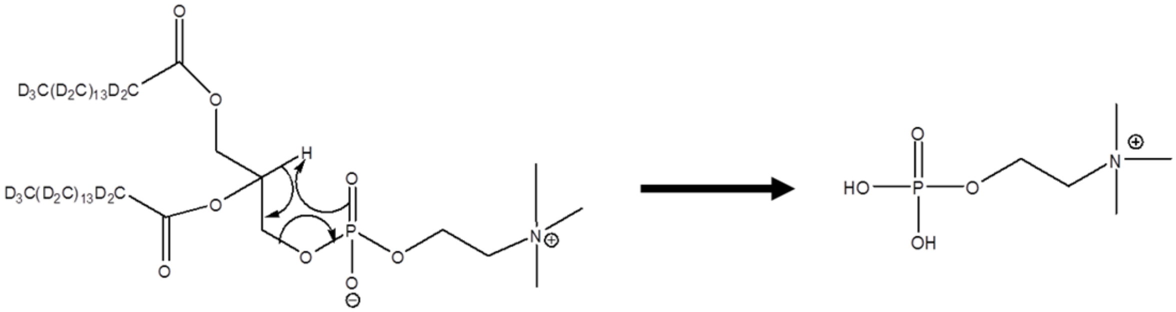

Figure 1. The previously proposed mechanism for the formation of the $C_5H_{15}NPO_4^+$ head group ion.[2]

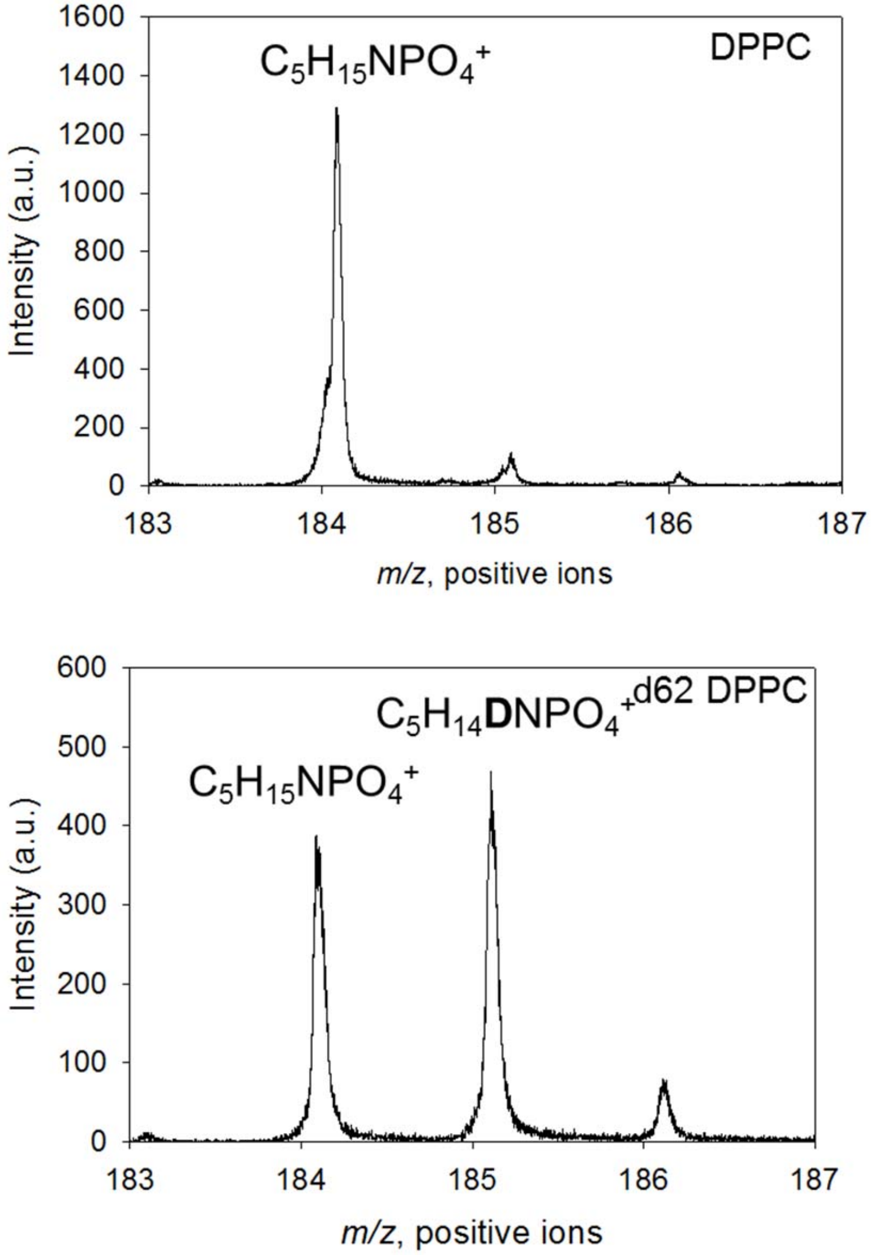

Figure 2. The head group spectra for a) DPPC and b) d62 DPPC. The deuterated head group ion is observed when the tail group is deuterated, suggesting an intramolecular transfer.

The $C_8H_{19}NPO_4^+$ ion forms via a differet pathway. The tail group does not impact a $C_8H_{18}DNPO_4^+$ fragment, but when the head group is deuterated there is an increase in the $C_8H_{18}DNPO_4^+$ ion intensity. This suggests that there are different reaction pathwats that can be monitored.

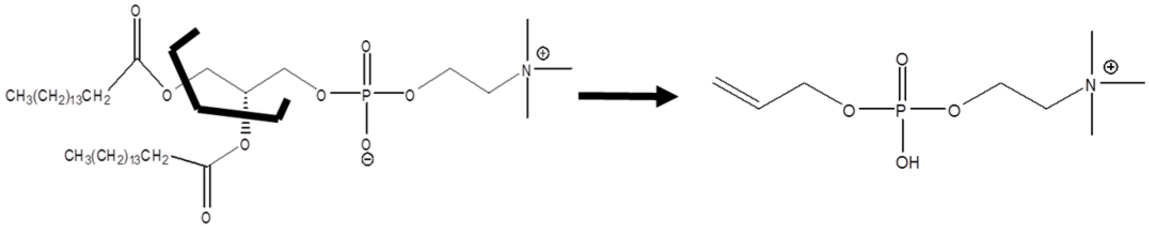

O
CH3(CH2)13CH2
O
O
CH3(CH2)13CH2
O
O
O
P
O
O
N
O
O
P
O
OH
N

Figure 3: Possible formation of the second head group fragment ion.

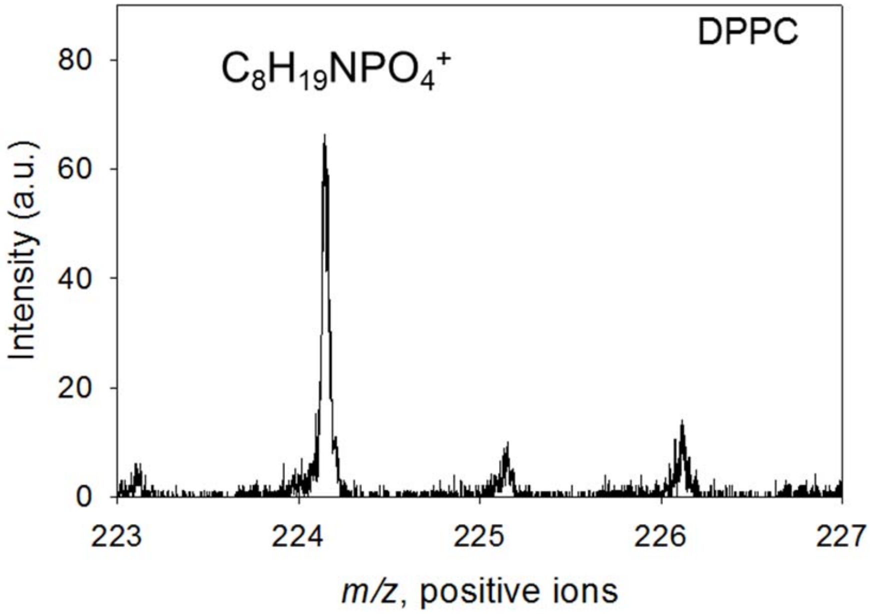

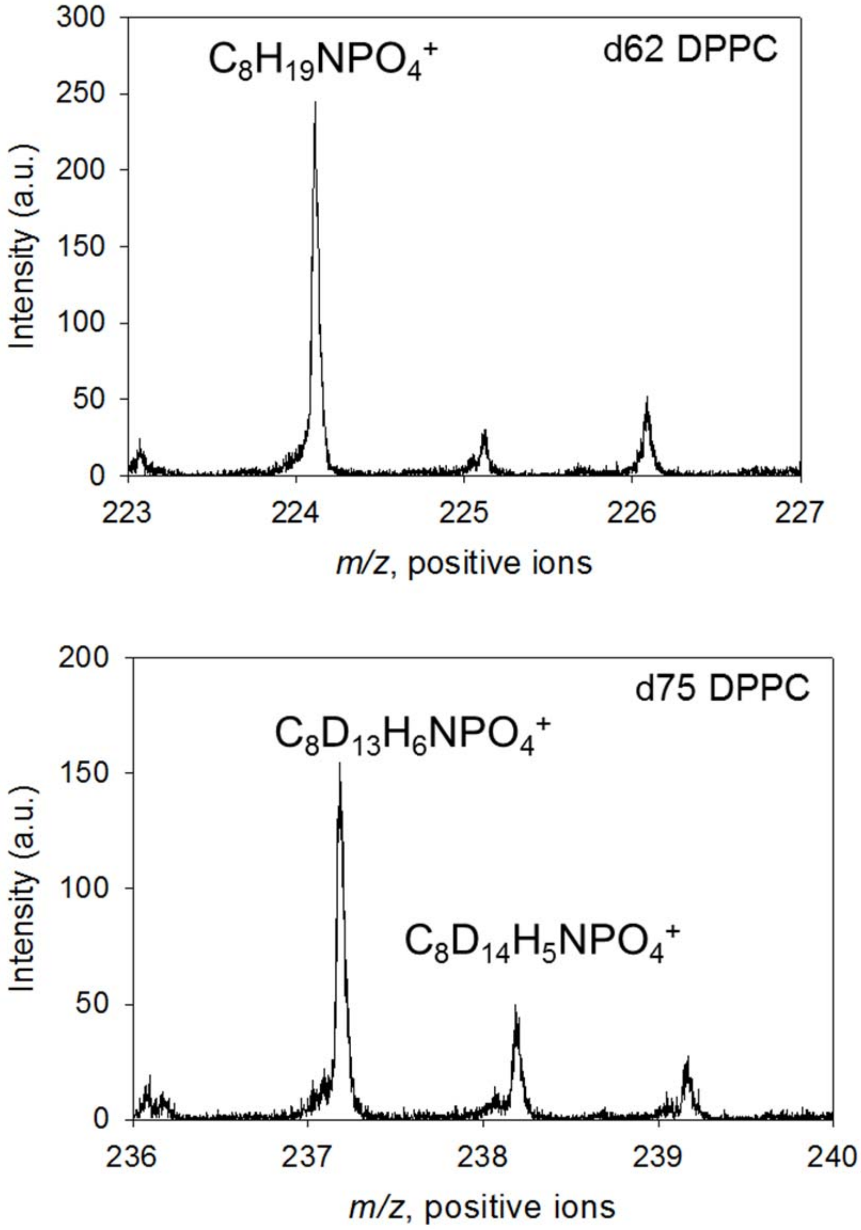

Figure 4. The head group spectra for a) DPPC, b) d62 DPPC, and c) d75 DPPC. The deuterated head group ion is observed only when the head group is deuterated, suggesting an intermolecular transfer.

Appendix 5 References

(1) Avanti Polar Lipids, I. 2012.

(2) Murphy, R. C. *Handbook of Lipid Research*; Plenium Press: New York, 1993; Vol. 7.